

NOVEL THERAPEUTIC TARGET AND DRUG DEVELOPMENT IN NEUROVASCULAR RETINAL DISEASES

EDITED BY: Amy Cheuk Yin Lo, Zhuo Shao, Zhongjie Fu and Zhongxiao Wang
PUBLISHED IN: Frontiers in Pharmacology





frontiers

Frontiers eBook Copyright Statement

The copyright in the text of individual articles in this eBook is the property of their respective authors or their respective institutions or funders. The copyright in graphics and images within each article may be subject to copyright of other parties. In both cases this is subject to a license granted to Frontiers.

The compilation of articles constituting this eBook is the property of Frontiers.

Each article within this eBook, and the eBook itself, are published under the most recent version of the Creative Commons CC-BY licence.

The version current at the date of publication of this eBook is CC-BY 4.0. If the CC-BY licence is updated, the licence granted by Frontiers is automatically updated to the new version.

When exercising any right under the CC-BY licence, Frontiers must be attributed as the original publisher of the article or eBook, as applicable.

Authors have the responsibility of ensuring that any graphics or other materials which are the property of others may be included in the CC-BY licence, but this should be checked before relying on the CC-BY licence to reproduce those materials. Any copyright notices relating to those materials must be complied with.

Copyright and source acknowledgement notices may not be removed and must be displayed in any copy, derivative work or partial copy which includes the elements in question.

All copyright, and all rights therein, are protected by national and international copyright laws. The above represents a summary only. For further information please read Frontiers' Conditions for Website Use and Copyright Statement, and the applicable CC-BY licence.

ISSN 1664-8714

ISBN 978-2-88966-868-7

DOI 10.3389/978-2-88966-868-7

About Frontiers

Frontiers is more than just an open-access publisher of scholarly articles: it is a pioneering approach to the world of academia, radically improving the way scholarly research is managed. The grand vision of Frontiers is a world where all people have an equal opportunity to seek, share and generate knowledge. Frontiers provides immediate and permanent online open access to all its publications, but this alone is not enough to realize our grand goals.

Frontiers Journal Series

The Frontiers Journal Series is a multi-tier and interdisciplinary set of open-access, online journals, promising a paradigm shift from the current review, selection and dissemination processes in academic publishing. All Frontiers journals are driven by researchers for researchers; therefore, they constitute a service to the scholarly community. At the same time, the Frontiers Journal Series operates on a revolutionary invention, the tiered publishing system, initially addressing specific communities of scholars, and gradually climbing up to broader public understanding, thus serving the interests of the lay society, too.

Dedication to Quality

Each Frontiers article is a landmark of the highest quality, thanks to genuinely collaborative interactions between authors and review editors, who include some of the world's best academicians. Research must be certified by peers before entering a stream of knowledge that may eventually reach the public – and shape society; therefore, Frontiers only applies the most rigorous and unbiased reviews. Frontiers revolutionizes research publishing by freely delivering the most outstanding research, evaluated with no bias from both the academic and social point of view. By applying the most advanced information technologies, Frontiers is catapulting scholarly publishing into a new generation.

What are Frontiers Research Topics?

Frontiers Research Topics are very popular trademarks of the Frontiers Journals Series: they are collections of at least ten articles, all centered on a particular subject. With their unique mix of varied contributions from Original Research to Review Articles, Frontiers Research Topics unify the most influential researchers, the latest key findings and historical advances in a hot research area! Find out more on how to host your own Frontiers Research Topic or contribute to one as an author by contacting the Frontiers Editorial Office: frontiersin.org/about/contact

NOVEL THERAPEUTIC TARGET AND DRUG DEVELOPMENT IN NEUROVASCULAR RETINAL DISEASES

Topic Editors:

Amy Cheuk Yin Lo, The University of Hong Kong, SAR China

Zhuo Shao, Hospital for Sick Children, Canada

Zhongjie Fu, Harvard Medical School, United States

Zhongxiao Wang, Harvard Medical School, United States

Citation: Lo, A. C. Y., Shao, Z., Fu, Z., Wang, Z., eds. (2021). Novel Therapeutic Target and Drug Development in Neurovascular Retinal Diseases. Lausanne: Frontiers Media SA. doi: 10.3389/978-2-88966-868-7

Table of Contents

- 05 Editorial: Novel Therapeutic Target and Drug Development in Neurovascular Retinal Diseases**
Zhuo Shao, Zhongxiao Wang, Amy C. Y. Lo and Zhongjie Fu
- 08 Metabolomic Profile of Posner–Schlossman Syndrome: A Gas Chromatography Time-of-Flight Mass Spectrometry-Based Approach Using Aqueous Humor**
Haiyan Wang, Ruyi Zhai, Qian Sun, Ying Wu, Zhujiang Wang, Junwei Fang and Xiangmei Kong
- 19 Inhibition of Pathological Retinal Neovascularization by a Small Peptide Derived from Human Tissue-Type Plasminogen Kringle 2**
Qian Sun, Yinchun Shen, Li Su and Xun Xu
- 29 LncRNA TDRG1-Mediated Overexpression of VEGF Aggravated Retinal Microvascular Endothelial Cell Dysfunction in Diabetic Retinopathy**
Qiaoyun Gong, Wenpei Dong, Ying Fan, Feng'e Chen, Xiaolan Bian, Xun Xu, Tianwei Qian and Ping Yu
- 40 MicroRNA-96 Promotes Vascular Repair in Oxygen-Induced Retinopathy—A Novel Uncovered Vasoprotective Function**
Michel Desjarlais, Maëlle Wirth, José Carlos Rivera, Isabelle Lahaie, Rabah Dabouz, Samy Omri, Pakiza Ruknudin, Celine Borrás and Sylvain Chemtob
- 54 High Glucose-Induced TRPC6 Channel Activation Decreases Glutamate Uptake in Rat Retinal Müller Cells**
Mingming Ma, Shuzhi Zhao, Jian Zhang, Tao Sun, Ying Fan and Zhi Zheng
- 64 Lactoferrin Has a Therapeutic Effect via HIF Inhibition in a Murine Model of Choroidal Neovascularization**
Mari Ibuki, Chiho Shoda, Yukihiro Miwa, Ayako Ishida, Kazuo Tsubota and Toshihide Kurihara
- 75 MicroRNA-18a-5p Administration Suppresses Retinal Neovascularization by Targeting FGF1 and HIF1A**
Ji-Tian Guan, Xin-Xin Li, De-Wei Peng, Wen-Meng Zhang, Jia Qu, Fan Lu, Robert J. D'Amato and Zai-Long Chi
- 86 Targeting Neuroinflammation in Neovascular Retinal Diseases**
Tianxi Wang, Demetrios I. Tsiurkis and Ye Sun
- 91 Arginase Pathway in Acute Retina and Brain Injury: Therapeutic Opportunities and Unexplored Avenues**
Abdelrahman Y. Fouda, Wael Eldahshan, S. Priya Narayanan, R. William Caldwell and Ruth B. Caldwell
- 98 Organoids and Microphysiological Systems: New Tools for Ophthalmic Drug Discovery**
Jing Bai and Chunming Wang
- 105 A Method for Developing Novel 3D Cornea-on-a-Chip Using Primary Murine Corneal Epithelial and Endothelial Cells**
Jing Bai, Haojie Fu, Lauren Bazinet, Amy E. Birsner and Robert J. D'Amato

114 Exploration of Oxygen-Induced Retinopathy Model to Discover New Therapeutic Drug Targets in Retinopathies

Maria Vähätupa, Tero A. H. Järvinen and Hannele Uusitalo-Järvinen

126 Protective Effects of Rapamycin on Trabecular Meshwork Cells in Glucocorticoid-Induced Glaucoma Mice

Xiaolu Zhu, Shengyu Wu, Wen Zeng, Xiaomin Chen, Tian Zheng, Jiangbo Ren and Min Ke

136 Mitochondrial Heme Synthesis Enzymes as Therapeutic Targets in Vascular Diseases

Trupti Shetty and Timothy W. Corson

142 EFEMP1 Overexpression Contributes to Neovascularization in Age-Related Macular Degeneration

Lu Cheng, Chong Chen, Wenke Guo, Kun Liu, Qianqian Zhao, Ping Lu, Fudong Yu and Xun Xu



Editorial: Novel Therapeutic Target and Drug Development in Neurovascular Retinal Diseases

Zhuo Shao¹, Zhongxiao Wang², Amy C. Y. Lo³ and Zhongjie Fu^{2*}

¹Division of Clinical and Metabolic Genetics, The Hospital for Sick Children, University of Toronto, Toronto, ON, Canada,

²Department of Ophthalmology, Boston Children's Hospital, Harvard Medical School, Boston, MA, United States, ³Department of Ophthalmology, LKS Faculty of Medicine, The University of Hong Kong, Hong Kong, China

Keywords: neovascularization, retina, retinopathy, metabolism, epigenetic modification, microfluidics, drug discovery, small peptide

Editorial on the Research Topic

Novel Therapeutic Target and Drug Development in Neurovascular Retinal Diseases

Pathological ocular angiogenesis leads to blindness in retinopathy of prematurity (ROP), diabetic retinopathy (DR), and age-related macular degeneration (AMD). Clinically approved anti-VEGF therapy has limited effectiveness and side effect profile unfit for some patients (Bressler et al., 2012; Jalali et al., 2013; Klufas and Chan, 2015; Zhao and Singh, 2018; Bakri et al., 2019). Therefore, further understanding of the disease pathogenesis and exploration of new therapeutics are required. In this research topic, we highlighted new drug targets, therapeutic approaches, and technologies for treatment of ocular neovascularization.

OPEN ACCESS

Edited and reviewed by:

Nicholas M. Barnes,
University of Birmingham,
United Kingdom

*Correspondence:

Zhongjie Fu
zhongjie.fu@childrens.harvard.edu

Specialty section:

This article was submitted to
Neuropharmacology,
a section of the journal
Frontiers in Pharmacology

Received: 23 January 2021

Accepted: 15 March 2021

Published: 15 April 2021

Citation:

Shao Z, Wang Z, Lo ACY and Fu Z
(2021) Editorial: Novel Therapeutic
Target and Drug Development in
Neurovascular Retinal Diseases.
Front. Pharmacol. 12:657684.
doi: 10.3389/fphar.2021.657684

METABOLISM AND CELL-CELL INTERACTION

Understanding the interaction of endothelial cells with the surrounding cells is essential for the development of effective and safe therapeutics (Wilson and Sapieha, 2016; Binet et al., 2020; Fu et al., 2020). Neuronal metabolism regulates retinal vascular function (Joyal et al., 2018; Fu et al., 2019). In this research topic, Fouda et al. provided a systematic overview of the arginase pathway in acute retina and brain injury, and discussed the possibility of modulating this pathway to treat ischemia-induced neurodegeneration. Shetty and Corson summarized the vulnerability of endothelial cells to mitochondrial heme loss, and proposed that targeting intracellular heme via inhibiting heme synthesis or blocking heme transport may be a novel strategy to decrease retinal neovascularization. Further exploration of neural-vascular metabolism and interaction is needed. Endothelial cells utilize glucose, fatty acid and glutamine as substrates for energy and biomass for cell homeostasis and growth (Falkenberg et al., 2019). On the other hand, photoreceptors require glucose and fatty acids for energy production and function (Joyal et al., 2016). Therefore, when considering interventions for metabolic modulation, it is necessary to take into account the overall impact on various retinal cell types.

In addition, the interaction of metabolic pathways in retinopathies also requires further investigation. Recently, low serine with increase in deoxysphingolipids is reported to correlate with macular disease (Gantner et al., 2019). Wang et al. revealed significant metabolic disturbances (such as amino acids and ketone bodies) in aqueous humor of patients with Posner-Schlossman syndrome that were identified with metabolomics. Further exploration of retinal metabolic interactions between amino acid, lipid pathways, and others would definitely attract great interests.

Inflammation and autophagy are induced in response to stressed conditions such as in retinal metabolic disorders (Tang and Kern, 2011; Mitter et al., 2012; Kauppinen et al., 2016). Wang et al. discussed that persistent neuroinflammation exacerbates ocular neovascularization. They further explored the potential involvement of SOCS3 and c-Fos in the disease pathogenesis of retinopathies. Zhu et al. demonstrated that rapamycin induced autophagy and preserved trabecular meshwork cells in glucocorticoid-induced glaucoma mice can be a potential therapeutic approach to glaucoma.

GENOMICS, TRANSCRIPTOME, AND PROTEOMICS FOR DRUG TARGET IDENTIFICATION

Recently, genomic analysis, transcriptome profiling, and proteomics have been used as a hypothesis free approach to identify drug targets in retinal neovascular diseases (Vahatupa et al., 2018; Desjarlais et al., 2019). Desjarlais et al. reported the discovery of down regulation of MicroRNA-96 in oxygen induced retinopathy (OIR) rats through next generation sequencing (NGS) screening. *In vitro* study demonstrated that overexpression of MicroRNA-96 stimulated tubulogenesis and migration against hyperoxia-induced endothelial dysfunction, while antagonizing microRNA-96 led to angiogenic impairment. Intravitreally supplementing microRNA-96 mimic preserved retinal/choroidal microvessels in the hyperoxic state of rat OIR model. Cheng et al. analyzed and compared transcriptome profiles in retinal-choroid tissues derived from donor patients with AMD and healthy controls. They identified that *EFEMP1* gene was upregulated in the AMD, especially wet-AMD patients. Elevation of *EFEMP1* product, fibulin-3, was confirmed in the serum of wet-AMD patients. *In vitro* overexpression and knockdown of *EFEMP1* in human umbilical vein endothelial cells (HUVECs) confirmed the proangiogenic effect of this gene. Vähätupa et al. reviewed the elevation of crystallins, small heat shock proteins, during early hypoxic state of OIR as well as an increase of actomyosin complex and Filamin A-R-Ras axis at the peak of neovascularization that were discovered through proteomic analysis using sequential window acquisition of all theoretical mass spectra (SWATH-MS). Some crystallins are neuroprotective while others play a prominent role in the pathology of neovascularization. The actomyosin complex and Filamin A-R-Ras axis regulates vascular permeability of the angiogenic blood vessels. These proteomic changes were also confirmed patients with proliferative diabetic retinopathy (PDR) and retinal vein occlusion (RVO).

RNA AND PEPTIDE BASED THERAPEUTIC APPROACHES

RNA based therapeutic approaches against retinal neovascular disease have gained significant interest in recent years. Ma et al. found that silencing *Trpc6* with RNA interference (RNAi) abolished high glucose-induced decreases in glutamate uptake and Müller glial cell death *in vitro*, suggesting that TRPC6 may be a promising target that deserves further investigation in animal

models. Protection of neurovascular supporting cells Müller glia and regulation of Müller gliosis may protect against diabetic retinopathy (Coughlin et al., 2017; Le, 2017). Additionally, Guan et al. reported that MicroRNA-18a-5p is increased during neovascularization of OIR mice retina, adding to the list of miRNAs that is involved in this process (Zhou et al., 2016; Xia et al., 2018). Antagonizing MicroRNA-18a-5p using agomiR-18a-5p suppressed neovascularization in OIR mice and Human Retinal Microvascular Endothelial Cell (HRMEC) proliferation, migration, and tube formation. miRNA mimics or inhibitors have been tested in clinical trials for treatment of viral infection (Janssen et al., 2013) and malignancy (Van Zandwijk et al., 2017). Moreover, long non coding RNAs (lncRNAs) have been shown to participate in transcription, post-transcription, translation, epigenetic regulation, splicing, and intracellular/extracellular trafficking (Wilusz et al., 2009). Gong et al. characterized the role of lncRNA human testis development-related gene 1 (TDRG1) in proliferative DR through modulation of VEGF. lncRNA TDRG1 was elevated in fibrovascular membranes (FVMs) from DR patients and hyperglycemic treated HRMECs. Knockdown of lncRNA TDRG1 reduced the VEGF level in HRMECs and protect against high-glucose-stimulated HRMEC migration.

In the area of peptide-based therapies, Sun et al. tested a small peptide derived from human tissue-type plasminogen kringle 2 (t-PA kringle 2) in HRMEC and mice model of OIR. Their study demonstrated that this peptide effectively inhibits HRMEC proliferation, migration and tube formation. It also inhibited retinal neovascularization in OIR mice retina. Compared to proteins, small peptides present the advantage of easier and relatively inexpensive synthesis, higher consistency between batches, lower immunogenicity, higher solubility in water, and better penetrating abilities. On the other hand, Ibuki et al. focused on Lactoferrin, a type of glycoprotein that is naturally present in body fluids. In this study, oral administration of Lactoferrin was shown to reduce laser-induced CNV in mice through inhibition of Hypoxia Induced Factor (HIF). Similarly, lactoferrin was shown to inhibit HIF in the 661W cone photoreceptor cell line.

ADVANCED TECHNOLOGIES

2D cell culture model has been widely used for mechanistic investigations and drug tests. However, this approach is limited by altered extracellular microenvironment, cell morphology and polarity, as well as nutrition depletion and waste product accumulation in media (Kapalczyńska et al., 2018). Bai and Wang summarized 3D organoid and microfluidic system as tools for the study of organ function and ophthalmic drug delivery. Bai et al. also reported the detailed methodology on the development of cornea-on-a-chip using primary murine corneal epithelial and endothelial cells. Taking the advantage of better modeling *in vivo* conditions, 3D culture is believed to improve the disease pathogenesis study and drug testing process.

In conclusion, this research topic includes original studies and reviews regarding novel therapeutic approaches to neurovascular

retinopathies. Improved understanding of the metabolic and inflammatory aspects of cell-cell interaction expands potential drug target for retinal neovascularization. Novel therapeutic approaches using RNA and peptide-based molecules diversifies the therapeutic approaches to these blinding diseases, where newly developed models such as 3D culture holds the promises of expediting and reducing the cost of drug discovery process. As Topic Editors of this special issue, we

sincerely thank all the authors and reviewers for their valuable contributions to this research topic.

AUTHOR CONTRIBUTIONS

All authors listed have made a substantial, direct and intellectual contribution to the work, and approved it for publication.

REFERENCES

- Bakri, S. J., Thorne, J. E., Ho, A. C., Ehlers, J. P., Schoenberger, S. D., Yeh, S., et al. (2019). Safety and efficacy of anti-vascular endothelial growth factor therapies for neovascular age-related macular degeneration. *Ophthalmology* 126, 55–63. doi:10.1016/j.ophtha.2018.07.028
- Binet, F., Cagnone, G., Crespo-Garcia, S., Hata, M., Neault, M., Dejda, A., et al. (2020). Neutrophil extracellular traps target senescent vasculature for tissue remodeling in retinopathy. *Science* 369. doi:10.1126/science.aay5356
- Bressler, N. M., Boyer, D. S., Williams, D. F., Butler, S., Francom, S. F., Brown, B., et al. (2012). Cerebrovascular accidents in patients treated for choroidal neovascularization with ranibizumab in randomized controlled trials. *Retina* 32, 1821–1828. doi:10.1097/iae.0b013e31825db6ba
- Coughlin, B. A., Feenstra, D. J., and Mohr, S. (2017). Müller cells and diabetic retinopathy. *Vis. Res.* 139, 93–100. doi:10.1016/j.visres.2017.03.013
- Desjarlais, M., Rivera, J. C., Lahaie, I., Cagnone, G., Wirt, M., Omri, S., et al. (2019). MicroRNA expression profile in retina and choroid in oxygen-induced retinopathy model. *PLoS One* 14, e0218282. doi:10.1371/journal.pone.0218282
- Falkenberg, K. D., Rohlenova, K., Luo, Y., and Carmeliet, P. (2019). The metabolic engine of endothelial cells. *Nat. Metab.* 1, 937–946. doi:10.1038/s42255-019-0117-9
- Fu, Z., Chen, C. T., Cagnone, G., Heckel, E., Sun, Y., Cakir, B., et al. (2019). Dyslipidemia in retinal metabolic disorders. *EMBO Mol. Med.* 11, e10473. doi:10.15252/emmm.201910473
- Fu, Z., Sun, Y., Cakir, B., Tomita, Y., Huang, S., Wang, Z., et al. (2020). Targeting neurovascular interaction in retinal disorders. *Int. J. Mol. Sci.* 21, 1503. doi:10.3390/ijms21041503
- Gantner, M. L., Eade, K., Wallace, M., Handzlik, M. K., Fallon, R., Trombley, J., et al. (2019). Serine and lipid metabolism in macular disease and peripheral neuropathy. *N. Engl. J. Med.* 381, 1422–1433. doi:10.1056/nejmoa1815111
- Jalali, S., Balakrishnan, D., Zeynalova, Z., Padhi, T. R., and Rani, P. K. (2013). Serious adverse events and visual outcomes of rescue therapy using adjunct bevacizumab to laser and surgery for retinopathy of prematurity. The Indian Twin Cities Retinopathy of Prematurity Screening database Report number 5. *Arch. Dis. Child. Fetal Neonatal. Ed.* 98, F327–F333. doi:10.1136/archdischild-2012-302365
- Janssen, H. L. A., Reesink, H. W., Lawitz, E. J., Zeuzem, S., Rodriguez-Torres, M., Patel, K., et al. (2013). Treatment of HCV infection by targeting microRNA. *N. Engl. J. Med.* 368, 1685–1694. doi:10.1056/nejmoa1209026
- Joyal, J.-S., Gantner, M. L., and Smith, L. E. H. (2018). Retinal energy demands control vascular supply of the retina in development and disease: the role of neuronal lipid and glucose metabolism. *Prog. Retin. Eye Res.* 64, 131–156. doi:10.1016/j.preteyeres.2017.11.002
- Joyal, J.-S., Sun, Y., Gantner, M. L., Shao, Z., Evans, L. P., Saba, N., et al. (2016). Retinal lipid and glucose metabolism dictates angiogenesis through the lipid sensor Ffar1. *Nat. Med.* 22, 439–445. doi:10.1038/nm.4059
- Kapalczynska, M., Kolenda, T., Przybyla, W., Zajackowska, M., Teresiak, A., Filas, V., et al. (2018). 2D and 3D cell cultures - a comparison of different types of cancer cell cultures. *Arch. Med. Sci.* 14, 910–919. doi:10.5114/aoms.2016.63743
- Kauppinen, A., Paterno, J. J., Blasiak, J., Salminen, A., and Kaarniranta, K. (2016). Inflammation and its role in age-related macular degeneration. *Cell. Mol. Life Sci.* 73, 1765–1786. doi:10.1007/s00018-016-2147-8
- Klufas, M. A., and Paul Chan, R. V. (2015). Intravitreal anti-VEGF therapy as a treatment for retinopathy of prematurity: what we know after 7 years. *J. Pediatr. Ophthalmol. Strabismus* 52, 77–84. doi:10.3928/01913913-20150216-01
- Le, Y.-Z. (2017). VEGF production and signaling in Müller glia are critical to modulating vascular function and neuronal integrity in diabetic retinopathy and hypoxic retinal vascular diseases. *Vis. Res.* 139, 108–114. doi:10.1016/j.visres.2017.05.005
- Mitter, S. K., Rao, H. V., Qi, X., Cai, J., Sugrue, A., Dunn, W. A., Jr., et al. (2012). Autophagy in the retina: a potential role in age-related macular degeneration. *Adv. Exp. Med. Biol.* 723, 83–90. doi:10.1007/978-1-4614-0631-0_12
- Tang, J., and Kern, T. S. (2011). Inflammation in diabetic retinopathy. *Prog. Retin. Eye Res.* 30, 343–358. doi:10.1016/j.preteyeres.2011.05.002
- Vähätupa, M., Nättinen, J., Jylhä, A., Aapola, U., Kataja, M., Kööbi, P., et al. (2018). SWATH-MS proteomic analysis of oxygen-induced retinopathy reveals novel potential therapeutic targets. *Invest. Ophthalmol. Vis. Sci.* 59, 3294–3306. doi:10.1167/jovs.18-23831
- Van Zandwijk, N., Pavlakis, N., Kao, S. C., Linton, A., Boyer, M. J., Clarke, S., et al. (2017). Safety and activity of microRNA-loaded minicells in patients with recurrent malignant pleural mesothelioma: a first-in-man, phase 1, open-label, dose-escalation study. *Lancet Oncol.* 18, 1386–1396. doi:10.1016/s1470-2045(17)30621-6
- Wilson, A., and Sapieha, P. (2016). Neurons and guidance cues in retinal vascular diseases. *Oncotarget* 7, 9618–9619. doi:10.18632/oncotarget.7413
- Wilusz, J. E., Sunwoo, H., and Spector, D. L. (2009). Long noncoding RNAs: functional surprises from the RNA world. *Genes Develop.* 23, 1494–1504. doi:10.1101/gad.1800909
- Xia, F., Sun, J.-J., Jiang, Y.-Q., and Li, C.-F. (2018). MicroRNA-384-3p inhibits retinal neovascularization through targeting hexokinase 2 in mice with diabetic retinopathy. *J. Cell Physiol* 234, 721–730. doi:10.1002/jcp.26871
- Zhao, Y., and Singh, R. P. (2018). The role of anti-vascular endothelial growth factor (anti-VEGF) in the management of proliferative diabetic retinopathy. *Drugs Context* 7, 212532. doi:10.7573/dic.212532
- Zhou, Q., Anderson, C., Hanus, J., Zhao, F., Ma, J., Yoshimura, A., et al. (2016). Strand and cell type-specific function of microRNA-126 in angiogenesis. *Mol. Ther.* 24, 1823–1835. doi:10.1038/mt.2016.108

Conflict of Interest: The authors declare that the research was conducted in the absence of any commercial or financial relationships that could be construed as a potential conflict of interest.

Copyright © 2021 Shao, Wang, Lo and Fu. This is an open-access article distributed under the terms of the Creative Commons Attribution License (CC BY). The use, distribution or reproduction in other forums is permitted, provided the original author(s) and the copyright owner(s) are credited and that the original publication in this journal is cited, in accordance with accepted academic practice. No use, distribution or reproduction is permitted which does not comply with these terms.



Metabolomic Profile of Posner–Schlossman Syndrome: A Gas Chromatography Time-of-Flight Mass Spectrometry-Based Approach Using Aqueous Humor

Haiyan Wang^{1,2,3†}, Ruyi Zhai^{4,5,6†}, Qian Sun^{1,2,3}, Ying Wu^{1,2,3}, Zhujuan Wang^{4,5,6}, Junwei Fang^{1,2,3,7*} and Xiangmei Kong^{4,5,6*}

¹ Department of Ophthalmology, Shanghai General Hospital, Shanghai Jiao Tong University School of Medicine, Shanghai, China, ² Shanghai Key Laboratory of Ocular Fundus Diseases, Shanghai Jiao Tong University, Shanghai, China, ³ Shanghai Engineering Center for Visual Science and Photomedicine, Shanghai, China, ⁴ Department of Ophthalmology and Visual Science, Eye, Ear, Nose and Throat Hospital, Shanghai Medical College, Fudan University, Shanghai, China, ⁵ Key Laboratory of Myopia, Ministry of Health, Fudan University, Shanghai, China, ⁶ Shanghai Key Laboratory of Visual Impairment and Restoration, Fudan University, Shanghai, China, ⁷ College of Basic Medical Sciences, Shanghai Jiao Tong University School of Medicine, Shanghai, China

OPEN ACCESS

Edited by:

Zhongxiao Wang,
Harvard Medical School,
United States

Reviewed by:

Yan Ni,
Zhejiang University, China
Yan-Nian Hui,
Fourth Military Medical
University, China

*Correspondence:

Junwei Fang
fangjunwei@shsmu.edu.cn
Xiangmei Kong
kongxm95@163.com

[†]These authors have contributed
equally to this work

Specialty section:

This article was submitted to
Neuropharmacology,
a section of the journal
Frontiers in Pharmacology

Received: 19 June 2019

Accepted: 15 October 2019

Published: 07 November 2019

Citation:

Wang H, Zhai R, Sun Q, Wu Y,
Wang Z, Fang J and Kong X (2019)
Metabolomic Profile of Posner–
Schlossman Syndrome: A Gas
Chromatography Time-of-Flight
Mass Spectrometry-Based Approach
Using Aqueous Humor.
Front. Pharmacol. 10:1322.
doi: 10.3389/fphar.2019.01322

The Posner–Schlossman syndrome (PSS) is a disease with clinically recurrent unilateral anterior uveitis with markedly elevated intraocular pressure (IOP) and subsequent progression to optic neuropathy. Retrospective studies have reported increased annual incidence of PSS, especially in China. While currently, the clinical management of PSS is still challenging. Metabolomics is considered to be a sensitive approach for the development of novel targeted therapeutics because of its direct elucidation of pathophysiological mechanisms. Therefore, we adopted gas chromatography time-of-flight mass spectrometry (GC-TOF-MS) technology-based non-targeted metabolomics approach to measure comprehensive metabolic profiles of aqueous humor (AH) samples obtained from patients with PSS, with an aim to demonstrate the underlying pathophysiology, identify potential biomarkers specific to PSS, and develop effective treatment strategies. A comparative analysis was used to indicate the distinct metabolites of PSS. Pathway analysis was conducted using MetaboAnalyst 4.0 to explore the metabolic reprogramming pathways involved in PSS. Logistic regression and receiver-operating characteristic (ROC) analyses were employed to evaluate the diagnostic capability of selected metabolites. Comparative analysis revealed a clear separation between PSS and control groups. Fourteen novel differentiating metabolites from AH samples obtained from patients with PSS were highlighted. Pathway analysis identified 11 carbohydrate, amino acid metabolism and energy metabolism pathways as the major disturbed pathways associated with PSS. The abnormal lysine degradation metabolism, valine–leucine–isoleucine biosynthesis, and citrate circle were considered to weigh the most in the development of PSS. The ROC analysis implied that the combination of glycine and homogentisic acid could serve as potential biomarkers for the discrimination of control and PSS groups. In conclusion, these results revealed for the first time the identity of important metabolites and pathways

contributing to the development/progression of PSS, enabled the better understanding of the mechanism of PSS, and might lead to the development of metabolic biomarkers and novel therapeutic strategies to restrict the development/progression of PSS.

Keywords: Posner–Schlossman syndrome, metabolism, mass spectrometry, gas chromatography time-of-flight mass spectrometry, aqueous humor

INTRODUCTION

Posner–Schlossman syndrome (PSS), also called glaucomatocyclitic crisis (GCC), is a disease with clinically recurrent unilateral anterior uveitis with markedly elevated intraocular pressure (IOP) and subsequent progression to optic neuropathy (Eissler, 1948; Moorthy et al., 1997). Retrospective studies have reported increased annual incidence of PSS, especially in China (Jiang et al., 2017). The clinical management of PSS is still challenging. Interventional measure for PSS is indicated for managing the associated inflammation and elevated IOP in order to prevent optic neuropathy. The use of corticosteroid can relieve the early stage symptoms; however, it fails to prevent the recurrence of PSS. Moreover, many patients develop corticoid dependence over shorter intervals gradually, complicating the management of PSS. Long-term administration of ganciclovir may control the symptoms of certain types of PSS (Miyana et al., 2010; Sobolewska et al., 2014; Su et al., 2014). However, the patients still experience progressive endothelium loss and a high relapse rate after the withdrawal of the drug (Moorthy et al., 1997; Chee and Jap, 2010; Miyana et al., 2010; Sobolewska et al., 2014; Su et al., 2014; Jiang et al., 2017). Eventually, repeated uncontrolled elevation of IOP can result in irreversible optic neuropathy and vision loss. Better understanding of the etiology and pathophysiological mechanism of PSS may aid in blunting the pathogenesis/progression of this disease. Several risk factors for PSS have been reported, such as inflammatory cytokines (Ohira et al., 2016; Pohlmann et al., 2018), vascular endothelial dysfunction (Shen et al., 2010), and primarily, human cytomegalovirus (HCMV) infection (Teoh et al., 2005; Chee and Jap, 2008; Van Gelder, 2008; Shazly et al., 2011; Su et al., 2014), which tops the list. Studies have demonstrated the participation of various metabolites in the inflammation process (Tannahill et al., 2013; Mills and O'Neill, 2014), including the HCMV-induced inflammatory response. Metabolites, as the downstream products of gene transcription, translation, and post-translational protein modification, are directly influenced by the physiological and pathological changes in tissues and accurately reflect the physiological changes (Oldiges et al., 2007; Baharum and Azizan, 2018). Therefore, studies investigating the change in endogenous metabolites and related metabolic pathways, underlying PSS, may provide a more sensitive approach to identify the pathophysiological mechanisms and, hopefully, lead to the identification of metabolic biomarkers for the prognosis of PSS and provide novel hypotheses for developing targeted therapeutics (Baharum and Azizan, 2018; Mayerle et al., 2018).

In metabolomic studies, mass spectrometry (MS) is the most preferred technique. Gas chromatography time-of-flight mass spectrometry (GC-TOF-MS) is perfectly suited for the identification and quantitation of low molecular weight metabolites (Phua et al., 2013; Jaeger et al., 2017; Yin et al., 2017) because of its key features, including higher sensitivity, selectivity, resolution, and accuracy of detection. Therefore, we adopted GC-TOF-MS technology-based non-targeted metabolomics approach and multivariate statistical analysis to measure comprehensive metabolic profiles of aqueous humor (AH) samples obtained from patients with PSS and cataract, with an aim to demonstrate the underlying pathophysiology, identify potential biomarkers specific to PSS, and develop effective treatment strategies.

METHODS

Research Design

The study was prospectively approved by the medical ethics committee of the Eye, Ear, Nose and Throat (EENT) Hospital of Fudan University (2017006–2), and research was conducted in accordance with the Declaration of Helsinki as revised in 2000. Signed informed consent was obtained from all participants enrolled in the study. We conducted this prospective, observational, and internal research project from June 2018 to December 2018 at EENT Hospital of Fudan University.

PSS was diagnosed based on the following clinical features: a) unilateral recurrent mild iridocyclitis; b) nonpigmented keratic precipitates (KPs) and corneal edema; c) cell and flare in the anterior chamber; d) elevated IOP; e) no posterior synechiae or peripheral anterior synechiae and posterior inflammation; and f) a relatively short attack duration. All participant data including gender, age, IOP, best-corrected visual acuity (BCVA), cornea endothelial cell density (CD), KP, Tyndall, and vertical ratio of cup to disk (C/D) were recorded and documented in the electronic case report form. In total, 43 participants were enrolled for this study, including 12 participants with PSS and 12 participants with cataract. All the PSS patients enrolled in this study were naïve patient without any treatment. All the PSS patients were at the acute onset stage.

Sample Collection

Paracentesis of anterior chamber was performed to collect AH sample for MS and anti-virus IgG concentration analysis. Meanwhile, serum sample was obtained in our central laboratory with the use of standardized procedures.

Analysis of Anti-Virus IgG Concentration in AH

Anti-virus IgG in AH and serum were detected by enzyme-linked immunosorbent assay (ELISA) kit (Virion\Serion, Germany). The test procedure was performed according to the kit instructions. Albumin was detected by scattering immunonephelometry (Guosai Biotechnology Co., Ltd, Shenzhen, China). The concentration of anti-virus IgG in AH was presented by a corrected ratio of (AH IgG/serum IgG) to (AH albumin/serum albumin), which was abbreviated as s/co. Mann–Whitney *U* test was performed to measure the significance of anti-virus IgG concentration between PSS and control groups.

Correlation Study Between Anti-Virus IgG Concentration and Clinical Variables

Spearman's rank correlation coefficient was performed to evaluate whether a correlation existed between both variables (anti-virus IgG concentration and clinical variables). Spearman's rank correlation coefficient value (Spearman's rho) ranged from 0 (no reliability) to 1 (perfect reliability). *p* values ≤ 0.05 were considered significant. All the analyses were carried out using SPSS 22.0 statistical software.

Mass Spectrometry Analysis

AH sample aliquots of 0.15 ml were transferred into cryovial tubes and stored at -80°C immediately. An Agilent 6890N gas chromatograph (Agilent Technologies) coupled to a Pegasus HT TOF MS (LECO Corp., St. Joseph, MI, USA) was used as the GC-TOF-MS platform. The sample preparation procedure and instrumental analysis were referred in the previously published methods (Qiu et al., 2014) with minor modifications, which was summarized in the **Supplementary Materials**.

Statistical and Data Analysis

For GC/MS data, data processing and identification are in accordance with our previously published work using XploreMET (Pan et al., 2010). The resulting data were exported into Microsoft Excel, and the peaks were normalized to the total sum of spectrum prior to multivariate analyses. The normalized data were analyzed by SIMCA-P (version 14.0 Umetrics AB, Umea, Sweden) for unsupervised principal component analysis (PCA) to obtain a general overview of the variance of metabolic phenotypes among different groups. In addition, supervised orthogonal projection to latent structure-discriminant analysis (OPLS-DA) was performed to obtain information about the variance of metabolic phenotypes that correspond to the classes. Student's *t*-test with Bonferroni's correction and fold change were performed afterwards to evaluate the significance of each metabolite. Significantly changed metabolites were identified by the parameters of OPLS-DA VIP > 1 , *t*-test *p* < 0.05 , and fold change > 1.2 or < 0.83 . The correlation between significantly disturbed metabolites and clinical variables of PSS patients was investigated by Spearman's rank correlation analysis using MetaboAnalyst 4.0 (<http://www.metaboanalyst.ca/>) (Xia and Wishart, 2016).

Pathway analysis was conducted using MetaboAnalyst 4.0 as well as the Kyoto Encyclopedia of Genes and Genomes

(KEGG) database (www.genome.jp/kegg/). Former collected metabolites were used as input. A logistic regression analysis and receiver-operating characteristic (ROC) analysis were performed using SPSS software version 18.0 (IBM Corp., Armonk, New York) to evaluate the diagnostic capability of selected metabolites. The area under the ROC curve (AUC) was calculated to quantify the performance of the diagnostic variables.

RESULTS

Sample Characteristics

The clinical characteristics of participants selected for discovery metabolomic profiling are shown in **Table 1**.

Anti-Virus IgG Concentration in AH

There was a significant difference of anti-HCMV IgG concentration between PSS and control groups (*p* value < 0.001) **Table 2**.

Correlation Analysis Between Anti-Virus IgG Concentration and Clinical Manifestations

In **Table 3**, Spearman's rank correlation coefficient indicated high agreement of HCMV and IOP ($r = 0.458$, *p* < 0.05), HCMV and

TABLE 1 | Clinical characteristics of participants in PSS and control groups.

	PSS	Control	<i>p</i> value
Number	12	12	
Gender (male, %)	5, 41.7	4, 33.3	0.673 Ψ
Age (years)	51.3 \pm 9.9	58.3 \pm 7.9	0.072
IOP (mmHg)	21.6 \pm 9.4	14.3 \pm 2.6	0.02*
BCVA	3.64 \pm 1.9	3.93 \pm 0.7	0.687
CD	2704.6 \pm 190.9	2626.7 \pm 282.3	0.486
KP (y/n)	12/0	0/12	$<0.001\mathbf{\Psi}^{**}$
Tyndall (y/n)	3/9	0/12	0.064 Ψ
Vertical C/D	0.4 (0.3–0.9)	0.3	$<0.001\mathbf{\#}^{***}$

PSS, Posner–Schlossman syndrome; BCVA, best-corrected visual acuity; IOP, intraocular pressure; CD, cell density; KP, keratic precipitate; C/D, ratio of cup to disk. $\mathbf{\#}$ by Mann–Whitney *U* test; Ψ , by χ^2 test. *, *p* value < 0.05 ; **, *p* value < 0.01 .

TABLE 2 | Anti-virus IgG concentration in AH from PSS and control groups.

	PSS	Control	<i>p</i> value
Number	12	12	
Anti-HCMV IgG (s/co)	0.45 (0.12–2.39)	0.01 (0–0.02)	$<0.001^{***}$
Anti-rubella virus IgG (s/co)	0.03 (0.01–0.08)	0.01 (0.01–0.03)	$<0.001^{***}$
Anti-VZV IgG (s/co)	0.02 (0.01–5.08)	0.01 (0–0.01)	0.024*
Anti-HSV1 IgG (s/co)	0.01 (0.01–0.04)	0.01 (0.01–0.02)	0.713

PSS, Posner–Schlossman syndrome; HCMV, human cytomegalovirus; VZV, varicella zoster virus; HSV, herpes simplex virus. Data were presented as median (range). Mann–Whitney *U* test was used to compare the anti-virus IgG concentration between PSS group and control group. *, *p* value < 0.05 ; ***, *p* value < 0.001 .

TABLE 3 | Spearman's correlation between anti-virus IgG concentration and clinical indexes.

	IOP	CD	CCT	C/D	KP	Tydall
Anti-HCMV IgG (s/co)	0.458*	−0.067	0.600	0.828***	0.879***	0.296
Anti-VZV IgG (s/co)	0.202	−0.174	−0.516	0.426*	0.533**	0.586**
Anti-rubella virus IgG (s/co)	0.233	−0.228	−0.261	0.535*	0.689***	0.563**
Anti-HSV1 IgG (s/co)	0.121	−0.501*	0.131	0.091	0.119	0.167

Correlation coefficient and *p* values are calculated by Spearman's correlation. HCMV, human cytomegalovirus; VZV, varicella zoster virus; HSV, herpes simplex virus; IOP, intraocular pressure; CD, cell density; CCT, central corneal thickness; C/D, ratio of cup to disk; KP, keratic precipitate. *, *p* value < 0.05; **, *p* value < 0.01; ***, *p* value < 0.001.

C/D ($r = 0.828$, $p < 0.001$), and HCMV and KP ($r = 0.879$, $p < 0.01$). Statistical correlation was also found between VZV and Tydall ($r = 0.586$, $p < 0.01$), VZV and C/D ($r = 0.426$, $p < 0.05$), and VZV and KP ($r = 0.533$, $p < 0.01$).

Global Metabolomic Profiles Between PSS and Control Groups

Evaluation of metabolomic profiles between PSS and control groups was conducted using unsupervised statistics, PCA. The PCA score plot with the first two (Figure 1A) and three (Figure 1B) principal components demonstrated a clear separation between the PSS and control groups, indicating that PSS caused gradual alterations in metabolism.

Significantly Disturbed Metabolites Between PSS and Control Groups

In the OPLS-DA model, clear differences were obtained for PSS versus control groups: cumulative R²_Y at 0.995 and Q²_Y at 0.445 (Figure 2A). VIP values and correlation coefficients (i.e., $p[\text{corr}]$) of each metabolite was shown in the V-plot, and 136 variables in red were found to have VIP values > 1 (Figure 2B). Metabolites with significant changes were easily isolated with the help of volcano plot, shown in Figure 2C. The permutation test results of OPLS-DA model are shown in Figure S1. The plot demonstrated as fold difference (*x*-axis) and *p* value (*y*-axis). Fourteen metabolites with significant abundance changes were defined and selected by the parameters of OPLS-DA VIP > 1, *t*-test $p < 0.05$, and fold change > 1.2 or < 0.83 (Table 4).

Spearman's Rank Correlation Analysis Between Disturbed Metabolites and Anti-Virus IgG Concentration in AH

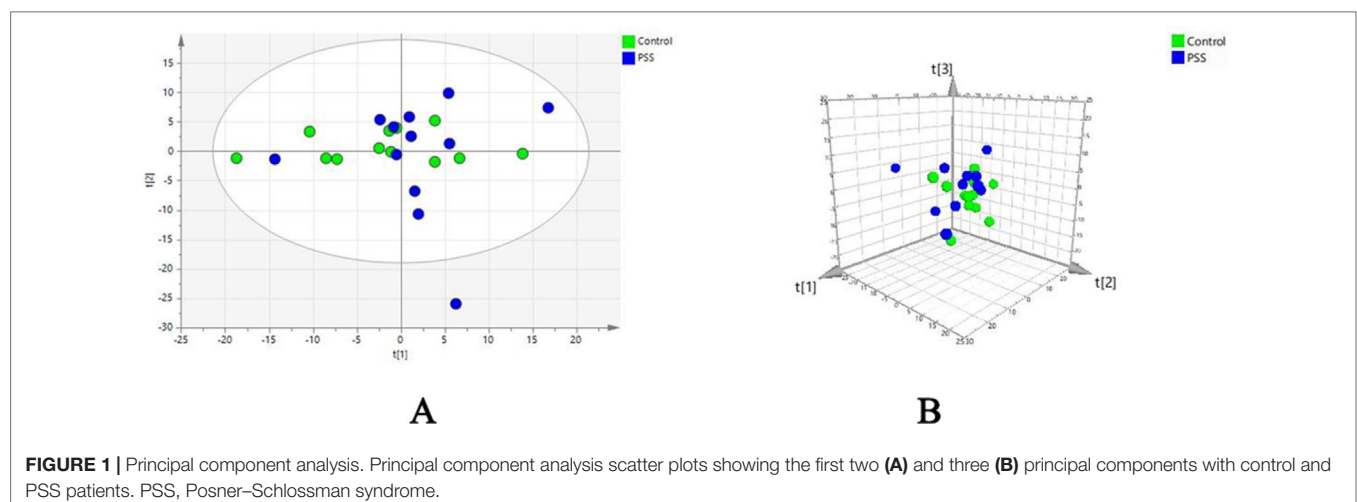
Spearman's rank correlation analysis indicated that there was strong positive correlation between anti-HCMV-IgG and glycine, phenylpyruvic acid, sorbitol, mannitol, aminoadipic acid, fumaric acid (FA), and 3-hydroxybutyric acid. Meanwhile, homogentisic acid and -arabinose exhibited notably negative correlation with anti-HCMV-IgG concentration (Figure 3).

Metabolic Pathway Analysis Associated With PSS

Pathways relevant to 14 differential metabolites in AH are shown in Figure 4 and Table 5. The abnormal of citrate cycle, valine–leucine–isoleucine biosynthesis, valine–leucine–isoleucine degradation, butanoate metabolism, fructose and mannose metabolism, lysine degradation metabolism, alanine, aspartate and glutamate metabolism, nitrogen metabolism, phenylalanine metabolism, tyrosine metabolism, and synthesis and degradation of ketone bodies metabolism were highlighted as the most important pathways in PSS group ($p < 0.05$).

Potential Biomarkers Analysis for Discrimination

We evaluated the impact of multiple metabolites and adopted a forward stepwise-regression selection procedure to select the best combination of potential biomarkers for discrimination. The



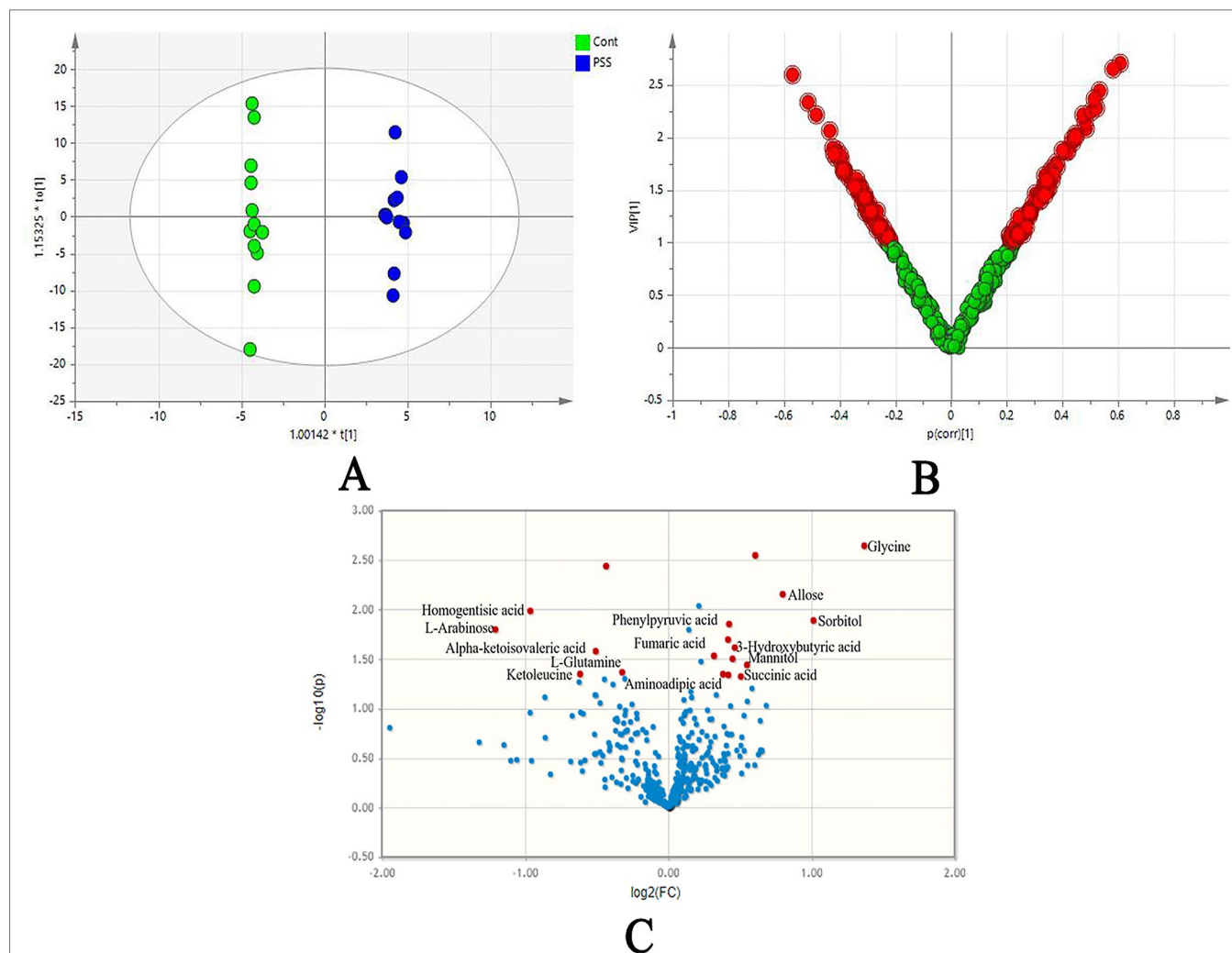


FIGURE 2 | The orthogonal projection to latent structure-discriminant analysis (OPLS-DA). OPLS-DA score plots **(A)** showed clear differences obtained for PSS versus control groups; loading plot **(B)** presented significantly disturbed metabolites in red (VIP 1); volcano plot **(C)** illustrated metabolites with their association with PSS, demonstrated as fold difference (x-axis) and p value (y-axis). PSS, Posner–Schlossman syndrome.

TABLE 4 | Significantly disturbed metabolites.

Name	VIP	p value	Fold change
3-Hydroxybutyric acid	1.739	0.024	1.38
Allose	1.809	0.007	1.74
Alpha-ketoisovaleric acid	1.531	0.026	0.704
Amino adipic acid	1.539	0.045	1.303
Fumaric acid	1.68	0.02	1.336
Glycine	2.104	0.002	2.582
Homogentisic acid	1.916	0.01	0.513
Ketoleucine	1.519	0.045	0.653
L-Arabinose	1.659	0.016	0.433
L-Glutamine	1.649	0.043	0.8
Mannitol	1.632	0.036	1.464
Phenylpyruvic acid	1.72	0.014	1.343
Sorbitol	1.865	0.013	2.02
Succinic acid	1.425	0.047	1.421

age was adjusted for the logistical regression model. The ROC presentation, on the basis of the logistic regression of metabolic biomarker panel, appears in **Figure 5**. The model containing panel metabolites showed very good discrimination between PSS and control groups. The AUC, sensitivity, and specificity of the logistic regression model established by glycine and homogentisic acid were 1 and 1 (**Figure 5**). Spearman's rank correlation analysis was conducted among 14 different metabolites with clinical variables. Glycine showed strong positive correlation with Tyndall, C/D ratio, and KP (**Figure 6**). Amino adipic acid and allose showed positive correlation with clinical indicators, including KP and IOP (**Figure 6**). Alpha-ketoisovaleric acid (KIV), -arabinose, ketoleucine, homogentisic, and allose showed negative correlation with clinical indicators, including IOP, KP, and C/D ratio (**Figure 6**).

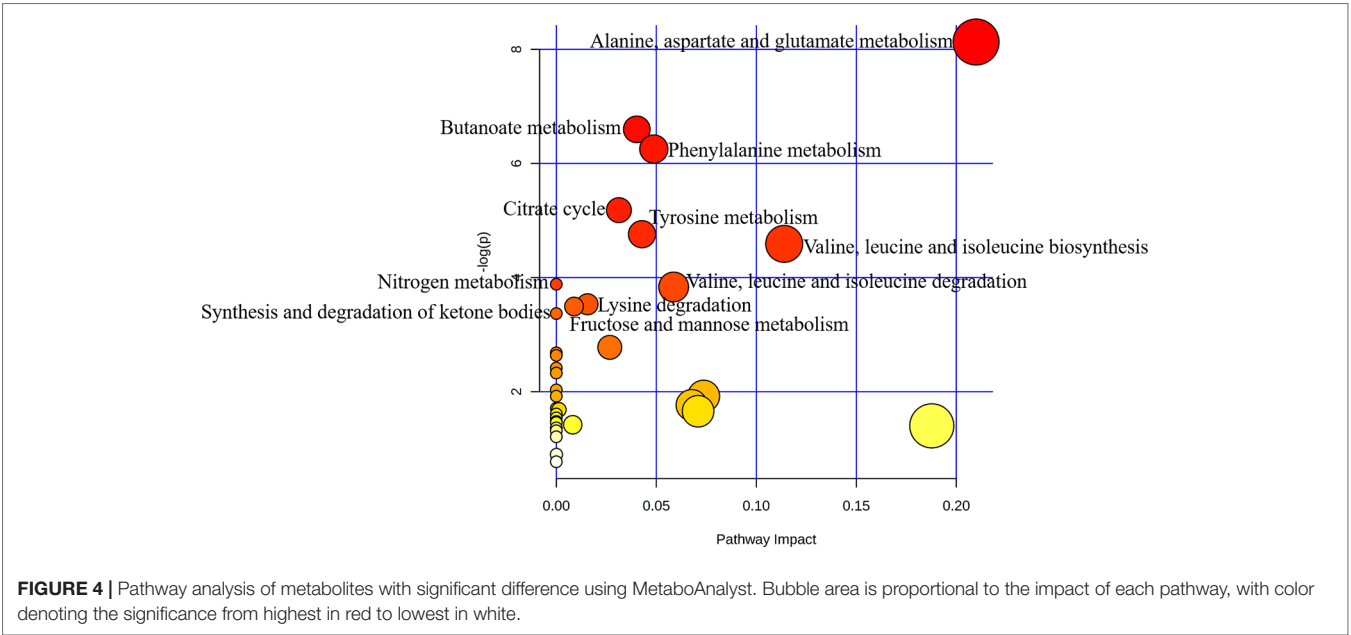
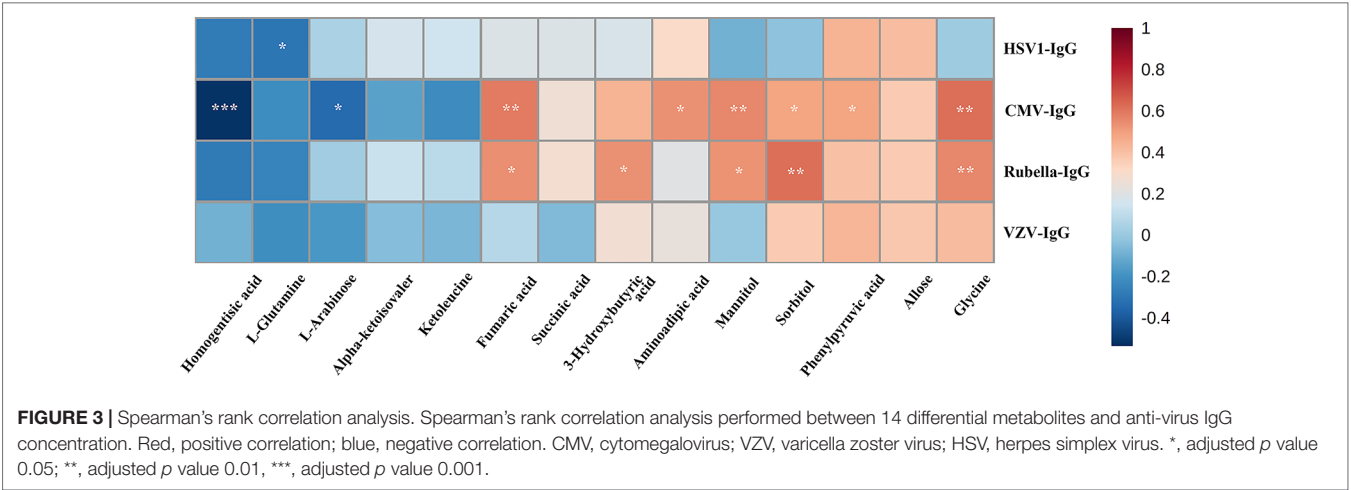


TABLE 5 | Pathways relevant to 14 differential metabolites.

Pathway	Metabolites	Total	Impact	Hits	<i>p</i> value
Alanine, aspartate, and glutamate metabolism	L-Glutamine, fumaric acid, succinic acid	24	0.1396	3	0.0003
Butanoate metabolism	(<i>R</i>)-3-Hydroxybutyric acid, succinic acid, fumaric acid	40	0.2327	3	0.0014
Citrate cycle (TCA cycle)	Succinic acid, fumaric acid	20	0.1163	2	0.0056
Fructose and mannose metabolism	Sorbitol, mannitol	48	0.2792	2	0.0304
Lysine degradation	Aminoadipic acid, glycine	47	0.2734	2	0.0293
Nitrogen metabolism	L-Glutamine	39	0.2268	2	0.0206
Phenylalanine metabolism	Phenylpyruvic acid, succinic acid, fumaric acid	45	0.2617	3	0.0019
Synthesis and degradation of ketone bodies	(<i>R</i>)-3-Hydroxybutyric acid	6	0.0349	1	0.0344
Tyrosine metabolism	Homogentisic acid, fumaric acid, succinic acid	76	0.442	3	0.0086
Valine, leucine, and isoleucine biosynthesis	Alpha-ketoisovaleric acid, 4-Methyl-2-oxopentanoate	27	0.157	2	0.0102
Valine, leucine, and isoleucine degradation	Alpha-ketoisovaleric acid, 4-Methyl-2-oxopentanoate	40	0.2327	2	0.0216

TCA, tricarboxylic acid.

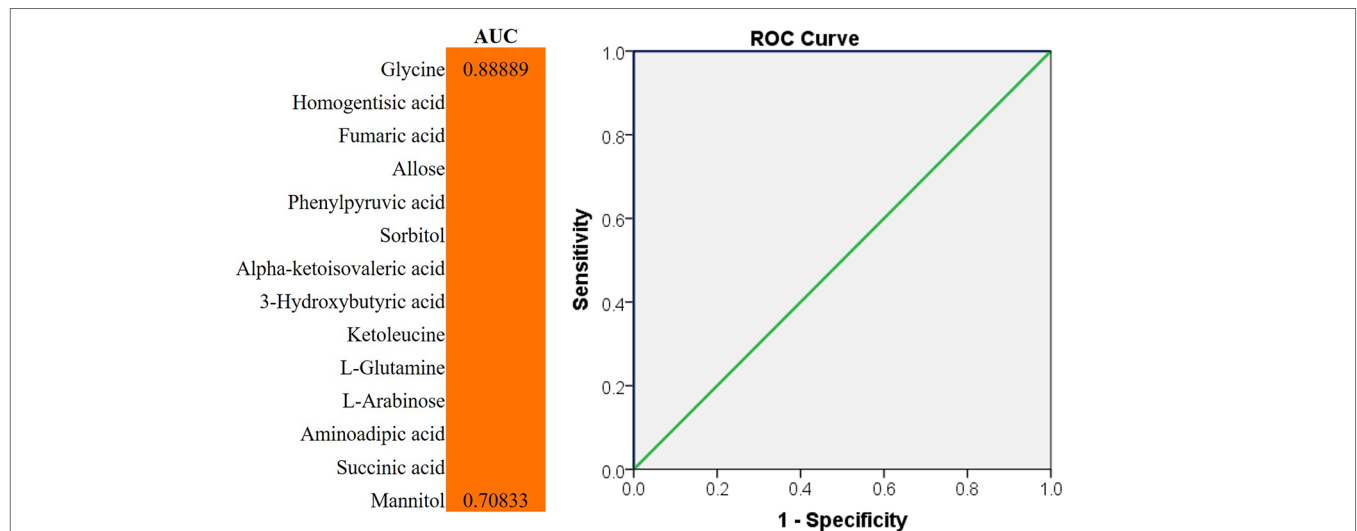


FIGURE 5 | ROC analysis for discrimination. The diagnostic outcomes of potential biomarkers were shown *via* the ROC curves for comparison between PSS versus control; ROC, receiver-operating characteristic; AUC, area under the receiver operating characteristic curve.

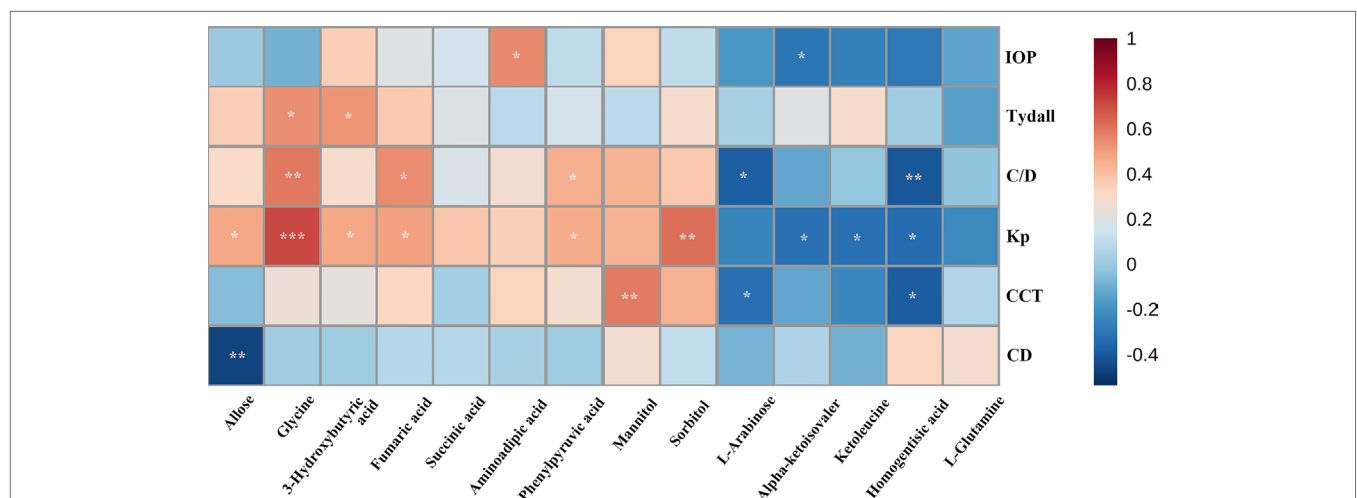


FIGURE 6 | Spearman's rank correlation analysis. Spearman's rank correlation analysis performed between 14 different metabolites and clinical indicators. Red, positive correlation; blue, negative correlation. CD, cell density; CCT, central corneal thickness; C/D, ratio of cup to disk; IOP, intraocular pressure; KP, keratic precipitate. *, adjusted *p* value 0.05; **, adjusted *p* value 0.01; ***, adjusted *p* value 0.001.

DISCUSSIONS

Metabolomics is a promising approach for the exploration of disease pathogenesis. The metabolomic profile of AH can directly indicate the physiological status of the eyes (Haines et al., 2018). In our study, 14 metabolites were discovered for the first time from AH samples obtained from patients with PSS—3-hydroxybutyric acid, allose, alpha-ketoisovaleric acid, aminoadipic acid, FA, glycine, homogentisic acid, ketoleucine, -arabinose, -glutamine, mannitol, phenylpyruvic acid, sorbitol, and succinic acid. Some of these metabolites have been recognized as node molecules in pathways associated with inflammation or neuroprotection (Effenberger-Neidnicht et al., 2014; Chen et al., 2016; Xu et al.,

2018; Liu et al., 2019). To advance our understanding of the pathophysiological patterns of these identified metabolites, we performed metabolic pathway analysis to identify pathway-based metabolomic features of these metabolites in PSS.

In our research, the lysine degradation metabolic pathway was significantly enriched in PSS (https://www.kegg.jp/kegg-bin/show_pathway?map00310). This enrichment was associated with the concomitant increase of glycine in the samples. Glycine, as a nutritionally important amino acid (AA), is highly essential for fetal and neonatal growth and development (Wang et al., 2014; Wu, 2014). Besides the generation of energy, studies have indicated that glycine can prevent the overproduction of pro-inflammatory cytokines (Li et al., 2001; Stoffels et al., 2011;

Effenberg-Neidnicht et al., 2014). Exogenous administration of glycine can modulate the toll-like receptor-4 (TLR4) and nucleotide-binding oligomerization domain protein inflammatory signaling pathway and subsequently downregulate the mRNA expression of related cytokines, such as interleukin-1 β (IL-1 β), tumor necrosis factor- α (TNF- α), nuclear factor kappa-B (NF- κ B) p65, and, especially, the mediator of macrophage recruitment, intercellular adhesion molecule-1 (ICAM-1), which regulates macrophage polarization and recruitment (Wheeler et al., 2000; Stoffels et al., 2011; Xu et al., 2018). We speculated that modulation of the unfavorable local resident macrophages by exogenous administration or endogenous upregulating of glycine might provide a valuable approach to mitigate macrophage-mediated inflammation in PSS. We also know that certain kinds of PSS are caused by HCMV infection. Researches have demonstrated that HCMV infection can induce the activation of the transcription factor NF- κ B, which is critical for transactivation of the major immediate-early promoter for HCMV [36]. Hence, downregulation of NF- κ B by glycine might be more efficient for treating HCMV-positive PSS. Spearman's rank correlation analysis confirmed significant strong positive correlation between anti-HCMV IgG and glycine (Figure 3). Based on the significant positive correlation between anti-HCMV IgG and glycine, we speculated that glycine might be a bioprobe for HCMV-derived PSS. In this circumstance, combined anti-HCMV therapy might be taken into consideration. Moreover, glycine has been well-documented as having the best neuroprotective effect among all AAs. Accumulated evidence indicates a direct role of glycine in neuroprotection and amelioration of hypoxia-ischemic brain injuries in adult and neonatal animals (Wheeler et al., 2000; Li et al., 2001; DeMeritt et al., 2004; Stoffels et al., 2011; Wang et al., 2014; Wu, 2014; Chen et al., 2016; Mori et al., 2017; Liu et al., 2019). This neuroprotective effect of glycine involved the suppression of inflammatory pathway associated with TNF- α or NF- κ B p65/hypoxia inducible factor-1 α (Hif-1 α) signalling (Wheeler et al., 1999; Liu et al., 2019). Stroke patients clinically treated with glycine-based modalities demonstrated favorable outcome and a reduced tendency for 30-day mortality (Gusev et al., 2000). Similar to cerebrospinal fluid, increased amount of glycine was detected in the AH of patients with PSS, which might confer a neuroprotection from optic neuropathy caused by marked elevation of IOP during the acute phase of PSS.

KIV was found decreased in the AH of patients with PSS. The associated valine–leucine–isoleucine biosynthesis pathway was highlighted during the *in silico* pathway analysis as an important pathway in PSS (https://www.kegg.jp/kegg-bin/show_pathway?map00290). Valine, leucine, and isoleucine from this pathway constitute the branched-chain AAs (BCAAs) family. BCAAs are strong nutritional stimuli that are able to regulate the inflammatory status by the regulation of glutamine production (Nicastro et al., 2012; Gameiro and Struhl, 2018). Under inflammatory circumstances, BCAAs can be transaminated to glutamate to meet the high requirement of glutamate in inflammatory cells, such as macrophages, and help maintain the cellular function (Pithon-Curi et al., 2004). Moreover, BCAAs have been widely known to activate mammalian target of rapamycin (mTOR), which can modulate autophagy and inflammatory

responses (Xu and Brink, 2016; Saxton and Sabatini, 2017; Sinclair et al., 2017). Reports have demonstrated that mTOR can facilitate PI3K/Akt-induced NF- κ B activation (Peppenelli et al., 2018; Altman et al., 2019), an important step in all the three stages of HCMV infection (Li et al., 2015; Peppenelli et al., 2018; Altman et al., 2019) (https://www.kegg.jp/kegg-bin/highlight_pathway?scale=1.0&map=map05163&keyword=human%20herpesvirus%203). Consequently, targeting the PIK/Akt/mTOR cascade might be more efficient for treating HCMV-positive PSS. Significantly decreased KIV was found in the AH of PSS. We speculated that KIV uptake increased significantly during the course of HCMV infection. Mammalian mitochondrial branched-chain α -keto acid dehydrogenase complex can catalyze the oxidative decarboxylation of KIV to yield the BCAA product, valine (Funchal et al., 2007). The metabolic stimulation of this step may be responsible for the decrease in KIV and accumulation of BCAA. This information provides a target for the metabolic inhibition of this step, which might reverse the result and diminish the activity of BCAAs and PIK/Akt/mTOR cascade.

Besides the PIK/Akt/mTOR pathway, BCAAs-induced mTOR activation can also significantly contribute to the upregulation of vascular endothelial growth factor (VEGF) level (Brugarolas et al., 2003; Klos et al., 2006), which has been found to be highly expressed in the AH of patients with uveitic glaucoma (Ohira et al., 2016). Recently, emerging evidences indicate that the VEGF–VEGF receptor (R) system is significantly involved in inflammation (Shibuya, 2015). Among the VEGFRs, VEGFR1 is expressed on the membrane of macrophage lineage cells and mediates the transduction of important cytokine/chemokine signaling in these cells (Shibuya, 2015). This VEGFR1–macrophage axis can trigger inflammatory responses in various tissues and might be a potential target for managing inflammation. Taken together, we surmised that the inhibition of BCAA/mTOR pathway could have beneficial therapeutic effects by preventing inflammation-mediated pathogenesis.

Marked increase in succinic acid and the associated pathways, citrate acid cycle (tricarboxylic acid [TCA] cycle) (https://www.kegg.jp/kegg-bin/show_pathway?map00020) was detected in the PSS group. TCA cycle has been considered to interact with the frontline innate leukocytes, such as macrophages and monocytes (Jha et al., 2015; Kelly and O'Neill, 2015; Murphy and O'Neill, 2018). The mechanism behind this process might involve the metabolic reprogramming of endogenous TCA cycle intermediates, namely, citric acid, which adopts regulatory features to harness inflammatory response. Typically, in the TCA cycle, citrate is converted to isocitrate, which is then diverted to succinate, a key marker of macrophage activation. Succinate has been found to be elevated in metabolic disorders associated with inflammation (Tannahill et al., 2013; Mills and O'Neill, 2014). Intracellular succinate accumulation is postulated to regulate the IL-1 β –HIF-1 α axis to exert pro-inflammatory function (Tannahill et al., 2013; Mills and O'Neill, 2014; Lampropoulou et al., 2016; Xiao et al., 2017). Meanwhile, we also detected increased FA in PSS AH, another well-known intermediate product of TCA. Recently, FA has shown its therapeutic potentials for the management of inflammatory clinical diseases, such as autoimmune myocarditis and multiple sclerosis (Wakkee

and Thio, 2007; Meili-Butz et al., 2008; Moharregg-Khiabani et al., 2009; Loewe et al., 2011). Hence, the regulation of TCA to generate favorable metabolites may have important clinical utility for the treatment of PSS.

Besides pathway analysis, ROC analysis was conducted to evaluate the diagnostic potential of selected metabolites. The results of ROC analysis implied that the combination of glycine and homogentisic acid could serve as potential biomarkers for the discrimination of control and PSS groups. Spearman's rank correlation analysis simultaneously revealed that these two metabolites, differentially expressed in patients with PSS, presented significant correlation with IOP, C/D, and anti-HCMV IgG titer in AH (Figures 3 and 6). This discovery demonstrated immense potential for PSS diagnosis. Most importantly, these metabolites could also provide valuable information regarding subtype identification and allow us to perform specific intervention for patients with PSS.

In conclusion, these results revealed for the first time the identity of important metabolites and pathways contributing to the development/progression of PSS. These discoveries enabled the better understanding of the mechanism of PSS and might lead to the development of metabolic biomarkers and novel therapeutic strategies to restrict the development/progression of PSS. Further investigations are needed to validate the role of these metabolites and relevant metabolic reprogramming pathways. We have realized there are limitations in our research. The following studies will recruit more participants and choose more suitable control group to support our results.

DATA AVAILABILITY STATEMENT

The raw data supporting the conclusions of this manuscript will be made available by the authors, without undue reservation, to any qualified researcher.

ETHICS STATEMENT

The studies involving human participants were reviewed and approved by the medical ethics committee of the Eye, Ear, Nose and Throat (ENT) Hospital of Fudan University (2017006–2). The patients/participants provided their written informed consent to participate in this study.

REFERENCES

- Altman, A. M., Mahmud, J., Nikolovska-Coleska, Z., and Chan, G. (2019). HCMV modulation of cellular PI3K/AKT/mTOR signaling: new opportunities for therapeutic intervention? *Antiviral. Res.* 163, 82–90. doi: 10.1016/j.antiviral.2019.01.009
- Baharum, S. N., and Azizan, K. A. (2018). Metabolomics in systems biology. *Adv. Exp. Med. Biol.* 1102, 51–68. doi: 10.1007/978-3-319-98758-3_4
- Brugarolas, J. B., Vazquez, F., Reddy, A., Sellers, W. R., and Kaelin, W. G. Jr. (2003). TSC2 regulates VEGF through mTOR-dependent and -independent pathways. *Cancer Cell* 4 (2), 147–158. doi: 10.1016/S1535-6108(03)00187-9

AUTHOR CONTRIBUTIONS

HW designed the study, evaluated of the results, and wrote the draft and final manuscript. RZ collected the clinical data of the subjects and analyzed statistical data. QS clinically evaluated the subjects and collected the AH sample. YW collected the metabolomic data. ZW performed the laboratory exams. JF evaluated of the original metabolomic data and edited the draft manuscript. XK evaluated the clinical characteristics of the subjects to establish the diagnosis, performed clinical procedures of the study, and edited the final manuscript. All authors approved the final manuscript.

FUNDING

This work was supported in part by grants from the National Natural Science Foundation of China (81870666), National Key R&D Program of China (2016YFC0904800), the Surface Project of National Natural Science Foundation of China (81770922), the project of Shanghai Municipal Commission of Health and Family Planning (201740204), the clinical science and technology innovation project of Shanghai Shengkang Hospital Development Center (SHDC12017X18), and the western medicine guidance project of Shanghai Committee of Science and Technology (19411961600). The open access publication fees were supported by the National Natural Science Foundation of China (81870666). The funders had no role in study design, data collection and analysis, decision to publish, or preparation of the manuscript. The authors declared that no conflicts of interest exist.

ACKNOWLEDGMENTS

We acknowledge Dr Xun Xu (MD) from our department for providing medical writing assistance.

SUPPLEMENTARY MATERIAL

The Supplementary Material for this article can be found online at: <https://www.frontiersin.org/articles/10.3389/fphar.2019.01322/full#supplementary-material>

FIGURE S1 | The validation plot from the 200-permutation test model. The Q2Y of the original model on the right were higher than the corresponding values of the permutation test models on the left.

- Chee, S. P., and Jap, A. (2008). Presumed fuchs heterochromic iridocyclitis and posner-schlossman syndrome: comparison of cytomegalovirus-positive and negative eyes. *Am. J. Ophthalmol.* 146 (6), 883–9 e1. doi: 10.1016/j.ajo.2008.09.001
- Chee, S. P., and Jap, A. (2010). Cytomegalovirus anterior uveitis: outcome of treatment. *Br. J. Ophthalmol* 94 (12), 1648–1652. doi: 10.1136/bjo.2009.167767
- Chen, J., Zhuang, Y., Zhang, Z. F., Wang, S., Jin, P., He, C., et al. (2016). Glycine confers neuroprotection through microRNA-301a/PTEN signaling. *Mol. Brain* 9 (1), 59. doi: 10.1186/s13041-016-0241-3
- DeMeritt, I. B., Milford, L. E., and Yurochko, A. D. (2004). Activation of the NF-kappaB pathway in human cytomegalovirus-infected cells is necessary for

- efficient transactivation of the major immediate-early promoter. *J. Virol.* 78 (9), 4498–4507. doi: 10.1128/JVI.78.9.4498-4507.2004
- Effenberger-Neidnicht, K., Jägers, J., Verhaegh, R., and de Groot, H. (2014). Glycine selectively reduces intestinal injury during endotoxemia. *J. Surg. Res.* 192 (2), 592–598. doi: 10.1016/j.jss.2014.06.016
- Eissler, R. (1948). Atrophy of the optic nerve due to malnutrition; report of two cases. *Arch. Ophthalmol.* 39 (4), 465–470. doi: 10.1001/archophth.1948.00900020473002
- Funchal, C., Tramontina, F., Quincozes dos Santos, A., Fraga de Souza, D., Gonçalves, C. A., Pessoa-Pureur, R., et al. (2007). Effect of the branched-chain alpha-keto acids accumulating in maple syrup urine disease on S100B release from glial cells. *J. Neurol. Sci.* 260 (1–2), 87–94. doi: 10.1016/j.jns.2007.04.011
- Gameiro, P. A., and Struhl, K. (2018). Nutrient deprivation elicits a transcriptional and translational inflammatory response coupled to decreased protein synthesis. *Cell Rep.* 24 (6), 1415–1424. doi: 10.1016/j.celrep.2018.07.021
- Gusev, E. I., Skvortsova, V. I., Dambinova, S. A., Raevskiy, K. S., Alekseev, A. A., Bashkatova, V. G., et al. (2000). Neuroprotective effects of glycine for therapy of acute ischaemic stroke. *Cerebrovasc. Dis.* 10 (1), 49–60. doi: 10.1159/000016025
- Haines, N. R., Manoharan, N., Olson, J. L., D'Alessandro, A. 2., and Reisz, J. A. (2018). Metabolomics analysis of human vitreous in diabetic retinopathy and rhegmatogenous retinal detachment. *J. Proteome Res.* 17 (7), 2421–2427. doi: 10.1021/acs.jproteome.8b00169
- Jaeger, C., Méret, M., Schmitt, C. A., and Lisec, J. (2017). Compound annotation in liquid chromatography/high-resolution mass spectrometry based metabolomics: robust adduct ion determination as a prerequisite to structure prediction in electrospray ionization mass spectra. *Rapid Commun. Mass Spectrom.* 31 (15), 1261–1266. doi: 10.1002/rcm.7905
- Jha, A. K., Huang, S. C., Sergushichev, A., Lampropoulou, V., Ivanova, Y., Loginicheva, E., et al. (2015). Network integration of parallel metabolic and transcriptional data reveals metabolic modules that regulate macrophage polarization. *Immunity* 42 (3), 419–430. doi: 10.1016/j.immuni.2015.02.005
- Jiang, J. H., Zhang, S. D., Dai, M. L., Yang, J. Y., Xie, Y. Q., Hu, C., et al. (2017). Posner-Schlossman syndrome in Wenzhou, China: a retrospective review study. *Br. J. Ophthalmol.* 101 (12), 1638–1642. doi: 10.1136/bjophthalmol-2016-309863
- Kelly, B., and O'Neill, L. A. (2015). Metabolic reprogramming in macrophages and dendritic cells in innate immunity. *Cell Res.* 25 (7), 771–784. doi: 10.1038/cr.2015.68
- Klos, K. S., Wyszomierski, S. L., Sun, M., Tan, M., Zhou, X., Li, P., et al. (2006). ErbB2 increases vascular endothelial growth factor protein synthesis via activation of mammalian target of rapamycin/p70S6K leading to increased angiogenesis and spontaneous metastasis of human breast cancer cells. *Cancer Res.* 66 (4), 2028–2037. doi: 10.1158/0008-5472.CAN-04-4559
- Lampropoulou, V., Sergushichev, A., Bambouskova, M., Nair, S., Vincent, E. E., Loginicheva, E., et al. (2016). Itaconate links inhibition of succinate dehydrogenase with macrophage metabolic remodeling and regulation of inflammation. *Cell Metab.* 24 (1), 158–166. doi: 10.1016/j.cmet.2016.06.004
- Li, X., Bradford, B. U., Wheeler, M. D., Stimpson, S. A., Pink, H. M., Brodie, T. A., et al. (2001). Dietary glycine prevents peptidoglycan polysaccharide-induced reactive arthritis in the rat: role for glycine-gated chloride channel. *Infect. Immun.* 69 (9), 5883–5891. doi: 10.1128/IAI.69.9.5883-5891.2001
- Li, Q., Wilkie, A. R., Weller, M., Liu, X., and Cohen, J. I. (2015). THY-1 cell surface antigen (CD90) has an important role in the initial stage of human cytomegalovirus infection. *PLoS Pathog.* 11 (7), e1004999. doi: 10.1371/journal.ppat.1004999
- Liu, R., Liao, X. Y., Pan, M. X., Tang, J. C., Chen, S. F., Zhang, Y., et al. (2019). Glycine exhibits neuroprotective effects in ischemic stroke in rats through the inhibition of M1 microglial polarization via the NF-kappaB p65/Hif-1alpha signaling pathway. *J. Immunol.* 202 (6), 1704–1714. doi: 10.4049/jimmunol.1801166
- Loewe, R., Pillinger, M., de Martin, R., Mrowietz, U., Gröger, M., Holnthoner, W., et al. (2011). Dimethylfumarate inhibits tumor-necrosis-factor-induced CD62E expression in an NF-kB-dependent manner. *J. Invest. Dermatol.* 117 (6), 1363–1368. doi: 10.1046/j.0022-022x.2001.01576.x
- Mayerle, J., Kalthoff, H., Reszka, R., Kamlage, B., Peter, E., Schniewind, B., et al. (2018). Metabolic biomarker signature to differentiate pancreatic ductal adenocarcinoma from chronic pancreatitis. *Gut* 67 (1), 128–137. doi: 10.1136/gutjnl-2016-312432
- Meili-Butz, S., Niermann, T., Fasler-Kan, E., Barbosa, V., Butz, N., John, D., et al. (2008). Dimethyl fumarate, a small molecule drug for psoriasis, inhibits Nuclear Factor-kB and reduces myocardial infarct size in rats. *Eur. J. Pharmacol.* 586 (1–3), 251–258. doi: 10.1016/j.ejphar.2008.02.038
- Mills, E., and O'Neill, L. A. (2014). Succinate: a metabolic signal in inflammation. *Trends Cell Biol.* 24 (5), 313–320. doi: 10.1016/j.tcb.2013.11.008
- Miyayama, M., Sugita, S., Shimizu, N., Morio, T., Miyata, K., Maruyama, K., et al. (2010). A significant association of viral loads with corneal endothelial cell damage in cytomegalovirus anterior uveitis. *Br. J. Ophthalmol.* 94 (3), 336–340. doi: 10.1136/bjo.2008.156422
- Moharreh-Khiabani, D., Linker, R. A., Gold, R., and Stangel, M. (2009). Fumaric acid and its esters: an emerging treatment for multiple sclerosis. *Curr. Neuropharm.* 7 (1), 60–64. doi: 10.2174/157015909787602788
- Moorthy, R. S., Mermoud, A., Baerveldt, G., Minckler, D. S., Lee, P. P., and Rao, N. A. (1997). Glaucoma associated with uveitis. *Surv. Ophthalmol.* 41 (5), 361–394. doi: 10.1016/S0039-6257(97)00006-4
- Mori, H., Momosaki, K., Kido, J., Naramura, T., Tanaka, K., Matsumoto, S., et al. (2017). Amelioration by glycine of brain damage in neonatal rat brain following hypoxia-ischemia. *Pediatr. Int.* 59 (3), 321–327. doi: 10.1111/ped.13164
- Murphy, M. P., and O'Neill, L. A. J. (2018). Krebs cycle reimagined: the emerging roles of succinate and itaconate as signal transducers. *Cell* 174 (4), 780–784. doi: 10.1016/j.cell.2018.07.030
- Nicastro, H., da Luz, C. R., Chaves, D. F., Bechara, L. R., Voltarelli, V. A., Rogero, M. M., et al. (2012). Does branched-chain amino acids supplementation modulate skeletal muscle remodeling through inflammation modulation? possible mechanisms of action. *J. Nutr. Metab.* 2012, 136937. doi: 10.1155/2012/136937
- Ohira, S., Inoue, T., Iwao, K., Takahashi, E., and Tanihara, H. (2016). Factors influencing aqueous proinflammatory cytokines and growth factors in uveitic glaucoma. *PLoS One* 11 (1), e0147080. doi: 10.1371/journal.pone.0147080
- Oldiges, M., Lütz, S., Pflug, S., Schroer, K., Stein, N., and Wiendahl, C. (2007). Metabolomics: current state and evolving methodologies and tools. *Appl. Microbiol. Biotechnol.* 76 (3), 495–511. doi: 10.1007/s00253-007-1029-2
- Pan, L., Qiu, Y., Chen, T., Lin, J., Chi, Y., Su, M., et al. (2010). An optimized procedure for metabolomic analysis of rat liver tissue using gas chromatography/time-of-flight mass spectrometry. *J. Pharm. Biomed. Anal.* 52 (4), 589–596. doi: 10.1016/j.jpba.2010.01.046
- Peppenelli, M. A., Miller, M. J., Altman, A. M., Cojohari, O., and Chan, G. C. (2018). Aberrant regulation of the Akt signaling network by human cytomegalovirus allows for targeting of infected monocytes. *Antiviral. Res.* 158, 13–24. doi: 10.1016/j.antiviral.2018.07.015
- Phua, L. C., Koh, P. K., Cheah, P. Y., Ho, H. K., and Chan, E. C. (2013). Global gas chromatography/time-of-flight mass spectrometry (GC/TOFMS)-based metabolomic profiling of lyophilized human feces. *J. Chromatogr. B. Analyt. Technol. Biomed. Life Sci.* 937, 103–113. doi: 10.1016/j.jchromb.2013.08.025
- Pithon-Curi, T. C., De Melo, M. P., and Curi, R. (2004). Glucose and glutamine utilization by rat lymphocytes, monocytes and neutrophils in culture: a comparative study. *Cell Biochem. Funct.* 22 (5), 321–326. doi: 10.1002/cbf.1109
- Pohlmann, D., Schlickeiser, S., Metzner, S., Lenglinger, M., Winterhalter, S., Pleyer, U. (2018). Different composition of intraocular immune mediators in Posner-Schlossman-Syndrome and Fuchs' Uveitis. *PLoS One* 13 (6), e0199301. doi: 10.1371/journal.pone.0199301
- Qiu, Y., Cai, G., Zhou, B., Li, D., Zhao, A., Xie, G., et al. (2014). A distinct metabolic signature of human colorectal cancer with prognostic potential. *Clin. Cancer Res.* 20 (8), 2136–2146. doi: 10.1158/1078-0432.CCR-13-1939
- Saxton, R. A., and Sabatini, D. M. (2017). mTOR signaling in growth, metabolism, and disease. *Cell* 168 (6), 960–976. doi: 10.1016/j.cell.2017.02.004
- Shazly, T. A., Aljajeh, M., and Latina, M. A. (2011). Posner-Schlossman glaucomatocyclitic crisis. *Semin. Ophthalmol.* 26 (4–5), 282–284. doi: 10.3109/08820538.2011.605821
- Shen, S. C., Ho, W. J., Wu, S. C., Yu, K. H., Lin, H. C., Lin, Y. S., et al. (2010). Peripheral vascular endothelial dysfunction in glaucomatocyclitic crisis: a preliminary study. *Invest. Ophthalmol. Vis. Sci.* 51 (1), 272–276. doi: 10.1167/iov.09-3849
- Shibuya, M. (2015). VEGF-VEGFR System as a target for suppressing inflammation and other diseases. *Endocr. Metab. Immune Disord. Drug Targets* 15 (2), 135–144. doi: 10.2174/1871530315666150316121956

- Sinclair, C., Bommakanti, G., Gardinassi, L., Loebbermann, J., Johnson, M. J., Hakimpour, P., et al. (2017). mTOR regulates metabolic adaptation of APCs in the lung and controls the outcome of allergic inflammation. *Science* 357 (6355), 1014–1021. doi: 10.1126/science.aaj2155
- Sobolewska, B., Deuter, C., Doycheva, D., Zierhut, M. (2014). Long-term oral therapy with valganciclovir in patients with Posner-Schlossman syndrome. *Graefes. Arch. Clin. Exp. Ophthalmol.* 252 (1), 117–124. doi: 10.1007/s00417-013-2535-9
- Stoffels, B., Türlér, A., Schmidt, J., Nazir, A., Tsukamoto, T., Moore, B. A., et al. (2011). Anti-inflammatory role of glycine in reducing rodent postoperative inflammatory ileus. *Neurogastroenterol. Motil.* 23 (1), 76–87, e8. doi: 10.1111/j.1365-2982.2010.01603.x
- Su, C. C., Hu, F. R., Wang, T. H., Huang, J. Y., Yeh, P. T., Lin, C. P., et al. (2014). Clinical outcomes in cytomegalovirus-positive Posner-Schlossman syndrome patients treated with topical ganciclovir therapy. *Am. J. Ophthalmol.* 158 (5), 1024–1031 e2. doi: 10.1016/j.ajo.2014.08.007
- Tannahill, G. M., Curtis, A. M., Adamik, J., Palsson-McDermott, E. M., McGettrick, A. F., Goel, G., et al. (2013). Succinate is an inflammatory signal that induces IL-1 β through HIF-1 α . *Nature* 496 (7444), 238–242. doi: 10.1038/nature11986
- Teoh, S. B., Thean, L., and Koay, E. (2005). Cytomegalovirus in aetiology of Posner-Schlossman syndrome: evidence from quantitative polymerase chain reaction. *Eye (Lond)* 19 (12), 1338–1340. doi: 10.1038/sj.eye.6701757
- Van Gelder, R. N. (2008). Idiopathic no more: clues to the pathogenesis of Fuchs heterochromic iridocyclitis and glaucomatocyclitic crisis. *Am. J. Ophthalmol.* 145 (5), 769–771. doi: 10.1016/j.ajo.2008.02.010
- Wakke, M., and Thio, H. B. (2007). Drug evaluation: BG-12, an immunomodulatory dimethylfumarate. *Curr. Opin. Invest. Drugs* 8 (11), 955–962.
- Wang, W., Dai, Z., Wu, Z., Lin, G., Jia, S., Hu, S., et al. (2014). Glycine is a nutritionally essential amino acid for maximal growth of milk-fed young pigs. *Amino Acids* 46 (8), 2037–2045. doi: 10.1007/s00726-014-1758-3
- Wheeler, M. D., Ikejima, K., Enomoto, N., Stacklewitz, R. F., Seabra, V., Zhong, Z., et al. (1999). Glycine: a new anti-inflammatory immunonutrient. *Cell Mol. Life Sci.* 56 (9–10), 843–856. doi: 10.1007/s000180050030
- Wheeler, M. D., Rose, M. L., Yamashima, S., Enomoto, N., Seabra, V., Madren, J., et al. (2000). Dietary glycine blunts lung inflammatory cell influx following acute endotoxin. *Am. J. Physiol. Lung Cell Mol. Physiol.* 279 (2), L390–L398. doi: 10.1152/ajplung.2000.279.2.L390
- Wu, G. (2014). Dietary requirements of synthesizable amino acids by animals: a paradigm shift in protein nutrition. *J. Anim. Sci. Biotechnol.* 5 (1), 34. doi: 10.1186/2049-1891-5-34
- Xia, J., and Wishart, D. S. (2016). Using metaboanalyst 3.0 for comprehensive metabolomics data analysis. *Curr. Protoc. Bioinf.* 55, 14 10 1–14 10 91. doi: 10.1002/cpbi.11
- Xiao, N., Lou, M. D., Lu, Y. T., Yang, L. L., Liu, Q., Liu, B., et al. (2017). Ginsenoside Rg5 attenuates hepatic glucagon response via suppression of succinate-associated HIF-1 α induction in HFD-fed mice. *Diabetologia* 60 (6), 1084–1093. doi: 10.1007/s00125-017-4238-y
- Xu, L., and Brink, M. (2016). mTOR, cardiomyocytes and inflammation in cardiac hypertrophy. *Biochim. Biophys. Acta.* 1863 (7), 1894–1903. doi: 10.1016/j.bbamcr.2016.01.003
- Xu, X., Wang, X., Wu, H., Zhu, H., Liu, C., Hou, Y., et al. (2018). Glycine relieves intestinal injury by maintaining mtor signaling and suppressing AMPK, TLR4, and NOD Signaling in Weaned piglets after lipopolysaccharide challenge. *Int. J. Mol. Sci.* 19 (7), 1980–1998. doi: 10.3390/ijms19071980
- Yin, S., Guo, P., Hai, D., Xu, L., Shu, J., Zhang, W., et al. (2017). Optimization of GC/TOF MS analysis conditions for assessing host-gut microbiota metabolic interactions: Chinese rhubarb alters fecal aromatic amino acids and phenol metabolism. *Anal. Chim. Acta* 995, 21–33. doi: 10.1016/j.aca.2017.09.042

Conflict of Interest: The authors declare that the research was conducted in the absence of any commercial or financial relationships that could be construed as a potential conflict of interest.

Copyright © 2019 Wang, Zhai, Sun, Wu, Wang, Fang and Kong. This is an open-access article distributed under the terms of the Creative Commons Attribution License (CC BY). The use, distribution or reproduction in other forums is permitted, provided the original author(s) and the copyright owner(s) are credited and that the original publication in this journal is cited, in accordance with accepted academic practice. No use, distribution or reproduction is permitted which does not comply with these terms.



Inhibition of Pathological Retinal Neovascularization by a Small Peptide Derived from Human Tissue-Type Plasminogen Kringle 2

Qian Sun^{1,2,3}, Yinchun Shen^{1,2,3}, Li Su^{1,2,3*} and Xun Xu^{1,2,3}

¹ Department of Ophthalmology, Shanghai General Hospital (Shanghai First People's Hospital), Shanghai Jiao Tong University School of Medicine, Shanghai, China, ² Shanghai Key Laboratory of Fundus Disease, Shanghai Jiao Tong University, Shanghai, China, ³ Shanghai Engineering Center for Visual Science and Photomedicine, Shanghai, China

OPEN ACCESS

Edited by:

Zhuo Shao,
University of Toronto, Canada

Reviewed by:

Lufei Sui,
Boston Children's Hospital,
United States
Haojie Fu,
Harvard Medical School,
United States

*Correspondence:

Li Su
sujilin615@163.com

Specialty section:

This article was submitted to
Neuropharmacology,
a section of the journal
Frontiers in Pharmacology

Received: 23 August 2019

Accepted: 16 December 2019

Published: 28 January 2020

Citation:

Sun Q, Shen Y, Su L and Xu X (2020)
Inhibition of Pathological Retinal
Neovascularization by a Small Peptide
Derived from Human Tissue-Type
Plasminogen Kringle 2.
Front. Pharmacol. 10:1639.
doi: 10.3389/fphar.2019.01639

Retinal neovascularization is a hallmark pathological process of numerous ocular diseases which comprise the most common causes of blindness and affect millions of people from infants to the elderly. Compared to large proteins, small peptides have advantages for therapeutic application in ocular diseases, especially for retinal diseases. In this study, we investigated a small peptide derived from human tissue-type plasminogen kringle 2 (t-PA kringle 2), named TKII-12, and investigated the effect of TKII-12 on various aspects of vascular endothelial growth factor (VEGF)-induced angiogenesis *in vitro* and *in vivo*. Our results showed that TKII-12 effectively inhibited VEGF-induced human retinal microvascular endothelial cell proliferation, migration and tube formation on Matrigel dose-dependently as well as sequence-dependently. TKII-12 inhibited VEGF-induced formation of actin stress fibers and focal adhesions in vascular endothelial cells. Moreover, TKII-12 effectively inhibited retinal neovascularization in a mouse oxygen-induced retinopathy (OIR) model. Our study demonstrated that TKII-12 could effectively inhibit retinal angiogenesis *in vitro* and *in vivo* by eliminating the formation of focal adhesion complexes and the organization of actin stress fibers. TKII-12 can serve as a prototype for retinal angiogenesis inhibitory drug development.

Keywords: peptides, tissue-type plasminogen activator, kringle, retinal angiogenesis, angiogenesis inhibitor

INTRODUCTION

Retinal neovascularization is a hallmark pathological process of numerous ocular diseases, such as proliferative diabetic retinopathy, ischemic retinal vein occlusion, and retinopathy of prematurity. Abnormal retinal neovascularization always leads to hemorrhage, retinal edema, fibrosis, and irreversible damages to the retinal tissue. Neovascular retinopathies collectively comprise the most common causes of blindness and affect millions of people from infants to the elderly (Lad et al., 2009; Wong et al., 2014; Lee et al., 2015; Ho et al., 2016).

In the past two decades, antivascular endothelial growth factor (VEGF) medications for neovascular ocular diseases have revolutionized the treatment paradigm for millions of patients and preserved their vision. However, there remain pitfalls and areas for improvement with these

anti-VEGF therapies. Currently, the most widely used retinal angiogenesis inhibitors, such as ranibizumab, aflibercept, and bevacizumab, are large and complex proteins, that are difficult to scavenge and expensive to manufacture (Avery et al., 2017). Compared to these proteins, small peptides have advantages for therapeutic application, due to their high solubility, increased bio-availability and lack of immune response in the host cell. Furthermore, the production of small peptides is controllable and much easier than that of proteins. Thus, designing and developing peptides for therapeutic application to inhibit angiogenesis is an important area in antiangiogenic drug development (Sulochana and Ge, 2007; Kaspar and Reichert, 2013; Agyei et al., 2017; Lau and Dunn, 2018).

Kringle domains are protein modules composed of 78–80 amino acids connected by a characteristic triple disulfide-linked loop. To date, many kringle-containing fragments from various endogenous proteins have been reported to inhibit angiogenesis *in vitro* and *in vivo*, such as angiostatin from plasminogen, KIV-9, KIV-10, and KV from human apolipoprotein (a), kringle 1 from hepatocyte growth factor, kringle-2 from prothrombin, and kringle 1-2 and K2P from human tissue-type plasminogen activator (t-PA) (Lim et al., 2012; Cho et al., 2013; Sun and Liu, 2019). Thus, the kringle structure has been considered as a conserved architecture that specifically inhibits angiogenesis. Kringle domains may provide a structural basis for identification of novel angiogenesis inhibitors.

In an effort to develop small peptide angiogenic inhibitors, we divided human t-PA kringle 2 amino acid sequences into 4 nonoverlapping small peptides by using the cysteine in disulfide bonds for cleavage sites (not including cysteine) (Figure 1). Our previous study demonstrated that one of these four peptides, TKII-10, which consisted of the Arg54-Trp63 amino acid of human t-PA kringle 2, inhibited VEGF stimulated migration and tube formation of human umbilical vein endothelial cells (HUVECs) *in vitro* and effectively inhibited angiogenesis in

chick chorioallantoic membrane and VEGF-induced corneal neovascularization (Su et al., 2010).

In this study, we investigated another small peptide derived from human t-PA kringle 2, named TKII-12, and explored the antiangiogenic effects of TKII-12 *in vitro* and *in vivo*, in an effort to search for a more effective antiangiogenic agent for the treatment of neovascular retinopathies. MTS assay, Transwell chamber assay and tube formation assay were performed to determine the inhibitory effects of TKII-12 on VEGF-induced vascular endothelial cells proliferation, migration, and tube formation *in vitro*. The *in vivo* antiangiogenic effect of TKII-12 was evaluated in mice with oxygen-induced retinopathy (OIR). The formation of actin stress fibers and focal adhesions in vascular endothelial cells were investigated to explore the antiangiogenic mechanism of TKII-12.

MATERIALS AND METHODS

Animals

All animals were cared for in accordance with the ARVO Statement for the Use of Animals in Ophthalmic and Vision Research. Neonatal C57BL/6J mice with nursing mothers were provided by Shanghai Laboratory Animal Center, Chinese Academy of Sciences. The animals were housed in an air-conditioned room with a 12-h light and dark cycle.

Cell Culture and Materials

HRMECs (cat. no. ACBRI 181) were purchased from Cell Systems (Kirkland, WA) and cells from passages 3–7 were used in the experiment. Cells were grown in M199 medium with 45 ng/ml bFGF and heparin and 20% fetal bovine serum. Confluent cells were switched to a serum-free medium for 24 h before treatment. Human VEGF165 was purchased from R&D Systems, Inc. (Minneapolis, MN). The Transwell chamber (8.0-μm

1
C-Y-F-G-N-G-S-A-Y-R-G-T-H-S-L-T-E-S-G-A-
S-C-L-P-W-N-S-M-I-L-I-G-K-V-Y-T-A-Q-N-P-
S-A-Q-A-L-G-L-G-K-H-N-Y-C-R-N-P-D-G-D-
A-K-P-W-C-H-V-L-K-N-R-R-L-T-W-E-Y-C-D-
V-P-S-C
 82

FIGURE 1 | Sequence of human t-PA kringle 2. The figure shows the primary sequences of the four t-PA kringle 2-derived peptides, highlighted in blue Peptide 1 (Tyr2–Ser21), green Peptide 2 (Leu23–Tyr52), purple Peptide 3 (Arg54–Trp63) (named TKII-10), and red Peptide 4 (His65–Tyr76)(named TKII-12), respectively.

pore size) was purchased from Costar (Corning, Cambridge, MA). Growth factor-reduced Matrigel was purchased from BD Biosciences (Bedford, MA).

Preparation of Peptides

The peptides TKII-12 (HVLKNRRLTWEY) and TKII-10 (RNPDGDAKPW) were synthesized by a high-efficiency solid-phase method using an automatic peptide synthesizer (Symphony; Protein Technologies, Tucson, AZ). The end product was characterized by high-performance liquid chromatography (HPLC, analytical; Shimadzu, Kyoto, Japan) and mass spectrometry (MS; Finnigan TSQ 7000; Thermo, Waltham, MA). To verify whether the effect of TKII-12 was sequence-dependent, we scrambled the amino acid sequence of TKII-12 and synthesized TKII-12S (KRYLTHNVRWLE). These peptides were freeze-dried and stored at -20°C until used. Immediately before use, the peptides were dissolved in phosphate-buffered saline (PBS). Both these peptides were water-soluble and stable in aqueous solutions.

Endothelial Cell Proliferation Assay

Endothelial cell proliferation assay was determined using the nonradioactive CellTiter 96[®] aqueous one solution (Promega, Madison, WI). Briefly, approximately 3,500 cells/well were added in triplicate into each well of 96-well cell culture plates and incubated at 37°C for 24 h. After 24 h, HRMECs were starved overnight and then incubated with or without 10 ng/ml of VEGF and various concentrations of peptide (1 nM, 10 nM, 100 nM, 1 μM , and 10 μM) for 24 h. Then, 20 μl of CellTiter 96[®] Aqueous One Solution was added to each well and incubated for another 3 h at 37°C . The absorbance at 490 nm, which correlates to the number of living cells, was measured with a microplate reader (Bio-Rad, Model 680, Hercules, CA). Each group was tested in triplicate. All the experiments were repeated 3 times.

Endothelial Cell Migration Assay

To determine the effect of TKII-12 peptide on endothelial cell migration toward VEGF, endothelial cell migration assay was performed using a disposable Transwell chamber as described previously with modifications (Sulochana et al., 2005). Briefly, HRMECs were starved overnight, trypsinized, and suspended at a final concentration of 8×10^5 cells/ml. Various concentrations of peptide (1 nM, 10 nM, 100 nM, 1 μM , and 10 μM) were preincubated with approximately 4×10^4 cells for 30 min at 37°C before seeding onto the cell culture inserts. VEGF (25 ng/ml) was placed into the lower chamber. The assembled cell culture insert chamber was then incubated at 37°C for 24 h. After removing the nonmigrating cells with a cotton swab in the upper chamber, migrated cells on the lower surface of the culture inserts were fixed with 4% paraformaldehyde, stained with hematoxylin, and photographed under a light microscope (Olympus, Tokyo, Japan). Five random fields ($\times 200$) were chosen in each insert, and the cell number was counted. Each group was tested in triplicate. All the experiments were repeated 3 times.

Endothelial Cell Tube Formation Assay

A tube formation assay was performed as previously described (Su et al., 2010). Growth factor-reduced Matrigel (50 μl) was added to each well of chilled 96-well plates and incubated for 30 min at 37°C . Approximately 3×10^4 cells were preincubated with various concentrations of peptide (1 nM, 10 nM, 100 nM, 1 μM , and 10 μM) at 37°C for 30 min before being seeded onto the solidified growth factor-reduced Matrigel in a 96-well plate. After incubating in media with or without 15 ng/ml of VEGF at 37°C for 6 h, tube formation was observed using an inverted phase contrast microscope (Olympus, Tokyo, Japan) and photographed with a digital camera (Olympus). Four random fields were chosen in each well, and the total tube length was quantified using the Image-Pro Plus Program (version 6.0; Media Cybernetics, Bethesda, MD). Each group was tested in triplicate. All the experiments were repeated 3 times.

Immunofluorescence Microscopy

For immunostaining, the cells were washed with PBS and fixed with 4% paraformaldehyde on ice for 15 min. For paxillin staining, cells were permeabilized by treatment with 0.4% Triton X-100. The cells were then treated with 1% fetal bovine serum (FBS) for 1 h at room temperature and incubated with a mouse monoclonal antibody against paxillin (Cell Signaling Technology). Unbound proteins were removed by washing, and the cells were subsequently incubated with fluorescein isothiocyanate (FITC)-labeled secondary antibody for 1 h. Tetramethylrhodamine (TRITC)-conjugated phalloidin (Sigma) was used to stain the actin cytoskeleton. The coverslips were then washed three times with Tris-buffered saline (TBS) containing 0.05% Tween 20 and examined using a fluorescence microscope (Model Axiophot2, Zeiss) (Kim et al., 2004).

Mouse OIR Assay

The mouse model of OIR was performed as previously described (Zhao et al., 2009). In our previous study (Zhao et al., 2009), we developed a small peptide KV11(YTMNPRKLFYD) from human apolipoprotein (a) KV which can effectively inhibit retinal pathologic angiogenesis at the dose of 50 mM (1 μl) in OIR model. Our newly developed peptide TKII-12 had a similar molecular weight as KV11. So we chose the dose of 50 mM (1 μl) for intravitreal injections in the OIR experiments. Neonatal C57BL/6J mice with their nursing mothers were randomly divided into five groups: room air plus PBS, room air plus TKII-12, oxygen plus PBS, oxygen plus TKII-12, and oxygen plus TKII-12S. Each group contained seven to nine pups. Briefly, on postnatal day 7 (P7), C57BL/6J mouse pups with their mothers were subjected to $75\% \pm 2\%$ oxygen for 5 days. At P12, they were returned to room air and raised for another 5 days. On P12 and P14, peptides were administered by intravitreal injections at the concentration of 50 mM (1 μl), respectively. Eyes of control mice were injected with 1 μl of PBS or TKII-12S (50 mM). Groups kept in room air received 1 μl of PBS or TKII-12 (50 mM) injections at the same time as those treated with oxygen. All the injections were performed in the

right eyes, and the left eyes were not injected. At P17, the mice were killed, and then, their eyes were enucleated and subjected to the following examinations.

To quantitatively analyze the areas of neovascularization and the avascular zone, retinal whole mounts were stained with Alexa Fluor 568 conjugated isolectin B4 (Molecular Probes, Eugene, OR) which showed strong affinity for vascular endothelial cells and perivascular cells. Briefly, the eyes were fixed in 4% paraformaldehyde at 4°C for 8 to 12 h. Then, the neuroretina was separated from the eye cup and fixed for another 2 h. The retinas were permeabilized in 1% Triton X-100 for 30 min, and then incubated with 5 µg/ml of isolectin B4 overnight at 4°C. The retinas were rinsed three times in PBS, mounted in PBS:glycerol (2:1), and covered with a coverslip. All fluorescence images were taken by a fluorescence microscope (Carl Zeiss Meditec), with a standardized technique at a magnification of $\times 5$. Flat-mounted retina images were assessed by image analysis software (Image-Pro Plus Program, version 6.0; Media Cybernetics, Bethesda, MD) to quantify the areas of avascular retina, retinal neovascularization, and normal vascularization. The total surface area of the retina was outlined using the outermost vessel of the arcade near the ora serrata as the border. Neovascularization, vaso-obliteration and normal vasculature were circumscribed based on their characteristic appearance, as described previously, and were normalized to the total retinal area. All images were examined in a blinded fashion.

Meanwhile, the eyes were fixed with 4% paraformaldehyde and embedded in paraffin. Ten sections, 30 µm apart, were cut sagittally through the cornea and parallel to the optic nerve and stained with hematoxylin and eosin. A blood vessel profile (BVP) was defined as an endothelial cell or a blood vessel with a lumen. BVPs were counted in the inner retina, which consists of the inner limiting membrane, the ganglion cell layer, the inner plexiform layer, and the inner nuclear layer. Five nonoverlapping fields per section were examined by two observers in a masked fashion. The mean of all 10 counted sections yield average retinal neovascular cell nuclei per eye.

Statistical Analysis

The experimental data were expressed as mean \pm SEM from at least three independent experiments. Analysis was performed with one-way analysis of variance (ANOVA) for multiple groups. For comparison of the differences between groups, a *post hoc* least significant difference (LSD) test was used. A *p* value <0.05 was considered to be statistically significant in all cases.

RESULTS

Inhibition of VEGF-Induced Endothelial Cell Proliferation by TKII-12

In cell proliferation assay, HRMECs were exposed to increasing concentrations of the peptides for 24 h in the presence of 10 ng/ml of VEGF as mitogenic stimulus. As shown in **Figure 2**, compared with control group, TKII-12 alone without VEGF

had no significant effect on HRMECs proliferation ($p > 0.05$). TKII-12 dose-dependently inhibited VEGF-induced HRMECs proliferation, and the concentration of TKII-12 required to reach 50% inhibition (ED50) was between 100 nM and 1 µM. However, TKII-10 did not show any significantly inhibitory effect on VEGF-induced HRMECs proliferation at the concentration of 10 µM, which was consistent with our previous results (Su et al., 2010). TKII-12S did not show any inhibitory effect on VEGF-induced HRMEC proliferation up to the concentration of 10 µM. Our results showed that TKII-12 can inhibit VEGF-induced HRMECs proliferation dose-dependently and sequence-dependently without significant toxic effect on endothelial cell proliferation.

Inhibition of VEGF-Induced Endothelial Cell Migration by TKII-12

Compared with control group, TKII-12 alone without VEGF had no significant effect on HRMECs migration ($p > 0.05$). Compared with the control group, the number of migration cells in the VEGF group increased significantly ($p < 0.05$). As shown in **Figure 3**, TKII-12 potentially inhibited VEGF-induced HRMECs migration in a dose-dependent as well as sequence-dependent manner with an estimated ED50 value between 100 nM and 1 µM, whereas TKII-12S had no such activity. TKII-10 inhibited VEGF-induced HRMECs migration at the concentration of 10 µM, but the inhibitory effect less effective than TKII-12.

Inhibition of VEGF-Induced Endothelial Cell Tube Formation by TKII-12

As shown in **Figure 4**, compared with control group, TKII-12 alone without VEGF had no significant effect on HRMECs tube formation ($p > 0.05$). VEGF (15 ng/ml) strongly stimulated HRMECs cell tube formation on Matrigel, compared with control group ($p < 0.05$). TKII-12 inhibited VEGF-induced HRMECs tube formation on Matrigel dose dependently, and at 10 µM concentration TKII-12 almost completely inhibited VEGF-induced HRMECs cells tube formation on Matrigel. TKII-12 inhibited VEGF-induced HRMECs tube formation sequence-dependently as TKII-12S was inactive. TKII-10 also inhibited VEGF-stimulated HRMECs tube formation, but the inhibitory effect was not as strong as TKII-12 at the concentration of 10 µM.

Inhibition of Actin Stress Fibers and Focal Adhesions Formation by TKII-12

The dynamic formation of actin stress fibers and focal adhesions played a crucial role in the regulation of cell adhesion and movement. As shown in **Figure 5**, VEGF significantly increased the formation of actin stress fibers and focal adhesions in vascular endothelial cells. Consistent with the effects of TKII-12 on VEGF-induced cell migration and tube formation, the formation of actin stress fibers and focal adhesions induced by VEGF was greatly decreased by TKII-12. The inhibitory effect was sequence-dependently as TKII-12S was inactive.

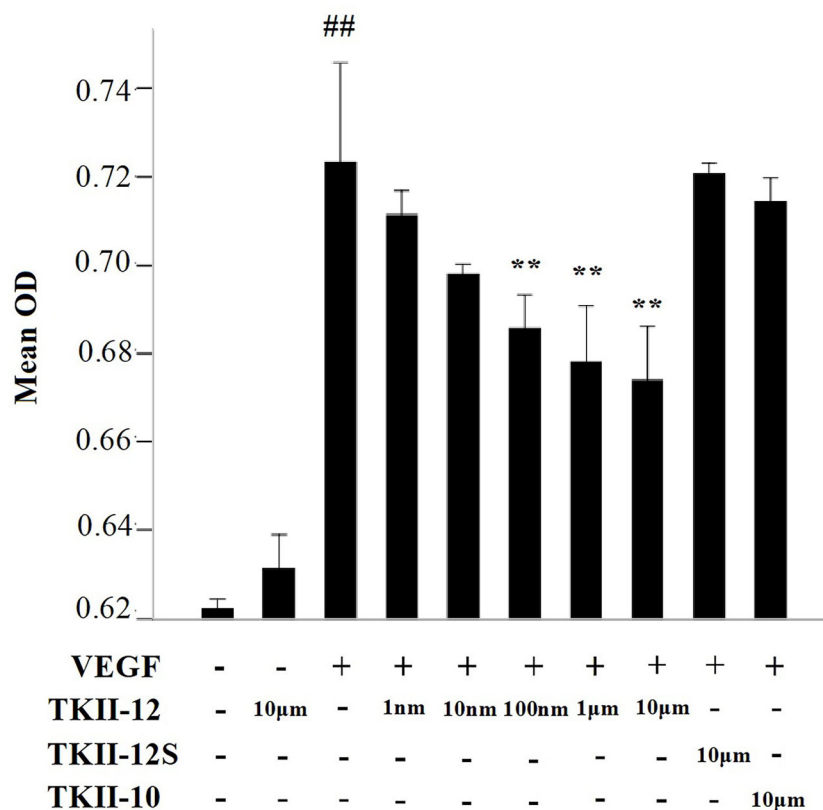


FIGURE 2 | Effects of TKII-12 on vascular endothelial growth factor (VEGF)-induced (HRMECs proliferation *in vitro*. Inhibitory effect of TKII-12 on endothelial cell proliferation was assessed by MTS method 24 h after treatment. Each value represents the mean \pm SEM of triplicate measurements. ** $p < 0.01$ versus the VEGF group. ## $p < 0.01$ versus the control group.

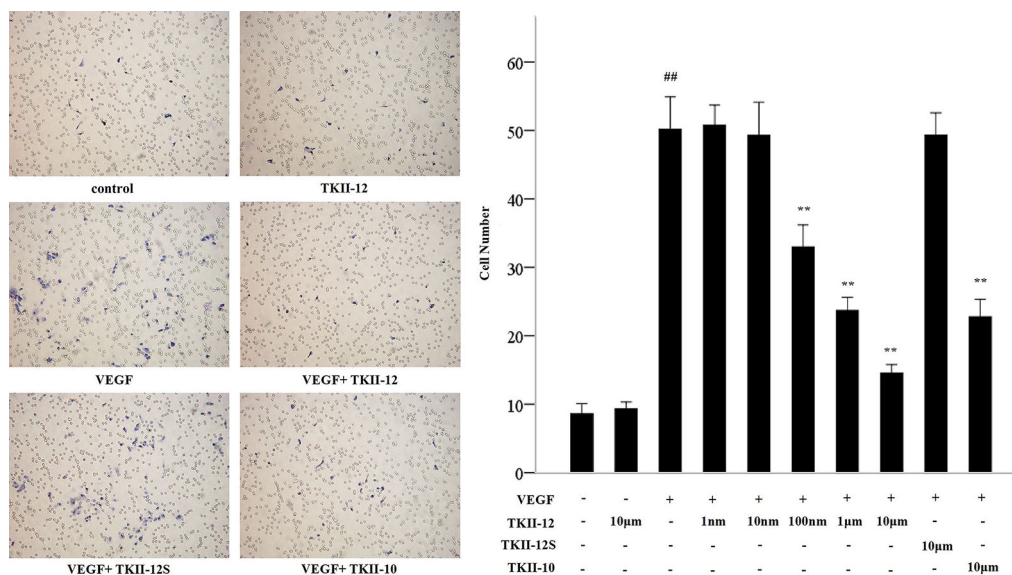


FIGURE 3 | Effects of TKII-12 on vascular endothelial growth factor (VEGF)-induced HRMECs migration *in vitro*. Inhibitory effect of TKII-12 on endothelial cell migration toward VEGF was assessed by a Transwell chamber 24 h after treatment. ** $p < 0.01$ versus the VEGF group. ## $p < 0.01$ versus the control group.

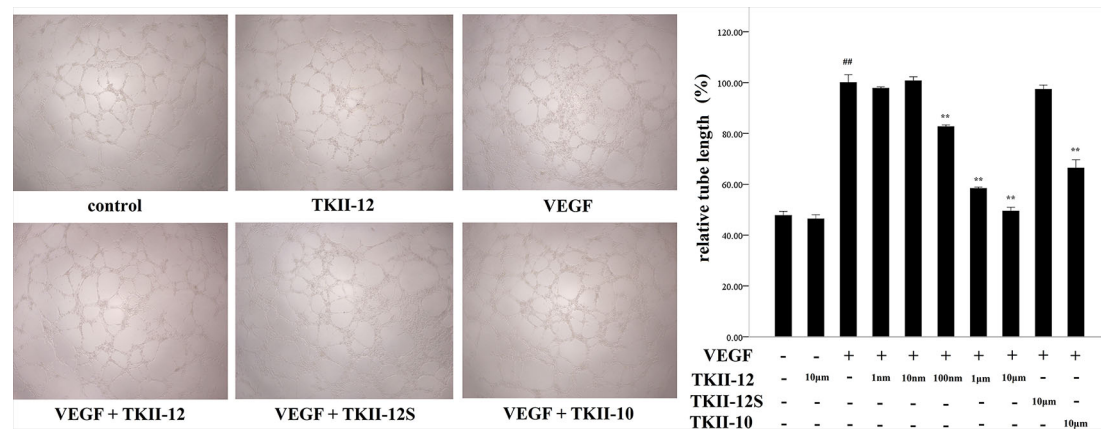


FIGURE 4 | Effects of TKII-12 on vascular endothelial growth factor (VEGF)-induced HRMECs tube formation on Matrigel. The left panel is the representative phase-contrast micrographs of HRMECs exposed to different culture medium at 6 h (magnification 20×). The right panel presents the quantitative graph of the relative percentage of tube length. Each value represents the mean \pm SEM of triplicate measurements. ** $p < 0.01$ versus the VEGF group. ## $p < 0.01$ versus the control group.

Inhibition of Oxygen-Induced Neovascular Retinopathy by TKII-12

The inhibitory effect of oxygen-induced retinal neovascularization by TKII-12 was quantitatively analyzed by isolectin B4 staining. The isolectin-stained retinal whole mounts were used to evaluate the neovascular, avascular, and normal vascular areas at P17. As shown in **Figure 6**, retinas of the room air plus TKII-12 group demonstrated normal retinal vascular development, without obvious differences from that of the room air plus PBS group, indicating that TKII-12 did not inhibit retinal vascular development under normal condition. Retinas of the oxygen plus PBS group exhibited obvious central vascular obliteration and extensive preretinal neovascular tuft formation located mainly at the junction between the central avascular and peripheral vascularized regions. Intravitreal TKII-12 injection significantly improved the pathological vascular responses. Compared with the oxygen plus PBS group, TKII-12 dramatically reduced the pericentral neovascular tuft area by up to 34% (from $17.37\% \pm 3.07\%$ to $11.45\% \pm 3.37\%$ of the whole retinal area) ($p < 0.01$). Meanwhile, TKII-12 also significantly reduced the central avascular area by up to 23% (from $31.70\% \pm 2.98\%$ to $24.51\% \pm 3.36\%$ of the whole retinal area) ($p < 0.01$), with a significant increase in the percentage of peripheral normal vascular area (from $50.93\% \pm 5.12\%$ to $64.04\% \pm 6.55\%$ of the whole retinal area) ($p < 0.01$) (**Figure 7**). These data indicated that TKII-12 potently inhibited pathological retinal neovascularization and enhanced physiological vascular regrowth in OIR. In contrast, intravitreal TKII-12S injection demonstrated no significant improvement in preretinal neovascular tuft formation and central vascular obliteration ($p > 0.05$), indicating that the angiogenic inhibitory effect of TKII-12 was sequence-dependent.

Histological examinations of the retinal sections further confirmed the preretinal neovascular tuft formation in the retinal flat mounts (**Figure 8**). The degree of retinal neovascular formation was quantified by counting BVPs in the inner retina in at least 10 sections per eye. Retinas in the room air plus TKII-12

group demonstrated few preretinal neovascular tuft, with no significant difference in BVP number compared with the room air plus PBS group ($p > 0.05$). Retinas in the oxygen plus PBS group showed obvious vascular lumen formation in the inner retina, and the BVP number significantly increased compared with the room air plus PBS group ($p < 0.01$). The BVP number significantly decreased in the oxygen plus TKII-12 group compared with the oxygen plus PBS group ($p < 0.01$). In contrast, the BVP number in the oxygen plus TKII-12S group showed no significant difference with that in the oxygen plus PBS group ($p > 0.05$), indicating that TKII-12 inhibited oxygen-induced retinal neovascularization sequence-dependently.

DISCUSSION

Retinal neovascularization is a major cause of vision loss in humans, and the potential therapeutic effects of angiogenic inhibitors in neovascular retinopathy are under intensive investigation. In this study, we observed that a small peptide, TKII-12, derived from human tissue-type plasminogen kringle 2 effectively inhibited VEGF-induced HRMECs proliferation, migration, and tube formation dose-dependently as well as sequence-dependently *in vitro*. TKII-12 decreased the formation of actin stress fibers and focal adhesions in vascular endothelial cells. Furthermore, TKII-12 effectively inhibited retinal neovascularization in a mouse OIR model. TKII-12 is a promising angiogenic inhibitor for the treatment of neovascular retinopathy.

In an effort to develop angiogenic inhibitors, we divided human t-PA kringle 2 into 4 nonoverlapping peptides (shown in **Figure 1**). In a series of studies, we analyzed the antiangiogenic effects of all these four peptides. Our previous study demonstrated that TKII-10 (Arg54-Trp63) inhibited VEGF stimulated migration and tube formation of vascular endothelial cells *in vitro* and corneal neovascularization *in vivo*

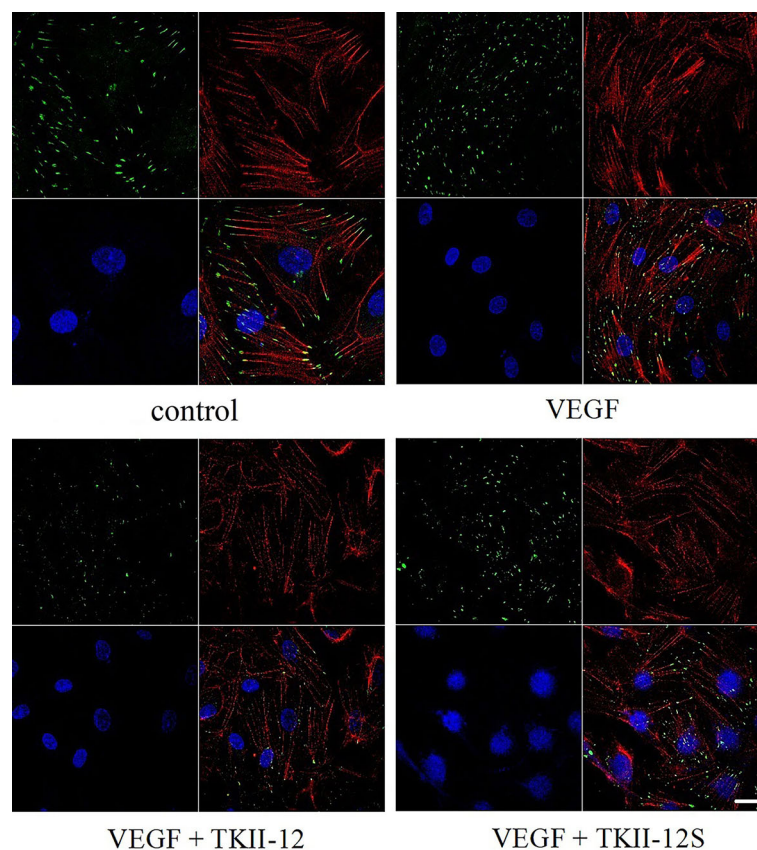


FIGURE 5 | Effects of TKII-12 on vascular endothelial growth factor (VEGF)-induced formation of actin stress fibers and focal adhesion complexes in HRMECs. HRMECs were immunostained with an antivinculin antibody and stained with TRITC-conjugated phalloidin and DAPI. The scale bar is 20 μ m.

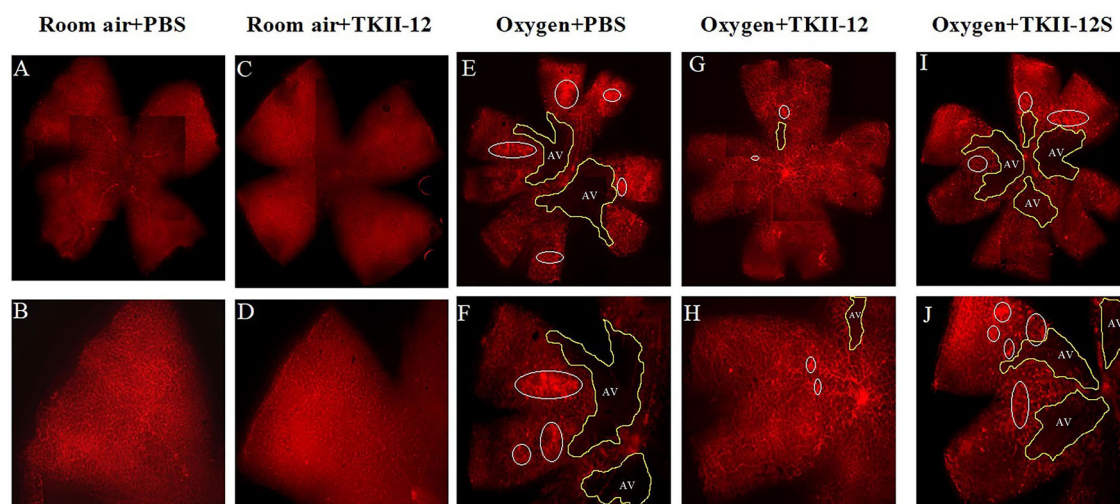


FIGURE 6 | Retina flat-mounts stained with isolectin B4 from each group at P17. The retinal vasculature in the room air plus TKII-12 group (C, D) was no different from that of the room air plus PBS group (A, B). Oxygen plus phosphate-buffered saline (PBS) (E, F) and oxygen plus the scrambled peptide (G, H) groups exhibited a remarkable avascular region and pathologic neovascular tufts. Oxygen plus TKII-12 group (I, J) showed a significant reduction in neovascularization and avascular region. Top row: whole retina montages created by four overlapping images containing one quadrant each; bottom row: a single image of the whole flat-mount, showing one quadrant. White circle: neovascular tufts. Yellow area: avascular region. Magnification, $\times 5$.

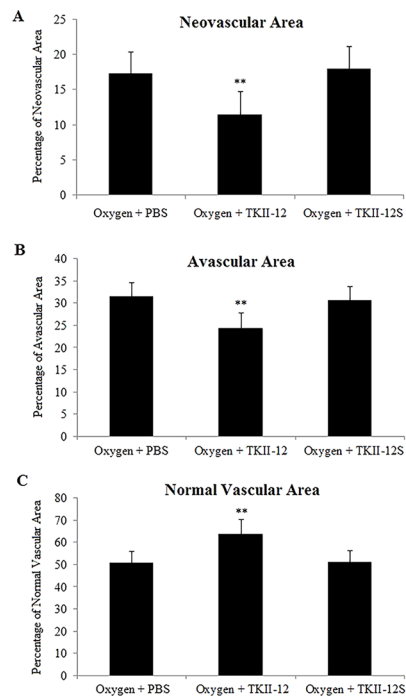


FIGURE 7 | Quantitative analysis of the effects of TKII-12 on oxygen-induced retinopathy in a mouse model. Quantification of neovascularization (A), avascularization (B), and normal vascularization (C) of each group were performed at P17. ** $p < 0.01$ versus the oxygen plus phosphate-buffered saline (PBS) group.

(Su et al., 2010). In this study, we demonstrated that TKII-12 (His65-Tyr76) inhibited VEGF-induced HRMECs proliferation, migration, and tube formation *in vitro* and pathological retinal neovascularization *in vivo*. Compared with TKII-10, the antiangiogenic effect of TKII-12 was stronger and more comprehensive. Besides TKII-12 and TKII-10, peptide Tyr2-Ser21 from human t-PA kringle 2 did not show any antiangiogenic effect *in vitro*. Peptide Leu23-Tyr52 from human t-PA kringle 2 inhibited VEGF-induced endothelial cell migration and tube formation *in vitro*, but the antiangiogenic effect was not as strong as TKII-12. Moreover, the solubility of peptide Leu23-Tyr52 was not as good as the other three peptides. Thus, we fully investigated the most promising antiangiogenic peptide TKII-12.

Angiogenesis is a multistep process that includes vascular endothelial cell proliferation and migration, capillary tube formation, and extracellular matrix degeneration and remodeling. Alteration of the cytoskeleton and the temporal-spatial organization of cell adhesion structures are central events in endothelial cell migration (Shen and Guan, 2001; Wozniak et al., 2004). Our results indicated that TKII-12 suppressed VEGF-stimulated formation of focal adhesion complexes and the consequent organization of actin stress fibers. The recombinant protein TK1-2 (kringle 1-2 from human t-PA) inhibited angiogenesis partly by the interaction with integrin $\alpha 2\beta 1$ (Kim et al., 2003; Kim et al., 2008). TKII-12 was derived from the extended antiparallel β -sheet within the t-PA kringle 2 domain which also demonstrated antiangiogenic activity (Byeon et al., 1991; Carroll et al., 2005). Another peptide, TP-7, derived from t-PA kringle 2 inhibited VEGF or FGF-induced

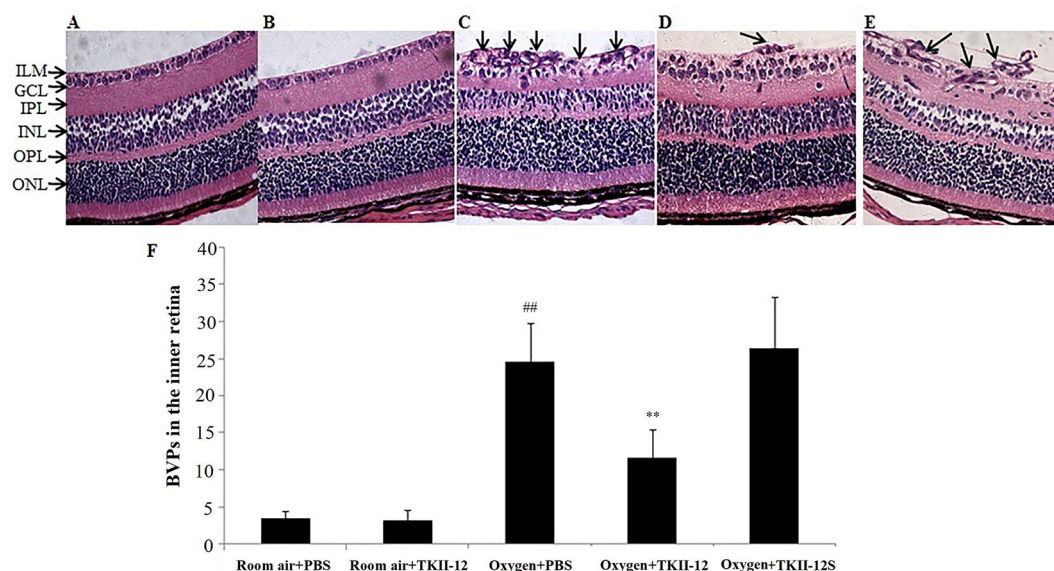


FIGURE 8 | Inhibitory effect of TKII-12 on oxygen-induced retinopathy in mice. Paraffin-embedded sections of the retina stained with hematoxylin and eosin. (A) Room air plus phosphate-buffered saline (PBS); (B) room air plus TKII-12; (C) oxygen plus PBS; (D) oxygen plus TKII-12; (E) oxygen plus the scrambled peptide. Arrows: blood vessel profiles (BVPs) in the inner retina or extending from the retina into the vitreous cavity. Magnification, $\times 100$. (F) Quantification of BVPs in the inner retina. ## $p < 0.01$ versus the room air plus PBS group. ** $p < 0.01$ versus the oxygen plus PBS group.

phosphorylation of ERK1/2 and FAK (Kim et al., 2017). Future studies are needed to identify the exact antiangiogenic mechanism of TKII-12.

Toxicity investigation is a critical part of antiangiogenic drug development. In this study, TKII-12 alone without VEGF did not show any potential toxicity to vascular endothelial cells as it had no significant effect on cell proliferation, migration or tube formation *in vitro*. In the OIR study, intravitreal TKII-12 injection in the room air plus TKII-12 group showed no obvious qualitative abnormalities such as vessel dilation, tortuosity, leakage, or hemorrhages, indicating that TKII-12 did not affect the normal retinal vessel development. These results indicated that TKII-12 had no obvious toxicity to the retinal vessel development, and its inhibitory effect on angiogenesis was specific to pathological retinal neovascularization. Our previous report also proved the safety of small peptides to retinal tissues. Intravitreal administration of KV11, even up to the concentration of 200 mM, did not display notable retinal toxicity as evaluated by electrophysiological and ultrastructural examinations (Zhao et al., 2009). Small peptides also show sufficient penetration capabilities. FITC-labeled KV11 could rapidly penetrate the whole retina. However, even after high-dose intravitreal injection, the plasma concentration of KV11 was still too low to induce evident systemic adverse reactions. TKII-12 has a similar molecular weight, isoelectric point, net charge, and good water solubility as KV11. Therefore, TKII-12 could be expected to have a similar favorable safety profile and penetration capability as KV11.

In previous studies, Kim et al. reported the recombinant protein TK1-2 and the t-PA kringle 2 domain alone inhibited angiogenesis *in vitro* and *in vivo* (Kim et al., 2003; Carroll et al., 2005; Kang et al., 2006; Kim et al., 2008). Kim also reported a peptide derived from t-PA kringle 2 (named TP-7) that inhibited angiogenesis and corneal neovascularization (Kim et al., 2017). TP-7 was derived from an extended antiparallel β -sheet motif of t-PA kringle 2. TP-7 can in part affect the integrin $\alpha 2\beta 1$ -dependent pathway and target VEGF and non-VEGF pathways. Our designed peptides (TKII-10 and TKII-12) were also derived from t-PA kringle 2, but they were designed using the cysteine in disulfide bonds for cleavage sites. TKII-10 can inhibit VEGF-stimulated migration and tube formation of HUVECs *in vitro* and effectively inhibited angiogenesis in chick chorioallantoic membrane and VEGF-induced corneal neovascularization. TKII-12 could effectively inhibit retinal angiogenesis *in vitro* and *in vivo* by eliminating the formation of focal adhesion complexes and the organization of actin stress fibers. Both of these peptides may serve as prototypes for antiangiogenic drug development.

While the widely-used anti-VEGF therapy has revolutionized the treatment of retinal neovascular diseases, it is still with some limitations. Anti-VEGF therapy effectively decreased retinal and

choroidal neovascular lesions; however, it can lead to ocular fundus fibrotic scarring and largely hinder the ultimate vision acuity improvement (Gemenetzi et al., 2017). With long-term studies, anti-VEGF resistance is now coming to our mind (Yang et al., 2016). This highlights the need for the development of new antiangiogenic drugs which can target different mechanism and reduce the necessity of invasive and repetitive intravitreal injections. Compared to proteins, low-molecular-weight small peptides, such as TKII-12, possessed its own incomparable superiority with easier and inexpensive synthesizing methods, improved consistency between batches, lower immunogenicity, higher solubility in water, and better penetrating abilities. Considering the hurdles in the clinical applications of large proteins, small peptides may provide promising candidates for new ocular antiangiogenic therapy.

CONCLUSION

In summary, TKII-12 can effectively inhibit VEGF-induced human retinal microvascular endothelial cell proliferation, migration, and tube formation *in vitro* and eliminate oxygen-induced retinal neovascularization *in vivo* by decreasing the formation of actin stress fibers and focal adhesions. TKII-12 may provide an effective approach for pathological retinal neovascularization therapy.

DATA AVAILABILITY STATEMENT

The raw data supporting the conclusions of this article will be made available by the authors, without undue reservation, to any qualified researcher.

ETHICS STATEMENT

The animal study was reviewed and approved by Shanghai General Hospital.

AUTHOR CONTRIBUTIONS

LS, QS, and XX designed the experiment. LS, YS, and QS performed the experiment. LS analyzed data and wrote the manuscript. XX conceived and supervised the study.

FUNDING

This project was sponsored by the National Key R&D Program of China (No. 2016YFC0904800) and the Program (No. 81302683 and 81570851) of the National Natural Science Foundation of China.

REFERENCES

- Agyei, D., Ahmed, I., Akram, Z., Iqbal, H. M., and Danquah, M. K. (2017). Protein and peptide biopharmaceuticals: an overview. *Protein Pept. Lett.* 24 (2), 94–101. doi: 10.2174/0929866523666161222150444
- Avery, R. L., Castellarin, A. A., Steinle, N. C., Dhoot, D. S., Pieramici, D. J., See, R., et al. (2017). Systemic pharmacokinetics and pharmacodynamics of intravitreal aflibercept, bevacizumab and ranibizumab. *Retina* 37 (10), 1847–1858. doi: 10.1097/IAE.0000000000001493

- Byeon, I. J., Kelley, R. F., and Llinás, M. (1991). Kringle-2 domain of the tissue-type plasminogen activator. 1H-NMR assignments and secondary structure. *Eur. J. Biochem.* 197 (1), 155–165. doi: 10.1111/j.1423-1033.1991.tb15894.x
- Carroll, V. A., Nikitenko, L. L., Bicknell, R., and Harris, A. L. (2005). Antiangiogenic activity of a domain deletion mutant of tissue plasminogen activator containing kringle 2. *Arterioscler. Thromb. Vasc. Biol.* 25 (4), 736–741. doi: 10.1161/01.ATV.0000157980.15710.2b
- Cho, C. F., Chen, P. K., Chang, P. C., Wu, H. L., and Shi, G. Y. (2013). Human plasminogen kringle 1-5 inhibits angiogenesis and induces thrombomodulin degradation in a protein kinase A-dependent manner. *J. Mol. Cell Cardiol.* 63, 79–88. doi: 10.1016/j.yjmcc.2013.07.009
- Gemenetzi, M., Lotery, A. J., and Patel, P. J. (2017). Risk of geographic atrophy in age-related macular degeneration patients treated with intravitreal anti-VEGF agents. *Eye (Lond)*. 31 (1), 1–9. doi: 10.1038/eye.2016.208
- Ho, M., Liu, D. T., Lam, D. S., and Jonas, J. B. (2016). Retinal vein occlusion, from basics to the latest treatment. *Retina* 36 (3), 432–448. doi: 10.1097/IAE.0000000000000843
- Kang, B. H., Shim, B. S., Lee, S. Y., Lee, S. K., Hong, Y. K., and Joe, Y. A. (2006). Potent anti-tumor and prolonged survival effects of E. coli-derived non-glycosylated kringle domain of tissue-type plasminogen activator. *Int. J. Oncol.* 28 (2), 361–367.
- Kaspar, A. A., and Reichert, J. M. (2013). Future directions for peptide therapeutics development. *Drug Discovery Today* 18 (17–18), 807–817. doi: 10.1016/j.drudis.2013.05.011
- Kim, H. K., Lee, S. Y., Oh, H. K., Kang, B. H., Ku, H. J., Lee, Y., et al. (2003). Inhibition of endothelial cell proliferation by the recombinant kringle domain of tissue-type plasminogen activator. *Biochem. Biophys. Res. Commun.* 304 (4), 740–746. doi: 10.1016/s0006-291x(03)00656-9
- Kim, J. S., Yu, H. K., Ahn, J. H., Lee, H. J., Hong, S. W., Jung, K. H., et al. (2004). Human apolipoprotein (a) kringle V inhibits angiogenesis *in vitro* and *in vivo* by interfering with the activation of focal adhesion kinases. *Biochem. Biophys. Res. Commun.* 313 (3), 534–540. doi: 10.1016/j.bbrc.2003.11.148
- Kim, H. K., Oh, D. S., Lee, S. B., Ha, J. M., and Joe, Y. A. (2008). Antimigratory effect of TKI-2 is mediated in part by interfering with integrin $\alpha 2\beta 1$. *Mol. Cancer Ther.* 7 (7), 2133–2141. doi: 10.1158/1535-7163.MCT-07-2405
- Kim, H. K., Choi, J. S., Lee, S. W., Joo, C. K., and Joe, Y. A. (2017). A novel peptide derived from tissue-type plasminogen activator potentially inhibits angiogenesis and corneal neovascularization. *J. Cell Biochem.* 118 (5), 1132–1143. doi: 10.1002/jcb.25732
- Lad, E. M., Hernandez-Boussard, T., Morton, J. M., and Moshfeghi, D. M. (2009). Incidence of retinopathy of prematurity in the United States: 1997 through 2005. *Am. J. Ophthalmol.* 148 (3), 451–458. doi: 10.1016/j.ajo.2009.04.018
- Lau, J. L., and Dunn, M. K. (2018). Therapeutic peptides: Historical perspectives, current development trends, and future directions. *Bioorg. Med. Chem.* 26 (10), 2700–2707. doi: 10.1016/j.bmc.2017.06.052
- Lee, R., Wong, T. Y., and Sabanayagam, C. (2015). Epidemiology of diabetic retinopathy, diabetic macular edema and related vision loss. *Eye Vis. (Lond)*. 2, 17. doi: 10.1186/s40662-015-0026-2
- Lim, Y., Jo, D. H., Kim, J. H., Ahn, J. H., Hwang, Y. K., Kang, D. K., et al. (2012). Human apolipoprotein (a) kringle V inhibits ischemia-induced retinal neovascularization via suppression of fibronectin-mediated angiogenesis. *Diabetes* 61 (6), 1599–1608. doi: 10.2337/db11-1541
- Shen, T. L., and Guan, J. L. (2001). Differential regulation of cell migration and cell cycle progression by FAK complexes with Src, PI3K, Grb7 and Grb2 in focal contacts. *FEBS Lett.* 499 (1–2), 176–181. doi: 10.1016/s0014-5793(01)02545-5
- Su, L., Xu, X., Zhao, H., Gu, Q., and Zou, H. D. (2010). *In vitro* and *in vivo* antiangiogenic activity of a novel deca-peptide derived from human tissue-type plasminogen activator kringle 2. *Biochem. Biophys. Res. Commun.* 369 (4), 1012–1017. doi: 10.1016/j.bbrc.2010.05.048
- Sulochana, K. N., and Ge, R. (2007). Developing antiangiogenic peptide drugs for angiogenesis-related diseases. *Curr. Pharm. Des.* 13 (20), 2074–2086. doi: 10.2174/138161207781039715
- Sulochana, K. N., Fan, H., Jois, S., Subramanian, V., Sun, F., Kini, R. M., et al. (2005). Peptides derived from human decorin leucine-rich repeat 5 inhibit angiogenesis. *J. Biol. Chem.* 280 (30), 27935–27948. doi: 10.1074/jbc.M414320200
- Sun, P., and Liu, Z. (2019). Overexpressing kringle 1 domain of hepatocyte growth factor with adeno-associated virus inhibits the pathological retinal neovascularization in an oxygen-induced retinopathy mouse model. *Biochem. Biophys. Res. Commun.* 508 (1), 130–137. doi: 10.1016/j.bbrc.2018.11.111
- Wong, W. L., Su, X., Li, X., Cheung, C. M., Klein, R., Cheng, C. Y., et al. (2014). Global prevalence of age-related macular degeneration and disease burden projection for 2020 and 2040: a systematic review and meta-analysis. *Lancet Glob. Health* 2 (2), e106–e116. doi: 10.1016/S2214-109X(13)70145-1
- Wozniak, M. A., Modzelewska, K., Kwong, L., and Keely, P. J. (2004). Focal adhesion regulation of cell behavior. *Biochim. Biophys. Acta* 1692 (2–3), 103–119. doi: 10.1016/j.bbamcr.2004.04.007
- Yang, S., Zhao, J., and Sun, X. (2016). Resistance to anti-VEGF therapy in neovascular age-related macular degeneration: a comprehensive review. *Drug Des. Devel. Ther.* 10, 1857–1867. doi: 10.2147/DDDT.S97653
- Zhao, H., Jin, H., Li, Q., Gu, Q., Zheng, Z., Wu, H., et al. (2009). Inhibition of pathologic retinal neovascularization by a small peptide derived from human apolipoprotein (a). *Invest. Ophthalmol. Vis. Sci.* 50 (11), 5384–5395. doi: 10.1167/iops.08-3163

Conflict of Interest: The authors declare that the research was conducted in the absence of any commercial or financial relationships that could be construed as a potential conflict of interest.

Copyright © 2020 Sun, Shen, Su and Xu. This is an open-access article distributed under the terms of the Creative Commons Attribution License (CC BY). The use, distribution or reproduction in other forums is permitted, provided the original author(s) and the copyright owner(s) are credited and that the original publication in this journal is cited, in accordance with accepted academic practice. No use, distribution or reproduction is permitted which does not comply with these terms.



LncRNA TDRG1-Mediated Overexpression of VEGF Aggravated Retinal Microvascular Endothelial Cell Dysfunction in Diabetic Retinopathy

OPEN ACCESS

Edited by:

Zhongxiao Wang,
Harvard Medical School,
United States

Reviewed by:

Ahmed Mousa,
Nourseen Charity Foundation for
Community Ophthalmology, Egypt
Jinling Yang,

Boston University, United States

Kehan Zhang,

Boston University, United States,

in collaboration with JY

*Correspondence:

Tianwei Qian
qtw6180@126.com

Ping Yu
zjypwz@163.com

Specialty section:

This article was submitted to
Neuropharmacology,
a section of the journal
Frontiers in Pharmacology

Received: 05 September 2019

Accepted: 31 December 2019

Published: 31 January 2020

Citation:

Gong Q, Dong W, Fan Y, Chen F,
Bian X, Xu X, Qian T and Yu P (2020)
LncRNA TDRG1-Mediated
Overexpression of VEGF Aggravated
Retinal Microvascular Endothelial Cell
Dysfunction in Diabetic Retinopathy.
Front. Pharmacol. 10:1703.
doi: 10.3389/fphar.2019.01703

**Qiaoyun Gong¹, Wenpei Dong², Ying Fan¹, Feng'e Chen¹, Xiaolan Bian³, Xun Xu¹,
Tianwei Qian^{1,4*} and Ping Yu^{3*}**

¹ Department of Ophthalmology, Shanghai General Hospital, National Clinical Research Center for Eye Diseases, Shanghai Key Laboratory of Ocular Fundus Diseases, Shanghai Engineering Center for Visual Science and Photomedicine, Shanghai Engineering Center for Precise Diagnosis and Treatment of Eye Diseases, Shanghai, China, ² Department of General Surgery, Hernia and Abdominal Wall Surgery Center of Shanghai Jiao Tong University, Shanghai Ninth People's Hospital, Shanghai Jiao Tong University School of Medicine, Shanghai, China, ³ Department of Pharmacy, Ruijin Hospital, Shanghai Jiao Tong University School of Medicine, Shanghai, China, ⁴ Department of Ophthalmology, Leiden University Medical Center, Leiden, Netherlands

Purpose: Diabetic retinopathy (DR), a neurovascular disease, is one of the leading causes of blindness in working-age adults. Long noncoding RNAs (lncRNAs) have attracted attention as indicators for DR. This study aimed to characterize the role of lncRNA human testis development-related gene 1 (TDRG1) and its modulation of vascular endothelial growth factor (VEGF) in deteriorating DR.

Methods: Tissue samples were obtained from patients with epiretinal membranes (EMs) or proliferative DR, and human retinal microvascular endothelial cells (HRECs) were cultured with high-glucose medium to mimic DR as the *in vitro* model. The expression of lncRNA TDRG1 and VEGF was determined by immunofluorescence staining, Western blotting, and RT-qPCR. Transfection of small-interfering RNA was conducted to knock down target gene expression. HREC functions were evaluated by cell viability, fluorescein isothiocyanate (FITC)-dextran extravasation, migration, and tube formation assays under different conditions.

Results: LncRNA TDRG1 and VEGF were found to be co-expressed and significantly upregulated in fibrovascular membranes (FVMs) from DR patients compared to those from EM patients. In the *in vitro* model, hyperglycemic treatment markedly increased the expression of lncRNA TDRG1 and VEGF at the mRNA and protein levels, which promoted cell proliferation and migration, enhanced permeability, and disrupted tube formation of HRECs. However, knockdown of lncRNA TDRG1 or VEGF notably decreased the expression of VEGF and reversed the impaired functions of high-glucose-treated HRECs.

Conclusions: LncRNA TDRG1 promoted microvascular cell dysfunction *via* upregulating VEGF in the progression of DR and may serve as a potential therapeutic target in DR treatment.

Keywords: LncRNA TDRG1, vascular endothelial growth factor, hyperglycemia, human retinal microvascular endothelial cells, diabetic retinopathy

INTRODUCTION

Diabetic retinopathy (DR) is one of the leading causes of blindness in working-age adults worldwide (Cheung et al., 2010). This type of retinopathy is a severe complication of diabetes mellitus (DM), and its prevalence is increasing dramatically due to the high incidence of DM (Antonetti et al., 2012). In 2010, the prevalence of DM in China was estimated to be 11.6% in the adult population (Xu et al., 2013). Based on a random-effects meta-analysis model in which data on the overall prevalence of DR in China in 2010 were pooled, the pooled prevalence rate of any DR in people with DM was 18.45% (Song et al., 2018). Then, according to a multi-hospital-based DR screening program of patients with diabetes in China from 2014 to 2016, the prevalence of any DR in DM patients was 27.9% (Zhang et al., 2017). The increasing rate of DR in DM patients requires an urgent and effective strategy to target DR as early as possible. Diabetic retinopathy is a chronic microvascular dysfunction that primarily results from long-term detrimental high-glucose exposure (Antonetti et al., 2006). The clinical stages of DR begin with microaneurysm, hemorrhage, cotton wool spot, and lipid exudates, which are non-proliferative characteristics. With the development of poorly controlled DR, proliferative manifestations, including neovascularization, vitreous hemorrhage, fibrovascular membrane (FVM) formation and even tractional retinal detachment, occur (Antonetti et al., 2012; Shin et al., 2014). The pathology of the clinical changes in DR is characterized by retinal microvascular dysfunction that leads to increased vascular permeability, destroyed vascular tubes, and breakdown of the blood-retinal barrier (BRB) (Antonetti et al., 2006). Endothelial cells (ECs) harboring tight junctions are essential for maintaining the inner BRB, and their impairment results in vascular hyperpermeability (Ciulla et al., 2003). Therefore, novel pharmacological therapies targeting biochemical mechanisms that promote EC function may effectively ameliorate DR.

Various vasoactive factors are involved in the microvascular dysfunction and angiogenesis of DR. Notably, vascular endothelial growth factor (VEGF), which mediates the structural and functional changes in the retina and in ECs in diabetic conditions (Kaur et al., 2009; Mima et al., 2012), has

attracted considerable attention due to its predominant role in deteriorating the progression of DR. Aberrant expression of VEGF aggravated pathological angiogenesis (Woolard et al., 2004) and then promoted the development of DR (Behl and Kotwani, 2015). Enhanced VEGF induced cellular and retina hyperpermeability, increased cell apoptosis, and promoted cell mobility through multiple signaling mechanisms in DR (Behl and Kotwani, 2015; Gong and Su, 2017). In the past decade, anti-VEGF therapy has been applied to treat DR and other neovascular ocular diseases. However, not all patients are responsive to anti-VEGF therapy, and some show side effects. Thus, other novel therapeutic strategies regulating VEGF are needed for DR treatment.

The role of transcriptional or post-transcriptional regulation is an emerging area of research that is expected to be involved in the pathogenesis of DR. Recent data have revealed that numerous noncoding RNAs (ncRNAs), which have little or no protein-coding potential, are expressed and function in both normal physiology and diseases such as cancers, genetic disorders, and neovascular diseases (Bartel, 2009; Wilusz et al., 2009; Conte et al., 2013). In particular, long ncRNAs (lncRNAs) have been shown to participate in different biological processes, including transcription, post-transcription, translation, epigenetic regulation, splicing, and intracellular/extracellular trafficking (Mercer et al., 2009; Wilusz et al., 2009). LncRNA transcripts are located in the nucleus and cytoplasm, and the transcription of lncRNAs can be modified post-transcriptionally, promoting temporal and cell-type-specific expression (Kapranov et al., 2007; Guttman et al., 2009; van Heesch et al., 2014). LncRNAs may guide transcription factors to, or sequester them from, a specific region of action, or they can interact with various components, thereby suppressing or activating gene expression (Wang and Chang, 2011). Human testis-specific gene testis developmental related gene 1 (TDRG1) is a newly identified lncRNA and encodes a 100 amino acid protein that does not possess any known protein domains (Wang et al., 2016). A previous report showed that lncRNA TDRG1 may enhance the proliferation of bone marrow mesenchymal stem cells *via* fibroblast growth factor 1 (FGF1) (Jiang et al., 2015). Additionally, lncRNA TDRG1 may promote endometrial carcinoma cell proliferation and invasion by positively targeting VEGF- α (Chen et al., 2018). Regarding the potentially important role of lncRNA TDRG1 in angiogenesis, we predicted that it may interact with VEGF and modulate EC functions to affect DR progression. Thus, this study aimed to explore the regulatory effects of lncRNA TDRG1 on VEGF actions in ameliorating DR. LncRNA TDRG1 may be a novel and effective target to inhibit the development of DR.

Abbreviations: DR, diabetic retinopathy; DM, diabetes mellitus; FVM, fibrovascular membrane; BRB, blood-retinal barrier; ECs, endothelial cells; VEGF, vascular endothelial growth factor; lncRNAs, long noncoding RNAs; TDRG1, testis-specific gene testis developmental related gene; HRECs, human retinal microvascular endothelial cells; PDR, proliferative diabetic retinopathy; NG, normal glucose; HG, high glucose; siRNA, small-interfering RNA; EMs, epiretinal membranes; NV, neovascularization.

MATERIALS AND METHODS

Tissue Samples

Tissue samples in this study included the epiretinal membranes (EM) of 12 healthy patients and FVMs of 12 proliferative DR (PDR) patients. All patients were 47–69 years old and received pars plana vitrectomy with membrane peeling. The six membrane specimens surgically obtained from the two groups of patients were fixed in 4% paraformaldehyde, embedded in paraffin and sectioned at 6 μ m for H&E staining and immunofluorescence staining. The remaining membranes in each group were extracted and processed with RT-qPCR for RNA detection. All procedures performed in this study involving human participants were in accordance with the 1964 Helsinki Declaration and its later amendments or comparable ethical standards and were approved by the ethics committee of Shanghai General Hospital. Informed consent was obtained from all individual participants included in the study.

Cell Culture and Treatment

Human retinal microvascular ECs (HRECs) were obtained from ANGIO-PRO TEOMIE (Boston, MA, USA) which were grown on polylysine-coated flask and cultured in EC medium containing 5% fetal bovine serum (FBS), 1% EC growth supplement, and 1% penicillin-streptomycin (Sciencell, Carlsbad, CA, USA) at 37°C in a humidified atmosphere containing 5% CO₂. HRECs were plated at 1×10^4 cells in 6-well plates (Corning; Acton, MA, USA) and treated with normal glucose (NG; 5.5 mmol/L) as a control or with high glucose (HG; 25 mmol/L) under normoxic conditions for 72 h to mimic the early stage of DR. For maintenance of uniform conditions, the medium was changed daily to eliminate metabolic byproducts and provide the nutrients necessary for the cells, and all of the *in vitro* experiments were carried out using HRECs at passages 3–8.

Small-Interfering RNA (siRNA) Transfection

Human retinal microvascular endothelial cells in the logarithmic growth phase were seeded in 6-well plates and exposed to normal or high-glucose medium. After reaching 70%–80% confluence, the cells were transfected with 50 nM siRNA (lncTDRG1 siRNA, VEGF siRNA, or NC siRNA) using Lipofectamine 3000 transfection reagent (Invitrogen, Carlsbad, CA, USA). After transfection for 6 h, fresh high-glucose medium or normal medium was replaced. The cells were harvested for further mRNA analysis after 48 h, and collected for protein analysis after 72 h. siRNAs were chemically synthesized by GenePharma (Shanghai, China).

Total RNA Isolation and Quantitative Analysis of mRNAs

Total RNA was extracted from HRECs cultured under different conditions and tissues using a TaKaRa Mini BEST Universal RNA Extraction Kit (TaKaRa Bio, Dalian, China) following the manufacturer's protocol. The A260/A280 value and concentration were measured by a NanoDrop 2000c Spectrophotometer

(Thermo, Waltham, MA, USA). An A260/A280 of approximately 2.0 was generally accepted for further analysis. Then, 500–1,000 ng of total RNA was reverse transcribed into cDNA using a Perfect Real Time RT reagent kit (TaKaRa Bio, Dalian, China) in a 20- μ L reaction volume.

To explore the expression and modulatory mechanism of lncRNA TDRG1 and VEGF in DR, real-time quantitative PCR (RT-qPCR) was performed to measure the levels of lncRNA TDRG1 and VEGF in human membrane samples and HRECs. The qPCR mixture contained 2 μ L cDNA, 10 μ mol gene-specific primers (forward and reverse mixed together), and 10 μ L of 2 \times Fast SYBR Green Master Mix (TaKaRa Bio, Dalian, China). Three replicates for each biological mixture were analyzed on a LightCycler 480 system (Roche Diagnostics). The data were normalized to the expression of the housekeeping gene GAPDH. Primer sequences are listed in **Table 1**. The relative expression levels were calculated using the $2^{-\Delta\Delta C_t}$ method, which was based on the ratio of gene expression between the experimental group and the control group.

Western Blotting

To confirm the protein expression and modulatory mechanism of lncRNA TDRG1 on VEGF in DR, total protein was collected from HRECs cultured under hyperglycemic conditions. The cells were lysed for 10 min on ice in radioimmunoprecipitation assay (RIPA) buffer complemented with protease inhibitor phenylmethylsulfonyl fluoride (PMSF, 1 mM, Beyotime, Jiangsu, China) according to the manufacturer's protocol and then sonicated. The lysates were collected at 12,000 rpm for 10 min at 4°C. Protein concentrations were evaluated using a Bicinchoninic Acid Protein Assay Kit (Thermo, IL, USA). Protein lysates were electrophoresed on 10% SDS polyacrylamide gels, transferred onto polyvinylidene difluoride (PVDF) membranes (Millipore, USA), and then blocked in 5% skim milk for 1 h. Primary antibodies against VEGF (1:1,000, Abcam #ab1316, USA) and GAPDH (1:1,000, CST Signaling #2118, USA) were applied separately at 4°C overnight. Blots were then treated with secondary antibodies (1:5,000; Millipore, USA) for 1 h. Finally, an Enhanced Chemiluminescence (ECL) Plus Kit (Thermo, IL, USA) was applied for visualization. The gray bands were calculated using ImageJ software.

Immunofluorescence and lncRNA TDRG1 FISH

To investigate the potential roles of lncRNA TDRG1 and VEGF in angiogenesis in the progression of DR, immunofluorescence staining of VEGF and lncRNA TDRG1 was performed using

TABLE 1 | Primer sequences of target genes.

Gene subtype	Oligonucleotide primers (5'–3')
Human VEGF	F: TTGCTGCTCTACCTCCACCA R: GCTGCGCTGATAGACATCCA
Human lncRNA TDRG1	F: TCTTCCCTGGCTTGGC R: TGGGCTCTTTCGTGGC
GAPDH	F: TGCACCACCAACTGCTTAGC R: GGCATGGACTGTGGTCATGAG

paraffin-embedded sections or cultured HRECs on poly-lysine-coated glass coverslips under hyperglycemic conditions. The slides were rinsed, and the cells were fixed with 4% paraformaldehyde, permeabilized with 0.5% Triton X-100 in PBS for 15 min at room temperature, and blocked (1% bovine serum albumin in PBS) for 1 h at 37°C. Subsequently, the sections were treated with primary rabbit polyclonal anti-VEGF antibody (1:100, Abcam #ab1316, USA), and RNA fluorescence *in situ* hybridization of lncRNA TDRG1-FISH (1:100, Servicebio, China) was performed at 4°C overnight. Slides were then incubated with Cy3-conjugated goat anti-rabbit or goat anti-mouse IgG DyLight 488-conjugated secondary antibodies (1:500, CST Signaling, USA) for 1 h at 37°C. Nuclei were stained with DAPI (1:5,000 diluted in PBS; Thermo, IL, USA). The slides were observed under a confocal laser scanning microscope (Leica, Germany). The primer sequence of lncRNA TDRG1-FISH was: 5'-CCTTGCCAGGTAAGTGAAAGTCGCTCCG-3'. The mean fluorescence intensities were calculated by ImageJ software. Five images for each group in the three independent experiments were evaluated. Specifically, the cell number was included in the calculation process.

Cell Viability Assessment

Human retinal microvascular endothelial cell viability was assessed by a Cell Counting Kit-8 (CCK-8, Dojindo, Japan) according to the manufacturer's protocol. HRECs were cultured under hyperglycemic conditions with transfections as described above and then seeded at a density of 2×10^3 cells/well in 96-well plates. Before detection, 90 μ L of fresh medium was replaced, and 10 μ L of CCK-8 was added to the cells. After incubation for 1.5 h at 37°C under normal oxygen, the absorbance was measured at 490 nm using a Varioskan Flash system (Thermo, USA). At each time point, the absorbance value was obtained, and then, calculations for each group were performed by comparing the value of each group to that of the responsive negative control (Ctr) group; the value of the control group was set to 1.

Monolayer Permeability Assay

For evaluating cell permeability, human retinal microvascular endothelial cells treated with different conditions were seeded at 1×10^5 cells/well in the upper chamber (6.5-mm diameter transwell with 0.4- μ m pore polycarbonate membrane inserts; Corning; USA) and cultured for 48 h to reach confluence. The upper chamber was washed three times with PBS and treated with FITC-dextran (1 mg/mL; Sigma; USA). The fluorescence intensity, equivalent to the relative amount of FITC-dextran in the lower chambers of the transwells, was measured over a 3-h incubation at 37°C and determined in triplicate using a Varioskan Flash system (excitation wavelength, 490 nm; emission wavelength, 520 nm; Thermo). The values were collected and calculated *via* comparisons to the responsive ctr group.

Cell Migration Assay

The migratory ability of HRECs under high glucose was determined using the transwell system. A total of 5×10^4 cells from each group were seeded in the top chambers of 6.5-mm diameter transwells with 8.0- μ m pore polycarbonate membrane

inserts (Corning; USA) and cultured in 100 μ L medium with 5% FBS. The bottom chambers were filled with 500 μ L medium with 20% FBS. After incubation for 24 h, the cells on the top chamber were removed, and the migrated cells were fixed with 4% paraformaldehyde for 30 min and stained in 0.1% crystal violet solution. Images were captured by microscopy. Cells were counted in five fields for each group and quantification was performed using ImageJ software.

Tube Formation Assay

The angiogenic formation of HRECs was measured using a tube formation assay. Firstly, 96-well plates were coated with 50 μ L of Matrigel Basement Membrane Matrix (BD Biosciences, USA) per well and polymerized for 1 h at 37°C. Then, human retinal microvascular endothelial cells were seeded in the Matrigel-coated plates at 7×10^3 cells per well in 100 μ L medium and incubated at 37°C for 6–8 h. The network of tubes was captured by microscopy. Quantification of tube formation was performed using ImageJ software.

Statistical Analysis

Data are presented as the mean \pm SEM from at least three independent experiments. One-way analysis of variance (one-way ANOVA) was used for multiple comparisons to assess the significant differences between groups. Comparisons between two groups were performed using Student's *t*-tests (GraphPad Prism 6.0; GraphPad Prism, USA). Two-sided *p* values < 0.05 were considered statistically significant.

RESULTS

Enhanced Coexpression of LncRNA TDRG1 and VEGF in FVMs

The coexpression of lncRNA TDRG1 and VEGF in FVMs from PDR patients and EMs from patients without DM was determined. HE staining showed the pathogenic structure of the EMs and FVMs. EMs had fibrous connective tissue, while FVMs showed both fibers and vascularity (**Figure 1A**). Immunofluorescence staining showed the lncRNA TDRG1 and VEGF were expressed in these two kinds of tissue samples, and high fluorescence was observed in the FVMs, especially in the vessel walls (**Figure 1B**). Moreover, expression of lncRNA TDRG1 and VEGF was increased in FVMs compared to EMs (**Figures 1C, D**), as shown by RT-qPCR and analyzed by Student's *t*-tests. These results revealed that lncRNA TDRG1 and VEGF were highly coexpressed around the vessels in FVMs at the stage of proliferative DR. Therefore, lncRNA TDRG1 and VEGF might cooperate to deteriorate the progression of DR.

Upregulated LncRNA TDRG1 and VEGF in HRECs Exposed to High Glucose

Consistent with the *in vivo* results, the mRNA levels of lncRNA TDRG1 and VEGF were enhanced by hyperglycemia in HRECs (**Figures 2A, B**), with observed increases of 2.0-fold in lncRNA TDRG1 and 2.5-fold in VEGF. At the post-transcriptional level, VEGF protein expression was upregulated concomitantly by

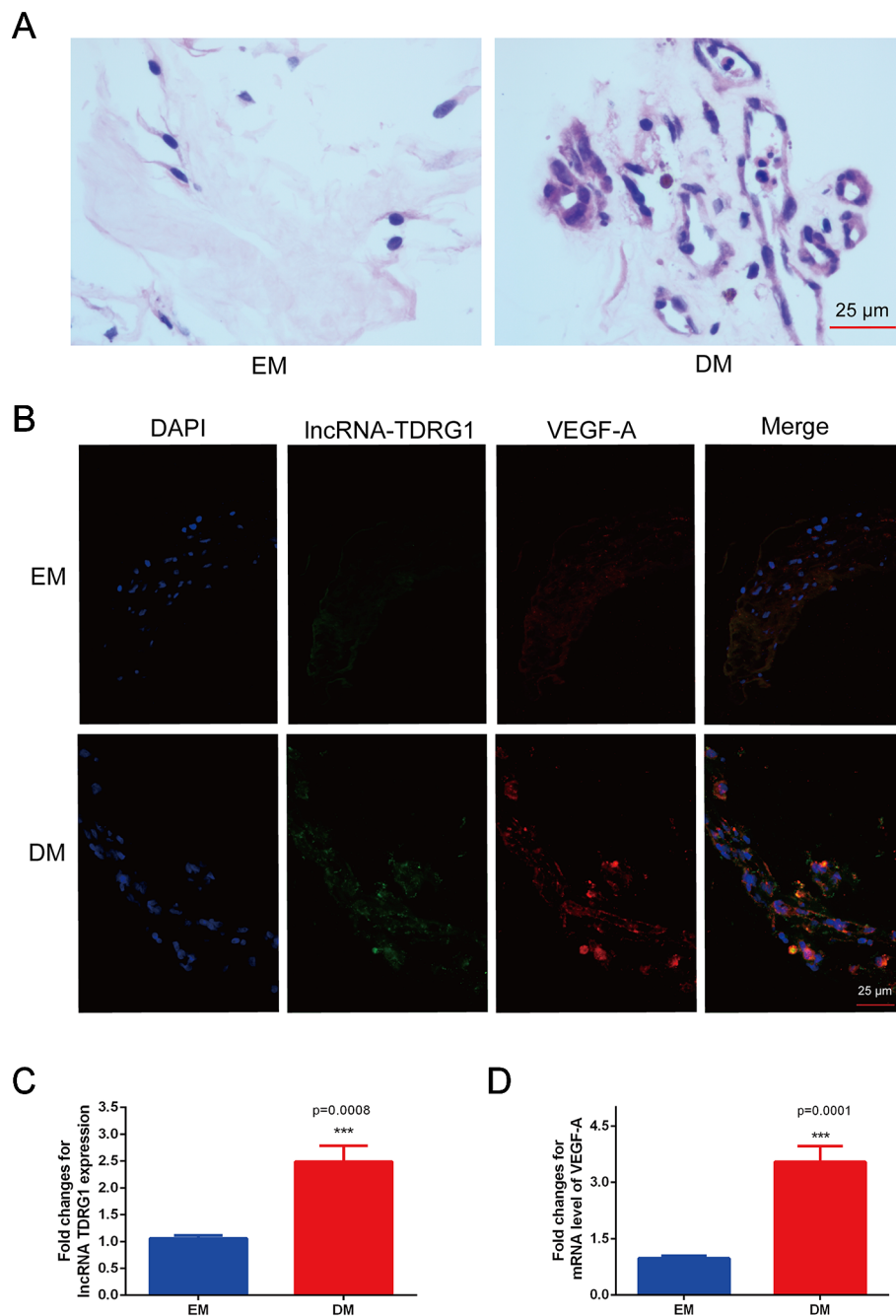


FIGURE 1 | Increased coexpression of lncRNA TDRG1 and VEGF in EMs and FVMs from patients. **(A)** HE staining demonstrated the fibrous connective tissue structure of EMs extracted from patients without DM and FVMs with vascularity from PDR patients with DM. **(B)** Double immunofluorescence staining of lncRNA TDRG1 (green) and VEGF (red) showed that coexpression of lncRNA TDRG1 and VEGF enhanced in the blood vessels of FVMs compared to EMs. **(C, D)** The expression level of lncRNA TDRG1 in FVMs was nearly 3.0-fold higher than that in EMs, while the VEGF mRNA level in FVMs was more than 3.0-fold higher than that in EMs. Bars, mean \pm SEM. *** $p < 0.001$ versus the EM group ($n = 6$).

high glucose (**Figures 2C, D**). Accordingly, lncRNA TDRG1 and VEGF were increased in HRECs in diabetic conditions.

Furthermore, double immunofluorescence staining was performed to determine the orientation and expression of lncRNA TDRG1 and VEGF in HRECs. lncRNA TDRG1 was

mainly expressed in the nucleus, while VEGF was detected in the nucleus and cytoplasm in HRECs (**Figure 2E**). The fluorescence of both lncRNA TDRG1 and VEGF under diabetic conditions was notably increased compared to that of the normal group. The quantitative analysis of the fluorescence showed a more than

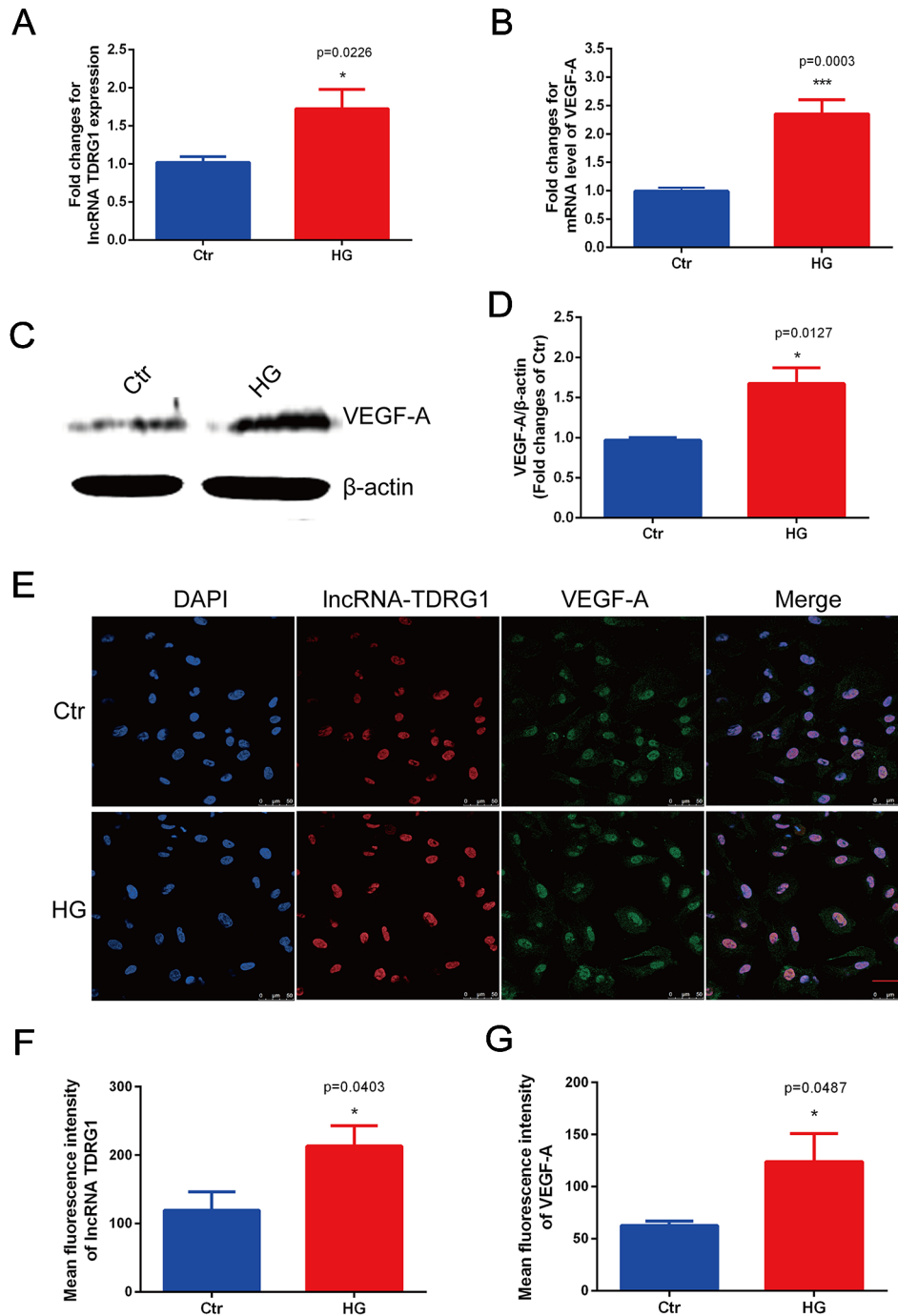


FIGURE 2 | Elevated expression levels of lncRNA TDRG1 and VEGF in HRECs exposed to hyperglycemia. **(A)** RT-qPCR showed that high glucose (HG) induced a 2.0-fold increase in lncRNA TDRG1 in HRECs at the transcriptional level. **(B)** HG significantly upregulated the expression of VEGF at the mRNA level ($n = 6$). **(C, D)** Western blot analysis demonstrated the protein level of VEGF in HRECs under hyperglycemic conditions. Similar to the transcript variation, VEGF protein was significantly increased after HG treatment ($n = 3$). **(E)** Dual immunostaining of lncRNA TDRG1 (red) and VEGF (green), merged with DAPI (blue) in HRECs under NG and HG. lncRNA TDRG1 was mainly located in the nucleus, while VEGF was expressed in the nucleus and cytoplasm. The fluorescence was enhanced by hyperglycemia. **(F, G)** Quantitative analysis of fluorescence in lncRNA TDRG1 and VEGF demonstrated a nearly 2.0-fold increase when HRECs were exposed to the HG condition ($n = 6$). Bars, mean \pm SEM. * $p < 0.05$, *** $p < 0.001$ versus the negative control group.

2.0-fold increase in both lncRNA TDRG1 and VEGF in HRECs under the HG condition (**Figures 2F, G**). These results revealed that the coexpression of lncRNA TDRG1 and VEGF in HRECs could be induced by hyperglycemia. The comparisons between NG and HG were performed using Student's *t*-tests.

Positive Regulation of VEGF by LncRNA TDRG1 in Hyperglycemic HRECs

The modulatory relationship between lncRNA TDRG1 and VEGF in DR progression was verified by siRNAs to silence the target genes. The lncTDRG1 siRNA sequences were as follows: sense: 5'-CCUCCCAGGUCUAGGUUCdTdT-3'; antisense: 5'-GAACCUAGACCUGGGAAGGdTdT-3'. The VEGF siRNA sequences were as follows: sense: 5'-GAAGUUCAUGGAUGUCUAUdTdT-3'; antisense: 5'-AUAGACAUCCAUGAACUCdTdT-3'.

Notably, hyperglycemia upregulated the mRNA levels of lncRNA TDRG1 and VEGF, with an increase of more than 1.5-fold in HRECs, but there was no distinct difference between the high-glucose group and the negative transfection group (**Figures 3A, B**). However, these changes were strongly suppressed by specific siRNAs, and the mRNA levels of lncRNA TDRG1 and VEGF decreased to the level of normal conditions. Moreover, VEGF was repressed following the downregulation of lncRNA TDRG1 in hyperglycemia-induced HRECs. Nevertheless, VEGF knockdown did not affect the expression of lncRNA TDRG1. Correspondingly, the enhanced protein level of VEGF induced by hyperglycemia was inhibited by separate transfection of lncRNA TDRG1 and VEGF siRNAs, while the negative control transfection resulted in no changes (**Figures 3C, D**). Thus, lncRNA TDRG1 positively modulated the expression of VEGF, while VEGF exerted no effects on the lncRNA TDRG1 level.

The changes in the fluorescence intensity of lncRNA TDRG1 and VEGF confirmed the consistent tendency with the mRNA and protein alterations (**Figure 3E**). The fluorescence intensities of lncRNA TDRG1 and VEGF were significantly decreased after transfection of siRNAs targeting lncRNA TDRG1 and VEGF in HRECs under hyperglycemic conditions. The quantitative analysis confirmed that knockdown of lncRNA TDRG1 repressed VEGF expression (**Figures 3F, G**). These data indicated that lncRNA TDRG1 could positively regulate VEGF expression in the progression of DR. One-way ANOVA was used for multiple comparisons to assess the significant differences between groups.

Effects of LncRNA TDRG1 or VEGF Knockdown on Hyperglycemia-Induced HREC Dysfunction

The pathological changes of diabetic microvascular complications are commonly characterized by abnormally functioning vascular ECs. The effects of lncRNA TDRG1 and VEGF on HRECs in DR conditions were then evaluated. CCK-8 assays showed that knockdown of lncRNA TDRG1 or VEGF could inhibit the accelerated cell proliferation induced by high glucose in ECs compared with that of the negative siRNA-transfected group (**Figure 4A**). A cell permeability assay demonstrated that hyperglycemia enhanced HREC leakage of FITC-dextran compared with that in the normal group. The monolayer

permeability of HRECs was rescued by lncRNA TDRG1 or VEGF downregulation compared with that of negative transfection (**Figure 4B**). The cell migration change under the DR condition was evaluated by transwell assays. The result revealed that diabetic conditions significantly promoted cell migration compared with the control conditions. However, exposure to high glucose, lncRNA TDRG1 intervention or VEGF siRNA could protect against high-glucose-stimulated HREC migration. The negative control cells under hyperglycemia did not show any significant difference in migration (**Figure 4C**). Both the lncRNA TDRG1 and VEGF interventions resulted in 2.0-fold decreases in migrated cells (**Figure 4E**). Matrigel tube formation was assessed in HRECs cultured under the same conditions as previously described. As demonstrated in **Figure 4D**, diabetic conditions caused a morphological change in HRECs and destroyed the tube network formation compared to the control conditions. In addition, lncRNA TDRG1 intervention distinctly improved the angiogenic ability of HRECs by increasing tube formation and tubule length relative to that of the negative transfection cells in hyperglycemic conditions as well as the effect of VEGF knockdown (**Figures 4F, G**). These results suggested that both lncRNA TDRG1 and VEGF depletion could prevent the breakdown of angiogenesis in HRECs induced by high-glucose conditions. One-way ANOVA was used for multiple comparisons to assess the significant differences between groups.

These findings indicated that modulation of VEGF by lncRNA TDRG1 knockdown had a protective role in HREC viability, cell permeability, motility, and tube integrity under DR conditions. Accordingly, inhibition of VEGF by lncRNA regulation improved HREC morphology in the progression of DR and might be a strategy in clinical therapy.

DISCUSSION

Diabetic retinopathy is one of the most serious microvascular complications of patients with long-term DM (Cheung et al., 2010; Antonetti et al., 2012), which is pathologically characterized by retinal inflammation, increased permeability, neovascularization, macular edema, and proliferative changes (Bandello et al., 2013). Hyperglycemia is the original and most important factor for diabetes and exerts adverse effects on vascular ECs during the development of microvascular complications (Antonetti et al., 2006). In addition to inflammatory mediators, neural dysfunction, and vascular growth factors, endothelial cells suffer from apoptosis, destroyed tight junctions, increased migration and enhanced permeability, which aggravate the progression of DR (Ciulla et al., 2003; Bandello et al., 2013). Therefore, protecting or reversing EC dysfunction is crucial for ameliorating DR and may be an effective therapeutic strategy.

The pivotal element in the development of DR from the non-proliferative to the proliferative stage is the occurrence and aggravation of neovascularization (NV). Angiogenic and antiangiogenic factors such as VEGF (Behl and Kotwani, 2015), pigment epithelium derived factor (PEDF) (Ibrahim et al., 2015),

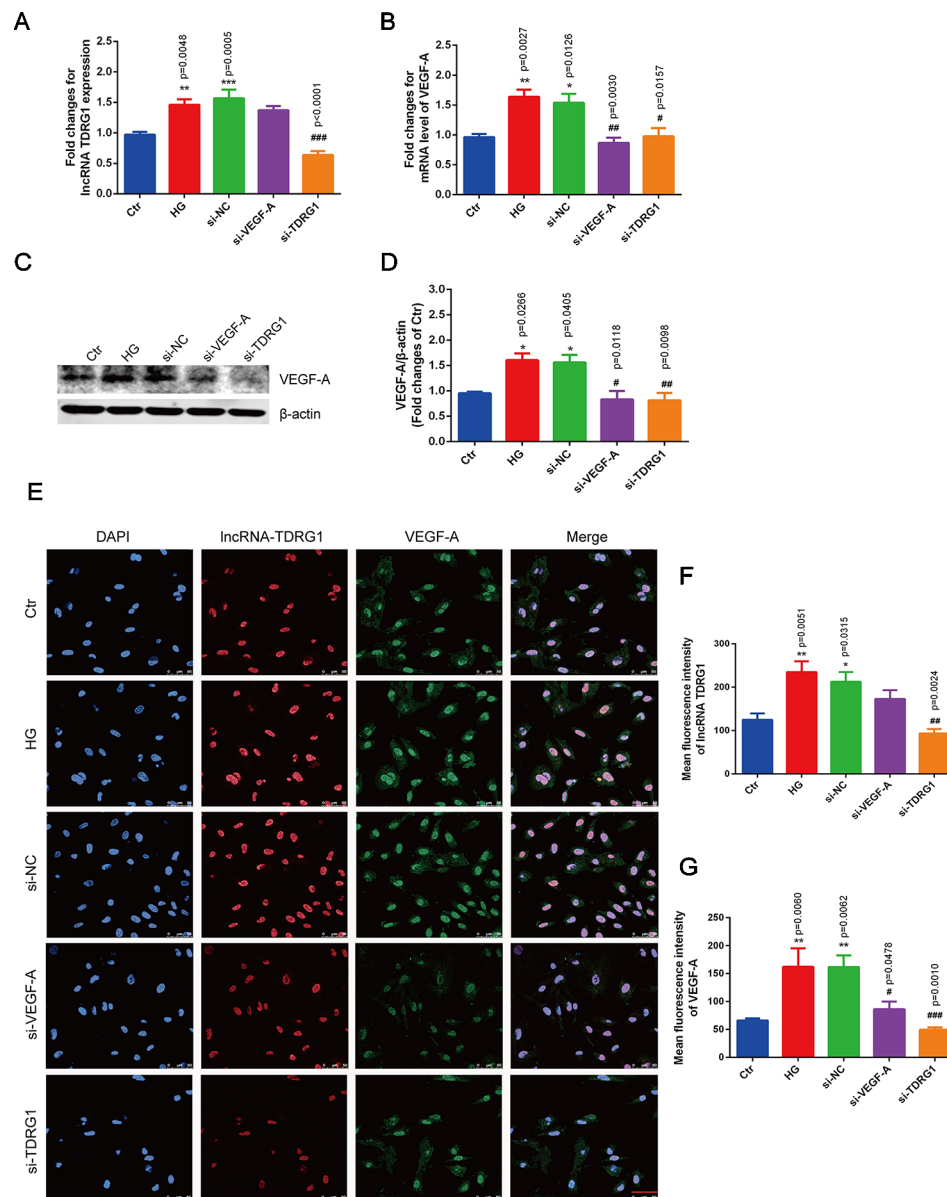


FIGURE 3 | Knockdown of lncRNA TDRG1 reversed the increased expression of VEGF in HRECs under high glucose. **(A)** The mRNA level of VEGF was inhibited by transfection with either VEGF siRNA or lncRNA TDRG1 siRNA. No significant change was observed between the negative transfection and HG groups. **(B)** Expression of lncRNA TDRG1 was suppressed by specific siRNAs in HRECs under HG but was not responsive to VEGF siRNA ($n = 6$). **(C, D)** The protein level of VEGF was consistent with the mRNA level. β -actin was used as a loading control ($n = 4$). **(E)** Immunofluorescence and **(F, G)** quantitative analysis revealed that high fluorescence of VEGF in HRECs induced by hyperglycemia could be repressed by knockdown of VEGF and lncRNA TDRG1, while HG-induced fluorescence of lncRNA TDRG1 was suppressed by lncRNA TDRG1 siRNA ($n = 5-10$). Bars, mean \pm SEM. * $p < 0.05$, ** $p < 0.01$, *** $p < 0.001$ versus the negative control group; # $p < 0.05$, ## $p < 0.01$, ### $p < 0.001$ versus the negative control siRNA transfection.

and angiopoietin (Bento et al., 2010) released by the retina under hyperglycemia act on NV. Most importantly, VEGF is a key stimulator in NV and closely correlates with the development of DR by causing retinal structural and functional dysfunction (Mima et al., 2012; Behl and Kotwani, 2015). Anti-VEGF therapy has been widely used to inhibit NV in retinal diseases that are not limited to DR. Due to the limitations of tolerance, side effects, and undesirable responsiveness of anti-VEGF

therapy, development of novel therapeutic targets to modulate VEGF to ameliorate DR and other neovascular retinal diseases is urgently needed.

With advancements in genome-wide analyses of the mammalian transcriptome, the functional significance of lncRNAs has been recognized (Carninci et al., 2005). An increasing number of studies have identified lncRNAs as a new class of modulatory molecules that affect various human diseases

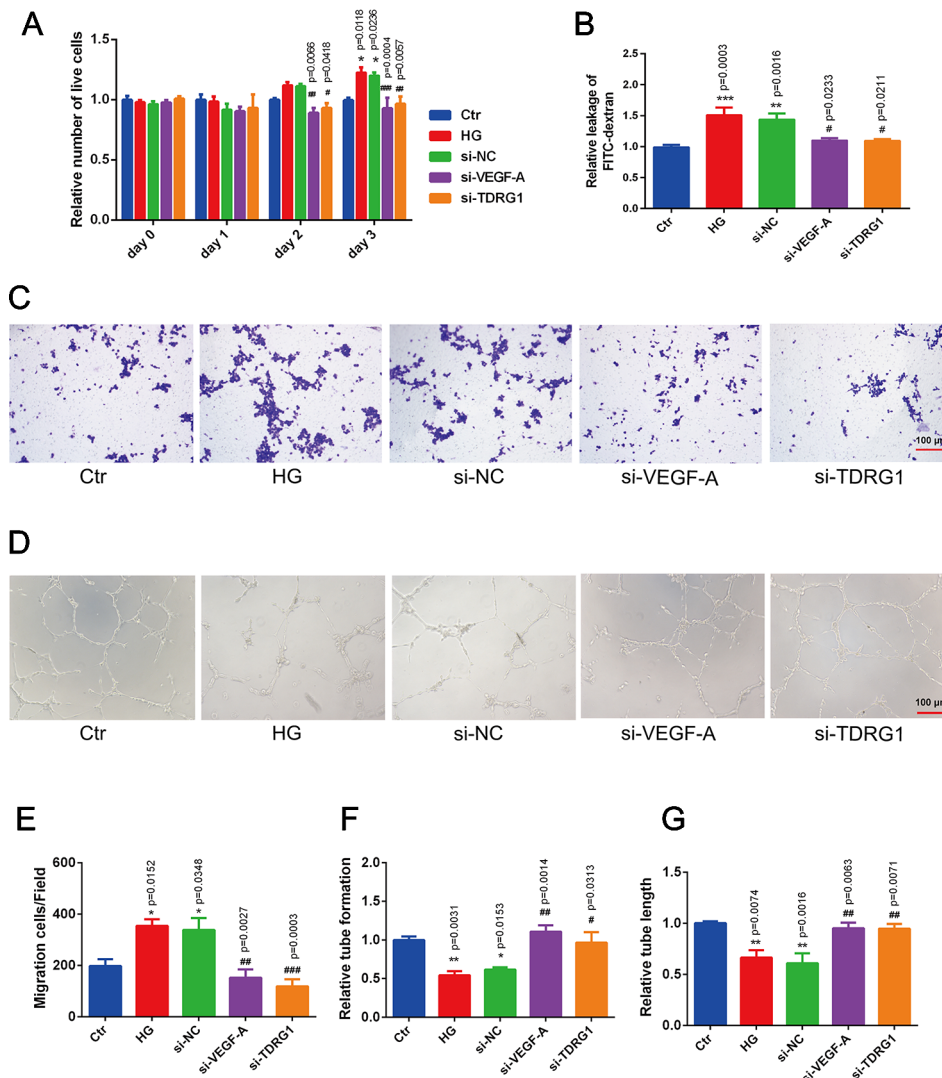


FIGURE 4 | Protective effects of VEGF depletion by lncRNA TDRG1 regulation on HREC dysfunction induced by hyperglycemia. **(A)** Increased proliferation of HRECs caused by HG was reduced by transfection of siRNAs targeting lncRNA TDRG1 and VEGF ($n = 5-7$). **(B)** Leakage of FITC-dextran demonstrated that hyperglycemia enhanced cell monolayer permeability, whereas this effect was reversed by VEGF or lncRNA TDRG1 knockdown ($n = 6$). **(C, E)** Increased migration of HRECs was observed under DR conditions, and VEGF or lncRNA TDRG1 inhibition exerted the opposite effects ($n = 8$). **(D, F, G)** Angiogenic ability of HRECs under different conditions. HG destroyed the tube network formation of HRECs compared to the negative control, while VEGF or lncRNA TDRG1 intervention improved the angiogenic ability of HRECs by enhancing tube formation and increasing tubule length. Negative siRNA transfection did not induce any distinct changes in HREC dysfunction. Relative tube formation and tube length were quantified by ImageJ software ($n = 6$). Bars, mean \pm SEM. * $p < 0.05$, ** $p < 0.01$, *** $p < 0.001$ versus the negative control group; # $p < 0.05$, ## $p < 0.01$, ### $p < 0.001$ versus the negative control siRNA transfection.

by regulating gene expression at the transcriptional, post-transcriptional, or epigenetic level (Wapinski and Chang, 2011; Mercer and Mattick, 2013). Especially in retinal diseases, the change in the abundance of lncRNAs has been assessed and detected by Yan et al. (2014). Altered expression of lncRNAs was identified in the retinas of streptozotocin-induced diabetic mice. Specifically, lncRNA MALAT1 (Liu et al., 2014; Liu et al., 2019), MIAT (Yan et al., 2015), MEG3 (Qiu et al., 2016), and ANRIL (Thomas et al., 2017) were studied *in vivo* in the retinas of diabetic models and *in vitro* in retinal ECs under DR conditions.

lncRNA TDRG1 was studied in vascularity in cancers and shown to modulate VEGF- α to aggravate the dysfunction of cancer cells (Wang et al., 2016), which is also a key step in the angiogenesis of DR, indicating the possible involvement of lncRNA TDRG1 in DR. Thus, we paid attention to the important roles of lncRNA TDRG1 in pathological angiogenesis by interacting with VEGF in microvascular diseases, such as DR.

In the present study, we found that lncRNA TDRG1 was strongly expressed in FVMs collected from PDR patients compared to EMs. Simultaneously, VEGF was found to be

coexpressed with lncRNA TDRG1 and enhanced in FVMs. Additionally, *in vitro* experiments in hyperglycemic HRECs confirmed the upregulated levels of lncRNA TDRG1 and VEGF. Immunofluorescence showed the coexpression and increase of lncRNA TDRG1 and VEGF in the nucleus of HRECs under DR conditions. Consistent with previous studies (Zhang et al., 2018; Gong et al., 2019), the increased expression of VEGF contributed to the progression of DR. However, to the best of our knowledge, this study shows that high levels of lncRNA TDRG1, which is coexpressed with VEGF, are tightly related to the development of DR. The expression of VEGF was positively regulated by lncRNA TDRG1 in hyperglycemic HRECs. Knockdown of lncRNA TDRG1 significantly suppressed the increased expression of lncRNA TDRG1 and VEGF induced by hyperglycemia, resulting in a level close to the normal level. In a previous study, RIP assays were conducted to confirm that lncRNA TDRG1 binds and targets the VEGF- α protein (Chen et al., 2018). Thus, in DR progression, lncRNA TDRG1 positively activated VEGF. Furthermore, genetic ablation of lncRNA TDRG1 *in vitro* rescued the EC dysfunction resulting from high glucose, including improving cell proliferation, decreasing cell permeability, inhibiting cell migration, and maintaining the integrity of tube formation of HRECs. Therefore, lncRNA TDRG1 could protect EC functions by modulating VEGF and thus ameliorating DR.

However, the limitation of this study is its lack of mechanistic experiments in animal models to confirm the modulatory effects of lncRNA TDRG1 on DR. Because lncRNA TDRG1 is not expressed in mice or rats, an animal model would be established with rabbits. Further *in vivo* studies will be conducted in a diabetic rabbit model, and the modulatory roles of lncRNA TDRG1 in DR will be confirmed in the future.

In conclusion, to the best of our knowledge, we showed that lncRNA TDRG1 and VEGF were coexpressed and enhanced in the FVMs of patients with PDR and hyperglycemic HRECs. Downregulation of lncRNA TDRG1 decreased VEGF expression directly and protected against microvascular cell dysfunction to alleviate the progression of DR. lncRNA TDRG1 may be an effective and novel therapeutic target for the treatment of DR *via* targeting VEGF.

REFERENCES

- Antonetti, D. A., Barber, A. J., Bronson, S. K., Freeman, W. M., Gardner, T. W., Jefferson, L. S., et al. (2006). Diabetic retinopathy: seeing beyond glucose-induced microvascular disease. *Diabetes* 55, 2401–2411. doi: 10.2337/db05-1635
- Antonetti, D. A., Klein, R., and Gardner, T. W. (2012). Diabetic retinopathy. *N. Engl. J. Med.* 366, 1227–1239. doi: 10.1056/NEJMra1005073
- Bandello, F., Lattanzio, R., Zucchiatti, I., and Turco, C. D. (2013). Pathophysiology and treatment of diabetic retinopathy. *Acta Diabetol.* 50, 1–20. doi: 10.1007/s00592-012-0449-3
- Bartel, D. P. (2009). MicroRNAs: target recognition and regulatory functions. *Cell* 136, 215–233. doi: 10.1016/j.cell.2009.01.002
- Behl, T., and Kotwani, A. (2015). Exploring the various aspects of the pathological role of vascular endothelial growth factor (VEGF) in diabetic retinopathy. *Pharmacol. Res.* 99, 137–148. doi: 10.1016/j.phrs.2015.05.013
- Bento, C. F., Fernandes, R., Matafome, P., Sena, C., Seica, R., and Pereira, P. (2010). Methylglyoxal-induced imbalance in the ratio of vascular endothelial growth factor

DATA AVAILABILITY STATEMENT

The datasets used and/or analyzed during the current study are available from the authors on reasonable request.

ETHICS STATEMENT

All procedures performed in studies involving human participants were in accordance with the ethical standards of the Shanghai Jiaotong University and National Research Committee and with the 1964 Helsinki Declaration and its later amendments or comparable ethical standards. Informed consent was obtained from all individual participants included in the study.

AUTHOR CONTRIBUTIONS

QG, PY, TQ, XB, and XX conceived and designed the experiments. WD and PY contributed to the acquisition of data. QG and PY analyzed and interpreted the data. YF and FC obtained tissue samples. QG and TQ contributed to drafting the article. All authors have revised the manuscript critically for important intellectual content and approved the final version to be published.

FUNDING

This work was supported by the National Science Foundation of China (No. 81800878), the Interdisciplinary Program of Shanghai Jiao Tong University (No. YG2017QN24), the Key Technological Research Projects of Songjiang District (No. 18sjkjgg24), and the Bethune Langmu Ophthalmological Research Fund for Young and Middle-aged People (No. BJ-LM2018002J).

ACKNOWLEDGMENTS

This study was supported by members of the Department of Ophthalmology in Shanghai General Hospital.

- to angiopoietin 2 secreted by retinal pigment epithelial cells leads to endothelial dysfunction. *Exp. Physiol.* 95, 955–970. doi: 10.1113/expphysiol.2010.053561
- Carninci, P., Kasukawa, T., Katayama, S., Gough, J., Frith, M. C., Maeda, N., et al. (2005). The transcriptional landscape of the mammalian genome. *Science* 309, 1559–1563. doi: 10.1126/science.1112014
- Chen, S., Wang, L. L., Sun, K. X., Liu, Y., Guan, X., Zong, Z. H., et al. (2018). lncRNA TDRG1 enhances tumorigenicity in endometrial carcinoma by binding and targeting VEGF-A protein. *Biochim. Biophys. Acta Mol. Basis Dis.* 1864, 3013–3021. doi: 10.1016/j.bbdis.2018.06.013
- Cheung, N., Mitchell, P., and Wong, T. Y. (2010). Diabetic retinopathy. *Lancet* 376, 124–136. doi: 10.1016/S0140-6736(09)62124-3
- Ciulla, T. A., Amador, A. G., and Zinman, B. (2003). Diabetic retinopathy and diabetic macular edema: pathophysiology, screening, and novel therapies. *Diabetes Care* 26, 2653–2664. doi: 10.2337/diacare.26.9.2653
- Conte, I., Banfi, S., and Bovolenta, P. (2013). Non-coding RNAs in the development of sensory organs and related diseases. *Cell. Mol. Life Sci.* 70, 4141–4155. doi: 10.1007/s00018-013-1335-z

- Gong, Q., and Su, G. (2017). Roles of miRNAs and long noncoding RNAs in the progression of diabetic retinopathy. *Biosci. Rep.* 37, BSR20171157. doi: 10.1042/BSR20171157
- Gong, Q., Li, F., Xie, J., and Su, G. (2019). Upregulated VEGF and Robo4 correlate with the reduction of miR-15a in the development of diabetic retinopathy. *Endocrine* 65, 35–45. doi: 10.1007/s12020-019-01921-0
- Guttman, M., Amit, I., Garber, M., French, C., Lin, M. F., Feldser, D., et al. (2009). Chromatin signature reveals over a thousand highly conserved large non-coding RNAs in mammals. *Nature* 458, 223–227. doi: 10.1038/nature07672
- Ibrahim, A. S., Tawfik, A. M., Hussein, K. A., Elshafey, S., Markand, S., Rizk, N., et al. (2015). Pigment epithelium-derived factor inhibits retinal microvascular dysfunction induced by 12/15-lipoxygenase-derived eicosanoids. *Biochim. Biophys. Acta* 1851, 290–298. doi: 10.1016/j.bbali.2014.12.017
- Jiang, S., Xia, M., Yang, J., Shao, J., Liao, X., Zhu, J., et al. (2015). Novel insights into a treatment for aplastic anemia based on the advanced proliferation of bone marrow-derived mesenchymal stem cells induced by fibroblast growth factor 1. *Mol. Med. Rep.* 12, 7877–7882. doi: 10.3892/mmr.2015.4421
- Kapranov, P., Cheng, J., Dike, S., Nix, D. A., Duttagupta, R., Willingham, A. T., et al. (2007). RNA maps reveal new RNA classes and a possible function for pervasive transcription. *Science* 316, 1484–1488. doi: 10.1126/science.1138341
- Kaur, C., Sivakumar, V., Foulds, W. S., Luu, C. D., and Ling, E. A. (2009). Cellular and vascular changes in the retina of neonatal rats after an acute exposure to hypoxia. *Invest. Ophthalmol. Vis. Sci.* 50, 5364–5374. doi: 10.1167/iovs.09-3552
- Liu, J. Y., Yao, J., Li, X. M., Song, Y. C., Wang, X. Q., Li, Y. J., et al. (2014). Pathogenic role of lncRNA-MALAT1 in endothelial cell dysfunction in diabetes mellitus. *Cell Death Dis.* 5, e1506. doi: 10.1038/cddis.2014.466
- Liu, P., Jia, S. B., Shi, J. M., Li, W. J., Tang, L. S., Zhu, X. H., et al. (2019). LncRNA-MALAT1 promotes neovascularization in diabetic retinopathy through regulating miR-125b/VE-cadherin axis. *Biosci. Rep.* 39. doi: 10.1042/BSR20181469
- Mercer, T. R., and Mattick, J. S. (2013). Structure and function of long noncoding RNAs in epigenetic regulation. *Nat. Struct. Mol. Biol.* 20, 300–307. doi: 10.1038/nsmb.2480
- Mercer, T. R., Dinger, M. E., and Mattick, J. S. (2009). Long non-coding RNAs: insights into functions. *Nat. Rev. Genet.* 10, 155–159. doi: 10.1038/nrg2521
- Mima, A., Qi, W., Hiraoka-Yamamoto, J., Park, K., Matsumoto, M., Kitada, M., et al. (2012). Retinal not systemic oxidative and inflammatory stress correlated with VEGF expression in rodent models of insulin resistance and diabetes. *Invest. Ophthalmol. Vis. Sci.* 53, 8424–8432. doi: 10.1167/iovs.12-10207
- Qiu, G. Z., Tian, W., Fu, H. T., Li, C. P., and Liu, B. (2016). Long noncoding RNA-MEG3 is involved in diabetes mellitus-related microvascular dysfunction. *Biochem. Biophys. Res. Commun.* 471, 135–141. doi: 10.1016/j.bbrc.2016.01.164
- Shin, E. S., Sorenson, C. M., and Sheibani, N. (2014). Diabetes and retinal vascular dysfunction. *J. Ophthalmic. Vis. Res.* 9, 362–373. doi: 10.4103/2008-322x.143378
- Song, P., Yu, J., Chan, K. Y., Theodoratou, E., and Rudan, I. (2018). Prevalence, risk factors and burden of diabetic retinopathy in China: a systematic review and meta-analysis. *J. Glob. Health* 8, 010803. doi: 10.7189/jogh.08.010803
- Thomas, A. A., Feng, B., and Chakrabarti, S. (2017). ANRIL: a regulator of VEGF in diabetic retinopathy. *Invest. Ophthalmol. Vis. Sci.* 58, 470–480. doi: 10.1167/iovs.16-20569
- van Heesch, S., van Itersson, M., Jacobi, J., Boymans, S., Essers, P. B., de Bruijn, E., et al. (2014). Extensive localization of long noncoding RNAs to the cytosol and mono- and polyribosomal complexes. *Genome. Biol.* 15, R6. doi: 10.1186/gb-2014-15-1-r6
- Wang, K. C., and Chang, H. Y. (2011). Molecular mechanisms of long noncoding RNAs. *Mol. Cell* 43, 904–914. doi: 10.1016/j.molcel.2011.08.018
- Wang, Y., Gan, Y., Tan, Z., Zhou, J., Kitazawa, R., Jiang, X., et al. (2016). TDRG1 functions in testicular seminoma are dependent on the PI3K/Akt/mTOR signaling pathway. *Onco. Targets Ther.* 9, 409–420. doi: 10.2147/OTT.S97294
- Wapinski, O., and Chang, H. Y. (2011). Long noncoding RNAs and human disease. *Trends Cell Biol.* 21, 354–361. doi: 10.1016/j.tcb.2011.04.001
- Wilusz, J. E., Sunwoo, H., and Spector, D. L. (2009). Long noncoding RNAs: functional surprises from the RNA world. *Genes Dev.* 23, 1494–1504. doi: 10.1101/gad.1800909
- Woolard, J., Wang, W. Y., Bevan, H. S., Qiu, Y., Morbidelli, L., Pritchard-Jones, R. O., et al. (2004). VEGF165b, an inhibitory vascular endothelial growth factor splice variant: mechanism of action, *in vivo* effect on angiogenesis and endogenous protein expression. *Cancer Res.* 64, 7822–7835. doi: 10.1158/0008-5472.CAN-04-0934
- Xu, Y., Wang, L., He, J., Bi, Y., Li, M., Wang, T., et al. (2013). Prevalence and control of diabetes in Chinese adults. *JAMA* 310, 948–959. doi: 10.1001/jama.2013.168118
- Yan, B., Tao, Z. F., Li, X. M., Zhang, H., Yao, J., and Jiang, Q. (2014). Aberrant expression of long noncoding RNAs in early diabetic retinopathy. *Invest. Ophthalmol. Vis. Sci.* 55, 941–951. doi: 10.1167/iovs.13-13221
- Yan, B., Yao, J., Liu, J. Y., Li, X. M., Wang, X. Q., Li, Y. J., et al. (2015). LncRNA-MIAT regulates microvascular dysfunction by functioning as a competing endogenous RNA. *Circ. Res.* 116, 1143–1156. doi: 10.1161/CIRCRESAHA.116.305510
- Zhang, G., Chen, H., Chen, W., and Zhang, M. (2017). Prevalence and risk factors for diabetic retinopathy in China: a multi-hospital-based cross-sectional study. *Br. J. Ophthalmol.* 101, 1591–1595. doi: 10.1136/bjophthalmol-2017-310316
- Zhang, D., Qin, H., Leng, Y., Li, X., Zhang, L., Bai, D., et al. (2018). LncRNA MEG3 overexpression inhibits the development of diabetic retinopathy by regulating TGF-beta1 and VEGF. *Exp. Ther. Med.* 16, 2337–2342. doi: 10.3892/etm.2018.6451

Conflict of Interest: The authors declare that the research was conducted in the absence of any commercial or financial relationships that could be construed as a potential conflict of interest.

Copyright © 2020 Gong, Dong, Fan, Chen, Bian, Xu, Qian and Yu. This is an open-access article distributed under the terms of the Creative Commons Attribution License (CC BY). The use, distribution or reproduction in other forums is permitted, provided the original author(s) and the copyright owner(s) are credited and that the original publication in this journal is cited, in accordance with accepted academic practice. No use, distribution or reproduction is permitted which does not comply with these terms.



MicroRNA-96 Promotes Vascular Repair in Oxygen-Induced Retinopathy—A Novel Uncovered Vasoprotective Function

Michel Desjarlais^{1*}, Maëlle Wirth¹, José Carlos Rivera^{1,2}, Isabelle Lahaie¹, Rabah Dabouz¹, Samy Omri¹, Pakiza Ruknudin¹, Celine Borrás¹ and Sylvain Chemtob^{1,2*}

¹ Department of Ophthalmology, Maisonneuve-Rosemont Hospital Research Center, University of Montreal, Montreal, QC, Canada, ² Departments of Pediatrics, Ophthalmology and Pharmacology, Centre Hospitalier Universitaire Sainte-Justine Research Center, Montreal, QC, Canada

OPEN ACCESS

Edited by:

Zhuo Shao,
University of Toronto,
Canada

Reviewed by:

Yan Gong,
Wuhan University,
China
Carlos Spuch,
Instituto de Investigación Sanitaria
Galicia Sur (IISGS), Spain

*Correspondence:

Michel Desjarlais
micheldesjarlais@gmail.com
Sylvain Chemtob
sylvain.chemtob@gmail.com

Specialty section:

This article was submitted to
Neuropharmacology,
a section of the journal
Frontiers in Pharmacology

Received: 15 November 2019

Accepted: 07 January 2020

Published: 03 February 2020

Citation:

Desjarlais M, Wirth M, Rivera JC, Lahaie I, Dabouz R, Omri S, Ruknudin P, Borrás C and Chemtob S (2020) MicroRNA-96 Promotes Vascular Repair in Oxygen-Induced Retinopathy—A Novel Uncovered Vasoprotective Function. *Front. Pharmacol.* 11:13. doi: 10.3389/fphar.2020.00013

Background and Aims: Vascular degeneration is a hallmark in the pathogenesis of oxygen-induced retinopathy (OIR). Dysregulation of microRNAs (miRNAs), key regulators of genes expressions, has been implicated in the regulation of ocular angiogenesis. However, miRNAs specific functions in impaired vascular development during OIR are poorly understood. Herein, we identified miR-96 as one of the most highly expressed miRNAs in the retina and choroid during vascular development and investigated the potential role of miR-96 on microvascular degeneration in a rat OIR model.

Methods and Results: Next generation sequencing (NGS) and qRT-PCR analysis showed that miR-96 maintain high levels of expression during ocular vascular development. Nevertheless, miR-96 was significantly downregulated in the retina and choroid of OIR rats (80% O₂ from P5 to P10) during the phase of microvascular degeneration. Similarly, human retinal microvascular endothelial cells (HRMEC) subjected to hyperoxia (80% O₂) showed a significant downregulation of miR-96 evaluated by qPCR. Interestingly, HRMEC supplemented with miR-96 regulated positively the expression of several key angiogenic factors including VEGF and ANG-2. To explore the angiogenic activity of miR-96 on HRMEC, we performed a gain/loss of function study. In a similar way to hyperoxia exposure, we observed a robust angiogenic impairment (tubulogenesis and migration) on HRMEC transfected with an antagonomiR-96. Conversely, overexpression of miR-96 stimulated the angiogenic activity of HRMEC and protected against hyperoxia-induced endothelial dysfunction. Finally, we evaluated the potential vasoprotective function of miR-96 in OIR animals. Rat pups intravitreally supplemented with miR-96 mimic (1 mg/kg) displayed a significant preservation of retinal/choroidal microvessels at P10 compared to controls. This result was consistent with the maintenance of physiologic levels of VEGF and ANG-2 in the OIR retina.

Conclusion: This study demonstrates that miR-96 regulates the expression of angiogenic factors (VEGF/ANG-2) associated to the maintenance of retinal and choroidal microvasculature during physiological and pathological conditions. Intravitreal

supplementation of miR-96 mimic could constitute a novel therapeutic strategy to improve vascular repair in OIR and other ischemic retinopathies.

Keywords: micro-RNA (miRNA), vascular degeneration, vascular repair and angiogenesis, oxygen-induced retinopathy (OIR), endothelial dysfunction

INTRODUCTION

Ocular vascular degeneration is an initial feature in the pathogenesis of several types of ischemic retinopathies, including retinopathy of prematurity (ROP) (Rivera et al., 2017). ROP is a well-known visual impairment in premature babies, characterized by an incomplete vascularization of the peripheral retina that causes ischemia and leading to an abnormal and excessive compensatory angiogenic response (pathological neovascularization [NV]) (Sapich et al., 2010; Wu et al., 2013; Rivera et al., 2017a). However, inner retinal vasculature is not the only affected area during OIR. Recent evidences showed that choroidal thinning is present in adolescents and adults formerly affected with ROP (Wu et al., 2013; Erol et al., 2016; Rivera et al., 2017b). Similarly, our group also detected a sustained choroidal thinning in different animal models of ROP (Shao et al., 2011; Zhou et al., 2016; Beaudry-Richard et al., 2018). To date, several studies have focused their effort in developing novel anti-angiogenic monotherapy against the aberrant NV, by using anti-growth factors such as anti-VEGF, -FGF, -IGF and their receptors (Cabral et al., 2017). However, a small number of studies have focused their efforts on attempting to promote and improve revascularization during the initial phase of ischemia, a strategy that should potentially limit subsequent pathologic NV.

Several mechanisms involved in the control of the angiogenic signaling response and vascular repair during ROP are reported to be altered, including those related to the expression of microRNAs (miRNAs), key regulators of gene expression (O'Connell et al., 2010; Caporali and Emanuelli, 2012; Paul et al., 2018). miRNAs are a family of small non-coding RNAs (20–25 nucleotides) involved in post-transcriptional regulation of genes by inhibiting protein translation or by degrading specific mRNA with a perfectly complementary target binding sequence (miRNA/mRNA). miRNAs regulate a wide range of targets essential for various biological processes such as growth, apoptosis/survival, immune response, cell migration, proliferation and stem cell function (O'Connell et al., 2010; Caporali and Emanuelli, 2012; Paul et al., 2018). Physiologic expression levels of miRNAs are altered in several pathological states, suggesting their critical role in the progression of various diseases such as cancer (Hosseini et al., 2018), cardiovascular diseases (Zhou et al., 2018), degenerative disorders (Qiu et al., 2015), and retinopathies (Wu et al., 2012; Wang et al., 2017; Desjarlais et al., 2019b).

miRNAs play a key regulatory role to maintain functional activity of endothelial cells (ECs), in particular in the control of angiogenic capacity (Desjarlais et al., 2017; Fernández-Hernando and Suárez, 2018). Endothelial cell dysfunction is characterized by impaired capacity to proliferate, migrate and form tubules—

critical components associated with insufficient post-ischemic revascularization (Isner and Asahara, 1999; Desjarlais et al., 2017). Some studies have shown changes in the expression of miRNAs in oxygen-induced retinopathy model (OIR). Our group recently reported a significant alteration in the expression level of several miRNAs in the retina and choroid associated with the vascular degeneration phase in a model of OIR in rats (Desjarlais et al., 2019b). However, the individual function of some specific miRNAs associated to the retinal and choroidal vascular degenerative process in OIR has not been investigated.

Next generation sequencing (NGS) revealed miR-96 as abundantly expressed during oculo-vascular development. Although implicated in development of the hindbrain (Schluter et al., 2018), and proliferation of cancer cells (Lin et al., 2010), its role in angiogenesis is unknown. In the present study, we identified miR-96 as an important vasoprotective miRNA that modulates VEGF and Ang-2 expression in the retina and choroid during physiological conditions. miR-96 downregulation was highly associated with impaired angiogenic process in endothelial cells exposed to hyperoxia *in vitro* and *in vivo* during vasoobliteration in OIR. Intravitreal supplementation of miR-96 prevented endothelial cell impairment induced by hyperoxia and microvascular degeneration in the retina and choroid during OIR. Altogether, these results suggest that miR-96 supplementation could be considered as a novel therapeutic strategy to improve and rescue retinal/choroidal vascular repair by promoting VEGF/Ang2 signaling in ischemic retinopathy.

MATERIALS AND METHODS

Animal Care

All animal experimental procedures were performed with strict adherence to the ARVO Statement for the Use of Animals in Ophthalmic and Vision Research and approved by the Animal Care Committee of the Hospital Maisonneuve-Rosemont in accordance with guidelines established by the Canadian Council on Animal Care.

50/10 Oxygen-Induced Retinopathy (OIR) Model in Rats

Cycling oxygen-induced retinopathy (OIR) in rats was used to evaluate the expression profile of miR-96 in the retina and choroid during the pathological progress of this disease. This model is characterized by a first phase of progressive microvascular degeneration that occurs between postnatal (P) days 1 and 14 (during cycling oxygen (50–10% every 24 h), followed by a second phase of abnormal pathological NV that

take place when pup rats are returned to room air between days 14 and 18 as previously described (Rivera et al., 2015; Desjarlais et al., 2019b). Briefly, a few hours after birth, litters of Sprague–Dawley albino rats (Charles River, St. Constant, QC, Canada) were placed with their mothers in an oxygen-regulated environment (OxyCycler A820CV; BioSpherix, Ltd., Redfield, NY, USA) adjusted to alternate between 50 and 10% oxygen every 24 h for 14 days (OIR group). At P14, rat pups were transferred to room air (21% O₂) for 3 days (P17). Age-matched normoxic control rat pups (NOR) were kept in room air (21% O₂) throughout the experiment. Retinal and choroidal samples were isolated at P7, P14 and P17 from OIR and control animals and evaluated by Next Generation Sequencing and qPCR as described (Desjarlais et al., 2019b).

Vaso-Obliteration Model (80% Constant Oxygen)

The angiogenic function of miR-96 in the retina and the potential vasoprotective effects of miR-based therapy during vascular degeneration were evaluated using a model favoring vaso-oblation in rats (Rivera et al., 2015). Retinal vaso-oblation (VO) was induced in Sprague–Dawley rat pups subjected to constant hyperoxia (80% O₂) in chambers controlled by a computer-assisted Oxycycler (BioSpherix, Ltd.) from P5 to P10. Age-matched normoxic control rat pups (NOR) were kept in room air (21% O₂) throughout the experiment. Thirty minutes before hyperoxia exposure at P5, the OIR pups were anesthetized and intravitreally injected or not, with 1 µl (1 mg/kg) of miR-96-5p mimic, or miR-mimic negative control (scrambled) (GE Healthcare Dharmacon, Lafayette, CO). This dose was chosen based on preliminary experiments showing the dose-range for optimal transfection efficiency in tissues (Desjarlais et al., 2017). miRNAs were administered in a mixture solution of InvivoFectamine 3.0 (Thermo Fisher, ON, Canada) according to the manufacturer's recommendations. For molecular analysis, the OIR and control animals were euthanatized, and retinas collected at P6, P8, P10. Vessel immunostaining analysis (retinal flat mounts and cryosection) was performed at P10.

Molecular Analysis

miRNA Isolation and Next Generation Sequencing Analyses

To explore the retinal/choroidal expression profile of miR-96 compare to the other miRNAs during OIR (OIR cycling model), total RNA was extracted from retinas and choroid tissues from OIR and NOR groups at P7, and P14, using the miRNeasy mini kit (Qiagen) according to the manufacturer's protocol. Quantification of total RNA was made with a nanodrop and 1 µg of total RNA was used for library preparation. Quality of total RNA was assessed with the BioAnalyzer Nano (Agilent) and all samples had a RIN above 8. Library preparation was done with the Truseq Small RNA library preparation kit (Illumina, Cat no. RS-200-0012). Eleven PCR cycles were required to amplify libraries. Libraries were quantified with a nanodrop and the quality was assessed with the BioAnalyzer High Sensitivity

(Agilent). All libraries were diluted to 10 nM, normalized and pooled (n = 5) to equimolar concentration based on Miseq v2 50 cycles using 7pM of pooled library. Sequencing was performed with the Illumina Hiseq2000 using the Hiseq Reagent Kit v3 (200 cycles, paired end) and 1.7 nM of the pooled library. Around 70 million paired-end reads were generated per sample. Quantification includes the raw read count, as well as normalized expression level as RPM values (reads per million reads mapped) to account for the variability in the library size.

qRT-PCT Validation of miR-96

To validate the effects of hyperoxia on miR-96 expression, total RNA where extracted from retinas of OIR and normoxia-raised (NOR) rats (OIR-vasooblation model) at P6, P8 and P10, and in human microvascular retinal endothelial cells (HRMEC) subjected or not to hyperoxia (80%O₂) for 1, 3, 6, 24 and 48h, using the miRNeasy mini kit (Qiagen) according to the manufacturer's protocol. RNA was reverse transcribed using with miScript II RT kit (Catalogue # 218161, QIAGEN, Hilden, Germany) according to manufacturer's guidelines. Real-time PCR was performed using 25 ng of cDNA sample by quantitative real-time PCR using iTaq Universal SYBR Green Supermix (BioRad) with 2 µM of miR-96-5p primers designed using Primer Bank and NCBI Primer Blast software (Alpha DNA, Montreal, Canada). Relative expression (RQ = delta/delta CT) was calculated using the detection system ABI Prism 7500 (Applied Biosystems, Foster City, CA, USA) and normalized to 18S and U6 snRNA.

Immunohistochemistry of Retinal and Choroidal Vessels

To analyze retinal vasculature, retinal flat mount dissection was performed on the enucleated eyes fixed in 4% paraformaldehyde for 1 h at room temperature and then stored in PBS until used. The retinas were incubated overnight in 1% Triton X100, 1 mM CaCl₂/PBS with the tetramethylrhodamine isothiocyanate-conjugated lectin endothelial cell marker Bandeiraea simplicifolia (1:100; Sigma-Aldrich Corp., St. Louis, MO, USA). Retinas were washed in PBS and mounted on microscope slides (Bio Nuclear Diagnostics, Inc., Toronto, ON, Canada) under coverslips with mounting media (Fluoro-Gel; Electron Microscopy Sciences, Hatfield, PA, USA). Retinas were photographed under an epifluorescence microscope (Zeiss AxioObserver; Carl Zeiss Canada, Toronto, ON, Canada), and the images were merged into a single file using the MosiaX option in the AxioVision 4.6.5 software (Zeiss). Retinal microvasculature has been quantified by the percentage of total retinal vasoblation, as well as the vascular density of the retina located in the same central and peripheral regions (Sapieha et al., 2008; Rivera et al., 2015). For choroidal vasculature, retinal cross-sections were performed. Eyes were collected, dehydrated by alcohol, and embedded in paraffin. Sagittal sections (7 µm thick) were cut by microtome (RM 2145; Leica, Wetzlar, Germany). Posterior eyecups were frozen in optimal cutting temperature medium and stained for choroidal vessels with TRITC-conjugated tetramethylrhodamine isothiocyanate-labeled lectin

(Sigma-Aldrich) in the cryosections. Sections were then visualized with an epifluorescence microscope (Eclipse E800; Nikon, Tokyo, Japan). In some experiment, cryosections of the different groups were co-stained by using rabbit antibody anti-VEGF (1:200, sc-152; Santa Cruz Biotechnology, Santa Cruz, CA, USA) by incubation overnight at 4°C in the blocking solution. Secondary antibodies such as Alexa Fluor 488 anti-rabbit (Life technologies) were used at a dilution of 1:1,000. Cell nuclei was identified with DAPI labeling. Incubation using rabbit or goat IgG as a primary antibody was conducted as a negative control. The image was split into the three-color channels (RGB Merge/split function) to obtain one image per channel.

Ex Vivo Choroidal Angiogenic Sprouting Assay

Angiogenic sprouting capacity of the choroid isolated from the different groups of rats were assessed as previously described (Shao et al., 2013). Briefly, choroid was isolated from rat pups at P10, sectioned into 1-mm rings, and placed into growth-factor-reduced Matrigel (Fisher Scientific, New Hampshire, USA) in 24-well plates and cultured at 37°C, 5% CO₂ and 95% air, for 5 days in endothelial growth medium; medium 200 (Life technologies) supplemented with 10% fetal bovine serum (FBS, Wisent, St-Jean-Baptiste, QC, Canada), 100 IU/ml penicillin/0.1 mg/ml streptomycin (Wisent) and low serum growth supplement (LSGS; 2% FBS, 3 ng/ml bFGF, 10 mg/ml heparin, 1 mg/ml hydrocortisone, and 10 ng/ml EGF; Life Technologies). Photomicrographs of individual explants were taken at day 5 using an inverted phase-contrast microscopy (AxioObserver; Zeiss), and microvascular sprouting area was quantified using Image J.

In Vitro Angiogenesis Analyses

Cell Culture

Human Retinal Microvascular Endothelial Cells (HRMECs) were purchased from Applied Biological Materials (cat #T4169) and cultured in medium 200 (Life technologies) supplemented with 10% fetal bovine serum (FBS, Wisent, St-Jean-Baptiste, QC, Canada), 100 IU/ml penicillin/0.1 mg/ml streptomycin (Wisent) and low serum growth supplement (LSGS; 2% FBS, 3 ng/ml bFGF, 10 mg/ml heparin, 1 mg/ml hydrocortisone, and 10 ng/ml EGF; Life Technologies). In some experiments, HRMECs were subjected or not to hyperoxia (80%) using oxygen monitoring chambers for different durations (1, 3, 6, 24 and 48h). HRMECs were grown at 37°C, 5% CO₂ and 95% air, and the medium was changed every 2 days and passaged when they reached 90% confluence; passages 3–6 were only used for experiments.

miRNA Transfection in HRMEC

Transfections were carried out at a concentration of 50 nM using Lipofectamine RNAiMAX Reagent (Thermo Fisher, ON, Canada) according to the manufacturer's protocol and as previously described. Briefly, HRMECs were transfected 24 h after being plated in 6-well plates with the following miRs purchased from Dharmacon (GE Healthcare Dharmacon, Lafayette, CO): miRIDIAN miR mimic negative control #1,

miRIDIAN miR mimic hsa-miR-96-5p, miRIDIAN antago-miR negative control #1, miRIDIAN antago-miR-96-5p. After 24 h, the transfection medium was replaced with antibiotic-free complete M200 medium and cells were subjected or not to hyperoxia (80%) for 24 h. Transfection efficiency was measured using mimic transfection control Dy547 (Dharmacon) and found to be 80–90% and also confirmed by qRT-PCR.

HMREC Capillary-Like Tubulogenesis on Matrigel

The angiogenic activity of HRMECs was determined using a Matrigel tube formation assay. Briefly, after transfection and exposure conditions, HRMECs were plated at a density of 30,000 cells/well in 96-well plates precoated with 50 µl of growth factor reduced Matrigel Matrix (Fisher Scientific, New Hampshire, USA) and cultured at 37°C for 6 h in complete endothelial growth medium. HRMECs were pre-transfected or not with miR-96-5p mimic, antagomiR-96-5p or appropriate miR controls for 24 h, and subjected or not to hyperoxia (80% O₂) for 6 h after plated in Matrigel. Capillary-like tubes were observed under a light microscope. Images were obtained at 10× magnification, and all tubes and branching point were counted.

Migration Scratch Assay

Measurement of cell migration was performed using an adapted scratch assay in confluent HRMECs. The cells were transfected and grown to near confluence in 24-well plates and subjected or not to hyperoxia (80% O₂). Mechanical disruption of the monolayer was realized by scraping with a pipette tip. Migration was assessed 24 h after mechanical disruption using an inverted microscope at a magnification of 200× and the area of migration and the cells density where quantified as previously described (Desjarlais et al., 2017; Desjarlais et al., 2019a). Six fields per well were evaluated and all experiments were performed in duplicate.

qRT-PCT Analyses of Angiogenic Factors Level

To explore the effects of miR-96-5p overexpression/inhibition on angiogenic factors mRNAs level in HMREC and in the rat retinas, total RNA was extracted using RNeasy mini kit (Qiagen) according to the manufacturer's protocol and was reverse transcribed using iScript-II RT kit (Qiagen) according to manufacturer's guidelines to generate cDNA. Quantitative real-time PCR reaction was performed using 25 ng of cDNA sample, 2 µM of specific primers for the selected mRNAs (Alpha DNA, Montreal, Canada) and Universal SYBR Green Supermix (BioRad). Relative expression ($RQ = 2^{-\Delta\Delta CT}$) was calculated using the instrument detection system; ABI Prism 7500 (Applied Biosystems, Foster City, CA, USA) and normalized to b-Actin and GAPDH.

Western Blot Analysis

Protein levels of VEGF, Ang2 and FGF-2 were analysed by Western blots in the retina of the different groups of rats and in HMREC extracts. For total protein extraction, isolated retina where rinsed in PBS, snap-frozen in liquid nitrogen, and stored at –80°C until use. Whole-cell protein extracts were obtained

after homogenization of the retina of the different groups of rats in ice cold RIPA buffer (pH = 8) containing 50 mM Tris-HCL, 150 mM NaCl, 5 mM EDTA, 1% Triton 100×, 0.5% sodium deoxycholate, 0.1% SDS with a cocktail of proteases and phosphatases inhibitors (MiniComplete, PhosphoStop and PMSF, Roche, Bâle, Switzerland). HRMECs were lysed with 50 µl of RIPA lysis buffer per well in 6-well plates, harvested and sonicated. 50 µg of protein per retina homogenate sample and 20 µg of protein per cell lysate sample were separated on an SDS-polyacrylamide gel and electroblotted on nitrocellulose membranes. Non-specific binding sites were blocked with 5% BSA for 1 h. The membranes were probed overnight at 4°C with the following antibodies: rabbit antibody VEGF (1:500, sc-152; Santa Cruz Biotechnology, Santa Cruz, CA, USA), goat antibody Ang2 (1:1,000, ab10601; ABCAM), mouse antibody FGF-2 (1:1,000, ab181; ABCAM) or GAPDH (1:2,000, ab181602; ABCAM). Membranes were then washed three times for 10 min with TBS-T and incubated with secondary antibodies for 1 h with 1:2,500 horseradish peroxidase (HRP)-conjugated anti-mouse or 1:2,000 HRP anti-goat or anti-rabbit secondary antibodies (Millipore). Specific proteins were detected by chemiluminescent reaction (GE Healthcare, Piscataway, NJ) by membranes exposure with LAS-3000 imager. Protein expression was quantified using ImageJ and the results are expressed as density values normalized to the loading control (GAPDH).

Statistical Analysis

All results are presented as mean ± SEM. Statistical significance was evaluated by a one- or two-way ANOVA followed by a Bonferroni *post hoc* test. A value of $P < 0.05$ was interpreted to denote statistical significance.

RESULTS

miR-96 Is Highly Expressed During Vascular Development But Downregulated During Hyperoxia-Induced Vessel Degeneration

We evaluated the expression profile of miR-96 in retinal and choroidal samples of animals exposed to normoxic (NOR) and during vasoobliteration phase in 50/10 oxygen-induced retinopathy model (50/10 OIR) at P7 and P14 by using next generation sequencing (NGS) analysis. During ocular vascular development, we found miR-96 to be highly expressed in the retina at P7 and choroid at P14 in normoxic animals (**Figure 1A**). However in 50/10 OIR animals, miR-96 was profoundly downregulated in the retinal/choroidal tissues at all time points evaluated (**Figure 1A**). To better validate the effect of hyperoxia on miR-96 expression, we also analyzed its levels of expression in the rat retina using a different vasoobliteration OIR model, specifically by constant exposure to 80% O₂. qRT-PCR analyses revealed that miR-96 expression was also significantly reduced in 80% OIR retina at P6, P8 and P10, compared to control (NOR) rats (**Figure 1B**). To assess whether miR-96 expression specifically affects endothelial cells during

hyperoxia, human retinal microvascular endothelial cells (HRMEC) were subjected to 80% oxygen for different periods of time (1, 3, 6, 24 and 48 h). Hyperoxia markedly suppressed miR-96 expression (**Figure 1C**). These results infer that decreased miR-96 levels may be associated with impaired endothelial cell function during OIR.

miR-96 Positively Regulates the Expression of Several Angiogenic Factors, Including VEGF, FGF-2 and Ang2, in Endothelial Cells

Based on expression profile of miR-96 in OIR we proceeded to determine if relevant angiogenic factors were regulated by miR-96, and whether maintaining miR-96 expression can prevent endothelial cell survival during OIR. Recent studies have reported an important correlation between miR-96 levels and tumor angiogenesis (Hong et al., 2016; Shi et al., 2017; Iwai et al., 2018). However, its potential role in OIR remains unknown. We investigated the effects of miR-96 up or down regulation on the expression of different angiogenic factors. We first determined the expression efficacy of miR-96 mimic or antagomiR-96 at different concentrations (10, 25 and 50 nM) for 24h in transfected HRMECs (**Figure 2A**). Transfection was highly efficient on endothelium at 50 nM for both miR-96 mimic (overexpression) and antagomiR-96 (suppression), and therefore, we used this concentration in all our experiments. We next evaluated if miR-96 mimic (50 nM) in cultured HRMECs affects the expression of angiogenic growth factors. Interestingly, increased miR-96 induced simultaneously and significantly the mRNA expression of several pro-angiogenic factors including, VEGF, Ang2, FGF-2, SFD-1 and VEGFR2 (**Figure 2B, C**). Conversely, inhibition of miR-96 expression by using an antagomiR (50 nM) downregulated expression of these factors (**Figure 2B, C**). In addition, miR-96 mimic reversed hyperoxia-induced mRNAs (**Figure 2D**) and protein suppression of VEGF, Ang2 and FGF-2 (**Figure 2E**). Hence, miR-96 is an important player in the control of gene expression of growth factors essential for maintenance and signaling on endothelium.

miR-96 Regulates the Angiogenic Function of HRMEC and Protects Against Hyperoxia-Induced Endothelial Dysfunction

The next step was to investigate the potential protective effect of increased miR-96 in tube formation and migration assays *in vitro* during hyperoxic exposure. We performed a gain and loss-of function experiment by transfecting HRMECs with a miR-96 mimic or antagomiR-96 in normoxic or hyperoxic conditions. In normoxic conditions, we found that augmented miR-96 significantly increased tubulogenesis (**Figure 3A**, upper panel) and endothelial cell migration (**Figure 3B**, upper panel). Conversely, miR-96 antagomiR resulted in failed HRMEC tubulogenesis and migration (**Figures 3A, B**, bottom panels), consistent with that seen during hyperoxia when miR-96 was down-regulated (**Figures 1C and 2D**); this inhibitory effect of antagomiR-96 is likely contributed at least in part by suppression

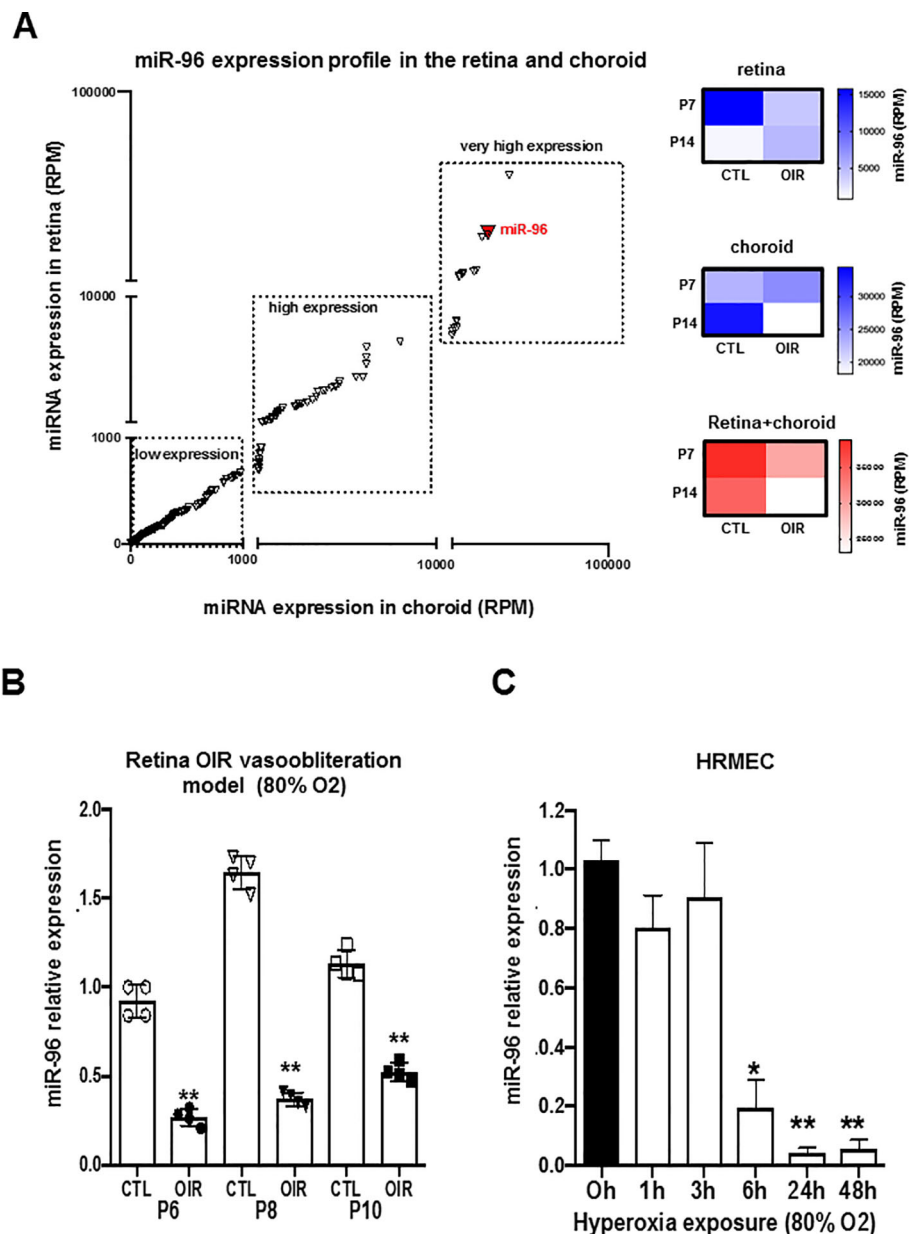


FIGURE 1 | miR-96 expression is downregulated in the retina and choroid of OIR rat and in human retinal endothelial cells subjected to hyperoxia. **(A)** NGS analyses showing miR-96 expression profile (RPM) in the retina and choroid during the vascular development of normoxic control rats vs OIR rats (OIR cycling-O₂ model). **(B, C)** qRT-PCR validation analysis of miR-96 expression in the retina of normoxic control rats vs OIR rats (vasoobliteration: constant-O₂ model) and respectively in Human Retinal Microvascular Endothelial Cell (HRMEC) subjected to hyperoxia (80% O₂). Data are mean \pm SEM. * $P < 0.05$ or ** $P < 0.01$ vs CTL (control). N = 4–5/group.

of VEGF/Ang2/FGF-2 proteins during hyperoxia (Figure 2D). On the other hand, treatment with miR-96 mimic significantly maintained endothelial cell tube formation and migration even under hyperoxic conditions (Figures 3A, B, bottom panel), probably also due to preservation of VEGF/Ang2/FGF-2 (Figure 2D).

Intravitreal Administration of miR-96 Prevents Retinal and Choroidal Vasoobliteration in Oxygen-Induced Retinopathy Rats

We evaluated if miR-96 mimic can preserve retinal and choroidal vessel integrity during OIR. miR-96 was

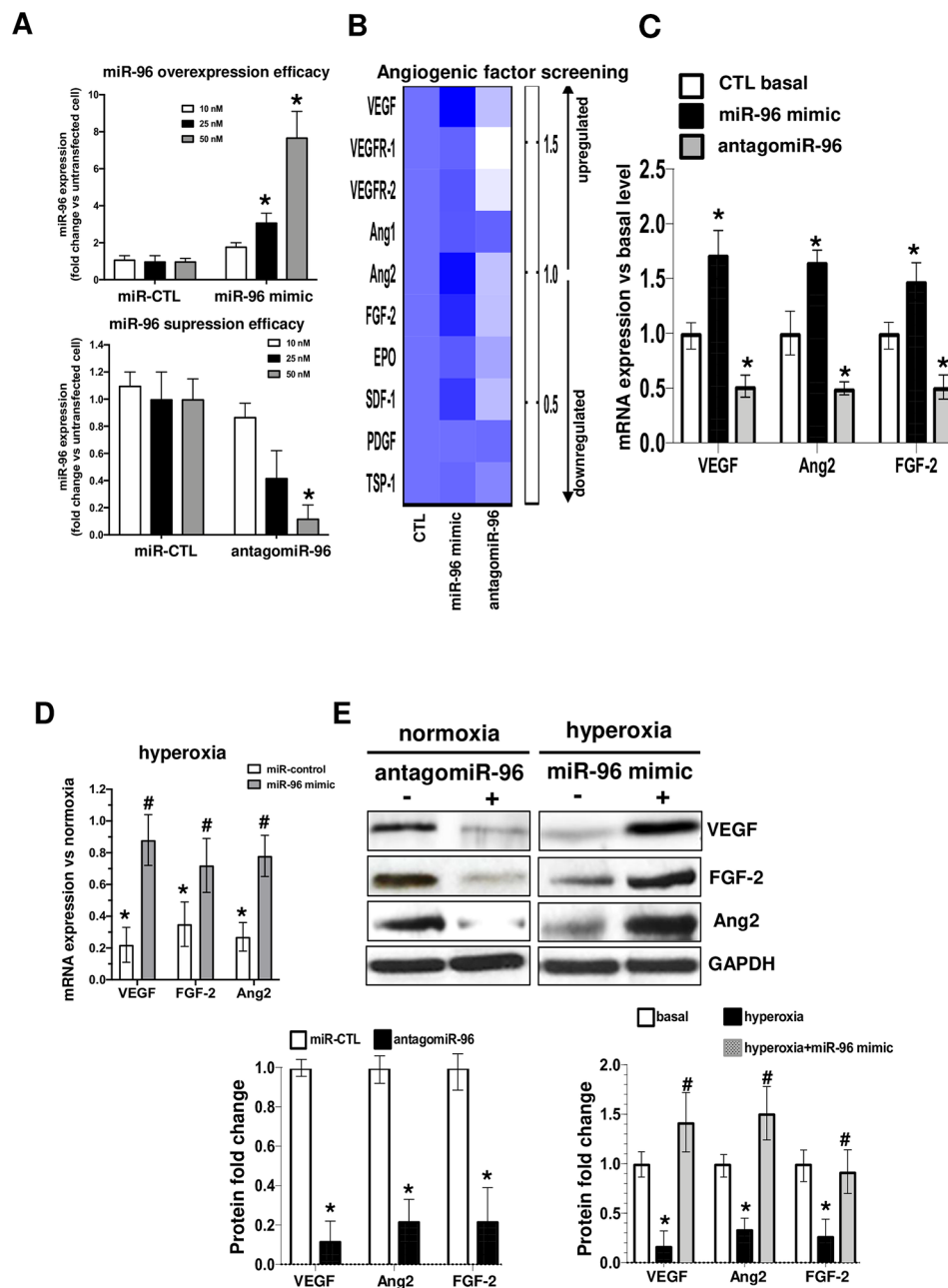


FIGURE 2 | miR-96 regulate simultaneous the expression level of VEGF/FGF-2/Ang2 in human retinal endothelial cells. To explore the regulatory function of miR-96 on HRMEC angiogenic factor production, cells were pre-transfected or not with 50 nM of miR-control (scrambled), miR-96 mimic or antagomiR-96 for 24 h, and subjected or not to hyperoxia (80% O₂) for an additional 24 h. **(A)** qRT-PCR analyses of miR-96 transfection efficacy, and **(B, C)** screening of angiogenic factor expression modulated by miR-96. **(D, E)** qRT-PCR analyses of miR-96 protective effects in HMREC subjected to hyperoxia **(D)** and western blot validation and compiled histogram analysis of the regulatory role of miR-96 on VEGF, FGF-2 and Ang2 proteins expression levels. N = 3–4 experiments. Data are mean ± SEM. **P* < 0.05 vs CTL (control) or #*P* < 0.05 vs hyperoxia.

maintained increased (till at least P10) following its intravitreal administration at P5 (**Figure 4A**). Retinal and choroidal microvascular decay is a feature of the first phase of OIR (Rivera et al., 2015; Zhou et al., 2016; Desjarlais et al., 2019b), as appreciated by an increase of total retinal vasoobliteration (**Figure 4B**), central avascular area (**Figure 4C**) and reduced

microvascular density in the peripheral retina (**Figure 4D**) after 5 days of exposure to hyperoxia (from P5 to P10); this was also associated with reduced choroidal thickness (**Figure 4E**). Interestingly, choroids from animals subjected to OIR exhibited a limited angiogenic ability (**Figure 4F**). Supplementation of miR-96 mimic (1 mg/kg, administered

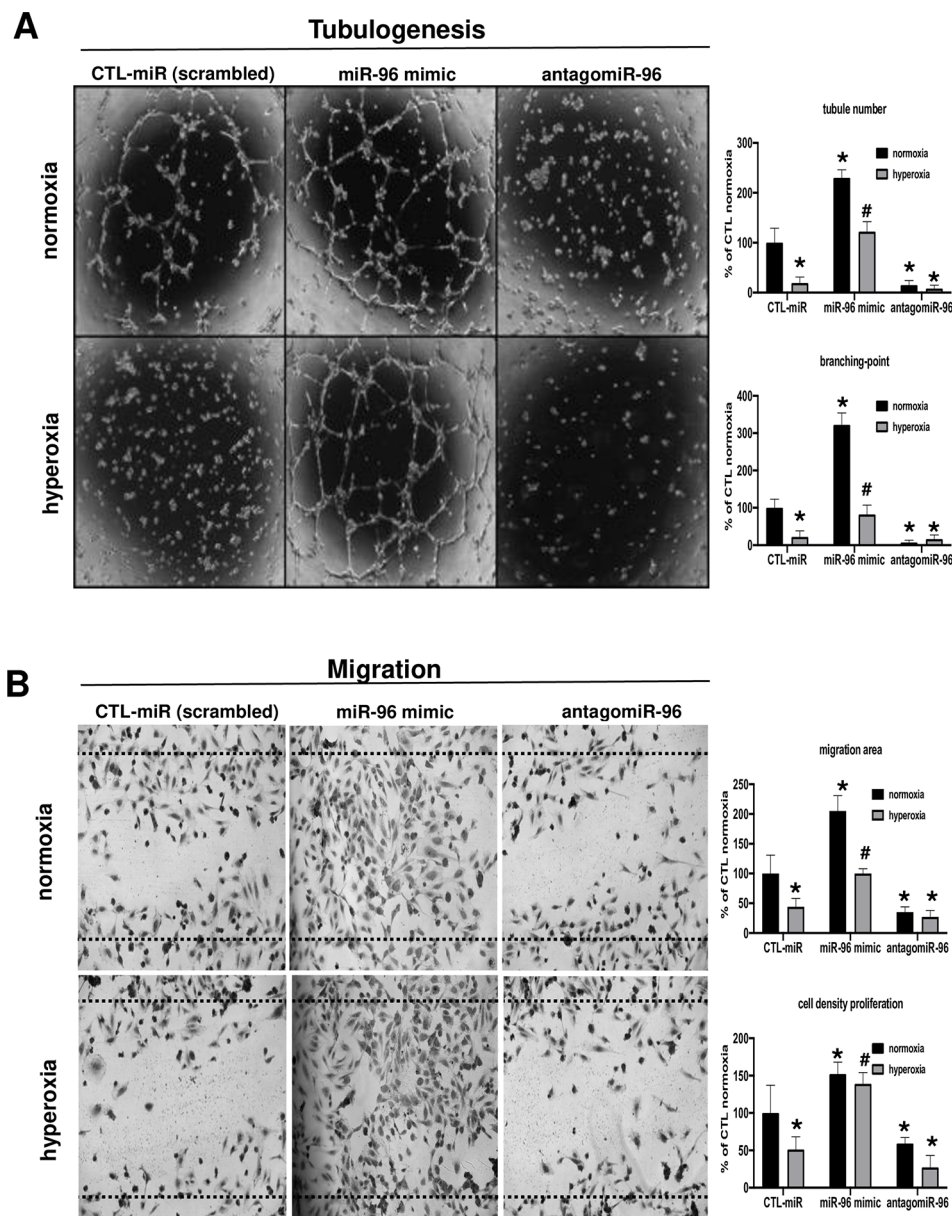


FIGURE 3 | Suppression of miR-96 leads to endothelial dysfunction, and miR-96 supplementation protects angiogenic properties of endothelial cells against hyperoxia. **(A)** *In vitro* evaluation of angiogenesis (tubulogenesis) using HRMEC cultured in Matrigel, and **(B)** cell migration scratch assay of HRMEC treated or not with a miR-control (scrambled), miR-96 mimic or antagomiR-96, and exposed or not to hyperoxia (80% O₂). Data are mean ± SEM. **P* < 0.05 vs CTL (control) or #*P* < 0.05 vs hyperoxia. N = 3–4 experiments.

intravitreally) 30 min before hyperoxic exposure, significantly prevented retinal and choroidal vasoobliteration (**Figures 4B–E**). Moreover, miR-96 mimic allowed the choroid of OIR-subjected rats to retain an angiogenic property (as seen in Matrigel) similar to that seen in normoxia-raised rats (**Figure 4F**). Consistent with physiologic angiogenic effects of miR-96, latter augmented mRNA and protein expression levels of VEGF and Ang2 in the retina of OIR rats at P8 and P10 (**Figures 5A, B, C**). Increased VEGF was also detected *in situ* in choroid of miR-96 mimic-treated animals (**Figure 5D**).

Together these observations highlight a beneficial angiogenic role of miR-96 and potential therapeutic value of this miR in preventing microvascular degeneration while preserving angiogenic capacity during OIR.

DISCUSSION

Although miRNAs are recognized as essential regulators of numerous genes resulting in the control of a variety of

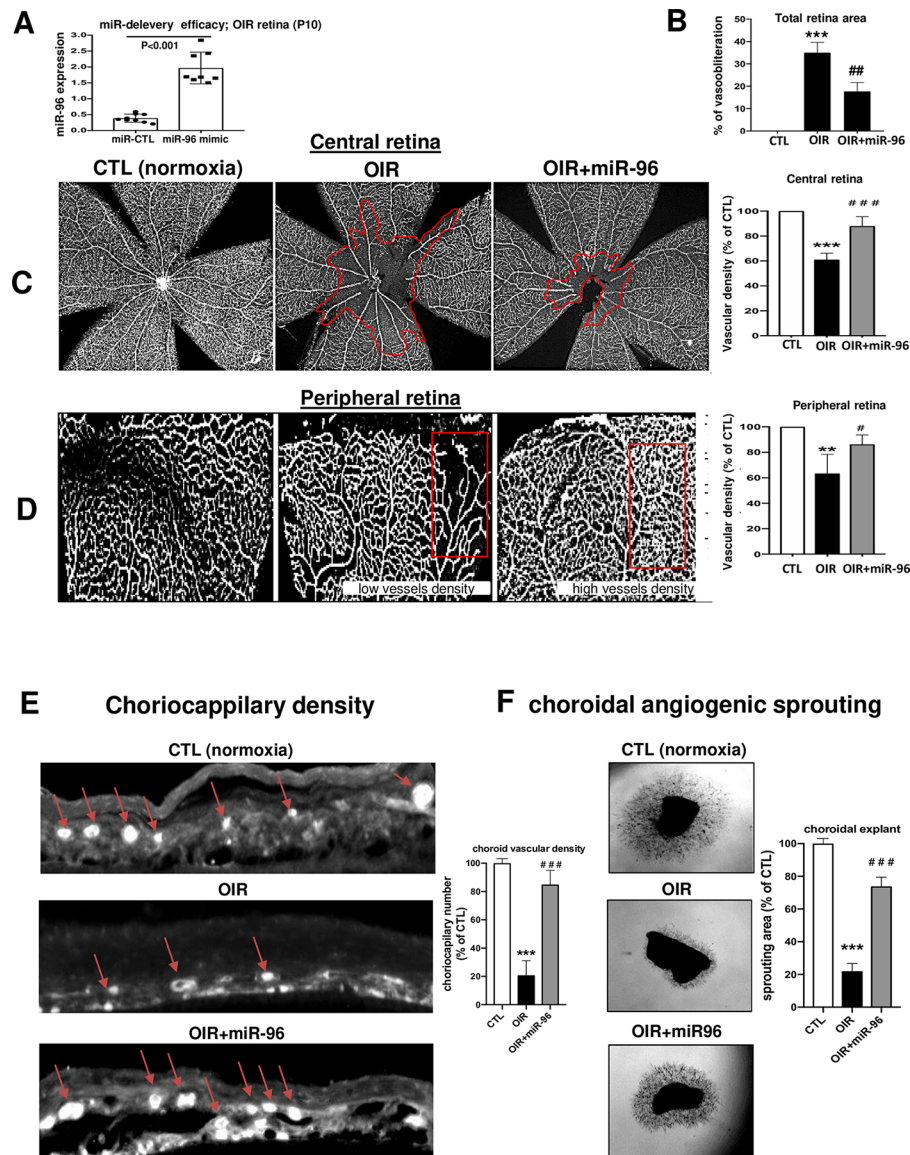


FIGURE 4 | Intraocular miR-96 (mimic) prevents retinal and choroidal vascular decay and facilitates revascularization in OIR model. OIR-subjected rats were injected intravitreally with a single dose (1 mg/kg) of miR-control or miR-96 mimic at P5 before hyperoxia exposure. Animals were then subjected to constant hyperoxia (80% O₂) until P10. **(A)** qRT-PCR analysis showing miR-96 treatment efficacy in raising miR-96 expression. **(B)** Quantification analyze of total retinal vasoobliteration in OIR-subjected rats treated or not with miR-96 mimic. **(C, D)** Representative flatmount images of central and peripheral vascularization; histogram on right show compiled analysis. **(E)** Isolectin staining of sub-retina showing choroidal vessels. **(F)** Photographic image of choroid explant vascular sprouting in Matrigel after 5 days of incubation, in tissues from normoxia- and OIR-raised animals treated or not with miR-96. Data are mean \pm SEM. ** $P < 0.01$ or *** $P < 0.001$ vs CTL; # $P < 0.05$ or ### $P < 0.01$ or #### $P < 0.001$ vs OIR. $N = 6-8/\text{group}$.

physiologic and pathologic processes (O'Connell et al., 2010; Caporali and Emanuelli, 2012; Paul et al., 2018), their specific individual functions during OIR remain mostly unexplored. Recently, our group published a complete profiling of miRNAs in the retina and choroid during OIR that identified a serial of differentially expressed miRNAs during the two characteristic pathological phases in OIR (Rivera et al., 2015; Zhou et al., 2016;

Desjarlais et al., 2019b). Here, we show that among these miRNAs, miR-96 was one of the most abundantly expressed miRNAs in the retina and choroid during ocular development. Furthermore, we found that miR-96 was downregulated in the retinal/choroidal tissues during the phase of vascular degeneration in OIR, inferring a potential critical role in the maintenance of ocular vasculature. Although previous studies

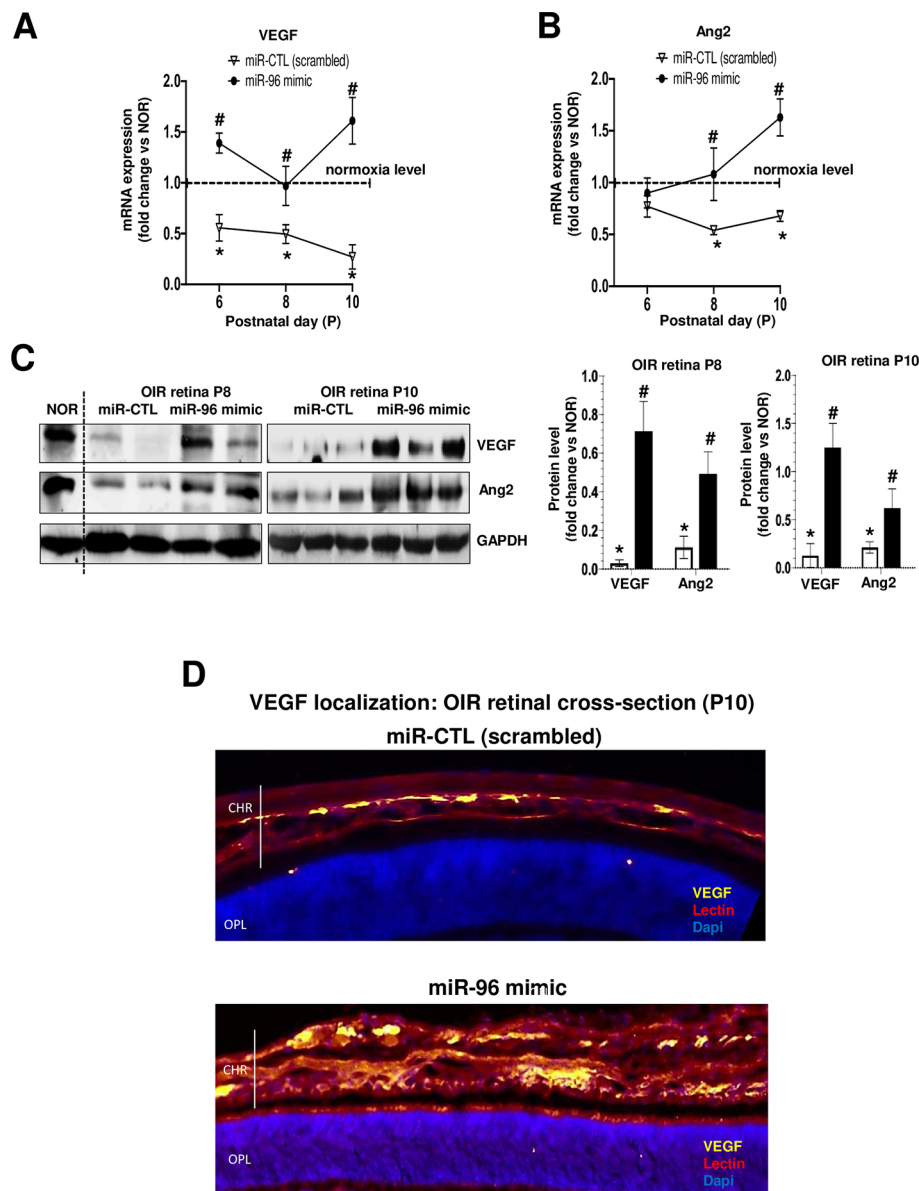
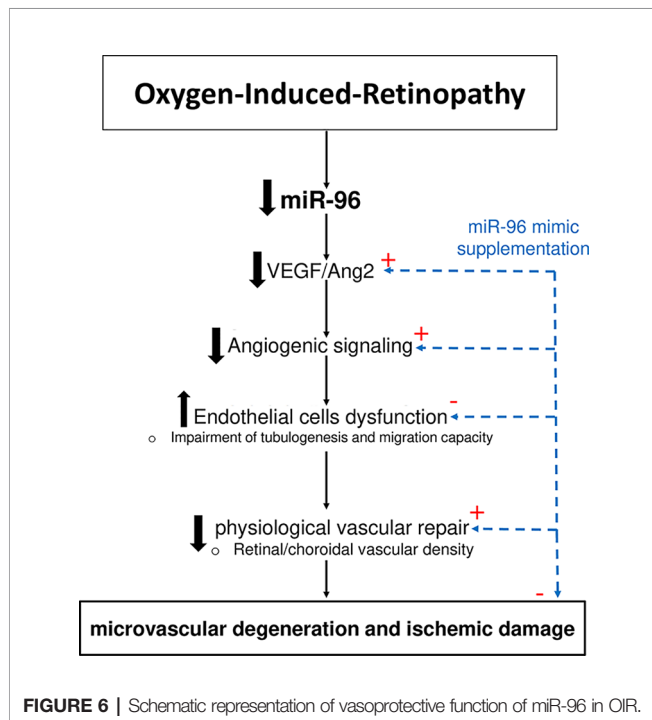


FIGURE 5 | miR-96 supplementation restores VEGF and Ang2 levels in retina of OIR-subjected rats. OIR rats were intravitreally injected with a single dose (1 mg/kg) of miR-CTL or miR-96 mimic at P5 before hyperoxia exposure. After treatments, the animals were subjected to constant hyperoxia (80% O₂) until P10. **(A, B, C)** Respectively, qRT-PCR and western blot analysis of VEGF and Ang2 expression in the retina of OIR-subjected rats treated or not with miR-96 mimic. **(D)** Immunostaining of VEGF in retinal cross-section reveals its expression co-localized on endothelium (lectin-staining) in OIR-subjected rats treated or not with miR-96 mimic. *P < 0.05 vs CTL or #vs OIR. N = 6–8 retinas/group.

have reported that miR-96 is essential for the normal development of the auditory hindbrain (Schluter et al., 2018), integrity and maturation of photoreceptors (Xiang et al., 2017) and proliferation of cancer cells (Lin et al., 2010), its implications in angiogenesis were still unknown. In the current study, we show that miR-96 is important for endothelial cell maintenance and proliferation. During hyperoxia-associated retinal and choroidal vascular decay, miR-96 is suppressed and along with its key angiogenic factors VEGF, Ang2 and FGF-2, resulting in

curtailed endothelial function; supplementation with miR-96 (using a mimic) restored retinal and choroidal vasculature *in vivo* in model of OIR, as well as its angiogenic capacity *ex vivo*, consistent with recently described restitution of choroidal angiogenic property by growth factors in OIR (Zhou et al., 2019). These properties of miR-96 in OIR are depicted in a schematic diagram (Figure 6).

miR-96 has been found to be modulated during various clinical conditions. For instance, miR-96 is upregulated in the retina of



streptozotocin-induced diabetes rats (Wu et al., 2012) and in the plasma of type-2 diabetic patients (Yang et al., 2017), while miR-96 is downregulated in the RHO-mouse retina, a model for common form of inherited blindness (Palfi et al., 2016). In addition, hypoxic conditions in cancer cells have shown to modify the expression profiling of miRNAs (Shen et al., 2013; Bandara et al., 2017). In breast and prostatic cancer cell lines, miR-96 has been found to be increased by hypoxia and play a role in the regulation of autophagy process (Ma et al., 2014; Shi et al., 2017). In another study a miR-183-96-182 cluster overexpressed the master regulator of angiogenesis HIF-1 α augmenting tumour progression and angiogenesis (Li et al., 2015). It is thus possible that augmented levels of VEGF/FGF-2/Ang2 in endothelial cells supplemented with miR-96 can be associated to the activation of miR-96/HIF-1 signalling; this has yet to be investigated.

Several miRNAs are modulated by reactive oxygen species (ROS) (He and Jiang, 2016; Banerjee et al., 2017), as reported in inflammation (Sonkoly and Pivarsci, 2009), cardiovascular conditions including stroke, and in post-occlusion revascularization (Magenta et al., 2013; Jaksik et al., 2014; Gong et al., 2018). Hyperoxia in the newborn leads to a systematic increase in ROS (Kwak et al., 2006). We postulate that these ROS can downregulate miR-96 as occurs with other miRNAs under oxidative stress conditions (Magenta et al., 2013; Jaksik et al., 2014). For instance, miR-96 in human retinal pigment epithelial cell stimulated with hydrogen peroxide (ROS inducer), was found to be strongly downregulated (Ayaz and Dinc, 2018). Conversely, overexpression of the miR-183/96/182 cluster resulted in a decreased production of nitrite and ROS by macrophage (Muraleedharan et al., 2019) and a neuroprotective role in the brain, by positively regulating glutathione (GSH) levels, a major

tissue antioxidant (Kinoshita et al., 2014). Collectively, these studies support the possibility that miR-96 can be decreased in hyperoxic/oxidative stress conditions; this does not exclude other mechanisms such as extracellular vesicles (Liu and Lu, 2015; Battaglia et al., 2019).

The present study is the first to show that miRNA-based therapy is beneficial in preserving vasculature during the (first) obliterative phase of OIR. Others have shown efficacy of miRNAs-based therapies to inhibit pathological neovascularization (Bai, Bai et al., 2011; Chen et al., 2017; Liu et al., 2019), but not in prevention of vascular decay. In this context miR-96-regulated VEGF and Ang2 play a critical role. Interestingly, studies have shown that VEGF and Ang-2 play a synergistic role in angiogenic stimulation (Bhaskar et al., 2013) and that conversely the dual inhibition of these factors leads to significant vascular failure (Coutelle et al., 2015; Regula et al., 2016). Consistently with our results, some studies have previously described a proangiogenic role of miR-96 in different cancer cell lines by targeting different genes with antiangiogenic functions. For example, miR-96 was reported to suppress PTPN9 (Hong et al., 2016), an important anti-angiogenic phosphatase involved in the inactivation of STAT3 (Yuan et al., 2010), a key proangiogenic transcriptional factor (Chen and Han, 2008). As is known a constitutive activation of STAT3 leads to upregulation of VEGF (Niu et al., 2002). Here, we observed a consistent increase on VEGF levels with miR-96 mimic stimulation. In addition, another study demonstrates that suppression of PTPN9 by miR-126 in endothelial cells in a mice model of angiogenesis and neurogenesis ischemia, induced the activation of AKT and ERK signaling, two major signaling pathway promoting cellular migration, proliferation and survival (Qu et al., 2019). As it is well known that HIF1 α acting as a key pro-angiogenic transcriptional factor activated by hypoxia and translocated to the nucleus to induce the production of several endothelial growth factors, a recent study reported that miR-182, a member of miR-96/182/183 cluster, directly suppresses the expression of prolyl hydroxylase domain enzymes (PHD) and the inhibiting factor HIF-1 (FIH1) in prostatic tumor cells causing a marked increase in HIF1 α activity (Li et al., 2015). Based on this finding, it's possible to speculate that miR-96 can also target varied negative regulators of HIF1 α activities. Other potential antiangiogenic factors regulated by miR-96 include OXO1, FOXO3, RECK, EphrinA5 and SAMD9 (Hong et al., 2016). In this context, FOX family can be negatively regulated in part by FGF-2/IGF-2, and other FOX members (Essaghir et al., 2009), suggesting a complex autoregulation mechanism between miR-96/FOX/angiogenic factor. While RECK represses the expression of MMP-2 and MMP-9 (Chang et al., 2008), and EphrinA5 (Wang et al., 2016) is important in regulating endothelial migration, survival and proliferation (Hara et al., 2010). The precise mechanism by which miR-96 regulates VEGF/Ang2/FGF-2 needs further investigations.

In summary, the current study demonstrates for the first time that miR-96 regulates the expression of angiogenic factors (VEGF/Ang-2) associated with the maintenance of retinal and choroidal microvasculature during physiological and pathological conditions that lead to vascular decay. Supplementation of miR-96 mimic could constitute a novel therapeutic strategy to improve vascular repair in OIR and other ischemic retinopathies.

DATA AVAILABILITY STATEMENT

The raw data generated for this article can be found in NCBI using the accession number GSE129995.

ETHICS STATEMENT

The animal study was reviewed and approved by Animal Care Committee of the Hospital Maisonneuve-Rosemont in accordance with guidelines established by the Canadian Council on Animal Care.

AUTHOR CONTRIBUTIONS

Conceived and designed the study: MD and SC. Wrote the manuscript: MD, SC, JR. Directed and planned the experiments:

MD. Performed the experiments: MD and MW, assisted by JR, RD, IL, PR, SO, CB. Analysed the data: MD, JR, SC.

FUNDING

MD is a recipient of a post-doctoral fellowship award from Hôpital Maisonneuve-Rosemont and from the Fonds de Recherche en Ophtalmologie de l'Université de Montréal. MW is a recipient of a bursary from Université de Lorraine, Nancy, France. JR was supported by the Heart and Stroke Foundation of Canada and the Canadian Stroke Network. RD is recipient of an award of Excellence from the Vision Health Network of Quebec. SC holds a Canada Research Chair (Vision Science) and the Leopoldine Wolfe Chair in translational research in age-related macular degeneration. The study was financed by grants from Canadian Institutes of Health Research (grant number—MOP12532), March of Dimes Birth Defects Foundation, Fonds de la Recherche en Santé—Québec (FRQS)/Québec Vision Health Network (grantee: SC).

REFERENCES

- Ayaz, L., and Dinc, E. (2018). Evaluation of microRNA responses in ARPE-19 cells against the oxidative stress. *Cutan Ocul. Toxicol.* 37 (2), 121–126. doi: 10.1080/15569527.2017.1355314
- Bai, Y., Bai, X., Wang, Z., Zhang, X., Ruan, C., and Miao, J. (2011). MicroRNA-126 inhibits ischemia-induced retinal neovascularization via regulating angiogenic growth factors. *Exp. Mol. Pathol.* 91 (1), 471–477. doi: 10.1016/j.yexmp.2011.04.016
- Bandara, K. V., Michael, M. Z., and Gleadle, J. M. (2017). MicroRNA biogenesis in hypoxia. *Microna* 6 (2), 80–96. doi: 10.2174/2211536606666170313114821
- Banerjee, J., Khanna, S., and Bhattacharya, A. (2017). MicroRNA regulation of oxidative stress. *Oxid. Med. Cell Longev.* 2017, 2872156. doi: 10.1155/2017/2872156
- Battaglia, R., Palini, S., Vento, M. E., La Ferlita, A., Lo Faro, M. J., Caroppo, E., et al. (2019). Identification of extracellular vesicles and characterization of miRNA expression profiles in human blastocoel fluid. *Sci. Rep.* 9 (1), 84. doi: 10.1038/s41598-018-36452-7
- Beaudry-Richard, A., Nadeau-Vallee, M., Prairie, E., Maurice, N., Heckel, E., Nezahy, M., et al. (2018). Antenatal IL-1-dependent inflammation persists postnatally and causes retinal and sub-retinal vasculopathy in progeny. *Sci. Rep.* 8 (1), 11875. doi: 10.1038/s41598-018-30087-4
- Bhaskar, A., Gupta, R., Sreenivas, V., Rani, L., Kumar, L., Sharma, A., et al. (2013). Synergistic effect of vascular endothelial growth factor and angiopoietin-2 on progression free survival in multiple myeloma. *Leuk. Res.* 37 (4), 410–415. doi: 10.1016/j.leukres.2012.12.014
- Cabral, T., Mello, L. G. M., Lima, L. H., Polido, J., Regatieri, C. V., Belfort, R. Jr., et al. (2017). Retinal and choroidal angiogenesis: a review of new targets. *Int. J. Retina Vitreous* 3, 31. doi: 10.1186/s40942-017-0084-9
- Caporali, A., and Emanueli, C. (2012). MicroRNAs in postischemic vascular repair. *Cardiol. Res. Pract.* 2012, 486702. doi: 10.1155/2012/486702
- Chang, C. K., Hung, W. C., and Chang, H. C. (2008). The Kazal motifs of RECK protein inhibit MMP-9 secretion and activity and reduce metastasis of lung cancer cells *in vitro* and *in vivo*. *J. Cell. Mol. Med.* 12 (6b), 2781–2789. doi: 10.1111/j.1582-4934.2008.00215.x
- Chen, Z., and Han, Z. C. (2008). STAT3: a critical transcription activator in angiogenesis. *Med. Res. Rev.* 28 (2), 185–200. doi: 10.1002/med.20101
- Chen, Q., Qiu, F., Zhou, K., Matlock, H. G., Takahashi, Y., Rajala, R. V. S., et al. (2017). Pathogenic role of microRNA-21 in diabetic retinopathy through downregulation of pparalpha. *Diabetes* 66 (6), 1671–1682. doi: 10.2337/db16-1246
- Coutelle, O., Schiffmann, L. M., Liwschitz, M., Brunold, M., Goede, V., Hallek, M., et al. (2015). Dual targeting of Angiopoietin-2 and VEGF potentiates effective vascular normalisation without inducing empty basement membrane sleeves in xenograft tumours. *Br. J. Cancer* 112 (3), 495–503. doi: 10.1038/bjc.2014.629
- Desjarlais, M., Dussault, S., Dhahri, W., Mathieu, R., and Rivard, A. (2017). MicroRNA-150 modulates ischemia-induced neovascularization in atherosclerotic conditions. *Arterioscler. Thromb. Vasc. Biol.* 37 (5), 900–908. doi: 10.1161/ATVBAHA.117.309189
- Desjarlais, M., Dussault, S., Rivard, F., Harel, S., Sanchez, V., Hussain, S. N. A., et al. (2019a). Forced expression of microRNA-146b reduces TRAF6-dependent inflammation and improves ischemia-induced neovascularization in hypercholesterolemic conditions. *Atherosclerosis* 289, 73–84. doi: 10.1016/j.atherosclerosis.2019.08.010
- Desjarlais, M., Rivera, J. C., Lahaie, I., Cagnone, G., Wirt, M., Omri, S., et al. (2019b). MicroRNA expression profile in retina and choroid in oxygen-induced retinopathy model. *PloS One* 14 (6), e0218282. doi: 10.1371/journal.pone.0218282
- Erol, M. K., Coban, D. T., Ozdemir, O., Dogan, B., Tunay, Z. O., and Bulut, M. (2016). Choroidal Thickness In Infants With Retinopathy Of Prematurity. *Retina* 36 (6), 1191–1198. doi: 10.1097/IAE.0000000000000866
- Essaghir, A., Dif, N., Marbehant, C. Y., Coffey, P. J., and Demoulin, J. B. (2009). The transcription of FOXO genes is stimulated by FOXO3 and repressed by growth factors. *J. Biol. Chem.* 284 (16), 10334–10342. doi: 10.1074/jbc.M808848200
- Fernández-Hernando, C., and Suárez, Y. (2018). MicroRNAs in endothelial cell homeostasis and vascular disease. *Curr. Opin. Hematol.* 25 (3), 227–236. doi: 10.1097/MOH.0000000000000424
- Gong, Y. Y., Luo, J. Y., Wang, L., and Huang, Y. (2018). MicroRNAs regulating reactive oxygen species in cardiovascular diseases. *Antioxid. Redox Signal* 29 (11), 1092–1107. doi: 10.1089/ars.2017.7328
- Hara, Y., Nomura, T., Yoshizaki, K., Frisen, J., and Osumi, N. (2010). Impaired hippocampal neurogenesis and vascular formation in ephrin-A5-deficient mice. *Stem Cells* 28 (5), 974–983. doi: 10.1002/stem.427
- He, J., and Jiang, B. H. (2016). Interplay between reactive oxygen species and MicroRNAs in cancer. *Curr. Pharmacol. Rep.* 2 (2), 82–90. doi: 10.1007/s40495-016-0051-4

- Hong, Y., Liang, H., Uzair Ur, R., Wang, Y., Zhang, W., Zhou, Y., et al. (2016). miR-96 promotes cell proliferation, migration and invasion by targeting PTPN9 in breast cancer. *Sci. Rep.* 6, 37421. doi: 10.1038/srep37421
- Hosseinali, N., Aghapour, M., Duijf, P. H. G., and Baradaran, B. (2018). Treating cancer with microRNA replacement therapy: a literature review. *J. Cell Physiol.* 233 (8), 5574–5588. doi: 10.1002/jcp.26514
- Isner, J. M., and Asahara, T. (1999). Angiogenesis and vasculogenesis as therapeutic strategies for postnatal neovascularization. *J. Clin. Invest.* 103 (9), 1231–1236. doi: 10.1172/JCI6889
- Iwai, N., Yasui, K., Tomie, A., Gen, Y., Terasaki, K., Kitaichi, T., et al. (2018). Oncogenic miR-96-5p inhibits apoptosis by targeting the caspase-9 gene in hepatocellular carcinoma. *Int. J. Oncol.* 53 (1), 237–245. doi: 10.3892/ijo.2018.4369
- Jaksik, R., Lalik, A., Skonieczna, M., Cieslar-Pobuda, A., Student, S., and Rzeszowska-Wolny, J. (2014). MicroRNAs and reactive oxygen species: are they in the same regulatory circuit? *Mutat. Res. Genet. Toxicol. Environ. Mutagen.* 764–765: 64–71. doi: 10.1016/j.mrgentox.2013.09.003
- Kinoshita, C., Aoyama, K., Matsumura, N., Kikuchi-Utsumi, K., Watabe, M., and Nakaki, T. (2014). Rhythmic oscillations of the microRNA miR-96-5p play a neuroprotective role by indirectly regulating glutathione levels. *Nat. Commun.* 5, 3823. doi: 10.1038/ncomms4823
- Kwak, D. J., Kwak, S. D., and Gauda, E. B. (2006). The effect of hyperoxia on reactive oxygen species (ROS) in rat petrosal ganglion neurons during development using organotypic slices. *Pediatr. Res.* 60 (4), 371–376. doi: 10.1203/01.pdr.0000239817.39407.61
- Li, Y., Zhang, D., Wang, X., Yao, X., Ye, C., Zhang, S., et al. (2015). Hypoxia-inducible miR-182 enhances HIF1 α signaling via targeting PHD2 and FIH1 in prostate cancer. *Sci. Rep.* 5, 12495. doi: 10.1038/srep12495
- Lin, H., Dai, T., Xiong, H., Zhao, X., Chen, X., Yu, C., et al. (2010). Unregulated miR-96 induces cell proliferation in human breast cancer by downregulating transcriptional factor FOXO3a. *PLoS One* 5 (12), e15797. doi: 10.1371/journal.pone.0015797
- Liu, Y., and Lu, Q. (2015). Extracellular vesicle microRNAs: biomarker discovery in various diseases based on RT-qPCR. *Biomark Med.* 9 (8), 791–805. doi: 10.2217/BMM.15.45
- Liu, C. H., Wang, Z., Huang, S., Sun, Y., and Chen, J. (2019). MicroRNA-145 regulates pathological retinal angiogenesis by suppression of TMOD3. *Mol. Ther. Nucleic Acids* 16, 335–347. doi: 10.1016/j.omtn.2019.03.001
- Ma, Y., Yang, H. Z., Dong, B. J., Zou, H. B., Zhou, Y., Kong, X. M., et al. (2014). Biphasic regulation of autophagy by miR-96 in prostate cancer cells under hypoxia. *Oncotarget* 5 (19), 9169–9182. doi: 10.18632/oncotarget.2396
- Magenta, A., Greco, S., Gaetano, C., and Martelli, F. (2013). Oxidative stress and microRNAs in vascular diseases. *Int. J. Mol. Sci.* 14 (9), 17319–17346. doi: 10.3390/ijms140917319
- Muraleedharan, C. K., McClellan, S. A., Ekanayaka, S. A., Francis, R., Zmejkoski, A., Hazlett, L. D., et al. (2019). The miR-183/96/182 cluster regulates macrophage functions in response to *Pseudomonas aeruginosa*. *J. Innate Immun.* 11 (4), 347–358. doi: 10.1159/000495472
- Niu, G., Wright, K. L., Huang, M., Song, L., Haura, E., Turkson, J., et al. (2002). Constitutive Stat3 activity up-regulates VEGF expression and tumor angiogenesis. *Oncogene* 21 (13), 2000–2008. doi: 10.1038/sj.onc.1205260
- O'Connell, R. M., Rao, D. S., Chaudhuri, A. A., and Baltimore, D. (2010). Physiological and pathological roles for microRNAs in the immune system. *Nat. Rev. Immunol.* 10 (2), 111–122. doi: 10.1038/nri2708
- Palfi, A., Hokamp, K., Hauck, S. M., Vencken, S., Millington-Ward, S., Chadderton, N., et al. (2016). microRNA regulatory circuits in a mouse model of inherited retinal degeneration. *Sci. Rep.* 6, 31431. doi: 10.1038/srep31431
- Paul, P., Chakraborty, A., Sarkar, D., Langthasa, M., Rahman, M., Bari, M., et al. (2018). Interplay between miRNAs and human diseases. *J. Cell Physiol.* 233 (3), 2007–2018. doi: 10.1002/jcp.25854
- Qiu, L., Tan, E. K., and Zeng, L. (2015). microRNAs and neurodegenerative diseases. *Adv. Exp. Med. Biol.* 888, 85–105. doi: 10.1007/978-3-31922671-2_6
- Qu, M., Pan, J., Wang, L., Zhou, P., Song, Y., Wang, S., et al. (2019). MicroRNA-126 regulates angiogenesis and neurogenesis in a mouse model of focal cerebral ischemia. *Mol. Ther. Nucleic Acids* 16, 15–25. doi: 10.1016/j.omtn.2019.02.002
- Regula, J. T., Lundh von Leithner, P., Foxton, R., Barathi, V. A., Cheung, C. M., Bo Tun, S. B., et al. (2016). Targeting key angiogenic pathways with a bispecific CrossMAB optimized for neovascular eye diseases. *EMBO Mol. Med.* 8 (11), 1265–1288. doi: 10.15252/emmm.201505889
- Rivera, J. C., Noueihed, B., Omri, S., Barrueco, J., Hilberg, F., and Chemtob, S. (2015). BIBF1120 (vargatef) inhibits preretinal neovascularization and enhances normal vascularization in a model of vasoproliferative retinopathy. *Invest. Ophthalmol. Vis. Sci.* 56 (13), 7897–7907. doi: 10.1167/iov.15-17146
- Rivera, J. C., Dabouz, R., Noueihed, B., Omri, S., Tahiri, H., and Chemtob, S. (2017a). Ischemic retinopathies: oxidative stress and inflammation. *Oxid. Med. Cell Longev.* 2017, 3940241. doi: 10.1155/2017/3940241
- Rivera, J. C., Holm, M., Austeng, D., Morken, T. S., Zhou, T. E., Beaudry-Richard, A., et al. (2017b). Retinopathy of prematurity: inflammation, choroidal degeneration, and novel promising therapeutic strategies. *J. Neuroinflammation* 14 (1), 165. doi: 10.1186/s12974-017-0943-1
- Sapieha, P., Sirinyan, M., Hamel, D., Zaniolo, K., Joyal, J. S., Cho, J. H., et al. (2008). The succinate receptor GPR91 in neurons has a major role in retinal angiogenesis. *Nat. Med.* 14 (10), 1067–1076. doi: 10.1038/nm.1873
- Sapieha, P., Joyal, J. S., Rivera, J. C., Kermorvant-Duchemin, E., Sennlaub, F., Hardy, P., et al. (2010). Retinopathy of prematurity: understanding ischemic retinal vasculopathies at an extreme of life. *J. Clin. Invest.* 120 (9), 3022–3032. doi: 10.1172/JCI42142
- Schluter, T., Berger, C., Rosengauer, E., Fieth, P., Krohs, C., Ushakov, K., et al. (2018). miR-96 is required for normal development of the auditory hindbrain. *Hum. Mol. Genet.* 27 (5), 860–874. doi: 10.1093/hmg/ddy007
- Shao, Z., Dorfman, A. L., Seshadri, S., Djavari, M., Kermorvant-Duchemin, E., Sennlaub, F., et al. (2011). Choroidal involution is a key component of oxygen-induced retinopathy. *Invest. Ophthalmol. Vis. Sci.* 52 (9), 6238–6248. doi: 10.1167/iov.10-6742
- Shao, Z., Friedlander, M., Hurst, C. G., Cui, Z., Pei, D. T., Evans, L. P., et al. (2013). Choroid sprouting assay: an ex vivo model of microvascular angiogenesis. *PLoS One* 8 (7), e69552. doi: 10.1371/journal.pone.0069552
- Shen, G., Li, X., Jia, Y. F., Piazza, G. A., and Xi, Y. (2013). Hypoxia-regulated microRNAs in human cancer. *Acta Pharmacol. Sin.* 34 (3), 336–341. doi: 10.1038/aps.2012.195
- Shi, Y., Zhao, Y., Shao, N., Ye, R., Lin, Y., Zhang, N., et al. (2017). Overexpression of microRNA-96-5p inhibits autophagy and apoptosis and enhances the proliferation, migration and invasiveness of human breast cancer cells. *Oncol. Lett.* 13 (6), 4402–4412. doi: 10.3892/ol.2017.6025
- Sonkoly, E., and Pivarcsi, A. (2009). microRNAs in inflammation. *Int. Rev. Immunol.* 28 (6), 535–561. doi: 10.3109/08830180903208303
- Wang, T. H., Yeh, C. T., Ho, J. Y., Ng, K. F., and Chen, T. C. (2016). OncomiR miR-96 and miR-182 promote cell proliferation and invasion through targeting ephrinA5 in hepatocellular carcinoma. *Mol. Carcinog.* 55 (4), 366–375. doi: 10.1002/mc.22286
- Wang, Y., Wu, S., Yang, Y., Peng, F., Li, Q., Tian, P., et al. (2017). Differentially expressed miRNAs in oxygen-induced retinopathy newborn mouse models. *Mol. Med. Rep.* 15 (1), 146–152. doi: 10.3892/mmr.2016.5993
- Wu, J. H., Gao, Y., Ren, A. J., Zhao, S. H., Zhong, M., Peng, Y. J., et al. (2012). Altered microRNA expression profiles in retinas with diabetic retinopathy. *Ophthalmic Res.* 47 (4), 195–201. doi: 10.1159/000331992
- Wu, W. C., Shih, C. P., Wang, N. K., Lien, R., Chen, Y. P., Chao, A. N., et al. (2013). Choroidal thickness in patients with a history of retinopathy of prematurity. *JAMA Ophthalmol.* 131 (11), 1451–1458. doi: 10.1001/jamaophthalmol.2013.5052
- Xiang, L., Chen, X. J., Wu, K. C., Zhang, C. J., Zhou, G. H., Lv, J. N., et al. (2017). miR-183/96 plays a pivotal regulatory role in mouse photoreceptor maturation and maintenance. *Proc. Natl. Acad. Sci. U. S. A.* 114 (24), 6376–6381. doi: 10.1073/pnas.1618757114
- Yang, Z. M., Chen, L. H., Hong, M., Chen, Y. Y., Yang, X. R., Tang, S. M., et al. (2017). Serum microRNA profiling and bioinformatics analysis of patients with type 2 diabetes mellitus in a Chinese population. *Mol. Med. Rep.* 15 (4), 2143–2153. doi: 10.3892/mmr.2017.6239
- Yuan, T., Wang, Y., Zhao, Z. J., and Gu, H. (2010). Protein-tyrosine phosphatase PTPN9 negatively regulates ErbB2 and epidermal growth factor receptor signaling in breast cancer cells. *J. Biol. Chem.* 285 (20), 14861–14870. doi: 10.1074/jbc.M109.099879

- Zhou, T. E., Rivera, J. C., Bhosle, V. K., Lahaie, I., Shao, Z., Tahiri, H., et al. (2016). Choroidal involution is associated with a progressive degeneration of the outer retinal function in a model of retinopathy of prematurity: early role for IL-1beta. *Am. J. Pathol.* 186 (12), 3100–3116. doi: 10.1016/j.ajpath.2016.08.004
- Zhou, S. S., Jin, J. P., Wang, J. Q., Zhang, Z. G., Freedman, J. H., Zheng, Y., et al. (2018). miRNAs in cardiovascular diseases: potential biomarkers, therapeutic targets and challenges. *Acta Pharmacol. Sin.* 39 (7), 1073–1084. doi: 10.1038/aps.2018.30
- Zhou, T. E., Zhu, T., Rivera, J. C., Omri, S., Tahiri, H., Lahaie, I., et al. (2019). The inability of the choroid to revascularize in oxygen-induced retinopathy results from increased p53/miR-Let-7b activity. *Am. J. Pathol.* 189 (11), 2340–2356. doi: 10.1016/j.ajpath.2019.07.009

Conflict of Interest: The authors declare that the research was conducted in the absence of any commercial or financial relationships that could be construed as a potential conflict of interest.

Copyright © 2020 Desjarlais, Wirth, Rivera, Lahaie, Dabouz, Omri, Ruknudin, Borrás and Chemtob. This is an open-access article distributed under the terms of the Creative Commons Attribution License (CC BY). The use, distribution or reproduction in other forums is permitted, provided the original author(s) and the copyright owner(s) are credited and that the original publication in this journal is cited, in accordance with accepted academic practice. No use, distribution or reproduction is permitted which does not comply with these terms.



High Glucose-Induced TRPC6 Channel Activation Decreases Glutamate Uptake in Rat Retinal Müller Cells

Mingming Ma^{1,2,3,4,5†}, Shuzhi Zhao^{1,2,3,4,5†}, Jian Zhang^{1,2,3,4,5}, Tao Sun^{1,2,3,4,5}, Ying Fan^{1,2,3,4,5*} and Zhi Zheng^{1,2,3,4,5*}

OPEN ACCESS

Edited by:

Zhongxiao Wang,
Harvard Medical School,
United States

Reviewed by:

Junwei Huang,
AbbVie, United States
Xiaomei Liu,
ShengJing Hospital of China
Medical University, China

*Correspondence:

Zhi Zheng
zhengzhi139@163.com
Ying Fan
mdfanying@sjtu.edu.cn

[†]These authors have contributed
equally to this work

Specialty section:

This article was submitted to
Neuropharmacology,
a section of the journal
Frontiers in Pharmacology

Received: 16 September 2019

Accepted: 20 December 2019

Published: 14 February 2020

Citation:

Ma M, Zhao S, Zhang J, Sun T,
Fan Y and Zheng Z (2020) High
Glucose-Induced TRPC6 Channel
Activation Decreases Glutamate
Uptake in Rat Retinal Müller Cells.
Front. Pharmacol. 10:1668.
doi: 10.3389/fphar.2019.01668

¹ Department of Ophthalmology, Shanghai General Hospital, Shanghai, China, ² National Clinical Research Center for Eye Diseases, Shanghai, China, ³ Shanghai Key Laboratory of Ocular Fundus Diseases, Shanghai Jiao Tong University, Shanghai, China, ⁴ Shanghai Engineering Center for Visual Science and Photomedicine, Shanghai General Hospital, Shanghai Jiao Tong University, Shanghai, China, ⁵ Shanghai Engineering Center for Precise Diagnosis and Treatment of Eye Diseases, Shanghai, China

High glucose (HG) increases the production of reactive oxygen species (ROS), leading to decreased glutamate uptake in Müller cells. The transient receptor potential cation channel 6 (TRPC6) channel, an oxidative stress-sensitive Ca^{2+} -permeable cationic channel, is readily detected in Müller cells and highly expressed under HG conditions. Yet, the effect of high glucose-induced TRPC6 channel activation in Müller cells is poorly understood. We hypothesized that TRPC6 channel activation mediates high glucose-induced decreases in Müller cell glutamate uptake. We found RNA interference (RNAi) of the TRPC6 channel abolished HG-induced decreases in glutamate uptake and cell death. HG also decreased the expression of the glutamate-aspartate transporter (GLAST), which is the most important transporter involved in glutamate uptake. The mRNA level of ciliary neurotrophic factor (CNTF) in rMC-1 cells and the release of CNTF in the culture media was decreased, but the mRNA levels of IL-6 and vascular endothelial growth factor (VEGF) were increased under HG conditions. After RNAi silencing in rMC-1 cells, the mRNA levels of CNTF increased, but IL-6 and VEGF levels decreased. Furthermore, TRPC6 knockdown (KD) decreased expression of glial fibrillary acidic protein (GFAP) and increased expression of Kir4.1, pointing to inhibition of HG-induced gliosis in rMC-1 cells. ROS and intracellular Ca^{2+} levels decreased after TRPC6 knockdown. Exposure to Hyp9 (10 μM), a highly selective TRPC6 channel agonist, can aggravate HG-induced pathological changes. Collectively, our results suggest TRPC6 channel activation is involved in HG-induced decreases in glutamate uptake in rMC-1 cells. These findings provide novel insights into the role of TRPC6 in HG-induced retinal neurovasculopathy and suggest TRPC6 is a promising target for drug development for diabetic retinopathy (DR).

Keywords: TRPC6 channel, diabetic retinopathy, Müller cells, glutamate uptake, reactive oxygen species

INTRODUCTION

Diabetic retinopathy (DR) is a leading cause of blindness in working-aged populations in developed countries and is traditionally regarded as a disorder of the retinal vessels. However, recent evidence demonstrates the pathogenesis of DR includes not only vascular changes, but also neuronal damage (Puro, 2002). It is becoming clear that changes in neuronal function and viability occur before blood-retina barrier (BRB) abnormalities in patients with diabetes and in diabetic animals (Martin et al., 2004; Barber et al., 1998). Unfortunately, the molecular and cellular mechanisms involved in the alteration and survival of retinal neurons in DR are poorly understood.

Retinas exposed to high glucose experience oxidative stress due to the increased production of reactive oxygen species (ROS), which is a key contributor to DR development (Lowell and Shulman, 2005). ROS target various mechanisms that contribute to DR, among which impairment of the glutamate-aspartate transporter (GLAST) in Müller cells has emerged as an important disease mechanism (Li and Puro, 2002). The GLAST is the only glial-type glutamate transporter in the retina (Harada et al., 1998). Therefore, glutamate clearance in the retina is mainly regulated by Müller cells. Glutamate is the major retinal excitatory neurotransmitter and is toxic when present at high concentrations, ultimately resulting in neurodegeneration (Sucher et al., 1997). Low extracellular glutamate levels in the retina are only possible with normally functioning Müller cells, which transport glutamate into cells through the GLAST on the cell membrane. It is clear diabetes-induced neuronal excitotoxicity damage is caused by excessive glutamate levels, which are typically the result of high levels of ROS in Müller cells (Puro, 2002; Jadhav et al., 2009). Some studies have shown reducing ROS production through the use of some antioxidants, such as superoxide dismutase (SOD), green tea, and taurine, can rescue the activity of the GLAST in Müller cells under HG conditions (Zeng et al., 2010; Silva et al., 2013). It is clear ROS generation is intracellular- Ca^{2+} dependent, and blocking Ca^{2+} influx can reduce the production of ROS (Yang et al., 2011).

The transient receptor potential canonical (TRPC) family (TRPC1–TRPC7) contributes to calcium influx, which is involved in the regulation of cell proliferation, differentiation, and various physiological functions (Pedersen et al., 2005). In particular, TRPC6 is one of the most extensively analyzed TRPC channels; its expression and function have been investigated in the retina, central nervous system, kidneys, and cardiovascular system (Onohara et al., 2006; Tai et al., 2008; Sachdeva et al., 2018). One study showed that TRPC6 expression levels were significantly higher in the retina of diabetic mice compared to normal mice, indicating an upregulation of TRPC6 transcripts under diabetic conditions, which was considered a response to the oxidative stress present under HG conditions (Sachdeva et al., 2018). At the cellular level, the TRPC6 channel has been identified in Müller cells (Da Silva et al., 2008), monocytes (Wuensch et al., 2010), platelets (Liu et al., 2008), podocytes (Yang et al., 2013), and hippocampal neurons (Liu et al., 2017). The ubiquitous distribution of TRPC6 indicates it may play roles in a wide range of physiological processes. TRPC6 activation contributes to the disease state, which is highlighted by the rescue of oxidative stress-induced

dysfunction via TRPC6 channel inhibition (Liu et al., 2017). Inhibition of the TRPC6 channel in THP-1 cells can reduce the production of ROS under HG conditions (Li et al., 2019). However, functional studies investigating the channel have not been performed in Müller cells. Müller cells, spanning the whole retina from the inner limiting membrane to the outer limiting membrane, are the predominant macroglia and retinal-supporting cells. Their structural characteristics make Müller cells ideal cellular regulators of physiological and pathological responses in the retinal vasculature and neurons (Reichenbach and Bringmann, 2013). Thus, the effect and mechanism by which TRPC6 channels function in Müller cells under HG conditions need to be investigated.

Here, we hypothesized that the TRPC6 channel mediates decreased glutamate uptake in Müller cells, because TRPC6 channel activation increases intracellular Ca^{2+} concentrations, which is required for ROS generation. To address our hypothesis, we selected rat Müller cells (rMC-1), which are known to express TRPC6. The levels of TRPC6, GLAST, Kir 4.1, and GFAP in rMC-1 cells under HG conditions were analyzed by Western blotting. Glutamate uptake assays were used to determine the activity of the GLAST. Cell viability was assayed by CCK-8 assays. Cell apoptosis was evaluated by TUNEL assays and caspase-3 activity. Intracellular ROS levels were measured using the CM-H₂DCFDA assay. A cell-based fluorometric assay was used to measure intracellular Ca^{2+} concentrations in rMC-1 cells loaded with a fluorescent Ca^{2+} indicator. The release of CNTF, IL-6, and VEGF from rMC-1 cells, and the mRNA levels of CNTF, IL-6, and VEGF in rMC-1 cells were evaluated by ELISA and qRT-PCR.

MATERIALS AND METHODS

Cell Culture and TRPC6 siRNA Transfection

A rat Müller cell line (rMC-1) was purchased from Kerfast Inc. (Boston, MA). Cells were cultured in DMEM media plus 10% fetal bovine serum and 1% penicillin streptomycin and maintained at 37°C in a humidified 5% CO_2 atmosphere. The medium was changed every 48 h. Cells cultured in 5 mmol/L glucose served as the control. Cells cultured in 25 mmol/L glucose represented the high glucose (HG) condition. rMC-1 cells grown in mannitol (20 mmol/L) served as the osmotic control. rMC-1 cells were used within passages 10 to 20.

To knock down the expression of TRPC6, we transfected the rMC-1 cells with siRNA, specifically targeting rat TRPC6 (sense, 5'-CAUACAUGUUAAUGAUCAtt-3', antisense, 5'-UGAUCAUUAAACAUGUAUGct-3') or negative control (NC) siRNA (sense, 5'-UUCUCCGAACGUGUCACGUTT-30, and antisense, 50-ACGUGACACGUUCGGAGAATT-3'). The oligonucleotides were mixed with the Lipofectamine RNAiMAX Transfection Reagent (Life Technologies, Grand Island, NY, USA) according to the manufacturer's protocol. After rMC-1 cells were grown to 50% confluency in different plates, cells were transfected. Media was replaced with HG media 7 h after transfection, and incubation continued for 48 h.

Analysis of Cell Viability

The viability of rMC-1 cells was evaluated by CCK-8 assays using a microplate reader. Briefly, rMC-1 cells were seeded in 96-well plates at a density of 10×10^3 cells/well and cultured for 48 h. Then, cells were incubated in DMEM in the presence or absence of high glucose combined with or without Hyp9 (5 and 10 μ M) for 48 h. Subsequently, the cells were incubated with the CCK-8 reagent for 2 h at 37°C. Finally, the optical density at 490 nm was measured with a microplate reader (Bio-Tek, Inc., Winooski, VT, USA). Measurements of each of these conditions were repeated three times in the same plate.

Enzyme-Linked Immunosorbent Assays (ELISAs)

Cells in 96-well plates were incubated in 50 μ l culture media with or without HG for 48 h, and the culture supernatants were collected. The concentrations of CNTF, VEGF, and IL-6 were determined by enzyme-linked immunosorbent assays (ELISAs) kits (R&D Systems, Minneapolis, MN, USA), according to the manufacturer's instructions.

Quantitative Real-Time PCR Analysis (qRT-PCR)

Total RNA was extracted from cultured rMC-1 cells using TRIzol (Life Technologies Inc., Gaithersburg, USA) according to the manufacturer's protocol. mRNA levels of CNTF, VEGF, and IL-6 were quantified by qRT-PCR. The sequences of the primers were as follows: CNTF (NCBI RefSeq NM_013166.1), F 5'-CGACTCCAAGAGAACCTCCA-3' and R 5'-CCTTCAGTTGGGGTGAATG-3', IL-6 (NCBI RefSeq NM_012589.2), F 5'-TCCTACCCCAACTTCCAATGCTC-3' and R 5'-TTGGATGGTCTTGGTCCTTAGCC-3', VEGF (NCBI RefSeq NM_031836.3), F 5'-GCACCCACGACAGAAGG-3' and R 5'-TGAACGCTCCAGGATTTA-3', β -actin (NCBI RefSeq NM_031144.3), F 5'-CACTGCCGATCCTCTTCCTC-3' and R 5'-TGCTGTGCGCTTCACCGTTCC-3'. β -actin served as the internal control. CNTF, VEGF, and IL-6 mRNA levels were normalized to β -actin levels, which served as the endogenous control to ensure equal starting amounts of cDNA. The control group was set as the calibrator with a value of 1, and the other groups were compared to this calibrator.

Western Blot Analyses

rMC-1 cells, treated as described previously, were homogenized in lysis buffer (0.05 M Tris-HCl, pH 7.4, 0.15 M NaCl, 0.25% deoxycholic acid, 1% NP-40, 1 mM EDTA). The protein samples were separated by SDS-PAGE and electroblotted onto a polyvinylidene fluoride membrane (Millipore, Bedford, MA, USA). After being blocked in 4% skim milk, the membrane was incubated at 4°C overnight with rabbit anti-TRPC6 (1:500; Abcam, Shatin, Hong Kong), rabbit anti-GLAST (1:500; Abcam, Shatin, Hong Kong), rabbit anti-Kir4.1 (1:1,000; Abcam, Shatin, Hong Kong), and rabbit anti-GFAP (1:5,000; Abcam, Shatin, Hong Kong) antibodies. Anti- β -actin (1:1,000 dilution, Cell Signaling Technology, Beverly, MA, US) was used as a loading control. The

intensity of the bands was quantified by densitometry using Image J software (NIH, USA).

Immunohistochemistry and Transferase-Mediated dUTP Nick-End Labeling Staining

To detect individual apoptotic cells, staining for transferase-mediated dUTP nick-end labeling staining (TUNEL) was carried out using a DeadEnd™ fluorometric TUNEL system kit (Promega, Madison, WI, US) according to the manufacturer's instructions. Cell nuclei were counterstained with DAPI (1 μ g/ml; Beyotime Institute of Biotechnology, Jiangsu, China). Samples were observed under a confocal laser scanning microscope (Zeiss LSM510; Carl Zeiss, Thornwood, NY). The numbers of total and TUNEL-positive nuclei were counted and analyzed using ImageJ/Imaris software.

Intracellular Ca²⁺ Measurements

Intracellular Ca²⁺ levels were quantitatively determined by Fluo3/AM fluorescence. rMC-1 cells were incubated with the Ca²⁺ indicator (Fluo3-AM; 10 μ M) for 0.5 h at 37°C in the dark, after which rMC-1 cells were washed twice to remove excess stain. Finally, the FLUO3-dependent fluorescence was determined by a FACScan at 488-nm excitation and 530-nm emission wavelengths.

Measurement of Intracellular ROS Generation

rMC-1 cells prepared with different treatments as described above were seeded in 96-well plates and grown to 85% confluence. The generation of intracellular ROS was detected by the dichlorodihydrofluorescein (DCF) method using 5-(and-6)-carboxy-2',7'-dichlorodihydrofluorescein diacetate (carboxy-H2DCFDA). The cells were gently washed with PBS and incubated with 3 μ M carboxy-H2DCFDA in phenol red-free medium at 37°C for 30 min. Cells were washed with and maintained in SBS before images were captured using a cell imaging system. Image J software was used for analysis of fluorescent intensity.

Glutamate Uptake Assay

rMC-1 cells were cultured in 24 well plates. The culture medium was removed, and the cells were incubated with medium containing mannitol and 5 mmol/L glucose or 25 mmol/L glucose for 24 h at 37°C. To determine the glutamate uptake capacity in rMC-1 cells after pretreatment, the cells were washed and incubated for 30 min in Krebs's solution containing 119 mM NaCl, 2.5 mM CaCl₂, 4.7 mM KCl, 1.0 mM MgCl₂, and 1.2 mM KH₂PO₄. Then, rMC-1 cells were exposed to 10 mmol/l unlabeled glutamate and 0.5 μ Ci/ml of L-[2,3-³H] glutamate (New England Nuclear, Boston, MA, USA) for 60 min. L-glutamate uptake was terminated by rapid removal of the incubation buffer, and the cells were washed twice with ice-cold PBS. rMC-1 cells were subsequently lysed, and small aliquots were removed from each well for the determination of protein content. L-[2,3-³H]-glutamate content was determined by scintillation counting.

Detection of Activated Caspase-3

The enzymatic activity of the caspase-3 class of proteases in rMC-1 cells was measured by a caspase-3 colorimetric assay kit (Promega, Madison, WI, USA) as previously described (Ma et al., 2018). The cleavage of a caspase-3 colorimetric substrate (DEVD-pNA) was measured at 405 nm using a microplate reader (Auto Bio Labtech Instruments, Co, Ltd, China).

Data Analysis

All experiments were performed at least three times, and the values were presented as mean \pm SD; statistical significance was assessed using two-tailed Student's *t* test or one-way ANOVA, followed by Tukey's *post hoc* test. *P* values are indicated with *, **, and ***, which correspond to values of 0.05, 0.01, and 0.001, respectively.

RESULTS

Effects of the TRPC6 Channel on Müller Cell Glutamate Uptake

The glutamate uptake assay showed that TRPC6 silencing (Supplementary Figure 1) could ameliorate glutamate uptake activity in retinal Müller cells under HG conditions. Exposure to 10 μ M Hyp9 reduced glutamate uptake activity under HG conditions (Figure 1).

The synaptic glutamate levels in the retina are mainly regulated by the GLAST in Müller cells. DR caused downregulation of the inwardly rectifying potassium channel Kir4.1, possibly resulting in dysfunction of the GLAST (Napper et al., 1999). To determine the effect of TRPC6 channel activation on the expression of the GLAST and Kir 4.1, Western blot analysis was performed. We determined GLAST and Kir4.1 expression in Müller cells decreased under HG conditions (Figure 2). TRPC6 knockdown increased GLAST and Kir 4.1 expression significantly (Figures 2 and 6).

Effect of the TRPC6 Channel on HG-Induced Müller Cell Viability and Apoptosis

To evaluate the influence of the TRPC6 channel on Müller cell viability, CCK-8 assays were used. Our results from three independent experiments are summarized in Figure 3. rMC-1 cells showed high cell viability under HG conditions after TRPC6 knockdown. Exposure to Hyp9 resulted in a concentration-dependent reduction in cell viability.

Consistent with previous reports, HG caused extensive cell apoptosis. In contrast, cells exposed to normal glucose concentrations or normal glucose plus mannitol (to exclude potential osmotic effects caused by excess glucose) underwent apoptosis at a much lower rate. HG caused significant cell apoptosis and increases in caspase-3 activity (Figure 5D). TRPC6 knockdown prevented cell apoptosis and decreased cellular caspase-3 activity (Figures 4 and 5C). These data indicate the TRPC6 channel plays a key role in HG-induced cell apoptosis.

Effect of the TRPC6 Channel on ROS Generation in Müller Cells

To examine the effects of the TRPC6 channel on Ca^{2+} concentrations in Müller cells, cells were loaded with a

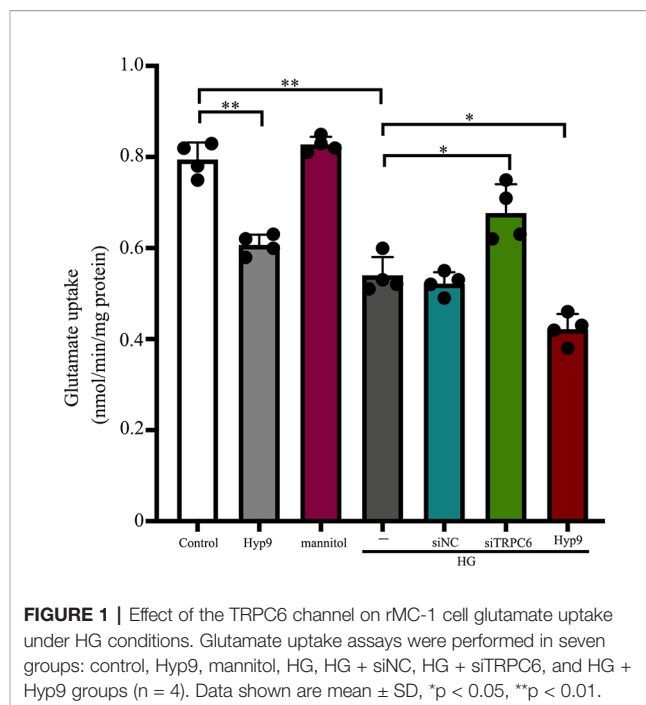


FIGURE 1 | Effect of the TRPC6 channel on rMC-1 cell glutamate uptake under HG conditions. Glutamate uptake assays were performed in seven groups: control, Hyp9, mannitol, HG, HG + siNC, HG + siTRPC6, and HG + Hyp9 groups (*n* = 4). Data shown are mean \pm SD, **p* < 0.05, ***p* < 0.01.

fluorescent Ca^{2+} indicator dye, and the fluorescence ratio (F420/F480) was measured after excitation at 420 and 480 nm and served as a direct index of Ca^{2+} concentration. As shown in Figure 5A, HG increased the Ca^{2+} concentration in normal cells, but TRPC6 knockdown significantly decreased Ca^{2+} concentrations.

Previous studies have shown that Ca^{2+} signaling is required for ROS production (Duan et al., 2007). As ROS are involved in apoptosis and glutamate excitotoxicity (Flora et al., 2007), ROS production due to HG conditions was studied using the ROS-sensitive fluorescent dye CM- H_2DCFDA . As shown in Figure 5B, HG promoted intracellular ROS accumulation in normal cells, but decreased concentrations in TRPC6 knockdown cells. Application of Hyp9 increased ROS accumulation under HG conditions in normal cells.

Effect of the TRPC6 Channel on HG-Induced Müller Cell Gliosis

The gliosis of Müller cells is characterized by an upregulation of the immunoreactivity against intermediate filament constituents vimentin and GFAP. GFAP protein was used as a key marker of Müller cell gliosis under HG conditions. The GFAP protein level in the HG group was higher than in the normal control group (Figure 2). TRPC6 knockdown significantly decreased the protein levels of GFAP under HG conditions (Figure 6).

Effect of the TRPC6 Channel on CNTF, IL-6, and VEGF Levels in Müller Cells and Supernatants

We sought to examine the effects of TRPC6 knockdown on the mRNA expression and release of CNTF, IL-6, and VEGF in rMC-1 cells using an RNAi approach to reduce TRPC6 levels.

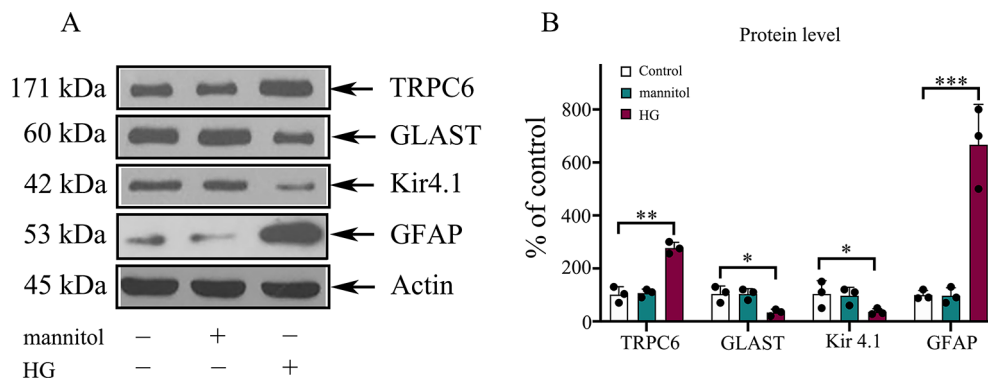


FIGURE 2 | The protein levels of GLAST, Kir4.1, and GFAP in rMC-1 cells under HG conditions. **(A)** Western blotting was used for TRPC6, GLAST, Kir4.1, GFAP, and actin in rMC-1 cells under HG conditions. **(B)** Densitometric analyses of TRPC6, GLAST, Kir4.1, and GFAP protein levels were standardized against actin protein levels. Data are expressed as mean \pm SD; $n = 3$ for each group; * $p < 0.05$, ** $p < 0.01$, *** $p < 0.001$.

HG treatment resulted in low mRNA expression and release of CNTF in or from rMC-1 cells (**Figures 7B and E**), but high levels of IL-6 (**Figures 7A and D**) and VEGF (**Figures 7C and F**). TRPC6 knockdown increased the mRNA expression and release of CNTF in or from rMC-1 cells and decreased the levels of IL-6 and VEGF. Exposure to 10 μ M Hyp9 under HG conditions enhanced the effects of HG-induced changes (**Figure 7**).

DISCUSSION

Hyperglycemia is a major risk factor for various human diseases. Multiple studies have reported that the excitotoxicity caused by elevated glutamate in the extracellular space in experimental models of diabetes plays an important role in the pathophysiology of DR (Lieth et al., 1998; Lieth et al., 2000; Kowluru et al., 2001). Our results indicate Müller cells treated with 25 mM glucose exhibit decreased glutamate uptake activity

because of decreased expression of the GLAST. The GLAST in Müller cells is mainly responsible for maintaining low synaptic glutamate levels in the retina. Significant decreases in glutamate transport mediated *via* the GLAST in Müller cells begins after just 4 weeks in diabetic rat models (Puro, 2002), which is consistent with reports showing significantly increased glutamate accumulation in diabetic rat retinas (Lieth et al., 1998; Lieth et al., 2000). Although the mechanism of dysfunction of the GLAST in Müller cells under HG remains unknown, Li et al. suggested that the dysfunction of GLAST is mainly caused by increased ROS levels (Li and Puro, 2002). In our study, inhibiting the generation of ROS under HG conditions by downregulating the TRPC6 channel enhanced the expression of the GLAST and improved the glutamate uptake activity of Müller cells under HG conditions. Some other studies showed that pro-inflammatory cytokines, such as IL-6 and TNF α , which trigger astrocyte activation, can cause a reduction in excitatory amino acid transporter (EAAT) expression. Activation of NF κ B

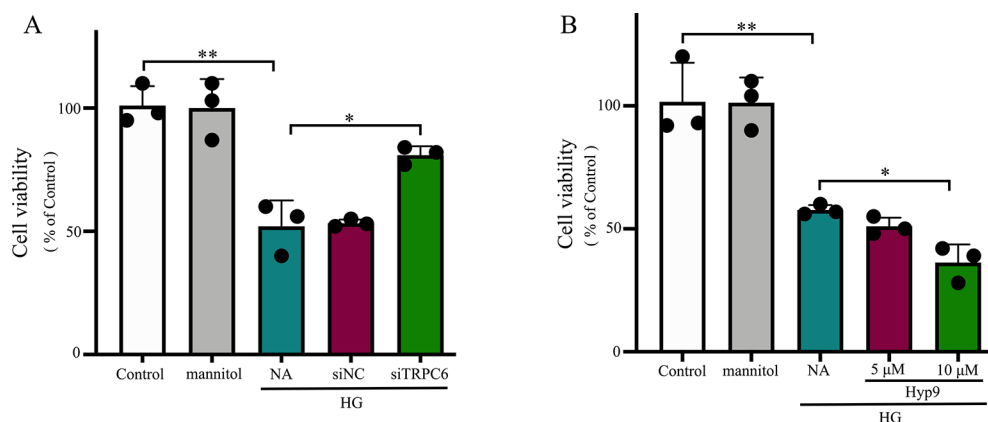


FIGURE 3 | The effect of the TRPC6 channel on rMC-1 cell viability under HG conditions. **(A)** Decreasing TRPC6 expression in rMC-1 cell prevents HG-induced reductions in cell viability. **(B)** rMC-1 cells were treated with different concentrations (5 and 10 μ M) of Hyp9. Activation of the TRPC6 channel by Hyp9 reduced cell viability, which was concentration dependent. The data are expressed as mean \pm SD, as a percentage of control; $n = 3$ for each group; * $p < 0.05$, ** $p < 0.01$.

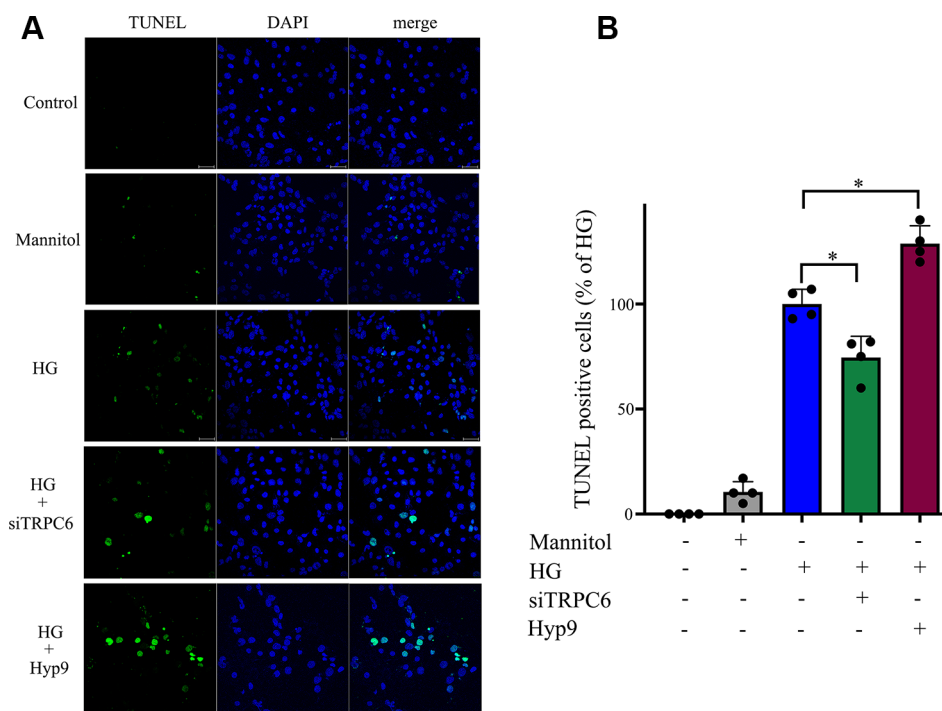


FIGURE 4 | HG-induced rMC-1 cell apoptosis was inhibited by silencing TRPC6. TUNEL assays were used to detect cell apoptosis in rMC-1 cells. **(A)** The green staining cells under HG conditions were found. **(B)** The percentage of TUNEL positive cells compared with the HG group. The HG group was set as 100%. The data are expressed as mean \pm SD; $n = 3$ for each group; * $p < 0.05$.

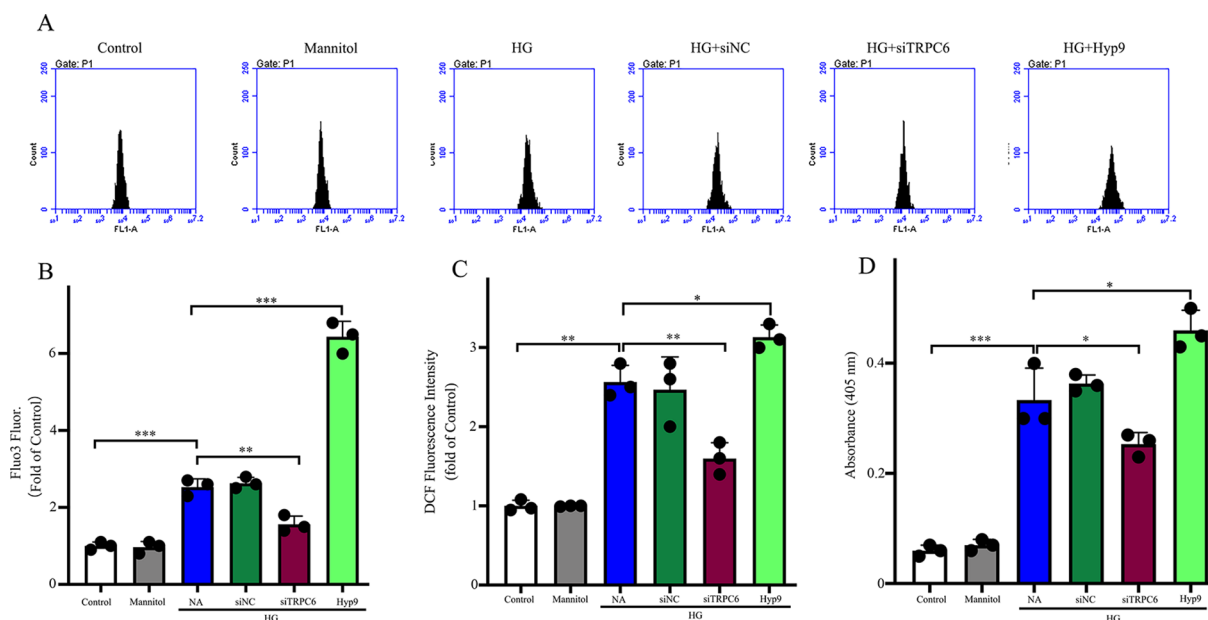


FIGURE 5 | The effect of the TRPC6 channel on intracellular Ca^{2+} concentrations, ROS generation, and caspase-3 activity under HG conditions. **(A)** Representative images showing Fluo3 fluorescence as a function of cytosolic free Ca^{2+} in rMC-1 cells in different groups. **(B)** Densitometric analyses between different groups in **(A)**. **(C)** Generation of intracellular ROS was detected by the DCF method using carboxy-H₂DCFDA. ROS production was inhibited by TRPC6 knockdown. **(D)** The high caspase-3 activities in rMC-1 cells under HG conditions were prevented by TRPC6 knockdown. The data are expressed as mean \pm SD; $n = 3$ for each group; * $p < 0.05$, ** $p < 0.01$, *** $p < 0.001$.

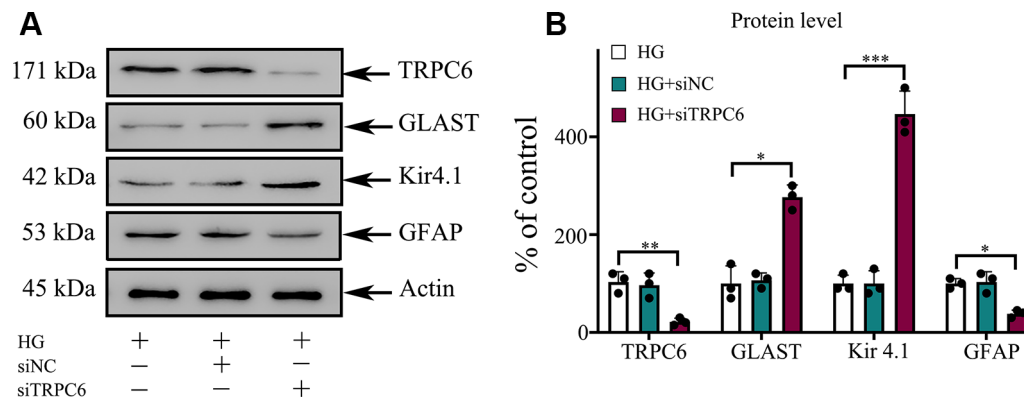


FIGURE 6 | TRPC6 knockdown enhanced the protein content of GLAST and Kir4.1, but decreased the protein content of GFAP in rMC-1 cells under HG conditions. **(A)** Western blotting was used for TRPC6, GLAST, Kir4.1, GFAP, and actin in rMC-1 cells. **(B)** Densitometric analyses of TRPC6, GLAST, Kir4.1, and GFAP protein levels were standardized against actin protein levels. The data are expressed as mean \pm SD, with the mean values for control set at 100%; $n = 3$ for each group; * $p < 0.05$, ** $p < 0.01$, *** $p < 0.001$.

suppresses the transcription of EAATs. Loss of EAAT protein is associated with reduced glutamate uptake (Furman and Norris, 2014). In this study, we found that the level of IL-6 under HG condition decreased with TRPC6 knockdown. However, whether the NF κ B pathway is involved in glutamate uptake is unknown and requires further research.

The Kir4.1 channel is the major inwardly rectifying channel in Müller cells and is widely thought to support K⁺ and glutamate uptake by Müller cells (Pannicke et al., 2006). Downregulation of the Kir4.1 channel when exposed to oxidative stress leads to an imbalance in K⁺ concentration, abnormal membrane depolarization, and subsequent swelling

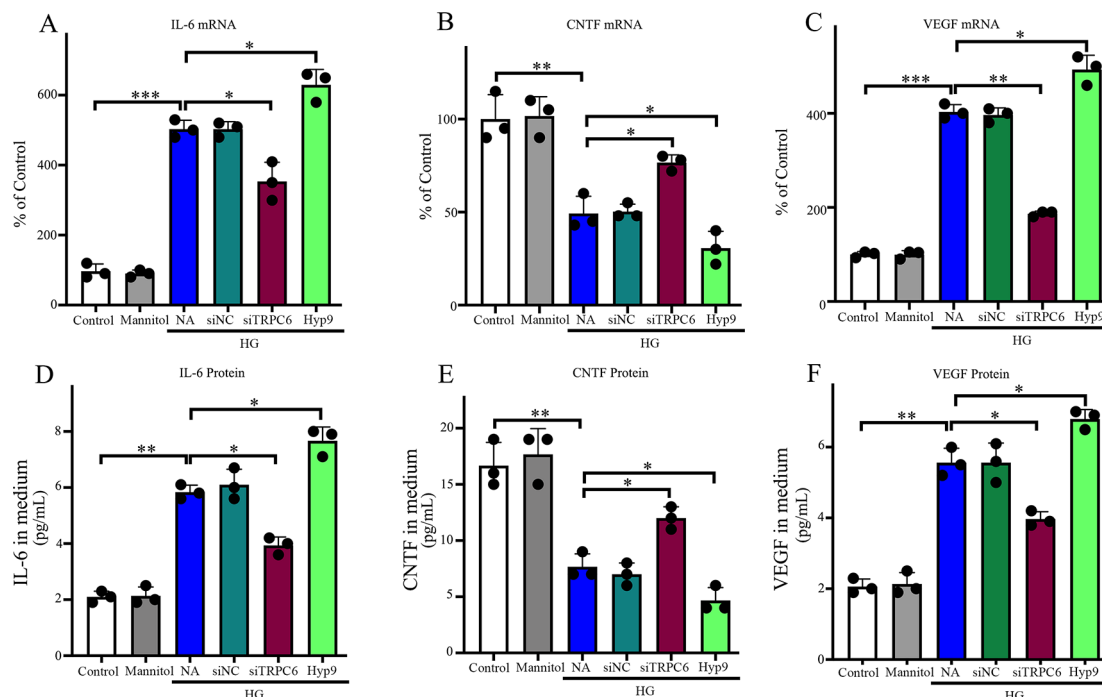


FIGURE 7 | Effect of the TRPC6 channel on IL-6, CNTF, and VEGF expression and production in rMC-1 cells under normal glucose or HG conditions. The protein levels of IL-6 **(D)**, CNTF **(E)**, and VEGF **(F)** secreted by rMC-1 in the medium were quantified by ELISA. mRNA levels of IL-6 **(A)**, CNTF **(B)**, and VEGF **(C)** were determined by real-time PCR, and their values were standardized to β -actin mRNA levels in the same RNA sample. The data are expressed as mean \pm SD; $n = 3$ for each group; * $p < 0.05$, ** $p < 0.01$, *** $p < 0.001$.

of Müller cells contributing to Müller cell dysfunction, resulting in gliosis and dysfunction of the GLAST, neuronal excitation, glutamate toxicity, and neuronal death (Francke et al., 2001; Pannicke et al., 2004; Olsen and Sontheimer, 2008). In our study, the Kir4.1 channel expression level decreased under HG conditions, GLAST expression levels decreased, and glutamate uptake was compromised simultaneously, which was consistent with previous studies.

The activity of Müller cells in response to oxidative stress may have cytoprotective properties in the early stages after damage and can be neuroprotective. However, this reaction can lead to a greater level of response described as gliosis, presenting as high levels of GFAP, which is detrimental to retinal tissue and exacerbates neuronal death, resulting in an increase in the retinal and vitreal levels of inflammatory factors, such as IL-6, while also decreasing levels of neuroprotective factors, such as CNTF (Bringmann et al., 2009). Some evidence indicates neuronal cell death is induced by the gliosis of Müller cells *via* the synthesis and secretion of inflammatory and neuroprotein factors. High IL-6 and decreased CNTF levels have been shown to contribute to retinal degeneration and neurodegeneration in DR (Bringmann et al., 2006; Bringmann et al., 2009). Furthermore, IL-6 has been found to be associated with vascular dysfunction and the promotion of angiogenesis, which suggest IL-6 may be a promising new therapeutic target to prevent diabetes-induced vascular damage (Rojas et al., 2010). In this study, we found the contents of CNTF secreted by Müller cells decreased under HG conditions. Knockdown of TRPC6 enhanced the secretion of CNTF and activation of TRPC6, while Hyp9 decreased the CNTF content. The opposite results were detected in the IL-6 content in the medium and expression of GFAP in Müller cells. The results showed that TRPC6 KD can prevent the gliosis of Müller cells and may provide a neuroprotective external environment for neurons in the retina.

Studies have suggested DR is a neurovascular disease of the retina, and the relationship between the excitotoxicity mediated by glutamate and the breakdown of the blood-retinal barrier (BRB) induced by VEGF is an interesting pathway linked to neurodegeneration with vascular impairment. Müller cells can produce many vasoactive growth factors. VEGF, a potent angiogenic and permeability growth factor, is known to be an important cause of BRB breakdown during the development and progression of retinal vascular diseases. It has been demonstrated that hyperglycemia induces an increase in extracellular glutamate levels in Müller cells, and subsequently, increased VEGF production and BRB breakdown was detected (Kusari et al., 2010; Shen et al., 2010). In this study, we have presented evidence that enhanced secretion of VEGF from Müller cells under HG conditions decreased with levels of extracellular glutamate, which were inhibited by silencing TRPC6. Application of Hyp9 increased the secretion of VEGF. Further study is warranted to establish whether TRPC6 KD can prevent BRB breakdown in DR.

Studies indicate Müller cells respond to oxidative stress and begin to die as DR progresses. Müller cells in the diabetic retina

show roughly 15% cell death after 7 months (Feenstra et al., 2013). The death of Müller cells in the diabetic retina is associated with decreases in protective growth factors (Fu et al., 2015). Müller cells participate in the establishment of the BRB, which is comprised of the tight junctions between vascular endothelial cells and pericytes (Bringmann et al., 2006). The loss of Müller cells in diabetes has also been associated with aneurysm formation, a clinical characteristic of DR (Hori and Mukai, 1980). The consequences of Müller cell death promote the loss of retinal blood barrier integrity and increase vascular permeability. However, the mechanism by which Müller cells die is not clear. In this study, the decreased cell viability of Müller cells under HG conditions was inhibited by TRPC6 knockdown. The cell viability decreased after application of Hyp9, which was concentration dependent. The apoptosis of Müller cells under HG conditions was caspase 3-dependent, and silencing TRPC6 reduced cell death and the activity of caspase 3. These results indicate the TRPC6 channel is involved in Müller cell death induced by HG.

In summary, we described the high expression of TRPC6 in retinal Müller cells under high glucose conditions and downregulation of TRPC6 expression could enhance GLAST expression and improve glutamate uptake. Decreased intracellular Ca^{2+} concentrations caused by downregulating TRPC6 expression can decrease the production of ROS. Furthermore, silencing TRPC6 under HG conditions prevented the apoptosis of Müller cells and reduced the secretion of IL-6 and VEGF from Müller cells, while increasing CNTF expression. Our results suggest the TRPC6 channel may play a key role in the pathophysiology of DR, and downregulation of the channel may act as an antioxidative agent against neurovascular changes in retinal Müller cells in DR by decreasing intracellular Ca^{2+} concentrations. Thus, this evidence suggests TRPC6 may be a promising target for further research and therapeutic development in DR.

DATA AVAILABILITY STATEMENT

The raw data supporting the conclusions of this manuscript will be made available by the authors, without undue reservation, to any qualified researcher.

AUTHOR CONTRIBUTIONS

All authors listed have made substantial, direct, and intellectual contribution to the work and approved it for publication.

FUNDING

This work was supported by the National Key R&D Program of China [2016YFC0904800 and 2019YFC0840607]; the National Science and Technology Major Project of China

[2017ZX09304010]; the Program of the National Natural Science Foundation of China [Grant No.81770947, 81700842]; the Excellent Medical Young Talent Projects of Shanghai General Hospital (Grant No.06N1702019).

ACKNOWLEDGMENTS

The authors would like to thank the DuoEase Scientific Service Center for the excellent language editing service and the suggestions for figure revision.

REFERENCES

- Barber, A. J., Lieth, E., Khin, S. A., Antonetti, D. A., Buchanan, A. G., and Gardner, T. W. (1998). Neural apoptosis in the retina during experimental and human diabetes. Early onset and effect of insulin. *J. Clin. Invest.* 102, 783–791. doi: 10.1172/JCI2425
- Bringmann, A., Pannicke, T., Grosche, J., Francke, M., Wiedemann, P., Skatchkov, S. N., et al. (2006). Müller cells in the healthy and diseased retina. *Prog. Retin. Eye Res.* 25, 397–424. doi: 10.1016/j.preteyeres.2006.05.003
- Bringmann, A., Iandiev, I., Pannicke, T., Wurm, A., Hollborn, M., Wiedemann, P., et al. (2009). Cellular signaling and factors involved in Müller cell gliosis: neuroprotective and detrimental effects. *Prog. Retin. Eye Res.* 28, 423–451. doi: 10.1016/j.preteyeres.2009.07.001
- Da Silva, N., Herron, C. E., Stevens, K., Jollimore, C. A., Barnes, S., and Kelly, M. E. (2008). Metabotropic receptor-activated calcium increases and store-operated calcium influx in mouse Müller cells. *Invest. Ophthalmol. Vis. Sci.* 49, 3065–3073. doi: 10.1167/iovs.07-1118
- Duan, Y., Gross, R. A., and Sheu, S. S. (2007). Ca²⁺-dependent generation of mitochondrial reactive oxygen species serves as a signal for poly(ADP-ribose) polymerase-1 activation during glutamate excitotoxicity. *J. Physiol.* 585, 741–758. doi: 10.1113/jphysiol.2007.145409
- Feenstra, D. J., Yego, E. C., and Mohr, S. (2013). Modes of retinal cell death in diabetic retinopathy. *J. Clin. Exp. Ophthalmol.* 4, 298. doi: 10.4172/2155-9570.1000298
- Flora, S. J., Saxena, G., and Mehta, A. (2007). Reversal of lead-induced neuronal apoptosis by chelation treatment in rats: role of reactive oxygen species and intracellular Ca²⁺. *J. Pharmacol. Exp. Ther.* 322, 108–116. doi: 10.1124/jpet.107.121996
- Francke, M., Faude, F., Pannicke, T., Bringmann, A., Eckstein, P., Reichelt, W., et al. (2001). Electrophysiology of rabbit Müller (glial) cells in experimental retinal detachment and PVR. *Invest. Ophthalmol. Vis. Sci.* 42, 1072–1079.
- Fu, S., Dong, S., Zhu, M., Sherry, D. M., Wang, C., You, Z., et al. (2015). Müller glia are a major cellular source of survival signals for retinal neurons in diabetes. *Diabetes* 64, 3554–3563. doi: 10.2337/db15-0180
- Furman, J. L., and Norris, C. M. (2014). Calcineurin and glial signaling: neuroinflammation and beyond. *J. Neuroinflamm.* 11, 158. doi: 10.1186/s12974-014-0158-7
- Harada, T., Harada, C., Watanabe, M., Inoue, Y., Sakagawa, T., Nakayama, N., et al. (1998). Functions of the two glutamate transporters GLAST and GLT-1 in the retina. *Proc. Natl. Acad. Sci. U.S.A.* 95, 4663–4666. doi: 10.1073/pnas.95.8.4663
- Hori, S., and Mukai, N. (1980). Ultrastructural lesions of retinal pericapillary Müller cells in streptozotocin-induced diabetic rats. *Albrecht Von Graefes Arch. Klin. Exp. Ophthalmol.* 213, 1–9. doi: 10.1007/bf02391205
- Jadhav, A. P., Roesch, K., and Cepko, C. L. (2009). Development and neurogenic potential of Müller glial cells in the vertebrate retina. *Prog. Retin. Eye Res.* 28, 249–262. doi: 10.1016/j.preteyeres.2009.05.002
- Kowluru, R. A., Engerman, R. L., Case, G. L., and Kern, T. S. (2001). Retinal glutamate in diabetes and effect of antioxidants. *Neurochem. Int.* 38, 385–390. doi: 10.1016/s0197-0186(00)00112-1
- Kusari, J., Zhou, S. X., Padillo, E., Clarke, K. G., and Gil, D. W. (2010). Inhibition of vitreoretinal VEGF elevation and blood-retinal barrier breakdown in

SUPPLEMENTARY MATERIAL

The Supplementary Material for this article can be found online at: <https://www.frontiersin.org/articles/10.3389/fphar.2019.01668/full#supplementary-material>

SUPPLEMENTARY FIGURE 1 | Effect of the siTRPC6 on TRPC6 expression in rMC-1 cells under normal glucose. The protein level of TRPC6 (A) was quantified by western blot. Densitometric analysis of TRPC6 protein levels was standardized against β -actin protein levels (B). mRNA level of TRPC6 (C) was determined by real-time PCR, and the value was standardized to β -actin mRNA levels in the same RNA sample. The data are expressed as mean \pm SD; n = 3 for each group; ***p < 0.001, vs control.

- streptozotocin-induced diabetic rats by brimonidine. *Invest. Ophthalmol. Vis. Sci.* 51, 1044–1051. doi: 10.1167/iovs.08-3293
- Li, Q., and Puro, D. G. (2002). Diabetes-induced dysfunction of the glutamate transporter in retinal Müller cells. *Invest. Ophthalmol. Vis. Sci.* 43, 3109–3116.
- Li, Z. Y., Tung, Y. T., Chen, S. Y., and Yen, G. C. (2019). Novel findings of 18beta-glycyrrhetic acid on sRAGE secretion through inhibition of transient receptor potential canonical channels in high-glucose environment. *Biofactors* 45, 607–615. doi: 10.1002/biof.1517
- Lieth, E., Barber, A. J., Xu, B., Dice, C., Ratz, M. J., Tanase, D., et al. (1998). Glial reactivity and impaired glutamate metabolism in short-term experimental diabetic retinopathy. Penn state retina research group. *Diabetes* 47, 815–820. doi: 10.1002/biof.1517
- Lieth, E., LaNoue, K. F., Antonetti, D. A., and Ratz, M. (2000). Diabetes reduces glutamate oxidation and glutamine synthesis in the retina. The penn state retina research group. *Exp. Eye Res.* 70, 723–730. doi: 10.1006/exer.2000.0840
- Liu, D., Maier, A., Scholze, A., Rauch, U., Boltzen, U., Zhao, Z., et al. (2008). High glucose enhances transient receptor potential channel canonical type 6-dependent calcium influx in human platelets via phosphatidylinositol 3-kinase-dependent pathway. *Arterioscler. Thromb. Vasc. Biol.* 28, 746–751. doi: 10.1161/ATVBAHA.108.162222
- Liu, Z., Ma, C., Zhao, W., Zhang, Q., Xu, R., Zhang, H., et al. (2017). High glucose enhances isoflurane-induced neurotoxicity by regulating TRPC-dependent calcium influx. *Neurochem. Res.* 42, 1165–1178. doi: 10.1007/s11064-016-2152-1
- Lowell, B. B., and Shulman, G. I. (2005). Mitochondrial dysfunction and type 2 diabetes. *Science* 307, 384–387. doi: 10.1126/science.1104343
- Ma, M., Xu, Y., Xiong, S., Zhang, J., Gu, Q., Ke, B., et al. (2018). Involvement of ciliary neurotrophic factor in early diabetic retinal neuropathy in streptozotocin-induced diabetic rats. *Eye (Lond)* 32, 1463–1471. doi: 10.1038/s41433-018-0110-7
- Martin, P. M., Roon, P., Van Ells, T. K., Ganapathy, V., and Smith, S. B. Death of retinal neurons in streptozotocin-induced diabetic mice. *Invest. Ophthalmol. Vis. Sci.* 45 (2004), 3330–3336. doi: 10.1167/iovs.04-0247
- Napper, G. A., Pianta, M. J., and Kalloniatis, M. (1999). Reduced glutamate uptake by retinal glial cells under ischemic/hypoxic conditions. *Vis. Neurosci.* 16, 149–158. doi: 10.1017/s0952523899161108
- Olsen, M. L., and Sontheimer, H. (2008). Functional implications for Kir4.1 channels in glial biology: from K⁺ buffering to cell differentiation. *J. Neurochem.* 107, 589–601. doi: 10.1111/j.1471-4159.2008.05615.x
- Onohara, N., Nishida, M., Inoue, R., Kobayashi, H., Sumimoto, H., Sato, Y., et al. (2006). TRPC3 and TRPC6 are essential for angiotensin II-induced cardiac hypertrophy. *EMBO J.* 25, 5305–5316. doi: 10.1038/sj.emboj.7601417
- Pannicke, T., Iandiev, I., Uckermann, O., Biedermann, B., Kutzer, F., Wiedemann, P., et al. (2004). A potassium channel-linked mechanism of glial cell swelling in the postischemic retina. *Mol. Cell Neurosci.* 26, 493–502. doi: 10.1016/j.mcn.2004.04.005
- Pannicke, T., Iandiev, I., Wurm, A., Uckermann, O., vom Hagen, F., Reichenbach, A., et al. (2006). Diabetes alters osmotic swelling characteristics and membrane conductance of glial cells in rat retina. *Diabetes* 55, 633–639. doi: 10.2337/diabetes.55.03.06.db05-1349
- Pedersen, S. F., Owsianik, G., and Nilius, B. (2005). TRP channels: an overview. *Cell Calcium* 38, 233–252. doi: 10.1016/j.ceca.2005.06.028

- Puro, D. G. (2002). Diabetes-induced dysfunction of retinal Muller cells. *Trans. Am. Ophthalmol. Soc.* 100, 339–352.
- Reichenbach, A., and Bringmann, A. (2013). New functions of Muller cells. *Glia* 61, 651–678. doi: 10.1002/glia.22477
- Rojas, M., Zhang, W., Lee, D. L., Romero, M. J., Nguyen, D. T., Al-Shabrawey, M., et al. (2010). Role of IL-6 in angiotensin II-induced retinal vascular inflammation. *Invest. Ophthalmol. Vis. Sci.* 51, 1709–1718. doi: 10.1167/iops.09-3375
- Sachdeva, R., Schlotterer, A., Schumacher, D., Matka, C., Mathar, I., Dietrich, N., et al. (2018). TRPC proteins contribute to development of diabetic retinopathy and regulate glyoxalase 1 activity and methylglyoxal accumulation. *Mol. Metab.* 9, 156–167. doi: 10.1016/j.molmet.2018.01.003
- Shen, W., Li, S., Chung, S. H., and Gillies, M. C. (2010). Retinal vascular changes after glial disruption in rats. *J. Neurosci. Res.* 88, 1485–1499. doi: 10.1002/jnr.22317
- Silva, K. C., Rosales, M. A., Hamassaki, D. E., Saito, K. C., Faria, A. M., Ribeiro, P. A., et al. (2013). Green tea is neuroprotective in diabetic retinopathy. *Invest. Ophthalmol. Vis. Sci.* 54, 1325–1336. doi: 10.1167/iops.12-10647
- Sucher, N. J., Lipton, S. A., and Dreyer, E. B. (1997). Molecular basis of glutamate toxicity in retinal ganglion cells. *Vision Res.* 37, 3483–3493. doi: 10.1016/S0042-6989(97)00047-3
- Tai, Y., Feng, S., Ge, R., Du, W., Zhang, X., He, Z., et al. (2008). TRPC6 channels promote dendritic growth via the CaMKIV-CREB pathway. *J. Cell Sci.* 121, 2301–2307. doi: 10.1242/jcs.026906
- Wuensch, T., Thilo, F., Krueger, K., Scholze, A., Ristow, M., and Tepel, M. (2010). High glucose-induced oxidative stress increases transient receptor potential channel expression in human monocytes. *Diabetes* 59, 844–849. doi: 10.2337/db09-1100
- Yang, D., Elner, S. G., Chen, X., Field, M. G., Petty, H. R., and Elner, V. M. (2011). MCP-1-activated monocytes induce apoptosis in human retinal pigment epithelium. *Invest. Ophthalmol. Vis. Sci.* 52, 6026–6034. doi: 10.1167/iops.10-7023
- Yang, H., Zhao, B., Liao, C., Zhang, R., Meng, K., Xu, J., et al. (2013). High glucose-induced apoptosis in cultured podocytes involves TRPC6-dependent calcium entry via the RhoA/ROCK pathway. *Biochem. Biophys. Res. Commun.* 434, 394–400. doi: 10.1016/j.bbrc.2013.03.087
- Zeng, K., Xu, H., Chen, K., Zhu, J., Zhou, Y., Zhang, Q., et al. (2010). Effects of taurine on glutamate uptake and degradation in Muller cells under diabetic conditions via antioxidant mechanism. *Mol. Cell Neurosci.* 45, 192–199. doi: 10.1016/j.mcn.2010.06.010

Conflict of Interest: The authors declare that the research was conducted in the absence of any commercial or financial relationships that could be construed as a potential conflict of interest.

Copyright © 2020 Ma, Zhao, Zhang, Sun, Fan and Zheng. This is an open-access article distributed under the terms of the Creative Commons Attribution License (CC BY). The use, distribution or reproduction in other forums is permitted, provided the original author(s) and the copyright owner(s) are credited and that the original publication in this journal is cited, in accordance with accepted academic practice. No use, distribution or reproduction is permitted which does not comply with these terms.



Lactoferrin Has a Therapeutic Effect via HIF Inhibition in a Murine Model of Choroidal Neovascularization

Mari Ibuki^{1,2}, Chiho Shoda^{1,3}, Yukihiro Miwa^{1,2}, Ayako Ishida¹, Kazuo Tsubota^{1,4*} and Toshihide Kurihara^{1,2*}

¹ Laboratory of Photobiology, Keio University School of Medicine, Tokyo, Japan, ² Department of Ophthalmology, Keio University School of Medicine, Tokyo, Japan, ³ Department of Ophthalmology, Nihon University, Tokyo, Japan, ⁴ Tsubota Laboratory, Inc., Tokyo, Japan

OPEN ACCESS

Edited by:

Zhongjie Fu,
Harvard Medical School,
United States

Reviewed by:

Haojie Fu,
Harvard Medical School,
United States
Akio Oishi,
University of Bonn, Germany

*Correspondence:

Kazuo Tsubota
tsubota@z3.keio.jp
Toshihide Kurihara
kurihara@z8.keio.jp

Specialty section:

This article was submitted to
Neuropharmacology,
a section of the journal
Frontiers in Pharmacology

Received: 26 November 2019

Accepted: 07 February 2020

Published: 28 February 2020

Citation:

Ibuki M, Shoda C, Miwa Y, Ishida A,
Tsubota K and Kurihara T (2020)
Lactoferrin Has a Therapeutic Effect via
HIF Inhibition in a Murine Model of
Choroidal Neovascularization.
Front. Pharmacol. 11:174.
doi: 10.3389/fphar.2020.00174

Background: Lactoferrin, a type of glycoprotein, is contained in exocrine fluids such as tears, breast milk, sweat, and saliva, and is known to have anti-microbial, antioxidant, and anti-cancer effects. In the ophthalmological field, topical administration of lactoferrin has been reported to have a therapeutic effect in a murine dry eye model. Hypoxia-inducible factor (HIF) regulates various gene expressions under hypoxia, including vascular endothelial growth factor (VEGF), and is considered as an alternative target for neovascular ocular diseases such as age-related macular degeneration (AMD). We previously screened natural products and identified lactoferrin as a novel HIF inhibitor. In this study, we confirmed that lactoferrin has an HIF inhibitory effect and a therapeutic effect in a murine model of neovascular AMD.

Methods: HIF inhibitory effects of lactoferrin were evaluated using a luciferase assay and western blotting *in vitro*. The quantified volume of choroidal neovascularization (CNV) induced by laser irradiation was compared with oral lactoferrin administration or conditional tissue specific *Hif1a* knockout mice.

Results: Lactoferrin administration showed a significant HIF inhibitory effect in the retinal neuronal cells. Oral administration of lactoferrin or conditional *Hif1a* gene deletion significantly reduced CNV volume compared to controls.

Conclusions: Lactoferrin has a therapeutic effect in a laser CNV model by suppressing the retinal HIF activity.

Keywords: lactoferrin, age-related macular degeneration, laser-induced choroidal neovascularization, hypoxia-inducible factor, retina, retinal pigment epithelium, choroid

INTRODUCTION

Lactoferrin, a type of glycoprotein, is contained in exocrine fluids such as nasal exudate, bronchial mucus, breast milk, tears, sweat, and saliva (Iigo et al., 2009). The concentration of lactoferrin varies in different human body fluids. Milk is the most abundant source of lactoferrin, with human colostrum containing up to 7 g/l (Masson and Heremans, 1971). The concentration in tears is 2 mg/ml, whereas

that in blood is normally only 1 $\mu\text{g/ml}$, although it can rise to 200 $\mu\text{g/ml}$ in an inflammatory situation (Masson and Heremans, 1971). It is reported that lactoferrin is responsible for several anti-infective, immunological, and gastrointestinal actions in neonates, infants, and young children (Manzoni et al., 2018). Lactoferrin is also known to have several biological functions, including antioxidant, anti-microbial, and anti-cancer effects (Kanwar et al., 2015). It is reported that oral administration of bovine lactoferrin inhibits carcinogenesis in the colon and other organs in rats, and lung metastasis in mice (Iigo et al., 2009). In the ophthalmological field, lactoferrin eye drops have been reported to have a therapeutic effect in a murine dry eye model by suppressing oxidative stress (Higuchi et al., 2012; Higuchi et al., 2016).

Age-related macular degeneration (AMD) is a leading cause of blindness globally. It is roughly classified into two types; atrophic type (dry AMD) and neovascular type (wet AMD). Wet AMD is characterized by neovascularization, and vascular endothelial growth factor (VEGF) is known as a major contributor to the pathogenesis. While treatment for wet AMD with anti-VEGF drugs is established and widely clinically performed, there exist some concerns of adverse effects with long-term administration, such as chorioretinal atrophy (Grunwald et al., 2014; Maguire et al., 2016).

Hypoxia-inducible factors (HIFs) are key molecules regulating various gene expressions, including VEGF, which are required for cell survival under hypoxia. HIFs are transcriptional factors that are stabilized and activated under hypoxic conditions (Wang and Semenza, 1995). Under normoxic conditions, α -subunits of HIFs are hydroxylated by prolyl hydroxylase, ubiquitinated by von Hippel-Lindau (VHL) protein recognition, and degraded in the proteasome. Under hypoxic conditions, the activity of HIF- α prolyl hydroxylase decreases and HIF- α s are stabilized (Kaelin and Ratcliffe, 2008). We have previously revealed physiological and pathological roles of HIFs in the developmental and adult retina (Kurihara et al., 2010; Kurihara et al., 2011; Kurihara et al., 2016). Retinal pigment epithelium (RPE) cells are important to maintain homeostasis in the retina, and contribute to the pathogenesis of AMD (de Jong, 2006). RPE-specific conditional *Vegf* knockout mice show choriocapillaris loss, RPE and photoreceptor cell degeneration, and subretinal deposit accumulation resembling human AMD phenotypes (Kurihara et al., 2012; Kurihara et al., 2016). In contrast, RPE-specific *Hif* knockout mice show no pathological phenotypes morphologically and functionally, although both *Vegf* and *Hif* RPE-specific knockout mice have a significant and similar reduction of laser-induced choroidal neovascularization (CNV) mimicking wet AMD (Kurihara et al., 2012).

To identify dietary factors inhibiting HIF and examine the functions against ocular diseases, we have screened natural products and reported their therapeutic effects in animal models of retinal disorders (Kunimi et al., 2019a; Kunimi et al., 2019b; Miwa et al., 2019). We further screened natural products from another library and revealed that administration of *Garcinia cambogia* extract and its main ingredient

hydroxycitric have HIF inhibitory effects, showing significant therapeutic effects in a murine laser-induced CNV model (Ibuki et al., 2019). Furthermore, another group also revealed that *in vivo* genome editing targeting HIF could suppress laser-CNV formation in mice, indicating that HIF inactivation in the retina may be a promising approach to treat the neovascular type of AMD (Kim et al., 2017).

From the screening test, we have identified lactoferrin can be a novel candidate to inhibit HIF. In this study, we confirmed that lactoferrin has an HIF inhibitory effect, especially in retinal neuronal cells. In addition, we revealed a pathological contribution of HIF, not only in RPE cells but also neuronal cells in sensory retina, by utilizing murine models of conditional gene deletion.

MATERIALS AND METHODS

Animals

We performed all procedures in accordance with the National Institute of Health (NIH) guidelines for work with laboratory animals, the ARVO Animal Statement for the Use of Animals in Ophthalmic and Vision Research, and the Animal Research: Reporting *in vivo* Experiments (ARRIVE) guidelines. Our all animal procedures were approved by the Institutional Animal Care and Use Committee at Keio University. Wild-type C57BL/6J mice (CLEA Japan, Tokyo, Japan) and other transgenic mice were raised in an air-conditioned room maintained at $23 \pm 3^\circ\text{C}$ under a 12 h dark/light cycle, with free access to food and water.

Transgenic mice expressing Cre recombinase under Best1 [Best1-Cre mice, (Iacovelli et al., 2011)] or Chx10 promoter [Chx10-Cre mice, (Muranishi et al., 2011)] were mated with *Hif1a*^{flox/flox} mice (Ryan et al., 1998) to obtain RPE or sensory retina specific *Hif1a* knockout mice, respectively. *Hif1a*^{flox/flox} mice without the Cre transgene were used as the control. The genetic background of all transgenic mice used in this study was C57BL/6J.

Luciferase Assay

We performed a luciferase assay as previously described (Ibuki et al., 2019). The luciferase assay was performed using the murine cone photoreceptor cell line (661W) and the human RPE cell line (ARPE19). HIF- α s were induced by 200 μM CoCl_2 . Lactoferrin (FUJIFILM Wako Pure Chemical) was dissolved in MQ so that its concentration was 1 mg/mL, and was added into the growth medium at the same time as CoCl_2 . After the administration, cells were incubated for 24 h and the luciferase expression was quantified. We used a total of 100 μM of topotecan (Cayman Chemical, Ann Arbor, MI, USA) as a positive control for an HIF inhibitor, and a medium without CoCl_2 and lactoferrin as a vehicle control.

Laser-Induced CNV

The laser irradiation was performed as previously described (Ibuki et al., 2019). We dilated the eyes of the mice and anesthetized them. We placed five laser spots (532 nm argon laser, 200 mW, 100 ms, 75 mm). We used the air bubble as an

index of Bruch's membrane disruption by laser irradiation and excluded laser spots without an occurrence of the air bubble from the data analysis. We also excluded laser spots with an occurrence of hemorrhage because those spots may vary in the development of CNV.

CNV Volume Measurement

We measured CNV volume as previously described (Ibuki et al., 2019). On the 7th day after the irradiation, we sacrificed the mice, and enucleated the eyeballs. The RPE-choroid-sclera complex was flat-mounted and stained with isolectin B4. We observed CNV with a laser microscope, generated three-dimensional images of the CNV, and measured the volume.

Administration of Lactoferrin to Mice

Lactoferrin was dissolved in PBS to a concentration of 1,600 mg/kg, and was administered to 3-week-old male mice 6 days/week for a total of 5 weeks. The control group was administered PBS. The mice were irradiated with a laser 4 weeks after the beginning of the administration.

Real-Time PCR

We performed real-time PCR as previously described (Ibuki et al., 2019). We extracted RNA from the ARPE19 cell line and the 661W cell lines. We calculated the relative amplification of the cDNA fragments using the $2^{-\Delta\Delta C_t}$ method. Real-time PCR primer sequences were as follows: human *Hif1a* forward: TTCACCTGAGCCTAATAGTCC, human *Hif1a* reverse: CAAGTCTAAATCTGTGTCCTG; human *Vegfa* forward: TCTACCTCCACCATGCCAAGT, human *Vegfa* reverse: GATGATTCTGCCCTCCTCCTT; human *Glut1* forward: CGGGCCAAGAGTGTGCTAAA, human *Glut1* reverse: TGACGATACCGGAGCCAATG; human *Pdk1* forward: ACAAGGAGAGCTTCGGGGTGGATC, human *Pdk1* reverse: CCACGTCGCAGTTTGGATTATGC; human *Bnip3* forward: GGACAGAGTAGTTCCAGAGGCAGTTC, human *Bnip3* reverse: GGTGTGCATTTCCACATCAAACAT; human *Gapdh* forward: TCCCTGAGCTGAACGGGAAG, human *Gapdh* reverse: GGAGGAGTGGGTGTCGCTGT; mouse *Hif1a* forward: GGTTCAGCAGACCCAGTTA, mouse *Hif1a* reverse: AGGCTCCTTGGATGAGCTTT; mouse *Vegfa*

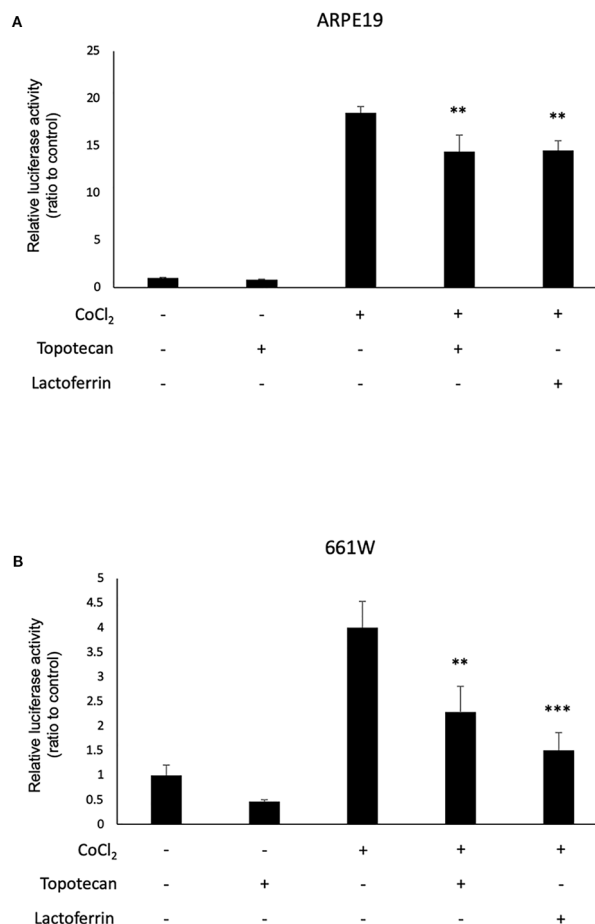


FIGURE 1 | Lactoferrin suppressed hypoxia-inducible factors (HIF) activation in a luciferase assay. **(A)** Administration of lactoferrin significantly suppressed CoCl₂-induced HIF activation in ARPE19 cells. **(B)** Administration of lactoferrin significantly suppressed CoCl₂-induced HIF activation in 661w cells. ** $p < 0.01$, *** $p < 0.001$, compared with CoCl₂ without topotecan and lactoferrin, $n = 3$.

forward: CCCTCTTAAATCGTGCCACC, mouse *Vegfa* reverse: CCTGTCCCTCTCTCTGTTTCG; mouse *Glut1* forward: CAGTTCGGCTATAACACTGGTG, mouse *Glut1* reverse: GCGGCTTTGTGATTTGTAT, mouse *Pdk1* forward: GCGGCTTTGTGATTTGTAT, mouse *Pdk1* reverse: ACCTGAATCGGGGATAAAC; mouse *Bnip3* forward: GCTCCCAGACACCACAAGAT, mouse *Bnip3* reverse: TGAGAGTAGCTGTGCGCTTC; mouse *Gapdh* forward: AGGAGCGAGACCCCACTAAC, and mouse *Gapdh* reverse: GATGACCCTTTTGGCTCCAC.

Western Blot

We performed Western Blot as previously described (Ibuki et al., 2019).

For *in vitro* experiments, we added 200 μ M CoCl₂ and 1 mg/mL lactoferrin to the ARPE19 cell line and 661W cell line. Six hours after the administration, we extracted protein from the cells and adjusted the protein concentration to 75 μ g/30 μ L.

For the *in vivo* experiments, we sacrificed the mice, and enucleated the eyes on the 3rd day after the laser irradiation. Six ocular samples from three mice were pooled per group. We adjusted the protein concentration to 55 μ g/42 μ L.

We incubated the membranes with rabbit monoclonal antibodies against HIF-1 α , or mouse monoclonal antibodies against β -actin. We washed incubated the membranes with a horseradish peroxidase (HRP)-labeled secondary antibody for HIF-1 α , or with a HRP-labeled secondary antibody for β -actin.

Statistics

We used a two-tail Student's *t*-test for the comparison of two groups. To compare multiple groups, we used a one-way analysis of variance (ANOVA) followed by Tukey's post hoc test. Probability values less than 0.05 was considered as being statistically significant. We expressed all results as the mean \pm standard deviation.

RESULTS

HIF Activation Was Suppressed by Lactoferrin Administration in a Luciferase Assay

We used 661W and ARPE19 to evaluate HIF activity with a luciferase assay. CoCl₂ was added to activate HIF signaling.

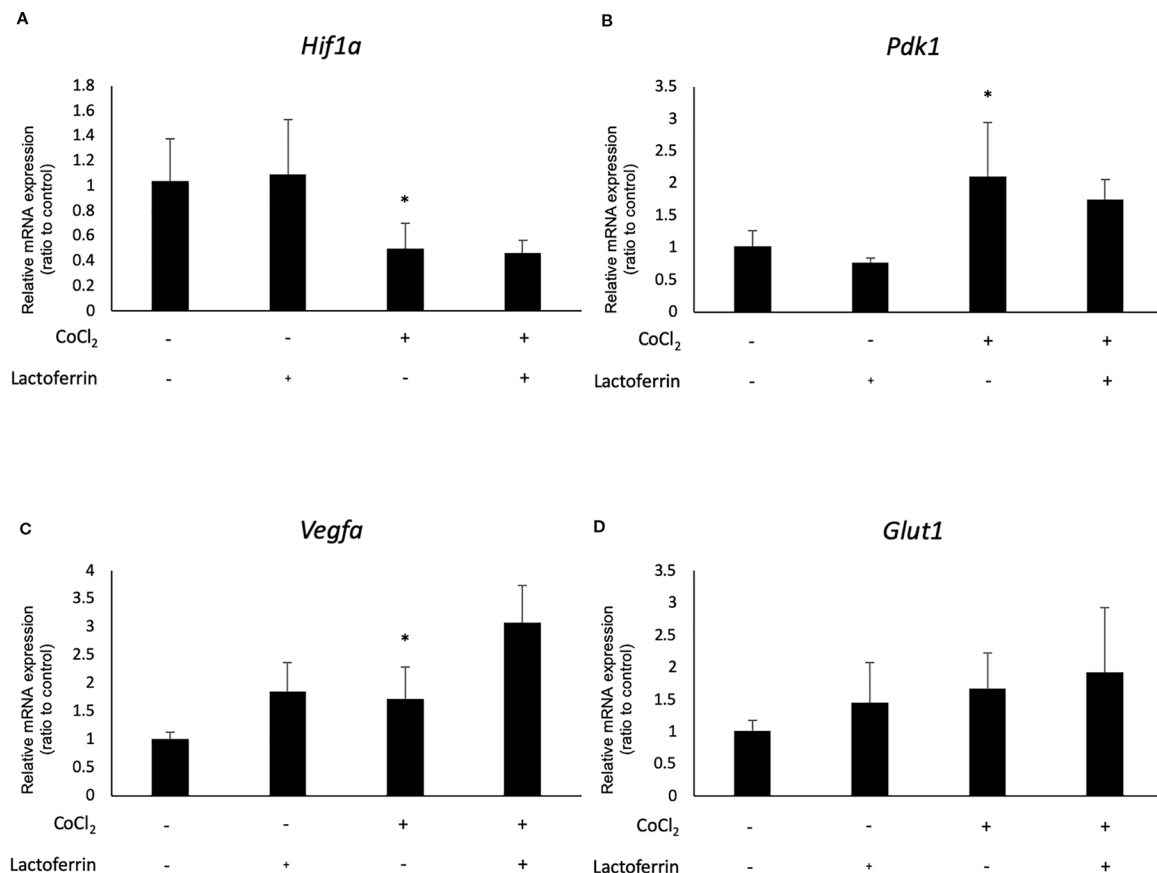


FIGURE 2 | *Hif1a* and the downstream genes were not affected by lactoferrin administration in ARPE19 cells. **(A)** *Hif1a* was downregulated by CoCl₂ administration in ARPE19 cells. The downstream genes of HIFs, including **(B)** *Pdk1*, **(C)** *Vegfa*, and **(D)** *Glut1* were upregulated by the administration of CoCl₂, but not changed by lactoferrin administration in ARPE19 cells. **p* < 0.05, compared with the control, *n* = 4–6.

Topotecan was used as a positive control of the HIF inhibitor. Lactoferrin showed an HIF inhibitory effect compared with the control group in ARPE19 cells (**Figure 1A**) and 661W cells (**Figure 1B**). Luciferase activity may be affected by magnesium concentration. To examine whether the chelate activity of lactoferrin changes magnesium concentration in the medium, we measured magnesium concentration in the medium with or without lactoferrin and there was no significant change observed (**Figure S4**).

Administration of Lactoferrin Downregulated *Hif1a* and Its Downstream Genes in 661W Cone Photoreceptor Cells

We examined how lactoferrin affects mRNA expression of *Hif1a* and its downstream genes. In general, HIF-1 α was stabilized and significantly increased in protein level followed by upregulation of the downstream genes after CoCl₂ administration. As a result of the negative feedback from the post translational protein modification, *Hif1a* was rather downregulated in mRNA level by CoCl₂ administration (Ibuki et al., 2019). Accordingly, in ARPE19 cells, *Hif1a* was significantly downregulated by

administration of CoCl₂ although administration of lactoferrin did not affect *Hif1a* expression (**Figure 2A**). The downstream genes of HIFs, such as *Pdk1*, *Vegfa*, and *Glut1* were upregulated by CoCl₂. These gene expressions were not changed by lactoferrin administration (**Figures 2B–D**). In contrast, *Pdk1*, *Vegfa*, and *Glut1* (**Figures 3B–D**) were downregulated significantly by lactoferrin administration in 661W cells. Lactoferrin did not affect HIF-1 α protein expression increased by CoCl₂ administration in ARPE19 cells (**Figures 4A and S1A, B**) and 661W cells (**Figures 4B and S2A, B**). These data suggested that HIF signaling is significantly suppressed by lactoferrin beyond protein expression in retinal neuronal cells.

Oral Administration of Lactoferrin Suppressed CNV Volume in the Laser CNV Model Mice

Lactoferrin was administered to the mice 6 days/week for a total of 5 weeks. We administered PBS for the vehicle group. We irradiated a laser 4 weeks after the beginning of the administration and evaluated the CNV volume on the seventh day after irradiation. A significant reduction in the CNV volume

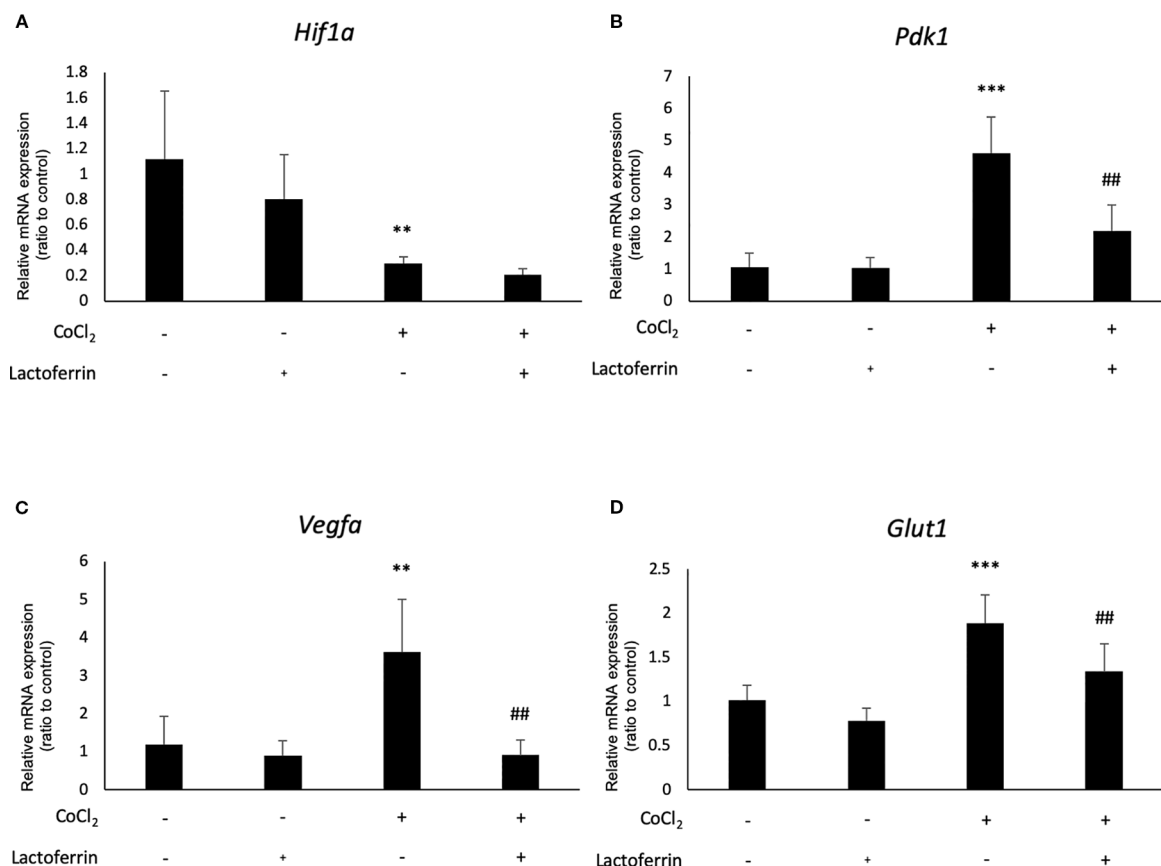


FIGURE 3 | *Hif1a* and the downstream genes were affected by lactoferrin administration in 661W cells. **(A)** *Hif1a* was downregulated by CoCl₂ administration in 661W cells. The downstream genes of HIFs, including **(B)** *Pdk1*, **(C)** *Vegfa*, and **(D)** *Glut1* were upregulated significantly by the administration of CoCl₂ and **(B)** *Pdk1*, **(C)** *Vegfa*, and **(D)** *Glut1* were suppressed significantly by lactoferrin administration in 661W cells. ***p* < 0.01, ****p* < 0.001, compared with the control. ##*p* < 0.01, compared with CoCl₂ without lactoferrin, *n* = 3–8.

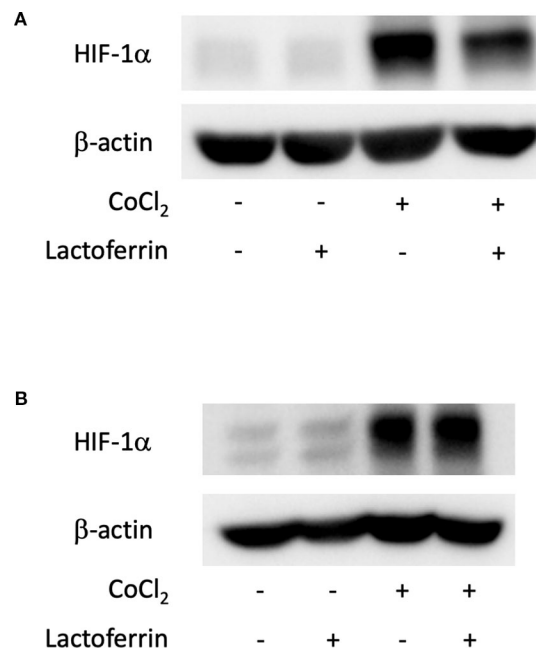


FIGURE 4 | HIF-1 α protein expression was not changed by lactoferrin administration in ARPE19 cells and 661W cells. **(A)** Western blot for HIF-1 α and β -actin in ARPE19 cells. **(B)** Western blot for HIF-1 α and β -actin in 661W cells.

was observed in the lactoferrin group compared with the vehicle group (**Figures 5A, B**). We measured the body weight of the mice before and after administration, and there is no significant change observed between the vehicle- and lactoferrin-administrated groups (**Figure 5C**).

Administration of Lactoferrin Suppressed HIF-1 α Expression *In Vivo*

Lactoferrin dissolved in PBS was orally administered to the mice for a total of 31 days, and the mice were irradiated with a laser on the fourth week of administration. In the choroid (**Figures 6A and S3A, B**) and the retina (**Figures 6B and S3C, D**), HIF-1 α protein was increased with the laser irradiation and suppressed by the administration of lactoferrin, even though the signal with the RPE/choroid tissue was weak (**Figure 6A**).

CNV Volume Was Reduced in Both RPE and Neural Retina Specific *Hif1a* Conditional Knockout Mice

To verify whether the CNV volume is regulated by HIF-1 α expression, we examined the pathological phenotype in tissue specific *Hif1a* conditional knockout model mice. To target RPE cells or retinal neuronal cells specifically, we generated *Hif1a*^{fl/fl}; Best1-Cre mice and *Hif1a*^{fl/fl}; Chx10-Cre mice, respectively. As same as the previous report by utilizing VMD2-Cre mice (Kurihara et al., 2012), RPE specific *Hif1a* knockout mice showed a significant reduction of the CNV volume even with a different Cre transgenic mice line (**Figures 7A, B**). We also

generated and examined sensory retina specific *Hif1a* knockout mice, showing a significant CNV reduction (**Figures 8A, B**). These data suggested that not only in RPE cells, but also in retinal neuronal cells, HIF-1 α expression significantly affects CNV formation.

DISCUSSION

In this study, we revealed that lactoferrin has an HIF inhibitory effect in the 661W cone photoreceptor cell line, suppressing HIF activity and the downstream genes (**Figures 1 and 3**). The results of the luciferase assay indicated that lactoferrin potentially suppresses HIF activity in RPE cells as well; however, the suppressive effect was limited according to the downstream evaluation (**Figure 2**), indicating that this suppressive effect may be actuated in a cell type dependent manner.

Lactoferrin is an iron-binding protein which is a monomeric, 80-kDa glycoprotein, with a single polypeptide chain of about 690 amino acid residues. Its amino acid sequence relationships place it in the wider transferrin family (Baker and Baker, 2005). It is known that lactoferrin regulates the quantity of iron absorbed in the intestine *via* its role in iron transport, and it can chelate iron, directly or indirectly (Hao et al., 2019). Lactoferrin has been used as an adjuvant therapy for some intestinal diseases and is now used in nutraceutical supplemented infant formula and other food products (Hao et al., 2019). Lactoferrin also has other numerous biological roles, such as the modulation of immune responses and anti-microbial, anti-viral, antioxidant, anti-cancer, and anti-inflammatory activities (Hao et al., 2019).

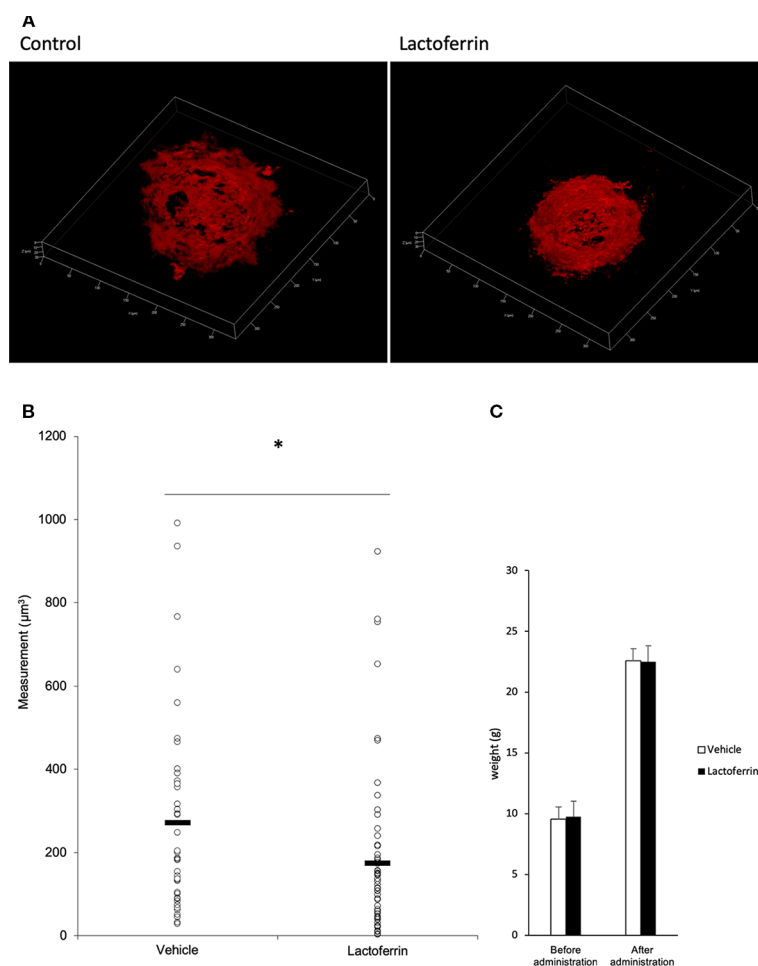


FIGURE 5 | Oral administration of lactoferrin suppressed laser-induced choroidal neovascularization (CNV) volume in mice. **(A)** Representative three-dimensional images of the CNV stained with isolectin B4 (IB4). **(B)** Quantification of the CNV volume. Note that the administration of lactoferrin significantly reduced the CNV volume compared with the vehicle group. Vehicle: $272.731 \pm 239.573 \mu\text{m}^3$, lactoferrin: $175.2 \pm 196.13 \mu\text{m}^3$, six mice for each, $*p < 0.05$. **(C)** The average of the body weight before and after administration. Note that there was no significant change between the two groups. $n = 6$.

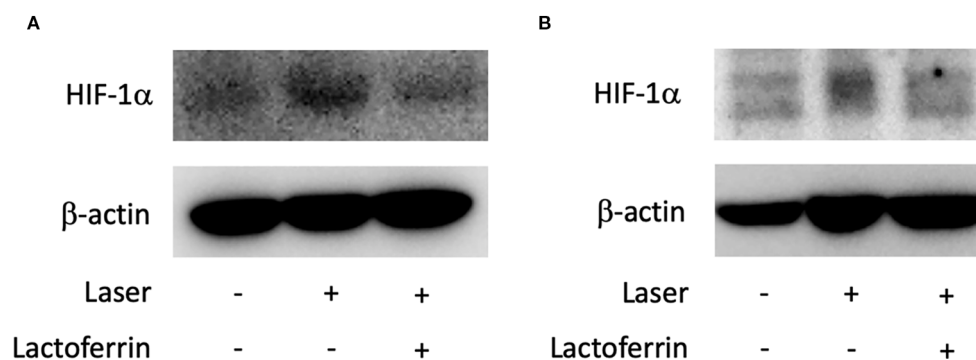


FIGURE 6 | HIF-1 α protein expression is suppressed by lactoferrin administration *in vivo*. Western blot for HIF-1 α with the tissue samples from the retinal pigment epithelium (RPE)/choroid **(A)** and the retina **(B)**. Note that administration of lactoferrin suppressed HIF-1 α expression, which increased with the laser irradiation in both the retina and RPE/choroid.

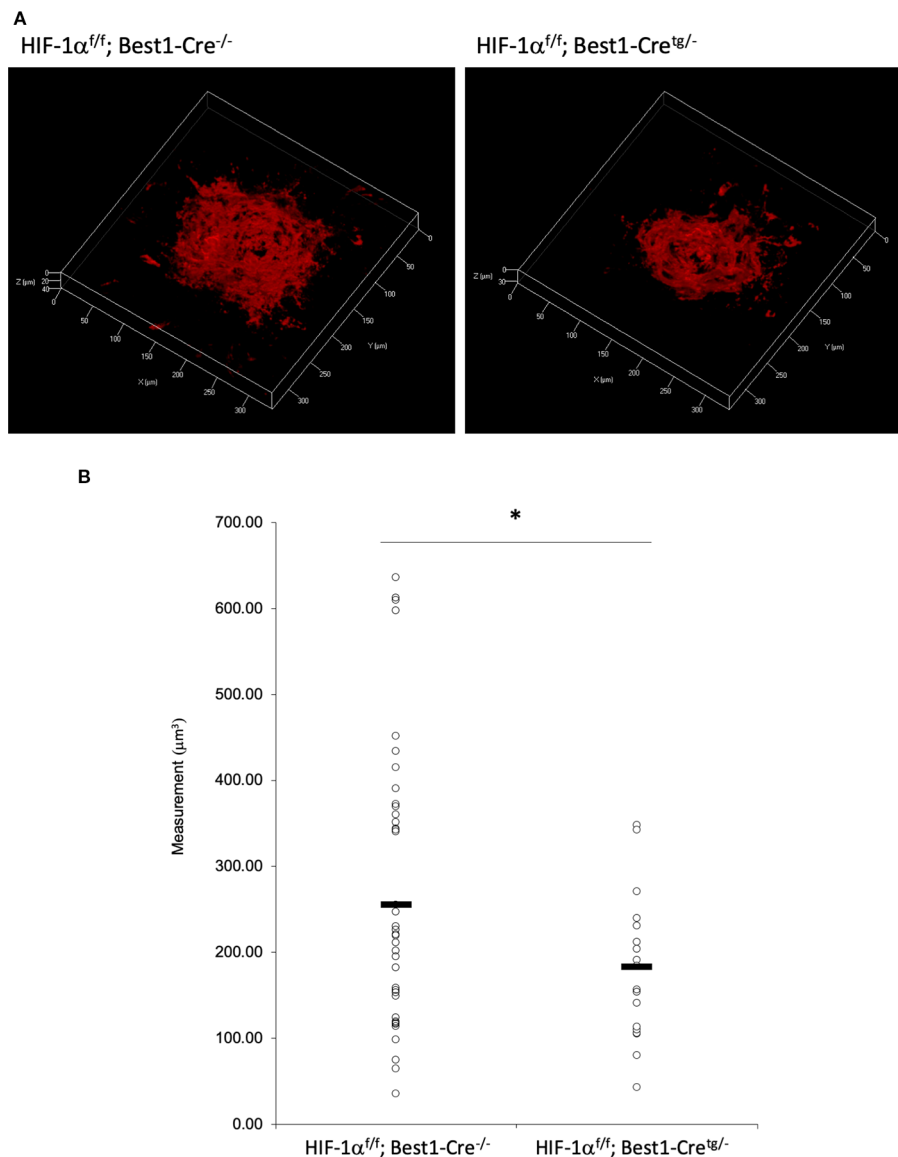


FIGURE 7 | A significant reduction of the CNV volume in RPE specific *Hif1a* conditional knockout mice. **(A)** Representative three-dimensional images of the CNV stained by IB4. **(B)** Quantification of the CNV volume. Note that the CNV volume in *Hif1a* $^{fl/fl}$; Best1-Cre $^{tg/-}$ mice was significantly reduced compared with the control. *Hif1a* $^{fl/fl}$; Best1-Cre $^{-/-}$: $256.14 \pm 160.37 \mu\text{m}^3$, *Hif1a* $^{fl/fl}$; Best1-Cre $^{tg/-}$: $183.89 \pm 91.26 \mu\text{m}^3$. Six mice for *Hif1a* $^{fl/fl}$; Best1-Cre $^{-/-}$ and *Hif1a* $^{fl/fl}$; Best1-Cre $^{tg/-}$, respectively. * $p < 0.05$. $n = 6$.

Lactoferrin is also known to bridge innate and adaptive immune functions in mammals. It is a pleiotropic molecule that directly assists in the influence of presenting cells for the development of T-helper cell polarization (Actor et al., 2009). It has been reported that lactoferrin reduces oxidative stress-induced apoptosis (Actor et al., 2009), and that *Streptococcus mutans* and *Vibrio cholerae*, but not *Escherichia coli*, were killed by incubation with purified human apolactoferrin (Arnold et al., 1977). It has also been reported that lactoferrin injection inhibits staphylococcal kidney infections (Bhimani et al., 1999). Lactoferrin at high concentrations has an ability to promote

growth and differentiation of the immature gut by enhancing proliferation of enterocytes and closure of enteric gap junctions, while at lower concentrations lactoferrin stimulates differentiation of enterocytes and expression of intestinal digestive enzymes (Buccigrossi et al., 2007). It has been reported that lactoferrin activates intestinal mucosal immunity in tumor-bearing mice (Wang et al., 2000). In addition, several *in vitro* studies have shown that lactoferrin is able to stimulate the growth of bifidobacteria; however, this effect is differentially exerted on different species and strains of bifidobacteria (Petschow et al., 1999; Liepke et al., 2002; Kim et al., 2004). In

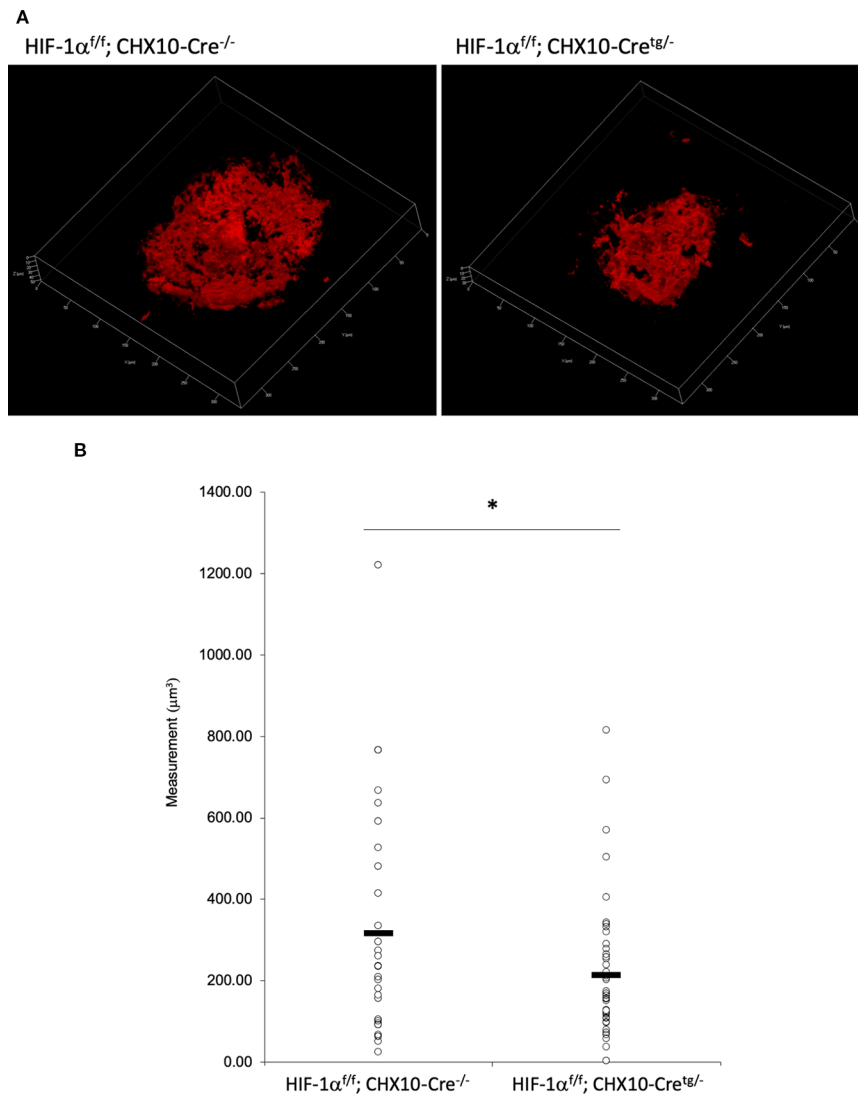


FIGURE 8 | A significant reduction of the CNV volume in neural retina specific *Hif1a* conditional knockout mice. **(A)** Representative three-dimensional images of the CNV stained by IB4. **(B)** Quantification of the CNV volume. Note that the CNV volume in *Hif1a^{fl/fl}; CHX10-Cre^{tg/-}* mice was significantly reduced compared with the control. *Hif1a^{fl/fl}; CHX10-Cre^{-/-}*: $317.84 \pm 282.97 \mu\text{m}^3$, *Hif1a^{fl/fl}; CHX10-Cre^{tg/-}*: $214.74 \pm 164.16 \mu\text{m}^3$. Six and four mice for *Hif1a^{fl/fl}; CHX10-Cre^{-/-}* and *Hif1a^{fl/fl}; CHX10-Cre^{tg/-}*, respectively. * $p < 0.05$. $n = 4-6$.

terms of anti-cancer effects, oral administration of bovine lactoferrin inhibits carcinogenesis in the colon and other organs in rats, and lung metastasis in mice (Iigo et al., 2009).

As described above, lactoferrin is known to have various roles. It has been reported that selenium-binding lactoferrin (Se-lactoferrin) eye drops suppress the upregulated expression of heme oxygenase-1, cyclooxygenase-2, matrix metalloproteinase-9, and interleukin-6, and also suppress 8-OHdG production in a murine dry eye model induced by surgical removal of the lacrimal glands (Higuchi et al., 2012). Se-lactoferrin eye drops have also been shown to have efficacy in a tobacco smoke exposure-induced rat dry eye model and a short-term rabbit dry eye model (Higuchi et al., 2016). It is also reported that oral lactoferrin administration preserves lacrimal gland function in aged mice by attenuating

oxidative damage and suppressing subsequent gland inflammation (Kawashima et al., 2012). In the current study, we found that oral administration of lactoferrin has a therapeutic effect in a laser-induced CNV model mimicking the neovascular type of AMD (Figure 5). This result is consistent with the previous report that the CNV volume is significantly increased in *lactoferrin* gene knockout mice (Montezuma et al., 2015). It has been reported that HIF downstream genes were upregulated in a laser-irradiated RPE/choroid (Kurihara et al., 2012). Oral administration of lactoferrin suppresses the increased HIF-1 α expression both in the RPE and the neural retina (Figure 6). Thus, there may be some dissociation of lactoferrin action against HIF-1 α between *in vitro* and *in vivo* observations in the current experiments. We speculate that this is because lactoferrin may

be metabolized in the body to directly suppress HIF-1 α protein expression in the eye. We further confirmed that not only in the RPE (**Figure 7**), but also in the neural retina (**Figure 8**), HIF-1 α expression significantly contributes to CNV formation. These results indicate that lactoferrin suppresses CNV formation by suppressing HIF-1 α in PRE and the neural retina.

In conclusion, HIF-1 α inactivation either in RPE or the neural retina can suppress CNV formation in a murine laser irradiation model. CNV formation is suppressed by oral administration of lactoferrin *via* HIF-1 α inactivation in the RPE and neural retina. These results suggest a potential clinical use of lactoferrin in daily life to prevent AMD.

DATA AVAILABILITY STATEMENT

All datasets generated for this study are included in the article/**Supplementary Material**.

ETHICS STATEMENT

The animal study was reviewed and approved by the Institutional Animal Care and Use Committee at Keio University.

AUTHOR CONTRIBUTIONS

MI performed all the experiments. CS and YM established the experimental protocols. AI prepared the experimental materials. MI and TK contributed to the conception and design of the

study. TK and KT supervised the project. All authors approved the final version for submission.

FUNDING

This work was funded by Grants-in-Aid for Scientific Research (KAKENHI, number 15K10881 and 18K09424) from the Ministry of Education, Culture, Sports, Science and Technology (MEXT) to TK. This study was conducted with financial support from ROHTO Pharmaceutical. The authors declare that this study received funding from ROHTO Pharmaceutical (Osaka, Japan). The funder was not involved in the study design, collection, analysis, interpretation of data, the writing of this article or the decision to submit it for publication.

ACKNOWLEDGMENTS

The authors thank K. Nishimaki, Y. Soejima, H. Aoyagi, and M. Shidomi at ROHTO Pharmaceutical Co. Ltd. for their critical discussion and H. Kunimi, K. Mori, S. Ikeda, X. Jiang, Y. Katada, Y. Hagiwara, K. Kurosaki, K. Takahashi, A. Kawabata, E. Yotsukura H. Torii, and N. Ozawa in the Laboratory of Photobiology, Keio University for their technical and administrative support.

SUPPLEMENTARY MATERIAL

The Supplementary Material for this article can be found online at: <https://www.frontiersin.org/articles/10.3389/fphar.2020.00174/full#supplementary-material>

REFERENCES

- Actor, J. K., Hwang, S. A., and Kruzel, M. L. (2009). Lactoferrin as a natural immune modulator. *Curr. Pharm. Des.* 15 (17), 1956–1973. doi: 10.2174/138161209788453202
- Arnold, R. R., Cole, M. F., and McGhee, J. R. (1977). A bactericidal effect for human lactoferrin. *Science* 197 (4300), 263–265. doi: 10.1126/science.327545
- Baker, E. N., and Baker, H. M. (2005). Molecular structure, binding properties and dynamics of lactoferrin. *Cell Mol. Life Sci.* 62 (22), 2531–2539. doi: 10.1007/s00018-005-5368-9
- Bhimani, R. S., Vendrov, Y., and Furmanski, P. (1999). Influence of lactoferrin feeding and injection against systemic staphylococcal infections in mice. *J. Appl. Microbiol.* 86 (1), 135–144. doi: 10.1046/j.1365-2672.1999.00644.x
- Buccigrossi, V., de Marco, G., Bruzzese, E., Ombrato, L., Bracale, I., Polito, G., et al. (2007). Lactoferrin induces concentration-dependent functional modulation of intestinal proliferation and differentiation. *Pediatr. Res.* 61 (4), 410–414. doi: 10.1203/pdr.0b013e3180332c8d
- de Jong, P. T. (2006). Age-related macular degeneration. *N. Engl. J. Med.* 355 (14), 1474–1485. doi: 10.1056/NEJMra062326
- Grunwald, J. E., Daniel, E., Huang, J., Ying, G. S., Maguire, M. G., Toth, C. A., et al. (2014). Risk of geographic atrophy in the comparison of age-related macular degeneration treatments trials. *Ophthalmology* 121 (1), 150–161. doi: 10.1016/j.optha.2013.08.015
- Hao, L., Shan, Q., Wei, J., Ma, F., and Sun, P. (2019). Lactoferrin: major physiological functions and applications. *Curr. Protein Pept. Sci.* 20 (2), 139–144. doi: 10.2174/1389203719666180514150921
- Higuchi, A., Inoue, H., Kawakita, T., Ogishima, T., and Tsubota, K. (2012). Selenium compound protects corneal epithelium against oxidative stress. *PLoS One* 7 (9), e45612. doi: 10.1371/journal.pone.0045612
- Higuchi, A., Inoue, H., Kaneko, Y., Oonishi, E., and Tsubota, K. (2016). Selenium-binding lactoferrin is taken into corneal epithelial cells by a receptor and prevents corneal damage in dry eye model animals. *Sci. Rep.* 6, 36903. doi: 10.1038/srep36903
- Iacovelli, J., Zhao, C., Wolkow, N., Veldman, P., Gollomp, K., Ojha, P., et al. (2011). Generation of Cre transgenic mice with postnatal RPE-specific ocular expression. *Invest. Ophthalmol. Vis. Sci.* 52 (3), 1378–1383. doi: 10.1167/iops.10-6347
- Ibuki, M., Shoda, C., Miwa, Y., Ishida, A., Tsubota, K., and Kurihara, T. (2019). Therapeutic effect of garcinia cambogia extract and hydroxycitric acid inhibiting hypoxia-inducible factor in a murine model of age-related macular degeneration. *Int. J. Mol. Sci.* 20 (20). doi: 10.3390/ijms20205049
- Iigo, M., Alexander, D. B., Long, N., Xu, J., Fukamachi, K., Futakuchi, M., et al. (2009). Anticarcinogenesis pathways activated by bovine lactoferrin in the murine small intestine. *Biochimie* 91 (1), 86–101. doi: 10.1016/j.biochi.2008.06.012
- Kaelin, W. G. Jr., and Ratcliffe, P. J. (2008). Oxygen sensing by metazoans: the central role of the HIF hydroxylase pathway. *Mol. Cell* 30 (4), 393–402. doi: 10.1016/j.molcel.2008.04.009
- Kanwar, J. R., Roy, K., Patel, Y., Zhou, S. F., Singh, M. R., Singh, D., et al. (2015). Multifunctional iron bound lactoferrin and nanomedicinal approaches to enhance its bioactive functions. *Molecules* 20 (6), 9703–9731. doi: 10.3390/molecules20069703

- Kawashima, M., Kawakita, T., Inaba, T., Okada, N., Ito, M., Shimmura, S., et al. (2012). Dietary lactoferrin alleviates age-related lacrimal gland dysfunction in mice. *PLoS One* 7 (3), e33148. doi: 10.1371/journal.pone.0033148
- Kim, W. S., Ohashi, M., Tanaka, T., Kumura, H., Kim, G. Y., Kwon, I. K., et al. (2004). Growth-promoting effects of lactoferrin on *L. acidophilus* and *Bifidobacterium* spp. *Biomaterials* 17 (3), 279–283. doi: 10.1023/b:biom.0000027705.57430.f1
- Kim, E., Koo, T., Park, S. W., Kim, D., Kim, K., Cho, H. Y., et al. (2017). In vivo genome editing with a small Cas9 orthologue derived from *Campylobacter jejuni*. *Nat. Commun.* 8, 14500. doi: 10.1038/ncomms14500
- Kunimi, H., Miwa, Y., Inoue, H., Tsubota, K., and Kurihara, T. (2019a). A novel HIF inhibitor halofuginone prevents neurodegeneration in a murine model of retinal ischemia-reperfusion. *Int. J. Mol. Sci.* 20 (13). doi: 10.3390/ijms20133171
- Kunimi, H., Miwa, Y., Katada, Y., Tsubota, K., and Kurihara, T. (2019b). HIF inhibitor topotecan has a neuroprotective effect in a murine retinal ischemia-reperfusion model. *PeerJ* 7, e7849. doi: 10.7717/peerj.7849
- Kurihara, T., Kubota, Y., Ozawa, Y., Takubo, K., Noda, K., Simon, M. C., et al. (2010). von Hippel-Lindau protein regulates transition from the fetal to the adult circulatory system in retina. *Development* 137 (9), 1563–1571. doi: 10.1242/dev.049015
- Kurihara, T., Westenskow, P. D., Krohne, T. U., Aguilar, E., Johnson, R. S., and Friedlander, M. (2011). Astrocyte pVHL and HIF- α isoforms are required for embryonic-to-adult vascular transition in the eye. *J. Cell Biol.* 195 (4), 689–701. doi: 10.1083/jcb.201107029
- Kurihara, T., Westenskow, P. D., Bravo, S., Aguilar, E., and Friedlander, M. (2012). Targeted deletion of Vegfa in adult mice induces vision loss. *J. Clin. Invest.* 122 (11), 4213–4217. doi: 10.1172/jci65157
- Kurihara, T., Westenskow, P. D., Gantner, M. L., Usui, Y., Schultz, A., Bravo, S., et al. (2016). Hypoxia-induced metabolic stress in retinal pigment epithelial cells is sufficient to induce photoreceptor degeneration. *Elife* 5. doi: 10.7554/eLife.14319
- Liepe, C., Adermann, K., Raida, M., Magert, H. J., Forssmann, W. G., and Zucht, H. D. (2002). Human milk provides peptides highly stimulating the growth of bifidobacteria. *Eur. J. Biochem.* 269 (2), 712–718. doi: 10.1046/j.0014-2956.2001.02712.x
- Maguire, M. G., Martin, D. F., Ying, G. S., Jaffe, G. J., Daniel, E., Grunwald, J. E., et al. (2016). Five-year outcomes with anti-vascular endothelial growth factor treatment of neovascular age-related macular degeneration: the comparison of age-related macular degeneration treatments trials. *Ophthalmology* 123 (8), 1751–1761. doi: 10.1016/j.ophtha.2016.03.045
- Manzoni, P., Dall'Agnola, A., Tome, D., Kaufman, D. A., Tavella, E., Pieretto, M., et al. (2018). Role of lactoferrin in neonates and infants: an update. *Am. J. Perinatol.* 35 (6), 561–565. doi: 10.1055/s-0038-1639359
- Masson, P. L., and Heremans, J. F. (1971). Lactoferrin in milk from different species. *Comp. Biochem. Physiol. B.* 39 (1), 119–129. doi: 10.1016/0305-0491(71)90258-6
- Miwa, Y., Hoshino, Y., Shoda, C., Jiang, X., Tsubota, K., and Kurihara, T. (2019). Pharmacological HIF inhibition prevents retinal neovascularization with improved visual function in a murine oxygen-induced retinopathy model. *Neurochem. Int.* 128, 21–31. doi: 10.1016/j.neuint.2019.03.008
- Montezuma, S. R., Dolezal, L. D., Rageh, A. A., Mar, K., Jordan, M., and Ferrington, D. A. (2015). Lactoferrin reduces chorioretinal damage in the murine laser model of choroidal neovascularization. *Curr. Eye Res.* 40 (9), 946–953. doi: 10.3109/02713683.2014.969808
- Muranishi, Y., Terada, K., Inoue, T., Katoh, K., Tsujii, T., Sanuki, R., et al. (2011). An essential role for RAX homeoprotein and NOTCH-HES signaling in Otx2 expression in embryonic retinal photoreceptor cell fate determination. *J. Neurosci.* 31 (46), 16792–16807. doi: 10.1523/jneurosci.3109-11.2011
- Petschow, B. W., Talbott, R. D., and Batema, R. P. (1999). Ability of lactoferrin to promote the growth of *Bifidobacterium* spp. *in vitro* is independent of receptor binding capacity and iron saturation level. *J. Med. Microbiol.* 48 (6), 541–549. doi: 10.1099/00222615-48-6-541
- Ryan, H. E., Lo, J., and Johnson, R. S. (1998). HIF-1 α is required for solid tumor formation and embryonic vascularization. *EMBO J.* 17 (11), 3005–3015. doi: 10.1093/emboj/17.11.3005
- Wang, G. L., and Semenza, G. L. (1995). Purification and characterization of hypoxia-inducible factor 1. *J. Biol. Chem.* 270 (3), 1230–1237. doi: 10.1074/jbc.270.3.1230
- Wang, W. P., Iigo, M., Sato, J., Sekine, K., Adachi, I., and Tsuda, H. (2000). Activation of intestinal mucosal immunity in tumor-bearing mice by lactoferrin. *Jpn. J. Cancer Res.* 91 (10), 1022–1027. doi: 10.1111/j.1349-7006.2000.tb00880.x

Conflict of Interest: Patents have been applied for field relating to the therapeutic effects of lactoferrin in ocular disorders. KT holds the position of CEO of Tsubota Laboratory, Inc.

The remaining authors declare that the research was conducted in the absence of any commercial or financial relationships that could be construed as a potential conflict of interest.

Copyright © 2020 Ibuki, Shoda, Miwa, Ishida, Tsubota and Kurihara. This is an open-access article distributed under the terms of the Creative Commons Attribution License (CC BY). The use, distribution or reproduction in other forums is permitted, provided the original author(s) and the copyright owner(s) are credited and that the original publication in this journal is cited, in accordance with accepted academic practice. No use, distribution or reproduction is permitted which does not comply with these terms.



MicroRNA-18a-5p Administration Suppresses Retinal Neovascularization by Targeting FGF1 and HIF1A

Ji-Tian Guan¹, Xin-Xin Li¹, De-Wei Peng¹, Wen-Meng Zhang¹, Jia Qu¹, Fan Lu^{1,2}, Robert J. D'Amato^{3,4} and Zai-Long Chi^{1,2*}

¹ State Key Laboratory of Ophthalmology, Optometry and Visual Science, Eye Hospital of Wenzhou Medical University, Wenzhou, China, ² International Joint Research Center for Regenerative Medicine and Neurogenetics, Wenzhou Medical University, Wenzhou, China, ³ Vascular Biology Program, Department of Surgery, Boston Children's Hospital, Boston, MA, United States, ⁴ Department of Ophthalmology, Harvard Medical School, Boston, MA, United States

OPEN ACCESS

Edited by:

Zhongjie Fu,
Harvard Medical School,
United States

Reviewed by:

Yan Gong,
Zhongnan Hospital of Wuhan
University, China
José Carlos Rivera,
University of Montreal, Canada

*Correspondence:

Zai-Long Chi
zailong.chi@eye.ac.cn

Specialty section:

This article was submitted to
Neuropharmacology,
a section of the journal
Frontiers in Pharmacology

Received: 27 November 2019

Accepted: 26 February 2020

Published: 10 March 2020

Citation:

Guan J-T, Li X-X, Peng D-W,
Zhang W-M, Qu J, Lu F, D'Amato RJ
and Chi Z-L (2020) MicroRNA-18a-5p
Administration Suppresses Retinal
Neovascularization by Targeting FGF1
and HIF1A. *Front. Pharmacol.* 11:276.
doi: 10.3389/fphar.2020.00276

Pathologic ocular neovascularization commonly results in visual impairment or even blindness in numerous fundus diseases, including proliferative diabetic retinopathy (PDR), retinopathy of prematurity (ROP), and age-related macular degeneration (AMD). MicroRNAs regulate angiogenesis through modulating target genes and disease progression, making them a new class of targets for drug discovery. In this study, we investigated the potential role of miR-18a-5p in retinal neovascularization using a mouse model of oxygen-induced proliferative retinopathy (OIR). We found that miR-18a-5p was highly expressed in the retina of pups as well as retinal endothelial cells, and was consistently down-regulated during retinal development. On the other hand, miR-18a-5p was increased significantly during pathologic neovascularization in the retinas of OIR mice. Moreover, intravitreal administration of miRNA mimic, agomiR-18a-5p, significantly suppressed retinal neovascularization in OIR models. Accordingly, agomiR-18a-5p markedly suppressed human retinal microvascular endothelial cell (HRMEC) function including proliferation, migration, and tube formation ability. Additionally, we demonstrated that miR-18a-5p directly down-regulated known vascular growth factors, fibroblast growth factor 1 (FGF1) and hypoxia-inducible factor 1- α (HIF1A), as the target genes. In conclusion, miR-18a-5p may be a useful drug target for pathologic ocular neovascularization.

Keywords: miR-18a-5p, neovascularization, proliferative retinopathy, FGF1, HIF1A

INTRODUCTION

The intraretinal vasculature supplies the inner part of the retina with oxygen and nutrients (Fruttiger, 2007). In mice, retinal vasculature development begins around birth and is completed in the third postnatal week (Stahl et al., 2010; Selvam et al., 2018). Dysfunctional angiogenesis is involved in many diseases, including cardiovascular diseases, tumorigenesis, and proliferative retinopathies (Folkman, 1995). Proliferative retinopathies such as proliferative diabetic retinopathy (PDR), retinopathy of prematurity (ROP), and retina vein occlusion (RVO) are characterized by pathological retinal neovascularization, which is the leading cause of blindness (Augustin and Koh, 2017). Retinal neovascularization is a very complicated pathophysiologic process, which is driven by the proangiogenic factors, such as vascular endothelial growth factor (VEGF), fibroblast

growth factor (FGF), and erythropoietin (Liu et al., 2016). Currently, the clinical treatments for proliferative retinopathy include laser photocoagulation, vitrectomy surgery, and anti-VEGF drugs. Laser photocoagulation, the standard treatment for proliferative retinopathy, has a high rate of visual and anatomic success (Wallace and Wu, 2013). Anti-VEGF drugs are widely used as the major treatment in both ROP and DR to achieve certain efficacy (Xu et al., 2018). However, despite these considerable advances, an increasing number of clinical studies have reported that laser treatment and anti-VEGF therapy does have some limitations and causes undesirable side effects (Potente et al., 2011; Xu et al., 2018). Therefore, it is critical to explore and identify additional factors that regulate pathological neovascularization in order to exploit new therapeutic drugs.

MicroRNAs (miRNAs) are small endogenous non-coding RNAs composed of 21–25 nucleotides that negatively regulate gene expression at the posttranscriptional level by mediating mRNA degradation and/or translational repression (He and Hannon, 2004; Bartel, 2009). MiRNAs have been reported to play a key role in retinal vascular development and disease progression (Shen et al., 2008; Sundermeier and Palczewski, 2012). Several miRNAs were identified to inhibit retinal neovascularization, such as miR-126, miR-150, miR-223, and miR-384-3p (Shi et al., 2013; Liu et al., 2015; Zhou et al., 2016; Xia et al., 2018). Until now, several miRNA mimics or inhibitors have been tested in clinical trials for treatment of various diseases (Bader, 2012; Janssen et al., 2013; van Zandwijk et al., 2017). There will undoubtedly be many more breakthroughs in the development of novel miRNA-based therapeutics for the treatment of neovascular eye diseases.

The miR-17-92 cluster is one of the first miRNAs found to be associated with tumor angiogenesis. This conserved miRNA cluster encodes miR-17, miR-18a, miR-19a/b, miR-20a, and miR-92a and is highly expressed in tumors (Kaluza et al., 2013). Several studies have proven that the miR-17-92 cluster serves an antiangiogenic role by targeting the proangiogenic factors (Bonauer et al., 2009; Nunes et al., 2015). MiR-18a and miR-19a have been shown to repress thrombospondin 1 (TSP1) and connective tissue growth factor (CTGF) (Dews et al., 2006; Chamorro-Jorganes et al., 2016). Ferreira et al. found that argonaute-2 can promote miR-18a entry in human brain endothelial cells (ECs), and miR-18a can modulate the EC proliferation and migration derived from human cerebral arteriovenous malformation (AVM), and produce aberrant tubule structure compared with normal brain ECs (Ferreira et al., 2014a,b). However, it is not completely understood whether miR-18a is altered in pathologic ocular neovascularization or whether it is useful as a new molecular target for the treatment of neovascular eye diseases.

Currently, the oxygen-induced retinopathy (OIR) mouse model has been widely used in studies ROP and PDR (Smith et al., 1994; Connor et al., 2009) to evaluating the efficacy of antiangiogenic agents. Neonatal mice are exposed to high oxygen levels (75% oxygen) from postnatal day 7 (P7) for 5 days. Hyperoxia inhibits retinal vessel growth, and relatively hypoxia (removed to room air) triggers both vascular regrowth and neovascularization. In this study, we investigated the effects of miR-18a-5p on the human retinal microvascular

endothelial cell (HRMEC) function and OIR models to elucidate the participation of miR-18a-5p in the initiation and progression of ocular neovascularization. Moreover, we explored the mechanism underlying miR-18a-5p activity in pathological angiogenesis through screening and validating the specific miR-18a-5p target genes. Taken together, these results might provide a reliable theoretical foundation to improve the treatment of neovascular ocular diseases.

MATERIALS AND METHODS

High-Throughput Sequencing

C57BL/6J mice were obtained from Beijing Vital River Laboratory Animal Technology Co., Ltd., Total RNA was extracted from fresh retinas isolated from mice in different developmental periods: postnatal day 1 (P1), P7, and P17. Briefly, the mice were euthanized, and retinas were isolated from the dissected eye and moved into the RNA-Solv Reagent (Omega Bio-tek, Norcross, GA, United States). T10 basic S25 ULTRA-TURRAX Disperser (IKA, Guangzhou, China) was used to homogenize retinas. Total RNA was extracted by miRNA Kit (Omega Bio-tek) according to the manufacturer's instructions. RNA quantity and quality were assessed by spectrophotometer 1510 (Thermo Fisher Scientific, Waltham, MA, United States). MiRNA libraries construction and sequencing on Illumina HiSeq 2500 (San Diego, CA, United States) were performed by RiboBio Co., Ltd. (Guangzhou, China). All animal experiments were performed strictly according to the ARVO Statement for the Use of Animals in Ophthalmic and Vision Research and approved by the Animal Care and Use Committee of Wenzhou Medical University.

Sequencing Data Analysis

For miRNA data analysis, clean reads were obtained from the 50-nt raw reads by removing the adaptor sequences and discarding low-quality reads. HISAT2 (Kim et al., 2015) was used to align the clean reads to the mouse reference genome mm10 with default parameters. Differential expression was assessed by DESeq using RPM (the number of reads per million) value as input. Differentially expressed miRNAs were chosen according to the criteria of fold change >2 and adjusted $P < 0.05$. All the differentially expressed miRNAs were used for temporal expression pattern analysis by STEM (Ernst and Bar-Joseph, 2006). Typical downregulated and upregulated miRNAs were clustered using the Amazing Heat Map function of TB tools (Chen et al., 2018). The differentially expressed miRNAs were clustered based on Euclidean distance using average linkage clustering with Cluster 3.0 software (Eisen Lab, University of California at Berkeley, United States). TreeView (Eisen Lab, University of California at Berkeley, United States) was used to visualize the clustered heat map.

OIR Mouse Model and Retinal Neovascularization Quantification

C57BL/6J mice were used to generate the oxygen-induced proliferative retinopathy (OIR) model as previously described

(Smith et al., 1994; Connor et al., 2009). Newborn mice and their nursing mother mice were exposed to 75% oxygen at P7 and returned to room air at P12. Mice were sacrificed at P17, followed by retina dissection and staining with Isolectin GS-IB₄ (Life Technologies, Eugene, OR, United States). The pups kept in room air throughout the experiments were used as the control. Intravitreal injection was conducted following previous protocols (Bai et al., 2011; Fu et al., 2017). Agomir-18a-5p at a dose of 1.5 μ g (RiboBio, Guangzhou, China) diluted in two microliter of phosphate-buffered saline (PBS, Biological Industries, Beit Haemek, Israel) was intravitreally injected into the eye of OIR mice at P12 using a 33-gauge needle (Hamilton, Reno, NV, United States). The contralateral eye injected with scrambled agomir diluted in PBS was used as the negative control (NC). Neovascularization (neovascular tuft) and vaso-oblivation in OIR were quantified by using Adobe Photoshop and ImageJ software. Quantification was performed with the identity of the samples masked, with *n* being the number of mice quantified.

Retinal Endothelial Cells (RECs) Isolation

The retinal cell suspension of mice was prepared using a modified method according to Su et al. (2003). Briefly, the retinas were dissected out from the mice eyes (6 to 7 pups from one litter), and minced into small pieces in Hanks' Balanced Salt Solution (HBSS; Thermo Fisher Scientific). Following digestion with collagenase type I (1 mg/ml) in Dulbecco's modified Eagle medium (DMEM, Thermo Fisher Scientific) for 30–45 min at 37°C, the cellular digests were filtered through the 40 μ m nylon mesh. DMEM with 10% fetal bovine serum (FBS; Thermo Fisher Scientific) was then added and centrifuged at 400 \times *g* for 10 min to pellet cells. The cells were resuspended and incubated with anti-CD31 MicroBeads (MicroBeads conjugated to monoclonal anti-mouse CD31 antibodies; Miltenyi Biotec GmbH, Bergisch Gladbach, Germany). Then, the cell suspension is loaded onto a MACS Column, which is placed in the magnetic field of a MACS Separator (Miltenyi Biotec GmbH). The magnetically labeled cells were washed and flushed out with the appropriate amount of PBS containing 0.5% bovine serum albumin (BSA) and 2 mM EDTA according to the manufacturer's protocol. The collected cells were plated in a 8.5 μ g/ml of Bovine Plasma Fibronectin (BPF; EMD Millipore) pre-coated 24-well plate and incubated in Endothelial Cell Medium (ECM; ScienCell, Carlsbad, CA, United States) containing 5% FBS, 20 μ g/ml of Endothelial Cell Growth Supplement (ECGS; EMD Millipore, Temecula, CA, United States), 100 μ g/ml streptomycin, and 100 U/ml penicillin at 37°C with 5% CO₂. Immunofluorescence (IF) staining was conducted to identify the RECs with anti-CD31 (BD Bioscience) and anti-VE-cadherin (CST, Beverly, MA, United States) antibodies.

Real-Time PCR

TRIzol Reagent (Thermo Fisher Scientific) was used to extract total RNA of retinas isolated from mice. Meanwhile, total RNA was extracted from the isolated RECs. To measurement of miR-18a-5p levels, real-time polymerase chain reaction (PCR) was performed using a miDETECT A Track miRNA qRT-PCR Starter Kit (RiboBio) according to the manufacturer's protocol. Total

RNA was added multiple Poly (A) using Poly (A) Polymerase, and reverse transcribed to cDNA using RTase mix and miDETECT A Track Uni-RT Primer. Real-time PCR was carried out on QuantStudio 5 Real-Time PCR Systems (Applied Biosystems, Foster City, CA, United States) using 2 \times SYBR Green Mix with miDETECT A Track miRNA-18a-5p Forward Primer. U6 was used as the control.

To detect target genes mRNA levels, total RNA was reversely transcribed to cDNA using the Reverse Transcription System (Promega, Madison, WI, United States). Real-time PCR was carried out using iTaq Universal SYBR Green Supermix (Bio-Rad, Hercules, CA, United States). GAPDH served as the internal control. All primers were synthesized by Invitrogen (Shanghai, China). The primer sequences used in this study were as follows: FGF1: 5'-ACACCGACGGGCTTTTATACG-3' (forward), 5'-CCCATTCTTCTTGAGGCCAAC-3' (reverse); HI F1A: 5'-TGTAATGCTCCCCTCACCCA-3' (forward), 5'-TGCA GGGTCAGCACTACTTC-3' (reverse); GAPDH: 5'-ATCGTGG AAGGATCATGACCACA-3' (forward), 5'-AGAGGCAGGGA TGATGTTCTGGA-3' (reverse). Each sample was detected in triplicate, and the specificity of PCR reaction was estimated by melt curve. Fold-change of miRNA level was calculated using the $\Delta\Delta$ CT method.

Cell Culture

HRMECs were obtained from Angio-Proteomie (Peabody, MA, United States). HRMECs were cultured in endothelial cell medium (ECM) supplemented with 5% Newborn Calf Serum (NCS; Life Technologies), 20 μ g/ml of ECGS, 100 μ g/ml streptomycin, and 100 U/ml penicillin in a T-25 flask coated with 8.5 μ g/ml of BPF at 37°C with 5% CO₂. When the cells became 90% confluent, they were subcultured at a 1:3 ratio. HEK293 cells were purchased from the American Type Culture Collection (ATCC, Manassas, VA, United States) and cultured in DMEM supplemented with 10% NCS and incubated at 37°C with 5% CO₂.

Proliferation Assay

Proliferation of HRMECs was detected by Cell Counting Kit-8 (CCK-8, Dojindo Molecular Technologies, Shanghai, China) assay. Cells were seeded in 96-well plates (3 \times 10³/well). Agomir-18a-5p (50 nM) or a scrambled negative control (NC) was transfected into HRMECs using Lipofectamine RNAiMAX Reagent (Invitrogen, Carlsbad, CA) following the manufacturer's instruction. After incubation for 1–5 days at 37°C with 5% CO₂, 10% CCK-8 solution was added to each well and incubated for 1 h. The absorbance value was measured at 450 nm using Multiscan GO (Thermo scientific).

Wound Healing Assay

The wound healing assay was carried out to explore the role of miR-18a-5p in HRMECs function. The cells were seeded in 12-well plates (2.5 \times 10⁵ cells per well) and grown to approximately 60% confluence. They were then transfected with agomir-18a-5p (50 nM) or NC and expanded until cells attained more than 90% confluence. A vertical scratch was created symmetrically across the confluent cell monolayer with a sterile 200- μ L

pipette tip. The floating cells and cellular debris were carefully removed by flushing them away with PBS and then replenishing each well with fresh culture medium. Closure of the denuded regions was monitored by capturing images of wound closure at 0 and 24 h observed with an inverted microscope (DMI8; Leica Microsystems Inc., Buffalo Grove, IL, United States). Cell migration areas were analyzed using ImageJ.

Transwell Assay

Transwell migration assay was performed with 8-mm pore size culture inserts (Transwell; Corning, NY, United States) placing into the wells of 24-well culture plates. Four hundred microliters of ECM containing 10% NCS were added in the lower chamber of each well. 1.5×10^5 cells (transfected with either miR-18a-5p or NC for 24 h) in 200 μ l of DMEM were then added to the upper chamber. At 48 h after transfection, 1.5×10^5 cells in 200 μ l of NCS-free ECM were then added to the upper chamber. After 24 h of incubation, the cells that had migrated through the pores were fixed by 4% paraformaldehyde, stained with crystal violet (Beyotime Biotechnology, Shanghai, China) for 15 min, respectively. The images were taken immediately using a microscope, and the cells were counted by ImageJ.

Tube Formation Assay

The HRMECs were plated in 6-well plates and transfected with 50 nM agomir-18a-5p or scrambled agomir (NC) for 48 h. The cells were harvested and cultured in a Matrigel Matrix (100 μ l/well; Corning, NY) pre-coated 48-well plate (4×10^4 /well). After 6 h of incubation, the cells were photographed using an inverted microscope. The parameters of tube formation by HRMECs were measured by ImageJ with the Angiogenesis Analyzer plugin. The number of mesh and total tube length were quantified and showed in this study.

Western Blot

Total proteins of HRMECs were extracted by RIPA Lysis Assay (Beyotime Biotechnology, Shanghai, China), and the concentration was measured by Pierce BCA Protein Assay Kit (Thermo Fisher Scientific, Rockford, IL, United States) according to the manufacturer's instructions. Fifty micrograms of total proteins were separated in 15% sodium dodecyl sulfate (SDS) polyacrylamide gels and transferred onto polyvinylidene difluoride (PVDF) membrane. The membrane was blocked in 5% skimmed milk for 2 h and subsequently incubated overnight at 4°C with primary antibodies against FGF1 (1:200; Abcam, CA, United States), HIF1A (1:200; CST, Boston, MA, United States), or β -actin (1:2,000; Invitrogen, Rockford, IL, United States). Horseradish peroxidase (HRP)-linked anti-rabbit IgG (1:1,000; Cell Signaling Technology) was used as the secondary antibody. Specific protein bands were detected with Clarity™ Western ECL Substrate Kit (Bio-Rad) and captured by FluorChem E system (Bio-Techne, Minneapolis, MN, United States). The gray intensity value of each protein band was analyzed by ImageJ.

Luciferase Reporter Assays

The 3' untranslated region (UTR) of human FGF1 was amplified and cloned into pmirGLO vector (Promega, Madison, WI,

United States). The mutated seed region was generated by a site-directed mutagenesis method to remove complementarity to nucleotides of miR-18a-5p. HEK293 cells were cultured in 96-well plates and co-transfected with 100 ng/well of recombinant pmirGLO vector and 50 nM of miR-18a-5p or NC with Lipofectamine 2000 transfection reagent (Thermo Fisher Scientific). The luciferase activity was detected with Dual-Glo Luciferase Assay System (Promega) according to the manufacturer's instructions.

Statistical Analysis

All data were analyzed and plotted using GraphPad Prism software and presented as the mean \pm standard error of the mean (SEM). Statistical differences were analyzed by Student's *t*-test or One-way ANOVA for multiple comparisons of mean values. $p < 0.05$ was considered statistically significant.

RESULTS

MiR-18a-5p Expression During Development and OIR Model

To identify miRNAs that are specifically regulated in developing retina, total RNAs isolated from pups retina at P1, P7, and P17, and performed high-throughput sequencing (GEO accession No. GSE142029). Based on the expression pattern analysis using STEM software, which implements a novel method for clustering short time series expression data that can differentiate between real and random patterns, miRNAs were mainly assigned to DD (down-regulated and down-regulated) profiles (Figure 1A). MiR-18a-5p was a typical miRNA that was consistently down-regulated during retinal development from P1 to P17 (Figure 1B). Moreover, miR-18a-5p was one of the most differentially expressed miRNAs (Figure 1C). Quantitative qPCR validated that miR-18a-5p was significantly down-regulated during retinal development (Figure 2A). Those the relative miR-18a-5p levels were decreased approximately 3-fold at P7, 125-fold at P17 and 300-fold at 8 weeks compared to P1 retina. On the other hand, the retinal miR-18a-5p levels were significantly up-regulated in OIR mice (Figure 2B). In order to verify that miR-18a-5p was expressed in the endothelium during retinal development, we have isolated RECs by MACS magnetic separation methods from retina and confirmed using pan-endothelial markers, anti-CD31 and anti-VE-Cadherin antibody (Figure 2C). In results, we showed that the miR-18a-5p expression levels in RECs of adult mice was significantly down-regulated compared to pups (Figure 2D), which is consistent with whole retinal expression pattern. Taken together, these results suggested that miR-18a-5p played a potential regulatory role in retinal physiologic and pathologic vascularization.

MiR-18a-5p Suppressed Neovascularization in OIR Mice

To determine whether miR-18a-5p contributes to modulating retinal neovascularization, the OIR mice model was established (Figure 3A) and were treated with intravitreal injection of

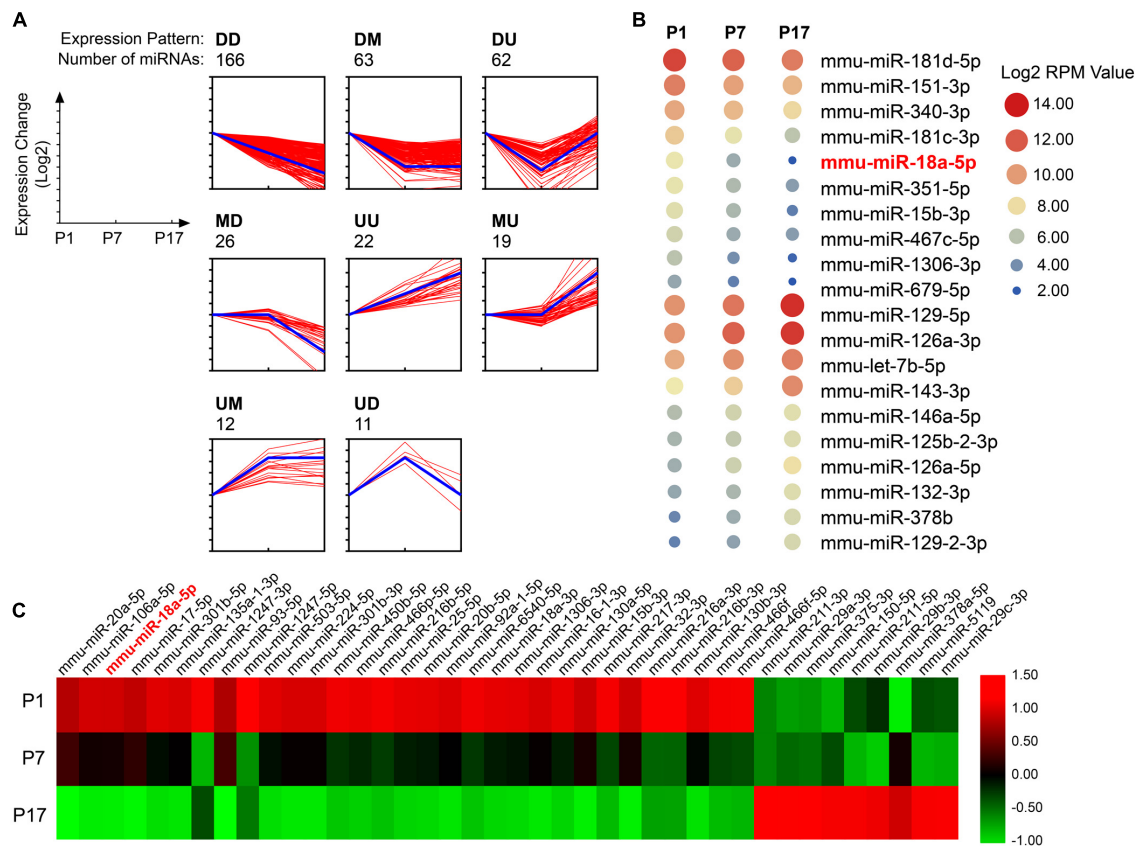


FIGURE 1 | Dynamic expression profiles of miRNA during retinal development. **(A)** The expression patterns of miRNAs specifically regulated in developing retinas ($n = 5$ per group). The miRNAs were assigned to the model profile that more closely matched its time series according to the correlation coefficient. D, down-regulated; M, maintain; U, up-regulated. Thick blue line, model profile of log of expression change ratio over time. Thin red line, all individual gene expression profiles. **(B)** Twenty typical continuously down-regulated or up-regulated miRNAs. RPM, the number of reads per million (RPM) clean tags. **(C)** The 40 most differentially expressed miRNAs during retinal development from postnatal day 1 (P1) to P17.

agomir-18a-5p (a type of chemically modified miR-18a-5p mimic) at P12. The expression level of miR-18a-5p at P17 was markedly increased in the agomir-18a-5p injected mice compared to scrambled agomir group (agomir-NC) (Figure 3B). At P17, agomir-18a-5p suppressed retinal neovascularization (~50%; Figures 3C,D) but not vaso-obliteration (Figures 3E,F) compared with agomir-NC control. Thus, miR-18a-5p showed therapeutic effect in retinal neovascularization in OIR model.

MiR-18a-5p Suppressed HRMECs Function

To further explore the inhibitory effect of miR-18a-5p on endothelial function, agomir-18a-5p was transfected into HRMECs and then evaluated its effect on cell proliferation and migration. The CCK-8 proliferation assay revealed that the cells treated with agomir-18a-5p showed significant reduction in absorbance compared with agomir-NC (Figure 4A). There was a significant decrease in cell number from day 2 to day 5 (Figure 4B), which indicated that agomir-18a-5p inhibited the viability of HRMECs. We then conducted wound healing and transwell assay to detect the migratory

capacity of HRMECs with agomir-18a-5p transfection. The agomir-18a-5p transfected cells showed 48% reduction in wound healing (Figures 4C,D) and 42% in transwell assay (Figures 4E,F) compared with agomir-NC. These results suggest that ectopic expression of miR-18a-5p restrains HRMECs migratory activity. To further evaluate the angiogenic effect of miR-18a-5p on HRMECs, we conducted the tube formation assay. As shown in Figure 4G, agomir-18a-5p substantially suppressed the tube formation of HRMECs, resulting in reductions of 73% in mesh numbers (Figure 4H) and 37% in total tubule length (Figure 4I). Taken together, miR-18a-5p up-regulation restrains the normal function of HRMECs including proliferation, migration, and the tube formation ability.

MiR-18a-5p Targeted Angiogenic Genes FGF1 and HIF1A

It has been reported that the effect of miRNAs on the endothelial cell function and vessel growth can be elucidated by regulating their target genes. To identify potential target genes of miR-18a-5p, we analyzed the seed sequence of miR-18a-5p (CGUGGAA),

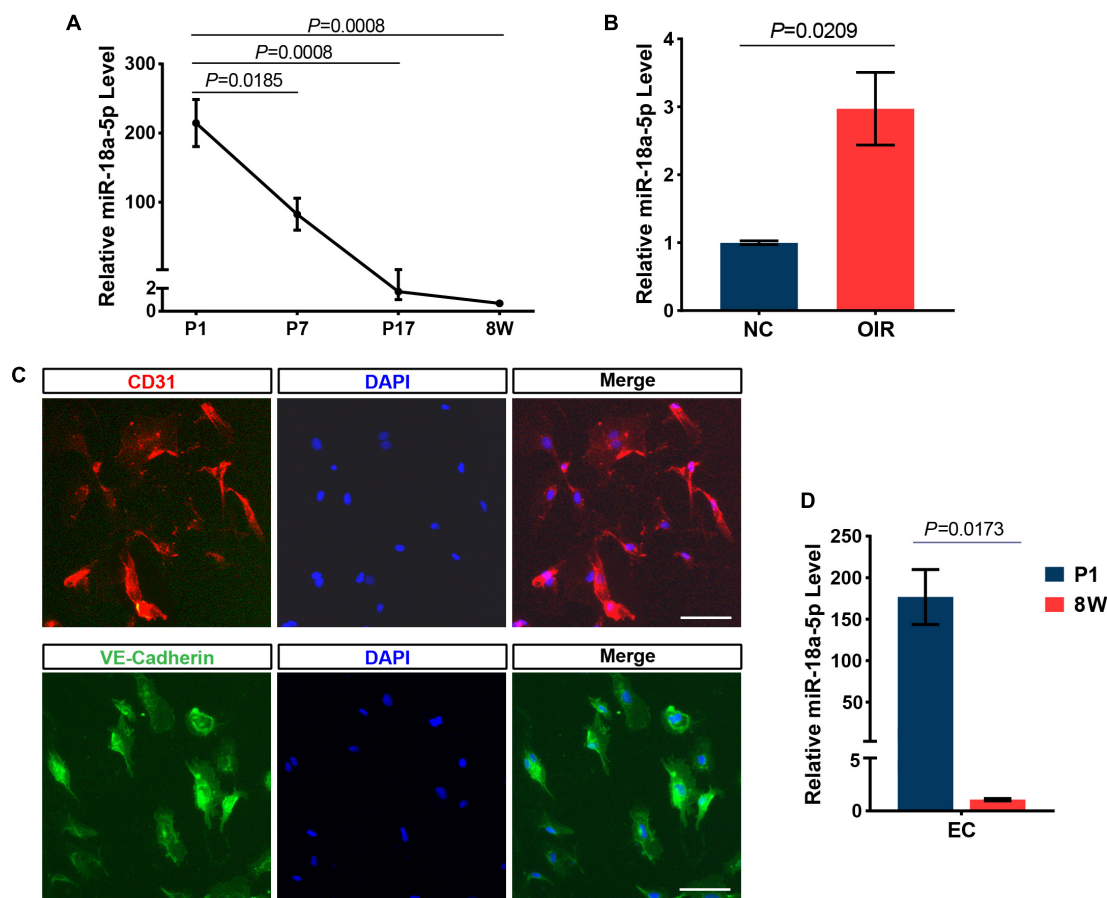


FIGURE 2 | MiR-18a-5p expression during development and OIR model. **(A)** MiR-18a-5p was significantly down-regulated during developing retina ($n = 5$ per group; One-way ANOVA with Bonferroni correction). **(B)** The miR-18a-5p expression level was increased by approximately 3-fold in OIR mice ($n = 6$ per group; unpaired t -test). **(C)** The isolated RECs were identified by immunostaining using pan-endothelial markers anti-CD31 and anti-VE-Cadherin antibody. Scale bar, 50 μ m. **(D)** MiR-18a-5p retinal endothelial cells (RECs) from 8-week-old (8W) mice was markedly down-regulated compared to newborn pups ($n = 3$ per group; unpaired t -test). OIR, oxygen-induced proliferative retinopathy; NC, normal control.

conserved in both human and murine subjects. These bases were complementarily paired with the 3' untranslated region (UTR) of FGF1 and HIF1A (**Figure 5A**). The mRNA levels of FGF1 and HIF1A in OIR retina were markedly decreased at P17 compared with normal control (NC) group (**Figure 5B**). Moreover, overexpression of miR-18a-5p in HRMECs significantly reduced the FGF1 and HIF1A expression both in mRNA and protein levels (**Figures 5C,D**). HIF1A has been identified as a target of miR-18a-5p (Krutilina et al., 2014). Consequently, luciferase reporter assay was carried out to determine the FGF1 is a novel target gene of miR-18a-5p. The wild-type or mutant 3' UTRs of FGF1 was successfully cloned into the luciferase reporter vector pmirGLO (**Figure 5E**). The result of the luciferase reporter assay revealed that agomir-18a-5p transfection significantly reduced the luciferase activity compared to the agomir-NC group (**Figure 5F**). Whereas, that the mutant reporter vector abolished the interactions between agomir-18a-5p and FGF1 3' UTRs. Our finding suggests those roles of miR-18a-5p in EC function and retinal neovascularization are through inhibiting the direct target genes FGF1 and HIF1A.

DISCUSSION

VEGF is a potent proangiogenic factor. Anti-VEGF drugs have been used to treat ocular neovascularization with certain efficacy. However, anti-VEGF therapy does have some limitations and may cause undesirable side effects. Several articles have reported that VEGF is necessary for vascular homeostasis (Carmeliet et al., 1996; Lee et al., 2007). Long-term clinical application of anti-VEGF drug may result in adverse ocular responses (Falavarjani and Nguyen, 2013). Due to continuous development of novel drugs, it will become more difficult to prove superiority of one drug versus another (Grossniklaus et al., 2010). However, it is still necessary to find new drugs to treat neovascular eye diseases as supplements to or even possible replacements for anti-VEGF drugs.

Non-coding RNAs (ncRNAs), including miRNA, long non-coding RNA (lncRNA) and circular RNA (circRNA), are related not only to tumorigenesis, but also to neurological, cardiovascular, developmental, and other diseases (Esteller, 2011). Dozens of miRNAs have been used as diagnostic

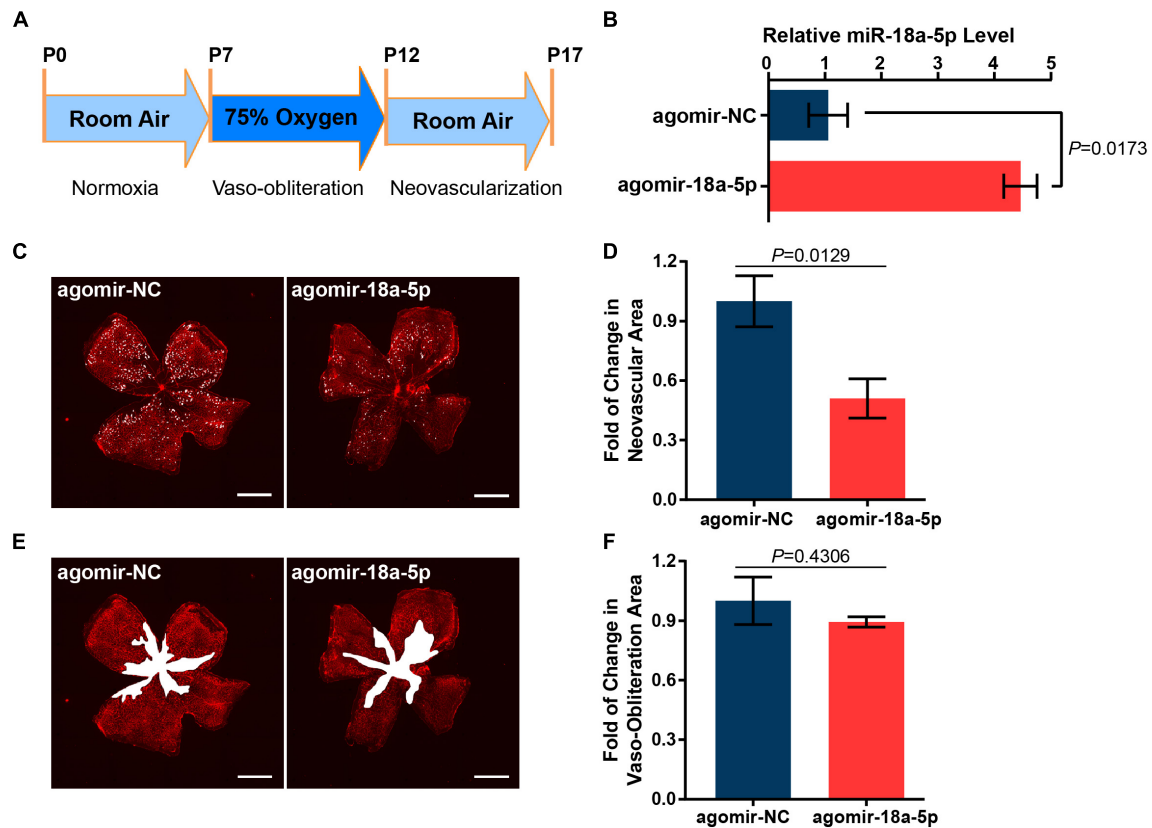


FIGURE 3 | MiR-18a-5p suppressed pathologic neovascularization in OIR. **(A)** Schematic of establishment of OIR mice model. **(B)** The relative miR-18a-5p expression level in OIR mice with intravitreal injection of agomir-18a-5p or agomir-NC. **(C,E)** Representative images of P17 OIR retinas injected with agomir-18a-5p or agomir-NC. Pathologic neovascularization and vaso-oblivation were labeled as white spot and area, respectively. Scale bar, 500 μ m. **(D,F)** Quantitative analysis of pathologic neovascularization and vaso-oblivation, respectively. The data are presented as mean \pm SEM ($n = 6$ per group; unpaired t -test). OIR, oxygen-induced proliferative retinopathy.

and prognostic biomarkers, and some miRNAs intended to treat diseases as varied as cancer, hepatitis, and scleroderma have reached clinical trials (Maurer et al., 2010; Bader, 2012; Janssen et al., 2013). It is easier to design and synthesize oligonucleotide-based drugs than to identify small molecules, and it makes the process of identifying active ncRNA drugs much faster than that of small-molecule drugs (Matsui and Corey, 2017; Nakamori et al., 2019). To utilize the mammalian RNAi pathway for potent and specific inhibition of putative therapeutic targets, RNAi drugs have the same advantages (Setten et al., 2019). To date, few RNAi-based drugs have received approval. Examples include Vitravene being applied to treat ocular/CMV retinitis (Roehr, 1998), and Kynamro being developed to treat systemic/familial hypercholesterolemia (Geary et al., 2015). Despite considerable progress, there are still some critical challenges in the development of oligonucleotide-based therapeutics, including identification of the best oligonucleotide drugs and delivery methods for each disease type, avoidance of non-specific toxicity caused by immunogenic reactions, off-target effects, and renal accumulation (Rupaimoole and Slack, 2017; Levin, 2019; Setten et al., 2019).

Recent studies have shown that multiple miRNAs were aberrantly expressed in pathological vessel growth and played vital roles in regulation of the neovascular eye diseases. Several specific miRNAs were highly expressed in ECs that curbed angiogenesis. These anti-angiogenic miRNAs include miR-126, miR-150, miR-184, and miR-342, whereas miR-132, miR-27, miR-155, and members of the let-7 family promoted angiogenesis (Zhang et al., 2017). The miR-17-92 cluster is one of the most extensively studied miRNAs, especially in tumor angiogenesis. Overexpression of the miR-17-92 cluster was shown to promote tumor angiogenesis (Dews et al., 2006). Transfection of ECs simultaneously with miR-18a, miR-17-5p, and miR-20a also rescued the defect in endothelial cell proliferation and morphogenesis initiated by the loss of Dicer (Suarez et al., 2008). On the contrary, Doebele et al. found that members of the microRNA-17-92 cluster exhibited a cell-intrinsic antiangiogenic function in ECs, and antagomir-17/20 selectively enhanced neovascularization of Matrigel plugs but did not affect tumor angiogenesis (Doebele et al., 2010). Based on the above information, the regulation of angiogenesis by miR-17-92 cluster is complex, and specific members of this cluster may mediate differential and context-dependent effects on neovascularization.

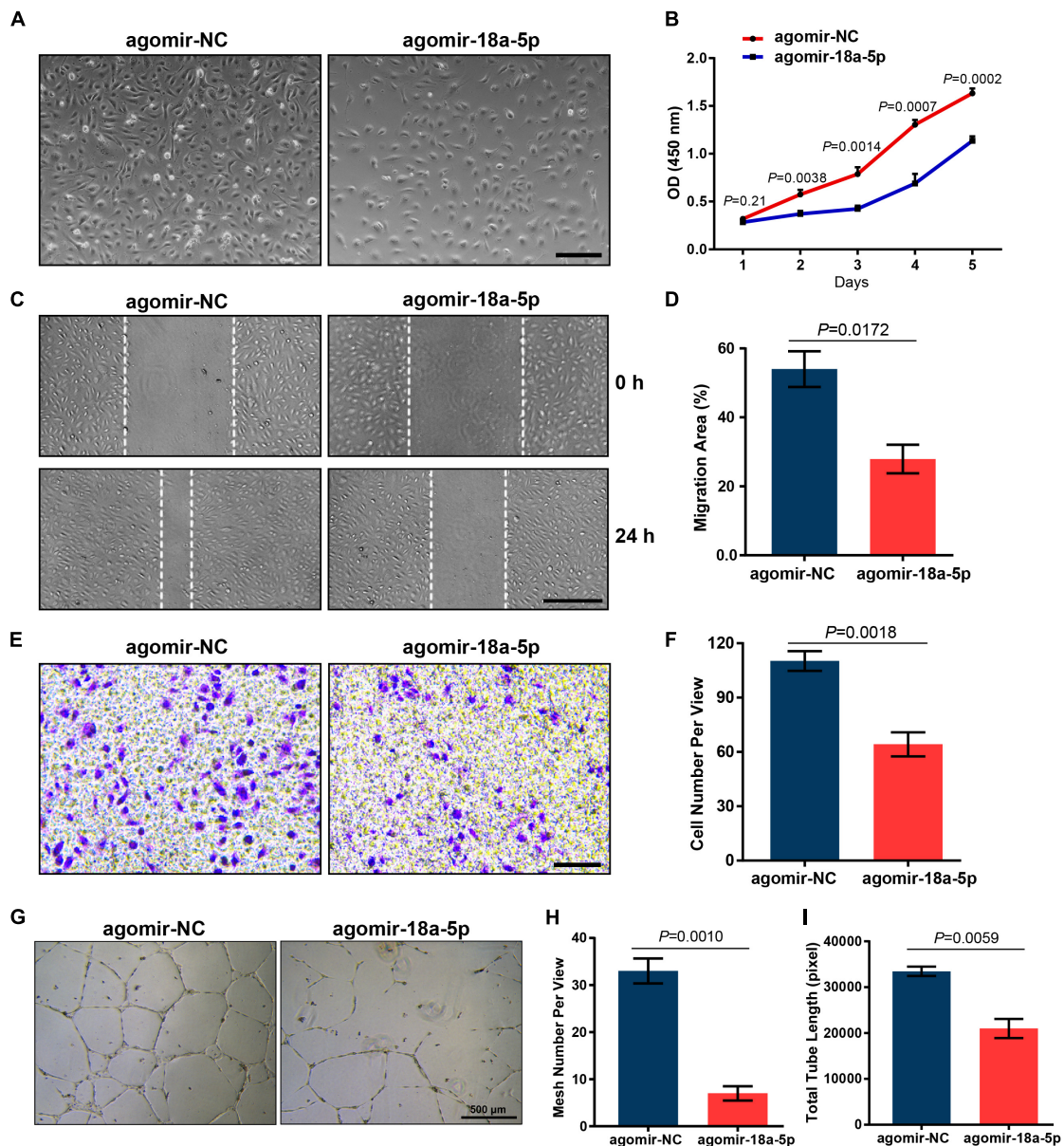


FIGURE 4 | Effect of miR-18a-5p on HRMECs function. **(A)** Representative images of HRMECs transfected with agomir-18a-5p or agomir-NC. Scale bar, 200 μ m. **(B)** HRMEC proliferation was suppressed by agomir-18a-5p treatment. The data are presented as mean \pm SEM ($n = 3$ per group; unpaired t -test). **(C,E)** Agomir-18a-5p treatment significantly suppressed the migratory ability of HRMECs wound healing or transwell assay. Scale bars, 200 μ m. **(D,F)** Quantitative analysis for HRMECs wound healing and transwell assay. The values are presented as mean \pm SEM ($n = 3$ per group; unpaired t -test). **(G)** Representative images of tube formation assay in HRMECs with agomir-18a-5p or agomir-NC transfection. Scale bar, 500 μ m. **(H,I)** Quantitative analysis of HRMECs in mesh numbers and total tubule length. The data are presented as mean \pm SEM ($n = 3$ per group; unpaired t -test). HRMECs, human retinal microvascular endothelial cells; CCK-8, Cell Counting Kit-8.

It seems more reasonable to target individual members of the miR-17-92 cluster to gain an accurate and deep understanding of their role in angiogenesis modulation.

In this study, miR-18a-5p was shown to be highly expressed in embryonic retinas and significantly down-regulated during the course of development. On the other hand, the expression level of miR-18a-5p in OIR retinas was higher than that of normal retinas. It can be speculated that miR-18a-5p may be involved

in the initiation and progression of angiogenesis. Therefore, we evaluated the potential role and anti-angiogenic efficacy of miR-18a-5p in treating retinal neovascularization. Our study showed that the upregulation of miR-18a-5p was capable of inhibiting pathological angiogenesis in an OIR model as well as HRMEC functions. Accumulating evidence shows that FGF1 and HIF1A are closely associated with angiogenesis, which are target genes of miR-18a-5p.

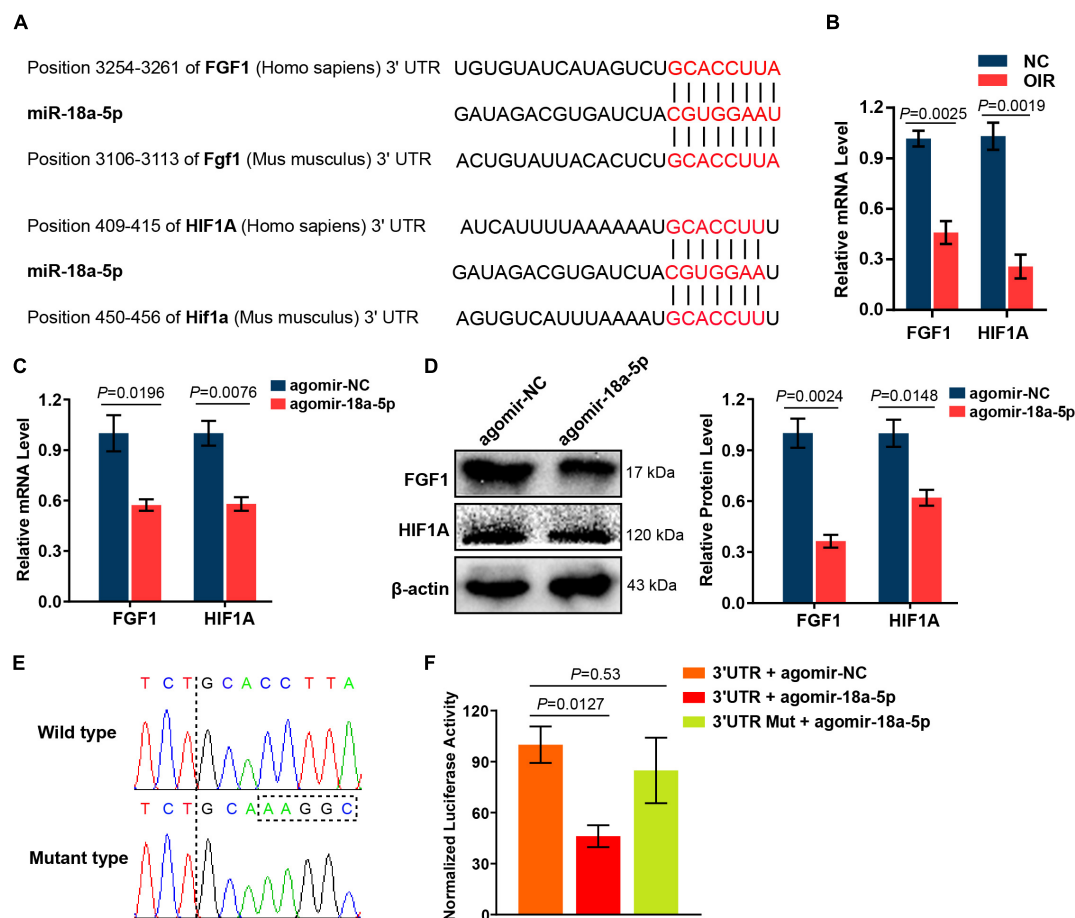


FIGURE 5 | miR-18a-5p targeted angiogenic genes FGF1 and HIF1A. **(A)** Alignment between the binding sites of miR-18a-5p and its targets. **(B)** FGF1 and HIF1A mRNA levels in OIR retinas at P17 ($n = 5-8$ per group; unpaired t -test). **(C)** FGF1 and HIF1A mRNA levels in HRMECs with agomir-18a-5p or agomir-NC transfection ($n = 3$ per group; unpaired t -test). **(D)** The protein levels of FGF1 and HIF1A in HRMECs with agomir-18a-5p or agomir-NC transfection ($n = 3$ per group; unpaired t -test). **(E)** Sequencing results of pmirGLO-FGF1 3' UTR and pmirGLO-FGF1 3' UTR-Mut. **(F)** Luciferase activity of HEK293 cells co-transfected with pmirGLO-FGF1 3' UTR or pmirGLO-FGF1 3' UTR-Mut, and agomir-18a-5p or agomir-NC ($n = 3$ per group; unpaired t -test). FGF1, fibroblast growth factor 1; HIF1A, hypoxia-inducible factor 1- α ; HRMECs, human retinal microvascular endothelial cells; HEK293, human embryonic kidney 293; NC, normal control; 3' UTR, 3' untranslated region; Mut, mutant.

FGF1 belongs to the FGF family and exerted a pro-angiogenic effect on ECs (Ding et al., 2003; Mori et al., 2013). FGF1 and VEGF have been demonstrated to be synergistic in the induction of angiogenesis as exposure of ECs to both FGF1 and VEGF in combination stimulated a greater angiogenic response than the response to either growth factor alone (Xue and Greisler, 2002). FGF1 also contributed to the increased number of blood vessels in the middle ear mucosa during otitis media (Husseman et al., 2012). In addition, controlled delivery of FGF1 and neuregulin-1 (NRG1) from biodegradable microparticles could promote cardiac repair in a rat myocardial infarction model through induction of tissue revascularization and activation of endogenous regeneration (Formiga et al., 2014).

HIF1A is an important transcription factor that tends to be activated in the hypoxia condition, in which it is known to increase the expression of VEGF and promote angiogenesis (Shweiki et al., 1992; Jones et al., 2002;

Ahluwalia and Tarnawski, 2012). HIF1A was also correlated to other genes in the angiogenesis pathway such as FGF2, and platelet-derived growth factor alpha (PDGFA) (Hoffmann et al., 2008). Non-steroidal anti-inflammatory drugs could inhibit hypoxia-induced *in vitro* angiogenesis in gastric microvascular ECs via reducing accumulation of HIF1A (Jones et al., 2002). Previous studies have revealed that HIF1A was overexpressed in multiple types of human cancer. Overexpression of HIF1A and HIF2A in squamous cell head-and-neck cancer (SCHNC) was related to locally aggressive behavior, intensification of angiogenesis, and resistance to carboplatin chemoradiotherapy (Koukourakis et al., 2002). There was a significant correlation between microvessel density and HIF1A expression in non-myoinvasive endometrioid carcinomas as well (Espinosa et al., 2010).

In the present study, overexpression of miR-18a-5p in HRMECs could significantly reduce the mRNA and protein levels

of FGF1 and HIF1A. Studies also confirmed that miR-18a-5p is a direct regulator of these genes in ECs through targeting their 3' UTR seed sequences. Therefore, miR-18a-5p might function as a suppressor of retinal neovascularization by targeting these two genes. Our study provides evidence of the association between miR-18a-5p and pathologic retinal angiogenesis. MiR-18a-5p is a potential therapeutic target for treatment neovascular ocular diseases.

DATA AVAILABILITY STATEMENT

The datasets generated for this study can be found in NCBI GEO accession GSE142029.

ETHICS STATEMENT

All animal experiments were performed strictly according to the ARVO Statement for the Use of Animals in Ophthalmic and

Vision Research and approved by the Animal Care and Use Committee of the Wenzhou Medical University.

AUTHOR CONTRIBUTIONS

Z-LC, RD'A, JQ, and FL conceptualized and designed the study. J-TG, X-XL, D-WP, and W-MZ acquisition of the data. J-TG, X-XL, D-WP, and Z-LC analyzed and interpreted the data. J-TG, D-WP, and Z-LC wrote, reviewed, and/or revised the manuscript. All authors have read and approved the final version of the manuscript.

FUNDING

This research was supported by the National Natural Science Foundation of China (81770918) and Zhejiang Provincial Natural Science Foundation of China (LY16H120006).

REFERENCES

- Ahluwalia, A., and Tarnawski, A. S. (2012). Critical role of hypoxia sensor-HIF-1alpha in VEGF gene activation. Implications for angiogenesis and tissue injury healing. *Curr. Med. Chem.* 19, 90–97. doi: 10.2174/092986712803413944
- Augustin, H. G., and Koh, G. Y. (2017). Organotypic vasculature: from descriptive heterogeneity to functional pathophysiology. *Science* 357:eaal2379. doi: 10.1126/science.aal2379
- Bader, A. G. (2012). miR-34 - a microRNA replacement therapy is headed to the clinic. *Front. Genet.* 3:120. doi: 10.3389/fgene.2012.00120
- Bai, Y., Bai, X., Wang, Z., Zhang, X., Ruan, C., and Miao, J. (2011). MicroRNA-126 inhibits ischemia-induced retinal neovascularization via regulating angiogenic growth factors. *Exp. Mol. Pathol.* 91, 471–477. doi: 10.1016/j.yexmp.2011.04.016
- Bartel, D. P. (2009). MicroRNAs: target recognition and regulatory functions. *Cell* 136, 215–233. doi: 10.1016/j.cell.2009.01.002
- Bonauer, A., Carmona, G., Iwasaki, M., Mione, M., Koyanagi, M., Fischer, A., et al. (2009). MicroRNA-92a controls angiogenesis and functional recovery of ischemic tissues in mice. *Science* 324, 1710–1713. doi: 10.1126/science.1174381
- Carmeliet, P., Ferreira, V., Breier, G., Pollefeyt, S., Kieckens, L., Gertsenstein, M., et al. (1996). Abnormal blood vessel development and lethality in embryos lacking a single VEGF allele. *Nature* 380, 435–439. doi: 10.1038/380435a0
- Chamorro-Jorganes, A., Lee, M. Y., Araldi, E., Landskroner-Eiger, S., Fernandez-Fuertes, M., Sahraei, M., et al. (2016). VEGF-Induced Expression of miR-17-92 Cluster in Endothelial Cells Is Mediated by ERK/ELK1 Activation and Regulates Angiogenesis. *Circ. Res.* 118, 38–47. doi: 10.1161/CIRCRESAHA.115.307408
- Chen, C., Chen, H., He, Y., and Xia, R. (2018). TBtools, a Toolkit for Biologists integrating various biological data handling tools with a user-friendly interface. *BioRxiv* [preprint]. doi: 10.1101/289660
- Connor, K. M., Krah, N. M., Dennison, R. J., Aderman, C. M., Chen, J., Guerin, K. I., et al. (2009). Quantification of oxygen-induced retinopathy in the mouse: a model of vessel loss, vessel regrowth and pathological angiogenesis. *Nat. Protoc.* 4, 1565–1573. doi: 10.1038/nprot.2009.187
- Dews, M., Homayouni, A., Yu, D., Murphy, D., Seignani, C., Wentzel, E., et al. (2006). Augmentation of tumor angiogenesis by a Myc-activated microRNA cluster. *Nat. Genet.* 38, 1060–1065. doi: 10.1038/ng1855
- Ding, L., Liu, W., Sun, J., Paoni, S. F., Hernady, E., Fenton, B. M., et al. (2003). FGF1 and VEGF mediated angiogenesis in KHT tumor-bearing mice. *Adv. Exp. Med. Biol.* 530, 603–609. doi: 10.1007/978-1-4615-0075-9_59
- Doebele, C., Bonauer, A., Fischer, A., Scholz, A., Reiss, Y., Urbich, C., et al. (2010). Members of the microRNA-17-92 cluster exhibit a cell-intrinsic antiangiogenic function in endothelial cells. *Blood* 115, 4944–4950. doi: 10.1182/blood-2010-01-264812
- Ernst, J., and Bar-Joseph, Z. (2006). STEM: a tool for the analysis of short time series gene expression data. *BMC Bioinformatics* 7:191. doi: 10.1186/1471-2105-7-191
- Espinosa, I., Jose Carnicer, M., Catasus, L., Canet, B., D'Angelo, E., Zannoni, G. F., et al. (2010). Myometrial invasion and lymph node metastasis in endometrioid carcinomas: tumor-associated macrophages, microvessel density, and HIF1A have a crucial role. *Am. J. Surg. Pathol.* 34, 1708–1714. doi: 10.1097/PAS.0b013e3181f32168
- Esteller, M. (2011). Non-coding RNAs in human disease. *Nat. Rev. Genet.* 12, 861–874. doi: 10.1038/nrg3074
- Falavarjani, K. G., and Nguyen, Q. D. (2013). Adverse events and complications associated with intravitreal injection of anti-VEGF agents: a review of literature. *Eye* 27, 787–794. doi: 10.1038/eye.2013.107
- Ferreira, R., Santos, T., Amar, A., Gong, A., Chen, T. C., Tahara, S. M., et al. (2014a). Argonaute-2 promotes miR-18a entry in human brain endothelial cells. *J. Am. Heart Assoc.* 3:e000968. doi: 10.1161/JAHA.114.000968
- Ferreira, R., Santos, T., Amar, A., Tahara, S. M., Chen, T. C., Giannotta, S. L., et al. (2014b). MicroRNA-18a improves human cerebral arteriovenous malformation endothelial cell function. *Stroke* 45, 293–297. doi: 10.1161/STROKEAHA.113.003578
- Folkman, J. (1995). Angiogenesis in cancer, vascular, rheumatoid and other disease. *Nat. Med.* 1, 27–31.
- Formiga, F. R., Pelacho, B., Garbayo, E., Imbuluzqueta, I., Diaz-Herraez, P., Abizanda, G., et al. (2014). Controlled delivery of fibroblast growth factor-1 and neuregulin-1 from biodegradable microparticles promotes cardiac repair in a rat myocardial infarction model through activation of endogenous regeneration. *J. Control. Release* 173, 132–139. doi: 10.1016/j.jconrel.2013.10.034
- Fruttiger, M. (2007). Development of the retinal vasculature. *Angiogenesis* 10, 77–88. doi: 10.1007/s10456-007-9065-1
- Fu, Z., Gong, Y., Liegl, R., Wang, Z., Liu, C. H., Meng, S. S., et al. (2017). FGF21 administration suppresses retinal and choroidal neovascularization in mice. *Cell Rep.* 18, 1606–1613. doi: 10.1016/j.celrep.2017.01.014
- Geary, R. S., Baker, B. F., and Crooke, S. T. (2015). Clinical and preclinical pharmacokinetics and pharmacodynamics of mipomersen (kynamro(R)): a second-generation antisense oligonucleotide inhibitor of apolipoprotein B. *Clin. Pharmacokinet.* 54, 133–146. doi: 10.1007/s40262-014-0224-4
- Grossniklaus, H. E., Kang, S. J., and Berglin, L. (2010). Animal models of choroidal and retinal neovascularization. *Prog. Retin. Eye Res.* 29, 500–519. doi: 10.1016/j.preteyeres.2010.05.003
- He, L., and Hannon, G. J. (2004). MicroRNAs: small RNAs with a big role in gene regulation. *Nat. Rev. Genet.* 5, 522–531. doi: 10.1038/nrg1379

- Hoffmann, A. C., Mori, R., Vallbohmer, D., Brabender, J., Klein, E., Drebber, U., et al. (2008). High expression of HIF1 α is a predictor of clinical outcome in patients with pancreatic ductal adenocarcinomas and correlated to PDGFA, VEGF, and bFGF. *Neoplasia* 10, 674–679. doi: 10.1593/neo.08292
- Hussemann, J., Palacios, S. D., Rivkin, A. Z., Oehl, H., and Ryan, A. F. (2012). The role of vascular endothelial growth factors and fibroblast growth factors in angiogenesis during otitis media. *Audiol. Neurotol.* 17, 148–154. doi: 10.1159/000333805
- Janssen, H. L., Reesink, H. W., Lawitz, E. J., Zeuzem, S., Rodriguez-Torres, M., Patel, K., et al. (2013). Treatment of HCV infection by targeting microRNA. *N. Engl. J. Med.* 368, 1685–1694. doi: 10.1056/NEJMoa1209026
- Jones, M. K., Szabo, I. L., Kawanaka, H., Husain, S. S., and Tarnawski, A. S. (2002). von Hippel Lindau tumor suppressor and HIF-1 α : new targets of NSAIDs inhibition of hypoxia-induced angiogenesis. *FASEB J.* 16, 264–266. doi: 10.1096/fj.01-0589fje
- Kaluza, D., Kroll, J., Gesierich, S., Manavski, Y., Boeckel, J. N., Doebele, C., et al. (2013). Histone deacetylase 9 promotes angiogenesis by targeting the antiangiogenic microRNA-17-92 cluster in endothelial cells. *Arterioscler. Thromb. Vasc. Biol.* 33, 533–543. doi: 10.1161/ATVBAHA.112.300415
- Kim, D., Langmead, B., and Salzberg, S. L. (2015). HISAT: a fast spliced aligner with low memory requirements. *Nat. Methods* 12, 357–360. doi: 10.1038/nmeth.3317
- Koukourakis, M. I., Giatromanolaki, A., Sivridis, E., Simopoulos, C., Turley, H., Talks, K., et al. (2002). Hypoxia-inducible factor (HIF1A and HIF2A), angiogenesis, and chemoradiotherapy outcome of squamous cell head-and-neck cancer. *Int. J. Radiat. Oncol. Biol. Phys.* 53, 1192–1202. doi: 10.1016/s0360-3016(02)02848-1
- Kruttila, R., Sun, W., Sethuraman, A., Brown, M., Seagroves, T. N., Pfeffer, L. M., et al. (2014). MicroRNA-18a inhibits hypoxia-inducible factor 1 α activity and lung metastasis in basal breast cancers. *Breast Cancer Res.* 16:R78. doi: 10.1186/bcr3693
- Lee, S., Chen, T. T., Barber, C. L., Jordan, M. C., Murdock, J., Desai, S., et al. (2007). Autocrine VEGF signaling is required for vascular homeostasis. *Cell* 130, 691–703. doi: 10.1016/j.cell.2007.06.054
- Levin, A. A. (2019). Treating disease at the RNA level with oligonucleotides. *N. Engl. J. Med.* 380, 57–70. doi: 10.1056/NEJMr1705346
- Liu, C. H., Sun, Y., Li, J., Gong, Y., Tian, K. T., Evans, L. P., et al. (2015). Endothelial microRNA-150 is an intrinsic suppressor of pathologic ocular neovascularization. *Proc. Natl. Acad. Sci. U.S.A.* 112, 12163–12168. doi: 10.1073/pnas.1508426112
- Liu, C. H., Wang, Z., Sun, Y., SanGiovanni, J. P., and Chen, J. (2016). Retinal expression of small non-coding RNAs in a murine model of proliferative retinopathy. *Sci. Rep.* 6:33947. doi: 10.1038/srep33947
- Matsui, M., and Corey, D. R. (2017). Non-coding RNAs as drug targets. *Nat. Rev. Drug Discov.* 16, 167–179. doi: 10.1038/nrd.2016.117
- Maurer, B., Stanczyk, J., Jungel, A., Akhmetshina, A., Trenkmann, M., Brock, M., et al. (2010). MicroRNA-29, a key regulator of collagen expression in systemic sclerosis. *Arthritis Rheum.* 62, 1733–1743. doi: 10.1002/art.27443
- Mori, S., Tran, V., Nishikawa, K., Kaneda, T., Hamada, Y., Kawaguchi, N., et al. (2013). A dominant-negative FGF1 mutant (the R50E mutant) suppresses tumorigenesis and angiogenesis. *PLoS One* 8:e57927. doi: 10.1371/journal.pone.0057927
- Nakamori, M., Junn, E., Mochizuki, H., and Mouradian, M. M. (2019). Nucleic Acid-Based Therapeutics for Parkinson's Disease. *Neurotherapeutics* 16, 287–298. doi: 10.1007/s13311-019-00714-7
- Nunes, D. N., Dias-Neto, E., Cardo-Vila, M., Edwards, J. K., Dobroff, A. S., Giordano, R. J., et al. (2015). Synchronous down-modulation of miR-17 family members is an early causative event in the retinal angiogenic switch. *Proc. Natl. Acad. Sci. U.S.A.* 112, 3770–3775. doi: 10.1073/pnas.1500008112
- Potente, M., Gerhardt, H., and Carmeliet, P. (2011). Basic and therapeutic aspects of angiogenesis. *Cell* 146, 873–887. doi: 10.1016/j.cell.2011.08.039
- Roehr, B. (1998). Fomivirsen approved for CMV retinitis. *J. Int. Assoc. Physicians AIDS Care* 4, 14–16.
- Rupaimoole, R., and Slack, F. J. (2017). MicroRNA therapeutics: towards a new era for the management of cancer and other diseases. *Nat. Rev. Drug Discov.* 16, 203–222. doi: 10.1038/nrd.2016.246
- Selvam, S., Kumar, T., and Fruttiger, M. (2018). Retinal vasculature development in health and disease. *Prog. Retin. Eye Res.* 63, 1–19. doi: 10.1016/j.preteyeres.2017.11.001
- Setten, R. L., Rossi, J. J., and Han, S. P. (2019). The current state and future directions of RNAi-based therapeutics. *Nat. Rev. Drug Discov.* 18, 421–446. doi: 10.1038/s41573-019-0017-14
- Shen, J., Yang, X., Xie, B., Chen, Y., Swaim, M., Hackett, S. F., et al. (2008). MicroRNAs regulate ocular neovascularization. *Mol. Ther.* 16, 1208–1216. doi: 10.1038/mt.2008.104
- Shi, L., Fisslthaler, B., Zippel, N., Fromel, T., Hu, J., Elghezawy, A., et al. (2013). MicroRNA-223 antagonizes angiogenesis by targeting beta1 integrin and preventing growth factor signaling in endothelial cells. *Circ. Res.* 113, 1320–1330. doi: 10.1161/CIRCRESAHA.113.301824
- Shweiki, D., Itin, A., Soffer, D., and Keshet, E. (1992). Vascular endothelial growth factor induced by hypoxia may mediate hypoxia-initiated angiogenesis. *Nature* 359, 843–845. doi: 10.1038/359843a0
- Smith, L. E., Wesolowski, E., McLellan, A., Kostyk, S. K., D'Amato, R., Sullivan, R., et al. (1994). Oxygen-induced retinopathy in the mouse. *Invest. Ophthalmol. Vis. Sci.* 35, 101–111.
- Stahl, A., Connor, K. M., Sapieha, P., Chen, J., Dennison, R. J., Krah, N. M., et al. (2010). The mouse retina as an angiogenesis model. *Invest. Ophthalmol. Vis. Sci.* 51, 2813–2826. doi: 10.1167/iov.10-5176
- Su, X., Sorenson, C. M., and Sheibani, N. (2003). Isolation and characterization of murine retinal endothelial cells. *Mol. Vis.* 9, 171–178.
- Suarez, Y., Fernandez-Hernando, C., Yu, J., Gerber, S. A., Harrison, K. D., Pober, J. S., et al. (2008). Dicer-dependent endothelial microRNAs are necessary for postnatal angiogenesis. *Proc. Natl. Acad. Sci. U.S.A.* 105, 14082–14087. doi: 10.1073/pnas.0804597105
- Sundermeier, T. R., and Palczewski, K. (2012). The physiological impact of microRNA gene regulation in the retina. *Cell Mol. Life Sci.* 69, 2739–2750. doi: 10.1007/s00018-012-0976-7
- van Zandwijk, N., Pavlakis, N., Kao, S. C., Linton, A., Boyer, M. J., Clarke, S., et al. (2017). Safety and activity of microRNA-loaded minicells in patients with recurrent malignant pleural mesothelioma: a first-in-man, phase 1, open-label, dose-escalation study. *Lancet Oncol.* 18, 1386–1396. doi: 10.1016/S1470-2045(17)30621-6
- Wallace, D. K., and Wu, K. Y. (2013). Current and future trends in treatment of severe retinopathy of prematurity. *Clin. Perinatol.* 40, 297–310. doi: 10.1016/j.clp.2013.02.005
- Xia, F., Sun, J. J., Jiang, Y. Q., and Li, C. F. (2018). MicroRNA-384-3p inhibits retinal neovascularization through targeting hexokinase 2 in mice with diabetic retinopathy. *J. Cell. Physiol.* 234, 721–730. doi: 10.1002/jcp.26871
- Xu, Y., Lu, X., Hu, Y., Yang, B., Tsui, C. K., Yu, S., et al. (2018). Melatonin attenuated retinal neovascularization and neuroglial dysfunction by inhibition of HIF-1 α -VEGF pathway in oxygen-induced retinopathy mice. *J. Pineal Res.* 64:e12473. doi: 10.1111/jpi.12473
- Xue, L., and Greisler, H. P. (2002). Angiogenic effect of fibroblast growth factor-1 and vascular endothelial growth factor and their synergism in a novel in vitro quantitative fibrin-based 3-dimensional angiogenesis system. *Surgery* 132, 259–267. doi: 10.1067/msy.2002.125720
- Zhang, Y., Cai, S., Jia, Y., Qi, C., Sun, J., Zhang, H., et al. (2017). Decoding non-coding RNAs: role of MicroRNAs and long non-coding RNAs in ocular neovascularization. *Theranostics* 7, 3155–3167. doi: 10.7150/thno.19646
- Zhou, Q., Anderson, C., Hanus, J., Zhao, F., Ma, J., Yoshimura, A., et al. (2016). Strand and cell type-specific function of microRNA-126 in angiogenesis. *Mol. Ther.* 24, 1823–1835. doi: 10.1038/mt.2016.108

Conflict of Interest: The authors declare that the research was conducted in the absence of any commercial or financial relationships that could be construed as a potential conflict of interest.

Copyright © 2020 Guan, Li, Peng, Zhang, Qu, Lu, D'Amato and Chi. This is an open-access article distributed under the terms of the Creative Commons Attribution License (CC BY). The use, distribution or reproduction in other forums is permitted, provided the original author(s) and the copyright owner(s) are credited and that the original publication in this journal is cited, in accordance with accepted academic practice. No use, distribution or reproduction is permitted which does not comply with these terms.



Targeting Neuroinflammation in Neovascular Retinal Diseases

Tianxi Wang, Demetrios I. Tsiurkis and Ye Sun*

Department of Ophthalmology, Boston Children's Hospital, Harvard Medical School, Boston, MA, United States

OPEN ACCESS

Edited by:

Zhuo Shao,
University of Toronto, Canada

Reviewed by:

José Carlos Rivera,
University of Montreal, Canada
Kyriaki Thermos,
University of Crete, Greece

*Correspondence:

Ye Sun
ye.sun@childrens.harvard.edu

Specialty section:

This article was submitted to
Neuropharmacology,
a section of the journal
Frontiers in Pharmacology

Received: 30 November 2019

Accepted: 20 February 2020

Published: 10 March 2020

Citation:

Wang T, Tsiurkis DI and Sun Y
(2020) Targeting Neuroinflammation
in Neovascular Retinal Diseases.
Front. Pharmacol. 11:234.
doi: 10.3389/fphar.2020.00234

Retinal blood vessels provide the necessary energy, nutrients and oxygen in order to support visual function and remove harmful particles from blood, thus acting to protect neuronal cells. The homeostasis of the retinal vessels is important for the maintenance of retinal visual function. Neovascularization is the most common cause of blindness in patients with retinopathy. Previous studies have shown that inflammatory mediators are known key regulators in retinopathy, but their causal link has been elusive. Although inflammation is often thought to arise from inflammatory cells like macrophages, neutrophils, and resident microglia, retinal neurons have also been reported to contribute to inflammation, through inflammatory signals, which mediate blood vessel growth. Therefore, it is important to explore the detailed mechanisms of neuroinflammation's effects on retinal neovascularization. This review looks to summarize current research on the relationship between retinal angiogenesis and neuroinflammation in retinopathy, as well as the potential effects of neuroinflammation on retinal neovascularization in different animal models.

Keywords: neuroinflammation, neovascularization, retina, retinal disease, pharmacology

RETINAL NEOVASCULAR DISEASES AND NEUROINFLAMMATION

The retina is part of the central nervous system and retinal blood vessels are functionally analogous to the cerebral blood vessels (Campbell and Humphries, 2012). The blood-retinal barrier (BRB) is formed by glial cells, pericytes and endothelial cells (Cunha-Vaz et al., 2011). Retinal blood vessels provide abundant energy and oxygen to neuronal and glial cells, while neuronal and glial cells provide growth factors for retinal blood vessels. In order to facilitate this, there is frequent and effective communication between neurons and vessels in the retina. Additionally, the BRB plays an important role in maintaining the function of the retina. An injury to the BRB causes neuroinflammation, which can result in BRB breakdown and neovascularization (NV). There is abundant evidence indicating that retinal NV is often accompanied by neuroinflammation (Connor et al., 2007; Sun et al., 2015, 2017), but how exactly neuroinflammation regulates retinal NV remains largely unknown.

Neuroinflammation causes neuronal damage, leading to the development and progression of a variety of neurodegenerative diseases such as Alzheimer's disease, Parkinson's disease, and retinal degeneration (Xing et al., 2016), as well as retinal neovascular diseases (Tonade et al., 2016; Sun et al., 2017). This damage triggers a rapid transformation of the retinal microglia into an activated state, switching its function from patrol to shield of the injured site (Chang et al., 2009). Activated microglia continue to secrete inflammatory mediators that act on other cells to induce and amplify

uncontrolled inflammatory responses. Retinal neurons, such as photoreceptors, have been recently reported to signal for blood vessel growth through inflammatory signals (Tonade et al., 2016; Sun et al., 2017). Pro-inflammatory cytokines and chemokines can cause neuronal apoptosis or death (Leung et al., 2016).

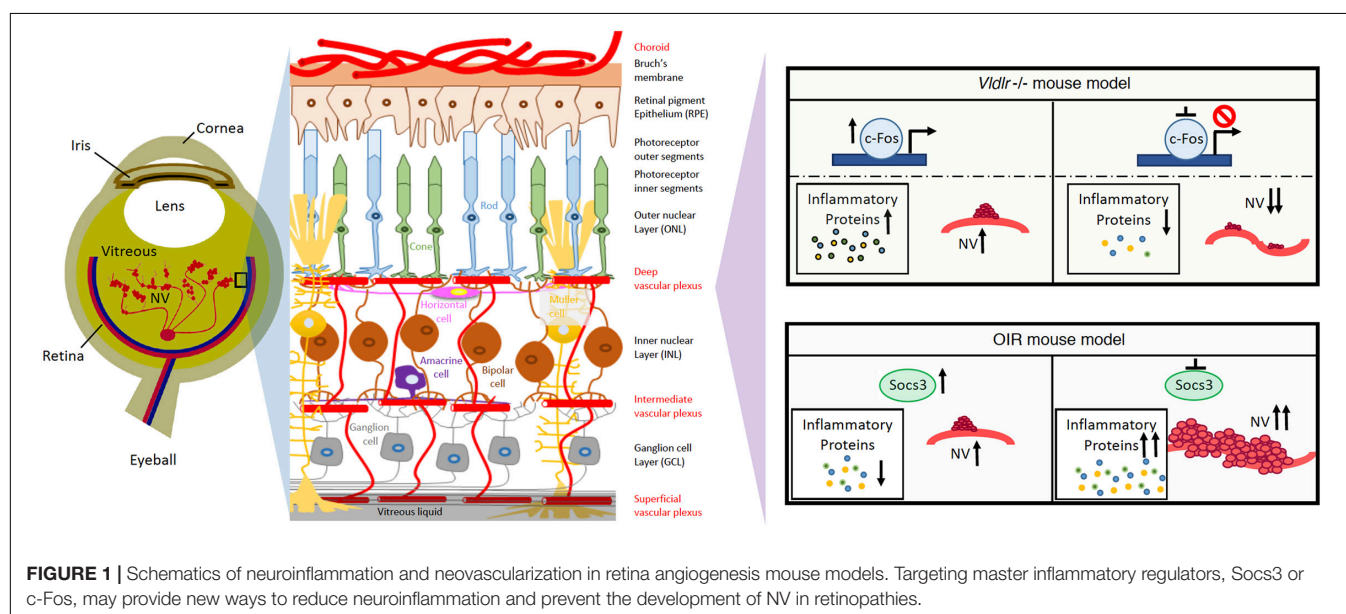
Neovascularization is the proliferation of new micro blood vessels in the retina. In clinic, these are called intraretinal microvascular abnormalities, as well as retinal NV when these new blood vessels grow to the surface of the retina (Campochiaro, 2013). The biggest difference between normal retinal vessels and new blood vessels is that the new blood vessels lack tight junction proteins, which means that the plasma in the NV leaks into the surrounding tissue, such as the vitreous, and causes the degeneration of the vitreous, resulting in vitreous hemorrhage. Furthermore, the subsequent pull on the retina by degraded vitreous may result in retinal detachment, which involves the macula and results in severe vision loss (Campochiaro, 2013). NV occurs in many ocular diseases, such as retinopathy of prematurity (ROP), age-related macular degeneration (AMD), and diabetic retinopathy (DR). However, the causes of retinal NV may be different among the different types of retinopathy.

Choroidal NV (CNV) is the major cause of vision loss in neovascular AMD. CNV is a process that involves the participation of vascular and extravascular components, such that CNV results in a complex tissue, which is composed of blood vessels, glial cells, myofibroblasts, retinal pigment epithelia, and inflammatory cells (Spaide, 2006). Immune dysregulation and inflammatory processes have been linked with CNV pathogenesis both clinically and experimentally (Ambati et al., 2013; Kumar et al., 2014; Chen et al., 2016). The release of a series of pro-angiogenic factors may be one of the causes of inflammatory cells triggering angiogenesis (Noel et al., 2007). Neutrophil or macrophage depletion was shown to reduce CNV formation (Espinosa-Heidmann et al., 2003; Zhou et al., 2005). Similarly, macrophage depletion was

associated with decreased vascular endothelial growth factor (VEGF) production in laser-induced CNV (Espinosa-Heidmann et al., 2003). The recruitment of blood-derived macrophages appears to be more associated with CNV than resident microglia by bone marrow transplantation experiments (Caicedo et al., 2005). In addition, photoreceptors can control proliferative angiogenesis by modulating photoreceptor inflammatory signals (Sun et al., 2017).

Retinopathy of prematurity is a major cause of blindness in children (Lutty et al., 2006; Tasman et al., 2006; Blencowe et al., 2012). With advances in neonatal care, smaller and more premature infants who are at high risk for ROP are saved; therefore, increasing the overall incidence of ROP. Currently there is no preventative treatment for ROP. To find new ROP treatments in addition to earlier preventative therapies, understanding the molecular mechanisms of ROP development becomes crucial. Photoreceptors have been reported to play an important role in the ROP pathogenesis (Akula et al., 2007a,b). Oxygen-induced retinopathy (OIR) is a classical and effective model for studying NV in the ROP (Smith et al., 1994; Connor et al., 2009). In this model, relative hypoxia leads to an increase in the expression of VEGF in the retina neurons and glial cells (Sun et al., 2015). At the same time, hypoxia can also cause neuroinflammation by activating microglia (Deliyanti et al., 2017). The continually activated microglia promote inflammation and VEGF expression, and eventually exacerbate NV.

Diabetic retinopathy is a common and complex diabetic complication. Hyperglycemia and dyslipidemia are closely related to the development of DR (Fu et al., 2016, 2018). NV often occurs in the later stages of DR (Klaassen et al., 2013; Hu et al., 2017). There are numerous angiogenic molecules that take part in regulated new-vessel formation in DR, including VEGF (Tanaka et al., 1997). The microglia in retinas are activated in animal diabetic models (Rungger-Brandle et al., 2000;



Kezic et al., 2013). Recent studies show that inflammatory changes in photoreceptors influence pathological angiogenesis in DR (Du et al., 2013; Kern and Berkowitz, 2015; Liu et al., 2016; Tonade et al., 2017). A dysregulation of communications among neurons including the photoreceptors, vascular cells, and glial cells plays a major role in the pathophysiology of proliferative DR (Antonetti et al., 2012), which is characterized by neovascularization, neuroinflammation and neurodegeneration.

TARGETING NEUROINFLAMMATION IN NEOVASCULAR RETINAL DISEASES

Although NV is the leading cause of blindness in eye diseases, including DR, AMD, and ROP, the detail mechanisms of the pathogenesis of NV are still not well understood (Zhang and Ma, 2007). Currently, ablation surgery, angiogenesis inhibitors and growth factor antibody therapy are the primary methods for NV treatment. Angiogenesis inhibitors include ranibizumab, bevacizumab and aflibercept. Bevacizumab is also known as Macugen, Avastin or Lucentis. All of the inhibitors have a similar function – they mainly inhibit the formation of new retinal blood vessels by inactivating VEGF (Avery et al., 2014; Fu et al., 2016). However, it is important to note that ablation surgery may cause damage to the retina, and anti-VEGF treatments may inhibit the growth of normal vessels and neurons (Fu et al., 2019). It is crucial to find new ways to treat retinal NV.

Because neuroinflammation is associated with retinal NV and promotes retinal NV (Fu et al., 2018), it may be possible to target neuroinflammation to treat retinal NV (Rivera et al., 2017). Recently, there have been attempts to suppress NV through controlling key regulators of inflammatory signals in the eye. Suppressor of cytokine signaling 3 (SOCS3) is an inducible negative feedback regulator of growth factor and inflammation signaling (Stahl et al., 2012), and plays a critical role in regulating inflammatory responses. SOCS3 is able to prevent pathological angiogenesis, and a conditional loss of SOCS3 in endothelial cells results in increased pathological NV (Stahl et al., 2012). The expression of SOCS3 is significantly increased in neuronal and glial cells in the OIR mouse model (Sun et al., 2015). A conditional knockout of SOCS3 in neuronal and glial cells exacerbates glial cell activation and neuroinflammation while promoting VEGFA expression and retinal NV (Sun et al., 2015). In addition, knocking out tumor necrosis factor alpha (TNF α), one of the inflammatory cytokines, appears to be protective in the OIR mouse model (Gardiner et al., 2005). Therefore, targeting the master regulator of cytokine signaling, SOCS3, may provide a new way to reduce neuroinflammation and suppress NV in the eye (Figure 1).

REFERENCES

- Akula, J. D., Hansen, R. M., Martinez-Perez, M. E., and Fulton, A. B. (2007a). Rod photoreceptor function predicts blood vessel abnormality in retinopathy of prematurity. *Invest. Ophthalmol. Vis. Sci.* 48, 4351–4359.
- Akula, J. D., Mocko, J. A., Moskowitz, A., Hansen, R. M., and Fulton, A. B. (2007b). The oscillatory potentials of the dark-adapted electroretinogram

c-Fos is a proto-oncogene and is also important for many cellular functions. In human photoreceptor cells, c-Fos expression occurs throughout the development process (Yu et al., 1994). c-Fos regulates the expression of the rod-specific gene (He et al., 1998) and apoptosis in photoreceptor (Hafezi et al., 1997; Hobson et al., 2000; Poon et al., 2000). Additionally, c-Fos is strongly related to metabolic demands (Sun et al., 2017). In a retinal angiogenesis mouse model of very low-density lipoprotein receptor (Vldlr) knockout mice, the expression levels of c-Fos and inflammatory cytokine (TNF α and Interleukin 6) are significantly increased in photoreceptors. Additionally, c-Fos controls retinal NV by modulating the neuroinflammation signals in this model (Sun et al., 2017). Therefore, targeting c-Fos may provide another way to reduce neuroinflammation in photoreceptors and prevent the development of NV in retinopathies (Figure 1).

In short, neuroinflammation is closely linked to angiogenesis, and improving the neuroinflammatory mechanism helps to inhibit retinal angiogenesis, while blocking inflammatory signals has also been reported to exacerbate retinal angiogenesis in the CNV model (Apte et al., 2006; Ambati et al., 2013). This happens because inflammation itself has two sides. In the early stages of neuroinflammation, activated glial cells work to clear damaged cells and protect the homeostasis of the retina. Persistent inflammation leads to a loss of control of glial cells, which in turn leads to an attack on their own cells through the secretion of inflammatory factors, exacerbating retinal angiogenesis. Therefore, inhibition of neuroinflammation to treat retinal angiogenesis is still controversial. To seek a better way to treat neuroinflammation, more investigation is needed to explore the detailed relationship between neuroinflammation and angiogenesis.

AUTHOR CONTRIBUTIONS

TW, DT, and YS contributed to the draft and edits of the manuscript. All authors approved the final manuscript.

ACKNOWLEDGMENTS

This work was supported by the NIH/NEI (R01EY030140 and R01EY029238), BrightFocus Foundation, Boston Children's Hospital Ophthalmology Foundation, and Boston Children's Hospital/IDDR (1U54HD090255) (YS). We thank Wenbo Li and Xudong Wang for their discussion.

in retinopathy of prematurity. *Invest. Ophthalmol. Vis. Sci.* 48, 5788–5797.

- Ambati, J., Atkinson, J. P., and Gelfand, B. D. (2013). Immunology of age-related macular degeneration. *Nat. Rev. Immunol.* 13, 438–451. doi: 10.1038/nri3459
- Antonetti, D. A., Klein, R., and Gardner, T. W. (2012). Diabetic retinopathy. *N. Engl. J. Med.* 366, 1227–1239.

- Apte, R. S., Richter, J., Herndon, J., and Ferguson, T. A. (2006). Macrophages inhibit neovascularization in a murine model of age-related macular degeneration. *PLoS Med.* 3:e310. doi: 10.1371/journal.pmed.0030310
- Avery, R. L., Castellarin, A. A., Steinle, N. C., Dhoot, D. S., Pieramici, D. J., See, R., et al. (2014). Systemic pharmacokinetics following intravitreal injections of ranibizumab, bevacizumab or aflibercept in patients with neovascular AMD. *Br. J. Ophthalmol.* 98, 1636–1641. doi: 10.1136/bjophthalmol-2014-305252
- Blencowe, H., Cousens, S., Oestergaard, M. Z., Chou, D., Moller, A. B., Narwal, R., et al. (2012). National, regional, and worldwide estimates of preterm birth rates in the year 2010 with time trends since 1990 for selected countries: a systematic analysis and implications. *Lancet* 379, 2162–2172. doi: 10.1016/S0140-6736(12)60820-4
- Caicedo, A., Espinosa-Heidmann, D. G., Pina, Y., Hernandez, E. P., and Cousins, S. W. (2005). Blood-derived macrophages infiltrate the retina and activate Muller glial cells under experimental choroidal neovascularization. *Exp. Eye Res.* 81, 38–47. doi: 10.1016/j.exer.2005.01.013
- Campbell, M., and Humphries, P. (2012). The blood-retina barrier: tight junctions and barrier modulation. *Adv. Exp. Med. Biol.* 763, 70–84. doi: 10.1007/978-1-4614-4711-5_3
- Campochiaro, P. A. (2013). Ocular neovascularization. *J. Mol. Med.* 91, 311–321.
- Chang, R. C., Chiu, K., Ho, Y. S., and So, K. F. (2009). Modulation of neuroimmune responses on glia in the central nervous system: implication in therapeutic intervention against neuroinflammation. *Cell. Mol. Immunol.* 6, 317–326. doi: 10.1038/cmi.2009.42
- Chen, M., Lechner, J., Zhao, J., Toth, L., Hogg, R., Silvestri, G., et al. (2016). STAT3 activation in circulating monocytes contributes to neovascular age-related macular degeneration. *Curr. Mol. Med.* 16, 412–423. doi: 10.2174/1566524016666160324130031
- Connor, K. M., Krah, N. M., Dennison, R. J., Aderman, C. M., Chen, J., Guerin, K. I., et al. (2009). Quantification of oxygen-induced retinopathy in the mouse: a model of vessel loss, vessel regrowth and pathological angiogenesis. *Nat. Protoc.* 4, 1565–1573. doi: 10.1038/nprot.2009.187
- Connor, K. M., SanGiovanni, J. P., Lofqvist, C., Aderman, C. M., Chen, J., Higuchi, A., et al. (2007). Increased dietary intake of omega-3-polyunsaturated fatty acids reduces pathological retinal angiogenesis. *Nat. Med.* 13, 868–873. doi: 10.1038/nm1591
- Cunha-Vaz, J., Bernardes, R., and Lobo, C. (2011). Blood-retinal barrier. *Eur. J. Ophthalmol.* 21(Suppl. 6), S3–S9. doi: 10.5301/EJO.2010.6049
- Deliyanti, D., Talia, D. M., Zhu, T., Maxwell, M. J., Agrotis, A., Jerome, J. R., et al. (2017). Foxp3(+) Tregs are recruited to the retina to repair pathological angiogenesis. *Nat. Commun.* 8:748. doi: 10.1038/s41467-017-00751-w
- Du, Y., Veenstra, A., Palczewski, K., and Kern, T. S. (2013). Photoreceptor cells are major contributors to diabetes-induced oxidative stress and local inflammation in the retina. *Proc. Natl. Acad. Sci. U.S.A.* 110, 16586–16591. doi: 10.1073/pnas.1314571110
- Espinosa-Heidmann, D. G., Suner, I. J., Hernandez, E. P., Monroy, D., Csaky, K. G., and Cousins, S. W. (2003). Macrophage depletion diminishes lesion size and severity in experimental choroidal neovascularization. *Invest. Ophthalmol. Vis. Sci.* 44, 3586–3592.
- Fu, Z., Chen, C. T., Cagnone, G., Heckel, E., Sun, Y., Cakir, B., et al. (2019). Dyslipidemia in retinal metabolic disorders. *EMBO Mol. Med.* 11:e10473. doi: 10.15252/emmm.201910473
- Fu, Z., Gong, Y., Lofqvist, C., Hellstrom, A., and Smith, L. E. (2016). Review: adiponectin in retinopathy. *Biochim. Biophys. Acta* 1862, 1392–1400. doi: 10.1016/j.bbdis.2016.05.002
- Fu, Z., Wang, Z., Liu, C. H., Gong, Y., Cakir, B., Liegl, R., et al. (2018). Fibroblast growth factor 21 protects photoreceptor function in type 1 diabetic mice. *Diabetes* 67, 974–985. doi: 10.2337/db17-0830
- Gardiner, T. A., Gibson, D. S., de Gooyer, T. E., de la Cruz, V. F., McDonald, D. M., and Stitt, A. W. (2005). Inhibition of tumor necrosis factor- α improves physiological angiogenesis and reduces pathological neovascularization in ischemic retinopathy. *Am. J. Pathol.* 166, 637–644. doi: 10.1016/s0002-9440(10)62284-5
- Hafezi, F., Steinbach, J. P., Marti, A., Munz, K., Wang, Z. Q., Wagner, E. F., et al. (1997). The absence of c-fos prevents light-induced apoptotic cell death of photoreceptors in retinal degeneration in vivo. *Nat. Med.* 3, 346–349. doi: 10.1038/nm0397-346
- He, L., Campbell, M. L., Srivastava, D., Blocker, Y. S., Harris, J. R., Swaroop, A., et al. (1998). Spatial and temporal expression of AP-1 responsive rod photoreceptor genes and bZIP transcription factors during development of the rat retina. *Mol. Vis.* 4:32.
- Hobson, A. H., Donovan, M., Humphries, M. M., Tuohy, G., McNally, N., Carmody, R., et al. (2000). Apoptotic photoreceptor death in the rhodopsin knockout mouse in the presence and absence of c-fos. *Exp. Eye Res.* 71, 247–254. doi: 10.1006/exer.2000.0878
- Hu, J., Dziumbla, S., Lin, J., Bibli, S. I., Zukunft, S., de Mos, J., et al. (2017). Inhibition of soluble epoxide hydrolase prevents diabetic retinopathy. *Nature* 552, 248–252. doi: 10.1038/nature25013
- Kern, T. S., and Berkowitz, B. A. (2015). Photoreceptors in diabetic retinopathy. *J. Diabetes Invest.* 6, 371–380. doi: 10.1111/jdi.12312
- Kezic, J. M., Chen, X., Rakoczy, E. P., and McMenamin, P. G. (2013). The effects of age and Cx3cr1 deficiency on retinal microglia in the Ins2(Akita) diabetic mouse. *Invest. Ophthalmol. Vis. Sci.* 54, 854–863. doi: 10.1167/iops.12-10876
- Klaassen, I., Van Noorden, C. J., and Schlingemann, R. O. (2013). Molecular basis of the inner blood-retinal barrier and its breakdown in diabetic macular edema and other pathological conditions. *Progress Retin. Eye Res.* 34, 19–48. doi: 10.1016/j.preteyeres.2013.02.001
- Kumar, A., Zhao, L., Fariss, R. N., McMenamin, P. G., and Wong, W. T. (2014). Vascular associations and dynamic process motility in perivascular myeloid cells of the mouse choroid: implications for function and senescent change. *Invest. Ophthalmol. Vis. Sci.* 55, 1787–1796. doi: 10.1167/iops.13-13522
- Leung, J. W., Lau, B. W., Chan, V. S., Lau, C. S., and So, K. F. (2016). Abnormal increase of neuronal precursor cells and exacerbated neuroinflammation in the corpus callosum in murine model of systemic lupus erythematosus. *Rest. Neurol. Neurosci.* 34, 443–453. doi: 10.3233/RNN-160638
- Liu, H., Tang, J., Du, Y., Saadane, A., Tonade, D., Samuels, I., et al. (2016). Photoreceptor cells influence retinal vascular degeneration in mouse models of retinal degeneration and diabetes. *Invest. Ophthalmol. Vis. Sci.* 57, 4272–4281. doi: 10.1167/iops.16-19415
- Lutty, G. A., Chan-Ling, T., Phelps, D. L., Adamis, A. P., Berns, K. I., Chan, C. K., et al. (2006). Proceedings of the third international symposium on retinopathy of prematurity: an update on rop from the lab to the nursery (November 2003, Anaheim, California). *Mol. Vis.* 12, 532–580.
- Noel, A., Jost, M., Lambert, V., Lecomte, J., and Rakic, J. M. (2007). Anti-angiogenic therapy of exudative age-related macular degeneration: current progress and emerging concepts. *Trends molecular Med.* 13, 345–352. doi: 10.1016/j.molmed.2007.06.005
- Poon, H. K., Tso, M. O., and Lam, T. T. (2000). c-Fos protein in photoreceptor cell death after photic injury in rats. *Invest. Ophthalmol. Vis. Sci.* 41, 2755–2758.
- Rivera, J. C., Holm, M., Austeng, D., Morken, T. S., Zhou, T., Beaudry-Richard, A., et al. (2017). Retinopathy of prematurity: inflammation, choroidal degeneration, and novel promising therapeutic strategies. *J. Neuroinflamm.* 14:165. doi: 10.1186/s12974-017-0943-1
- Rungger-Brandle, E., Dosso, A. A., and Leuenberger, P. M. (2000). Glial reactivity, an early feature of diabetic retinopathy. *Invest. Ophthalmol. Vis. Sci.* 41, 1971–1980.
- Smith, L. E., Wesolowski, E., McLellan, A., Kostyk, S. K., D'Amato, R., Sullivan, R., et al. (1994). Oxygen-induced retinopathy in the mouse. *Invest. Ophthalmol. Vis. Sci.* 35, 101–111.
- Spaide, R. F. (2006). Rationale for combination therapies for choroidal neovascularization. *Am. J. Ophthalmol.* 141, 149–156. doi: 10.1016/j.ajo.2005.07.025
- Stahl, A., Joyal, J. S., Chen, J., Sapieha, P., Juan, A. M., Hatton, C. J., et al. (2012). SOCS3 is an endogenous inhibitor of pathologic angiogenesis. *Blood* 120, 2925–2929. doi: 10.1182/blood-2012-04-422527
- Sun, Y., Ju, M., Lin, Z., Fredrick, T. W., Evans, L. P., Tian, K. T., et al. (2015). SOCS3 in retinal neurons and glial cells suppresses VEGF signaling to prevent pathological neovascular growth. *Sci. Signal.* 8:ra94. doi: 10.1126/scisignal.aaa8695
- Sun, Y., Lin, Z., Liu, C. H., Gong, Y., Liegl, R., Fredrick, T. W., et al. (2017). Inflammatory signals from photoreceptor modulate pathological retinal

- angiogenesis via c-Fos. *J. Exp. Med.* 214, 1753–1767. doi: 10.1084/jem.20161645
- Tanaka, Y., Katoh, S., Hori, S., Miura, M., and Yamashita, H. (1997). Vascular endothelial growth factor in diabetic retinopathy. *Lancet* 349:1520. doi: 10.1016/s0140-6736(05)62099-5
- Tasman, W., Patz, A., McNamara, J. A., Kaiser, R. S., Trese, M. T., and Smith, B. T. (2006). Retinopathy of prematurity: the life of a lifetime disease. *Am. J. Ophthalmol.* 141, 167–174.
- Tonade, D., Liu, H., and Kern, T. S. (2016). Photoreceptor cells produce inflammatory mediators that contribute to endothelial cell death in diabetes. *Invest. Ophthalmol. Vis. Sci.* 57, 4264–4271.
- Tonade, D., Liu, H., Palczewski, K., and Kern, T. S. (2017). Photoreceptor cells produce inflammatory products that contribute to retinal vascular permeability in a mouse model of diabetes. *Diabetologia* 60, 2111–2120. doi: 10.1007/s00125-017-4381-5
- Xing, X., Liu, F., Xiao, J., and So, K. F. (2016). Neuro-protective mechanisms of *Lycium barbarum*. *Neuromol. Med.* 18, 253–263. doi: 10.1007/s12017-016-8393-y
- Yu, M. C., Li, W. W., Liu, K., and Yew, D. T. (1994). An immunohistochemical study of the c-fos protooncogene in the developing human retina. *Neuroscience* 60, 983–987. doi: 10.1016/0306-4522(94)90277-1
- Zhang, S. X., and Ma, J. X. (2007). Ocular neovascularization: implication of endogenous angiogenic inhibitors and potential therapy. *Prog. Retin. Eye Res.* 26, 1–37. doi: 10.1016/j.preteyeres.2006.09.002
- Zhou, J., Pham, L., Zhang, N., He, S., Gamulescu, M. A., Spee, C., et al. (2005). Neutrophils promote experimental choroidal neovascularization. *Mol. Vis.* 11, 414–424.

Conflict of Interest: The authors declare that the research was conducted in the absence of any commercial or financial relationships that could be construed as a potential conflict of interest.

Copyright © 2020 Wang, Tsirikis and Sun. This is an open-access article distributed under the terms of the Creative Commons Attribution License (CC BY). The use, distribution or reproduction in other forums is permitted, provided the original author(s) and the copyright owner(s) are credited and that the original publication in this journal is cited, in accordance with accepted academic practice. No use, distribution or reproduction is permitted which does not comply with these terms.



Arginase Pathway in Acute Retina and Brain Injury: Therapeutic Opportunities and Unexplored Avenues

Abdelrahman Y. Fouda^{1,2,3,4*}, Wael Eldahshan⁵, S. Priya Narayanan^{1,2,3,6},
R. William Caldwell^{2,5} and Ruth B. Caldwell^{1,2,3,7*}

¹ Vascular Biology Center, Medical College of Georgia, Augusta University, Augusta, GA, United States, ² Culver Vision Discovery Institute, Medical College of Georgia, Augusta University, Augusta, GA, United States, ³ Charlie Norwood VA Medical Center, Augusta, GA, United States, ⁴ Clinical Pharmacy Department, Faculty of Pharmacy, Cairo University, Giza, Egypt, ⁵ Department of Pharmacology and Toxicology, Medical College of Georgia, Augusta University, Augusta, GA, United States, ⁶ Department of Clinical and Administrative Pharmacy, University of Georgia, Athens, GA, United States, ⁷ Department of Cellular Biology and Anatomy, Medical College of Georgia, Augusta University, Augusta, GA, United States

OPEN ACCESS

Edited by:

Zhongjie Fu,
Harvard Medical School,
United States

Reviewed by:

Chenxi Qiu,
Harvard Medical School,
United States
Juan Zhou,
Dalhousie University, Canada

*Correspondence:

Abdelrahman Y. Fouda
afouda@augusta.edu
Ruth B. Caldwell
rcaldwel@augusta.edu

Specialty section:

This article was submitted to
Neuropharmacology,
a section of the journal
Frontiers in Pharmacology

Received: 04 December 2019

Accepted: 26 February 2020

Published: 17 March 2020

Citation:

Fouda AY, Eldahshan W,
Narayanan SP, Caldwell RW and
Caldwell RB (2020) Arginase Pathway
in Acute Retina and Brain Injury:
Therapeutic Opportunities
and Unexplored Avenues.
Front. Pharmacol. 11:277.
doi: 10.3389/fphar.2020.00277

Ischemic retinopathies represent a major cause of visual impairment and blindness. They include diabetic retinopathy (DR), acute glaucoma, retinopathy of prematurity (ROP), and central (or branch) retinal artery occlusion (CRAO). These conditions share in common a period of ischemia or reduced blood supply to the retinal tissue that eventually leads to neuronal degeneration. Similarly, acute brain injury from ischemia or trauma leads to neurodegeneration and can have devastating consequences in patients with stroke or traumatic brain injury (TBI). In all of these conditions, current treatment strategies are limited by their lack of effectiveness, adverse effects or short time window for administration. Therefore, there is a great need to identify new therapies for acute central nervous system (CNS) injury. In this brief review article, we focus on the pathway of the arginase enzyme as a novel therapeutic target for acute CNS injury. We review the recent work on the role of arginase enzyme and its downstream components in neuroprotection in both retina and brain acute injury models. Delineating the similarities and differences between the role of arginase in the retina and brain neurodegeneration will allow for better understanding of the role of arginase in CNS disorders. This will also facilitate repurposing the arginase pathway as a new therapeutic target in both retina and brain diseases.

Keywords: arginase, polyamines, retina, brain, ischemic injury, traumatic injury

INTRODUCTION

The brain and the retina are primary components of the central nervous system (CNS). In fact, the retina is developed from the brain tissue during embryogenesis. Therefore, it is considered an extension of the brain (London et al., 2013). Both the retina and the brain are neurovascular organs with supporting glia cells. It has been recently appreciated that disease mechanisms in the brain can be extended to the retina and vice versa (London et al., 2013; Jindal, 2015). With the retina and the brain being windows to each other, reviewing the literature on both organs greatly improves our understanding of the mechanisms of CNS injury and neurodegeneration.

Arginase is an important enzyme that has been conserved across species, including plants, bacteria, invertebrates, and vertebrates (Dzik, 2014). It has long been known for its central role in ammonia detoxification in the urea cycle of the liver (Wu and Morris, 1998). Furthermore, arginase has been shown to play an important role in different pathological conditions of the kidney, cardiovascular system, immune system, neurovascular system and certain types of cancers (Caldwell et al., 2018).

Several studies have linked arginase to CNS disorders such as Alzheimer's, multiple sclerosis, diabetic retinopathy (DR), retinopathy of prematurity (ROP), among others. In this brief review, we focus on the role of arginase in acute retina and brain injury. In addition, we briefly discuss the recent literature on the role of arginase in Alzheimer's disease (AD) and tauopathies, which is an area of increasing interest in recent years. The reader is referred to our recent reviews for discussion of the role of arginase in other chronic CNS disorders (Caldwell et al., 2015, 2018).

THE ARGINASE PATHWAY

Arginase is the enzyme that converts the amino acid, arginine, to ornithine and urea. Ornithine, the product of the arginase enzymatic reaction is further converted by ornithine decarboxylase (ODC) to form the polyamines, putrescine, spermine and spermidine and by the ornithine aminotransferase pathway to form proline (Caldwell et al., 2018). Ornithine can also be produced from glutamate via ornithine aminotransferase independent of arginase (Ginguay et al., 2017). There are two isoforms of arginase, arginase 1 (A1) and arginase 2 (A2) that are encoded by two different genes. Human A1 is a 322 amino acid protein while A2 has 354 amino acids (Dizikes et al., 1986; Gotoh et al., 1996). A1 and A2 amino acids sequences share more than 60% homology, however, they are identical in the enzyme catalytic site (Vockley et al., 1996). While the two isoforms mediate the same enzymatic reaction, they differ in their tissue and cell-specific expression as well as subcellular localization. A1 is cytosolic and it is highly expressed in liver tissue where it plays a major role in ammonia detoxification through the urea cycle. A2 is present in the mitochondria. It is highly expressed in the kidney. Both isoforms are expressed in other peripheral tissues and in the CNS, including the retina and the brain. The arginase isoforms and their downstream products polyamines and proline play diverse physiological roles and are induced or downregulated under pathological conditions (Morris, 2009; Caldwell et al., 2018). The polyamines can play important roles in cell proliferation, ion channel function, and neuroprotection. Proline is involved in collagen formation which can contribute to wound healing and/or fibrosis (Wu and Morris, 1998; Caldwell et al., 2018). Apart from their role in generation of polyamines and prolines, the arginases can compete with the nitric oxide synthase (NOS) enzyme for the common substrate arginine. Therefore, arginase can regulate the function of the three NOS isoforms, endothelial (eNOS), inducible (iNOS), and neuronal (nNOS).

ROLE OF THE ARGINASE PATHWAY IN ACUTE RETINA INJURY

For the sake of this review, we focus on two acute models of retinal injury, ischemia-reperfusion injury (IR) and optic nerve crush (ONC), a model for traumatic optic neuropathy (TON). Both models involve neurodegeneration in the form of loss of inner retinal neurons within one to 2 weeks of injury. Our work using both the IR injury and ONC models showed retinal neuroprotection in A2 knockout (KO) mice (Shosha et al., 2016; Xu et al., 2018). These studies show that A2 plays a central role in the pathophysiology of acute retinal injury. In the IR injury model, which leads to both neuronal and microvascular degeneration, A2 deletion reduced neurodegeneration and limited the formation of acellular capillaries. Furthermore, A2 deletion reduced oxidative stress and cell death by necroptosis. This protective effect of A2 deletion after IR injury was confirmed by the improved retina function as shown by electroretinographic recording in A2 KO mice (Shosha et al., 2016).

In the ONC model, A2 deletion reduced death of the retinal ganglion cells (RGCs) and prevented degeneration of their axons, while enhancing axonal sprouting. In addition to the decreased inflammatory response, A2 KO retinas showed increases in the neurotrophin, brain derived neurotrophic factor (BDNF) and its downstream signaling following ONC. In both the IR injury and ONC models, A2 deletion preserved retinal structure and reduced glial activation.

In contrast to A2, our studies with A1 knockout mice showed a worsened neurovascular outcome after IR injury with A1 deletion either globally or specifically in myeloid cells (Fouda et al., 2018). This worsened outcome was manifested in the form of retinal neurodegeneration and thinning as well as increased acellular capillaries. A1 deletion was also associated with increased retinal inflammatory response and cell death by necroptosis after IR. On the other hand, Intravitreal treatment with pegylated A1 (PEG-A1), a stable form of the enzyme, improved neuronal survival in WT mice after IR. Our *in vitro* studies showed an increased inflammatory response in A1KO macrophages which was ameliorated with PEG-A1 treatment. Intravitreal administration of A1KO macrophages worsened the retinal IR injury (Fouda et al., 2018). Collectively these data show a protective role of myeloid A1 against retinal IR injury. Interestingly, when A1 competes with inducible NOS (iNOS) and reduces L-arginine available to it, it dampens iNOS-induced inflammation and oxidative stress (Kleinert et al., 2003; Fouda et al., 2018). A recent report has indicated that A1 expression in macrophages is critical for suppression of iNOS expression (Suwanpradid et al., 2017). The role of A1 in the ONC model is yet to be elucidated.

Unlike A1, A2 is upregulated in pro-inflammatory macrophage and has been shown to promote the macrophage inflammatory response (Ming et al., 2012; Yang and Ming, 2014). However, the role of A2 in macrophages is still controversial, with some reports suggesting an anti-inflammatory role of A2 in macrophages (Johann et al., 2007; Lewis et al., 2011; Hardbower et al., 2016). Therefore, the role of A2 in macrophages is as

yet unclear. It is possible that there is a reciprocal regulation between A1 and A2 in macrophages and other cell types that can explain the opposite roles of the two isoforms in retinal IR injury. This interaction between the two isoforms needs to be further explored.

Polyamines in Acute Retinal Injury

Given that both arginase isoforms mediate the same enzymatic reaction, a central unanswered question about the differential roles of A1 and A2 in acute retinal injury is how each isoform affects the downstream polyamine metabolism in different cell types. The role of polyamines has been studied in ONC and retinal excitotoxicity models. In the ONC model, oral administration of the polyamine, spermidine, in drinking water protected against retinal ganglion cell (RGC) loss and retinal degeneration while enhancing optic nerve regeneration. The spermidine treatment decreased the ONC-induced apoptotic signaling, reduced iNOS expression and limited microglia accumulation (Noro et al., 2015b). Similarly, oral administration of spermidine has been shown to ameliorate neurodegeneration in a genetic mouse model of normal tension glaucoma that involves glutamate neurotoxicity (Noro et al., 2015a). Polyamine treatment is also protective against monosodium glutamate neurotoxicity in the newborn rat retinas (Gilad and Gilad, 1989). However, another study showed that intravitreal injection of the polyamines, putrescine or spermine exacerbated RGC loss in a model of N-methyl-D-aspartate (NMDA)-induced excitotoxic injury. This damage was attributed to binding of polyamines to the NMDA receptor (Pernet et al., 2007). Taken together, the role of polyamines in acute retinal injury seems to be dependent on the injury model and route of administration, and therefore needs further elucidation.

In addition, polyamine metabolism can be dysregulated under pathological conditions via induction of certain enzymes such as polyamine oxidase (PAO) leading to increases in toxic polyamine oxidative products. The role of PAO in retinopathy has been recently reviewed by Narayanan et al. (2019). Studies performed by Pichavaram et al. demonstrated the critical involvement of polyamine oxidation in a model of excitotoxicity-induced retinal neuronal damage (Pichavaram et al., 2018). In that study, expression of the PAO, spermine oxidase, was shown to be upregulated in response to NMDA treatment. Furthermore, loss of RGCs, degeneration of synaptic contacts, and loss of inner retinal neurons were evident in NMDA-treated retinas. Treatment with MDL 72527, a selective enzyme-activated irreversible inhibitor of PAO significantly reduced these effects and improved neuronal survival.

ROLE OF THE ARGINASE PATHWAY IN ACUTE BRAIN INJURY

There have been few studies that directly addressed the role of arginase after acute brain injury that occurs with stroke or traumatic brain injury (TBI). Both arginase isoforms have been shown to be expressed in rat brain neurons at basal conditions. After photothrombotic stroke, A1 expression was

increased in macrophages and astrocytes in the vicinity of the ischemic lesion while A2 expression was unchanged. Moreover, A1 expression co-localized with the neurotrophin, BDNF, in activated astrocytes. This was associated with an increase in overall arginase activity post-stroke (Quirie et al., 2013). A more recent study showed exclusive expression of A1 in infiltrating myeloid cells (macrophages) but not microglia in the spinal cord after contusion injury or experimental autoimmune encephalomyelitis (EAE) induction (Greenhalgh et al., 2016). Similarly, the same group showed that A1 is expressed by macrophages rather than microglia after permanent middle cerebral artery occlusion (Zarruk et al., 2018).

A1 has been used extensively in stroke studies as a marker for the M2-like anti-inflammatory macrophages with its expression in myeloid cells being correlated with better outcomes. After experimental stroke, the number of A1 positive macrophages correlated with neuroprotection and functional recovery (Hamzei Taj et al., 2016). However, the direct role of A1 in stroke pathophysiology has not been rigorously examined to our knowledge. On the other hand, Ahmad et al. (2016) tested the role of A2 in ischemic stroke using a permanent middle cerebral artery occlusion model. A2 KO mice showed increased brain infarction and worse neurological deficit at 7 days after stroke as compared to wild type (WT) but there was no significant difference in cerebral blood flow between the two groups post-ischemia. The authors further confirmed the protective role of A2 using the NMDA-induced acute excitotoxicity model. However, the study did not address the underlying mechanism of this protective effect of A2. A more recent study showed upregulation of both arginase isoforms in rat brain after stroke and improvement of stroke outcomes with the indirect arginase inhibitors, L-citrulline, L-ornithine, and L-norvaline (Barakat et al., 2018). However, while these amino acids can modulate arginase activity, they are not specific for arginase and can have other off-target effects.

Similar to stroke, A1 has been shown to be upregulated in macrophages but not microglia after TBI (Hsieh et al., 2013). Treatments that improved TBI outcomes also increased M2-like, A1 positive macrophages (Gao et al., 2017; Xu et al., 2017). Overexpression of A1, but not A2, in brain neurons protected against TBI (Madan et al., 2018). Another study showed improved recovery of cerebral blood flow after TBI in A2 knockout mice (Bitner et al., 2010). Taken together, the role of arginase in acute brain injury and the interplay between the two enzyme isoforms still require further investigation.

The Polyamines and Brain Injury

In mice subjected to experimental stroke, polyamines were found to be decreased within the infarct area but increased systemically in plasma at 24 h (Saiki et al., 2009). Inhibition of ODC with DFMO (difluoromethylornithine) reduced stroke infarct volume in rats, suggesting a deleterious role of polyamines in stroke (Muszynski et al., 1993). However, DFMO also inhibits arginase due to feed-back inhibition associated with the accumulation of ornithine (Selamnia et al., 1998). In contrast, treatment with spermine but not putrescine or spermidine was neuroprotective in a neonatal rat model of hypoxia-ischemia. Interestingly,

spermine treatment was associated with inhibition of arginase activity and increased NOS activity, suggesting involvement of arginase in the pathology (Clarkson et al., 2004). In TBI models, polyamine catabolism has been found to be increased in the brain with a six-fold increase in putrescine levels but not spermine and spermidine within the first 3 days after injury (Shohami et al., 1992; Henley et al., 1996; Doğan et al., 1999a; Zahedi et al., 2010). Treatment with DFMO improved the neurological outcome after TBI in rats but did not affect edema formation or blood-brain barrier breakdown (Shohami et al., 1992). Further study is needed to elucidate the specific mediator(s) of these DFMO effects.

Again, as with retinal injury, the role of polyamines in acute brain injury is further complicated by the induction of PAO enzyme activity, leading to the formation of the toxic products, acrolein, and 3-aminopropanal that have been shown to strongly correlate with stroke pathology (Ivanova et al., 1998; Saiki et al., 2009). Acrolein is a highly reactive aldehyde and a potent mediator of oxidative damage. DNA adduction, inflammation, membrane disruption, protein adduction, and endoplasmic reticulum stress are the major mechanisms of acrolein-induced toxicity (Moghe et al., 2015). Expression of spermine oxidase was found to be increased in a rat model of stroke (Fan et al., 2019), and this increase has been shown to be positively correlated with the severity of brain injury following excitotoxic damage (Cervetto et al., 2016; Pietropaoli et al., 2018). Earlier studies demonstrated that blockade of polyamine oxidation using the PAO inhibitor, MDL 72527, was neuroprotective in a rat stroke model (Doğan et al., 1999b). Similarly, MDL 72527 reduced traumatic injury volume and brain edema in a rat model of TBI (Doğan et al., 1999a). Collectively, these studies show a deleterious role of PAO in acute brain injury.

CLINICAL STUDIES EXAMINING THE ARGINASE-POLYAMINE PATHWAY IN ACUTE RETINA AND BRAIN INJURY

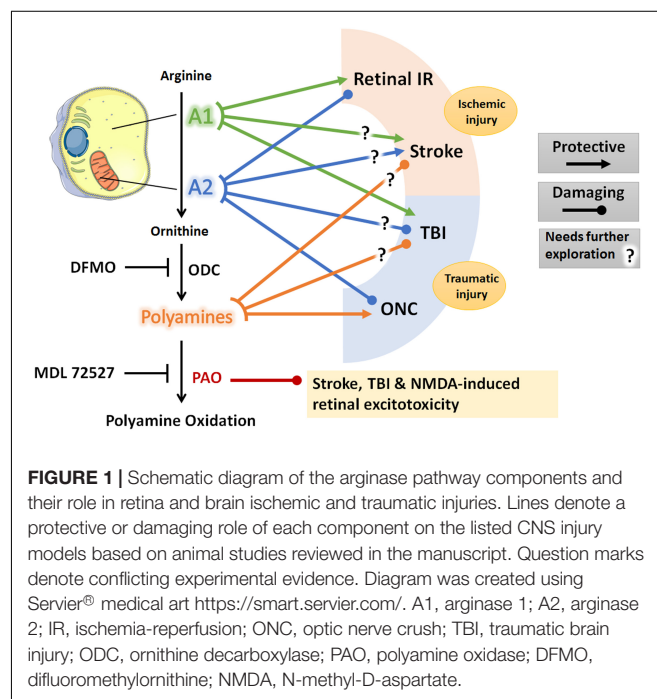
To our knowledge, the role of arginase pathway in CNS injury has not been tested clinically and only a few studies have described changes in the pathway in patient samples. A1 mRNA was shown to be acutely upregulated in peripheral blood of ischemic stroke and mild TBI patients (Petrone et al., 2017; Yoo et al., 2019). Furthermore, increased serum A1 levels were found to be correlated with ischemic stroke severity and post-stroke immune suppression as measured by neutrophil-lymphocyte ratio (NLR) (Petrone et al., 2016). Similarly, plasma polyamine, PAO, and acrolein levels were shown to be upregulated acutely after ischemic stroke and this effect was correlated with infarct volume and clinical outcome (Els et al., 2001; Tomitori et al., 2005). Therefore, the use polyamine metabolites as biochemical markers for stroke has been proposed (Igarashi and Kashiwagi, 2011).

To our knowledge, levels of the two different arginase isoforms have not been studied in patients with any form of retinopathy. However, metabolomic profiling of vitreous samples from patients with proliferative DR revealed increases in arginase pathway metabolites, including arginine, ornithine, and proline with the later showing the most pronounced

increase (Paris et al., 2015). Furthermore, L-arginine pathway is dysregulated in plasma samples from type 2 diabetic patients with PDR (Sumarriva et al., 2019; Zhu et al., 2019). In addition, another study of vitreous samples collected from patients with proliferative DR found increases in spermine and spermidine levels as compared to non-diabetic controls while putrescine was reduced (Nicoletti et al., 2003). Collectively, these studies show the strong involvement of the arginase pathway in the pathophysiology of retinopathy in humans.

ARGINASE IN ALZHEIMER'S DISEASE AND TAUOPATHIES

Alzheimer's disease is a neurodegenerative disorder characterized by the accumulation of β -amyloid (A β) peptides, and hyperphosphorylated and aggregated tau in the brain. Tau is a protein that promotes microtubule assembly and stabilization in axons (Hunt et al., 2015). Post-translational modifications of tau result in its dysfunction and a group of neurodegenerative diseases termed tauopathies (Lee et al., 2001; Hunt et al., 2015). Overexpression of A1 in the hippocampus of a mouse model of tauopathy resulted in a decrease in tau pathology and hippocampal atrophy. One mechanism is through inhibiting mTOR signaling pathway and stimulation of autophagy (Hunt et al., 2015). A second mechanism could be through the formation of polyamines which stabilize already destabilized microtubules in tau pathology (Hunt et al., 2015; Vemula et al., 2019). Surprisingly, A1 has been shown to accumulate at sites of A β deposition (Kan et al., 2015). In murine models of AD, inhibition of arginase using DFMO or L-norvaline reduced A β deposition (Kan et al., 2015; Polis et al., 2018). However, these



compounds inhibit both isoforms of arginase making it difficult to study the effect of individual isoforms on AD pathology.

There is evidence from clinical studies that the urea cycle is involved in the pathophysiology of AD (Hansmannel et al., 2010). Of all the urea cycle enzymes, ornithine transcarboxylase (OTC), is differentially expressed in vascular endothelial cells of AD brains compared to controls indicating an active urea cycle (Bensemain et al., 2009). The increase in OTC expression could be a compensation for the decrease in glutamine synthase (GS) activity in the frontal pole of AD brains that results in ammonia build up (Smith et al., 1991). Additionally, an increase in arginase activity is reported in AD brains consistent with an increase in A2 expression and no significant change in A1 (Hansmannel et al., 2010; Liu et al., 2014). In the plasma, however, a decrease in arginase activity has been reported in patients with AD (Vural et al., 2009). The expression of plasma arginase isoforms was not measured in this study. These data indicate the overall involvement of arginase in AD pathology in humans. DFMO use did not slow cognitive decline in a single-case study of an AD patient (Alber et al., 2018). Short term L-arginine administration improved cognitive function in a small group of elderly (Ohtsuka and Nakaya, 2000). A Recent clinical trial in cognitively intact older adults showed enhanced memory performance with spermidine supplementation (Wirth et al., 2018). Despite this, the role of arginase and polyamines in AD has not been directly tested in clinical trials and there is no evidence so far that related therapies can stop the progression of AD in humans.

Taken together and based on clinical and pre-clinical data, we speculate that the build-up of A1 at sites of A β deposition and tau dysfunction could be a compensatory mechanism to halt disease progression. Accumulation of A2, however, could be a negative consequence that further exacerbates the disease pathology.

ARGINASE PATHWAY AS A THERAPY FOR ACUTE CNS INJURY AND AD

Based on the above reviewed work, arginase pathway represents a potential therapeutic target in acute CNS injury. The role of arginase pathway components in acute brain and retinal injury is summarized in **Figure 1**. Specifically, use of A1 as a therapy for acute CNS ischemia and AD is an appealing approach since PEG-A1 is already being clinically tested in patients with advanced hepatocellular carcinoma and melanoma, and it appears to be safe and well-tolerated (Yau et al., 2013,

2015; De Santo et al., 2018). However, possible systemic adverse effects on endothelial cell function and immune responses should also be tested and considered. One study showed that experimental TBI induces endothelial dysfunction in the systemic microcirculation via A1 upregulation and eNOS uncoupling (Villalba et al., 2017). Similarly, another study showed that A1 release by neutrophils induced peripheral immunosuppression in a murine stroke model (Sippel et al., 2015). This was echoed by clinical data showing a correlation between increased serum A1 levels and post-stroke immune suppression (Petrone et al., 2016). Therefore, the timing and duration of the administration of arginase needs to be studied in detail in order to harness the protective effect of this drug in CNS disease with a high efficacy and safety profile. In addition to A1, manipulation of A2, polyamine levels, or PAO can also be targeted to limit acute CNS injury. However, there is no clinically tested drug that can specifically target A2 or PAO. DFMO, which inhibits ODC and therefore can reduce polyamine levels, has been tested in neuroblastoma patients and found to be protective (Sholler et al., 2018). As was noted above, DFMO lacks specificity and can also inhibit arginase activity. More research into the definitive role of polyamines in acute CNS injury is warranted before further pursuing this pathway as a therapeutic target.

AUTHOR CONTRIBUTIONS

AF drafted the main body of the mini-review. RWC, SN, and WE helped with drafting and editing. RBC revised and approved the final version.

FUNDING

This review was supported by grants from the National Institute of Health (NIH grant R01-EY11766 to RBC and RWC), the Department of Veterans Affairs, Veterans Health Administration, Office of Research and Development, Biomedical Laboratory Research and Development (BX001233 to RBC), the National Institute of Health K99 award (1K99EY029373-01A1 to AF), NIH R01EY028569 to SN and the Culver Vision Discovery Institute at Augusta University. RBC is the recipient of a Research Career Scientist Award from the Department of Veterans Affairs. The contents do not represent the views of the Department of Veterans Affairs or the United States Government. The funders had no role in preparation of the manuscript, or decision to publish.

REFERENCES

- Ahmad, A. S., Shah, Z. A., and Dore, S. (2016). Protective role of arginase ii in cerebral ischemia and excitotoxicity. *J. Neurol. Neurosci.* 7:88.
- Alber, J., McGarry, K., Noto, R. B., and Snyder, P. J. (2018). Use of eflornithine (dfmo) in the treatment of early alzheimer's disease: a compassionate use, single-case study. *Front. Aging. Neurosci.* 10:60. doi: 10.3389/fnagi.2018.00060
- Barakat, W., Fahmy, A., Askar, M., and El-Kannishy, S. (2018). Effectiveness of arginase inhibitors against experimentally induced stroke. *Naunyn Schmiedeberg's Arch. Pharmacol.* 391, 603–612. doi: 10.1007/s00210-018-1489-1
- Bensemain, F., Hot, D., Ferreira, S., Dumont, J., Bombois, S., Maurage, C. A., et al. (2009). Evidence for induction of the ornithine transcarbamylase expression in alzheimer's disease. *Mol. Psychiatry* 14, 106–116.
- Bitner, B. R., Brink, D. C., Mathew, L. C., Pautler, R. G., and Robertson, C. S. (2010). Impact of arginase ii on cbf in experimental cortical impact injury in mice using mri. *J. Cereb. Blood Flow Metab.* 30, 1105–1109. doi: 10.1038/jcbfm.2010.47
- Caldwell, R. B., Toque, H. A., Narayanan, S. P., and Caldwell, R. W. (2015). Arginase: an old enzyme with new tricks. *Trends Pharmacol. Sci.* 36, 395–405. doi: 10.1016/j.tips.2015.03.006

- Caldwell, R. W., Rodriguez, P. C., Toque, H. A., Narayanan, S. P., and Caldwell, R. B. (2018). Arginase: a multifaceted enzyme important in health and disease. *Physiol. Rev.* 98, 641–665. doi: 10.1152/physrev.00037.2016
- Cervetto, C., Vergani, L., Passalacqua, M., Ragazzoni, M., Venturini, A., Cecconi, F., et al. (2016). Astrocyte-dependent vulnerability to excitotoxicity in spermine oxidase-overexpressing mouse. *Neuromol. Med.* 18, 50–68. doi: 10.1007/s12017-015-8377-3
- Clarkson, A. N., Liu, H., Pearson, L., Kapoor, M., Harrison, J. C., Sammut, I. A., et al. (2004). Neuroprotective effects of spermine following hypoxic-ischemic-induced brain damage: a mechanistic study. *FASEB J.* 18, 1114–1116. doi: 10.1096/fj.03-1203fje
- De Santo, C., Cheng, P., Beggs, A., Egan, S., Bessudo, A., and Mussai, F. (2018). Metabolic therapy with peg-arginase induces a sustained complete remission in immunotherapy-resistant melanoma. *J. Hematol. Oncol.* 11:68.
- Dizikes, G. J., Grody, W. W., Kern, R. M., and Cederbaum, S. D. (1986). Isolation of human liver arginase cDNA and demonstration of non-homology between the two human arginase genes. *Biochem. Biophys. Res. Commun.* 141, 53–59. doi: 10.1016/s0006-291x(86)80333-3
- Doğan, A., Rao, A. M., Baskaya, M. K., Hatcher, J., Temiz, C., Rao, V. L., et al. (1999a). Contribution of polyamine oxidase to brain injury after trauma. *J. Neurosurg.* 90, 1078–1082. doi: 10.3171/jns.1999.90.6.1078
- Doğan, A., Rao, A. M., Hatcher, J., Rao, V. L., Baskaya, M. K., and Dempsey, R. J. (1999b). Effects of md1 72527, a specific inhibitor of polyamine oxidase, on brain edema, ischemic injury volume, and tissue polyamine levels in rats after temporary middle cerebral artery occlusion. *J. Neurochem.* 72, 765–770. doi: 10.1046/j.1471-4159.1999.0720765.x
- Dzik, J. M. (2014). Evolutionary roots of arginase expression and regulation. *Front. Immunol.* 5:544. doi: 10.3389/fimmu.2014.00544
- Els, T., Bruckmann, J., Röhn, G., Daffertshofer, M., Mönning, J. S., Ernestus, R. I., et al. (2001). Spermidine: a predictor for neurological outcome and infarct size in focal cerebral ischemia? *Stroke* 32, 43–46. doi: 10.1161/01.str.32.1.43
- Fan, J., Chen, M., Wang, X., Tian, Z., Wang, J., Fan, D., et al. (2019). Targeting smox is neuroprotective and ameliorates brain inflammation in cerebral ischemia/reperfusion rats. *Toxicol. Sci.* 168, 381–393. doi: 10.1093/toxsci/kfy300
- Fouda, A. Y., Xu, Z., Shosha, E., Lemtalsi, T., Chen, J., Toque, H. A., et al. (2018). Arginase 1 promotes retinal neurovascular protection from ischemia through suppression of macrophage inflammatory responses. *Cell Death Dis.* 9:1001.
- Gao, W., Li, F., Zhou, Z., Xu, X., Wu, Y., Zhou, S., et al. (2017). IL-2/anti-IL-2 complex attenuates inflammation and bbb disruption in mice subjected to traumatic brain injury. *Front. Neurol.* 8:281. doi: 10.3389/fneur.2017.00281
- Gilad, G. M., and Gilad, V. H. (1989). Treatment with polyamines can prevent monosodium glutamate neurotoxicity in the rat retina. *Life Sci.* 44, 1963–1969. doi: 10.1016/0024-3205(89)90409-8
- Ginguay, A., Cynober, L., Curis, E., and Nicolis, I. (2017). Ornithine aminotransferase, an important glutamate-metabolizing enzyme at the crossroads of multiple metabolic pathways. *Biology (Basel)* 6:18. doi: 10.3390/biology6010018
- Gotoh, T., Sonoki, T., Nagasaki, A., Terada, K., Takiguchi, M., and Mori, M. (1996). Molecular cloning of cDNA for non-hepatic mitochondrial arginase (arginase ii) and comparison of its induction with nitric oxide synthase in a murine macrophage-like cell line. *FEBS Lett.* 395, 119–122. doi: 10.1016/0014-5793(96)01015-0
- Greenhalgh, A. D., Passos Dos Santos, R., Zarruk, J. G., Salmon, C. K., Kroner, A., et al. (2016). Arginase-1 is expressed exclusively by infiltrating myeloid cells in CNS injury and disease. *Brain Behav. Immun.* 56, 61–67. doi: 10.1016/j.bbi.2016.04.013
- Hamzei Taj, S., Kho, W., Riou, A., Wiedermann, D., and Hoehn, M. (2016). Mirna-124 induces neuroprotection and functional improvement after focal cerebral ischemia. *Biomaterials* 91, 151–165. doi: 10.1016/j.biomaterials.2016.03.025
- Hansmann, F., Sillaire, A., Kamboh, M. I., Lendon, C., Pasquier, F., Hannequin, D., et al. (2010). Is the urea cycle involved in Alzheimer's disease? *J. Alzheimer's Dis.* 21, 1013–1021.
- Hardbower, D. M., Asim, M., Murray-Stewart, T., Casero, R. A. Jr., Verriere, T., Lewis, N. D., et al. (2016). Arginase 2 deletion leads to enhanced m1 macrophage activation and upregulated polyamine metabolism in response to *Helicobacter pylori* infection. *Amino Acids* 48, 2375–2388. doi: 10.1007/s00726-016-2231-2
- Henley, C. M., Muszynski, C., Cherian, L., and Robertson, C. S. (1996). Activation of ornithine decarboxylase and accumulation of putrescine after traumatic brain injury. *J. Neurotrauma* 13, 487–496. doi: 10.1089/neu.1996.13.487
- Hsieh, C. L., Kim, C. C., Ryba, B. E., Niemi, E. C., Bando, J. K., Locksley, R. M., et al. (2013). Traumatic brain injury induces macrophage subsets in the brain. *Eur. J. Immunol.* 43, 2010–2022. doi: 10.1002/eji.201243084
- Hunt, J. B. Jr., Nash, K. R., Placides, D., Moran, P., Selenica, M. L., Abuqalbeen, F., et al. (2015). Sustained arginase 1 expression modulates pathological tau deposits in a mouse model of tauopathy. *J. Neurosci.* 35, 14842–14860. doi: 10.1523/jneurosci.3959-14.2015
- Igarashi, K., and Kashiwagi, K. (2011). Use of polyamine metabolites as markers for stroke and renal failure. *Methods Mol. Biol.* 720, 395–408. doi: 10.1007/978-1-61779-034-8_25
- Ivanova, S., Botchkina, G. I., Al-Abed, Y., Meistrell, M. III, Batliwalla, F., Dubinsky, J. M., et al. (1998). Cerebral ischemia enhances polyamine oxidation: identification of enzymatically formed 3-aminopropanal as an endogenous mediator of neuronal and glial cell death. *J. Exp. Med.* 188, 327–340. doi: 10.1084/jem.188.2.327
- Jindal, V. (2015). Interconnection between brain and retinal neurodegenerations. *Mol. Neurobiol.* 51, 885–892. doi: 10.1007/s12035-014-8733-6
- Johann, A. M., Barra, V., Kuhn, A. M., Weigert, A., von Knethen, A., and Brune, B. (2007). Apoptotic cells induce arginase ii in macrophages, thereby attenuating no production. *FASEB J.* 21, 2704–2712. doi: 10.1096/fj.06-7815com
- Kan, M. J., Lee, J. E., Wilson, J. G., Everhart, A. L., Brown, C. M., Hoofnagle, A. N., et al. (2015). Arginine deprivation and immune suppression in a mouse model of Alzheimer's disease. *J. Neurosci.* 35, 5969–5982. doi: 10.1523/jneurosci.4668-14.2015
- Kleinert, H., Schwarz, P. M., and Förstermann, U. (2003). Regulation of the expression of inducible nitric oxide synthase. *Biol. Chem.* 384, 1343–1364.
- Lee, V. M., Goedert, M., and Trojanowski, J. Q. (2001). Neurodegenerative tauopathies. *Annu. Rev. Neurosci.* 24, 1121–1159. doi: 10.1146/annurev.neuro.24.1.1121
- Lewis, N. D., Asim, M., Barry, D. P., de Sablet, T., Singh, K., Piazzuelo, M. B., et al. (2011). Immune evasion by *Helicobacter pylori* is mediated by induction of macrophage arginase ii. *J. Immunol. (Baltimore, Md.: 1950)* 186, 3632–3641. doi: 10.4049/jimmunol.1003431
- Liu, P., Fletee, M. S., Jing, Y., Collie, N. D., Curtis, M. A., Waldvogel, H. J., et al. (2014). Altered arginine metabolism in Alzheimer's disease brains. *Neurobiol. Aging* 35, 1992–2003. doi: 10.1016/j.neurobiolaging.2014.03.013
- London, A., Benhar, I., and Schwartz, M. (2013). The retina as a window to the brain—from eye research to CNS disorders. *Nat. Rev. Neurol.* 9, 44–53. doi: 10.1038/nrneurol.2012.227
- Madan, S., Kron, B., Jin, Z., Al Shamy, G., Campeau, P. M., Sun, Q., et al. (2018). Arginase overexpression in neurons and its effect on traumatic brain injury. *Mol. Genet. Metab.* 125, 112–117. doi: 10.1016/j.ymgme.2018.07.007
- Ming, X.-F., Rajapakse, A. G., Yepuri, G., Xiong, Y., Carvas, J. M., Ruffieux, J., et al. (2012). Arginase ii promotes macrophage inflammatory responses through mitochondrial reactive oxygen species, contributing to insulin resistance and atherogenesis. *J. Am. Heart Assoc.* 1:e000992.
- Moghe, A., Ghare, S., Lamoreau, B., Mohammad, M., Barve, S., McClain, C., et al. (2015). Molecular mechanisms of acrolein toxicity: relevance to human disease. *Toxicol. Sci.* 143, 242–255. doi: 10.1093/toxsci/kfu233
- Morris, S. M. Jr. (2009). Recent advances in arginine metabolism: roles and regulation of the arginases. *Br. J. Pharmacol.* 157, 922–930. doi: 10.1111/j.1476-5381.2009.00278.x
- Muszynski, C. A., Robertson, C. S., Goodman, J. C., and Henley, C. M. (1993). Dfmo reduces cortical infarct volume after middle cerebral artery occlusion in the rat. *J. Cereb. Blood Flow Metab.* 13, 1033–1037. doi: 10.1038/jcbfm.1993.131
- Narayanan, S. P., Shosha, E., and D Palani, C. (2019). Spermine oxidase: a promising therapeutic target for neurodegeneration in diabetic retinopathy. *Pharmacol. Res.* 147:104299. doi: 10.1016/j.phrs.2019.104299
- Nicoletti, R., Venza, I., Ceci, G., Visalli, M., Teti, D., and Reibaldi, A. (2003). Vitreous polyamines spermidine, putrescine, and spermine in human proliferative disorders of the retina. *Br. J. Ophthalmol.* 87, 1038–1042. doi: 10.1136/bjo.87.8.1038
- Noro, T., Namekata, K., Azuchi, Y., Kimura, A., Guo, X., Harada, C., et al. (2015a). Spermidine ameliorates neurodegeneration in a mouse model of normal tension glaucoma. *Investig. Ophthalmol. Vis. Sci.* 56, 5012–5019.

- Noro, T., Namekata, K., Kimura, A., Guo, X., Azuchi, Y., Harada, C., et al. (2015b). Spermidine promotes retinal ganglion cell survival and optic nerve regeneration in adult mice following optic nerve injury. *Cell Death Dis.* 6:e1720. doi: 10.1038/cddis.2015.93
- Ohtsuka, Y., and Nakaya, J. (2000). Effect of oral administration of L-arginine on senile dementia. *Am. J. Med.* 108, 439–439.
- Paris, L. P., Johnson, C. H., Aguilar, E., Usui, Y., Cho, K., Hoang, L. T., et al. (2015). Global metabolomics reveals metabolic dysregulation in ischemic retinopathy. *Metabolomics* 12, 15.
- Pernet, V., Bourgeois, P., and Di Polo, A. (2007). A role for polyamines in retinal ganglion cell excitotoxic death. *J. Neurochem.* 103, 1481–1490. doi: 10.1111/j.1471-4159.2007.04843.x
- Petrone, A. B., Gionis, V., Giersch, R., and Barr, T. L. (2017). Immune biomarkers for the diagnosis of mild traumatic brain injury. *NeuroRehabilitation* 40, 501–508. doi: 10.3233/nre-171437
- Petrone, A. B., O'Connell, G. C., Regier, M. D., Chantler, P. D., Simpkins, J. W., and Barr, T. L. (2016). The role of arginase 1 in post-stroke immunosuppression and ischemic stroke severity. *Transl. Stroke Res.* 7, 103–110. doi: 10.1007/s12975-015-0431-9
- Pichavaram, P., Palani, C. D., Patel, C., Xu, Z., Shosha, E., Fouda, A. Y., et al. (2018). Targeting polyamine oxidase to prevent excitotoxicity-induced retinal neurodegeneration. *Front. Neurosci.* 12:956. doi: 10.3389/fnins.2018.00956
- Pietropaoli, S., Leonetti, A., Cervetto, C., Venturini, A., Mastrantonio, R., Baroli, G., et al. (2018). Glutamate excitotoxicity linked to spermine oxidase overexpression. *Mol. Neurobiol.* 55, 7259–7270. doi: 10.1007/s12035-017-0864-0
- Polis, B., Srikanth, K. D., Elliott, E., Gil-Henn, H., and Samson, A. O. (2018). L-norvaline reverses cognitive decline and synaptic loss in a murine model of alzheimer's disease. *Neurotherapeutics* 15, 1036–1054. doi: 10.1007/s13311-018-0669-5
- Quirie, A., Demougeot, C., Bertrand, N., Mossiat, C., Garnier, P., Marie, C., et al. (2013). Effect of stroke on arginase expression and localization in the rat brain. *Eur. J. Neurosci.* 37, 1193–1202. doi: 10.1111/ejn.12111
- Saiki, R., Nishimura, K., Ishii, I., Omura, T., Okuyama, S., Kashiwagi, K., et al. (2009). Intense correlation between brain infarction and protein-conjugated acrolein. *Stroke* 40, 3356–3361. doi: 10.1161/strokeaha.109.553248
- Selamnia, M., Mayeur, C., Robert, V., and Blachier, F. (1998). Alpha-difluoromethylornithine (dfmo) as a potent arginase activity inhibitor in human colon carcinoma cells. *Biochem. Pharmacol.* 55, 1241–1245. doi: 10.1016/s0006-2952(97)00572-8
- Shohami, E., Nates, J. L., Glantz, L., Trembovler, V., Shapira, Y., and Bachrach, U. (1992). Changes in brain polyamine levels following head injury. *Exp. Neurol.* 117, 189–195. doi: 10.1016/0014-4886(92)90126-b
- Sholler, G. L. S., Ferguson, W., Bergendahl, G., Bond, J. P., Neville, K., Eslin, D., et al. (2018). Maintenance dfmo increases survival in high risk neuroblastoma. *Sci. Rep.* 8, 14445.
- Shosha, E., Xu, Z., Yokota, H., Saul, A., Rojas, M., Caldwell, R. W., et al. (2016). Arginase 2 promotes neurovascular degeneration during ischemia/reperfusion injury. *Cell Death Dis.* 7:e2483. doi: 10.1038/cddis.2016.295
- Sippel, T. R., Shimizu, T., Strnad, F., Traystman, R. J., Herson, P. S., and Waziri, A. (2015). Arginase i release from activated neutrophils induces peripheral immunosuppression in a murine model of stroke. *J. Cereb. Blood Flow Metab.* 35, 1657–1663. doi: 10.1038/jcbfm.2015.103
- Smith, C. D., Carney, J. M., Starke-Reed, P. E., Oliver, C. N., Stadtman, E. R., Floyd, R. A., et al. (1991). Excess brain protein oxidation and enzyme dysfunction in normal aging and in alzheimer disease. *Proc. Natl. Acad. Sci. U.S.A.* 88, 10540–10543. doi: 10.1073/pnas.88.23.10540
- Sumarriva, K., Uppal, K., Ma, C., Herren, D. J., Wang, Y., Chocron, I. M., et al. (2019). Arginine and carnitine metabolites are altered in diabetic retinopathy. *Investig. Ophthalmol. Vis. Sci.* 60, 3119–3126.
- Suwanpradit, J., Shih, M., Pontius, L., Yang, B., Birukova, A., Guttman-Yassky, E., et al. (2017). Arginase1 deficiency in monocytes/macrophages upregulates inducible nitric oxide synthase to promote cutaneous contact hypersensitivity. *J. Immunol.* 199, 1827–1834. doi: 10.4049/jimmunol.1700739
- Tomitori, H., Usui, T., Saeki, N., Ueda, S., Kase, H., Nishimura, K., et al. (2005). Polyamine oxidase and acrolein as novel biochemical markers for diagnosis of cerebral stroke. *Stroke* 36, 2609–2613. doi: 10.1161/01.str.0000190004.36793.2d
- Vemula, P., Jing, Y., Zhang, H., Hunt, J. B. Jr., Sandusky-Beltran, L. A., Lee, D. C., et al. (2019). Altered brain arginine metabolism in a mouse model of tauopathy. *Amino Acids* 51, 513–528. doi: 10.1007/s00726-018-02687-x
- Villalba, N., Sackheim, A. M., Nunez, I. A., Hill-Eubanks, D. C., Nelson, M. T., and Wellman, G. C. (2017). Traumatic brain injury causes endothelial dysfunction in the systemic microcirculation through arginase-1-dependent uncoupling of endothelial nitric oxide synthase. *J. Neurotrauma* 34, 192–203. doi: 10.1089/neu.2015.4340
- Vockley, J. G., Jenkinson, C. P., Shukla, H., Kern, R. M., Grody, W. W., and Cederbaum, S. D. (1996). Cloning and characterization of the human type ii arginase gene. *Genomics* 38, 118–123. doi: 10.1006/geno.1996.0606
- Vural, H., Sirin, B., Yilmaz, N., Eren, I., and Delibas, N. (2009). The role of arginine-nitric oxide pathway in patients with alzheimer disease. *Biol. Trace Element Res.* 129, 58–64. doi: 10.1007/s12011-008-8291-8
- Wirth, M., Benson, G., Schwarz, C., Köbe, T., Grittner, U., Schmitz, D., et al. (2018). The effect of spermidine on memory performance in older adults at risk for dementia: a randomized controlled trial. *Cortex* 109, 181–188. doi: 10.1016/j.cortex.2018.09.014
- Wu, G., and Morris, S. M. Jr. (1998). Arginine metabolism: nitric oxide and beyond. *Biochem. J.* 336(Pt 1), 1–17. doi: 10.1042/bj3360001
- Xu, X., Gao, W., Cheng, S., Yin, D., Li, F., Wu, Y., et al. (2017). Anti-inflammatory and immunomodulatory mechanisms of atorvastatin in a murine model of traumatic brain injury. *J. Neuroinflamm.* 14, 167–167.
- Xu, Z., Fouda, A. Y., Lemtalsi, T., Shosha, E., Rojas, M., Liu, F., et al. (2018). Retinal neuroprotection from optic nerve trauma by deletion of arginase 2. *Front. Neurosci.* 12:970. doi: 10.3389/fnins.2018.00970
- Yang, Z., and Ming, X.-F. (2014). Functions of arginase isoforms in macrophage inflammatory responses: impact on cardiovascular diseases and metabolic disorders. *Front. Immunol.* 5:533. doi: 10.3389/fimmu.2014.00533
- Yau, T., Cheng, P. N., Chan, P., Chan, W., Chen, L., Yuen, J., et al. (2013). A phase 1 dose-escalating study of pegylated recombinant human arginase 1 (peg-rharg1) in patients with advanced hepatocellular carcinoma. *Invest New Drugs* 31, 99–107. doi: 10.1007/s10637-012-9807-9
- Yau, T., Cheng, P. N., Chan, P., Chen, L., Yuen, J., Pang, R., et al. (2015). Preliminary efficacy, safety, pharmacokinetics, pharmacodynamics and quality of life study of pegylated recombinant human arginase 1 in patients with advanced hepatocellular carcinoma. *Invest. New Drugs* 33, 496–504. doi: 10.1007/s10637-014-0200-8
- Yoo, H., Kim, J., Lee, A.-R., Lee, J.-M., Kim, O.-J., Kim, J.-K., et al. (2019). Alteration of microRNA 340-5p and arginase-1 expression in peripheral blood cells during acute ischemic stroke. *Mol. Neurobiol.* 56, 3211–3221. doi: 10.1007/s12035-018-1295-2
- Zahedi, K., Huttinger, F., Morrison, R., Murray-Stewart, T., Casero, R. A., and Strauss, K. I. (2010). Polyamine catabolism is enhanced after traumatic brain injury. *J. Neurotrauma* 27, 515–525. doi: 10.1089/neu.2009.1097
- Zarruk, J. G., Greenhalgh, A. D., and David, S. (2018). Microglia and macrophages differ in their inflammatory profile after permanent brain ischemia. *Exp. Neurol.* 301, 120–132. doi: 10.1016/j.expneurol.2017.08.011
- Zhu, X. R., Yang, F. Y., Lu, J., Zhang, H. R., Sun, R., Zhou, J. B., et al. (2019). Plasma metabolomic profiling of proliferative diabetic retinopathy. *Nutr. Metab. (Lond)* 16:37.

Conflict of Interest: AF, RBC, and RWC have a pending patent on the use of arginase 1 as a treatment for ischemic retinopathies.

The remaining authors declare that the research was conducted in the absence of any commercial or financial relationships that could be construed as a potential conflict of interest.

Copyright © 2020 Fouda, Eldahshan, Narayanan, Caldwell and Caldwell. This is an open-access article distributed under the terms of the Creative Commons Attribution License (CC BY). The use, distribution or reproduction in other forums is permitted, provided the original author(s) and the copyright owner(s) are credited and that the original publication in this journal is cited, in accordance with accepted academic practice. No use, distribution or reproduction is permitted which does not comply with these terms.



Organoids and Microphysiological Systems: New Tools for Ophthalmic Drug Discovery

Jing Bai¹ and Chunming Wang^{2*}

¹ Department of Mechanical Engineering, Massachusetts Institute of Technology, Cambridge, MA, United States, ² State Key Laboratory of Quality Research in Chinese Medicine, Institute of Chinese Medical Sciences, University of Macau, Taipa, Macau

OPEN ACCESS

Edited by:

Zhongjie Fu,
Boston Children's Hospital,
United States

Reviewed by:

Lin Cheng,
The University of Iowa,
United States
Kevin Eade,
Lowy Medical Research Institute
(LMRI), United States

*Correspondence:

Chunming Wang
cmwang@um.edu.mo

Specialty section:

This article was submitted to
Neuropharmacology,
a section of the journal
Frontiers in Pharmacology

Received: 30 November 2019

Accepted: 18 March 2020

Published: 03 April 2020

Citation:

Bai J and Wang C (2020) Organoids and Microphysiological Systems: New Tools for Ophthalmic Drug Discovery. *Front. Pharmacol.* 11:407. doi: 10.3389/fphar.2020.00407

Organoids are adept at preserving the inherent complexity of a given cellular environment and when integrated with engineered micro-physiological systems (MPS) present distinct advantages for simulating a precisely controlled geometrical, physical, and biochemical micro-environment. This then allows for real-time monitoring of cell-cell interactions. As a result, the two aforementioned technologies hold significant promise and potential in studying ocular physiology and diseases by replicating specific eye tissue microstructures *in vitro*. This miniaturized review begins with defining the science behind organoids/MPS and subsequently introducing methods for generating organoids and engineering MPS. Furthermore, we will discuss the current state of organoids and MPS models in retina, cornea surrogates, and other ocular tissue, in regards to physiological/disease conditions. Finally, future prospective on organoid/MPS will be covered here. Organoids and MPS technologies closely recapture the *in vivo* microenvironment and thusly will continue to provide new understandings in organ functions and novel approaches to drug development.

Keywords: organoid, microphysiological system, ocular, organ-on-a-chip, 3D tissue constructs

INTRODUCTION

Organoid and microphysiological system are two emerging techniques to recapitulate the key organ features. Most of the current conventional cell culture systems, for example, Transwells are considered as oversimplified *in vitro* models, and thus are not appropriate platforms to study organ functions. Organoids, which are miniaturized organs with a three-dimensional structure and multiple cell layers, have advantages over two-dimensional models by maintaining organ anatomic microstructure and basic organ functions (Lancaster and Knoblich, 2014). Organoids are either generated from primary tissue cells, embryonic stem cells, or induced pluripotent stem cells (iPSCs). They possess the capability of self-assembly, self-renewal, and differentiation, ranging in size from micrometer to millimeter scale, with the potential to address the limitations of conventional cell culture system, such as random configuration (Liu et al., 2019).

Microphysiological system (MPS), also known as organ-on-a-chip technology, is an integrative, microfabricated platform designed to recapitulate functional units of human organs *in vitro* (Huh et al., 2011). Conventional 3D models, where cells are growing within the extracellular matrix (ECM), fail to reflect critical aspects of human organs, including cell-tissue interface and physical

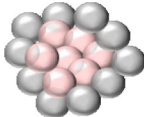

and biochemical stimuli, such as flow and pressure. MPS provides essential advantages in this regard. First, fluid is restrained in micro-scale channels, enabling close contact between different cell types (e.g., between epithelium and vascular endothelium) to capture the dynamic cell-cell interplay. Next, microenvironment cues, including spatiotemporal gradients of chemicals and mechanical strain that are critical to mimic the organ functions, can be examined in a single microfluidic setup. In addition, vasculature-on-a-chip enables emulating pulsatile blood luminal flow and interstitial flow, the key determinants of tissue functions (Kim et al., 2017); and these vascular modules are embedded in interconnected multiple tissue units for blood supply. Lastly, in MPS, the optical transparency of microfluidic devices allows for real-time monitoring. Optical tracking of cell migration and cell-cell interaction presents an indispensable tool for analyzing tissue functions, such as monitoring the dynamic process of tissue development, repair, and regeneration (Tkachenko et al., 2009). **Table 1** compares organoids and MPS in their definition, functions, and applications. These two techniques are conceptually different, yet complementary toward the same goal of recapitulation organ functions *in vitro* (Park et al., 2019).

The technical advancement on microfluidics, 3D printing, tissue engineering materials, and microfabrication has paved the way for the development of novel MPS. This easy-to-use platform can be replicated in standard biological labs for development and tissue regeneration study, and enable clinical researchers to optimize drug treatment. In addition, there is

growing recognition in industrial partners that this technique is suitable for pre-clinic drug screening and toxicology evaluation. The benefits of this 3D miniaturized assays include reducing animal test, evaluating targeted drug delivery and accelerating drug development process.

Eye diseases like macular degeneration, glaucoma, and cataracts are not self-healing and can cause severe visual impairment. Common retinal disorders, including age-related macular degeneration (AMD), retinitis pigmentosa, and diabetic retinopathy (Zhang et al., 2015), affect millions of people worldwide. Meanwhile, ocular surface diseases remain another therapeutic challenge for vision restoration. It is crucial to investigate the pathogenesis of ocular diseases and to develop novel drugs. Considerable progress has been achieved on developing physiological and pathological ocular models, aiming to recapitulate key aspects in the ocular development and diseases. Despite that organoids and MPS models in major organs has been developed, such as liver (Wu et al., 2019), heart (Nugraha et al., 2019), brain (Qian et al., 2019), and pathological phenotypes like cancer (Niu et al., 2014; Tu et al., 2014; Bai et al., 2015a; Adriani et al., 2016) and Alzheimer's disease (Gonzalez et al., 2018), remarkable achievement has been made to study ocular organoids and MPS. Although these techniques are still simplified methods, they have shown the potential to capture key features of basic ocular tissues like cornea, retina, and lens (**Figure 1A**). In this review, we will discuss the methods to generate organoids and MPS in ophthalmic research and focus

TABLE 1 | Comparison of organoids and microphysiological systems (MPS) on their definition, functions, and applications.

	Organoids 	Microphysiological systems 
Structure	3D <i>in vitro</i> , • Self-organized functional organotypic units	3D <i>in vitro</i> • Microfabricated cell culture device recapitulating organ functional units
Size	µm–mm	µm–mm
Easy-to-culture	Moderate • Timely activation of cell-fate specification signaling pathways	Easy–moderate • Explicit structuring patterning—e.g., bioprinting, bio lithography
Culture time	Moderate • Weeks	Short–moderate • Days to weeks
Co-culture ability	Yes	Yes • Limited cell types in device
Reproducibility	Moderate • Lack of understanding and guide of their differentiation	Yes • Appropriate culture conditions and microfabrication
High-throughput	Low	Moderate–low
Microenvironment	Absent • Oversimplified models in absent of flow, physical and chemical cues	Present • Complex models replicating organ functions, e.g., muscle contractions, blood flow
Vasculature and blood perfusion	Highly possible	Highly possible
<i>In vivo</i>-like function	Moderate • Recapitulating basic organ functions	High • Emulating complex organ functions
Genetic manipulation	Applicable • Inherited key genetic features from iPSCs	Applicable
Application to personalized medicine and drug screening	Yes	Yes

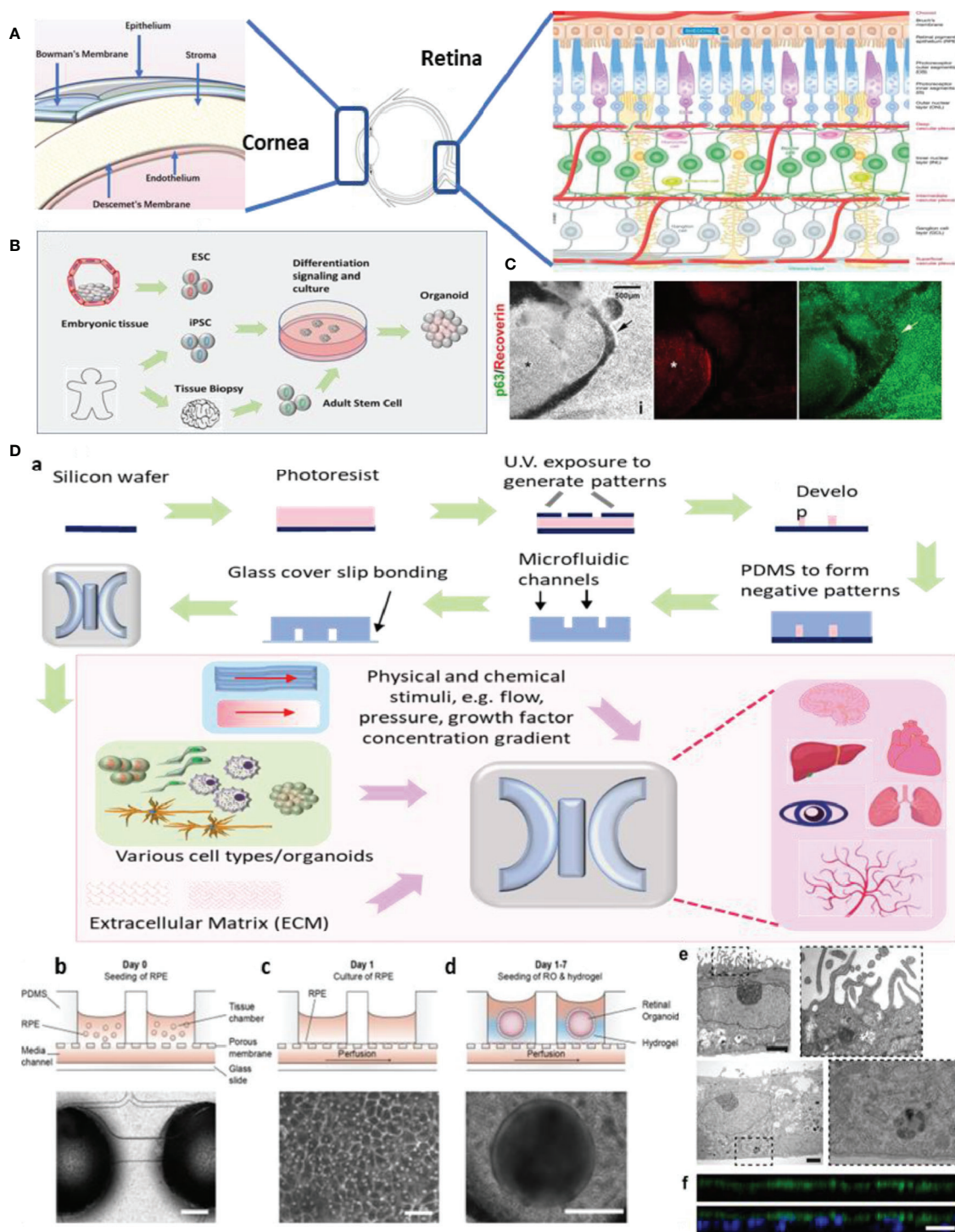


FIGURE 1 | Continued

FIGURE 1 | Ocular organoids and microphysiological systems (MPS). **(A)** Structure of eye, cornea, and retina. Retina structure was adapted from (Fu et al., 2019). **(B)** Schematic representation on the stepwise generation of organoids. **(C)** Differentiation of human iPSCs into retinal and corneal organoids. Distinct circular to oval-shaped eye field primordial (EFP) encompassed a centrally located p63⁺ Recoverin⁺ neuroretinal (NR) cup (asterisks), adapted from (Susaimanickam et al., 2017). **(D)** a. Schematic representation of photolithography for polydimethylsiloxane (PDMS)-based microfluidic device fabrication and essential components in a standard MPS model. b.c.d.e.f. An representative example of merging organoid and MPS technology in a human retina-on-a-chip platform: b.c.d. microfluidic platform enabling co-culture of human induced pluripotent stem cell (hiPSC)-derived retinal pigment epithelium (RPE) and ROs (retinal organoids) in a defined physiological structure (the top layer has compartments for the ROs and RPE, and the bottom layer with a channel for a vasculature); e.f. electron microscopic image of polarized RPE cells. RPE cells display apical microvilli (top row) and a basal membrane (bottom row), and immunohistochemical staining for ezrin (green), an apical microvilli marker, indicated polarized RPE, adapted from (Achberger et al., 2019).

on the most promising models, including retinal, corneal, and other ocular tissue models. We also acknowledge the future prospective of these novel technologies and benefits on drug discovery.

Generating Organoids and Engineering Micro-Physiological Systems

Organoids are generated from either primary cells or progenitor cells isolated from biopsy, or pluripotent stem cells (PSCs) (Figure 1B). With sequential differentiation steps, the cells would be capable to retain the intrinsic developmental features of an organ. The most commonly used cells are iPSCs. These cells are PSCs that can be generated directly from adult cells with four reprogramming factors Oct3/4, Sox2, Klf4, and c-Myc (Takahashi and Yamanaka, 2006). The advantage of iPSCs is their high potential to differentiate into all major tissues, cell lineages, and high degree of biomimicry. A review has summarized organoid generation methods and discussed a promising approach of “human on a dish” (McCauley and Wells, 2017). Briefly, iPSCs were differentiated and self-assembled to generate organotypic constructs with extrinsic signals, including growth factors, extracellular matrix, and culture media. The 3D cellular structures could recapitulate the developmental features after 2 weeks and could be maintained in culture for months.

Technical advances in organoid fabrication provide hope for generating more complex MPS prototypes. MPS assembles the microphysical and chemical microenvironment. Successful fabrication of MPS requires two major techniques: microfluidics which precisely control a small amount of fluid to mimic interstitial flow in the organs; and microfabrication which assembles the essential 3D compartments and microchannel networks for organoids/cells to grow. Previous microfabrication method used silicon until soft lithography of polydimethylsiloxane (PDMS) replica became the most dominant method for organ-on-a-chip applications (Figure 1D). This is because of its easy fabrication, outstanding optical transparency and minimum cytotoxicity (Huh et al., 2011; Ghaemmaghami et al., 2012). A detailed review article has discussed PDMS for organ-on-a-chip applications (Sia and Whitesides, 2003). More recently, 3D bioprinting has been widely applied to the fabrication of organ microstructures. This technology has streamlined the fabrication process of microfluidic compartments to one single step (Ho et al., 2015). 3D bioprinting is capable of integrating multiple cells, matrix components, and growth factors, allowing for cells to assemble along more exact layer-by-layer printed microstructures. Typical

3D bioprinting methods involve micro-extrusion, inkjet, and laser-assisted printing (Yi et al., 2017), while micro-extrusion is the most common method for microfluidic chips fabrication. Another benefit of 3D bioprinting is that the printing ink can consist of any natural or synthetic biocompatible material (depending on the requirement of the design).

Retina Models

The retina is the innermost layer of the eye with a complex light-sensing structure. A good review has described the anatomy and function of retina by Hoon et al. (2014) (Figure 1A, right). Approaches have emerged for developing retinal organoids and MPS. One of the most well-known ocular organoid models is the self-organizing optic-cup (Eiraku et al., 2011) differentiated from mouse embryonic stem cell.

Modeling retinal organoids and MPS is challenging because the retina has one of the most complex and fine structures in the body with a high variety of cell types. Therefore, only partial aspects of its functions are capable to be recapitulated in a single model. Thus far, efforts have been made to develop two perspectives of retinal structure. First, the neurosensory structure including photoreceptor cells, ganglion cells, and optic nerve; second, the dynamics of choriocapillaris and retinal pigment epithelium (RPE) interactions and blood-retina barrier (BRB) functions. Several promising studies have demonstrated the development of retinal neuronal organoids and MPS, from mouse stem cells (Eiraku et al., 2011) to human stem cells (Nakano et al., 2012), from generating photoreceptors (Zhong et al., 2014) to retinal ganglion cells (Ohlemacher et al., 2016). Retinal organoids have, to this point, been developed by isolating human photoreceptor precursors and self-assembling of layers of differentiated photoreceptors (Chen et al., 2016; Lakowski et al., 2018), or from human iPSCs (Zhong et al., 2014). Most of the retinal neuronal cells have limited capacity for regeneration where iPSCs cells have the capability to differentiate into functional retinal neuronal cells. By using retinal organoids, precursor cells, and their microenvironment, the retinal MPS models are emerging to recapitulate parts of retinal functions. A microfluidic chip to study synaptic regeneration has been developed (Su et al., 2015). In the study, retinal precursor cells were isolated and cultured in a microfluidic chip with multiple arrays of microchannels to restore the retinal neuronal synapse. Another study utilized multi-passage mouse retinal progenitor cells, leading to the development of a μ Retina chip (Mishra et al., 2015). By coupling computer simulations and experimental validations, chemical concentration gradients are monitored with real-time imaging on cell migration.

Next, to emulate retinal vasculature/RPE interactions and BRB functions, MPS has the advantage of retaining the vasculature structure and co-culturing with RPE cells. An early model consisted of a simple co-culture chip with human RPE cell line ARPE-19 and human umbilical vein endothelial cells (HUVEC) (Kaji et al., 2014), and was followed up by a choroid chip with an artificial Bruch's membrane (Chen et al., 2017). In recent times, an angiogenesis model is established with perfusable blood vessel networks, enabling the observation of pathological retinal angiogenesis (Chung et al., 2018). Another study has featured a BRB model using microfluidic system and evaluate the integrity of the epithelial and endothelial barrier function (Yeste et al., 2017). To date, new processes are emerging that seek to combine organoids and MPS to generate complex multi-layer retinal vasculature and RPE models (**Figure 1D**). One novel MPS, in particular, is being developed by integrating more than seven human iPSCs-derived retinal cell types (Achberger et al., 2019). This allows for the formation of outer segment-like structures and the establishment of *in vivo*-like physiological processes such as outer segment phagocytosis and calcium dynamics.

Remarkably, besides physiological models, some retinal organoid models have been shown to have an impact on investigating disease mechanisms. A 3D retina organoid has been established for studying X-linked retinitis pigmentosa (Megaw et al., 2017) and another organoid model has been recreated to study glaucoma using patient-derived samples (Ohlemacher et al., 2016). In addition, an AMD model has been employed to mimic chronic and acute mechanical stress on RPE cells during different stages of AMD (Farjood and Vargis, 2018). However, there is still only a limited number of retinal organoids and MPS models that are present.

Cornea Models

Compared to the retina, the corneal structure is less complicated. There are critical design principles to generate functional corneal organoids. These principles involve: semitransparency, structural retaining corneal epithelium, stroma (organized collagen fibrils), Bowman's membrane/Descemet's membrane, and endothelium (**Figure 1A**, left). Limbal stem cells/progenitor cells which reside in the peripheral of cornea, are the major source of corneal cell regenerations and tissue repair. iPSCs become an important alternative source of corneal cells. It is the first generation of corneal epithelial cells from iPSCs which are derived from dermal fibroblasts and the corneal limbal epithelium was reported in 2012 (Hayashi et al., 2012). A number of contemporary studies describe a novel method to generate three-dimensional corneal organoids from human iPSCs (Foster et al., 2017; Susaimanickam et al., 2017) (**Figure 1C**). These mini-corneal organoids, that ranging in size from one to seven millimeters in diameter, reproduce the early developmental events *in vitro* and duplicate similar anatomical features and gene expression profiles of corneas (Foster et al., 2017; Susaimanickam et al., 2017). However, more accurate differentiation protocol is needed in order to better mimic corneal functions and conditions like Fuch's dystrophy or Keratoconus.

Besides organoids, corneal MPS are powerful models in studying corneal physiology and pathology. The first corneal-on a chip assay was in 2009, where the study developed a microfluidic device containing collagen vitrigel (CV) for the development of corneal microtissue patches (Puleo et al., 2009). Another example is an eye-on-a-chip that models blinking by integrating a hydrogel "eyelid" (Seo et al., 2019) to evaluate cornea therapeutic drugs and provided a realistic platform to prevent dry eye disease. The further development of these models would greatly benefit future pharmacological ocular drug topical delivery.

Lens and Other Ocular Tissue Models

The advancement of novel retinal and corneal models has opened new ways for the development of other ocular tissue counterparts. Nonetheless, there are even fewer organoids and MPS models on lens and other ocular tissue, in comparison to corneal and retinal models. There is an organoid lens model for defining molecular disease mechanisms caused by cataract risk factors (Murphy et al., 2018). This study, in question, demonstrated the generation of light-focusing human micro-lenses from spheroidal masses of human lens epithelial cells purified from differentiating pluripotent stem cells. One further example involved a contact lens-on-a-chip system. The design facilitated the study of different disinfection agents to prevent severe eye infections (Guan et al., 2016). There are great potentials for these physiological and pathological models in accelerating the identification and screening of ophthalmic drug targets, to address such pathological conditions as cataract and glaucoma.

Prospective and Future Directions

To date, there is still a lack of a perfect organoid or MPS model to capture the development process of an entire organ. Researchers are now seeking ways to develop more advanced models without sacrificing their reproducibility. Besides organoids and MPS applications in regenerative medicine (Sasai, 2013), another major pharmaceutical application is in drug screening, hit identifications, and lead optimizations. There are 3D high content drug screening models based on organoids and MPS (Aref et al., 2013; Bai et al., 2015b; Kim et al., 2015) that have been constituted for various other organs. The methodological concepts from the aforementioned studies could be applied to ophthalmic organoids and MPS models. It is imperative to generate robust ocular disease models to facilitate the evaluation of preclinical candidates, such as drug effects, toxicology, pharmacokinetics, and pharmacodynamics, for both synthetic drug candidates (Kondo and Inoue, 2019) and natural compounds (Bai et al., 2019; Sun and Zhang, 2019).

In addition to an integrative "organoid-on-a-chip" (Park et al., 2019), a future direction of ocular MPS design should focus on mirroring the development of eye tissue on-chip, with special tissue fidelity features, such as vascularized tissue, ECM, immune cell interactions. Possibly, integration of complex functions, such as light-sensing and circuit structure in the vision system, would allow for capturing electric signals from the eye for probing

vision problems in a noninvasive manner and toward more precise and controllable models.

The development of new technologies sheds new light on the understanding of ophthalmic disease mechanisms with the use of organoids and MPS models. Patient-derived stem cell organoid models would benefit personalized medicine. CRISPR/Cas9 technology and single-cell sequencing on-chip would subsequently enable complementary assay on basic research and clinical trials, moving toward a revolution in the conventional drug development pipeline. Finally, refined protocols of organoids and advances on microfluidic technology, 3D printing, biomaterials would potentially lead to integrative tissue models to recapitulate the physiological hallmarks of an entire eye. Although challenges still exist, more opportunities have arisen to improve the basic understanding of the ocular diseases and drug development to prevent vision loss.

REFERENCES

- Achberger, K., Probst, C., Haderspeck, J., Bolz, S., Rogal, J., Chuchuy, J., et al. (2019). Merging organoid and organ-on-a-chip technology to generate complex multi-layer tissue models in a human retina-on-a-chip platform. *Elife* 8, e46188. doi: 10.7554/eLife.46188
- Adriani, G., Bai, J., Wong, S., Kamm, R. D., and Thiery, J. P. (2016). M2a macrophages induce contact-dependent dispersion of carcinoma cell aggregates. *Macrophage* 3, e1222. doi: 10.14800/Macrophage.1222
- Aref, A. R., Huang, R. Y., Yu, W., Chua, K. N., Sun, W., Tu, T. Y., et al. (2013). Screening therapeutic EMT blocking agents in a three-dimensional microenvironment. *Integr. Biol. (Camb)* 5, 381–389. doi: 10.1039/C2IB20209C
- Bai, J., Adriani, G., Dang, T. M., Tu, T. Y., Penny, H. X., Wong, S. C., et al. (2015a). Contact-dependent carcinoma aggregate dispersion by M2a macrophages via ICAM-1 and beta2 integrin interactions. *Oncotarget* 6, 25295–25307. doi: 10.18632/oncotarget.4716
- Bai, J., Tu, T. Y., Kim, C., Thiery, J. P., and Kamm, R. D. (2015b). Identification of drugs as single agents or in combination to prevent carcinoma dissemination in a microfluidic 3D environment. *Oncotarget* 6, 36603–36614. doi: 10.18632/oncotarget.5464
- Bai, J., Kwok, W. C., and Thiery, J. P. (2019). Traditional Chinese Medicine and regulatory roles on epithelial-mesenchymal transitions. *Chin. Med.* 14, 34. doi: 10.1186/s13020-019-0257-6
- Chen, H. Y., Kaya, K. D., Dong, L., and Swaroop, A. (2016). Three-dimensional retinal organoids from mouse pluripotent stem cells mimic in vivo development with enhanced stratification and rod photoreceptor differentiation. *Mol. Vis.* 22, 1077–1094.
- Chen, L. J., Ito, S., Kai, H., Nagamine, K., Nagai, N., Nishizawa, M., et al. (2017). Microfluidic co-cultures of retinal pigment epithelial cells and vascular endothelial cells to investigate choroidal angiogenesis. *Sci. Rep.* 7, 3538. doi: 10.1038/s41598-017-03788-5
- Chung, M., Lee, S., Lee, B. J., Son, K., Jeon, N. L., and Kim, J. H. (2018). Wet-AMD on a Chip: Modeling Outer Blood-Retinal Barrier In Vitro. *Adv. Healthc. Mater.* 7, 1700028. doi: 10.1002/adhm.201700028
- Eiraku, M., Takata, N., Ishibashi, H., Kawada, M., Sakakura, E., Okuda, S., et al. (2011). Self-organizing optic-cup morphogenesis in three-dimensional culture. *Nature* 472, 51–56. doi: 10.1038/nature09941
- Farjood, F., and Vargis, E. (2018). Novel devices for studying acute and chronic mechanical stress in retinal pigment epithelial cells. *Lab. Chip* 18, 3413–3424. doi: 10.1039/C8LC00659H
- Foster, J. W., Wahlin, K., Adams, S. M., Birk, D. E., Zack, D. J., and Chakravarti, S. (2017). Cornea organoids from human induced pluripotent stem cells. *Sci. Rep.* 7, 41286. doi: 10.1038/srep41286
- Fu, Z., Chen, C. T., Cagnone, G., Heckel, E., Sun, Y., Cakir, B., et al. (2019). Dyslipidemia in retinal metabolic disorders. *EMBO Mol. Med.* 11, e10473. doi: 10.15252/emmm.201910473

AUTHOR CONTRIBUTIONS

JB and CW designed the review paper structure and layout. JB and CW contributed to the preparation of the manuscript.

FUNDING

This study was funded by the Science and Technology Development Fund, Macau SAR (The additional fund to State Key Laboratory of Quality Research in Chinese Medicine).

ACKNOWLEDGMENTS

We thank Brian A. Zappella for the English editing.

- Ghaemmaghami, A. M., Hancock, M. J., Harrington, H., and Kaji, H. (2012). Khademhosseini, Biomimetic tissues on a chip for drug discovery. *Drug Discovery Today* 17, 173–181. doi: 10.1016/j.drudis.2011.10.029
- Gonzalez, C., Armijo, E., Bravo-Alegria, J., Becerra-Calixto, A., Mays, C. E., and Soto, C. (2018). Modeling amyloid beta and tau pathology in human cerebral organoids. *Mol. Psychiatry* 23, 2363–2374. doi: 10.1038/s41380-018-0229-8
- Guan, A., Wang, Y., Phillips, K. S., and Li, Z. (2016). A contact-lens-on-a-chip companion diagnostic tool for personalized medicine. *Lab. Chip* 16, 1152–1156. doi: 10.1039/C6LC00034G
- Hayashi, R., Ishikawa, Y., Ito, M., Kageyama, T., Takashiba, K., Fujioka, T., et al. (2012). Generation of corneal epithelial cells from induced pluripotent stem cells derived from human dermal fibroblast and corneal limbal epithelium. *PLoS One* 7, e45435. doi: 10.1371/journal.pone.0045435
- Ho, C. M., Ng, S. H., Li, K. H., and Yoon, Y. J. (2015). 3D printed microfluidics for biological applications. *Lab. Chip* 15, 3627–3637. doi: 10.1039/C5LC00685F
- Hoon, M., Okawa, H., Della Santina, L., and Wong, R. O. (2014). Functional architecture of the retina: development and disease. *Prog. Retin Eye Res.* 42, 44–84. doi: 10.1016/j.preteyeres.2014.06.003
- Huh, D., Hamilton, G. A., and Ingber, D. E. (2011). From 3D cell culture to organs-on-chips. *Trends Cell Biol.* 21, 745–754. doi: 10.1016/j.tcb.2011.09.005
- Kaji, S., Ito, H., Nagamine, H., Nishizawa, K., Nagai, M., and N. and Abe, T. (2014). Characterization of retinal pigment epithelial cells and endothelial cells within a microfluidic device towards a retina on a chip, 18th International Conference on Miniaturized Systems for Chemistry and Life Sciences (San Antonio, Texas, USA: Royal Society of Chemistry).
- Kim, C., Kasuya, J., Jeon, J., Chung, S., and Kamm, R. D. (2015). A quantitative microfluidic angiogenesis screen for studying anti-angiogenic therapeutic drugs. *Lab. Chip* 15, 301–310. doi: 10.1039/C4LC00866A
- Kim, S., Kim, W., Lim, S., and Jeon, J. S. (2017). Vasculature-On-A-Chip for In Vitro Disease Models. *Bioeng. (Basel)* 4 (1), E8. doi: 10.3390/bioengineering4010008
- Kondo, J., and Inoue, M. (2019). Application of Cancer Organoid Model for Drug Screening and Personalized Therapy. *Cells* 8 (5), 470. doi: 10.3390/cells8050470
- Lakowski, J., Welby, E., Budinger, D., Di Marco, F., Di Foggia, V., Bainbridge, J. W. B., et al. (2018). Isolation of Human Photoreceptor Precursors via a Cell Surface Marker Panel from Stem Cell-Derived Retinal Organoids and Fetal Retinae. *Stem Cells* 36, 709–722. doi: 10.1002/stem.2775
- Lancaster, M. A., and Knoblich, J. A. (2014). Organogenesis in a dish: modeling development and disease using organoid technologies. *Science* 345, 1247125. doi: 10.1126/science.1247125
- Liu, H., Wang, Y., Cui, K., Guo, Y., Zhang, X., and Qin, J. (2019). Advances in Hydrogels in Organoids and Organs-on-a-Chip. *Adv. Mater.* 31, e1902042. doi: 10.1002/adma.201902042
- McCauley, H. A., and Wells, J. M. (2017). Pluripotent stem cell-derived organoids: using principles of developmental biology to grow human tissues in a dish. *Development* 144, 958–962. doi: 10.1242/dev.140731

- Megaw, R., Abu-Arafah, H., Jungnickel, M., Mellough, C., Gurniak, C., Witke, W., et al. (2017). Gelsolin dysfunction causes photoreceptor loss in induced pluripotent cell and animal retinitis pigmentosa models. *Nat. Commun.* 8, 271. doi: 10.1038/s41467-017-00111-8
- Mishra, S., Thakur, A., Redenti, S., and Vazquez, M. (2015). A model microfluidics-based system for the human and mouse retina. *BioMed. Microdevices* 17, 107. doi: 10.1007/s10544-015-0002-6
- Murphy, P., Kabir, M. H., Srivastava, T., Mason, M. E., Dewi, C. U., Lim, S., et al. (2018). Light-focusing human micro-lenses generated from pluripotent stem cells model lens development and drug-induced cataract in vitro. *Development* 145 (1), dev155838. doi: 10.1242/dev.155838
- Nakano, T., Ando, S., Takata, N., Kawada, M., Muguruma, K., Sekiguchi, K., et al. (2012). Self-formation of optic cups and storable stratified neural retina from human ESCs. *Cell Stem Cell* 10, 771–785. doi: 10.1016/j.stem.2012.05.009
- Niu, Y., Bai, J., Kamm, R. D., Wang, Y., and Wang, C. (2014). Validating antimetastatic effects of natural products in an engineered microfluidic platform mimicking tumor microenvironment. *Mol. Pharm.* 11, 2022–2029. doi: 10.1021/mp500054h
- Nugraha, B., Buono, M. F., von Boehmer, L., Hoerstrup, S. P., and Emmert, M. Y. (2019). Human Cardiac Organoids for Disease Modeling. *Clin. Pharmacol. Ther.* 105, 79–85. doi: 10.1002/cpt.1286
- Ohlemacher, S. K., Sridhar, A., Xiao, Y., Hochstetler, A. E., Sarfarazi, M., Cummins, T. R., et al. (2016). Stepwise Differentiation of Retinal Ganglion Cells from Human Pluripotent Stem Cells Enables Analysis of Glaucomatous Neurodegeneration. *Stem Cells* 34, 1553–1562. doi: 10.1002/stem.2356
- Park, S. E., Georgescu, A., and Huh, D. (2019). Organoids-on-a-chip. *Science* 364, 960–965. doi: 10.1126/science.aaw7894
- Puleo, C. M., McIntosh Ambrose, W., Takezawa, T., Elisseff, J., and Wang, T. H. (2009). Integration and application of vitrified collagen in multilayered microfluidic devices for corneal microtissue culture. *Lab. Chip* 9, 3221–3227. doi: 10.1039/b908332d
- Qian, X., Song, H., and Ming, G. L. (2019). Brain organoids: advances, applications and challenges. *Development* 146 (8), dev166074. doi: 10.1242/dev.166074
- Sasai, Y. (2013). Next-generation regenerative medicine: organogenesis from stem cells in 3D culture. *Cell Stem Cell* 12, 520–530. doi: 10.1016/j.stem.2013.04.009
- Seo, J., Byun, W. Y., Alisafaei, F., Georgescu, A., Yi, Y. S., Massaro-Giordano, M., et al. (2019). Multiscale reverse engineering of the human ocular surface. *Nat. Med.* 25, 1310–1318. doi: 10.1038/s41591-019-0531-2
- Sia, S. K., and Whitesides, G. M. (2003). Microfluidic devices fabricated in poly (dimethylsiloxane) for biological studies. *Electrophoresis* 24, 3563–3576. doi: 10.1002/elps.200305584
- Su, P. J., Liu, Z., Zhang, K., Han, X., Saito, Y., Xia, X., et al. (2015). Retinal synaptic regeneration via microfluidic guiding channels. *Sci. Rep.* 5, 13591. doi: 10.1038/srep13591
- Sun, Z., and Zhang, B. (2019). High-throughput screening (HTS) of natural products with triple-negative breast cancer (TNBC) organoids. *J. Clin. Oncol.* 37, e12558–e12558. doi: 10.1200/JCO.2019.37.15_suppl.e12558
- Susaimanickam, P. J., Maddileti, S., Pulimamidi, V. K., Boyinpally, S. R., Naik, R. R., Naik, M. N., et al. (2017). Generating minicorneal organoids from human induced pluripotent stem cells. *Development* 144, 2338–2351. doi: 10.1242/dev.143040
- Takahashi, K., and Yamanaka, S. (2006). Induction of pluripotent stem cells from mouse embryonic and adult fibroblast cultures by defined factors. *Cell* 126, 663–676. doi: 10.1016/j.cell.2006.07.024
- Tkachenko, E., Gutierrez, E., Ginsberg, M. H., and Groisman, A. (2009). An easy to assemble microfluidic perfusion device with a magnetic clamp. *Lab. Chip* 9, 1085–1095. doi: 10.1039/b812184b
- Tu, T. Y., Wang, Z., Bai, J., Sun, W., Peng, W. K., Huang, R. Y., et al. (2014). Rapid prototyping of concave microwells for the formation of 3D multicellular cancer aggregates for drug screening. *Adv. Healthc. Mater.* 3, 609–616. doi: 10.1002/adhm.201300151
- Wu, L. J., Chen, Z. Y., Wang, Y., Zhao, J. G., Xie, X. Z., and Chen, G. (2019). Organoids of liver diseases: From bench to bedside. *World J. Gastroenterol.* 25, 1913–1927. doi: 10.3748/wjg.v25.i16.1913
- Yeste, J., Garcia-Ramirez, M., Illa, X., Guimera, A., Hernandez, C., Simo, R., et al. (2017). A compartmentalized microfluidic chip with crisscross microgrooves and electrophysiological electrodes for modeling the blood-retinal barrier. *Lab. Chip* 18, 95–105. doi: 10.1039/C7LC00795G
- Yi, H. G., Lee, H., and Cho, D. W. (2017). 3D Printing of Organs-On-Chips. *Bioeng. (Basel)* 4 (1), E10. doi: 10.3390/bioengineering4010010
- Zhang, J., Tuo, J., Wang, Z., Zhu, A., Machalinska, A., and Long, Q. (2015). Pathogenesis of Common Ocular Diseases. *J. Ophthalmol.* 2015, 734527. doi: 10.1155/2015/734527
- Zhong, X., Gutierrez, C., Xue, T., Hampton, C., Vergara, M. N., Cao, L. H., et al. (2014). Generation of three-dimensional retinal tissue with functional photoreceptors from human iPSCs. *Nat. Commun.* 5, 4047. doi: 10.1038/ncomms5047

Conflict of Interest: The authors declare that the research was conducted in the absence of any commercial or financial relationships that could be construed as a potential conflict of interest.

Copyright © 2020 Bai and Wang. This is an open-access article distributed under the terms of the Creative Commons Attribution License (CC BY). The use, distribution or reproduction in other forums is permitted, provided the original author(s) and the copyright owner(s) are credited and that the original publication in this journal is cited, in accordance with accepted academic practice. No use, distribution or reproduction is permitted which does not comply with these terms.



A Method for Developing Novel 3D Cornea-on-a-Chip Using Primary Murine Corneal Epithelial and Endothelial Cells

Jing Bai^{1,2*}, Haojie Fu¹, Lauren Bazinet¹, Amy E. Birsner¹ and Robert J. D'Amato^{1,3}

¹ The Vascular Biology Program and Department of Surgery, Boston Children's Hospital, Harvard Medical School, Boston, MA, United States, ² Department of Mechanical Engineering, Massachusetts Institute of Technology, Cambridge, MA, United States, ³ Department of Ophthalmology, Harvard Medical School, Boston, MA, United States

OPEN ACCESS

Edited by:

Amy C. Lo,
The University of Hong Kong,
Hong Kong

Reviewed by:

Harshini Sarojini,
University of Louisville,
United States
Yau Kei Chan,
The University of Hong Kong,
Hong Kong

*Correspondence:

Jing Bai
bajj0005@e.ntu.edu.sg

Specialty section:

This article was submitted to
Neuropharmacology,
a section of the journal
Frontiers in Pharmacology

Received: 30 November 2019

Accepted: 23 March 2020

Published: 28 April 2020

Citation:

Bai J, Fu H, Bazinet L, Birsner AE and
D'Amato RJ (2020) A Method for
Developing Novel 3D Cornea-on-a-
Chip Using Primary Murine Corneal
Epithelial and Endothelial Cells.
Front. Pharmacol. 11:453.
doi: 10.3389/fphar.2020.00453

Microfluidic-based organ-on-a-chip assays with simultaneous coculture of multi-cell types have been widely utilized for basic research and drug development. Here we describe a novel method for a primary cell-based corneal microphysiological system which aims to recapitulate the basic functions of the *in vivo* cornea and to study topically applied ocular drug permeation. In this study, the protocols for isolating and cultivating primary corneal epithelial cells and endothelial cells from mouse inbred strain C57BL/6J were optimized, to allow for the development of a primary-cell based microfluidic 3D micro-engineered cornea. This tissue unit, by overcoming the limitations of 2D conventional cell culture, supports new investigations on cornea function and facilitates drug delivery testing.

Keywords: microfluidic, primary cells, organ-on-a-chip, 3D cell-based models, cornea

INTRODUCTION

The cornea is an avascular and transparent mucosal tissue, and serves as one of the body's major mechanical barriers (DeMonte and Kim, 2011; Sridhar, 2018). Topical application of ocular drug to the cornea of the eye is the ideal route to treat diseases such as uveitis as well as retinal diseases, with maximal convenience and minimal invasiveness. It has been shown that topically administered antibody can quickly reach therapeutic levels in the anterior and posterior segment without the need for a penetration enhancer (Ottiger et al., 2009). As well, new approaches on ocular drug delivery, such as targeted drug delivery system (TDDS) (Xu et al., 2015) have accelerated the topical applications of liposome-, nanoparticle-, emulsion- and microspheres-based drug delivery, allowing for drugs to be concentrated on the target site with high efficacy and reduced side-effects (Kaluzhny et al., 2018). This may result in a shift of the current ocular drug delivery paradigm. However, developing an accurate corneal tissue models remains one of the major challenges to the study of drug permeation and delivery (Wright et al., 2020).

The human cornea is composed of 5 complex layers, namely, epithelium, the Bowman's layer, stroma, the Descemet's membrane and endothelium. The apical layer of epithelium contains tight junctions and is considered as one of the rate-limiting steps of topical administrations. Next, the stroma, composed of collagen fibers, serves as a diffusion barrier to lipophilic compounds. Lastly, a monolayer of endothelial cells also contributes to the restrictions on drug diffusion (Sosnova-

Netukova et al., 2007). Certain drug-metabolizing enzymes and transporters which alter ophthalmological drug availability are present in the cornea (Shirasaki, 2008). Specifically, cornea primary cells express those important enzymes and transporters (Kaluzhny et al., 2018; Sridhar, 2018). Since these physiological features can be depleted during continuous *in vitro* passages, corneal primary cell-based, three-dimensional (3D) corneal models are critical to recapitulate unique physiological functions of the cornea.

Microfluidic-based 3D cell assays can mimic tissue/organ functions and cellular interactions, with the advantage of controllable geometrical, physical and biochemical microenvironment, and real-time imaging (Aref et al., 2013; Bai et al., 2015). This technology is emerging for *in vitro* testing platforms of ocular biological events (Guan et al., 2016; Seo et al., 2016; Bennet et al., 2018; Lu et al., 2019). There are previous studies reporting cornea-on-a-chip assays (Bennet et al., 2018; Seo et al., 2019) for testing drug delivery. However, it is still necessary to address the problem of drug diffusion within a controllable genetic background. Herein, we described a novel method to isolate and culture mouse primary corneal epithelial and endothelial cells, which are used to create a 3D microfluidic based cellular model.

In this study, mouse cornea was first dissected and epithelial/endothelial cells were isolated. Afterwards, the cells were cultivated separately in the two peripheral channels of a 3-channel microfluidic device with collagen matrix in the central channel to form a 3D model. To model the *in vivo* system, a condensed collagen layer was formed in the epithelium channel to mimic Bowman's layer with the concept of viscous finger (Bischel et al., 2012), a method to produce hydrogel lumen structure (Chin et al., 2002). This design is highly accessible to most of the standard biological labs and would provide a precise model to study physiological/pathological conditions of cornea tissues for ophthalmological drug discovery, potentially leading to development of novel ocular drug delivery methods across the anterior chamber.

MATERIALS AND EQUIPMENT

Reagents

Device Fabrication

Polydimethylsiloxane, PDMS, Dow Corning Sylgard 184 Silicone Elastomer base and curing agent (Ellesworth, Cat. No. 184).

Cell Culture

PCT Corneal Epithelium Medium, Low BPE (Zenbio, Cat. No. CnT-50).

Ham's F12 (Thermo Fisher Scientific, Cat. No. 11765047).

M199 (Thermo Fisher Scientific, Cat. No. 11150067).

DMEM GlutaMAX (Thermo Fisher Scientific, Cat. No. 10566-016).

HyClone Fetal Bovine Serum (Fisher Scientific, Cat. No. SH3007103).

1x insulin, transferrin, selenium (ITS) (Millipore-Sigma, Cat. No. I3146).

Ascorbic acid (Millipore-Sigma, Cat. No. A4403).

bFGF (STEMCELL Technologies, Cat. No. 78003.1).

1x Phosphate Buffer Saline (PBS), sterile.

1× anti-biotic/anti-mycotic solution in PBS.

10x PBS with Phenol Red.

1M NaOH in 1x PBS, sterile.

100% ethanol.

5% Bovine Serum Albumin.

Corning Matrigel Matrix (Corning, Cat. No. 354234).

Cell culture grade water.

Ethanol, 70% (vol/vol).

Dispase (Worthington, Cat. No. 9001-92-7).

Collagenase A (Sigma-Aldrich/Roche, Cat. No. 10103586001).

ACCUTASE™ (STEMCELL Technologies, Cat. No. 07920).

Corning® Collagen I, Rat Tail (Corning, Cat. No. 354236).

Human Collagen Type IV (Sigma-Aldrich, Cat. No. C5533-5MG).

For immunofluorescent experiment (optional):

- Collagen-Fluorescein (FITC) Conjugate (Biovision, Cat. No. M1304-5).
- 4% Paraformaldehyde (PFA) (Sigma-Aldrich).
- 0.1% Triton-X (Sigma-Aldrich).
- ZO-1 polyclonal antibody (Invitrogen, Cat. No. 617300).
- Fluorescent dextran 70kDa Texas Red (Life Tech, Cat. No. D-1830).
- Fluorescent dextran 40kDa Texas Red (Thermo Fisher Scientific, Cat. No. D1829).
- Fluorescent dextran 10kDa (Thermo Fisher Scientific, Cat. No. D1828).
- K12 polyclonal antibody (Biorbyt, Cat. No. orb418611).
- Alexa Fluo 405 Goat anti-Rabbit IgG (H+L) (Invitrogen, Cat. No. A-31556).
- Alexa Fluo 594 Goat anti-Rabbit IgG (H+L) (Invitrogen, Cat. No. A-11037).
- Cell Tracker™ Red (Thermo Fisher Scientific, Cat. No. C34552).
- Cell Tracker™ Blue (Thermo Fisher Scientific, Cat. No. C12881).

Equipment

Hemocytometer for cell counting.

Ophthalmic scissors, forceps.

CO2 Chamber for mouse euthanasia.

Stereomicroscope.

24-well tissue culture plate.

10-cm tissue culture dish.

0.45µm syringe filter.

15ml Falcon Tube.

Scotch tape.
 Glass coverslip.
 Drying oven (60–80°C).
 Vacuum desiccator.
 Benchtop centrifuge.
 Tissue culture incubator with 37°C and 5% CO₂.
 Water bath with 37°C.
 Autoclave equipment.
 Humid chamber prepared by autoclaved water filled in 1000μl pipet tip box for collagen gelation, kept in 37°C.
 Plasma cleaner (Harrick Plasma, cat. no. PDC-001).
 Confocal microscope.

METHODS

Microfluidic Device Preparation

Wafers were designed with AutoCAD and made by established SU-8 micropatterning methods (Shin et al., 2012; Levario et al., 2013) or by outsourcing. The wafer pattern contains 3 channels with one middle gel channel and two peripheral cell channels (**Figure 1**). To prepare the PDMS device, a disposable plastic cup was filled with Sylgard 184 silicone elastomer base and the curing agent in a 10:1

weight ratio. The solution was mixed and poured into a petri dish containing the SU-8 wafer and degassed for 40mins, before being transferred to a 70°C oven for 2h for curing. Afterwards, the PDMS negative pattern was carefully removed from the wafer and holes were punched through at the inlet- and outlet- of channels using dermal biopsy punches (1.5mm and 2.5mm). Scotch tape was used to remove small debris on the surface of device before autoclaving (120°C for 20 min). The sterile devices were dried in an oven at 80°C for at least 4 h and the devices were ready to bond on glass coverslip. The devices can be stored for up to 1 month at room temperature prior to bonding (Time: 8h).

On the subsequent day of preparation, glass coverslips were cleaned by immersing into 100% ethanol, air-dried, and then plasma treated together with the PDMS devices (pattern facing up). The treated surface was bonded together by applying light manual pressure. The bonded devices were kept in sterile dishes at 70°C oven overnight. The devices can be stored for up to 2 weeks at room temperature before seeding cells (Time: overnight).

Isolation of Mouse Primary Corneal Epithelial and Endothelial Cells Solution Preparing

- 0.8U/ml dispase and 1mg/ml collagenase A in DMEM was prepared separately and then filtered separately into

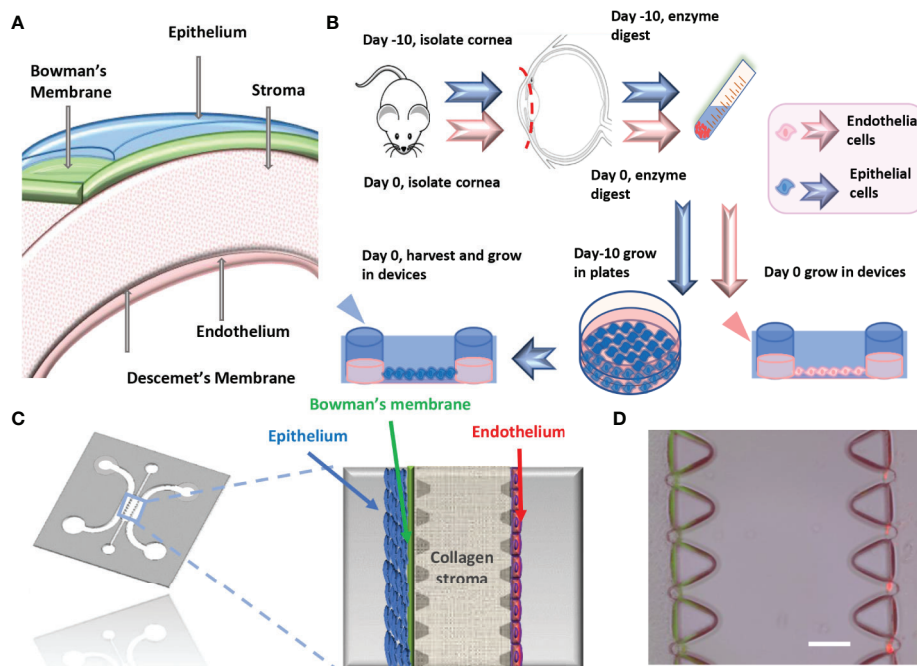


FIGURE 1 | Microfluidic platform for cornea-on-a-chip. **(A)**. The structure of the cornea. **(B)**. Flow chart of mouse primary corneal endothelial cells/epithelial cell isolation and method for growing into devices, epithelial cells were cultured *in vitro* before being seeded into device while endothelial cells were isolated and cultured. **(C)**. Microfluidic cornea-on-a-chip device layout, red: endothelial cells, blue: epithelial cells. Corneal epithelium has 5-7 layers of cells and endothelium has a monolayer of cells, with Bowman's membrane represented as a condensed thin layer of green collagen gel. **(D)**. Representative phase contrast image for cornea-on-a-chip. Scale: 100μm.

individual 15ml tubes using syringes and 0.45um syringe filters, respectively.

- DMEM+10%FBS+1x pen/strep.
- 1x anti-biotic/anti-mycotic solution in 1x sterile PBS.
- 50 µg/ml collagen IV in 1x PBS.
- 10 ng/ml bFGF.
- 1:50 Matrigel in DMEM.
- Cornea endothelial cell culture media: F99 medium containing 1:1 Ham's F12 and M199, supplemented with 5% FBS, 20 µg/ml ascorbic acid, 1x ITS, 1x anti-biotic/anti-mycotic and 10 ng/ml bFGF (Li et al., 2007; Peh et al., 2013).
- PCT Corneal Epithelium Medium, Low BPE, prepared according to manufacturer's instruction.

Common Steps

All mouse experiments were conducted in compliance with the protocols approved by the Institutional Animal Care and Use Committee of Boston Children's Hospital (approval number 15-08-2998R for mouse experiments). Five C57BL/6J adult male mice (age 7-8 weeks) were euthanized by CO₂, and intact eye globes were enucleated using a pair of fine curved forceps. The isolated eyes were placed into a 15ml tube containing 5ml of DMEM without serum and transferred to a new 10cm dish. Under a stereomicroscope, each eye was carefully dissected to eyecups by making a circumferential incision around the ora serrata (limbus), cut to include the limbus. Afterward, the lens was removed and posterior eye cup was discarded, leaving behind the cornea (time: 1.5 -2h).

The corneas were transferred to a new 15ml tube and washed three times in a 1x anti-biotic/anti-mycotic solution in PBS (wash buffer) for a total of 15 minutes. After wash buffer was removed, the corneas were resuspended in 6-7ml of serum free DMEM containing 0.8U/ml dispase. Corneas were then incubated for 1h at 37°C in water bath and the tube inverted every 15 min to ensure good digestion. Once the digestion has completed, enzyme solution was discarded by pipetting, and reaction was stopped by addition of 10ml of cold DMEM containing 10% FBS and 1x pen/strep. (time: 1h 30mins).

Corneal Epithelial Cells

Corneal epithelial cells were isolated by a combination of enzyme digestion and tissue explant methods. 5 wells of a 6-well plate were coated with 1:50 Matrigel for 1h at 37°C. Each digested cornea piece was carefully dissected equally into two pieces using ophthalmic scissors. The edge of curved cornea pieces was further cut halfway through to allow flat plating, and corneas from each mouse were attached in one well with epithelium facing up. Upon plating, one drop of media was applied on top of each corneal piece to prevent the tissue from drying out. 15 mins later, 2ml fresh corneal epithelium medium was added onto each well. Cells were grown without disturbance for 3 days before the corneal tissues were removed. Attached cells were grown to 80%-90% confluency for 5 to 7 days before

accutase digestion. For digestion, 3ml accutase was applied to the cell culture for 10 min incubation. Cells were then harvested by washing with 6ml DMEM containing 10% FBS and 1x pen/strep. The suspension was then centrifuged at 800rpm for 5mins and cell pellet collected before growing into microfluidic devices (time: 8 -10 days).

Corneal Endothelial Cells

One day prior to seeding endothelial cells into microfluidic devices, the peripheral microfluidic channel was coated with collagen IV solution for at least 1h in 37°C incubator. Then the channels were washed twice with 100µl cell culture grade water and allowed to air-dry. The devices can be kept at room temperature for usage the following day (time: 1h).

On the subsequent day, 5 additional mice were euthanized and corneas were obtained and digested as previously described. Descemet's membrane and corneal endothelial cells were stripped from the posterior surface of the cornea under a stereomicroscope and suspended in 3-5ml of 1mg/ml collagenase A with a new 15ml tube and digested for additional 40mins in 37°C water bath. Afterward, the cell pellet was washed with 2-3ml 100% FBS and collected by centrifugation at 800rpm for 5 minutes before plating in the endothelial cell channel on the previously collagen IV-coated microfluidic device (time: 2h 30mins).

Cornea-on-a-Chip Setup Solution Preparation

- 200µl 2mg/ml and 4.5mg/ml collagen type-I, respectively, pH=7.2-7.4, was prepared separately by: a concentrated collagen type-I, sterile water, 10x PBS with phenol red to indicate the PH, 0.5M NaOH for pH adjustment (a pink-yellowish tone indicates a correct pH value). Keep all solutions on ice.
- 5% BSA dissolved in 1xPBS (for immunostaining, optional).
- Fluorescent dextran 70kDa, 40kDa and 10kDa Texas Red each 12.5µg/ml in DMEM (for diffusive experiment, optional).
- Cell Tracker™ Red and Blue, 1:200 diluted in serum free DMEM, separately (for visualization, optional).

Corneal Stroma and Bowman's Layer Formation

Up to 15 cornea-on-a-chip devices were able to be established with this protocol. For each device, the middle gel channel was filled with 10µl of 2mg/ml collagen type-I, pH=7.2-7.4 solution and the devices were put into a humid chamber in 37°C for 30 min to allow collagen gelation. To form the Bowman's layer, a condensed collagen gel thin layer was created along the epithelial side channel by viscous finger patterning. Briefly, 10µl of 4.5mg/ml collagen type-I solution was added in the epithelial cell channel and incubated in 37°C for 1min, before a droplet of DMEM with a volume of 50µl was added on from the 1.5mm diameter inlet. The less viscous

fluid displaces the center of the collagen gel solution, leaving a thin lumen structure after the DMEM was removed. The device was incubated in 37°C incubator with humidity chamber again until polymerization was completed for 45mins. Then DMEM was removed and the devices were ready for cell seeding. (Time: 1h 30mins).

Cell Seeding in the Microfluidic Devices

Corneal epithelial and endothelial cells were harvested as described above. Endothelial cells were seeded with a density of 1×10^5 /ml (each device 30 μ l) and flipped 90° immediately to allow for the cells adhering to the stroma and an endothelial cell monolayer to be formed by gravity. The device was flipped back after 30mins and 70 μ l endothelial cell culture media was added to the media channel. Then the devices were left for another 30mins in 37°C incubator without disturbance. For epithelial cells, the seeding procedure was identical as with endothelial cells, except for the cell density at 3×10^5 /ml and seeded twice. Epithelial cell culture media (CnT-50) was applied on this media channel. Cell culture media on both channels were changed daily for another 48h (Time: 48h).

Cell Immunofluorescent Staining

Primary corneal endothelial cells and epithelial cells were stained with ZO-1 (Invitrogen) and cytokeratin 12 (Biorbyt), respectively. The on-chip staining protocol could be found in our previous studies (Niu et al., 2014; Bai et al., 2015; Adriani et al., 2016). Briefly, cell culture media was removed from the side channels, and cells were washed with PBS once and fixed in 4% Paraformaldehyde (PFA) for 15min at room temperature. 0.1% Triton-X was used for membrane permeabilization for 15mins before blocking with 5% BSA dissolved in 1xPBS for 45mins-1h at room temperature. Afterward, cells were stained with primary antibodies (1:100) overnight at 4°C and secondary antibodies for 1h at room temperature. The secondary antibody (1:200) used in this study were Alexa Fluor 405 and Alexa Fluor 594 (goat anti-rabbit, Invitrogen). Fluorescent images were obtained by confocal microscopy (Olympus FV1000). For cell tracker staining experiments, epithelial cells and endothelial cells were incubated separately with blue and red solution for 15mins before rinsed by fresh DMEM. Then the cells were centrifuged and grown in the microfluidic devices.

Characterization of Corneal Model Permeability

60 μ l of fluorescent dextran at a concentration of 12.5 μ g/mL (10kDa, 40kDa and 70kDa, Texas Red, respectively) was applied to the epithelial channel and allowed to flow across the stroma. Meanwhile, equal volume of non-fluorescent DMEM was applied through the endothelial cells channel to equate the pressure and to allow for dextran diffusion. Using fluorescence microscopy, the concentration fields in the endothelial channel were captured at 0min and 30mins, respectively. Their raw intensity profiles were analyzed using ImageJ (LOCI, University of Wisconsin). And diffusive permeability was calculated by

$$P_D = \beta \cdot D \frac{dC/dx}{\Delta C}$$

C = dextran fluorescence intensity, ΔC = the intensity drops across the vessel, β = area correction factor, dC/dx = slope of the concentration profile, D = dextran diffusion coefficient in collagen gel.

RESULTS AND DISCUSSION

In this study, we present a new method to develop a novel cornea-on-a-chip assay. Compared to established cornea-on-a-chip models, we have utilized isolated primary mouse corneal endothelial cells and epithelial cells in the setup. First, we have improved the current corneal epithelial cell culture protocol by an integration of tissue explant and enzyme digestion methods and accommodated these cells to grow in microfluidic chambers. Secondly, we have created the cornea-on-a-chip model with functional analysis *via* determining dextran diffusion permeability across the corneal barriers. The advantage of our model over the existing models is retaining *in vivo* characteristics, both genetically and phenotypically, to mimic corneal functions and drug diffusion processes. Thus, by utilizing rodent primary cells, it will better model genetic susceptibility to ocular diseases and enhance our understanding of genes function in a distinct genetic background. Furthermore, isolating rodent cells would allow for future on-chip studies on developmental and age-related ocular diseases.

Isolation of Corneal Epithelial and Endothelial Cells

Cornea physiological structure was demonstrated in **Figure 1A** and a descriptive sketch on isolating corneal epithelial and endothelial cell procedure is shown in **Figure 1B**. To isolate corneal epithelial cells, the limbus where corneal epithelial stem/progenitor cells reside was isolated together with the corneal epithelial sheets (Li et al., 2017). These progenitor cells provide major resources and are critical for epithelial cell proliferation *in vitro*. The tissue explant method is a cell culture technique which involves growing cells *ex vivo* from pieces of tissue. Collagen or Matrigel coating is usually necessary for enhancing cell adhesion and migration. This technique has advantages in terms of cell numbers and viability over cell suspension culture (Ma and Liu, 2011), which tissue is completely digested into a single cell suspension by specific enzymes before being seeded into cell culture plates. In our method, we have further improved the current tissue explant method by an additional partial enzyme digestion step before the corneal tissue was attached and by growing this in a tissue culture plate (**Figure 2A**). Our results suggest that a combination of Matrigel plate coating with partial dispase digestion on the explanted cornea tissue (EM group) maximizes the yield of mouse corneal epithelial cells (**Figure 2B**). On day 4, significant increase in the cell numbers in the EM group was observed, conversely, no cells were

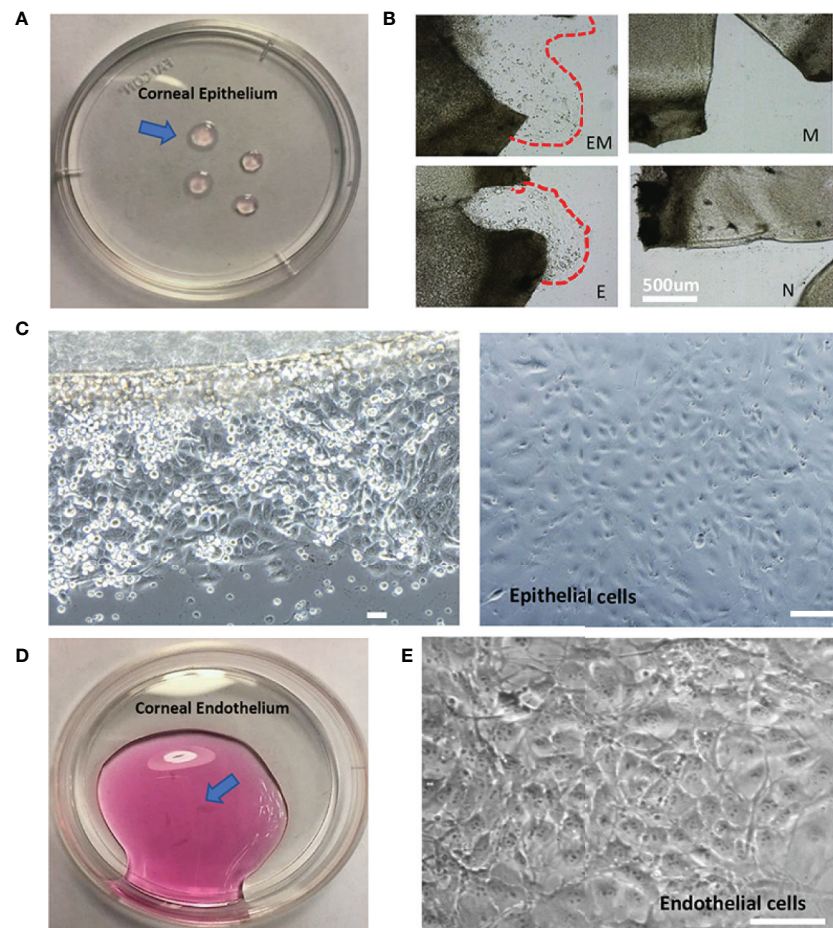


FIGURE 2 | Morphology of isolated mouse corneal epithelial and endothelial cells. **(A).** Isolated corneal epithelium (arrow). **(B).** Comparison of four methods to culture corneal epithelial cells at day 3, EM = Enzyme digested+ Matrigel coated, E = Enzyme digested alone, M = Matrigel coated, N = No coating + no enzyme digestion. **(C).** Epithelial cells cultured by tissue explant method at day 3 (left), day 10 (right). **(D).** Isolated corneal endothelium (arrow). **(E).** Morphology of corneal endothelial cells isolated and cultured. Scale: 200µm.

migrating out in the groups without enzyme digestion. We have used the EM method throughout the study for culturing corneal epithelial cells.

After the corneal tissue was harvested, digested, and plated, epithelial cells began to migrate out onto the tissue culture plates within 3 days (**Figure 2C**, left). The cells display a cobblestone-like appearance and became confluent at day 10 (**Figure 2C**, right). The amount of epithelial cell harvested was up to 2.5×10^5 cells in total. A previous study has optimized corneal epithelial cell culture by using CnT-50 media, a low-calcium, low bovine pituitary extract (BPE), serum-free medium (Kobayashi et al., 2009). Our findings also indicated that CnT-50 enables reproducible corneal epithelial cell expansion.

It is important to note that corneal endothelial cells are a type of slow-cycling cell and their proliferation *in vitro* is minimal. Therefore, in our study, we were only culturing the *in vitro* single

endothelial cell suspension into microfluidic devices to form endothelium monolayer. 10 mouse corneas were able to yield 5×10^4 live endothelial cells in total. Extracted corneal endothelium (**Figure 2D**) and phase-contrast images indicated that corneal endothelial cells retained their unique hexagonal cellular morphology (**Figure 2E**).

Cornea-on-a-Chip Development

The microfluidic cornea-on-a-chip setup was shown in **Figure 1C**, and a representative phase-contrast image was shown in **Figure 1D**. It recapitulates the corneal tissue structures with an epithelial layer and an endothelial layer on the two peripheral channels. A 3D collagen gel matrix (2mg/ml) is formed in the middle channel representing corneal stroma which forms the bulk of the cornea framework and comprises 80%–85% of its

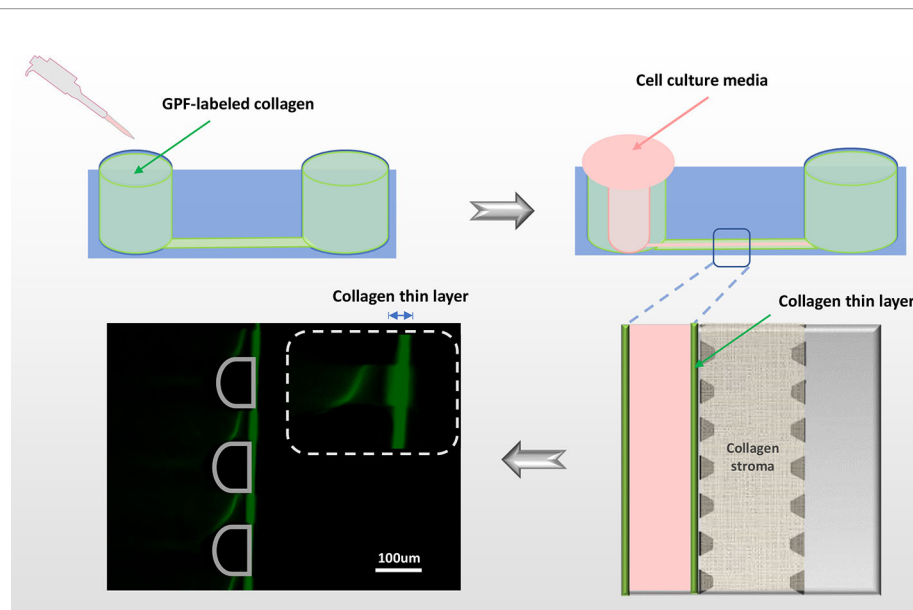


FIGURE 3 | Viscous finger patterning to assemble Bowman's membrane. The side microchannel is filled with 4.5mg/ml collagen I solution, and incubated in 37°C for 1min before applying DMEM media to the same channel from one inlet. A lumen is formed by DMEM displacing the collagen solution in the center of the microchannel, leaving a thin layer of condensed collagen (green fluorescent line) which mimics the Bowman's membrane. To demonstrate the collagen thin layer, GFP-labeled collagen was mixed with non-fluorescent collagen in 1:10. Green: collagen; pink: cell culture media.

thickness (DelMonte and Kim, 2011). Bowman's membrane has critical functions for drug transport and diffusion. It acts as a thick supporting collagen matrix layer for the epithelium with a thickness of $17.7 \pm 1.6 \mu\text{m}$ (Sridhar, 2018). In this study, a denser but thinner collagen layer (4.5mg/ml), formed by viscous finger patterning, is designed to mimic the Bowman's membrane. Viscous finger patterning is designed with the concept of a less viscous fluid replacing a more viscous fluid and thereby forming “finger-like” projections of the less viscous fluid (Walker and Beebe, 2002; Bischel et al., 2012). **Figure 3** has illustrated the viscous finger patterning process. Microchannels were 160µm tall and 400µm wide. A droplet of culture media with a volume of 50µl would create enough surface energy and pressure to pump the liquid through a microchannel with 1.5mm inlet diameters and 2.5 mm outlet diameters.

After collagen gelation, DMEM was removed from the microchannel and corneal epithelial cells were seeded on top of the Bowman's membrane which formed cell layers in 48h. We observed that epithelial cells continued to grow in the microfluidic chips and formed a structure of 5-7 cell layers [**Figures 4A** (left), **B**, **D**(right)], which mimics the corneal epithelial sheets *in vivo*. Cytokeratin 12 immunostaining for corneal epithelial cells was shown in **Figure 4B** (left: phase contrast image; right: immunofluorescent image). For the endothelium, immunofluorescent staining on the intact monolayer is shown in **Figures 4A** (ZO-1, right) and **D** (right). A surpass view as well as a 3-section view of the setup was shown in **Figures 4C**, **D** (left). The established microfluidic platform was functional through two weeks after seeding.

To further validate the model, we have performed dextran diffusion assay with 3 different molecular weights (10kDa, 40kDa and 70kDa) to determine the diffusive permeability in this model. The purpose of this assay was to mimic drug diffusion across the corneal barrier (**Figure 4E**). With or without endothelial cell monolayer, there was a minimal difference on permeability for all three dextrans. However, in the absence of epithelial cell clusters, a significant increase in the permeability indicated that epithelium is the major determinant of drug diffusion transportation rates. The results are in agreement with previous findings (Bennet et al., 2018).

In this study, we have described a 3D microfluidic-based cell assay to recapitulate the basic corneal functional unit. The prototype allows for the study of corneal function/pathology as well as ocular drug diffusion into the anterior chamber.

LIMITATION OF THIS STUDY

The microfluidic setup has advantages over 2D cell culture assays in terms of a small scale and important 3D features. However, this study has limitations to be considered. Normal corneal epithelium is a 5–6 layers structure with three types of cells: superficial cells, wing cells, and basal cells (Sridhar, 2018). It is difficult to distinguish and isolate individual epithelial cell subtypes and to restructure them *in vitro*. In addition, while the predominant component of the stroma is collagen type I, type VI and type XII. This study did not address the differences of the various collagen types.

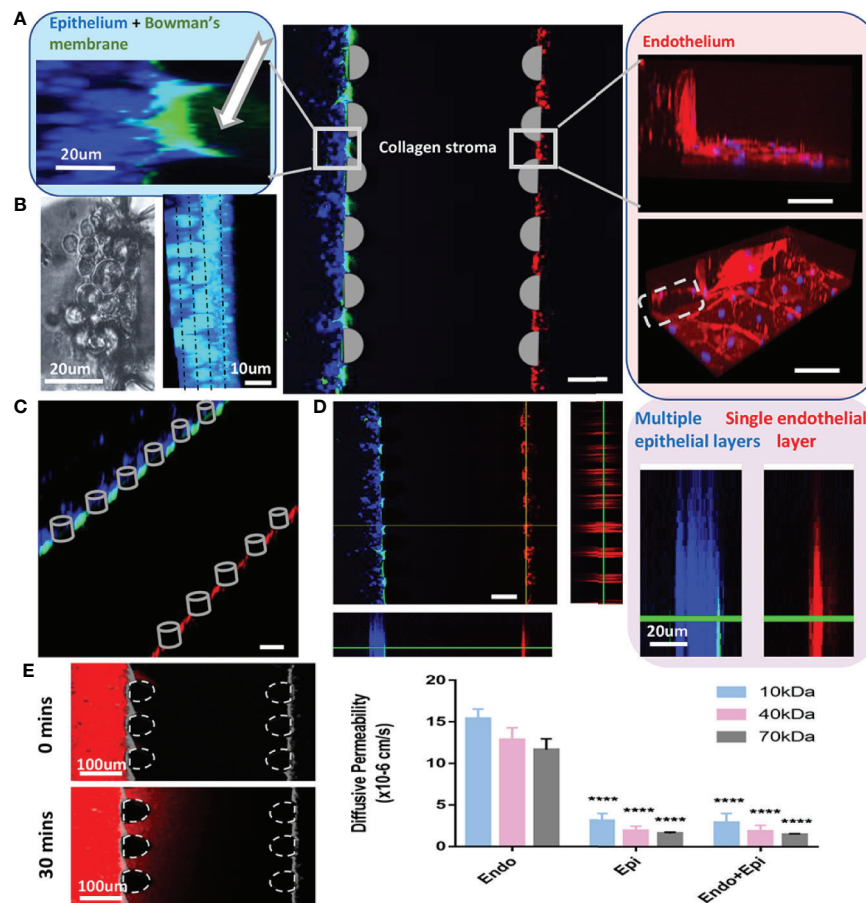


FIGURE 4 | Cornea-on-a-chip setup. **(A)** Immunofluorescent image of the device structure and cells 24h after seeding; middle: a 3D projection view of the cornea-on-a-chip assay; left: higher magnification on the corneal epithelial side, Bowman's layer as GFP-labeled condensed collagen (white arrow), epithelial cells (blue); right: endothelial cells monolayer was stained by ZO-1 (red), nuclei (blue), gray dotted line: PDMS pillar in the microfluidic device. **(B)** Phase-contrast (left) and immunofluorescent image (right) on corneal epithelial cells stained with cytokeratin 12 at 48h after seeding. Cells form 4-5 layers as indicated by dotted line. Blue: cytokeratin 12, cyan: nuclei. **(C)** Immunofluorescent surpass view image showing the overlay of the cornea-on-a-chip setup. **(D)** A 3-section view (left) and a comparison of epithelial multiple layer and endothelial monolayer (right). Endothelial cells were labeled with CellTracker™ Red and epithelial cells were labeled with CellTracker™ Blue. Bowman's membrane was shown in GFP-labeled collagen. **(E)** Dextran diffusion assay for 10kDa, 40kDa and 70kDa dextran label with Texas red and diffusive permeability was calculated from the fluorescent intensity across epithelial, endothelial layer and the entire cornea. Left, an example of dextran intensity images for the entire cornea at 0min and 30mins, respectively. Right, diffusive permeability in three conditions for three dextran molecules: epi = only epithelial cells present; endo = only endothelial cells present; endo+epi = co-culture of endothelial and epithelial cells. All data are expressed as mean \pm S.E.M. Comparison between multiple groups was performed by one-way-ANOVA and indicated by following Tukey means comparison tests (defined as: **** $p < 0.0001$). Analysis performed by Prism 7 (GraphPad). Scale:100um.

DATA AVAILABILITY STATEMENT

The datasets generated for this study are available on request to the corresponding author.

AUTHOR CONTRIBUTIONS

JB, RD'A designed research. JB, LB, and HF performed research and analyzed data. JB wrote the manuscript. JB, RD'A, HF, and AB contributed to the preparation of the manuscript.

ETHICS STATEMENT

The animal study was reviewed and approved by Institutional Animal Care and Use Committee of Boston Children's Hospital.

FUNDING

This study was supported, in part, by the NIH National Eye Institute under Award Number R01EY012726-12 (to RD'A).

REFERENCES

- Adriani, G., Bai, J., Wong, S. C., Kamm, R. D., and Thiery, J. P. (2016). M2a macrophages induce contact-dependent dispersion of carcinoma cell aggregates. *Macrophage* 3, e1222. doi: 10.14800/Macrophage.1222
- Aref, A. R., Huang, R. Y., Yu, W., Chua, K. N., Sun, W., Tu, T. Y., et al. (2013). Screening therapeutic EMT blocking agents in a three-dimensional microenvironment. *Integr. Biol. (Camb)* 5, 381–389. doi: 10.1039/C2IB20209C
- Bai, J., Adriani, G., Dang, T. M., Tu, T. Y., Penny, H. X., Wong, S. C., et al. (2015). Contact-dependent carcinoma aggregate dispersion by M2a macrophages via ICAM-1 and beta2 integrin interactions. *Oncotarget* 6, 25295–25307. doi: 10.18632/oncotarget.4716
- Bai, J., Tu, T. Y., Kim, C., Thiery, J. P., and Kamm, R. D. (2015). Identification of drugs as single agents or in combination to prevent carcinoma dissemination in a microfluidic 3D environment. *Oncotarget* 6, 36603–36614. doi: 10.18632/oncotarget.5464
- Bennet, D., Estlack, Z., Reid, T., and Kim, J. (2018). A microengineered human corneal epithelium-on-a-chip for eye drops mass transport evaluation. *Lab. Chip* 18, 1539–1551. doi: 10.1039/C8LC00158H
- Bischel, L. L., Lee, S. H., and Beebe, D. J. (2012). A practical method for patterning lumens through ECM hydrogels via viscous finger patterning. *J. Lab. Autom.* 17, 96–103. doi: 10.1177/2211068211426694
- Chin, J., Boek, E. S., and Coveney, P. V. (2002). Lattice Boltzmann simulation of the flow of binary immiscible fluids with different viscosities using the Shan-Chen microscopic interaction model. *Philos. Trans. A Math. Phys. Eng. Sci.* 360, 547–558. doi: 10.1098/rsta.2001.0953
- DelMonte, D. W., and Kim, T. (2011). Anatomy and physiology of the cornea. *J. Cataract Refract. Surg.* 37, 588–598. doi: 10.1016/j.jcrs.2010.12.037
- Guan, A., Wang, Y., Phillips, K. S., and Li, Z. (2016). A contact-lens-on-a-chip companion diagnostic tool for personalized medicine. *Lab. Chip* 16, 1152–1156. doi: 10.1039/C6LC00034G
- Kaluzhny, Y., Kinuthia, M. W., Truong, T., Lapointe, A. M., Hayden, P., and Klausner, M. (2018). New Human Organotypic Corneal Tissue Model for Ophthalmic Drug Delivery Studies. *Invest. Ophthalmol. Vis. Sci.* 59, 2880–2898. doi: 10.1167/iops.18-23944
- Kobayashi, T., Yoshioka, R., Shiraishi, A., and Ohashi, Y. (2009). New technique for culturing corneal epithelial cells of normal mice. *Mol. Vis.* 15, 1589–1593.
- Levario, T. J., Zhan, M., Lim, B., Shvartsman, S. Y., and Lu, H. (2013). Microfluidic trap array for massively parallel imaging of Drosophila embryos. *Nat. Protoc.* 8, 721–736. doi: 10.1038/nprot.2013.034
- Li, W., Sabater, A. L., Chen, Y. T., Hayashida, Y., Chen, S. Y., He, H., et al. (2007). A novel method of isolation, preservation, and expansion of human corneal endothelial cells. *Invest. Ophthalmol. Vis. Sci.* 48, 614–620. doi: 10.1167/iops.06-1126
- Li, J., Chen, S. Y., Zhao, X. Y., Zhang, M. C., and Xie, H. T. (2017). Rat Limbal Niche Cells Prevent Epithelial Stem/Progenitor Cells From Differentiation and Proliferation by Inhibiting Notch Signaling Pathway In Vitro. *Invest. Ophthalmol. Vis. Sci.* 58, 2968–2976. doi: 10.1167/iops.16-20642
- Lu, Y., Chan, Y. K., Lau, L. H., Chao, Y., Shih, K. C., Lai, S. M., et al. (2019). Adhesion of silicone oil and emulsification: an *in vitro* assessment using a microfluidic device and 'Eye-on-a-Chip'. *Acta Ophthalmol.* 97, 313–318. doi: 10.1111/aos.13982
- Ma, X. L., and Liu, H. Q. (2011). Comparison of cell-suspension and explant culture of mouse corneal epithelial cells in mice. *Int. J. Ophthalmol.* 11, 939–942. doi: 10.3969/j.issn.1672-5123.2011.06.001
- Niu, Y., Bai, J., Kamm, R. D., Wang, Y., and Wang, C. (2014). Validating antimetastatic effects of natural products in an engineered microfluidic platform mimicking tumor microenvironment. *Mol. Pharm.* 11, 2022–2029. doi: 10.1021/mp500054h
- Ottiger, M., Thiel, M. A., Feige, U., Lichtlen, P., and Urech, D. M. (2009). Efficient intraocular penetration of topical anti-TNF-alpha single-chain antibody (ESBA105) to anterior and posterior segment without penetration enhancer. *Invest. Ophthalmol. Vis. Sci.* 50, 779–786. doi: 10.1167/iops.08-2372
- Peh, G. S., Toh, K. P., Ang, H. P., Seah, X. Y., George, B. L., and Mehta, J. S. (2013). Optimization of human corneal endothelial cell culture: density dependency of successful cultures *in vitro*. *BMC Res. Notes* 6, 176. doi: 10.1186/1756-0500-6-176
- Seo, W. B., Frank, A., Massaro-Giordano, M., Lee, V., Bunya, V. Y., and Huh, D. (2016). Human blinking 'eye-on-a-chip'. *Investig. Ophthalmol. Vis. Sci.* 57, 3872.
- Seo, J., Byun, W. Y., Alisafaei, F., Georgescu, A., Yi, Y. S., Massaro-Giordano, M., et al. (2019). Multiscale reverse engineering of the human ocular surface. *Nat. Med.* 25, 1310–1318. doi: 10.1038/s41591-019-0531-2
- Shin, Y., Han, S., Jeon, J. S., Yamamoto, K., Zervantonakis, I. K., Sudo, R., et al. (2012). Microfluidic assay for simultaneous culture of multiple cell types on surfaces or within hydrogels. *Nat. Protoc.* 7, 1247–1259. doi: 10.1038/nprot.2012.051
- Shirasaki, Y. (2008). Molecular design for enhancement of ocular penetration. *J. Pharm. Sci.* 97, 2462–2496. doi: 10.1002/jps.21200
- Sosnova-Netukova, M., Kuchynka, P., and Forrester, J. V. (2007). The suprabasal layer of corneal epithelial cells represents the major barrier site to the passive movement of small molecules and trafficking leukocytes. *Br. J. Ophthalmol.* 91, 372–378. doi: 10.1136/bjo.2006.097188
- Sridhar, M. S. (2018). Anatomy of cornea and ocular surface. *Indian J. Ophthalmol.* 66, 190–194. doi: 10.4103/ijo.IJO_646_17
- Walker, G. M., and Beebe, D. J. (2002). A passive pumping method for microfluidic devices. *Lab. A Chip* 2, 131–134. doi: 10.1039/b204381e
- Wright, C. B., Becker, S. M., Low, L. A., Tagle, D. A., and Sieving, P. A. (2020). Improved Ocular Tissue Models and Eye-On-A-Chip Technologies Will Facilitate Ophthalmic Drug Development. *J. Ocular Pharmacol. Ther.* 36 (1), 25–29. doi: 10.1089/jop.2018.0139
- Xu, W., Xing, F. J., Dong, K., You, C., Yan, Y., Zhang, L., et al. (2015). Application of traditional Chinese medicine preparation in targeting drug delivery system. *Drug Delivery* 22, 258–265. doi: 10.3109/10717544.2014.892545

Conflict of Interest: The authors declare that the research was conducted in the absence of any commercial or financial relationships that could be construed as a potential conflict of interest.

Copyright © 2020 Bai, Fu, Bazinet, Birsner and D'Amato. This is an open-access article distributed under the terms of the Creative Commons Attribution License (CC BY). The use, distribution or reproduction in other forums is permitted, provided the original author(s) and the copyright owner(s) are credited and that the original publication in this journal is cited, in accordance with accepted academic practice. No use, distribution or reproduction is permitted which does not comply with these terms.



Exploration of Oxygen-Induced Retinopathy Model to Discover New Therapeutic Drug Targets in Retinopathies

Maria Vähätupa¹, Tero A. H. Järvinen^{1,2} and Hannele Uusitalo-Järvinen^{1,3*}

¹ Faculty of Medicine and Health Technology, Tampere University, Tampere, Finland, ² Department of Orthopedics and Traumatology, Tampere University Hospital, Tampere, Finland, ³ Eye Centre, Tampere University Hospital, Tampere, Finland

OPEN ACCESS

Edited by:

Zhuo Shao,
Hospital for Sick Children, Canada

Reviewed by:

Maurizio Cammalleri,
University of Pisa, Italy
Massimo Dal Monte,
University of Pisa, Italy

*Correspondence:

Hannele Uusitalo-Järvinen
hannele.uusitalo-jarvinen@tuni.fi

Specialty section:

This article was submitted to
Neuropharmacology,
a section of the journal
Frontiers in Pharmacology

Received: 01 December 2019

Accepted: 27 May 2020

Published: 11 June 2020

Citation:

Vähätupa M, Järvinen TAH and
Uusitalo-Järvinen H (2020) Exploration
of Oxygen-Induced Retinopathy Model
to Discover New Therapeutic Drug
Targets in Retinopathies.
Front. Pharmacol. 11:873.
doi: 10.3389/fphar.2020.00873

Oxygen-induced retinopathy (OIR) is a pure hypoxia-driven angiogenesis model and the most widely used model for ischemic retinopathies, such as retinopathy of prematurity (ROP), proliferative diabetic retinopathy (PDR), and retinal vein occlusion (RVO). OIR model has been used to test new potential anti-angiogenic factors for human diseases. We have recently performed the most comprehensive characterization of OIR by a relatively novel mass spectrometry (MS) technique, sequential window acquisition of all theoretical fragment ion mass spectra (SWATH-MS) proteomics and used genetically modified mice strains to identify novel molecular drug targets in angiogenic retinal diseases. We have confirmed the relevance of the identified molecular targets to human diseases by determining their expression pattern in neovascular membranes obtained from PDR and RVO patients. Based on our results, crystallins were the most prominent proteins induced by early hypoxic environment during the OIR, while actomyosin complex and Filamin A-R-Ras axis, that regulates vascular permeability of the angiogenic blood vessels, stood out at the peak of angiogenesis. Our results have revealed potential new therapeutic targets to address hypoxia-induced pathological angiogenesis and the associated vascular permeability in number of retinal diseases.

Keywords: hypoxia, angiogenesis, vascular permeability, R-Ras, filamin, myosin, retinopathy of prematurity (ROP), diabetic retinopathy

INTRODUCTION

The formation of new blood vessels, angiogenesis, is essential for normal development, and functional blood vessels are needed for the maintenance of tissue homeostasis (**Figure 1**). Angiogenesis is controlled by a delicate balance of pro- and anti-angiogenic factors in human body. The formation of pathological neovascularization (NV) can be induced when the balance between pro- and antiangiogenic factors shifts. NV is a common factor in several retinal diseases, such as retinopathy of prematurity (ROP), diabetic retinopathy (DR), and the wet form of age-related macular degeneration (AMD) (Campochiaro, 2013). These retinal diseases are major causes of severe visual impairment and blindness in developed countries. Due to aging population, incidence of retinal diseases involving ocular NV is constantly increasing.

NV can arise either from retina or choroid in the eye. Retinal NV is seen in ischemic retinopathies, such as ROP, DR, and retinal vein occlusion (RVO), whereas choroidal NV develops in wet AMD, where choroidal neovessels grow through Bruch's membrane toward subretinal space and outer retina (Campochiaro, 2015). The neovessels are unstable and hyperpermeable, and accordingly, they leak causing hemorrhages and edema. Ultimately in wet AMD subretinal and intraretinal leakage from the neovessels leads to scarring and permanent photoreceptor damage in the retina resulting in vision loss. In DR, ROP, and RVO, retinal neovascularization is associated with hemorrhages, fibrovascular proliferation, and subsequent contraction of neovascular membranes ultimately leading to retinal detachment and blindness.

Vascular endothelial growth factor-A (VEGF-A) is a major proangiogenic factor driving angiogenesis. When the cells experience hypoxia, it stabilizes hypoxia inducible factor-1 α (HIF-1 α) (Lee et al., 2019; Yeo, 2019; Liao and Zhang, 2020). Stabilized HIF-1 α translocates to the cell nucleus and forms a complex with HIF-1 β , creating HIF-1 transcription factor. HIF-1 transcription factor then binds to hypoxia response element in the genes that promote survival in low-oxygen conditions. Active HIF-1 signaling triggers the production of large number of angiogenic growth factors, among them VEGF. These soluble growth factors direct the sprouting of the new blood vessel, i.e., angiogenesis, to deliver oxygen and address the hypoxia in the tissue (Lee et al., 2019; Yeo, 2019; Liao and Zhang, 2020). VEGF also induces vascular permeability and leakage in ocular NV diseases (Ferrara et al., 2003; Penn et al., 2008). The use of VEGF inhibitors as an antiangiogenic treatment for ocular neovascular diseases has revolutionized the treatment of these diseases and improved their prognosis dramatically. Despite the progress, there are nonresponsive patients as well as many unwanted side-effects (Yang et al., 2016). Furthermore, eradication of the neovessels by VEGF inhibitors may worsen the underlying ischemia and drive the formation of new, leaky blood vessels by alternative molecular mechanism. On the other hand, we have learned to understand that the persistency of angiogenic blood vessels leads to the progression of NV retinal diseases instead of resolving them (Mishra, 2016). Thus, the

proposed molecular mechanism for future antiangiogenic therapies is one where the angiogenic blood vessels are “normalized” to stable ones to alleviate the hypoxia and stop the detrimental aberrant vascular leakage which leads scarring in retinal NV diseases (Goel et al., 2012). Thus, more effective and specific therapies that address the permeability are needed for neovascular diseases.

Vascular permeability is strictly controlled during physiological conditions, but this control is lost in many diseases and the blood vessels become hyperpermeable. VEGF-A is the most potent growth factor in inducing vascular permeability. As a matter of fact, it was first discovered as a vascular permeability factor, a soluble protein secreted by tumors and shown to significantly increase vascular permeability (Senger et al., 1983). It is still considered as the major growth factor regulating vascular permeability in tumors and NV diseases. Features of hyperpermeable blood vessels, such as damage to the glycocalyx lining the inner lumen of endothelial cells, disorganization of cell-cell junctions and the dropout of pericytes and discontinuous endothelial cells, are well-established (Sawada et al., 2012; Butler et al., 2020). VE-cadherin is a dimeric transmembrane protein that clusters at cell-cell contacts, where it forms complexes with other signaling proteins, such as β -catenin, p120, and plakoglobin (Dejana et al., 2008) (Figure 2). VE-cadherin is needed for the maintenance of a stable vascular system. It controls endothelial vascular permeability and prevents excess vascular growth (Giannotta et al., 2013) (Figure 2).

Oxygen-Induced Retinopathy (OIR)

In order to find out completely novel and specific drug targets for retinal NV diseases, we have explored the most common *in vivo* model for retinal NV, the mouse oxygen-induced retinopathy (OIR) model (Smith et al., 1994) (Figure 3). The OIR model is widely used to study retinal NV diseases, because it shares many hallmarks with human ischemic retinopathies (Scott and Fruttiger, 2010; Stahl et al., 2010; Vessey et al., 2011; Vähätupa et al., 2016; Liu et al., 2017; Sun and Smith, 2018). The practicability of mouse OIR model has been demonstrated as it was widely used to test new potential antiangiogenic factors for human diseases and proved to provide similar outcome of the treatment as was later obtained in humans.

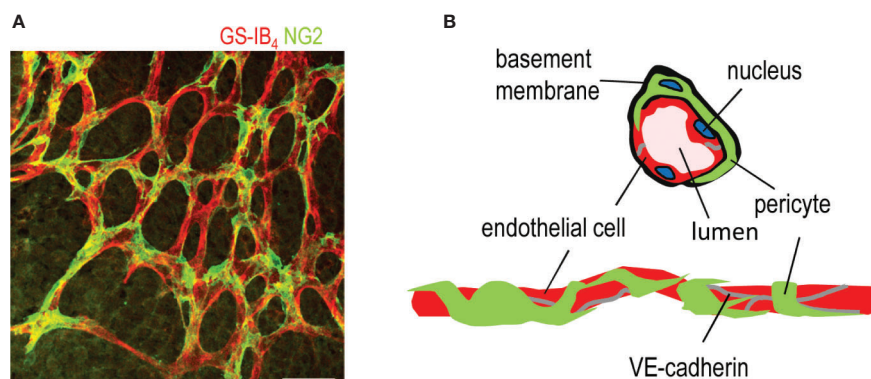


FIGURE 1 | Structure of a capillary blood vessel in retina. **(A)** Capillary plexus of the mouse retina, where ECs are stained in red (Isolectin B₄), and pericytes are stained in green (NG2 antibody). Scale bar is 50 μ m. **(B)** Structure of capillary blood vessels in retina. This figure is reproduced from Vähätupa, 2019 with the permission of the copyright holder.

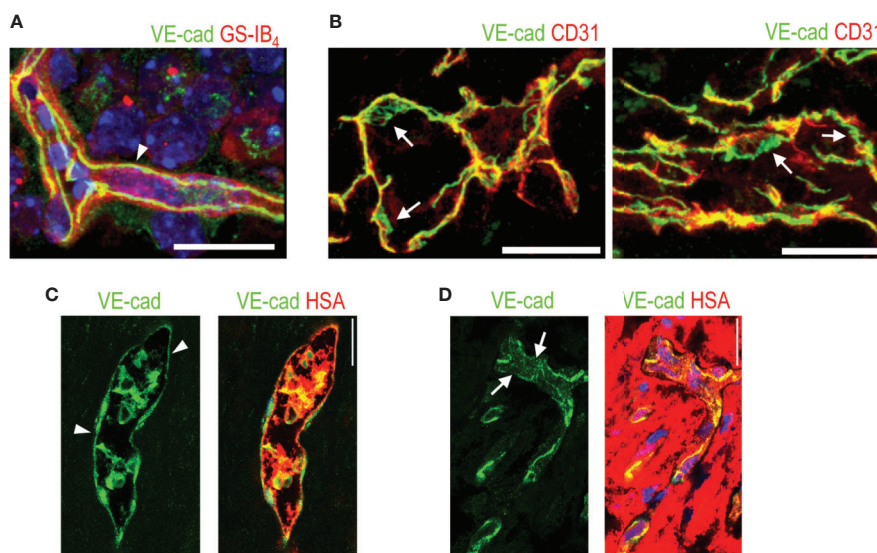


FIGURE 2 | VE-cadherin expression in normal retina and in human PDR. **(A)** VE-cadherin (arrowhead, green) exhibits uniform expression in healthy mouse retina ECs (red). **(B)** VE-cadherin expression is aberrant in the vasculature of human PDR samples, (arrow). **(C)** In blood vessels where normal or continuous (arrowhead) VE-cadherin expression is seen, human serum albumin (HSA, red) is seen inside the blood vessels. **(D)** In the areas of discontinuous or absent VE-cadherin (arrows), HSA is seen around the blood vessels, indicating leakage. Scale bar is 200 μ m. This figure is reproduced from Vähätupa, 2019 with the permission of the copyright holder.

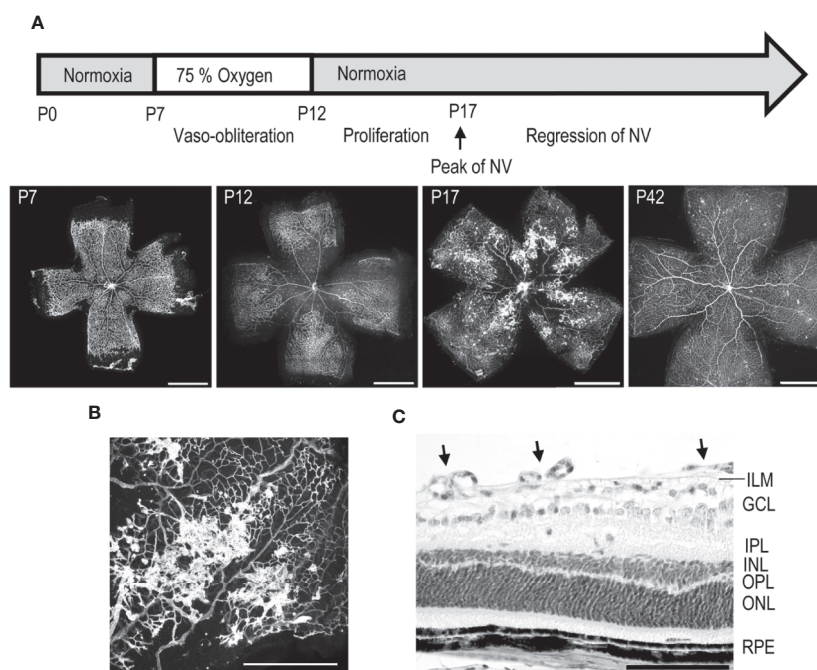


FIGURE 3 | Mouse oxygen-induced retinopathy model. **(A)** Timeline of the OIR model. Induction; mice are exposed to 75% oxygen from P7 to P12 in hyperoxia chamber and returned to normal room air. Avascular area in the central retina (at P12) induces revascularization, and peak of preretinal NV is seen at P17. **(B)** Preretinal neovascular tufts form at the border between the vascular and avascular retina. **(C)** Retinal cross-section of OIR retina at P17, where preretinal tufts are sprouting towards the vitreous. Moreover, thinning of INL and OPL layers is seen. Scale bars are 1 mm in A, 500 μ m in B, and 100 μ m in C. This figure is reproduced from Vähätupa, 2019 with the permission of the copyright holder.

Furthermore, it has proved feasible to test the effect of specific genes in the pathogenesis in retinal NV diseases as genetically modified mouse strains (knockout or transgenic) can be tested in it. We have performed the most comprehensive proteomics characterization of the OIR to date in order to understand molecular processes that drive the pathological neovessel formation in the model and correlated these findings with samples from human NV retinal diseases (Vähätupa et al., 2018a).

The mouse OIR model, takes advantage of plasticity of the neonatal mouse retinal blood vessels which undergo regression when the mouse is exposed to hyperoxic stimulus (Benjamin et al., 1998; Vähätupa et al., 2020). In the OIR model, neonatal mice are placed to 75% hyperoxic chamber at postnatal day 7 (P7) for five days, after which they are returned to normal room air (Smith et al., 1994; Vähätupa et al., 2016; Vähätupa et al., 2020) (**Figure 3**). Upon return to normoxic conditions, the avascular retina becomes hypoxic triggering revascularization of the retina from the periphery towards the central retina. Due to excessive hypoxic stimuli, some of the retinal blood vessels start to sprout towards the vitreous, forming preretinal NV, called preretinal tufts, that are immature and hyperpermeable (**Figure 3**). Using the OIR model, both the rate of revascularization and the amount of pathological NV can be measured (Connor et al., 2009; Stahl et al., 2010; Vähätupa et al., 2020) (**Figure 3**).

To understand the complex molecular events that drive pathological angiogenesis in the OIR model and to hopefully identify novel therapeutic target molecules for human NV retinal diseases, we investigated the pathogenesis of the mouse OIR model using the SWATH-MS full proteome-based approach (Vähätupa et al., 2018a). Overall, we were able to quantify almost 3,000 unique proteins and their expression levels during the OIR pathogenesis. Quite strikingly, the proteomics analysis revealed that the strongest cause for the differences in the protein expression levels appears to be the developmental stage of the retina. On the other hand, the pathway analysis identified angiogenesis as a mechanism that induced the changes in the protein expression levels at P17, i.e., the peak of angiogenesis in OIR (Vähätupa et al., 2018a).

Hypoxia-Induced Expression of Crystallins in OIR

To gain more insight to the role of hypoxia in human retinopathies, we explored protein expression profile in OIR 24 h after return to normoxia. We detected a family of proteins, crystallins that were greatly upregulated (based on fold-change) by sudden hypoxia placed on retina (Vähätupa et al., 2018a). Remarkably, the crystallin family clearly stands out from the rest of the proteome by the strong hypoxia-induced expression (Vähätupa et al., 2018a). Crystallins are small heat-shock proteins that play roles in neuroprotection, because they protect cells from hypoxia and maintain mitochondrial homeostasis (Diokmetzidou et al., 2016; Kannan et al., 2016). Crystallins are expressed in the retina, where they participate in various biological processes, among them the development of retinal vasculature (Zhang et al., 2005; Sinha et al., 2008). α -

crystallins may have therapeutic value in the retina. The administration of α -crystallins inhibited retinal degeneration, protected retinal ganglion cells from apoptosis, and promoted axonal regeneration in experimental animal models (Nagaraj et al., 2016). It is thought that α A-crystallin might be useful in the treatment of early DR, because adenovirus-mediated delivery of α A-crystallin inhibited pericyte dropout and vascular leakage from angiogenic blood vessels (Kim et al., 2012).

In addition to their roles in neuroprotection and development, some of the crystallins have been reported to play a prominent role in pathology of retinal NV diseases. Namely, α B-crystallin is a modulator of angiogenesis because it functions as a chaperone for VEGF and is needed for its adequate folding and secretion (Kase et al., 2010; Kannan et al., 2012). Accordingly, α B-crystallin is expressed in pathological blood vessels in PDR and is also found in vitreous fluid, and its levels correlate with VEGF levels (Chen et al., 2017). Mice deficient for α B-crystallin had less VEGF and NV compared to WT mice in the OIR model. α B-crystallin has also been reported to participate in the epithelial-mesenchymal transition (EMT), leading to TGF- β driven subretinal fibrosis in experimental AMD (Ishikawa et al., 2016). The expression of crystallins is greatly increased in many ocular diseases, such as AMD, DR, mechanical trauma, and ischemic insults (Kase et al., 2011; Thanos et al., 2014; Kannan et al., 2016). To make the matters even more complicated, an experimental diabetes study reported overexpression of α , β , and γ -crystallins in the diabetic retina, but they had lost their neuroprotective functions due to diabetes (Losiewicz and Fort, 2011).

In view of the animal studies and clinical data as well as the opposite functions of different individual crystallins and the fact that the expression levels of almost all crystallin family members are increased by the hypoxia in OIR, their potential therapeutic value is complicated (Vähätupa et al., 2018a). It seems that the therapeutic potential of crystallins needs to be investigated individually to identify the potential therapeutic crystallins among the family. Furthermore, their opposing biological functions indicate that while some members might have therapeutic value, some might have to be inhibited to treat the NV retinal diseases.

Leakage of Plasma Proteins From Pathological Blood Vessels in OIR—Important Players in Pathobiology?

Pathological vascular permeability is a hallmark of the angiogenic blood vessels also in human retinopathies. Among the most upregulated proteins at the peak of angiogenesis in OIR (at P17) were plasma proteins such as Vitamin-D-binding protein (Gc), Albumin, and Apolipoprotein A1 (Apoa1) (Vähätupa et al., 2018a). This is most likely due to increased plasma leakage from hyperpermeable, angiogenic blood vessels. However, these proteins might also have biological functions in the OIR pathogenesis. The most upregulated protein based on fold change at P17 was Gc, a vitamin D-binding protein. It was substantially more upregulated than serum albumin, the most abundant blood protein in mammals, which may indicate

selective accumulation (Vähätupa et al., 2018a). Gc is a multifunctional glycoprotein and a member of the albumin superfamily of binding proteins. It is an important carrier of vitamin D metabolites, such as calcitriol, the active form of vitamin D (Delanghe et al., 2015; Duchow et al., 2019). Interestingly, calcitriol has been reported to be antiangiogenic in a dose dependent manner in the OIR model (Albert et al., 2007). Other vitamin D receptor agonists also attenuated ocular angiogenesis in a zebrafish larvae model (Merrigan and Kennedy, 2017). Gc can also modulate inflammatory functions since it can be converted to a vitamin-D-binding protein-macrophage activating factor (DBP-MAF), which may have antitumorigenic and antiangiogenic effects (Kanda et al., 2002; Kisker et al., 2003). The antiangiogenic functions of DBP-MAF are based on its ability to inhibit VEGF signaling by decreasing the phosphorylation of VEGFR2 and ERK1/2 (Kalkunte et al., 2005). Vitamin D metabolism has been linked to ocular disease pathology and low serum levels of vitamin D represent a risk factor for AMD, DR, and glaucoma (Layana et al., 2017; Skowron et al., 2018). Vitamin D receptor (VDR) is expressed in neurons, retinal, and choroidal ECs, and especially strongly in pericytes (Jamali et al., 2017; Layana et al., 2017). Mice deficient for VDR had an increased number of pericytes and impaired NV and were resistant to the antiangiogenic functions of calcitriol in OIR (Jamali et al., 2017). It has also been suggested that vitamin D could work by protecting against oxidation and inflammation in NV retinal diseases (Layana et al., 2017; Skowron et al., 2018).

Based on the results obtained, it is possible that the upregulation of Gc in OIR at P17 could be an endogenous signal to suppress angiogenesis or a response to low levels of vitamin D metabolites in the retina. A proteomic study of ROP showed that Gc was one of the proteins found in the vitreous of ROP patients but not in the healthy controls (Sugioka et al., 2017). On the other hand, the increased amount of Gc in NV Retina could also be outcome of the increased expression, not just the product of enhanced leakage, because ECs release Gc under stress, but not during normal growth (Raymond et al., 2005). Gc works as a growth factor in blood vessels and induces cell migration and proliferation of vascular SMCs at the site of vascular injury (Raymond et al., 2005). Recently published meta-analysis indicated that Gc polymorphisms play important roles in cancer pathogenesis (Zhu et al., 2019). The role of Gc in ocular angiogenesis and OIR has not been investigated. Thus, further studies are needed to find out whether its enhanced accumulation is the by-product of leakage or whether it is produced by the ECs in angiogenic blood vessels. These issues would clarify its role in neovascular ocular diseases.

Proteins Involved in Mechanotransduction Are Upregulated in OIR and Angiogenesis in OIR May Involve Endothelial-to-Mesenchymal Transition (EndMT)

When we focused on the peak of angiogenesis in OIR, i.e., P17, majority of the upregulated proteins were involved in the mechanotransduction, cell adhesion, and actin cytoskeleton signaling (Vähätupa et al., 2018a). Proteins associated to actin

cytoskeleton play an important role in cell-cell adhesion (Hoelzle and Svitkina, 2012) and actin cytoskeleton remodeling is implicated as an important factor in angiogenesis (Keezer et al., 2003; Kilarski et al., 2003). In order to change shape, cells need to sense and respond to external mechanical stimulus and forces. These molecules are thought to be part of the mechanobiome, which includes molecules ranging from cell adhesion to ECM to the contractile molecules in the cytosol (Kothari et al., 2019). Together they form a network of proteins, where some act either as a sensors or actuators. Some of the proteins, like non-muscle myosin II, can act both as a sensor and an actuator, and further link to other proteins like scaffolding proteins and transcription factors (Luo et al., 2012; Kothari et al., 2019). Notably, the actomyosin network is a significant driver of cellular processes by regulating gene expression and has been implicated as an important regulator in angiogenesis (Angulo-Urarte et al., 2018; Kothari et al., 2019).

Actomyosin (complex of myosin and actin) contraction-based pulling forces at the cell junctions are regulating the switch between stable and unstable EC junctions (Angulo-Urarte et al., 2018).

One of the molecules involved in this process is Vinculin, a focal adhesion protein connecting cell adhesions to the actin cytoskeleton (Ziegler et al., 2008). Vinculin associates with VE-cadherin on the EC junctions as a regulator force-dependent remodeling (Huveneers et al., 2012) and deregulation of Vinculin is associated with enhanced cancer cell migration (Goldmann et al., 2013). Interestingly, Vinculin was one of the proteins upregulated at the angiogenic phase in OIR (Vähätupa et al., 2018a).

Among the mechanobiome proteins upregulated in OIR (Vähätupa et al., 2018a), Myh9 is especially relevant (Figure 4). We demonstrated strong induction of Myh9 in OIR at the peak of angiogenesis, i.e., at P17 (Vähätupa et al., 2018a). Strikingly, the strong Myh9 expression took place selectively in angiogenic blood vessels in the OIR (Vähätupa et al., 2018a) (Figure 4). Myh9 encodes for a myosin IIA heavy chain, a cytoskeletal contractile/motor protein, which participates in a variety of processes requiring contractile force, such as cytokinesis, cell migration, polarization and adhesion, and the maintenance of cell shape (Pecci et al., 2018). Its expression levels are considered to reflect the stiffness of the tissue, such that the stiffest tissues express high levels of Myh9 (Irianto et al., 2016). When cells are migrating, they adhere to the extracellular matrix, which transmits forces inside the cell, and the nonmuscle myosins balance the mechanical forces. The stiffer the tissue, the more contractility the migrating cells need. ECs form contact with each other with lamellipodia like structures. Then they retract and remain in contact with thin bridges formed by filopodia-like protrusions, which connect to neighboring ECs by VE-cadherin-rich junctions. Actin bundles in bridges recruit nonmuscle myosin II and mature into stress fibers. Myosin II activity is important for bridge formation and accumulation of VE-cadherin in nascent adherens junctions (Hoelzle and Svitkina, 2012). When the ECs are migrating, these myosin IIA-generated forces destabilize endothelial cell-

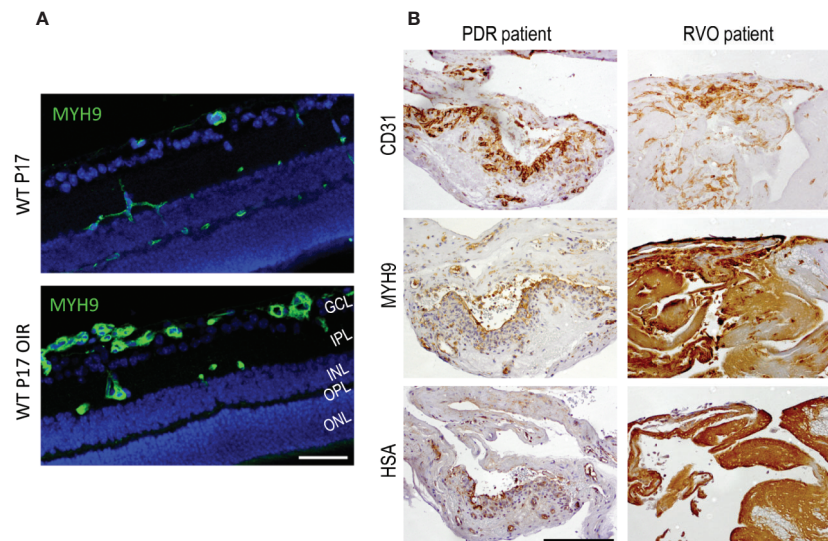


FIGURE 4 | Myosin IIA (Myh9) is expressed in OIR retinas and human PDR and RVO fibrovascular membranes. **(A)** Mouse retinal sections stained for Myh9 (green) exhibit increased expression in the blood vessels in OIR retinas. **(B)** The blood vessels (CD31) had HSA restricted inside the blood vessels when Myh9 expression was low. Strong Myh9 expression is associated with strong HSA accumulation throughout the sample in fibrotic RVO sample. In PDR samples with low Myh9 expression in the blood vessels (CD31) had HSA restricted inside the blood vessels. In fibrotic RVO sample strong Myh9 expression together with strong HSA accumulation throughout the sample was seen. Scale bar is 50 μ m in A and 200 μ m in B. This figure is reproduced from Vähätupa, 2019 with the permission of the copyright holders.

cell junctions and increase vascular permeability (Huynh et al., 2011; Bordeleau et al., 2017; Lampi and Reinhart-King, 2018). Myh9 is overexpressed in many cancers, and its high expression is associated with poor prognosis indicating very aggressive phenotype of the tumor (Newell-Litwa et al., 2015). The complex interactions between the stiffness of the tissue and myosin IIA was recently elegantly demonstrated in glioblastoma (Picariello et al., 2019; Surcel and Robinson, 2019). The deletion of Myh9 led to the inhibition of tumor cell invasion, but its effects on cell proliferation are different depending on environmental mechanics, i.e., whether the cells are on soft or stiff surface (Picariello et al., 2019). In addition to regulating the endothelial cell-cell junctions, Myh9 regulates cell migration in angiogenesis (Vicente-Manzanares et al., 2009; Yoon et al., 2019). Myh9 is required for sprouting angiogenesis as it is crucial for mediating mechanical forces and maintaining cell-cell contacts between tip and stalk cells (Yoon et al., 2019). This is the likeliest explanation for the induction Myh9 during sprouting angiogenesis in OIR (Vähätupa et al., 2018a) (**Figure 4**).

As the mechanobiome is an important regulator of gene expression, the activation of Myh9 led to elevated VEGF expression and induction of arteriogenesis in the ischemia-driven arteriogenesis (Morrison et al., 2014). Myh9 has also been shown to control the translocalization of nucleolin, which is primarily a nuclear protein but translocates to the EC surface in angiogenesis (Christian et al., 2003; Huang et al., 2006; Fogal et al., 2009; Li et al., 2018). Therapies that antagonize nucleolin or block Myh9 inhibit angiogenesis by causing EC apoptosis and normalizing the vasculature (Fogal et al., 2009). In our proteomic

study, we observed only a modest increase in the nucleolin expression (Vähätupa et al., 2018a). However, the gene expression levels are not relevant to function of nucleolin in angiogenesis, because its function is related to its translocation to cell surface. It was recently shown that nucleolin is translocated to the EC surface in neovascular blood vessels in OIR, whereas it stayed nuclear in the normoxic conditions (Garfias et al., 2019). Similar nucleolin translocation takes place in corneal neovascularization and nucleolin-binding DNA aptamer was able to inhibit corneal neovascularization (Vivanco-Rojas et al., 2020).

We also studied Myh9 expression in human NV retinal diseases. Strong Myh9 expression correlated with HSA accumulation (i.e., leakage) in PDR and RVO membranes (Vähätupa et al., 2018a) (**Figure 4**). This indicates increased EC contractility, which in turn, results in increased vascular permeability. Myh9 is also expressed in fibroblast like cells that have undergone endothelial to mesenchymal transition (EndMT) (Evrard et al., 2016). Actin cytoskeleton remodeling is well characterized process in epithelial to mesenchymal transition in cancer invasion and metastasis (Peng et al., 2018).

In EndMT, cells start to express mesenchymal markers, gain increased motility, and begin the secretion of extracellular matrix proteins. This phenomenon is reported to contribute to endothelial dysfunction during inflammation (Cho et al., 2018) and it is involved in a variety of disease processes, such as vascular or tissue fibrosis, and in the tumor environment (Hong et al., 2018). Upstream regulator analysis of OIR proteomics data indicates TGF- β , Mkl2, and Mknk1 as potential enhancers of increased angiogenesis in OIR. In addition, TGF- β is known for its roles in

the induction of EMT and myofibroblast transformation. Mkl2 (and Mkl1) are key regulators in these cellular processes (Crider et al., 2011; Gasparics and Sebe, 2018). Increased TGF- β signaling leads to EndMT in the vasculature, which shares many features with EMT (Dejana et al., 2017; Schwartz et al., 2018). Enhanced vascular TGF- β signaling may also induce fibrosis to surrounding tissue. EndMT takes place in glucose-treated retinal ECs, where EC damage leads to a decrease in endothelial markers and an increase in mesenchymal markers, processes which is induced by TGF- β (Cao et al., 2014; Thomas et al., 2019). In light of the recent finding that TGF- β together with α b-crystallin is associated with EMT and with subretinal scarring (Ishikawa et al., 2016), simultaneous up-regulation of both molecules could provide hints about the potential events that ultimately lead to fibrosis in angiogenic retinal diseases. Furthermore, it was recently demonstrated that myeloid cell-derived furin, TGF- β activator, is crucial for the angiogenesis in OIR (Vähätupa et al., 2018b), but furin also aggravates hypoxia-induced blood-brain barrier dysfunction (Baumann et al., 2019). Taking together, the upregulation of proteins involved in mechanotransduction and actomyosin network as well as in the TGF- β signaling in OIR during the angiogenic phase may suggest that these processes could be important for angiogenesis, and thus provide a potential therapeutic target.

R-Ras and Filamin A Axis in Vascular Stabilization of Angiogenic Blood Vessels in OIR

One of the proteins predicted to be causing enhanced angiogenesis in the OIR model was Flna, which is the most abundant member of the filamins. Filamins act as actin binding scaffold proteins that maintain ECM connections. They act as mechanoresponsive actin crosslinkers and are important players in the actomyosin network and crucial for mechanotransduction (Baudier et al., 2018; Balassy et al., 2019). Thus, they modulate

the interactions between actin cytoskeleton and the ECM, enabling changes in the transmission of forces at the cell periphery (Razinia et al., 2012).

We showed that Flna was expressed in the retinal blood vessels and the expression was increased in OIR (**Figure 5**). In addition to the increase in the levels of total Flna, a 14-fold induction of C-terminal Flna fragment (Flna^{CT}) was detected (Vähätupa et al., 2018a) (**Figure 5**). In hypoxia, Flna is rapidly upregulated and then interacts with HIF-1 α and promotes angiogenesis (Zheng et al., 2014). In hypoxia, Flna undergoes calpain dependent cleavage, and its 90 kDa C-terminal fragment (Flna^{CT}) accumulates into the nucleus, enhancing HIF-1 α (but not HIF-2 α) accumulation there. Flna^{CT} interaction with HIF-1 α localizes the HIF-1 complex to the promoter regions of HIF-1 target genes and enhances their transcription/expression (Zheng et al., 2014). Upregulation of Flna has been found in many cancers, and tumor cells lacking Flna exhibits impaired growth and angiogenesis, as well as the reduced expression of HIF target genes (Nallapalli et al., 2012; Zheng et al., 2014). Targeting Flna has been proposed as a target for cancer therapy (Nallapalli et al., 2012). Considering that N-terminal Flna is needed for the stability of the EC barrier, specific inhibition of Flna^{CT} could provide a more potent antiangiogenic therapeutic effect than general Flna inhibition. Indeed, it was recently shown that blocking the calpain-dependent cleavage of Flna hinders the growth of tumor cells (Salimi et al., 2018).

Concerning molecular mechanism by which Flna induces its effects on blood vessels, it interacts with small GTPase R-Ras to control cell migration and maintain vascular barrier function (Griffiths et al., 2011). R-Ras is a member of the Ras superfamily of known oncogenes. However, R-Ras maintains cellular quiescence and inhibits cell proliferation, effects that are opposite to the biological functions of other Ras family members, which play a prominent role in cancer progression

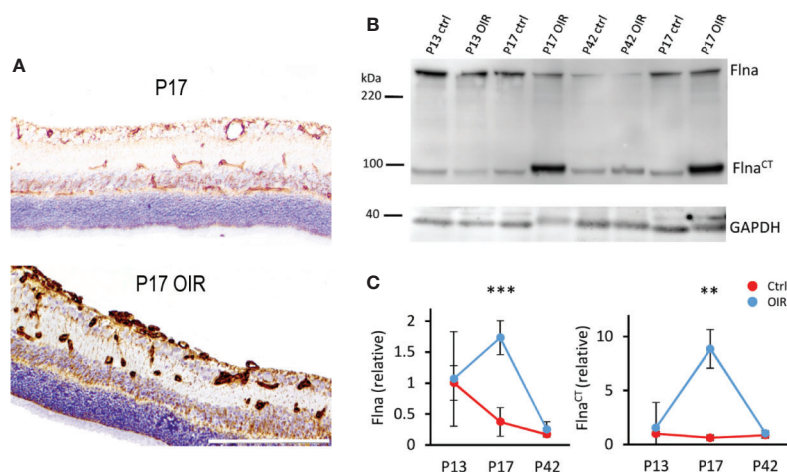


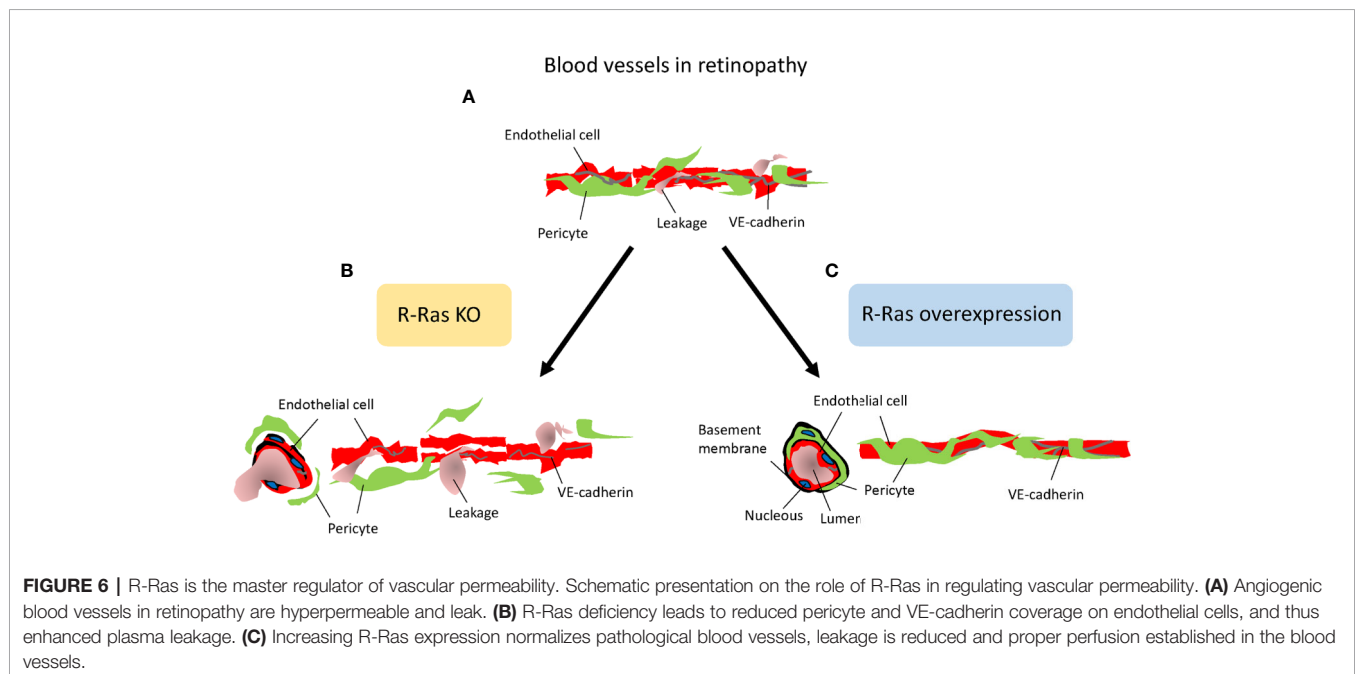
FIGURE 5 | Filamin A upregulation in OIR retinal blood vessels. **(A)** Retinal sections stained for Flna (brown) show induction of Flna in retinal blood vessels in OIR. **(B)** Western blot of control and OIR retinas at different time points shows increase of cleaved Flna fragment, Flna^{CT} in OIR at P17. **(C)** Quantification of total Flna and Flna^{CT} in control and OIR retinas. Scale bar is 200 μ m. This figure is adapted from Vähätupa, 2019 with the permission of the copyright holders. ** $P < 0.01$, *** $P < 0.001$.

(Prior et al., 2012; May et al., 2015). Generation of R-Ras deficient mice revealed that the primary function of R-Ras is in the regulation blood vessel maturation and angiogenesis (Komatsu and Ruoslahti, 2005; Sawada et al., 2012; Sawada and Komatsu, 2012) (**Figure 6**). R-Ras inhibits vessel sprouting and branching and EC migration (Sawada et al., 2012; Sawada et al., 2015b). Most importantly, it is a crucial gene to regulate vascular permeability not only during pathological tumor angiogenesis, but also in physiological tissue repair, that is, in skin wounds as it stabilizes blood vessel walls (Komatsu and Ruoslahti, 2005; Sawada et al., 2012; Sawada et al., 2015a; Ketomäki et al., 2019; Järvinen, 2020) (**Figure 6**). R-Ras is also integral for the proper lumenization of the angiogenic blood vessels, i.e., it restores proper lumen formation and normal perfusion and most importantly addresses the hypoxia (Li et al., 2017). Taken together, R-Ras is considered as a master regulator of vascular permeability in angiogenesis (**Figure 6**).

R-Ras is crucial for blood vessel integrity and stabilization in the OIR model, where R-Ras deficient mice have a hyper-permeable phenotype (Vähätupa et al., 2016) (**Figure 6**). Although the revascularization rates are identical between WT and R-Ras KO mice, the neovascular blood vessels leak twice as much in the KO mice than in the WT mice. The pericyte coverage is reduced in the angiogenic blood vessels in OIR in the R-Ras KO mice, and VE-cadherin expression is reduced (Vähätupa et al., 2016). R-Ras expression in human DR samples showed that the immature, pathological VEGFR2+ blood vessels lack R-Ras expression and R-Ras expression correlates inversely with leakage from the immature blood vessels, i.e., more leakage in human DR, less R-Ras is expressed in the blood vessels (Vähätupa et al., 2016). The molecular mechanisms by which R-Ras exerts its function on vascular permeability are not known in detail, but our understanding on its function is rapidly

emerging as its central role in regulating vascular permeability is appreciated. R-Ras is functionally different from classic antiangiogenic agents as it does not induce endothelial cell apoptosis, but it actually promotes endothelial cell survival (Komatsu and Ruoslahti, 2005; Takino et al., 2019).

Concerning endothelial cell death, Ras guanyl nucleotide releasing protein 2 (RasGRP2) inhibits EC apoptosis *via* R-Ras (Takino et al., 2019). Furthermore, R-Ras interacts with Flna and co-localizes into plasma membrane (Griffiths et al., 2011). Disrupting this interaction promotes disorganization of VE-cadherin at adherens junctions and leads to leaky blood vessels. R-Ras binds to Flna in its N-terminus (Griffiths et al., 2011). Thus, the selective blockage of either the cleavage of Flna (that creates angiogenic Flna^{CT}) or Flna^{CT} fragment itself could be a potential therapeutic approach in ischemic retinopathies involving NV, because it should not interfere with the physical interaction between R-Ras and N-terminus of Flna that maintains vascular stability in blood vessels. Interestingly, we showed that the induction of Flna^{CT} is almost 15-fold in OIR (Vähätupa et al., 2018a), making it viable molecular target to inhibit sprouting angiogenesis. Furthermore, actin-binding protein Girdin/GIV regulates transendothelial permeability by also controlling VE-cadherin trafficking through R-Ras (Ichimiya et al., 2015). The mechanism of action regulating vascular permeability could also be related to R-Ras being also an integrin activator (Zhang et al., 1996). Notch activates in R-Ras – $\beta 1$ integrin pathway in radial glia (Fujita et al., 2020). Notch signaling tells endothelial cells to stop migrating and proliferating in angiogenesis (Luo et al., 2019). Notch induced activation of R-Ras – $\beta 1$ integrin pathway could be the mechanism for the appearance of R-Ras during blood vessel maturation (Komatsu and Ruoslahti, 2005; Vähätupa et al., 2016). Flna, in turn, interacts with $\beta 1$, $\beta 2$, and $\beta 7$ integrin tails



(Toomer et al., 2019). R-Ras regulates integrin dependent cell migration through Flna (Gawecka et al., 2010). Sandri et al. showed integrin-activated R-Ras recruits RIN2 to focal adhesions and induces RIN2 conversion to a Rab5-docking protein (Fernandez-Borja, 2012; Sandri et al., 2012). Subsequently, the complex promotes actin polymerization and formation of new focal contacts (Fernandez-Borja, 2012; Sandri et al., 2012). Finally, the vascular stabilizing functions of R-Ras also involve pericytes, as R-Ras is needed for their recruitment to the angiogenic blood vessels (Sawada et al., 2012) (**Figure 6**). Pericyte loss, in turn, leads to pathological angiogenesis, and their loss is considered as a key feature in the progression of DR (Beltramo and Porta, 2013; Mishra, 2016).

Our understanding on role of R-Ras as a master regulator of vascular permeability is currently increasing in diseased states. It was recently demonstrated that R-Ras induced different phosphoinositide 3-kinase-(PI3K)-Akt signaling than VEGF-A and these two different PI3K-Akt signaling “phenotypes” lead to totally different phenotypes in angiogenic blood vessels in hypoxia (Li et al., 2017). Whereas VEGF-A induced PI3K-Akt signaling leads to sprouting angiogenesis, R-Ras induced signaling leads to upregulation of podocalyxin and proper lumenogenesis of the angiogenic blood vessels (Li et al., 2017). Podocalyxin, in turn, is required for maintaining vascular permeability in blood-brain barrier (Cait et al., 2019), which could be the mechanism by which R-Ras exerts its effects in OIR and retinopathy. Interestingly, increased R-Ras palmitoylation is the mechanism by which R-Ras can be inactivated in vascular diseases (Wei et al., 2020). R-Ras is the molecular target of epalmitoylation enzyme acyl-protein thioesterase 1 (APT1). APT1 deficiency leads to enhanced palmitoylation of R-Ras and inhibits lumen formation, whereas the inhibition of R-Ras palmitoylation rescues vessel lumen formation (Wei et al., 2020).

The expression of another filamin-family member, Filamin B (Flnb) was increased at P17 OIR. Whereas Flna is more ubiquitously expressed in vascular mural cells and ECs, the expression of Flnb is restricted to ECs (Del Valle-Perez et al., 2010). Disruption of Flnb, but not Flna, leads to inhibition of EC migration after VEGF induction (Del Valle-Perez et al., 2010). Flnb deficiency led to an impaired microvascular network in the central nervous system (Zhou et al., 2007), whereas gain of function of Flnb is proposed to modulate the interaction between Flna and Flnb and impair filamins function in the regulation of angiogenesis, which could lead to abnormal angiogenesis. VEGF and protein kinase C promote the ubiquitination of Flnb, which leads to angiogenic-promoting HDAC7 phosphorylation (Su et al., 2013). Taking together, these results suggest, that the increased expression of Flna may play a role in the regulation of vascular permeability *via*

N-terminal Flna, whereas Flna^{CT} and Flnb may drive angiogenesis and the migration of ECs in OIR. Similar to our results in OIR (Vähätupa et al., 2018a), the enhanced expression of Flna has been reported in proteomics-based studies from other models of retinal diseases (Murugesan et al., 2019; Christakopoulos et al., 2019).

CONCLUSION

OIR is a hypoxia-induced angiogenesis model and a representative experimental model for several human neovascular retinal diseases. As it is acknowledged that the angiogenic blood vessels actually support the persistency of hypoxia in the tissue and lead to the progression of NV diseases instead of resolving the pathology (Mishra, 2016), it has become absolute necessity to understand their biology in detail. The most comprehensive proteomics-based analysis of the OIR to date delineates the possible molecular mechanisms that may drive angiogenesis in this model (Vähätupa et al., 2018a). Together with studies using genetically modified mice strain we were able to identify not just proteins induced in the hypoxic environment of retina, but also molecular interplay between the proteins induced by hypoxia and then by subsequent angiogenesis as well as the R-Ras – Filamin A axis that regulates vascular permeability in OIR. Interestingly, the sprouting angiogenesis in OIR needs an EC specific induction of genes involved in the mechanotransduction of forces generated by migrating cells. This network may present completely novel drug targets for future therapies. We hope that the better understanding of the molecules involved in the OIR will lead to new drug therapies for the human NV retinal diseases.

AUTHOR CONTRIBUTIONS

MV made the figures. All authors reviewed the literature, wrote and edited the manuscript.

ACKNOWLEDGMENTS

This study was supported by Academy of Finland, Finnish Diabetic Research Foundation, Diabetes Wellness Foundation, Tampere Tuberculosis Foundation, Pirkanmaa Hospital District Research Foundation, Finnish Eye Foundation, Finnish Cultural Foundation, Mary and Georg C. Ehrnrooth's Foundation, Päivikki and Sakari Sohlberg Foundation and Tays Research Foundation.

REFERENCES

- Albert, D. M., Scheef, E. A., Wang, S., Mehraein, F., Darjatmoko, S. R., Sorenson, C. M., et al. (2007). Calcitriol is a potent inhibitor of retinal neovascularization. *Invest. Ophthalmol. Visual Sci.* 48 (5), 2327–2334. doi: 10.1167/iops.06-1210
- Angulo-Urarte, A., Casado, P., Castillo, S. D., Kobialka, P., Kotini, M. P., Figueiredo, A. M., et al. (2018). Endothelial cell rearrangements during vascular patterning require PI3-kinase-mediated inhibition of actomyosin contractility. *Nat. Commun.* 9 (1), 4826–018-07172-3. doi: 10.1038/s41467-018-07172-3
- Balassy, Z., Lauzon, A.-M., and Hilbert, L. (2019). Spreading of perturbations in myosin group kinetics along actin filaments. *Proc. Natl. Acad. Sci. United States America* 116 (35), 17336–17344. doi: 10.1073/pnas.1904164116
- Baudier, J., Jenkins, Z. A., and Robertson, S. P. (2018). The filamin-B-refilin axis - spatiotemporal regulators of the actin-cytoskeleton in development and disease. *J. Cell Sci.* 131 (8), 10.1242/jcs.213959. doi: 10.1242/jcs.213959

- Baumann, J., Huang, S.-F., Gassmann, M., Tsao, C.-C., and Ogunshola, O. O. (2019). Furin inhibition prevents hypoxic and TGF β -mediated blood-brain barrier disruption. *Exp. Cell Res.* 383 (2), 111503 doi: 10.1016/j.yexcr.2019.111503
- Beltramo, E., and Porta, M. (2013). Pericyte loss in diabetic retinopathy: mechanisms and consequences. *Curr. Med. Chem.* 2026, 3218–3225. doi: 10.2174/09298673113209990022
- Benjamin, L. E., Hemo, I., and Keshet, E. (1998). A plasticity window for blood vessel remodelling is defined by pericyte coverage of the preformed endothelial network and is regulated by PDGF-B and VEGF. *Development (Cambridge England)* 125 (9), 1591–1598.
- Bordeleau, F., Mason, B. N., Lollis, E. M., Mazzola, M., Zanotelli, M. R., Somasegar, S., et al. (2017). Matrix stiffening promotes a tumor vasculature phenotype. *Proc. Natl. Acad. Sci. United States America* 114 (3), 492–497. doi: 10.1073/pnas.1613855114
- Butler, M. J., Down, C. J., Foster, R. R., and Satchell, S. C. (2020). The pathological relevance of increased endothelial glycocalyx permeability. *Am. J. Pathol.* 190 (4), 742–751. doi: 10.1016/j.ajpath.2019.11.015
- Cait, J., Hughes, M. R., Zeglinski, M. R., Chan, A. W., Osterhof, S., Scott, R. W., et al. (2019). Podocalyxin is required for maintaining blood-brain barrier function during acute inflammation. *Proc. Natl. Acad. Sci. United States America* 116 (10), 4518–4527. doi: 10.1073/pnas.1814766116
- Campochiaro, P. A. (2013). Ocular neovascularization. *J. Mol. Med. (Berlin Germany)* 91 (3), 311–321. doi: 10.1007/s00109-013-0993-5
- Campochiaro, P. A. (2015). Molecular pathogenesis of retinal and choroidal vascular diseases. *Prog. Retinal Eye Res.* 49, 67–81. doi: 10.1016/j.preteyeres.2015.06.002
- Cao, Y., Feng, B., Chen, S., Chu, Y., and Chakrabarti, S. (2014). Mechanisms of endothelial to mesenchymal transition in the retina in diabetes. *Invest. Ophthalmol. Visual Sci.* 55 (11), 7321–7331. doi: 10.1167/jovs.14-15167
- Chen, W., Lu, Q., Lu, L., and Guan, H. (2017). Increased levels of α B-crystallin in vitreous fluid of patients with proliferative diabetic retinopathy and correlation with vascular endothelial growth factor. *Clin. Exp. Ophthalmol.* 454, 379–384. doi: 10.1111/ceo.12891
- Cho, J. G., Lee, A., Chang, W., Lee, M. S., and Kim, J. (2018). Endothelial to Mesenchymal Transition Represents a Key Link in the Interaction between Inflammation and Endothelial Dysfunction. *Front. Immunol.* 9, 294. doi: 10.3389/fimmu.2018.00294
- Christakopoulos, C., Cehofski, L. J., Christensen, S. R., Vorum, H., and Honoré, B. (2019). Proteomics reveals a set of highly enriched proteins in epiretinal membrane compared with inner limiting membrane. *Exp. Eye Res.* 186, 107722. doi: 10.1016/j.yexcr.2019.107722
- Christian, S., Pilch, J., Akerman, M. E., Porkka, K., Laakkonen, P., and Ruoslahti, E. (2003). Nucleolin expressed at the cell surface is a marker of endothelial cells in angiogenic blood vessels. *J. Cell Biol.* 163 (4), 871–878. doi: 10.1083/jcb.200304132
- Connor, K. M., Krah, N. M., Dennison, R. J., Aderman, C. M., Chen, J., Guerin, K. I., et al. (2009). Quantification of oxygen-induced retinopathy in the mouse: a model of vessel loss, vessel regrowth and pathological angiogenesis. *Nat. Protoc.* 4 (11), 1565–1573. doi: 10.1038/nprot.2009.187
- Crider, B. J., Risinger, G., Haaksma, C. J., Howard, E. W., and Tomasek, J. J. (2011). Myocardin-related transcription factors A and B are key regulators of TGF- β 1-induced fibroblast to myofibroblast differentiation. *J. Invest. Dermatol.* 131 (12), 2378–2385. doi: 10.1038/jid.2011.219
- Dejana, E., Orsenigo, F., and Lampugnani, M. G. (2008). The role of adherens junctions and VE-cadherin in the control of vascular permeability. *J. Cell Sci.* 121 (Pt 13), 2115–2122. doi: 10.1242/jcs.017897
- Dejana, E., Hirschi, K. K., and Simons, M. (2017). The molecular basis of endothelial cell plasticity. *Nat. Commun.* 8, 14361. doi: 10.1038/ncomms14361
- Del Valle-Perez, B., Martinez, V. G., Lacasa-Salavert, C., Figueras, A., Shapiro, S. S., Takafuta, T., et al. (2010). Filamin B plays a key role in vascular endothelial growth factor-induced endothelial cell motility through its interaction with Rac-1 and Vav-2. *J. Biol. Chem.* 285 (14), 10748–10760. doi: 10.1074/jbc.M109.062984
- Delanghe, J. R., Speckaert, R., and Speckaert, M. M. (2015). Behind the scenes of vitamin D binding protein: more than vitamin D binding. *Best Pract. Res. Clin. Endocrinol. Metab.* 29 (5), 773–786. doi: 10.1016/j.beem.2015.06.006
- Diokmetzidou, A., Soumaka, A., Kloukina, I., Tskitis, M., Makridakis, M., Varela, A., et al. (2016). Desmin and α B-crystallin interplay in the maintenance of mitochondrial homeostasis and cardiomyocyte survival. *J. Cell Sci.* 129 (20), 3705–3720. doi: 10.1242/jcs.192203
- Duchow, E. G., Cooke, N. E., Seeman, J., Plum, L. A., and DeLuca, H. F. (2019). Vitamin D binding protein is required to utilize skin-generated vitamin D. *Proc. Natl. Acad. Sci. United States America* 116 (49), 24527–24532. doi: 10.1073/pnas.1915442116
- Evrard, S. M., Lecce, L., Michelis, K. C., Nomura-Kitabayashi, A., Pandey, G., Purushothaman, K. R., et al. (2016). Endothelial to mesenchymal transition is common in atherosclerotic lesions and is associated with plaque instability. *Nat. Commun.* 7, 11853. doi: 10.1038/ncomms11853
- Fernandez-Borja, M. (2012). A tale of three GTPases and a RIN in endothelial cell adhesion. *Cell Res.* 22 (10), 1426–1428. doi: 10.1038/cr.2012.118
- Ferrara, N., Gerber, H. P., and LeCouter, J. (2003). The biology of VEGF and its receptors. *Nat. Med.* 9 (6), 669–676. doi: 10.1038/nm0603-669
- Fogal, V., Sugahara, K. N., Ruoslahti, E., and Christian, S. (2009). Cell surface nucleolin antagonist causes endothelial cell apoptosis and normalization of tumor vasculature. *Angiogenesis* 12 (1), 91–100. doi: 10.1007/s10456-009-9137-5
- Fujita, I., Shitamukai, A., Kusumoto, F., Mase, S., Suetsugu, T., Omori, A., et al. (2020). Endfoot regeneration restricts radial glial state and prevents translocation into the outer subventricular zone in early mammalian brain development. *Nat. Cell Biol.* 22 (1), 26–37. doi: 10.1038/s41556-019-0436-9
- Garfias, Y., Iturriaga-Goyon, E., Castro, I., Magana-Guerrero, F. S., Dominguez-Lopez, A., Vivanco-Rojas, O., et al. (2019). Characterization of retinal nucleolin expression in an oxygen-induced retinopathy model. *Invest. Ophthalmol. Visual Sci.* 60 (9), 1650. doi: 10.1016/j.yexcr.2020.107977
- Gasparics, A., and Sebe, A. (2018). MRTFs- master regulators of EMT. *Dev. Dynamics* 247 (3), 396–404. doi: 10.1002/dvdy.24544
- Gawecka, J. E., Griffiths, G. S., Ek-Rylander, B., Ramos, J. W., and Matter, M. L. (2010). R-Ras regulates migration through an interaction with filamin A in melanoma cells. *PLoS One* 5 (6), e11269. doi: 10.1371/journal.pone.0011269
- Giannotta, M., Trani, M., and Dejana, E. (2013). VE-cadherin and endothelial adherens junctions: active guardians of vascular integrity. *Dev. Cell* 265, 441–454. doi: 10.1016/j.devcel.2013.08.020
- Goel, S., Wong, A. H., and Jain, R. K. (2012). Vascular normalization as a therapeutic strategy for malignant and nonmalignant disease. *Cold Spring Harbor Perspect. Med.* 2 (3), a006486. doi: 10.1101/cshperspect.a006486
- Goldmann, W. H., Auernheimer, V., Thievsen, I., and Fabry, B. (2013). Vinculin, cell mechanics and tumour cell invasion. *Cell Biol. Int.* 37 (5), 397–405. doi: 10.1002/cbin.10064
- Griffiths, G. S., Grundl, M., Allen, J., and Matter, M. L. (2011). R-Ras interacts with filamin A to maintain endothelial barrier function. *J. Cell. Physiol.* 226 (9), 2287–2296. doi: 10.1002/jcp.22565
- Hoelzle, M. K., and Svitkina, T. (2012). The cytoskeletal mechanisms of cell-cell junction formation in endothelial cells. *Mol. Biol. Cell* 23 (2), 310–323. doi: 10.1091/mbc.e11-08-0719
- Hong, L., Du, X., Li, W., Mao, Y., Sun, L., and Li, X. (2018). EndMT: A promising and controversial field. *Eur. J. Cell Biol.* 97 (7), 493–500. doi: 10.1016/j.jecb.2018.07.005
- Huang, Y., Shi, H., Zhou, H., Song, X., Yuan, S., and Luo, Y. (2006). The angiogenic function of nucleolin is mediated by vascular endothelial growth factor and nonmuscle myosin. *Blood* 107 (9), 3564–3571. doi: 10.1182/blood-2005-07-2961
- Huveneers, S., Oldenburg, J., Spanjaard, E., van der Krogt, G., Grigoriev, I., Akhmanova, A., et al. (2012). Vinculin associates with endothelial VE-cadherin junctions to control force-dependent remodeling. *J. Cell Biol.* 196 (5), 641–652. doi: 10.1083/jcb.201108120
- Huynh, J., Nishimura, N., Rana, K., Ploquin, J. M., Califano, J. P., Montague, C. R., et al. (2011). Age-related intimal stiffening enhances endothelial permeability and leukocyte transmigration. *Sci. Trans. Med.* 3 (112), 112ra122. doi: 10.1126/scitranslmed.3002761
- Ichimiya, H., Maeda, K., Enomoto, A., Weng, L., Takahashi, M., and Murohara, T. (2015). Girdin/GIV regulates transendothelial permeability by controlling VE-cadherin trafficking through the small GTPase, R-Ras. *Biochem. Biophys. Res. Commun.* 461 (2), 260–267. doi: 10.1016/j.bbrc.2015.04.012
- Irianto, J., Pfeifer, C. R., Xia, Y., and Discher, D. E. (2016). SnapShot: Mechanosensing Matrix. *Cell* 165 (7), 1820–1820.e1. doi: 10.1016/j.cell.2016.06.002

- Ishikawa, K., Sreekumar, P. G., Spee, C., Nazari, H., Zhu, D., Kannan, R., et al. (2016). α B-Crystallin Regulates Subretinal Fibrosis by Modulation of Epithelial-Mesenchymal Transition. *Am. J. Pathol.* 186 (4), 859–873. doi: 10.1016/j.ajpath.2015.11.014
- Järvinen, T. A. H. (2020). Neovascularization in tendinopathy: from eradication to stabilization. *Br. J. Sports Med.* 54 (1), 1–2. doi: 10.1136/bjsports-2019-100608
- Jamali, N., Wang, S., Darjatmoko, S. R., Sorenson, C. M., and Sheibani, N. (2017). Vitamin D receptor expression is essential during retinal vascular development and attenuation of neovascularization by 1, 25(OH)2D3. *PLoS One* 12 (12), e0190131. doi: 10.1371/journal.pone.0190131
- Kalkunte, S., Brard, L., Granai, C. O., and Swamy, N. (2005). Inhibition of angiogenesis by vitamin D-binding protein: characterization of anti-endothelial activity of DBP-maf. *Angiogenesis* 8 (4), 349–360. doi: 10.1007/s10456-005-9024-7
- Kanda, S., Mochizuki, Y., Miyata, Y., Kanetake, H., and Yamamoto, N. (2002). Effects of vitamin D(3)-binding protein-derived macrophage activating factor (GcMAF) on angiogenesis. *J. Natl. Cancer Institute* 94 (17), 1311–1319. doi: 10.1093/jnci/94.17.1311
- Kannan, R., Sreekumar, P. G., and Hinton, D. R. (2012). Novel roles for α -crystallins in retinal function and disease. *Prog. Retinal Eye Res.* 31 (6), 576–604. doi: 10.1016/j.preteyeres.2012.06.001
- Kannan, R., Sreekumar, P. G., and Hinton, D. R. (2016). α crystallins in the retinal pigment epithelium and implications for the pathogenesis and treatment of age-related macular degeneration. *Biochim. Biophys. Acta* 1860 (1 Pt B), 258–268. doi: 10.1016/j.bbagen.2015.05.016
- Kase, S., He, S., Sonoda, S., Kitamura, M., Spee, C., Wawrousek, E., et al. (2010). α B-crystallin regulation of angiogenesis by modulation of VEGF. *Blood* 115 (16), 3398–3406. doi: 10.1182/blood-2009-01-197095
- Kase, S., Ishida, S., and Rao, N. A. (2011). Increased expression of α A-crystallin in human diabetic eye. *Int. J. Mol. Med.* 28 (4), 505–511. doi: 10.3892/ijmm.2011.708
- Keezer, S. M., Ivie, S. E., Kruttsch, H. C., Tandle, A., Libutti, S. K., and Roberts, D. D. (2003). Angiogenesis inhibitors target the endothelial cell cytoskeleton through altered regulation of heat shock protein 27 and cofilin. *Cancer Res.* 63 (19), 6405–6412.
- Ketomäki, T., Vähätupa, M., May, U., Pemmari, T., Ruikka, E., Hietamo, J., et al. (2019). R-Ras regulates vascular permeability, but not overall healing in skin wounds. *Exp. Dermatol.* 28 (2), 202–206. doi: 10.1111/exd.13851
- Kilarski, W. W., Jura, N., and Gerwins, P. (2003). Inactivation of Src family kinases inhibits angiogenesis in vivo: implications for a mechanism involving organization of the actin cytoskeleton. *Exp. Cell Res.* 291 (1), 70–82. doi: 10.1016/S0014-4827(03)00374-4
- Kim, Y. H., Park, S. Y., Park, J., Kim, Y. S., Hwang, E. M., Park, J. Y., et al. (2012). Reduction of experimental diabetic vascular leakage and pericyte apoptosis in mice by delivery of α A-crystallin with a recombinant adenovirus. *Diabetologia* 55 (10), 2835–2844. doi: 10.1007/s00125-012-2625-y
- Kisker, O., Onizuka, S., Becker, C. M., Fannon, M., Flynn, E., D'Amato, R., et al. (2003). Vitamin D binding protein-macrophage activating factor (DBP-maf) inhibits angiogenesis and tumor growth in mice. *Neoplasia (New York N.Y.)* 5 (1), 32–40. doi: 10.1016/S1476-5586(03)80015-5
- Komatsu, M., and Ruoslahti, E. (2005). R-Ras is a global regulator of vascular regeneration that suppresses intimal hyperplasia and tumor angiogenesis. *Nat. Med.* 11 (12), 1346–1350. doi: 10.1038/nm1324
- Kothari, P., Johnson, C., Sandone, C., Iglesias, P. A., and Robinson, D. N. (2019). How the mechanobiome drives cell behavior, viewed through the lens of control theory. *J. Cell Sci.* 132 (17), jcs234476. doi: 10.1242/jcs.234476
- Lampi, M. C., and Reinhart-King, C. A. (2018). Targeting extracellular matrix stiffness to attenuate disease: From molecular mechanisms to clinical trials. *Sci. Trans. Med.* 10 (422), jcs216010. doi: 10.1126/scitranslmed.aao0475
- Layana, A. G., Minnella, A. M., Garhofer, G., Aslam, T., Holz, F. G., Leys, A., et al. (2017). “Vitamin D and Age-Related Macular Degeneration. *Nutrients* 9, 1120. doi: 10.3390/nu9101120
- Lee, J. W., Ko, J., Ju, C., and Eltzschig, H. K. (2019). Hypoxia signaling in human diseases and therapeutic targets. *Exp. Mol. Med.* 51 (6), 68. doi: 10.1038/s12276-019-0235-1
- Li, F., Sawada, J., and Komatsu, M. (2017). R-Ras-Akt axis induces endothelial lumenogenesis and regulates the patency of regenerating vasculature. *Nat. Commun.* 8 (1), 1720–017-01865-x. doi: 10.1038/s41467-017-01865-x
- Li, S., Jiang, Q., Liu, S., Zhang, Y., Tian, Y., Song, C., et al. (2018). A DNA nanorobot functions as a cancer therapeutic in response to a molecular trigger in vivo. *Nat. Biotechnol.* 36 (3), 258–264. doi: 10.1038/nbt.4071
- Liao, C., and Zhang, Q. (2020). Understanding the oxygen sensing pathway and its therapeutic implications in diseases. *Am. J. Pathol.* doi: 10.1016/j.ajpath.2020.04.003
- Liu, C. H., Wang, Z., Sun, Y., and Chen, J. (2017). Animal models for ocular angiogenesis: from developments to pathologies. *FASEB J.* 31 (11), 4665–4681. doi: 10.1096/fj.201700336R
- Losiewicz, M. K., and Fort, P. E. (2011). Diabetes impairs the neuroprotective properties of retinal α -crystallins. *Invest. Ophthalmol. Visual Sci.* 52 (9), 5034–5042. doi: 10.1167/iiov.10-6931
- Luo, T., Mohan, K., Srivastava, V., Ren, Y., Iglesias, P. A., and Robinson, D. N. (2012). Understanding the cooperative interaction between myosin II and actin cross-linkers mediated by actin filaments during mechanosensation. *Biophys. J.* 102 (2), 238–247. doi: 10.1016/j.bpj.2011.12.020
- Luo, Z., Shang, X., Zhang, H., Wang, G., Massey, P. A., Barton, S. R., et al. (2019). Notch signaling in osteogenesis, osteoclastogenesis and angiogenesis. *Am. J. Pathol.* 189 (8), 1495–1500. doi: 10.1016/j.ajpath.2019.05.005
- May, U., Prince, S., Vähätupa, M., Laitinen, A. M., Nieminen, K., Uusitalo-Järvinen, H., et al. (2015). Resistance of R-Ras knockout mice to skin tumour induction. *Sci. Rep.* 5, 11663. doi: 10.1038/srep11663
- Merrigan, S. L., and Kennedy, B. N. (2017). Vitamin D receptor agonists regulate ocular developmental angiogenesis and modulate expression of dre-miR-21 and VEGF. *Br. J. Pharmacol.* 174 (16), 2636–2651. doi: 10.1111/bph.13875
- Mishra, A. (2016). Angiogenic neovessels promote tissue hypoxia. *Proc. Natl. Acad. Sci. United States America* 113 (38), 10458–10460. doi: 10.1073/pnas.1612427113
- Morrison, A. R., Yarovsky, T. O., Young, B. D., Moraes, F., Ross, T. D., Ceneri, N., et al. (2014). Chemokine-coupled β 2 integrin-induced macrophage Rac2-Myosin IIA interaction regulates VEGF-A mRNA stability and arteriogenesis. *J. Exp. Med.* 21110, 1957–1968. doi: 10.1084/jem.20132130
- Murugesan, N., Fickweiler, W., Clermont, A. C., Zhou, Q., and Feener, E. P. (2019). Retinal proteome associated with bradykinin-induced edema. *Exp. Eye Res.* 186, 107744. doi: 10.1016/j.exer.2019.107744
- Nagaraj, R. H., Nahomi, R. B., Mueller, N. H., Raghavan, C. T., Ammar, D. A., and Petrash, J. M. (2016). Therapeutic potential of α -crystallin. *Biochim. Biophys. Acta* 1860 (1 Pt B), 252–257. doi: 10.1016/j.bbagen.2015.03.012
- Nallapalli, R. K., Ibrahim, M. X., Zhou, A. X., Bandaru, S., Sunkara, S. N., Redfors, B., et al. (2012). Targeting filamin A reduces K-RAS-induced lung adenocarcinomas and endothelial response to tumor growth in mice. *Mol. Cancer* 11, 50. doi: 10.1186/1476-4598-11-50
- Newell-Litwa, K. A., Horwitz, R., and Lamers, M. L. (2015). Non-muscle myosin II in disease: mechanisms and therapeutic opportunities. *Dis. Models Mech.* 8 (12), 1495–1515. doi: 10.1242/dmm.022103
- Pecci, A., Ma, X., Savoia, A., and Adelstein, R. S. (2018). MYH9: Structure, functions and role of non-muscle myosin IIA in human disease. *Gene* 664, 152–167. doi: 10.1016/j.gene.2018.04.048
- Peng, J. M., Bera, R., Chiou, C. Y., Yu, M. C., Chen, T. C., Chen, C. W., et al. (2018). Actin cytoskeleton remodeling drives epithelial-mesenchymal transition for hepatoma invasion and metastasis in mice. *Hepatology (Baltimore Md.)* 67 (6), 2226–2243. doi: 10.1002/hep.29678
- Penn, J. S., Madan, A., Caldwell, R. B., Bartoli, M., Caldwell, R. W., and Hartnett, M. E. (2008). Vascular endothelial growth factor in eye disease. *Prog. Retinal Eye Res.* 27 (4), 331–371. doi: 10.1016/j.preteyeres.2008.05.001
- Picariello, H. S., Kenchappa, R. S., Rai, V., Crish, J. F., Dovas, A., Pogoda, K., et al. (2019). Myosin IIA suppresses glioblastoma development in mechanically sensitive manner. *Proc. Natl. Acad. Sci. United States America* 116 (31), 15550–15559. doi: 10.1073/pnas.1902847116
- Prior, I. A., Lewis, P. D., and Mattos, C. (2012). A comprehensive survey of Ras mutations in cancer. *Cancer Res.* 72 (10), 2457–2467. doi: 10.1158/0008-5472.CAN-11-2612
- Raymond, M. A., Desormeaux, A., Labelle, A., Soulez, M., Soulez, G., Langelier, Y., et al. (2005). Endothelial stress induces the release of vitamin D-binding protein, a novel growth factor. *Biochem. Biophys. Res. Commun.* 3383, 1374–1382. doi: 10.1016/j.bbrc.2005.10.105
- Razinia, Z., Makela, T., Ylanne, J., and Calderwood, D. A. (2012). Filamins in mechanosensing and signaling. *Annu. Rev. Biophys.* 41, 227–246. doi: 10.1146/annurev-biophys-050511-102252

- Salimi, R., Bandaru, S., Devarakonda, S., Gokalp, S., Ala, C., Alvandian, A., et al. (2018). Blocking the Cleavage of Filamin A by Calpain Inhibitor Decreases Tumor Cell Growth. *Anticancer Res.* 38 (4), 2079–2085. doi: 10.21873/anticancer.12447
- Sandri, C., Caccavari, F., Valdembrì, D., Camillo, C., Veltel, S., Santambrogio, M., et al. (2012). The R-Ras/RIN2/Rab5 complex controls endothelial cell adhesion and morphogenesis via active integrin endocytosis and Rac signaling. *Cell Res.* 22 (10), 1479–1501. doi: 10.1038/cr.2012.110
- Sawada, J., and Komatsu, M. (2012). Normalization of tumor vasculature by R-Ras. *Cell Cycle (Georgetown Tex.)* 11 (23), 4285–4286. doi: 10.4161/cc.22465
- Sawada, J., Urakami, T., Li, F., Urakami, A., Zhu, W., Fukuda, M., et al. (2012). Small GTPase R-Ras regulates integrity and functionality of tumor blood vessels. *Cancer Cell* 22 (2), 235–249. doi: 10.1016/j.ccr.2012.06.013
- Sawada, J., Li, F., and Komatsu, M. (2015a). R-Ras Inhibits VEGF-Induced p38MAPK Activation and HSP27 Phosphorylation in Endothelial Cells. *J. Vasc. Res.* 52 (5), 347–359. doi: 10.1159/000444526
- Sawada, J., Li, F., and Komatsu, M. (2015b). R-Ras protein inhibits autophosphorylation of vascular endothelial growth factor receptor 2 in endothelial cells and suppresses receptor activation in tumor vasculature. *J. Biol. Chem.* 290 (13), 8133–8145. doi: 10.1074/jbc.M114.591511
- Schwartz, M. A., Vestweber, D., and Simons, M. (2018). A unifying concept in vascular health and disease. *Sci. (New York N.Y.)* 360 (6386), 270–271. doi: 10.1126/science.aat3470
- Scott, A., and Fruttiger, M. (2010). Oxygen-induced retinopathy: a model for vascular pathology in the retina. *Eye (London England)* 24 (3), 416–421. doi: 10.1038/eye.2009.306
- Senger, D. R., Galli, S. J., Dvorak, A. M., Perruzzi, C. A., Harvey, V. S., and Dvorak, H. F. (1983). Tumor cells secrete a vascular permeability factor that promotes accumulation of ascites fluid. *Sci. (New York N.Y.)* 219 (4587), 983–985. doi: 10.1126/science.6823562
- Sinha, D., Klise, A., Sergeev, Y., Hose, S., Bhutto, I. A., Hackler, L., et al. (2008). β A3/A1-crystallin in astroglial cells regulates retinal vascular remodeling during development. *Mol. Cell. Neurosci.* 37 (1), 85–95. doi: 10.1016/j.mcn.2007.08.016
- Skowron, K., Pawlicka, I., and Gil, K. (2018). The role of vitamin D in the pathogenesis of ocular diseases. *Folia Med. Cracoviensia* 58 (2), 103–118. doi: 10.24425/fmc.2018.124662
- Smith, L. E., Wesolowski, E., McLellan, A., Kostyk, S. K., D'Amato, R., Sullivan, R., et al. (1994). Oxygen-induced retinopathy in the mouse. *Invest. Ophthalmol. Visual Sci.* 35 (1), 101–111.
- Stahl, A., Connor, K. M., Sapieha, P., Chen, J., Dennison, R. J., Krah, N. M., et al. (2010). The mouse retina as an angiogenesis model. *Invest. Ophthalmol. Visual Sci.* 51 (6), 2813–2826. doi: 10.1167/iovs.10-5176
- Su, Y. T., Gao, C., Liu, Y., Guo, S., Wang, A., Wang, B., et al. (2013). Monoubiquitination of filamin B regulates vascular endothelial growth factor-mediated trafficking of histone deacetylase 7. *Mol. Cell. Biol.* 33 (8), 1546–1560. doi: 10.1128/MCB.01146-12
- Sugioka, K., Saito, A., Kusaka, S., Kuniyoshi, K., and Shimomura, Y. (2017). Identification of vitreous proteins in retinopathy of prematurity. *Biochem. Biophys. Res. Commun.* 488 (3), 483–488. doi: 10.1016/j.bbrc.2017.05.067
- Sun, Y., and Smith, L. E. H. (2018). Retinal vasculature in development and disease. *Annu. Rev. Visual Sci.* 15 (4), 101–122. doi: 10.1146/annurev-vision-091517-034018
- Surcel, A., and Robinson, D. N. (2019). Meddling with myosin's mechanobiology in cancer. *Proc. Natl. Acad. Sci. U.S.A.* 116 (31), 15322–15323. doi: 10.1073/pnas.1909995116
- Takino, J. I., Sato, T., Nagamine, K., and Hori, T. (2019). The inhibition of Bax activation-induced apoptosis by RasGRP2 via R-Ras-PI3K-Akt signaling pathway in the endothelial cells. *Sci. Rep.* 9 (1), 16717. doi: 10.1038/s41598-019-53419-4
- Thanos, S., Bohm, M. R., Meyer zu Horste, M., Prokosch-Willing, V., Hennig, M., Bauer, D., et al. (2014). Role of crystallins in ocular neuroprotection and axonal regeneration. *Prog. Retinal Eye Res.* 42, 145–161. doi: 10.1016/j.preteyeres.2014.06.004
- Thomas, A. A., Biswas, S., Feng, B., Chen, S., Gonder, J., and Chakrabarti, S. (2019). lncRNA H19 prevents endothelial-mesenchymal transition in diabetic retinopathy. *Diabetologia* 62 (3), 517–530. doi: 10.1007/s00125-018-4797-6
- Toomer, K., Sauls, K., Fulmer, D., Guo, L., Moore, K., Glover, J., et al. (2019). Filamin-A as a Balance between Erk/Smad Activities During Cardiac Valve Development. *Anatomical record (Hoboken N.J.: 2007)* 302 (1), 117–124. doi: 10.1002/ar.23911
- Vähätupa, M., Prince, S., Vataja, S., Mertimo, T., Kataja, M., Kinnunen, K., et al. (2016). Lack of R-Ras Leads to Increased Vascular Permeability in Ischemic Retinopathy. *Invest. Ophthalmol. Visual Sci.* 57 (11), 4898–4909. doi: 10.1167/iovs.16-19212
- Vähätupa, M., Nättinen, J., Jylhä, A., Aapola, U., Kataja, M., Kööbi, P., et al. (2018a). SWATH-MS Proteomic Analysis of Oxygen-Induced Retinopathy Reveals Novel Potential Therapeutic Targets. *Invest. Ophthalmol. Visual Sci.* 59 (8), 3294–3306. doi: 10.1167/iovs.18-23831
- Vähätupa, M., Cordova, Z. M., Barker, H., Aittomäki, S., Uusitalo, H., Järvinen, T. A. H., et al. (2018b). Furin deficiency in myeloid cells leads to attenuated revascularization in a mouse-model of oxygen-induced retinopathy. *Exp. Eye Res.* 166, 160–167. doi: 10.1016/j.exer.2017.10.013
- Vähätupa, M., Jääskeläinen, N., Cerrada-Gimenez, M., Thana, R., Järvinen, T. A. H., Kalesnykas, G., et al. (2020). Oxygen-induced retinopathy (OIR) in rodents: a pathological neovascularization model for ischemic retinal diseases. *J. Visual Exp.*
- Vähätupa, M. (2019). *Regulation of Angiogenesis: Role of R-Ras, furin and syndecan 4 in retinal angiogenesis* (Tampere, Finland: Tampere University Dissertations), 115.
- Vessey, K. A., Wilkinson-Berka, J. L., and Fletcher, E. L. (2011). Characterization of retinal function and glial cell response in a mouse model of oxygen-induced retinopathy. *J. Comp. Neurol.* 519 (3), 506–527. doi: 10.1002/cne.22530
- Vicente-Manzanares, M., Ma, X., Adelstein, R. S., and Horwitz, A. R. (2009). Non-muscle myosin II takes centre stage in cell adhesion and migration. *Nat. Rev. Mol. Cell Biol.* 10 (11), 778–790. doi: 10.1038/nrm2786
- Vivanco-Rojas, O., García-Bermúdez, M. Y., Iturriaga-Goyon, E., Rebollo, W., Buentello-Volante, B., Magaña-Guerrero, F. S., et al. (2020). Corneal neovascularization is inhibited with nucleolin-binding aptamer, As1411. *Exp. Eye Res.* 193, 107977. doi: 10.1016/j.exer.2020.107977
- Wei, X., Adak, S., Zayed, M. A., Yin, L., Feng, C., Speck, S. L., et al. (2020). Endothelial palmitoylation cycling coordinates vessel remodeling in peripheral artery disease. *Circ. Res.* doi: 10.1161/CIRCRESAHA.120.316752
- Yang, S., Zhao, J., and Sun, X. (2016). Resistance to anti-VEGF therapy in neovascular age-related macular degeneration: a comprehensive review. *Drug Design Dev. Ther.* 10, 1857–1867. doi: 10.2147/DDDT.S97653
- Yeo, E. J. (2019). Hypoxia and aging. *Exp. Mol. Med.* 51 (6), 67. doi: 10.1038/s12276-019-0233-3
- Yoon, C., Choi, C., Stapleton, S., Mirabella, T., Howes, C., Dong, L., et al. (2019). Myosin IIA-mediated forces regulate multicellular integrity during vascular sprouting. *Mol. Biol. Cell* 30 (16), 1974–1984. doi: 10.1091/mbc.E19-02-0076
- Zhang, Z., Vuori, K., Wang, H., Reed, J. C., and Ruoslahti, E. (1996). Integrin activation by R-ras. *Cell* 85 (1), 61–69. doi: 10.1016/S0092-8674(00)81082-X
- Zhang, C., Gehlbach, P., Gongora, C., Cano, M., Fariss, R., Hose, S., et al. (2005). A potential role for β - and γ -crystallins in the vascular remodeling of the eye. *Dev. Dynamics* 234 (1), 36–47. doi: 10.1002/dvdy.20494
- Zheng, X., Zhou, A. X., Rouhi, P., Uramoto, H., Boren, J., Cao, Y., et al. (2014). Hypoxia-induced and calpain-dependent cleavage of filamin A regulates the hypoxic response. *Proc. Natl. Acad. Sci. United States America* 111 (7), 2560–2565. doi: 10.1073/pnas.1320815111
- Zhou, X., Tian, F., Sandzen, J., Cao, R., Flaberg, E., Szekely, L., et al. (2007). Filamin B deficiency in mice results in skeletal malformations and impaired microvascular development. *Proc. Natl. Acad. Sci. United States America* 104 (10), 3919–3924. doi: 10.1073/pnas.0608360104
- Zhu, M., Tan, Z., Luo, Z., Hu, H., Wu, T., Fang, S., et al. (2019). Association of the vitamin D metabolism gene GC and CYP27B1 polymorphisms with cancer susceptibility: a meta-analysis and trial sequential analysis. *Biosci. Rep.* 39 (9), BSR20190368. doi: 10.1042/BSR20190368. Print 2019 Sep 30.
- Ziegler, W. H., Gingras, A. R., Critchley, D. R., and Emsley, J. (2008). Integrin connections to the cytoskeleton through talin and vinculin. *Biochem. Soc. Trans.* 36 (Pt 2), 235–239. doi: 10.1042/BSOT360235

Conflict of Interest: The authors declare that the research was conducted in the absence of any commercial or financial relationships that could be construed as a potential conflict of interest.

Copyright © 2020 Vähätupa, Järvinen and Uusitalo-Järvinen. This is an open-access article distributed under the terms of the Creative Commons Attribution License (CC BY). The use, distribution or reproduction in other forums is permitted, provided the original author(s) and the copyright owner(s) are credited and that the original publication in this journal is cited, in accordance with accepted academic practice. No use, distribution or reproduction is permitted which does not comply with these terms.



Protective Effects of Rapamycin on Trabecular Meshwork Cells in Glucocorticoid-Induced Glaucoma Mice

Xiaolu Zhu, Shengyu Wu, Wen Zeng, Xiaomin Chen, Tian Zheng, Jiangbo Ren and Min Ke*

Department of Ophthalmology, Zhongnan Hospital of Wuhan University, Wuhan, China

OPEN ACCESS

Edited by:

Zhongxiao Wang,
Boston Children's Hospital
and Harvard Medical School,
United States

Reviewed by:

Haojie Fu,
Boston Children's Hospital
and Harvard Medical School,
United States
Junwei Huang,
AbbVie, United States

*Correspondence:

Min Ke
keminyk@163.com

Specialty section:

This article was submitted to
Neuropharmacology,
a section of the journal
Frontiers in Pharmacology

Received: 23 March 2020

Accepted: 22 June 2020

Published: 02 July 2020

Citation:

Zhu X, Wu S, Zeng W, Chen X,
Zheng T, Ren J and Ke M (2020)
Protective Effects of Rapamycin on
Trabecular Meshwork Cells in
Glucocorticoid-Induced
Glaucoma Mice.
Front. Pharmacol. 11:1006.
doi: 10.3389/fphar.2020.01006

Glucocorticoid-induced glaucoma (GIG) is a chronic optic neuropathy caused by systemic or topical glucocorticoid (GC) treatment, which could eventually lead to permanent vision loss. To investigate the protective effects of rapamycin (RAP) on the trabecular cells during the development of GIG in mice, the effects of RAP on intraocular pressure (IOP), trabecular ultrastructure, and retinal ganglion cells (RGCs) were examined in C57BL/6J female mice treated with dexamethasone acetate (Dex-Ace). The expression of α -actin in trabecular tissue was detected by immunofluorescence, and the autophagic activity of trabecular cells and the expression of GIG-related myocilin and α -actin were detected by immunoblotting. Our results indicated that Dex-Ace significantly increased IOP at the end of the third week ($p < 0.05$), while RAP treatment neutralized this elevation of IOP by Dex-Ace. Dex-Ace treatment significantly decreased the RGC numbers ($p < 0.05$), while synchronous RAP treatment kept the number comparable to control. The outer sheath of elastic fibers became thicker and denser, and the mitochondria of lesions increased in Dex-Ace-treated groups at 4 weeks, while no significant change was observed in the RAP-treated trabecular tissues. Dex-Ace induced myocilin, α -actin, Beclin-1, and LC3-II/LC-I ratio, and lowered p62, while synchronous RAP treatment further activated autophagy and neutralized the induction of myocilin and α -actin. Our studies suggested that RAP protected trabecular meshwork cells by further inducing autophagy way from damages of GC treatment.

Keywords: glucocorticoid-induced glaucoma, trabecular meshwork, dexamethasone, autophagy, rapamycin

INTRODUCTION

The therapeutic use of glucocorticoids (GCs) in susceptible individuals increases intraocular pressure (IOP) (Fini et al., 2017), which is a major risk factor for GC-induced glaucoma (GIG), an ocular diseases featured with progressive degeneration of retinal ganglion cells (RGCs) (Kwon et al., 2009). In addition, GIG is similar to primary open angle glaucoma (POAG). Increased IOP can cause vascular insufficiency (Ster et al., 2014). and will further lead to vascular endothelial

metabolic disorders (Gong et al., 2016a; Fu et al., 2018a). GC-induced ocular hypertension results from increased aqueous outflow pathway resistance, morphological and biochemical changes in trabecular meshwork (TM) (Clark and Wordinger, 2009). Therefore, the effects of GCs on TM cells and other ocular tissues drew increasing attention during last decades. Previous researches suggested that GCs promoted the deposition of TM extracellular matrices (such as fibronectin and type IV collagen), cytosolic protein (such as α -smooth muscle actin), and altered cell cytoskeleton to form cross-linked actin networks (Chan, 2006; Deng et al., 2013). However, the exact pathological mechanisms are still unclear at present. A comprehensive knowledge on the pathogenesis of steroid responders will improve our prevention of IOP elevation and enhance our understanding of steroid induction mechanisms in glaucoma.

Autophagy is an important process to promote cell survival under various stressful conditions, during which various stromal and organelles in the cell are degraded by the lysosomal system. TM cells belong to the post-dividing cells and cannot be removed by re-splitting to remove excess harmful substances. TM cells are continuously under mechanical stress and cell deformation stress due to IOP fluctuations and eye movement (Hirt and Liton, 2017). Autophagy, as a mechanism of intracellular self-adaptation protection, maintains TM cell homeostasis and normal function. Previous reviews stated that GCs affected autophagy of various cells, such as osteoblasts, fibroblasts, muscle cells, and lymphocytes (Eisenberg-Lerner et al., 2009; Zhu and Zhang, 2018). Researches also showed that the autophagy homeostasis of TM cells in the glaucoma aqueous humor outflow pathway changed (Eskelinen and Saftig, 2009). In primary cultures of porcine and human TM cells, sustained IOP elevation activated autophagy to response pressure and restore balance (Porter et al., 2014).

Our previous researches suggested that the dexamethasone acetate (Dex-Ace) treatment activated autophagy in a time-dependent manner and that the autophagy activity peaked at the fourth week with a plateau of increased IOP for 4 weeks. Thereafter, the continued DEX-Ace treatment did not affect IOP value reduction, but the autophagy activity gradually decreased (Zeng et al., 2019). Decreased autophagy activity might cause the accumulation of diseased organelles, and produce oxidative damage as well (Levine and Klionsky, 2004), and might be an indication of progressive dysregulation of TM function.

Rapamycin (RAP), a lipophilic macrolide antibiotic, was created as an antifungal agent, and also has multifunctional nonantibiotic properties (Prevel et al., 2013). Related researches showed that RAP played an important role in neurological diseases, like Parkinson's disease (Malagelada et al., 2010), nerve injury, Alzheimer disease, and so on (Caccamo et al., 2009). Previous studies stated that RAP improved the survival rate of RGCs in a rat chronic ocular hypertension model of glaucoma (Su et al., 2014) and significantly enhanced autophagy in a monkey chronic hypertensive model (Deng et al., 2013). However, the role of RAP in GIG is still unclear.

Studies using systemically or topically treated C57BL/6J mice with DEX showed increased IOP and ultrastructural changes looked like those stated in humans after GC therapy (Overby et al., 2014; Zode et al., 2014; Patel et al., 2017; Faralli et al., 2018).

This research, we used a GIG mouse model to explore the relationship between elevated levels of autophagy and hormonal glaucoma. The effects of RAP, as an mTOR inhibitor and autophagy inducer (Levine and Klionsky, 2004), on the autophagy levels in GIG mice were investigated. Our results indicated that RAP protected the functions of TM cells *via* upregulating autophagy in GIG.

MATERIALS AND METHODS

Animal Experiment

Female C57BL/6J mice (6–8 weeks old) were purchased from Beijing HFK Bioscience company and housed at the Center for Animal Experiment/Animal Biosafety Level-III laboratory of Wuhan University. Animal experiment complied with the Association for Research in Vision and Ophthalmology Statement of the Use of Animals in Ophthalmic and Vision Research and carried out according to the regulation of Wuhan University Health Science Center Institutional Animal Care and Use Committee. The mice (16–18 g) were housed under a 12-h light/12-h dark cycle with a free access to standard rodent food and water. The condition of temperature was controlled (22–28°C), as well as the humidity (45–75%).

Reagents

One hundred and six C57BL/6J mice were divided into four groups randomly: control (vehicle suspension +DMSO), Dex-Ace-treated (Dex-Ace+DMSO), RAP-treated (vehicle suspension +RAP), and Dex-Ace+RAP-treated groups (Dex-Ace+RAP). Dex-Ace (10 mg/ml) or vehicle suspension solution (20 μ l) was conjunctival fornix (CF) injected into the tenon of the right eye every 4 d. RAP (4 mg/kg) or 0.1% dimethyl sulfoxide (DMSO, 100 μ l) was injected intraperitoneally every other day. Vehicle suspension and DEX-Ace formulation were introduced as a preview study (Patel et al., 2017). RAP formulation (0.25 mg/ml in 0.1% DMSO) was stored at -20°C (working fluid).

Periocular CF Injection

Mice were put into an anesthesia chamber filled with 0.8 L/min oxygen and 2.5% isoflurane to induce general anesthesia. After anesthesia, mice got 1–2 drops of 0.5% proparacaine HCL (S.A. Alcon-couvreur N.V., Belgium) in both eyes. The CF injection was performed as previously noted (Patel et al., 2017). Briefly, after lower eyelid was retracted, 20 μ l DEX-Ace (10 mg/ml) or vehicle suspension were injected by a 29-gauge insulin syringe immediately under the CF of the right eye in the process of 5–10 s. A 1-ml syringe (Sinopharm, China) was used to inject 100 μ l RAP (4 mg/kg) or DMSO (0.1%) into the abdominal cavity.

IOP Measurement

Mice were put into the Decapicone, a plastic bag especially for the mouse, which could fully expose the head but restrict its movement (Wang et al., 2005). The head of conscious mice was exposed in the hole at the top of the cone and IOP was measured as soon as the mice stayed stable. An effective reading of daytime IOP was obtained weekly at 10 am and 2 pm by applying a probe

of tonometer (TonoLab, Colonial Medical, USA) to gently flatten an area of the corneal surface. After baseline IOP was obtained, the right eye was then treated with DEX-Ace or vehicle suspension every 4 d. The IOP of each eye was taken from the average of 3 test values.

Weight Measurement

The mice were gently placed on the digital electronic scales (BY-dzc, China) and the weight was measured immediately after the mice stayed stable. Recorded effective reading of body weight weekly at 10 am to an accuracy of 0.01 g. The body weight of each mice was taken from the average of three test values.

RGC Staining

To estimate changes in the RGC numbers after GIG mice were induced, we counted the number of RGCs in the retinas. BRN3a were used to detect the RGCs in the retina, and the method of retina dissection was as previously described (Li et al., 2014; Vidal-Sanz et al., 2015; Wang et al., 2016; Gong et al., 2016b). Briefly, after the mice were sacrificed, the enucleated eyes were fixed in 4% paraformaldehyde for 1 h and flushed in PBS. The retinas were then cut into 4 quadrants and flattened with a fine brush. After incubated with 0.5% Triton X-100 for 15 min, the retinas were incubated with BRN3a antibody (1:200, Millipore, USA) at 4°C overnight. After incubating, the retinas were flushed in PBS three times and then incubated with IgG Cy3 antibody (1:200) for 2 h. Non-overlapping images containing most of the retina in four quadrants were obtained by confocal 155 microscope (zoom = 1,600 folds; TCS SP5 CLSM, Leica, Germany), and the average RGC numbers for four quadrants were quantified.

Transmission Electron Microscopy

Unperfused mouse eyes were immediately fixed *via* 2.5% glutaraldehyde (Ted Pella, USA) in phosphate buffer at 4°C for 2 h. The fixative was injected into the eye from a tiny incision in the posterior sclera. Tissues were then fixed with OsO₄, dehydrated using ascending alcohol series, and embedded in Epon resin. Ultrathin sections on trabecular organization were cut with an ultramicrotome (EM UC7, Leica), examined using an electron microscope (Tecnai G2 20 TWIN, FEI, USA), and then obtained as described previously (Zeng et al., 2019).

Immunofluorescence, Hematoxylin and Eosin (H&E) Staining

Mouse eyeballs were enucleated and immediately fixed in 4% paraformaldehyde at 4°C overnight as previously described (Fu et al., 2018b). After rinsed three times with PBS, the eyes were dehydrated and embedded in paraffin (Paraplast, Sigma-Aldrich, USA). Tissue slices (5 µm) were obtained using a rotation microtome (Thermo Fisher, USA), deparaffinized, and then rehydrated with graded ethanol for 5 min twice each. Antigen retrieval was conducted in citrate buffer. Once cooled, tissue sections were blocked with 10% goat serum and 0.2% Triton-X 100 in a dark and humid chamber for 2 h. After rinse briefly with PBS, the sections were immunolabeled with rabbit polyclonal antibody (α -smooth muscle actin, 1:100, Abcam) and incubated

at 4°C overnight. After flushing, the samples were incubated with corresponding secondary antibodies (Alexa goat anti-rabbit 568, 1:500, Thermo Fisher) for 2 h. DAPI (Vector, CA) was used to visualize cellular nuclear. The slices were examined by the Keyence all-in-one fluorescence microscope (Itasca, USA) (Kasetti et al., 2016). For H&E staining, the paraffin section of mice TM tissues were sequentially deparaffinized, rehydrated, stained with hematoxylin and eosin (Sigma-Aldrich), dehydrated and sealed. The slices were visualized and photographed with phase contrast microscope (DMI 1, Leica).

Western Blotting

Anterior segment tissues were dissected detailedly and then placed in RIPA lysis buffer (Cell Signaling Technology, USA) (Zode et al., 2015). Whole section of the TM with small part of ciliary muscle, iris, and cornea, were contained in the tissues. The BCA Protein Assay kit (Beyotime, China) was used to detect the concentration of total protein. Total protein (40 µg) was analyzed by sodium dodecyl sulfate polyacrylamide gel electrophoresis (Beyotime) and transferred to polyvinylidene fluoride membranes (Millipore, USA) followed by the manufacturer's protocol. Membranes were blocked by PBS containing 5% BSA (Cell Signaling) at room temperature for 1 h, and then incubated with primary antibodies (p62, 1:1,000, Cell Signaling; Beclin-1, 1:1,000, Abcam; α -actin, 1:1000, Abcam; Myocilin, 1:500, Abcam; GAPDH, 1:1000, Boster, China) at 4°C overnight. The membranes were washed, incubated with corresponding secondary antibodies (1:3,000, Cell Signaling), and detected by ChemiDoc™ XRS+ Imaging System (Bio-Rad, USA). The band intensities were analyzed by ImageJ software.

Statistical Analysis

Statistical analyses were performed with using Prism version 7.0 (GraphPad, USA). Statistical analyses among groups were evaluated *via* one-way analysis of variance (ANOVA), and two groups' comparisons were using unpaired t-test. All data were presented as mean \pm SEM for multiple independent experiments. $P < 0.05$ was considered as statistical significance.

RESULTS AND DISCUSSION

RAP Inhibited the Elevated IOP Caused by Dex-Ace CF Injection

The CF injection of Dex-Ace was reported to repeatedly caused obvious and persistent IOP elevation, which related to reduced outflow facility (Patel et al., 2017). As our previous researches proved, Dex-Ace induced rapid and significant IOP increase, which peaked at week 4 (Zeng et al., 2019). In this study, we founded that the IOP in the Dex-Ace-treated group increased at 3 weeks and sustained until 4 weeks. However, IOP had little change in the other three groups. Conscious daytime IOP value was 13.54 ± 0.45 mmHg ($n = 18$) in the control group, 22.33 ± 0.77 mmHg ($n = 18$) in the Dex-Ace-treated group, 14.23 ± 0.65 mmHg ($n = 18$) in the RAP-treated group, and 14.23 ± 0.68 mmHg ($n = 18$) in the DEX-Ace+RAP-treated group at week 4.

Since the third week of treatment, the conscious mouse IOP in the DEX-Ace-treated group continued to be higher than the other three groups by about 4–8 mmHg ($P < 0.05$) (Figure 1).

RAP Did Not Affect the Body Weight in Mice

In order to evaluate the effect of Dex-Ace treatment and RAP treatment on the whole body of mice, we selected mice with no statistically significant difference ($P > 0.05$) in initial body weight comparison. After different treatments, we measured the body weight of mice weekly, and chosen body weight at the end of 0 week, 1 week, 2 week, 3 week, and 4 week for statistical analysis. There was no statistically significant difference between the body weight of each group at 1–4 weeks with its initial weight ($P > 0.05$). And no significant difference was seen in body weight comparison between the four groups at 1–4 weeks ($P > 0.05$) (Figure 2).

RAP Protected RGCs From Damages by Dex-Ace Treatment

Our previous researches suggested that IOP elevation caused by Dex-Ace treatment in mice resulted in RGC loss by BRN3a immunostaining (Zeng et al., 2019). In this study, no significant difference was seen in the number of RGCs in the 4 groups of mice at 1 week. At 4 weeks, the number of RGCs in the Dex-Ace-treatment group was significantly decreased ($p = 0.023$), but not in the other three groups. Compared with the Dex-Ace-treated group (326.38 ± 42.86), Dex-Ace+RAP-treated eyes maintained normal RGC numbers in 4 weeks after treatment (388.87 ± 37.25 , Figure 3).

RAP Recovered Dex-Ace-Induced Ultrastructural and Histological Changes of the TM Cells

Dex treatment led to many ultrastructural and histological changes in the TM cells, such as rougher cell membrane edge, poor integrity of the cell membrane, increased bundle-like collagen fibers, and inconspicuous trabecular space. Abnormal mitochondria could also

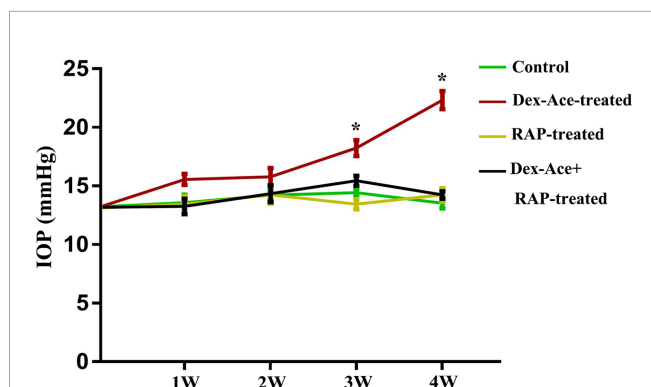


FIGURE 1 | RAP reduced Dex-Ace-induced IOP elevation. The conscious mouse IOP was induced significantly by Dex-Ace at 3–4 weeks, but RAP treatment decreased this increase. ($n = 20$; *, $p < 0.05$).

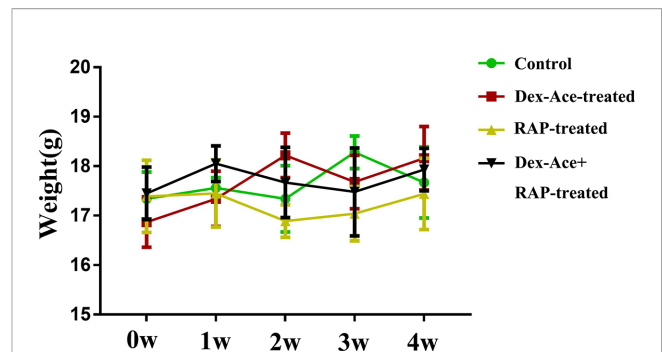


FIGURE 2 | At 0–4 weeks, compared with the other three groups, there was no significant change and fluctuation in the body weight of the Dex-Ace +RAP-treated group. ($n = 20$; $p > 0.05$).

be observed in the cytoplasm. Elastic fibers were increased and disordered, and the outer sheath of the elastic fibers was thick and dense (Figure 4B). However, synchronous RAP treatment maintained TM cells a normal morphology with no significant difference compared to the control and RAP-treated groups. The cell membrane of TM cells was smooth and intact, the nuclear staining was uniform, and the basement membrane was relatively intact and continuous. The elastic fibers were surrounded by the thin sheaths, and a large number of collagen fibers were arranged neatly (Figures 4A–D).

In Dex-Ace-treated group, mitochondrial arrangement was disordered, the outline was blurred, the membrane was damaged and dissolved, and the crest disappeared (Figure 5A). In addition, it also could be observed that the mitochondria were fused and merge into giant mitochondria, which were rod-shaped and swollen (Figure 5B). However, synchronous RAP treatment kept the mitochondria in a normal elliptical shape, with a clear outline and crest, and a normal arrangement (Figures 5C, D).

RAP Downregulated Dex-Ace-Induced α -Actin Expression

Dex-Ace treatment promoted the deposition of extracellular matrix such as fibronectin (Steely et al., 1992), collagens (Zhou et al., 1998), and α -action (Clark et al., 2005) in the trabecular tissues. To assess whether Dex-Ace treatment led to these biochemical changes in GIG mice, we experimented α -smooth muscle actin in the anterior segment tissues. Only the Dex-Ace treatment group showed obvious deposition of α -actin in the trabecular tissues. The Dex-Ace+RAP-treated group did not show an increased expression of α -actin compared to the other groups (Figure 6).

RAP Upregulated TM Cell Autophagy and Downregulated Dex-Ace-Induced GIG-Related Protein Expression

Our previous studies suggested that numerous autophagy-related structures were discovered in the TM cells after Dex-Ace treatment (Zeng et al., 2019). Related studies demonstrated RAP increased autophagy *via* inhibiting mTOR (Hosokawa et al., 2009). To investigate whether RAP improved the autophagy in the GIG

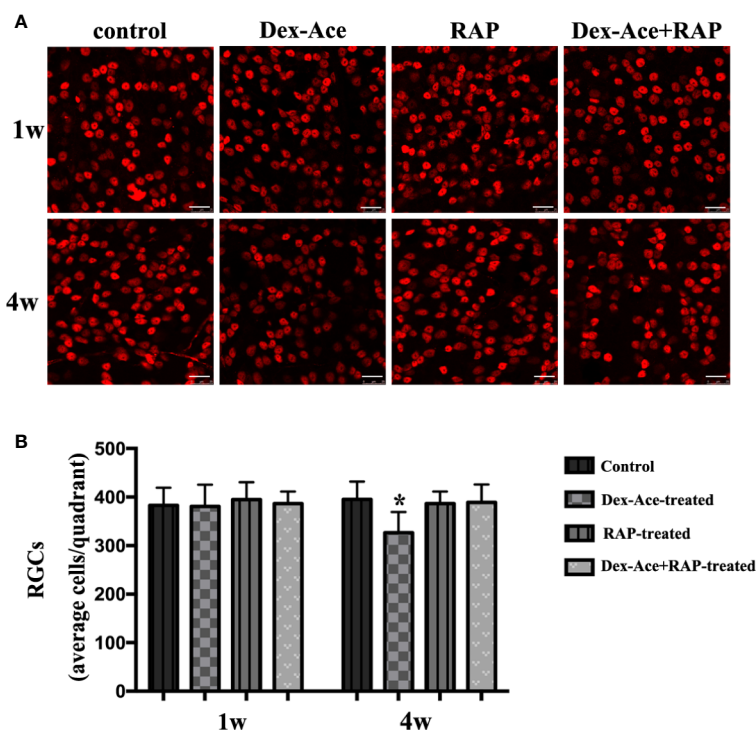


FIGURE 3 | RAP increased Dex-Ace-induced reduction of RGCs at 4 weeks. **(A)** Representative BRN3a staining at 1 and 4 weeks. **(B)** Quantification of RGC survival in average four quadrants. There was no statistical difference of RGC number between groups at 1 week ($p > 0.05$). Compared with the other three groups, the RGCs were significantly reduced in the Dex-Ace group at 4 weeks (scale bar: 25 μ m; $n = 5$; *, $p < 0.05$).

trabecular tissues, autophagy-associated proteins Beclin-1, p62 and LC3 were examined in TM cells. It has been reported that Beclin-1 was an important factor in autophagy, and its autophagic work requires adequate levels of Beclin-1 (Wirawan et al., 2012). p62, as a marker of autophagic flux, accumulates when autophagy is inhibited (Bjorkoy et al., 2009). When autophagosomes were produced, LC3-I transitioned to LC3-II, which indicated that the content of the LC3-II can laterally reflect the number of autophagosomes (Mizushima et al., 2010). Compared with the control group, the other three groups all showed a gradual increase of Beclin-1 and LC3-II/LC3-I ratio along with a decrease of p62 expression. Furthermore, Beclin-1 and LC3-II/LC3-I ratio were significantly increased and p62 was significantly decreased in the Dex-Ace+RAP-treated group compared to the Dex-Ace-treated group (**Figures 7A–D**). These results demonstrated that autophagy was activated in TM cells of GIG mice, suggesting that RAP upregulated TM cell autophagy in GIG mice.

Dex treatment also induces several biochemical modifications in the TM cells, such as enhanced accumulation of collagens, fibronectin, and α -smooth muscle actin (Patel et al., 2017). RAP downregulated α -actin expression, we next assessed the GIG-related proteins myocilin and α -actin in TM cells. Only the Dex-Ace-treated group showed increased expression of myocilin and α -actin. There was no significant difference of myocilin and α -actin expression in the other three groups (**Figures 7A, E, F**), suggesting that RAP inhibited overexpression of myocilin and α -actin after Dex-Ace treatment.

DISCUSSION

GIG is a secondary open angle glaucoma owing to the increased outflow resistance of the trabecular mesh water outflow channel. Many studies explored the effects of GCs on TM tissues and cells. Recently, more and more studies suggested that the autophagy homeostasis of TM cells in the glaucoma outflow pathway changed (Kitaoka et al., 2013). Our previous researches indicated that autophagy and the damaging histological changes in the TM tissues were increased in the GIG mice model. In this study, we employed this female GIG mice model to assess whether the use of Dex combined with autophagy activator RAP affected GIG progression. In female mice, hormone injection induced less stress response, such as fight and bite, resulting in less mortality rate. Our results indicated that Dex-Ace treatment induced a fast and obvious elevation of IOP, and increased α -actin and autophagy level in the TM tissues. Moreover, the loss of RGCs after DEX-Ace treatment suggested that the GIG mice model might be able to construct optic neuropathy.

Autophagy, a cellular self-digestion mechanism, is a process that catalyzes the degradation of injured organelles and protein owing to metabolism on body (Knoferle et al., 2010; Kroemer et al., 2010; Dash et al., 2019), and will further cause cell apoptosis. Induction of autophagy helps cells adapt to environmental changes by increasing the turnover of proteins and organelles, which in turn affects other cells and metabolic stress, and assist in rebalancing cell and organelle functions,

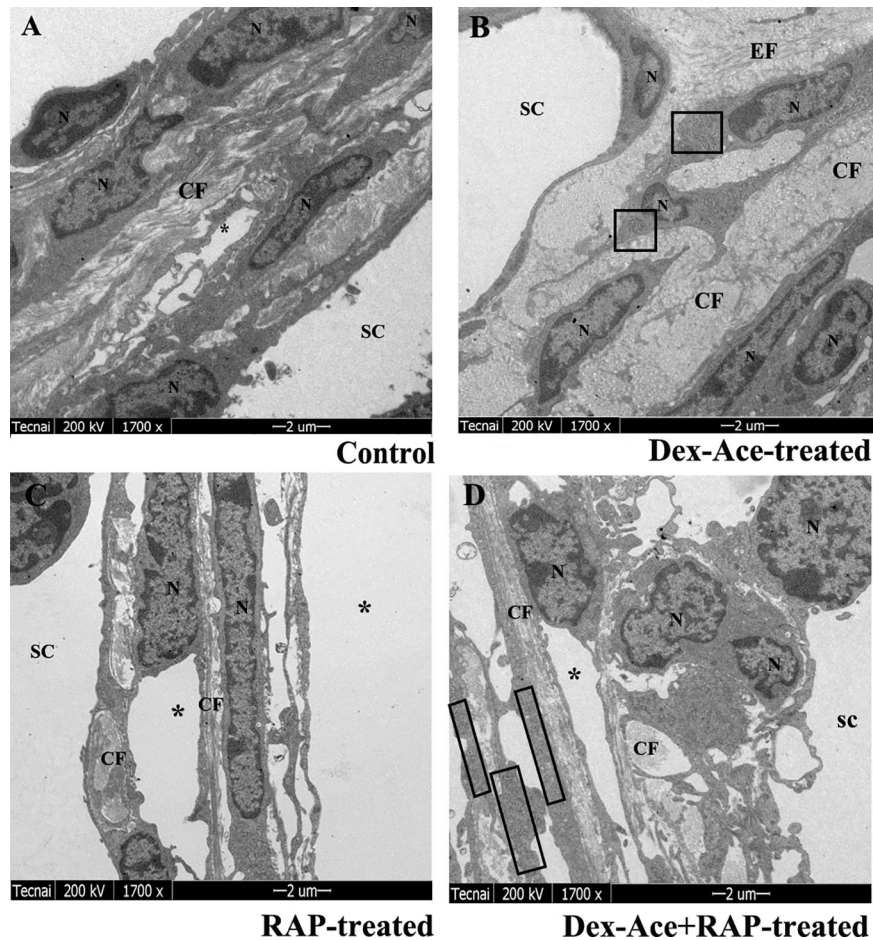


FIGURE 4 | RAP normalized Dex-Ace-induced ultrastructural changes of trabecular tissues at 4 weeks. In the control and RAP-treated group (**A, C**), the cell membrane was intact, the nuclear staining was uniform, and the normal mitochondria were arranged in a bundle of collagen fibers. In the Dex-Ace-treated group (**B**) the trabecular space was not obvious. The cytoplasm showed abnormal swelling of the mitochondria, increased and disorderly arranged elastic fibers, thicker, and denser outer sheath of the elastic fibers. In the Dex-Ace+RAP-treated group (**D**), abnormal swelling of the mitochondria were also showed in the cytoplasm, but the disorderly arranged elastic fibers didn't been found. (*: trabecular mesh gap; N, nucleus; CF, collagen fiber; EF, elastic fibers; boxes indicate swollen mitochondria; n=5; magnification; 1,700x).

suggesting that activation of autophagy may be the TM cellular original response to stress and balance (Kumari et al., 2012).

In our studies, mTOR inhibitor RAP was used as an autophagy activator to treat GIG mice. RAP was reported to bind FKBP12 and block the active site of mTOR, resulting in suppressed mTORC1 activity (Heitman J and Hall, 1991; Caron et al., 2010). GIG mice had no IOP elevation under RAP treatment, indicating that RAP-induced autophagy under Dex-Ace-treated conditions controlled IOP in mice. The number of RGCs was significantly increased in Dex-Ace+RAP-treated GIG mice, suggesting RAP protected RGCs from Dex-Ace-induced cell apoptosis, which might inhibit the release of neurotoxic mediators by modulating NF- κ B signaling and directly inhibiting RGC apoptosis (Mizushima et al., 2010; Su et al., 2014). Besides, Han et al. pointed out that activated autophagy took part in RAP-mediated inhibition of BV2 microglia activation, suggesting that RAP mediated neuroprotection *via* enhancing

autophagy in glaucoma (Han et al., 2013). Moreover, previous studies stated that RAP rescued RGCs *via* downregulating retinal protein REDD1 and working on the mTOR/HIF-1 pathway to vascular endothelial growth factor (VEGF) production in the photoreceptors and retinal pigment epithelial cells case (Bird, 2010).

Electron microscope observation and immunohistochemical analysis indicated that swollen and increased mitochondria accompanied by overexpressed extracellular matrix were observed in the Dex-Ace-treated mice, but not in Dex-Ace+RAP-treated mice. Damaged mitochondrial quality emphasized the impaired mitochondrial dynamics and mitophagy. Cell damage caused dynamic change in mitochondrial fission, leading to fragmental division of mitochondria and ultimately resulting in cell death (Saxena et al., 2019). Several publications reported that mitochondria affected oxidative stress (Osborne et al., 2014). It was also reported that these swollen mitochondria induced

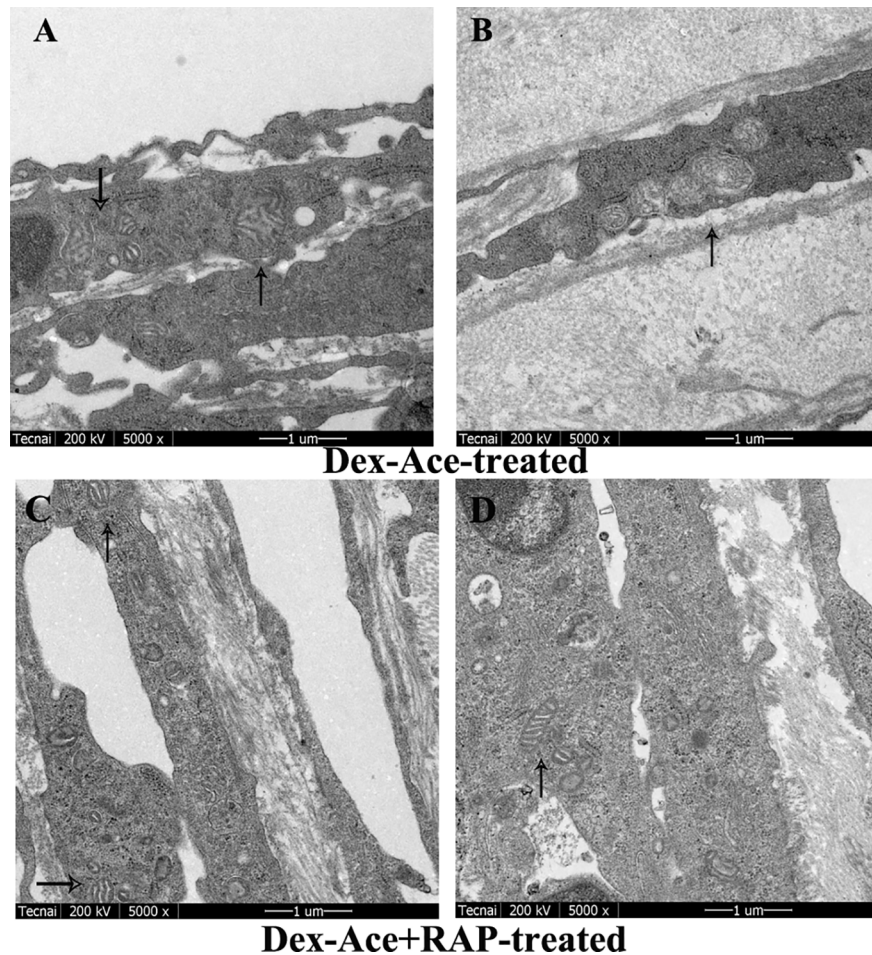


FIGURE 5 | RAP normalized Dex-Ace-induced ultrastructural changes of mitochondria at 4 weeks. In the Dex-Ace-treated group (**A, B**), the mitochondria were swollen and deformed, mitochondrial crests disappeared, and autophagic mitochondria fused into huge autophagosomes. In the Dex-Ace+RAP-treated group (**C, D**), the mitochondria maintained normal shape and arrangement, and the mitochondrial membrane and crests were clearly visible. (arrows indicate mitochondria; $n=5$; magnification: 5,000 \times).

transient elevation of cytosolic calcium concentration, which in turn activated the calmodulin-dependent pathways (Kfir-Erenfeld et al., 2010). The mechanism of mitochondrial regulation by RAP is complex and multiplex. RAP might inhibit cytoplasmic mTORC1, causing a reduced hypoxia-inducible factor (HIF)-1 α and glycolytic flux to elevate mitochondrial oxygen consumption simultaneously (Hudson et al., 2002). Another research showed that mTORC1 improved mitochondrial biogenesis and metabolism through transcription factors YY-1 and PGC-1 α (Cunningham et al., 2007). Moreover, RAP significantly induced autophagy, and suppressed oxidative stress as well as apoptosis, possibly *via* eliminating injured mitochondria (He et al., 2019).

In our previous study, Dex-Ace treatment induced autophagy to dispose of damaged TM cells. However, increased abnormal mitochondria indicated that autophagy was insufficient to resolve GC-induced damage (Zeng et al., 2019). In our current study, the subsequent rise of Beclin-1 and LC3-II/LC3-I ratio, together with the reduction of the autophagic substrate p62/SQSTM-1, highly

suggested the outcome of an ascending autophagic flux after RAP treatment in GIG mice. Previous research stated that p62 might be involved in the neurodegenerative processes because the overexpression of p62 promoted apoptosis through increasing production of caspase-8, and the knockdown of p62 reduced human glioma cell death (Zhang et al., 2013). Further studies reported that RAP-induced autophagy inhibited axonal growth in cortical neurons and that autophagy negatively regulated axonal extension through the RhoA-ROCK pathway, resulting axonal regeneration of RGCs (Ban et al., 2013; Munemasa and Kitaoka, 2015). Myocilin in TM cells is a short-lived protein (Mizushima, 2007; Su et al., 2017). The mutation of myocilin induced a toxic gain in cellular function in the endoplasmic reticulum stress of TM cells through misfolding and abnormal amyloidosis of myocilin protein (Suntharalingam et al., 2012). In conclusion, an abnormal increase in extracellular matrix caused by Dex-Ace treatment resulted in increased IOP, dysfunctional aqueous humor outflow, TM cell death, and ultimately optic

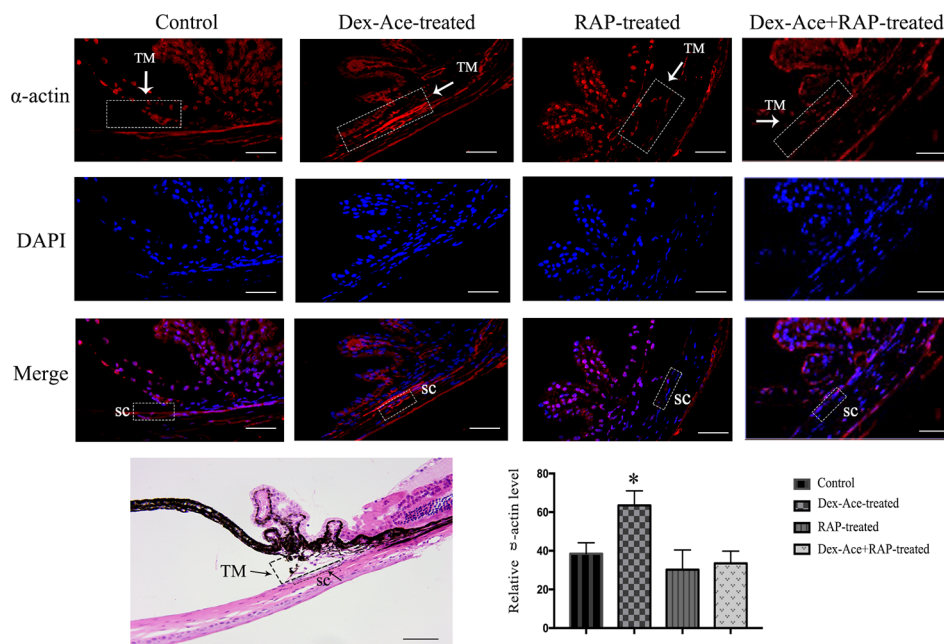


FIGURE 6 | RAP decreased Dex-Ace-induced α -actin expression in mouse trabecular tissues. The fluorescence intensity of α -actin in trabecular tissues was increased in the Dex-Ace-treated group at 4 weeks. (Immunofluorescence: SC, Schlemm's canal; magnification: 400 \times ; scale bar: 50 μ m; $n = 5$; *, $p < 0.05$; H&E: Magnification: 200 \times ; scale bar: 50 μ m; $n = 3$).

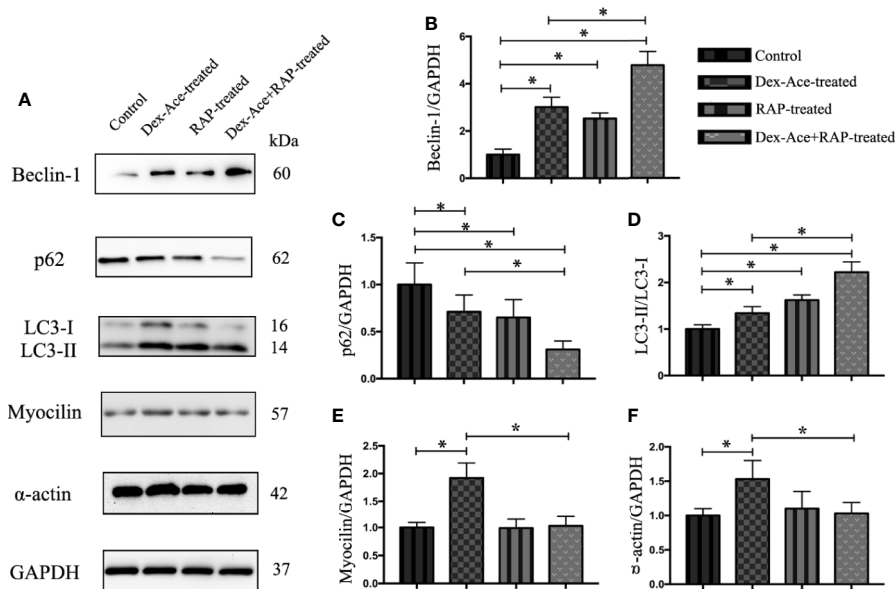


FIGURE 7 | RAP enhanced Dex-Ace-reduced TM cell autophagy and Dex-Ace-induced GIG-related protein expression at the 4th week. The relative protein expression levels of Beclin-1 and LC3-II/LC3-I ratio were upregulated, and p62 was downregulated in the Dex-Ace-treated group. RAP treatment further increased beclin-1 and LC3-II/LC3-I ratio, and downregulated p62 (A, B, C, D). Myocilin and α -actin were upregulated in the Dex-Ace-treated group and neutralized by RAP treatment (A, E, F). ($n = 6$; *, $p < 0.05$).

nerve damage (Jacobson et al., 2001). Therefore, enhanced autophagy, which degraded the misfolded myocilin and other increased extracellular matrix, might restore TM function and reduce pathological changes in glaucoma.

CONCLUSIONS

In this study, the relationship between autophagy and GIG was further observed by using autophagy activators. Our results indicated that RAP ameliorated increased IOP, damaged RGCs, and TM ultrastructure changes induced by Dex-Ace. Our results further elucidated the neuroprotective function of RAP, which supported the concept that RAP was potentially therapeutic target for GIG patients.

DATA AVAILABILITY STATEMENT

All datasets presented in this study are included in the article/supplementary material.

REFERENCES

- Ban, B. K., Jun, M. H., Ryu, H. H., Jang, D. J., Ahmad, S. T., and Lee, J. A. (2013). Autophagy negatively regulates early axon growth in cortical neurons. *Mol. Cell Biol.* 33 (19), 3907–3919. doi: 10.1128/MCB.00627-13
- Bird, A. C. (2010). Therapeutic targets in age-related macular disease. *J. Clin. Invest.* 120 (9), 3033–3041. doi: 10.1172/JCI42437
- Bjorkoy, G., Lamark, T., Pankiv, S., Overvatn, A., Brech, A., and Johansen, T. (2009). Monitoring autophagic degradation of p62/sqstm1. *Methods Enzymol.* 452, 181–197. doi: 10.1016/S0076-6879(08)03612-4
- Caccamo, A., Majumder, S., Deng, J. J., Bai, Y., Thornton, F. B., and Oddo, S. (2009). Rapamycin rescues tdp-43 mislocalization and the associated low molecular mass neurofilament instability. *J. Biol. Chem.* 284 (40), 27416–27424. doi: 10.1074/jbc.M109.031278
- Caron, E., Ghosh, S., Matsuoka, Y., Ashton-Beaucage, D., Therrien, M., Lemieux, S., et al. (2010). A comprehensive map of the mtor signaling network. *Mol. Syst. Biol.* 2010 (6), 453. doi: 10.1038/msb.2010.108
- Chan, D. C. (2006). Mitochondria: Dynamic organelles in disease, aging, and development. *Cell* 125 (7), 1241–1252. doi: 10.1016/j.cell.2006.06.010
- Clark, A. F., and Wordinger, R. J. (2009). The role of steroids in outflow resistance. *Exp. Eye Res.* 88 (4), 752–759. doi: 10.1016/j.exer.2008.10.004
- Clark, A. F., Brothie, D., Read, A. T., Hellberg, P., English-Wright, S., Pang, I. H., et al. (2005). Dexamethasone alters f-actin architecture and promotes cross-linked actin network formation in human trabecular meshwork tissue. *Cell Motil. Cytoskeleton.* 60 (2), 83–95. doi: 10.1002/cm.20049
- Cunningham, J. T., Rodgers, J. T., Arlow, D. H., Vazquez, F., Mootha, V. K., and Puigserver, P. (2007). Mtor controls mitochondrial oxidative function through a yy1-pgc-1 α transcriptional complex. *Nature* 450 (7170), 736–740. doi: 10.1038/nature06322
- Dash, S., Aydin, Y., and Wu, T. (2019). Integrated stress response in hepatitis c promotes nr1f2-related chaperone-mediated autophagy: A novel mechanism for host-microbe survival and hcc development in liver cirrhosis. *Semin. Cell Dev. Biol.* 101, 20–35. doi: 10.1016/j.semdb.2019.07.015
- Deng, S., Wang, M., Yan, Z., Tian, Z., Chen, H., Yang, X., et al. (2013). Autophagy in retinal ganglion cells in a rhesus monkey chronic hypertensive glaucoma model. *PLoS One* 8 (10), e77100. doi: 10.1371/journal.pone.0077100
- Eisenberg-Lerner, A., Bialik, S., Simon, H. U., and Kimchi, A. (2009). Life and death partners: Apoptosis, autophagy and the cross-talk between them. *Cell Death Differ.* 16 (7), 966–975. doi: 10.1038/cdd.2009.33

ETHICS STATEMENT

The animal study was reviewed and approved by Association for Research in Vision and Ophthalmology Statement of the Use of Animals in Ophthalmic and Vision Research.

AUTHOR CONTRIBUTIONS

XZ designed, conducted the project. XZ and SW carried out the experiments. WZ and TZ collected and analyzed the data. JR and MK assisted with the preparation of the experiments. XZ and XC prepared this manuscript. All authors contributed to the article and approved the submitted version.

FUNDING

This research was supported by National Natural Science Foundation of China (81970802).

- Eskelinen, E. L., and Saftig, P. (2009). Autophagy: A lysosomal degradation pathway with a central role in health and disease. *Biochim. Biophys. Acta* 1793 (4), 664–673. doi: 10.1016/j.bbamcr.2008.07.014
- Faralli, J. A., Dimeo, K. D., Trane, R. M., and Peters, D. (2018). Absence of a secondary glucocorticoid response in c57bl/6j mice treated with topical dexamethasone. *PLoS One* 13 (3), e0192665. doi: 10.1371/journal.pone.0192665
- Fini, M. E., Schwartz, S. G., Gao, X., Jeong, S., Patel, N., Itakura, T., et al. (2017). Steroid-induced ocular hypertension/glaucoma: Focus on pharmacogenomics and implications for precision medicine. *Prog. Retin. Eye Res.* 56, 58–83. doi: 10.1016/j.preteyeres.2016.09.003
- Fu, Z., Löfqvist, C. A., Liegl, R., Wang, Z., Sun, Y., Gong, Y., et al. (2018a). Photoreceptor glucose metabolism determines normal retinal vascular growth. *EMBO Mol. Med.* 10 (1), 76–90. doi: 10.15252/emmm.201707966
- Fu, Z., Wang, Z., Liu, C. H., Gong, Y., Cakir, B., Liegl, R., et al. (2018b). Fibroblast growth factor 21 protects photoreceptor function in type 1 diabetic mice. *Diabetes* 67 (5), 974–985. doi: 10.2337/db17-0830
- Gong, Y., Fu, Z., Edin, M. L., Liu, C., Wang, Z., Shao, Z., et al. (2016a). Cytochrome p450 oxidase 2c inhibition adds to omega-3 long-chain polyunsaturated fatty acids protection against retinal and choroidal neovascularization. *Arterioscler. Thromb. Vasc. Biol.* 36 (9), 1919–1927. doi: 10.1161/ATVBAHA.116.307558
- Gong, Y., Shao, Z., Fu, Z., Edin, M. L., Sun, Y., Liegl, Y., et al. (2016b). Fenofibrate inhibits cytochrome p450 epoxygenase 2c activity to suppress pathological ocular angiogenesis. *EBioMedicine* 13, 201–211. doi: 10.1016/j.ebiom.2016.09.025
- Han, H. E., Kim, T. K., Son, H. J., Park, W. J., and Han, P. L. (2013). Activation of autophagy pathway suppresses the expression of inos, il6 and cell death of lps-stimulated microglia cells. *Biomol. Ther. (Seoul)* 21 (1), 21–28. doi: 10.4062/biomolther.2012.089
- He, J. N., Zhang, S. D., Qu, Y., Wang, H. L., Tham, C. C., Pang, C. P., et al. (2019). Rapamycin removes damaged mitochondria and protects human trabecular meshwork (tm-1) cells from chronic oxidative stress. *Mol. Neurobiol.* 56 (9), 6586–6593. doi: 10.1007/s12035-019-1559-5
- Heitman, J. M. N., and Hall, M. N. (1991). Targets for cell cycle arrest by the immunosuppressant rapamycin in yeast. *Science* 253, 905–909. doi: 10.1126/science.1715094
- Hirt, J., and Liton, P. B. (2017). Autophagy and mechanotransduction in outflow pathway cells. *Exp. Eye Res.* 158, 146–153. doi: 10.1016/j.exer.2016.06.021
- Hosokawa, N., Hara, T., Kaizuka, T., Kishi, C., Takamura, A., Miura, Y., et al. (2009). Nutrient-dependent mtorc1 association with the ulk1-atg13-fip200 complex

- required for autophagy. *Mol. Biol. Cell* 20 (7), 1981–1991. doi: 10.1091/mbc.e08-12-1248
- Hudson, C. C., Liu, M., Chiang, G. G., Otterness, D. M., Loomis, D. C., Kaper, F., et al. (2002). Regulation of hypoxia-inducible factor 1 expression and function by the mammalian target of rapamycin. *Mol. Cell. Biol.* 22 (20), 7004–7014. doi: 10.1128/MCB.22.20.7004-7014.2002
- Jacobson, N., Andrews, M., Shepard, A. R., Nishimura, D., Searby, C., Fingert, J. H., et al. (2001). Non-secretion of mutant proteins of the glaucoma gene myocilin in cultured trabecular meshwork cells and in aqueous humor. *Hum. Mol. Genet.* 10 (2), 117–125. doi: 10.1093/hmg/10.2.117
- Kasetti, R. B., Phan, T. N., Millar, J. C., and Zode, G. S. (2016). Expression of mutant myocilin induces abnormal intracellular accumulation of selected extracellular matrix proteins in the trabecular meshwork. *Invest. Ophthalmol. Visual Sci.* 57 (14), 6058–6069. doi: 10.1167/iov.16-19610
- Kfir-Erenfeld, S., Sionov, R. V., Spokoini, R., Cohen, O., and Yefenof, E. (2010). Protein kinase networks regulating glucocorticoid-induced apoptosis of hematopoietic cancer cells: Fundamental aspects and practical considerations. *Leuk. Lymphoma* 51 (11), 1968–2005. doi: 10.3109/10428194.2010.506570
- Kitaoka, Y., Munemasa, Y., Kojima, K., Hirano, A., Ueno, S., and Takagi, H. (2013). Axonal protection by nmnat3 overexpression with involvement of autophagy in optic nerve degeneration. *Cell Death Dis.* 4, e860. doi: 10.1038/cddis.2013.391
- Knoferle, J., Koch, J. C., Ostendorf, T., Michel, U., Planchamp, V., Vutova, P., et al. (2010). Mechanisms of acute axonal degeneration in the optic nerve in vivo. *Proc. Natl. Acad. Sci. U.S.A.* 107 (13), 6064–6069. doi: 10.1073/pnas.0909794107
- Kroemer, G., Marino, G., and Levine, B. (2010). Autophagy and the integrated stress response. *Mol. Cell* 40 (2), 280–293. doi: 10.1016/j.molcel.2010.09.023
- Kumari, S., Mehta, S. L., and Li, P. A. (2012). Glutamate induces mitochondrial dynamic imbalance and autophagy activation: Preventive effects of selenium. *PLoS One* 7 (6), e39382. doi: 10.1371/journal.pone.0039382
- Kwon, Y. H., Fingert, J. H., Kuehn, M. H., and Alward, W. L. (2009). Primary open-angle glaucoma. *N Engl. J. Med.* 360 (11), 1113–1124. doi: 10.1056/NEJMra0804630
- Levine, B., and Klionsky, D. J. (2004). Development by self-digestion: Molecular mechanisms and biological functions of autophagy. *Dev. Cell* 6 (4), 463–477. doi: 10.1016/S1534-5807(04)00099-1
- Li, J., Liu, C. H., Sun, Y., Gong, Y., Fu, Z., Evans, L. P., et al. (2014). Endothelial twist1 promotes pathological ocular angiogenesis. *Invest. Ophthalmol. Visual Sci.* 55 (12), 8267–8277. doi: 10.1167/iov.14-15623
- Malagelada, C., Jin, Z. H., Jackson-Lewis, V., Przedborski, S., and Greene, L. A. (2010). Rapamycin protects against neuron death in in vitro and in vivo models of parkinson's disease. *J. Neurosci.* 30 (3), 1166–1175. doi: 10.1523/JNEUROSCI.3944-09.2010
- Mizushima, N., Yoshimori, T., and Levine, B. (2010). Methods in mammalian autophagy research. *Cell* 140 (3), 313–326. doi: 10.1016/j.cell.2010.01.028
- Mizushima, N. (2007). Autophagy: Process and function. *Genes Dev.* 21 (22), 2861–2873. doi: 10.1101/gad.1599207
- Munemasa, Y., and Kitaoka, Y. (2015). Autophagy in axonal degeneration in glaucomatous optic neuropathy. *Prog. Retin. Eye Res.* 47, 1–18. doi: 10.1016/j.preteyeres.2015.03.002
- Osborne, N. N., Álvarez, C. N., and del Olmo Aguado, S. (2014). Targeting mitochondrial dysfunction as in aging and glaucoma. *Drug Discovery Today* 19 (12), 1613–1622. doi: 10.1016/j.drudis.2014.05.010
- Overby, D. R., Bertrand, J., Tektas, O. Y., Boussommier-Calleja, A., Schicht, M., Ethier, C. R., et al. (2014). Ultrastructural changes associated with dexamethasone-induced ocular hypertension in mice. *Invest. Ophthalmol. Visual Sci.* 55 (8), 4922–4933. doi: 10.1167/iov.14-14429
- Patel, G. C., Phan, T. N., Maddineni, P., Kasetti, R. B., Millar, J. C., Clark, A. F., et al. (2017). Dexamethasone-induced ocular hypertension in mice. *Am. J. Pathol.* 187 (4), 713–723. doi: 10.1016/j.ajpath.2016.12.003
- Porter, K. M., Jeyabalan, N., and Liton, P. B. (2014). Mtor-independent induction of autophagy in trabecular meshwork cells subjected to biaxial stretch. *Biochim. Biophys. Acta* 1843 (6), 1054–1062. doi: 10.1016/j.bbamcr.2014.02.010
- Prevel, N., Allenbach, Y., Klatzmann, D., Salomon, B., and Benveniste, O. (2013). Beneficial role of rapamycin in experimental autoimmune myositis. *PLoS One* 8 (11), e74450. doi: 10.1371/journal.pone.0074450
- Saxena, S., Mathur, A., and Kakkar, P. (2019). Critical role of mitochondrial dysfunction and impaired mitophagy in diabetic nephropathy. *J. Cell. Physiol.* 234 (11), 19223–19236. doi: 10.1002/jcp.28712
- Steely, H. T., Browder, S. L., Julian, M. B., Miggans, S. T., Wilson, K. L., and Clark, A. F. (1992). The effects of dexamethasone on fibronectin expression in cultured human trabecular meshwork cells. *Invest. Ophthalmol. Visual Sci.* 33 (7), 2242–2250.
- Ster, A. M., Popp, R. A., Petrisor, F. M., Stan, C., and Pop, V. I. (2014). The role of oxidative stress and vascular insufficiency in primary open angle glaucoma. *Chujul. Med.* 87 (3), 143–146. doi: 10.15386/cjmed-295
- Su, W., Li, Z., Jia, Y., and Zhuo, Y. (2014). Rapamycin is neuroprotective in a rat chronic hypertensive glaucoma model. *PLoS One* 9 (6), e99719. doi: 10.1371/journal.pone.0099719
- Su, Y., Wu, J., He, J., Liu, X., Chen, X., Ding, Y., et al. (2017). High insulin impaired ovarian function in early pregnant mice and the role of autophagy in this process. *Endocr. J.* 64 (6), 613–621. doi: 10.1507/endocrj.EJ16-0494
- Suntharalingam, A., Abisambra, J. F., O'Leary, J. C., Koren, J., Zhang, B., Joe, M. K., et al. (2012). Glucose-regulated protein 94 triage of mutant myocilin through endoplasmic reticulum-associated degradation subverts a more efficient autophagic clearance mechanism. *J. Biol. Chem.* 287 (48), 40661–40669. doi: 10.1074/jbc.M112.384800
- Vidal-Sanz, M., Valiente-Soriano, F. J., Ortín-Martínez, A., Nadal-Nicolás, F. M., Jiménez-López, M., Salinas-Navarro, M., et al. (2015). Retinal neurodegeneration in experimental glaucoma. *Prog. Brain. Res.* 220, 1–35.
- Wang, W. H., Millar, J. C., Pang, I. H., Wax, M. B., and Clark, A. F. (2005). Noninvasive measurement of rodent intraocular pressure with a rebound tonometer. *Invest. Ophthalmol. Visual Sci.* 46 (12), 4617–4621. doi: 10.1167/iov.05-0781
- Wang, Z., Liu, C. H., Sun, Y., Gong, Y., Favazza, T. L., Morss, P. C., et al. (2016). Pharmacologic activation of wnt signaling by lithium normalizes retinal vasculature in a murine model of familial exudative vitreoretinopathy. *Am. J. Pathol.* 186 (10), 2588–2600. doi: 10.1016/j.ajpath.2016.06.015
- Wirawan, E., Lippens, S., Vanden Bergh, T., Romagnoli, A., Fimia, G. M., Piacentini, M., et al. (2012). Beclin1: A role in membrane dynamics and beyond. *Autophagy* 8 (1), 6–17. doi: 10.4161/auto.8.1.16645
- Zeng, W., Wang, W., Wu, S., Zhu, X., Zheng, T., Chen, X., et al. (2019). Mitochondria and autophagy dysfunction in glucocorticoid-induced ocular hypertension/glaucoma mice model. *Curr. Eye Res.* 45 (2), 190–198. doi: 10.1080/02713683.2019.1657462
- Zhang, Y. B., Gong, J. L., Xing, T. Y., Zheng, S. P., and Ding, W. (2013). Autophagy protein p62/sqstm1 is involved in hamlet-induced cell death by modulating apoptosis in u87mg cells. *Cell Death Dis.* 4, e550. doi: 10.1038/cddis.2013.77
- Zhou, L., Li, Y., and Yue, B. Y. (1998). Glucocorticoid effects on extracellular matrix proteins and integrins in bovine trabecular meshwork cells in relation to glaucoma. *Int. J. Mol. Med.* 1 (2), 339–346. doi: 10.3892/ijmm.1.2.339
- Zhu, H., and Zhang, Y. (2018). Life and death partners in post-pci restenosis: Apoptosis, autophagy, and the cross-talk between them. *Curr. Drug Targets* 19 (9), 1003–1008. doi: 10.2174/1389450117666160625072521
- Zode, G. S., Sharma, A. B., Lin, X., Searby, C. C., Bugge, K., Kim, G. H., et al. (2014). Ocular-specific stress reduction rescues glaucoma in murine glucocorticoid-induced glaucoma. *J. Clin. Invest.* 124 (5), 1956–1965. doi: 10.1172/JCI69774
- Zode, G. S., Kuehn, M. H., Nishimura, D. Y., Searby, C. C., Mohan, K., Grozdanic, S. D., et al. (2015). Reduction of stress via a chemical chaperone prevents disease phenotypes in a mouse model of primary open angle glaucoma. *J. Clin. Invest.* 125 (8), 3303. doi: 10.1172/JCI82799

Conflict of Interest: The authors declare that the research was conducted in the absence of any commercial or financial relationships that could be construed as a potential conflict of interest.

Copyright © 2020 Zhu, Wu, Zeng, Chen, Zheng, Ren and Ke. This is an open-access article distributed under the terms of the Creative Commons Attribution License (CC BY). The use, distribution or reproduction in other forums is permitted, provided the original author(s) and the copyright owner(s) are credited and that the original publication in this journal is cited, in accordance with accepted academic practice. No use, distribution or reproduction is permitted which does not comply with these terms.



Mitochondrial Heme Synthesis Enzymes as Therapeutic Targets in Vascular Diseases

Trupti Shetty^{1,2} and Timothy W. Corson^{1,2,3*}

¹ Department of Ophthalmology, Eugene and Marilyn Glick Eye Institute, Indiana University School of Medicine, Indianapolis, IN, United States, ² Department of Pharmacology and Toxicology, Indiana University School of Medicine, Indianapolis, IN, United States, ³ Department of Biochemistry and Molecular Biology, Indiana University School of Medicine, Indianapolis, IN, United States

Keywords: age-related macular degeneration, diabetic retinopathy, angiogenesis, neovascularization, ferrochelatase, electron transport chain, endothelial nitric oxide synthase, heme synthesis

OPEN ACCESS

Edited by:

Zhongjie Fu,
Boston Children's Hospital and
Harvard Medical School, United States

Reviewed by:

Yuqing Huo,
Augusta University, United States
Keisuke Yanagida,
National Center For Global Health and
Medicine, Japan

*Correspondence:

Timothy W. Corson
tcorson@iu.edu

Specialty section:

This article was submitted to
Neuropharmacology,
a section of the journal
Frontiers in Pharmacology

Received: 30 November 2019

Accepted: 23 June 2020

Published: 15 July 2020

Citation:

Shetty T and Corson TW (2020)
Mitochondrial Heme Synthesis
Enzymes as Therapeutic Targets in
Vascular Diseases.
Front. Pharmacol. 11:1015.
doi: 10.3389/fphar.2020.01015

INTRODUCTION: SYNTHESIS AND FUNCTIONS OF HEME

Mitochondrial function in endothelial cells (EC) is interconnected by a mesh of signaling molecules that cross pathways often (Kluge et al., 2013). One such versatile biomolecule is heme. Heme is important for respiration, curbing oxidative stress, drug metabolism, and oxygen transport (Dailey and Meissner, 2013). The heme synthesis pathway and intermediates have been studied in detail over decades, with crystal structures and cloned genes available (Poulos, 2014). Intriguingly, heme is an important prosthetic moiety of key proteins of EC (Chiabrando et al., 2014b).

In mammalian cells, heme synthesis is accomplished in the mitochondria and cytosol over a series of eight enzymatic reactions, followed by modification of heme in a couple of sub-hemylation steps (Nilsson et al., 2009; Hamza and Dailey, 2012; Dailey et al., 2017). Heme biosynthesis in cells other than erythrocytes is initiated by the rate-limiting enzyme aminolevulinic acid synthase (ALAS1) that catalyzes formation of 5-aminolevulinic acid (ALA) from succinyl-CoA and glycine (Figure 1A). ALA is exported into the cytosol and converted *via* several intermediates into coproporphyrinogen-III (CPO) by coproporphyrinogen oxidase (CPOX); CPO is then transported back into the mitochondria for the last two steps of the pathway. In the final step, ferrochelatase (FECH) incorporates ferrous iron into protoporphyrin IX (PPIX), synthesizing protoheme. Heme is then available to enable cellular processes by combining with enzyme subunits as a prosthetic group. For example, heme-iron is part of the catalytically active form of endothelial nitric oxide synthase (eNOS) (Raman et al., 1998). Similarly, different forms of heme are incorporated into mitochondrial respiratory complexes I–IV of the electron transport chain (ETC) (Kim et al., 2012). Of course, the majority of heme is used for incorporation into hemoglobin during erythropoiesis (Korolnek and Hamza, 2014) and some (primarily in the liver) for the synthesis of cytochrome P450s, responsible for xenobiotic metabolism (Correia et al., 2011).

Apart from being a prosthetic cofactor for enzymes, heme's regulated production ensures that active iron is sequestered before it can promote formation of reactive oxygen species (ROS) (Ryter and Tyrrell, 2000). Hence, heme plays a crucial role in ROS homeostasis in the mitochondria, without which many mitochondrial processes would be damaged (Alonso et al., 2003). One key regulator involved in detoxification of ROS and stimulating mitochondrial biogenesis is

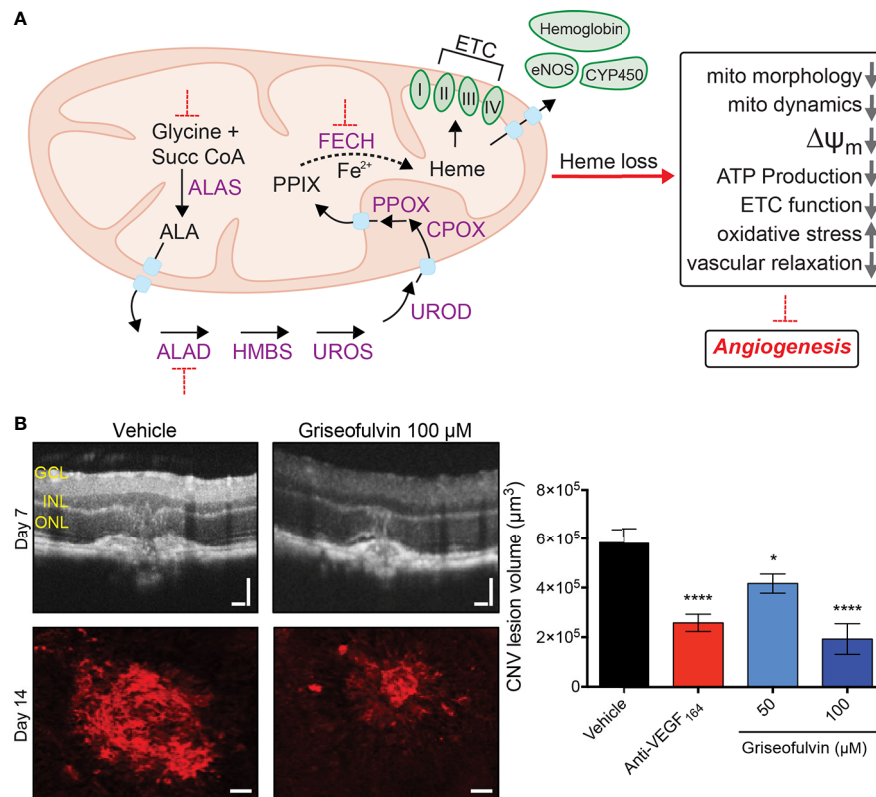


FIGURE 1 | Schematic diagram of the heme synthesis pathway in the mitochondrion and effect of *Fech* inhibition *in vivo*. **(A)** Eight sequential steps in the heme synthesis pathway are depicted, along with some heme-containing proteins. Red dotted lines indicate blockade. **(B)** *Fech* inhibition using griseofulvin in the laser-induced choroidal neovascularization (CNV) mouse model. CNV was confirmed by optical coherence tomography (OCT). Griseofulvin treated eyes had significantly smaller neovascular lesions as seen in red agglutinin staining for vasculature. Retinal layers indicated: GCL, ganglion cell layer; INL, inner nuclear layer; ONL, outer nuclear layer; Scale bars for OCT images and agglutinin immunostaining are 100 and 50 μm, respectively. **p* = 0.015; ****p* = 0.0001 versus vehicle, ANOVA with Dunnett's *post hoc* tests (*n* = 11–13 eyes per group). Anti-VEGF₁₆₄ is a positive control antibody therapy. Figure modified from Basavarajappa et al., 2017 © 2017 The Authors, CC BY 4.0. Succ CoA, succinyl-CoA, ALA, 5-aminolevulinic acid; ALAS, ALA synthase; ALAD, ALA dehydratase; HMBS, hydroxymethylbilane synthase; UROS, uroporphyrinogen synthase; UROD, uroporphyrinogen decarboxylase; CPOX, coproporphyrinogen oxidase; PPOX, protoporphyrinogen oxidase; FECH, ferrochelatase; PPIX, protoporphyrin IX; eNOS, endothelial nitric oxide synthase; CYP450, cytochrome P450; ETC, electron transport chain; $\Delta\Psi_m$ = mitochondrial membrane potential; mito, mitochondria.

proliferator-activated receptor gamma coactivator 1 α (PGC1 α) (Austin and St-Pierre, 2012). PGC1 α regulates ALAS1 expression in the liver, linking heme synthesis directly to the nutritional state of cells (Handschin et al., 2005). Fasting-induced PGC1 α was found to be essential for vascular growth and pathological angiogenesis (Saint-Geniez et al., 2013). Here, we review recent studies that have identified an unexpected link between angiogenesis and heme synthesis, offering exciting therapeutic relevance to vascular diseases like retinopathy of prematurity (ROP), proliferative diabetic retinopathy (PDR), and wet age-related macular degeneration (AMD).

HEME SYNTHESIS PROTEINS AS ANGIOGENESIS MEDIATORS

The terminal heme synthesis enzyme, ferrochelatase, encoded by *FECH*, was the first heme pathway component to be identified as

a druggable target in pathological angiogenesis. FECH blockade (both genetically and pharmacologically) reduced proliferation, migration and endothelial tube formation in microvascular ECs. This effect was specific to ECs; FECH inhibition had a negligible effect on non-endothelial ocular cell proliferation. This anti-angiogenic effect was also seen *in vivo*: mice with a partial loss-of-function *Fech*^{m1Pas} point mutation formed reduced neovascular lesions in the eye in the laser-induced choroidal neovascularization (L-CNV) model with features of wet AMD, as did mice with ocular *Fech* knockdown or inhibition (Figure 1B). In addition, FECH was overexpressed in and around these lesions, and in human wet age-related macular degeneration eyes (Basavarajappa et al., 2017). Moreover, FECH was upregulated, particularly in neovascular tufts, in the oxygen-induced retinopathy (OIR) mouse model of ROP (Pran Babu et al., 2020). The mechanisms of how heme contributes to EC physiology and drives angiogenesis are now beginning to be understood.

MECHANISMS OF HEME REGULATION OF ANGIOGENESIS

Mitochondrial Function

Inhibition of heme synthesis has varying impact on the hemoproteins of the ETC (Vijayasarathy et al., 1999; Atamna et al., 2001). Heme *b* and *c* are present in complexes II and III, whereas complex IV has two groups of heme *a*, made after two consecutive modifications to protoheme (Kim et al., 2012). We recently showed that loss of heme *via* blockade of the terminal enzyme FECH in retinal ECs specifically causes complex IV dysfunction with negligible effects on other complexes of the ETC (Shetty et al., 2020). Complex IV protein and activity were significantly decreased by small molecule or genetic inhibition of FECH, but partially restored after heme supplementation. This loss in complex IV was accompanied by a depolarized mitochondrial membrane. Furthermore, heme depletion damaged both oxidative phosphorylation and glycolysis in retinal and choroidal ECs, along with a decrease in mitochondrial fusion and elevated ROS. This work characterized the direct effect of heme blockade on EC metabolism for the first time (Shetty et al., 2020).

Another recent study elucidated the contribution of the serine synthesis pathway to heme and EC metabolism (Vandekeere et al., 2018). Inhibition of the serine synthesis enzyme phosphoglycerate dehydrogenase (PHGDH) reduced glycine (substrate for the first step of the heme synthesis pathway), leading to an indirect decrease of heme enzymes and an eventual reduction in heme production in ECs. This also caused mitochondrial defects like reduced respiration, smaller mitochondria, increased fission, reduced fusion, and elevated mitophagy. Neonatal mice with silenced PHGDH had reduced retinal vascularization and reduced vessel area in the brain, heart, and kidney. Additionally, another group demonstrated that complex III is essential for EC proliferation (but not migration) in macrovascular ECs. Conditional knockout of EC-specific complex III led to reduced retinal, lung, and tumor neovascular blood vessels (Diebold et al., 2019). Loss of FECH activity was anti-proliferative for brain microvascular ECs, with no effect on macrovascular ECs (Basavarajappa et al., 2017). This was in contrast to reduced heme synthesis seen in macrovascular ECs as a result of aberrant serine synthesis (Vandekeere et al., 2018). The differential phenotypes of heme loss in microvasculature versus macrovasculature remain unclear and solicit further studies (Ghitescu and Robert, 2002; Sandoo et al., 2011).

Sprouting human umbilical vein ECs are highly glycolytic, producing up to 85% of ATP through the glycolysis pathway. During angiogenesis, endothelial tip and stalk cells dynamically switch their glycolytic activity depending on the energy demands of the tip cells and the proliferating stalk cells (De Bock et al., 2013). Recently, endothelial tip cells were reported to be less glycolytic during angiogenic cell differentiation (Yetkin-Arik et al., 2019), however more studies are warranted to validate such observations. Additionally, mitochondrial fatty acid oxidation has a role in proliferation of sprouting ECs (Schoors et al., 2015). While blocking heme production diminishes

glycolytic capacity of retinal ECs (Shetty et al., 2020), it is as yet unclear whether heme regulation of EC metabolism varies between tip and non-tip ECs. Recent genomic analysis of murine choroidal ECs from neovascularization revealed potential metabolic candidates not found in healthy cells, suggesting targeting endothelial metabolism could be the way forward in vascular therapeutics (Rohlenova et al., 2020).

Cytosolic Effects

Lack of heme synthesis also leads to incomplete formation of eNOS and reduced activity (Feng, 2012). Heme depletion *via* FECH inhibition led to decreased expression, hemylation, and activity of eNOS in retinal microvascular ECs (Basavarajappa et al., 2017). Heme inhibition by chemically blocking the second synthesis enzyme aminolevulinic acid dehydratase (ALAD) in rats led to reduced eNOS and downstream mediator soluble guanylyl cyclase (sGC), both important in maintaining regular cardiovascular function. These effects did not affect vascular tension and resulted in no change to arterial blood pressure (Bourque et al., 2010). But heme depletion-driven eNOS dysfunction led to impaired NO mediated vascular relaxation in bovine coronary arteries (Zhang et al., 2018). NO, a potent vasodilator, is pro-angiogenic and NO itself is known to inhibit hemylation of extramitochondrial *apo*-hemoproteins (Waheed et al., 2010).

It is important to note that heme overload in ECs also leads to abnormal angiogenesis. Silencing of the heme transporter FLVCR1a led to intracellular heme accumulation in microvascular ECs, but not in macrovascular ECs. This heme accumulation in microvascular ECs led to impaired angiogenesis, damaged vessel formation and embryonic lethality *in vivo* (Petrillo et al., 2018). Heme toxicity has been investigated previously in hemolytic diseases like sickle cell disease and thalassemia, where heme scavengers are helpful in reducing heme-induced ROS accumulation (Vinci et al., 2013). In non-small cell lung cancer, tumor cells had elevated heme synthesis activity, increasing respiratory function of the ETC and enhancing tumorigenic properties like migration and invasiveness (Sohoni et al., 2019). This suggests in addition to heme loss being anti-angiogenic, heme synthesis overdrive can increase mitochondrial function, but this remains to be validated in ECs. It would be interesting to investigate whether heme mediates EC metabolism in neovascularized tumors in a similar fashion and whether heme synthesis blockers could be valuable as cancer therapies.

THERAPEUTIC POTENTIAL OF TARGETING HEME SYNTHESIS IN NEOVASCULARIZATION

Current therapeutic strategies targeting mitochondria involve key functions like mitochondrial division (Cassidy-Stone et al., 2008), ROS formation (Dhanasekaran et al., 2004), and metabolism (Mather et al., 2001; Csiszar et al., 2009) for age-related neurodegenerative diseases like Alzheimer's, Parkinson's, and

Huntington's (Lane et al., 2015). Meanwhile, anti-vascular endothelial growth factor (VEGF) therapies remain classic biologics used for neovascular diseases such as wet AMD, PDR, and multiple cancers (Jain, 2014). Until our and others' work described above, there was no rationale for targeting heme synthesis as neovascularization therapy. But given the specific antiproliferative effects of FECH blockade in microvascular ECs, FECH inhibitors like *N*-methylprotoporphyrin have demonstrated potential in targeting neovascular pathologies, both *in vitro* and in the OIR mouse model (Basavarajappa et al., 2017; Pran Babu et al., 2020). Novel, drug-like FECH inhibitors are also a possibility (Corson et al., 2019; Sishtla et al., 2019).

Repurposing existing drugs for pathological angiogenesis also holds promise towards this end. Griseofulvin, an FDA-approved anti-fungal drug, has a long-known off-target effect of FECH inhibition (Brady and Lock, 1992; Liu et al., 2015). It has anti-angiogenic effects in retinal ECs, blocking proliferation, migration, and tube formation *in vitro* and reducing neovascularization *in vivo* comparable to intraocular anti-VEGF treatment, in both OIR and L-CNV mouse models (**Figure 1B**) (Basavarajappa et al., 2017; Pran Babu et al., 2020). Isoniazid, an anti-mycobacterial drug, decreases FECH expression while upregulating ALAS1 (Brewer et al., 2019), and thus could be tested for potential anti-angiogenic activity in neovascularization models. Other inhibitors of heme synthesis used *in vitro* include succinylacetone and salicylic acid that block ALAD and FECH respectively (Giger and Meyer, 1983; Gupta et al., 2013), however their use in preclinical angiogenesis models remains to be investigated.

Targeting mitochondrial proteins directly involved in ETC activity has limitations as well, with a direct consequence on mitochondrial function. However, extracellular supplementation of hemin (a more stable form of heme) is able to normalize some of the mitochondrial physiology, like eNOS levels, complex IV activity, and ETC function (Basavarajappa et al., 2017; Vandekeere et al., 2018; Shetty et al., 2020). Effect of FECH blockade can be titrated, with a dose dependent decrease in angiogenesis features observed in animal models and ECs in culture. Homozygous *Fech*^{m1Pas} mice have significantly reduced neovascular lesions, compared to heterozygous *Fech*^{m1Pas} mice. And heterozygotes themselves have reduced lesions compared to wild-type (Basavarajappa et al., 2017), suggesting a window of FECH antiangiogenic effects without toxicity. However, complete loss of *Fech* and *Alas1* are embryonically lethal to mice (Magness et al., 2002; Chiabrando et al., 2014a), highlighting the importance of modulating heme inhibition carefully.

Oral supplementation of heme, while still achieving therapeutic antiangiogenic effects of inhibitors, could be considered (Luan et al., 2017). In order to limit systemic toxicity, it would be helpful to localize therapeutic formulations to pathological tissue wherever possible. For example, in ocular neovascularization, therapeutic agents could be delivered through intravitreal or subretinal injection (Basavarajappa et al., 2017), or even as eyedrops if formulation allows; this is a promising area for future work. Therapeutic targeting specific to ECs could be included in drug delivery

systems (Kawahara et al., 2013), since systemic deficiency in heme synthesis enzymes can lead to porphyrias. For example, erythropoietic protoporphyria is caused by toxic buildup of PPIX (Gouya et al., 1999). The phototoxic PPIX can be detrimental to cells, and is manipulated in photodynamic therapy (PDT) (Krammer and Plaetzer, 2008). However, it is unlikely that PPIX itself mediates anti-angiogenic effects, as ALA-PDT relies heavily on uptake of ALA (Wachowska et al., 2011). Moreover, as noted, hemin is able to rescue anti-angiogenic effects in ECs, even in the presence of PPIX build-up, suggesting that this mechanism is heme dependent and not due to PPIX toxicity.

CONCLUSIONS AND FUTURE PROSPECTS

Targeting intracellular heme, either *via* inhibition of synthesis through intermediary enzymes or blocking heme transport (through FLVCR) provides for a novel therapeutic strategy, one that is primed to be explored in detail in vascular biology. Key questions that need to be addressed are: Is the role of heme in angiogenesis limited to ETC and eNOS or do other heme-containing proteins aid in anti-angiogenic effects? Which enzymes in the heme synthesis pathway are the most effectively targetable for treating pathological angiogenesis? What are the key differences in microvascular and macrovascular heme synthesis, and can we manipulate these therapeutically? Proliferative ECs appear to be particularly sensitive to heme loss, but is this sensitivity only relevant in vascular tissues? Most importantly, we also need to elucidate the contribution of heme and heme pathway intermediates in maintaining normal endothelial cellular physiology, to devise better strategies for future therapeutic interventions.

AUTHOR CONTRIBUTIONS

TS, TC: wrote the paper, edited the paper, and approved final version.

FUNDING

Related work in the Corson laboratory is supported by NIH/NEI R01EY025641, NIH/NCATS UL1TR001108, the Retina Research Foundation, the International Retinal Research Foundation, the BrightFocus Foundation, the Carl Marshall and Mildred Almen Reeves Foundation, and the Ralph and Grace Showalter Research Trust.

ACKNOWLEDGMENTS

We thank members of the Corson laboratory for comments on the manuscript.

REFERENCES

- Alonso, J. R., Cardellach, F., Lopez, S., Casademont, J., and Miro, O. (2003). Carbon monoxide specifically inhibits cytochrome c oxidase of human mitochondrial respiratory chain. *Pharmacol. Toxicol.* 93, 142–146. doi: 10.1034/j.1600-0773.2003.930306.x
- Atamna, H., Liu, J., and Ames, B. N. (2001). Heme deficiency selectively interrupts assembly of mitochondrial complex IV in human fibroblasts: Relevance to aging. *J. Biol. Chem.* 276, 48410–48416. doi: 10.1074/jbc.M108362200
- Austin, S., and St-Pierre, J. (2012). PGC1 α and mitochondrial metabolism: Emerging concepts and relevance in ageing and neurodegenerative disorders. *J. Cell Sci.* 125, 4963–4971. doi: 10.1242/jcs.113662
- Basavarajappa, H. D., Sulaiman, R. S., Qi, X., Shetty, T., Sheik Pran Babu, S., Sishtla, K. L., et al. (2017). Ferrochelatase is a therapeutic target for ocular neovascularization. *EMBO Mol. Med.* 9, 786–801. doi: 10.15252/emmm.201606561
- Bourque, S. L., Benjamin, C. D., Adams, M. A., and Nakatsu, K. (2010). Lack of hemodynamic effects after extended heme synthesis inhibition by succinylacetone in rats. *J. Pharmacol. Exp. Ther.* 333, 290–296. doi: 10.1124/jpet.109.162966
- Brady, A. M., and Lock, E. A. (1992). Inhibition of ferrochelatase and accumulation of porphyrins in mouse hepatocyte cultures exposed to porphyrinogenic chemicals. *Arch. Toxicol.* 66, 175–181. doi: 10.1007/BF01974011
- Brewer, C. T., Yang, L., Edwards, A., Lu, Y., Low, J., Wu, J., et al. (2019). The isoniazid metabolites hydrazine and pyridoxal isonicotinoyl hydrazone modulate heme biosynthesis. *Toxicol. Sci.* 168, 209–224. doi: 10.1093/toxsci/kfy294
- Cassidy-Stone, A., Chipuk, J. E., Ingberman, E., Song, C., Yoo, C., Kuwana, T., et al. (2008). Chemical inhibition of the mitochondrial division dynamin reveals its role in Bax/Bak-dependent mitochondrial outer membrane permeabilization. *Dev. Cell* 14, 193–204. doi: 10.1016/j.devcel.2007.11.019
- Chiabrando, D., Mercurio, S., and Tolosano, E. (2014a). Heme and erythropoiesis: More than a structural role. *Haematologica* 99, 973–983. doi: 10.3324/haematol.2013.091991
- Chiabrando, D., Vinchi, F., Fiorito, V., Mercurio, S., and Tolosano, E. (2014b). Heme in pathophysiology: A matter of scavenging, metabolism and trafficking across cell membranes. *Front. Pharmacol.* 5, 61. doi: 10.3389/fphar.2014.00061
- Correia, M. A., Sinclair, P. R., and De Matteis, F. (2011). Cytochrome P450 regulation: The interplay between its heme and apoprotein moieties in synthesis, assembly, repair, and disposal. *Drug Metab. Rev.* 43, 1–26. doi: 10.3109/03602532.2010.515222
- Corson, T. W., Seo, S. Y., Lee, B., and Sishtla, K. (2019). *Ferrochelatase inhibitors and methods of use*, International Patent Application PCT/US19/29909.
- Csiszar, A., Labinskyy, N., Pinto, J. T., Ballabh, P., Zhang, H., Losonczy, G., et al. (2009). Resveratrol induces mitochondrial biogenesis in endothelial cells. *Am. J. Physiol. Heart Circ. Physiol.* 297, H13–H20. doi: 10.1152/ajpheart.00368.2009
- Dailey, H. A., and Meissner, P. N. (2013). Erythroid heme biosynthesis and its disorders. *Cold Spring Harb. Perspect. Med.* 3, a011676. doi: 10.1101/cshperspect.a011676
- Dailey, H. A., Dailey, T. A., Gerdes, S., Jahn, D., Jahn, M., O'Brian, M. R., et al. (2017). Prokaryotic heme biosynthesis: Multiple pathways to a common essential product. *Microbiol. Mol. Biol. Rev.* 81, e00048–16. doi: 10.1128/MMBR.00048-16
- De Bock, K., Georgiadou, M., Schoors, S., Kuchnio, A., Wong, B. W., Cantelmo, A. R., et al. (2013). Role of PFKFB3-driven glycolysis in vessel sprouting. *Cell* 154, 651–663. doi: 10.1016/j.cell.2013.06.037
- Dhanasekaran, A., Kotamraju, S., Kalivendi, S. V., Matsunaga, T., Shang, T., Keszler, A., et al. (2004). Supplementation of endothelial cells with mitochondria-targeted antioxidants inhibit peroxide-induced mitochondrial iron uptake, oxidative damage, and apoptosis. *J. Biol. Chem.* 279, 37575–37587. doi: 10.1074/jbc.M404003200
- Diebold, L. P., Gil, H. J., Gao, P., Martinez, C. A., Weinberg, S. E., and Chandel, N. S. (2019). Mitochondrial complex III is necessary for endothelial cell proliferation during angiogenesis. *Nat. Metab.* 1, 158–171. doi: 10.1038/s42255-018-0011-x
- Feng, C. (2012). Mechanism of nitric oxide synthase regulation: electron transfer and interdomain interactions. *Coord. Chem. Rev.* 256, 393–411. doi: 10.1016/j.ccr.2011.10.011
- Ghitescu, L., and Robert, M. (2002). Diversity in unity: The biochemical composition of the endothelial cell surface varies between the vascular beds. *Microsc. Res. Tech.* 57, 381–389. doi: 10.1002/jemt.10091
- Giger, U., and Meyer, U. A. (1983). Effect of succinylacetone on heme and cytochrome P450 synthesis in hepatocyte culture. *FEBS Lett.* 153, 335–338. doi: 10.1016/0014-5793(83)80637-1
- Gouya, L., Puy, H., Lamoril, J., Da Silva, V., Grandchamp, B., Nordmann, Y., et al. (1999). Inheritance in erythropoietic protoporphyria: A common wild-type ferrochelatase allelic variant with low expression accounts for clinical manifestation. *Blood* 93, 2105–2110. doi: 10.1182/blood.V93.6.2105.406k28_2105_2110
- Gupta, V., Liu, S., Ando, H., Ishii, R., Tateno, S., Kaneko, Y., et al. (2013). Salicylic acid induces mitochondrial injury by inhibiting ferrochelatase heme biosynthesis activity. *Mol. Pharmacol.* 84, 824–833. doi: 10.1124/mol.113.087940
- Hamza, I., and Dailey, H. A. (2012). One ring to rule them all: trafficking of heme and heme synthesis intermediates in the metazoans. *Biochim. Biophys. Acta* 1823, 1617–1632. doi: 10.1016/j.bbamcr.2012.04.009
- Handschin, C., Lin, J., Rhee, J., Peyer, A. K., Chin, S., Wu, P. H., et al. (2005). Nutritional regulation of hepatic heme biosynthesis and porphyria through PGC-1 α . *Cell* 122, 505–515. doi: 10.1016/j.cell.2005.06.040
- Jain, R. K. (2014). Antiangiogenesis strategies revisited: from starving tumors to alleviating hypoxia. *Cancer Cell* 26, 605–622. doi: 10.1016/j.ccr.2014.10.006
- Kawahara, H., Naito, H., Takara, K., Wakabayashi, T., Kidoya, H., and Takakura, N. (2013). Tumor endothelial cell-specific drug delivery system using apelin-conjugated liposomes. *PLoS One* 8, e65499. doi: 10.1371/journal.pone.0065499
- Kim, H. J., Khalimonchuk, O., Smith, P. M., and Winge, D. R. (2012). Structure, function, and assembly of heme centers in mitochondrial respiratory complexes. *Biochim. Biophys. Acta* 1823, 1604–1616. doi: 10.1016/j.bbamcr.2012.04.008
- Kluge, M. A., Fetterman, J. L., and Vita, J. A. (2013). Mitochondria and endothelial function. *Circ. Res.* 112, 1171–1188. doi: 10.1161/CIRCRESAHA.111.300233
- Korolnek, T., and Hamza, I. (2014). Like iron in the blood of the people: The requirement for heme trafficking in iron metabolism. *Front. Pharmacol.* 5, 126. doi: 10.3389/fphar.2014.00126
- Krammer, B., and Plaetzer, K. (2008). ALA and its clinical impact, from bench to bedside. *Photochem. Photobiol. Sci.* 7, 283–289. doi: 10.1039/B712847A
- Lane, R. K., Hilsabeck, T., and Rea, S. L. (2015). The role of mitochondrial dysfunction in age-related diseases. *Biochim. Biophys. Acta* 1847, 1387–1400. doi: 10.1016/j.bbmbio.2015.05.021
- Liu, K., Yan, J., Sachar, M., Zhang, X., Guan, M., Xie, W., et al. (2015). A metabolomic perspective of griseofulvin-induced liver injury in mice. *Biochem. Pharmacol.* 98, 493–501. doi: 10.1016/j.bcp.2015.09.002
- Luan, Y., Zhang, F., Cheng, Y., Liu, J., Huang, R., Yan, M., et al. (2017). Hemin improves insulin sensitivity and lipid metabolism in cultured hepatocytes and mice fed a high-fat diet. *Nutrients* 9, 805. doi: 10.3390/nu9080805
- Magness, S. T., Maeda, N., and Brenner, D. A. (2002). An exon 10 deletion in the mouse ferrochelatase gene has a dominant-negative effect and causes mild protoporphyria. *Blood* 100, 1470–1477. doi: 10.1182/blood-2001-12-0283
- Mather, K. J., Verma, S., and Anderson, T. J. (2001). Improved endothelial function with metformin in type 2 diabetes mellitus. *J. Am. Coll. Cardiol.* 37, 1344–1350. doi: 10.1016/S0735-1097(01)01129-9
- Nilsson, R., Schultz, I. J., Pierce, E. L., Soltis, K. A., Naranuntarat, A., Ward, D. M., et al. (2009). Discovery of genes essential for heme biosynthesis through large-scale gene expression analysis. *Cell Metab.* 10, 119–130. doi: 10.1016/j.cmet.2009.06.012
- Petrillo, S., Chiabrando, D., Genova, T., Fiorito, V., Ingoglia, G., Vinchi, F., et al. (2018). Heme accumulation in endothelial cells impairs angiogenesis by triggering paraptosis. *Cell Death Differ.* 25, 573–588. doi: 10.1038/s41418-017-0001-7
- Poulos, T. L. (2014). Heme enzyme structure and function. *Chem. Rev.* 114, 3919–3962. doi: 10.1021/cr400415k
- Pran Babu, S. P. S., White, D., and Corson, T. W. (2020). Ferrochelatase regulates retinal neovascularization. *FASEB J.* in press. doi: 10.1096/fj.202000964R
- Raman, C. S., Li, H., Martasek, P., Kral, V., Masters, B. S., and Poulos, T. L. (1998). Crystal structure of constitutive endothelial nitric oxide synthase: A paradigm for pterin function involving a novel metal center. *Cell* 95, 939–950. doi: 10.1016/S0092-8674(00)81718-3

- Rohlenova, K., Goveia, J., Garcia-Caballero, M., Subramanian, A., Kalucka, J., Treps, L., et al. (2020). Single-cell RNA sequencing maps endothelial metabolic plasticity in pathological angiogenesis. *Cell Metab.* 31, 862–877 e814. doi: 10.1016/j.cmet.2020.03.009
- Ryter, S. W., and Tyrrell, R. M. (2000). The heme synthesis and degradation pathways: role in oxidant sensitivity. Heme oxygenase has both pro- and antioxidant properties. *Free Radic. Biol. Med.* 28, 289–309. doi: 10.1016/S0891-5849(99)00223-3
- Saint-Geniez, M., Jiang, A., Abend, S., Liu, L., Sweigard, H., Connor, K. M., et al. (2013). PGC-1 α regulates normal and pathological angiogenesis in the retina. *Am. J. Pathol.* 182, 255–265. doi: 10.1016/j.ajpath.2012.09.003
- Sandoo, A., Carroll, D., Metsios, G. S., Kitas, G. D., and Veldhuijzen Van Zanten, J. J. (2011). The association between microvascular and macrovascular endothelial function in patients with rheumatoid arthritis: a cross-sectional study. *Arthritis Res. Ther.* 13, R99. doi: 10.1186/ar3374
- Schoors, S., Bruning, U., Missiaen, R., Queiroz, K. C., Borgers, G., Elia, I., et al. (2015). Fatty acid carbon is essential for dNTP synthesis in endothelial cells. *Nature* 520, 192–197. doi: 10.1038/nature14362
- Shetty, T., Sishtla, K., Park, B., Repass, M. J., and Corson, T. W. (2020). Heme synthesis inhibition blocks angiogenesis via mitochondrial dysfunction. *iScience*. in press. Preprint: *bioRxiv*. 836304. doi: 10.1101/836304.
- Sishtla, K., Lee, S., Lee, J. E., Seo, S. Y., and Corson, T. W. (2019). Discovery of ferrochelatase inhibitors as antiangiogenic agents. *Invest. Ophthalmol. Vis. Sci.* 60, E-abstract 5405.
- Sohoni, S., Ghosh, P., Wang, T., Kalainayakan, S. P., Vidal, C., Dey, S., et al. (2019). Elevated heme synthesis and uptake underpin intensified oxidative metabolism and tumorigenic functions in non-small cell lung cancer cells. *Cancer Res.* 79, 2511–2525. doi: 10.1158/0008-5472.CAN-18-2156
- Vandekeere, S., Dubois, C., Kalucka, J., Sullivan, M. R., Garcia-Caballero, M., Goveia, J., et al. (2018). Serine synthesis via PHGDH is essential for heme production in endothelial cells. *Cell Metab.* 28, 573–587 e513. doi: 10.1016/j.cmet.2018.06.009
- Vijayarath, C., Damle, S., Lenka, N., and Avadhani, N. G. (1999). Tissue variant effects of heme inhibitors on the mouse cytochrome c oxidase gene expression and catalytic activity of the enzyme complex. *Eur. J. Biochem.* 266, 191–200. doi: 10.1046/j.1432-1327.1999.00843.x
- Vinchi, F., De Franceschi, L., Ghigo, A., Townes, T., Cimino, J., Silengo, L., et al. (2013). Hemopexin therapy improves cardiovascular function by preventing heme-induced endothelial toxicity in mouse models of hemolytic diseases. *Circulation* 127, 1317–1329. doi: 10.1161/CIRCULATIONAHA.112.130179
- Wachowska, M., Muchowicz, A., Firczuk, M., Gabrysiak, M., Winiarska, M., Wańczyk, M., et al. (2011). Aminolevulinic acid (ALA) as a prodrug in photodynamic therapy of cancer. *Molecules* 16 (5), 4140–4164. doi: 10.3390/molecules16054140
- Waheed, S. M., Ghosh, A., Chakravarti, R., Biswas, A., Haque, M. M., Panda, K., et al. (2010). Nitric oxide blocks cellular heme insertion into a broad range of heme proteins. *Free Radic. Biol. Med.* 48, 1548–1558. doi: 10.1016/j.freeradbiomed.2010.02.038
- Yetkin-Arik, B., Vogels, I. M. C., Neyazi, N., Van Duinen, V., Houtkooper, R. H., Van Noorden, C. J. F., et al. (2019). Endothelial tip cells in vitro are less glycolytic and have a more flexible response to metabolic stress than non-tip cells. *Sci. Rep.* 9, 10414. doi: 10.1038/s41598-019-46503-2
- Zhang, B., Alruwaili, N., Kandhi, S., Deng, W., Huang, A., Wolin, M. S., et al. (2018). Inhibition of ferrochelatase impairs vascular eNOS/NO and sGC/cGMP signaling. *PLoS One* 13, e0200307. doi: 10.1371/journal.pone.0200307

Conflict of Interest: TC is a named inventor on patent applications related to this topic.

The remaining author declares that the research was conducted in the absence of any commercial or financial relationships that could be construed as a potential conflict of interest.

Copyright © 2020 Shetty and Corson. This is an open-access article distributed under the terms of the Creative Commons Attribution License (CC BY). The use, distribution or reproduction in other forums is permitted, provided the original author(s) and the copyright owner(s) are credited and that the original publication in this journal is cited, in accordance with accepted academic practice. No use, distribution or reproduction is permitted which does not comply with these terms.



EFEMP1 Overexpression Contributes to Neovascularization in Age-Related Macular Degeneration

Lu Cheng^{1†}, Chong Chen^{1†}, Wenke Guo^{2†}, Kun Liu¹, Qianqian Zhao², Ping Lu², Fudong Yu^{2*} and Xun Xu^{1*}

¹Shanghai Key Laboratory of Ocular Fundus Diseases, Department of Ophthalmology, Shanghai General Hospital, Shanghai Jiaotong University, National Clinical Research Center for Eye Diseases, Shanghai Engineering Center for Visual Science and Photomedicine, Shanghai Engineering Center for Precise Diagnosis and Treatment of Eye Diseases, Shanghai, China, ²NHC Key Lab of Reproduction Regulation, Shanghai Institute of Planned Parenthood Research, Fudan University, Shanghai, China

OPEN ACCESS

Edited by:

Zhongxiao Wang,
Boston Children's Hospital and
Harvard Medical School, United States

Reviewed by:

Kehan Zhang,
Boston University, United States
Haojie Fu,
Boston Children's Hospital and
Harvard Medical School, United States

*Correspondence:

Xun Xu
drxuxun@sjtu.edu.cn
Fudong Yu
fdyush@163.com

[†]These authors have contributed
equally to this work

Specialty section:

This article was submitted to
Neuropharmacology,
a section of the journal
Frontiers in Pharmacology

Received: 31 March 2020

Accepted: 01 December 2020

Published: 15 January 2021

Citation:

Cheng L, Chen C, Guo W, Liu K,
Zhao Q, Lu P, Yu F and Xu X (2021)
EFEMP1 Overexpression Contributes
to Neovascularization in Age-Related
Macular Degeneration.
Front. Pharmacol. 11:547436.
doi: 10.3389/fphar.2020.547436

Purpose: Age-related macular degeneration (AMD) is one of the leading causes of blindness, and choroidal neovascularization (CNV) in AMD can lead to serious visual impairment. Gene expression profiling of human ocular tissues have a great potential to reveal the pathophysiology of AMD. This study aimed to identify novel molecular biomarkers and gene expression signatures of AMD.

Methods: We analyzed transcriptome profiles in retinal-choroid tissues derived from donor patients with AMD in comparison with those from healthy controls using a publicly available dataset (GSE29801). We focused on the EFEMP1 gene, which was found to be differentially upregulated in AMD, especially in wet AMD eyes. Serological validation analysis was carried out to verify the expression of EFEMP1 in 39 wet AMD patients and 39 age- and gender-matched cataract controls, using an enzyme-linked immunosorbent assay (ELISA). We then investigated the role of EFEMP1 in angiogenesis through *in vitro* experiments involving EFEMP1 overexpression (OE) and knockdown in human umbilical vein endothelial cells (HUVECs).

Results: An increase in EFEMP1 expression was observed in the retinal-choroid tissues of eyes with AMD, which was more significant in wet AMD than in dry AMD. In addition, there was a significant increase in serum fibulin-3 (EFEMP1 encoded protein) concentration in patients with wet AMD compared with that in the controls. Tube formation and proliferation of EFEMP1-OE HUVECs increased significantly, whereas those of EFEMP1 knockdown HUVECs decreased significantly compared with those of the control. Additional extracellular fibulin-3 treatments did not increase tube formation and proliferation of wildtype and EFEMP1 knockdown HUVECs, indicating that the proangiogenic properties of EFEMP1 are of cell origin. We also found that vascular endothelial growth factor expression in HUVECs was upregulated by EFEMP1 overexpression and downregulated by EFEMP1 knockdown.

Conclusion: Our findings demonstrate EFEMP1 as a novel biomarker for CNV in AMD, providing a new target for the development of wet AMD-directed pharmaceuticals and diagnostics.

Keywords: Age-related macular degeneration, EFEMP1, fibulin-3, choroidal neovascularization, biomarker, gene expression profiling

INTRODUCTION

Age-related macular degeneration (AMD) is one of the leading causes of blindness in patients beyond 55 years. The number of AMD-affected patients is predicted to reach nearly 200 million by 2020 globally, increasing to approximately 300 million by 2040 (Wong et al., 2014). In advanced cases, wet AMD is often associated with abnormal choroidal neovascularization (CNV), a phenotype that can cause fluid and lipid leakage under the macula and fibrous scar formation and ultimately lead to serious visual impairment (Schmidt-Erfurth and Waldstein, 2016).

Although it is well-known that aging is the prevailing risk factor for AMD, genetic factors may contribute to AMD occurrence and progression (Smith et al., 2001). In recent years, genetic linkage analysis and genome-wide association studies have identified several important genetic risk factors, including complement-related genes (CFH, C2, CFB, CFHR1/3, C3, etc.) as well as non-complement-related genes, such as ARMS2 and HTRA1, and lipid metabolism-related loci (Zarepari et al., 2004; Edwards et al., 2005; Hageman et al., 2005; Gold et al., 2006; Yang et al., 2006; Maller et al., 2007; Fritsche et al., 2016). Despite these important discoveries, we still lack a detailed insight into the molecular mechanism responsible for the specific AMD phenotype. Although the introduction of treatments targeting vascular endothelial growth factor (VEGF) has decreased the incidence of legal blindness and visual impairment caused by wet AMD (Mehta et al., 2018), the underlying CNV pathophysiology and a comprehensive understanding of the biological pathways that mediate wet AMD development and progression have not yet been clarified.

Compared to research strategies that depend on indirect and reductionist experimental approaches, gene expression profiling of human ocular tissues has great potential to resolve AMD-associated molecular signaling pathways more precisely and comprehensively (Newman et al., 2012). Therefore, in this study, we analyzed the transcriptome profiles of differentially expressed genes in ocular tissues derived from AMD donor patients and compared the results with those of healthy donor controls using published public datasets and focused on the differentially upregulated epidermal growth factor-containing fibrillin-like extracellular matrix protein 1 (EFEMP1) gene. To elucidate the possible role of EFEMP1 in wet AMD and its biological function, serological validation analysis was carried out to verify the expression of EFEMP1 in wet AMD patients and cataract controls using enzyme-linked immunosorbent assay (ELISA). The phenotype was detected in EFEMP1 overexpressing and EFEMP1 knockdown human umbilical vein endothelial cells (HUVECs). Our findings might reveal a potential new target for the development of wet AMD-directed pharmaceuticals and diagnostics.

MATERIALS AND METHODS

Screening Differentially Expressed Proteins Through Published Datasets

DNA-free RNA levels of differentially expressed proteins in retinal-choroid samples from human donor eyes were screened in two published datasets, the University of Iowa and the Lions

Eye Bank of Oregon. Unlike the Iowa samples, which were expertly graded (normal, pre-AMD, dry AMD, and wet AMD), the Oregon samples received only a general AMD classification based on medical histories confirmed by ophthalmological records (Newman et al., 2012). Since Oregon samples received a less rigorous AMD classification than the Iowa samples, only normal and pre-AMD data were included. Donor-specific details (e.g., age, sex, and AMD phenotype) can be evaluated using the Gene Expression Omnibus (GEO: GSE29801).

Patient Samples

This study was reviewed and approved by the Medical Ethics Committee at Shanghai General Hospital affiliated to Shanghai Jiao Tong University (No.2016KY115-2) and conformed to the tenets of the Declaration of Helsinki. Written informed consent was obtained from all participants.

Patients were screened for enrollment in Shanghai General Hospital from October 2018 to December 2018. Patients diagnosed with wet AMD were included, assessed independently by two trained ophthalmologists (Dr. Xun X and Dr. Kun L). Patients were excluded if 1) they had intraocular surgeries or other pathologies, including congenital ocular diseases, glaucoma, and fundus diseases except for AMD according to self-reported history or ophthalmic examination; 2) they had systematic diseases including liver damage, kidney failure, lung disease, mental illness, autoimmune diseases, or cancer; and 3) the participant was unwilling or unable to give written consent or verbal assent. After the enrollment, each participant underwent a comprehensive ophthalmic examination, including a best-corrected visual acuity (BCVA) evaluation, slit-lamp biomicroscopy, tonometry, fundus examination, and optical coherence tomography (OCT). BCVA was measured using a retroilluminated Early Treatment of Diabetic Retinopathy Study chart from a distance of 4 m. For the control group, we enrolled age- and gender-matched cataract patients without fundus diseases who planned to undergo cataract surgery at Shanghai General Hospital. All serum samples were collected from wet AMD patients and cataract controls and stored in a -80°C refrigerator for no more than three months after quick-freezing in liquid nitrogen.

Serological Validation Analysis: ELISA-Based EFEMP1 Quantification

ELISA for EFEMP1 coding protein fibulin-3 was conducted according to the manufacturer's instructions using the Human EFEMP1 Assay ELISA Kit (#SEF422Hu, USCN Life Science Inc., Wuhan, China). Absorbance was measured at 450 nm using a microplate reader (Model 680, Bio-Rad, Hercules, CA, United States), and the results were calculated using GraphPad PRISM 5.0 (GraphPad Software Inc., La Jolla, CA, United States). Log transformation was performed for all analyses. Fibulin-3 levels were calculated and expressed as ng/mg. All samples were tested in duplicate.

Cells and Reagents

Primary HUVECs from pooled donors were obtained from Lonza (Portsmouth, NH) and maintained in endothelial cell medium

TABLE 1 | Sequences of primers used in this study.

Gene Name	Direction	Sequence 5' to 3'
EFEMP1	Forward	CAGGCTACGAGCAAAGTGAAC
	Reverse	ACAGTTGAGCCTGTCACTGCT
VEGF	Forward	CAACTTCTGGGCTGTTCTCGCT
	Reverse	CCCCCTCTCCTCTTCTCTCTCT

(ECM, ScienCell, San Diego, CA, United States). To mimic the AMD-associated EFEMP1 transcriptional level increase, we constructed EFEMP1 overexpressing (EFEMP1-OE) HUVECs using a recombinant lentivirus vector GV492 containing the human EFEMP1 gene (GenBank: NM_002775; SIRION Biotech). The lentivirus vector for EFEMP1 knockdown was achieved by cloning small hairpin RNAs using a recombinant lentivirus vector GV248, described as shEFEMP1 (target sequence: 5'-gcGTAGACATAGATGAATGTA-3'). CON335 and CON077 modification-containing enzymatically inactive variants were used separately as controls for EFEMP1-OE and shEFEMP1, respectively. Green fluorescent protein (GFP) was also inserted into the vector to instantly monitor the transfection rate. After 2 weeks of culture, when the HUVEC monolayer was completely established, cells were infected with GV492-EFEMP1, GV492-CON335, GV248-shEFEMP1, and GV248-CON077 overnight at 37°C. The medium was then changed, and the cells were cultured for three more weeks before performing any experiment.

Quantitative Real-Time Polymerase Chain Reaction

Total RNA was extracted using TRIzol (Invitrogen, Carlsbad, CA, United States), and reverse transcription was performed through M-MLV and cDNA amplification using the SYBR Green Master Mix kit (Takara, Otsu, Japan). Total RNA was isolated using a High Pure miRNA isolation kit (Roche) and the reverse transcription reaction was performed using a TaqMan MicroRNA Reverse Transcription kit (Life Technologies). Nuclear and cytoplasmic fractions were isolated using NE-PER Nuclear and Cytoplasmic Extraction Reagents (Thermo Scientific). Primer sequences are listed in **Table 1**. qRT-PCR results were analyzed using the LightCycler480 (Roche). The results shown represent the average of three independent experiments.

Western Blot Analysis

HUVECs were harvested and extracted using a lysis buffer (100 mM Tris-HCl, 2% SDS, 1 mM mercaptoethanol, 25% glycerol). Cell extracts were boiled in SDS sample buffer (Invitrogen, Carlsbad, CA, United States) and equal amounts of cell extracts were separated on 15% SDS-PAGE gels. Separated protein bands were transferred onto polyvinylidene fluoride membranes (Millipore, Billerica, MA, United States). The primary antibodies, including anti-fibulin-3 (ab70561, rabbit polyclonal antibody, Abcam, Cambridge, MA, United States), anti-VEGF (ab53465, rabbit polyclonal antibody, Abcam,

Cambridge, MA, United States), and anti-tubulin (ab153802, rabbit polyclonal antibody, Abcam, Cambridge, MA, United States), were diluted at a ratio of 1:1,000 according to the manufacturer's instructions and incubated overnight at 4°C. Horseradish peroxidase-linked secondary antibodies (Cell Signaling Technology) were added at a dilution ratio of 1:10,000 and incubated at room temperature for 1 h. The membranes were washed with PBS three times and the immunoreactive bands were visualized using ECL-PLUS/Kit (GE Healthcare, Piscataway, NJ, United States) according to the manufacturer's instructions.

Human Umbilical Vein Endothelial Cell Tube Formation Assay

We used a HUVEC tube formation assay, which measures the ability of endothelial cells plated at subconfluent densities with the appropriate extracellular matrix support, to form capillary-like structures (tubes) to model the reorganization stage of angiogenesis. Experiments were performed using a μ -Slide Angiogenesis kit (81,506, Ibidi, Martin Reid, Germany). Precooled growth factor-reduced Matrigel was added to each inner well of cooled μ -Slide plates and incubated at 37°C for 60 min. HUVECs were preincubated at 37°C for 30 min before seeding. In some cases, WT or shEFEMP1 HUVECs were preincubated in ECM with different concentrations of recombinant human fibulin-3 protein (8416-FB-050, R&D Systems, Minneapolis, MN). 50 μ l cell suspension (2×10^5 cells/ml) with or without fibulin-3 protein was applied to each upper well. After incubation at 37°C for 12 h, the samples were stained with diluted calcein (6.25 μ g/ml), fluorescent images were captured using an Olympus FSX100 microscope (Olympus, Tokyo, Japan), and the images were analyzed using the ImageJ software (National Institutes of Health, Bethesda, MA, United States). Four fields were randomly selected from each well, then the total tube length, number of branch points, and total number of networks were quantified.

Human Umbilical Vein Endothelial Cell 5-Ethynyl-2'-Deoxyuridine Proliferation Assay

HUVECs were seeded onto a 96-well plate at a density of 1×10^4 cells per well in ECM with or without fibulin-3 protein and allowed to adhere overnight. 5-Ethynyl-2'-deoxyuridine (EdU) assay was carried out with a Click-iT™ Plus EdU Cell Proliferation Kit (C10638, Thermo Fisher Scientific, Waltham, MA, United States). After incubation with 50 μ M EdU for 2 h, the cells were fixed in 4% paraformaldehyde and stained with Apollo Dye Solution. Hoechst-33,342 was used to stain nucleic acids within the cells. Images were acquired with an Olympus FSX100 microscope (Olympus, Tokyo, Japan), and the percentage of EdU-positive cells was quantified using the ImageJ software (National Institutes of Health, Bethesda, MA, United States).

Statistical Analyses

Results for continuous variables with normal distribution are presented as mean \pm SD and were analyzed using one-way analysis of variance (ANOVA) and Student's t-test. Bonferroni correction was used for multiple comparisons. Results for

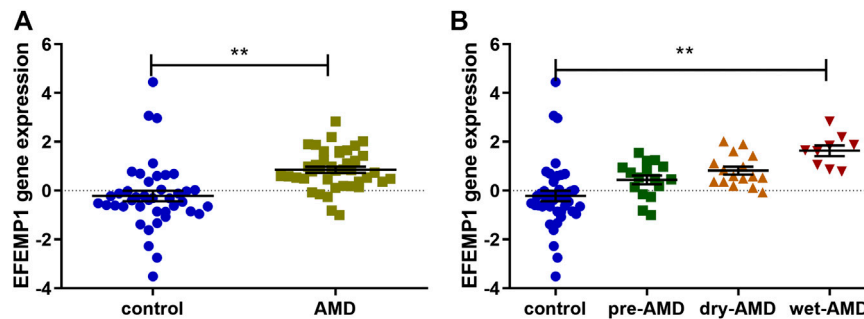


FIGURE 1 | EFEMP1 gene expression in ocular tissues derived from patients with age-related macular degeneration (AMD) and healthy controls from GSE29801. **(A)** EFEMP1 expression increased in AMD-affected eyes compared with that in the control group. **(B)** EFEMP1 expression in wet AMD-affected eyes was higher than that in the control group as well as in the pre-AMD and dry AMD groups. ** $p < 0.01$.

continuous but non-normally distributed variables were presented as medians and interquartile ranges and analyzed using nonparametric tests. Binary variables were presented as absolute numbers or percentages and were analyzed using the chi-squared test. Statistical analyses were performed using SPSS 22.0 (Statistical Software, Los Angeles, CA, United States) and GraphPad PRISM 5.0. p -values < 0.05 were considered statistically significant.

RESULTS

Identification of EFEMP1 in Age-Related Macular Degeneration

To identify the differentially expressed genes in AMD, we performed transcriptome profiling from GSE29801 (containing retinal-choroid tissue samples from 42 normal eyes and 41 eyes with AMD, including 16 pre-AMD eyes, 16 dry AMD eyes, and nine wet AMD eyes) after data preprocessing and quality assessment using R software. We identified 827 upregulated genes and 592 downregulated genes; the top 100 most significant DEGs of GSE29801 have been identified in another study of ours (not published yet). Furthermore, tissue specific expression analysis of these DEGs was conducted to obtain retinal-choroid specific proteins. EFEMP1/fibulin-3, the expression of which is significantly higher in retinal-choroid than in other tissues, was finally found. Compared with the control group, EFEMP1 gene was upregulated in ocular tissues of patients with AMD, as well as in patients with pre-AMD, dry AMD, and wet AMD. Furthermore, the expression of EFEMP1 in wet AMD eyes was higher than that in patients with pre-AMD and dry AMD, but there was no significant difference between pre-AMD and dry AMD patients. (Figure 1; Table 2).

Serum Fibulin-3 Level Increases in Patients With Wet Age-Related Macular Degeneration

To validate whether the serum concentration of EFEMP1 coding protein fibulin-3 was also upregulated in patients with wet AMD, serum samples from 39 wet AMD patients and 39 age- and gender-matched cataract controls were collected for ELISA. The mean levels of fibulin-3 in serum from patients with wet AMD and controls were 3.989 ± 1.852 ng/ml and 2.793 ± 1.847 ng/ml, respectively. There was a

statistically significant increase in circulating fibulin-3 levels in patients with wet AMD compared with those in controls ($p = 0.0056$, Figure 2).

Effects of EFEMP1 on Human Umbilical Vein Endothelial Cell Tube Formation

EFEMP1-OE and EFEMP1 knockdown (shEFEMP1) HUVECs were constructed (Figure 3). Next, we employed *in vitro* HUVEC tube formation assays to directly determine the effect of EFEMP1 on angiogenesis. In the absence of any additional stimulation in ECM with growth factor-reduced Matrigel, EFEMP1-OE HUVECs exhibited significantly enhanced tube formation activities, with increased mean HUVEC tube length, number of branch points, and total number of networks compared with those of the control CON335 HUVECs (Figure 4A, $p < 0.01$). In contrast, shEFEMP1 HUVECs exhibited markedly decreased tube formation capacities, with shorter mean tube length, fewer branch points, and smaller networks than those of the CON077 HUVECs (Figure 4B).

Effects of EFEMP1 on Human Umbilical Vein Endothelial Cell Proliferation

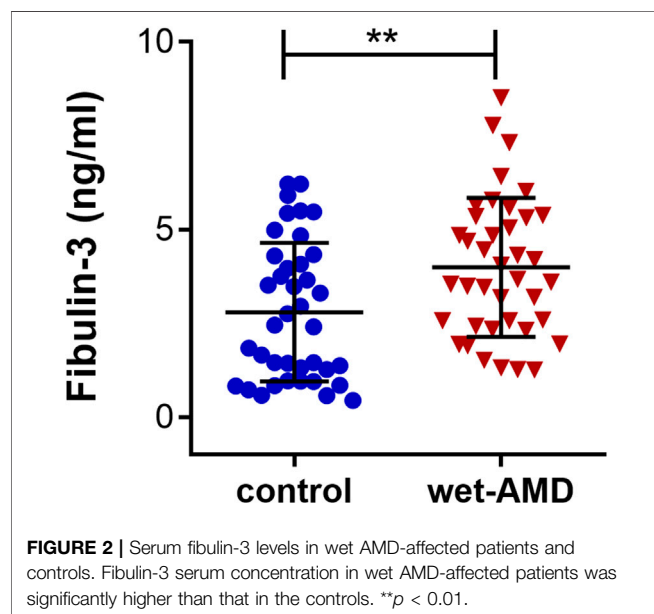
The proliferation of EFEMP1-OE HUVECs increased significantly compared to that of CON335 HUVECs, whereas the proliferation of shEFEMP1 HUVECs decreased significantly compared to that of CON077 HUVECs (Figure 5). This indicated that fibulin-3 played an important role in promoting cell proliferation in HUVECs.

Origin of the Proangiogenesis Property of EFEMP1

EFEMP1 is a member of the secreted extracellular glycoprotein family, and its overexpression increases both the intracellular and extracellular fibulin-3 levels. Therefore, to reveal whether the origin of the proangiogenesis property of EFEMP1 is extracellular or intracellular, the effects of extracellular fibulin-3 on wildtype (WT) and shEFEMP1 HUVECs were examined. It seemed that WT HUVECs treated with different concentrations of recombinant human fibulin-3 protein exhibited similar tube formation capacities and no significant differences in mean tube length, number of branch points, and total number of

TABLE 2 | EFEMP1 gene expression data in ocular tissues of patients with age-related macular degeneration (AMD) and healthy controls from GSE29801.

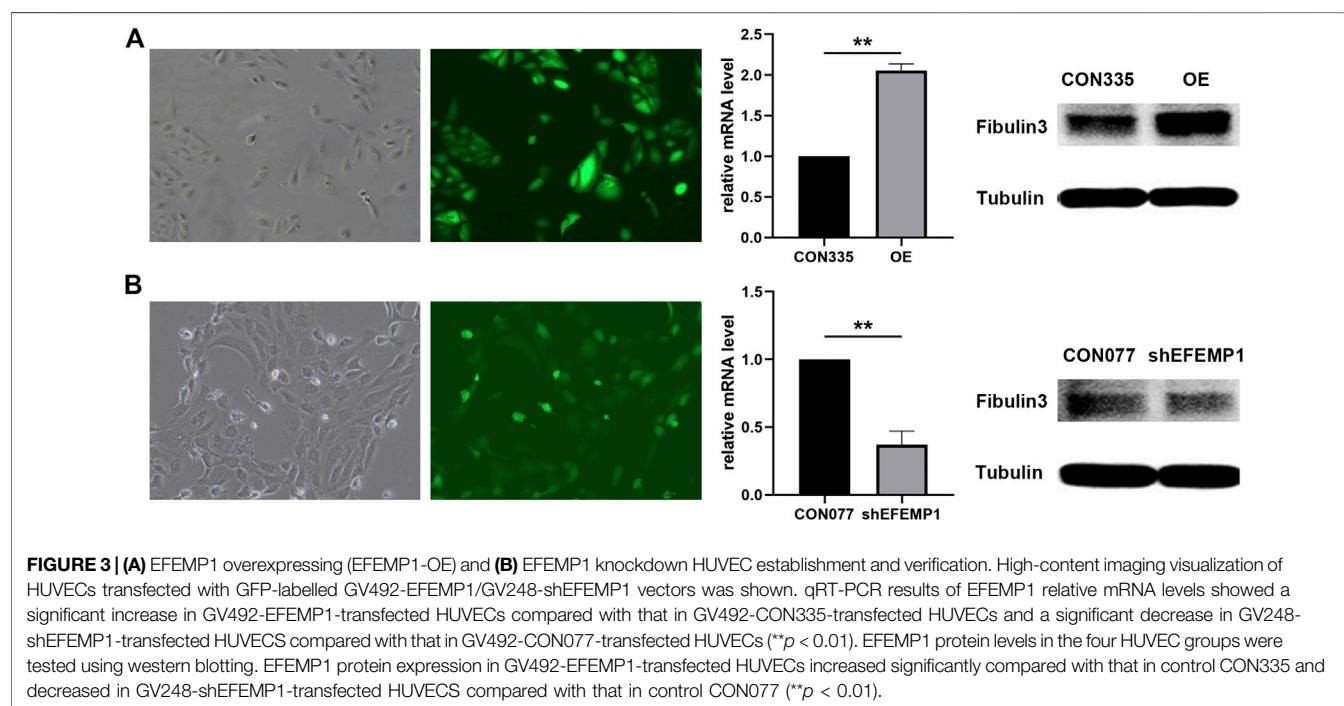
EFEMP1	AMD			
	Pre-AMD (n = 16)	Dry AMD (n = 16)	Wet AMD (n = 9)	Total (n = 41)
Control (n = 42)	$p = 0.0229$	$p = 0.0003$	$p < 0.0001$	$p < 0.0001$
Pre-AMD	—	$p = 0.1295$	$p = 0.0005$	—
Dry AMD	—	—	$p = 0.0059$	—



networks were found among groups. In addition, the addition of fibulin-3 in ECM could not recover the inhibited tube formation capacity of shEFEMP1 HUVECs (**Figure 6A**). Similarly, the proliferation of WT HUVECs was not affected by different concentrations of extracellular fibulin-3, and no significant differences in proliferation capacities were found between WT HUVECs in fibulin-3 coated or uncoated plates (**Figure 6B**). Moreover, the proliferation of shEFEMP1 HUVECs was not increased by the addition of extracellular fibulin-3 (**Figure 6B**). The results indicated that intracellular, but not extracellular, increase in fibulin-3 could promote angiogenesis in HUVECs.

Effects of EFEMP1 on the Expression of Vascular Endothelial Growth Factor in Human Umbilical Vein Endothelial Cell

As shown in **Figure 7**, VEGF mRNA and protein levels were significantly increased by overexpression of fibulin-3, whereas knockdown of fibulin-3 inhibited the expression of VEGF at the mRNA and protein levels. This indicated that VEGF signaling



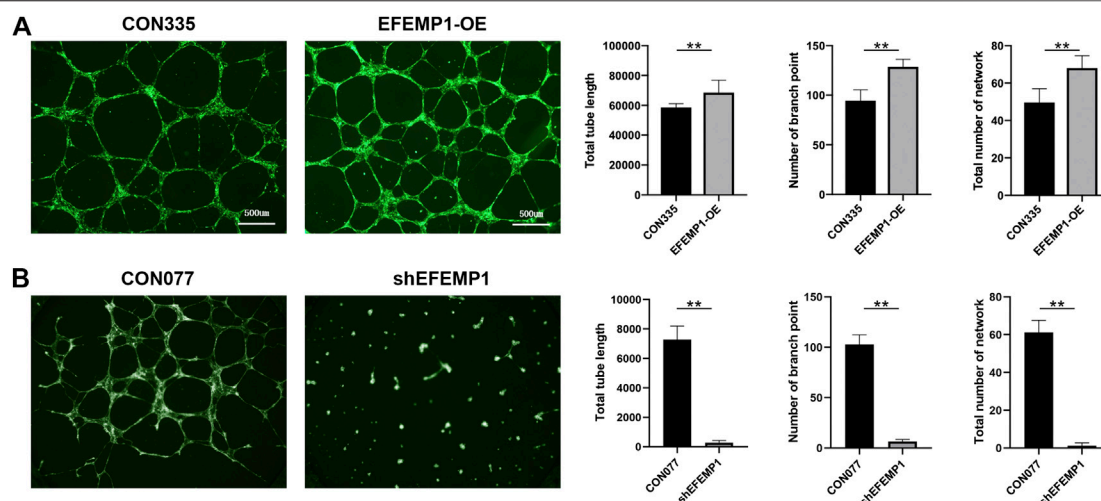


FIGURE 4 | Effects of EFEMP1 on HUVEC tube formation. **(A)** Control CON335 HUVECs, EFEMP1-OE HUVECs, **(B)** control CON077 HUVECs, and shEFEMP1 HUVECs seeded on Matrigel were allowed to form tubes for 12 h in the absence of any additional stimulation. Total tube length, number of branch points, and total number of networks in captured images were measured using MetaMorph. The data represent the average of five independent replicates and the experiments were performed three times. ** $p < 0.01$.

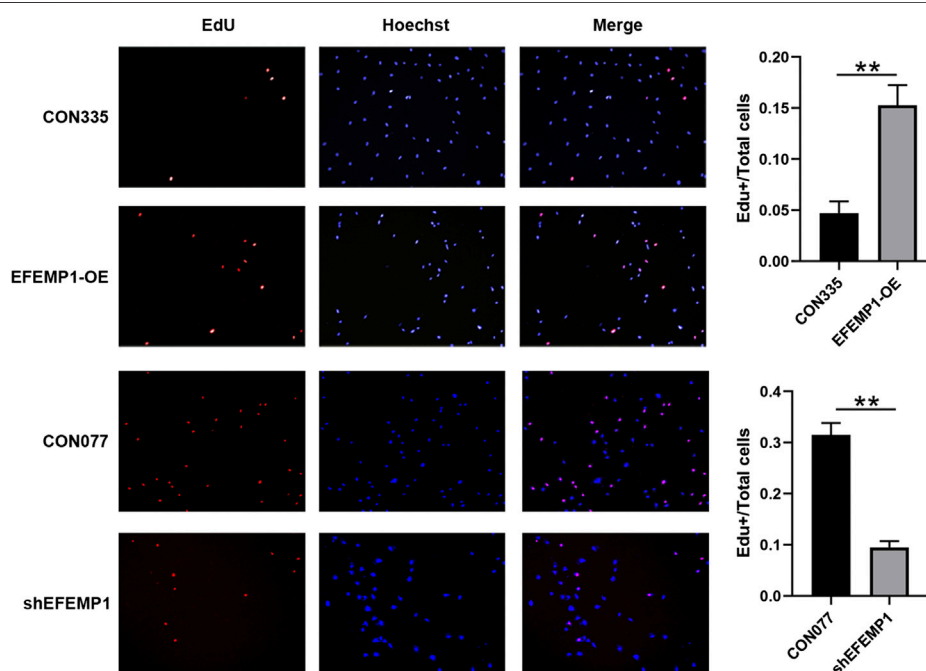


FIGURE 5 | Effects of EFEMP1 on HUVEC proliferation. CON335 HUVECs, EFEMP1-OE HUVECs, CON077 HUVECs, and shEFEMP1 HUVECs were stained using EdU and Hoechst. EdU-positive cells were highlighted in red and nuclei in blue, following Hoechst staining. Proliferation capacities were analyzed by calculating the percentage of EdU-positive cells. Three independent experiments were performed, and five fields were randomly selected for statistical analysis in each experiment. ** $p < 0.01$.

may participate in the proangiogenesis process induced by fibulin-3. These results are also consistent with the findings in a previous study whereby CNV cases with R345W mutation in EFEMP1 were sensitive to anti-VEGF treatment (Sohn et al., 2011).

DISCUSSION

AMD is a disease with complex inheritance and epigenetic changes (DeAngelis et al., 2017). CNV development is a common and sight-threatening complication. Based on

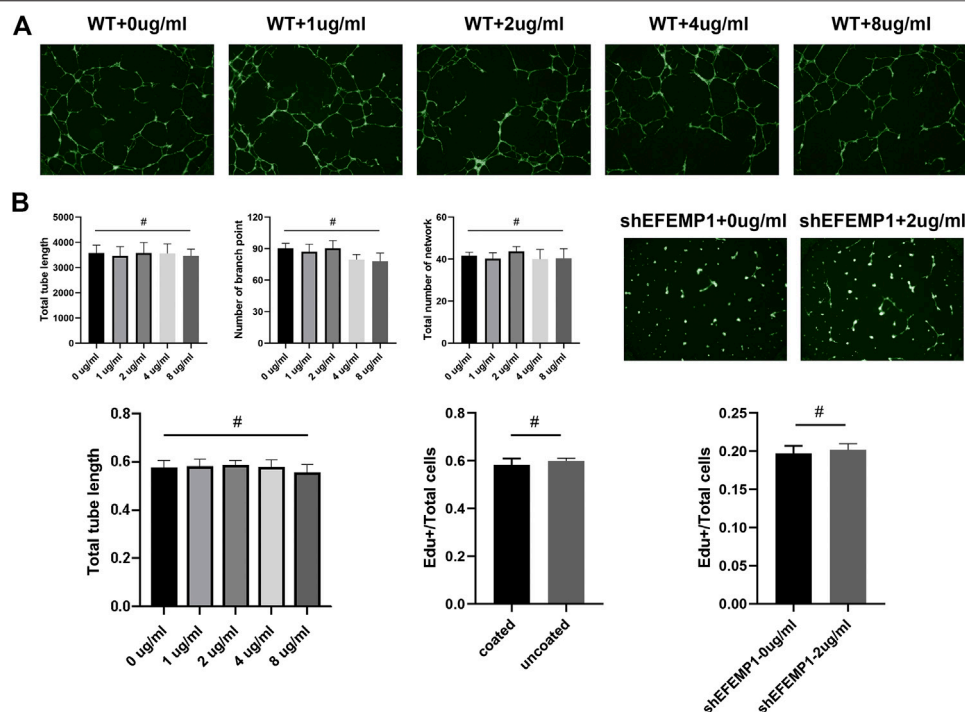


FIGURE 6 | Origin of the proangiogenesis property of EFEMP1. **(A)** Tube formation of wild type (WT) HUVECs treated with different concentrations (0 μ g/ml, 1 μ g/ml, 2 μ g/ml, 4 μ g/ml, and 8 μ g/ml) of recombinant human fibulin-3 protein and shEFEMP1 HUVECs treated with or without fibulin-3 protein was tested. **(B)** Proliferation of wild type (WT) HUVECs treated with different concentrations (0 μ g/ml, 1 μ g/ml, 2 μ g/ml, 4 μ g/ml, and 8 μ g/ml) of recombinant human fibulin-3 protein, WT HUVECs in fibulin-3 coated or uncoated plates, and shEFEMP1 HUVECs treated with or without fibulin-3 protein was tested using EdU assay. $^{\#}p > 0.05$.

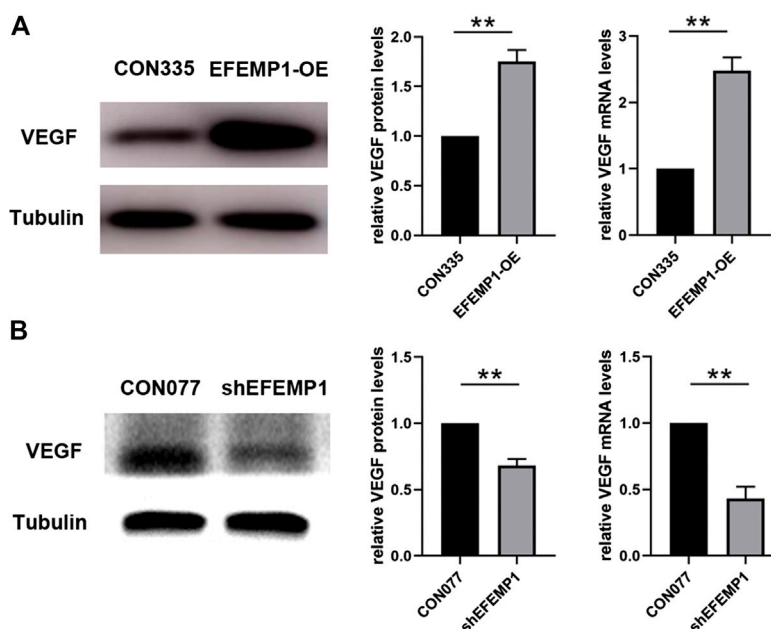


FIGURE 7 | Effects of EFEMP1 on VEGF expression. VEGF mRNA and protein level alterations in **(A)** CON335 HUVECs, EFEMP1-OE HUVECs, **(B)** CON077 HUVECs, and shEFEMP1 HUVECs were detected using qRT-PCR and western blotting, respectively. $^{**}p < 0.01$.

numerous genetic studies of AMD, approximately 50% of the heritability of AMD can be explained by two major loci harboring coding and noncoding variation at chromosomes 1q (CFH) and 10q (ARMS2/HTRA1) (Klein et al., 2005; Hageman et al., 2005; Rivera et al., 2005; Deangelis et al., 2008). Recently, a large sample genome-wide association study (GWAS) has highlighted new genes and pathways in the development of AMD, including complement activation, collagen synthesis, lipid metabolism/cholesterol transport, endodermal cell differentiation, and extracellular matrix organization, indicating that many unknown genetic changes remain to be discovered in the initiation and development of AMD (Fritsche et al., 2016). Compared to previous GWAS studies, gene expression profiling of human ocular tissues has great potential to identify gene coexpression modules, to build molecular models with predictive utility, and to elucidate functional networks of AMD (Newman et al., 2012). In the present study, we aimed to screen novel biomarkers from the perspective of transcriptome profiling of AMD patients' RPE-choroid and retina tissue samples (GSE29801), using integrated bioinformatic analysis, verify its expression in peripheral blood, and elucidate its possible biological function. To our knowledge, no similar studies have been conducted previously.

In this study, we downloaded the RNA sequencing microarray data from the GEO database. NCBI-GEO is a free database for microarray/gene profiling and next-generation sequencing. Furthermore, we analyzed the transcriptome of differentially expressed genes in ocular tissues derived from AMD donor patients compared with normal donor controls. As a result, the differentially upregulated EFEMP1 gene was screened.

It is generally believed that the human EFEMP1 cDNA encodes a secreted extracellular protein named fibulin-3, which consists of 493 amino acids with a predicted molecular weight of 55 kDa (Lecka-Czernik et al., 1995). Fibulin-3 is one of seven highly conserved members of the fibulin family of extracellular matrix (ECM) proteins (Zhang and Marmorstein, 2010), which is implicated in extracellular matrix remodeling, cell proliferation, and organogenesis (Chen et al., 2018). Although EFEMP1 is a broadly expressed gene throughout the body (Marmorstein et al., 2002; Kobayashi et al., 2007; Zhang and Marmorstein, 2010), its expression in the retina is significantly higher than in other tissues (**Figure 1**). A missense mutation R345W was found to be associated with Malattia Leventinese/Doyne honeycomb retinal dystrophy (ML/DHRD) (Stone et al., 1999). In normal eyes, EFEMP1 accumulated predominantly in the nerve fiber layer and the photoreceptor inner and outer segments; less intense accumulation was observed in the outer nuclear layer (ONL) and the inner (IPL) and outer (OPL) plexiform layers. No accumulation was observed in the RPE, Bruch's membrane, the choroid (CH), or the inner nuclear layer (INL). Nevertheless, in both ML and AMD eyes, abnormally accumulated EFEMP1 is seen beneath the RPE overlaying sub-RPE deposits and accelerates the process of drusen formation (Marmorstein et al., 2002). Recent studies have shown that EFEMP1 knockout has protective effects on the progress of sub-RPE deposits in mouse eyes (Stanton et al., 2017), suggesting that the existence of EFEMP1 may be required for

sub-RPE deposit formation. Nevertheless, the association between EFEMP1 and wet AMD has not been reported thus far, and the function of EFEMP1 in CNV, especially in vascular endothelial cells, is still unclear.

According to the present study, the expression of EFEMP1 was upregulated in the retinal-choroid tissue of both dry AMD and wet AMD patients. Moreover, the increase in wet AMD was more significant than that in dry AMD. We also described higher levels of serum fibulin-3 in wet AMD compared to controls. This may emphasize an important role of EFEMP1 in the advanced CNV stage of the disease, and not only in the early drusen formation phase, indicating that EFEMP1 might be a novel biomarker of wet AMD that could be detected through peripheral blood examination.

Recently, an increasing number of studies have implicated that EFEMP1 plays an important but contradictory role in regulating angiogenesis, as it appears to have different functions in different tissues. In lung, liver, breast, ovarian, and prostate cancers, fibulin-3 acts as an angiogenesis antagonist (Sadr-Nabavi et al., 2009; Hu et al., 2011; Chen et al., 2013). Downregulation of fibulin-3 results in tumor angiogenesis (Albig et al., 2006). However, in cervical carcinoma, pancreatic cancer, high-grade gliomas, and psoriasis, overexpressed fibulin-3 was shown to upregulate VEGF expression and induce angiogenesis (Seeliger et al., 2009; Song et al., 2011; Nandhu et al., 2014; Wang et al., 2019). This property may be correlated with its context-specific manner (Albig et al., 2006). However, its role in the development of ocular angiogenesis has not been investigated. The higher EFEMP1 expression level in the retinal-choroid tissues with CNV lesions was demonstrated in the current study, indicating that EFEMP1 plays a proangiogenic role in wet AMD eyes. The current study also highlights the active role of EFEMP1 in HUVECs *in vitro*. We found that overexpression of EFEMP1 promoted tube formation and cell proliferation of HUVECs, whereas knockdown of EFEMP1 inhibited tube formation and proliferation capacities. One possible explanation for these results is the change in extracellular fibulin-3 levels, which was caused by the increase or decrease in fibulin-3 secretion in HUVECs transfected with fibulin-3 cDNA or shRNA. Indeed, higher extracellular fibulin-3 levels secreted by tumor cells could induce proangiogenic behavior in endothelial cells (Nandhu et al., 2014; Wang et al., 2019). Therefore, we reexamined the angiogenic behavior of HUVECs using highly purified fibulin-3. Remarkably, extracellular fibulin-3 was insufficient to increase HUVEC tube formation and proliferation. Moreover, tubulogenesis and proliferation inhibited by shEFEMP1 was not recovered in the presence of additional fibulin-3. Taken together, these results suggest that the proangiogenic effects of EFEMP1 in HUVECs are, at least in part, dependent on intracellular modulation. In addition, the expression of VEGF in HUVECs was upregulated by EFEMP1 overexpression and downregulated by EFEMP1 knockout, providing indirect evidence that the VEGF signaling pathway may participate in the proangiogenesis of EFEMP1.

Although R345W mutations have been reported in ML, no mutation in EFEMP1 has been reported to be associated with AMD (Stone et al., 1999). In the absence of a mutation, it is

possible that modifications due to aging, cigarette smoking, or oxidative, thermal, or other stress cause overexpression of EFEMP1 (Giasson et al., 2000; Stanton et al., 2017) in RPE cells and vascular endothelial cells in the retina of AMD eyes. On one hand, secreted fibulin-3 could partially drain into the blood through disrupted blood–retina barriers, resulting in an increase in serum fibulin-3 levels. On the other hand, increased fibulin-3 may promote angiogenesis, which is common in tumor angiogenesis. In the present study, upregulated ocular expression of EFEMP1 and increased serum level of fibulin-3 have been verified in patients with wet AMD. We also demonstrated that HUVECs-origin fibulin-3 contributes to endothelial cell tube formation, proliferation, and VEGF production. Although extracellular matrix origin fibulin-3 promotes sub-RPE deposits and accelerates the process of drusen formation (Marmorstein et al., 2002; Stanton et al., 2017), the proangiogenic properties of EFEMP1 are of endothelium origin according to the present study. The angiogenesis modulation mechanism by fibulin-3 needs to be studied in more detail through both *in vivo* and *in vitro* experiments in the future. One possible explanation would be that, as an extracellular glycoprotein, fibulin-3 is translated into the endoplasmic reticulum, where it is folded and processed before transport to the Golgi and eventually secreted. Overexpression of fibulin-3 and its accumulation in the endoplasmic reticulum could lead to the activation of the unfolded protein response on demand and further induce transcriptional upregulation of VEGF, which has been reported in RPE cells (Roybal et al., 2005).

The current study is interesting owing to two principal reasons. First, we revealed for the first time that EFEMP1 gene expression is upregulated in wet AMD eyes, which could be detected through serum examination, providing new molecular biomarkers and gene expression signatures of AMD. Second, we discovered that EFEMP1 could promote angiogenesis of endothelial cells to foster CNV development in the eye, providing new insights into the landscape of AMD pathophysiology and new targets for CNV treatment. This study also has some limitations and shortcomings. First, the sample size, especially in the wet AMD group in the current study, was limited; therefore, the results of this study are preliminary and larger sample sizes are needed to produce a solid confirmation. Second, only *in vitro* experiments were conducted in the present study; thus, further *in vivo* experiments are needed to provide more direct evidence of the role of EFEMP1 in CNV formation.

CONCLUSION

In summary, we have demonstrated several important findings. First, an increase in EFEMP1 expression was observed in the retinal-choroid tissues of eyes with AMD, which was more significant in wet AMD than in dry AMD. Second, higher levels of serum fibulin-3 were detected in wet AMD. Finally,

cell-origin EFEMP1 substantially promoted tube formation, enhanced cell proliferation, and increased the expression of VEGF in HUVECs. These results may offer novel insights into AMD pathogenesis and represent new targets for the development of AMD-directed therapeutics and diagnostics, but they need further confirmation by *in vivo* experiments.

DATA AVAILABILITY STATEMENT

The original contributions presented in the study are included in the article/Supplementary Materials, further inquiries can be directed to the corresponding authors.

ETHICS STATEMENT

The studies involving human participants were reviewed and approved by the Medical Ethics Committee at the Shanghai General Hospital affiliated to the Shanghai Jiao Tong University (No.2016KY115-2). The patients/participants provided their written informed consent to participate in this study.

AUTHOR CONTRIBUTIONS

LC and CC conceived and coordinated the project, enrolled participants, collected samples, and performed serological analysis, compiled the figures and the tables, and wrote the manuscript. WG performed cell experiments and statistical analysis of all data and compiled functional enrichment analysis and protein–protein interaction network analysis. KL helped to collect participants and coordinate data analysis. QZ and PL helped with data curation and searching information in different databases. FY sourced the database and screened the hub genes. XX conceived and directed the project and wrote the manuscript. All authors reviewed the manuscript.

FUNDING

This study was supported by the National Key R&D Program of China (2016YFC0904800, 2019YFC0840607); National Science and Technology Major Project of China (2017ZX09304010); National Natural Science Foundation of China (81800831, 81800835, and 82000880); Shanghai Sailing Program (18YF1419700 and 19YF1439400); Shanghai “Rising Stars of Medical Talent” Youth Development Program (Youth Medical Talents Specialist Program), and Cross-Research Foundation of Shanghai Jiaotong University (ZH2018QNA13). No author has a financial or proprietary interest in any material or method mentioned.

REFERENCES

- Albig, A. R., Neil, J. R., and Schieman, W. P. (2006). Fibulins 3 and 5 antagonize tumor angiogenesis *in vivo*. *Canc. Res.* 66, 2621–2629. doi:10.1158/0008-5472.CAN-04-4096
- Chen, J., Wei, D. Y., Zhao, Y. R., Liu, X. Y., and Zhang, J. (2013). Overexpression of EFEMP1 correlates with tumor progression and poor prognosis in human ovarian carcinoma. *PLoS One*. 8, e7878. doi:10.1371/journal.pone.0078783
- Chen, Y., Gilbert, M. A., Grochowski, C. M., McEldrew, D., Llewellyn, J., Waisbourd-Zinman, O., et al. (2018). A genome-wide association study identifies a susceptibility locus for biliary atresia on 2p16.1 within the gene EFEMP1. *PLoS Genet.* 14, e1007532. doi:10.1371/journal.pgen.1007532
- DeAngelis, M. M., Ji, F., Adams, S., Morrison, M. A., Harring, A. J., Sweeney, M. O., et al. (2008). Alleles in the HtrA serine peptidase 1 gene alter the risk of neovascular age-related macular degeneration. *Ophthalmology*. 115, 1209–1215. doi:10.1016/j.ophtha.2007.10.032
- DeAngelis, M. M., Owen, L. A., Morrison, M. A., Morgan, D. J., Li, M., Shikoor, A., et al. (2017). Genetics of age-related macular degeneration (AMD). *Hum. Mol. Genet.* 26, R45–R50. doi:10.1093/hmg/ddx22810.1093/hmg/ddx343
- Edwards, A. O., Ritter, R., Abel, K. J., Manning, A., Panhuysen, C., and Farrer, L. A. (2005). Complement factor H polymorphism and age-related macular degeneration. *Science*. 308, 421–424. doi:10.1126/science.1110189
- Fritsche, L. G., Igl, W., Bailey, J. N., Grassmann, F., Sengupta, S., Bragg-Gresham, J. L., et al. (2016). A large genome-wide association study of age-related macular degeneration highlights contributions of rare and common variants. *Nat. Genet.* 48, 34–43. doi:10.1038/ng.3448
- Giasson, B. I., Duda, J. E., Murray, I. V., Chen, Q., Souza, J. M., Hurtig, H. I., et al. (2000). Oxidative damage linked to neurodegeneration by selective alpha-synuclein nitration in synucleinopathy lesions. *Science*. 290, 985–989. doi:10.1126/science.290.5493.985
- Gold, B., Merriam, J. E., Zernant, J., Hancox, L. S., Taiber, A. J., Gehrs, K., et al. (2006). Variation in factor B (BF) and complement component 2 (C2) genes is associated with age-related macular degeneration. *Nat. Genet.* 38, 458–462. doi:10.1038/ng1750
- Hageman, G. S., Anderson, D. H., Johnson, L. V., Hancox, L. S., Taiber, A. J., Hardisty, L. I., et al. (2005). A common haplotype in the complement regulatory gene factor H (HF1/CFH) predisposes individuals to age-related macular degeneration. *Proc. Natl. Acad. Sci. U. S. A.* 102, 7227–7232. doi:10.1073/pnas.050153610210.1073/pnas.0501536102
- Hu, Y., Pioli, P. D., Siegel, E., Zhang, Q., Nelson, J., Chaturvedi, A., et al. (2011). EFEMP1 suppresses malignant glioma growth and exerts its action within the tumor extracellular compartment. *Mol. Canc.* 10, 123. doi:10.1186/1476-4598-10-123
- Klein, R. J., Zeiss, C., Chew, E. Y., Tsai, J. Y., Sackler, R. S., Haynes, C., et al. (2005). Complement factor H polymorphism in age-related macular degeneration. *Science*, 308: 385–389. doi:10.1126/science.1109557
- Kobayashi, N., Kostka, G., Garbe, J. H., Keene, D. R., Bächinger, H. P., Hanisch, F. G., et al. (2007). A comparative analysis of the fibulin protein family. Biochemical characterization, binding interactions, and tissue localization. *J. Biol. Chem.* 282, 11805–11816. doi:10.1074/jbc.M611029200
- Lecka-Czernik, B., Lumpkin, C. K., Jr, and Goldstein, S. (1995). An overexpressed gene transcript in senescent and quiescent human fibroblasts encoding a novel protein in the epidermal growth factor-like repeat family stimulates DNA synthesis. *Mol. Cell Biol.* 15, 120–128. doi:10.1128/mcb.15.1.120
- Maller, J. B., Fagerness, J. A., Reynolds, R. C., Neale, B. M., Daly, M. J., and Seddon, J. M. (2007). Variation in complement factor 3 is associated with risk of age-related macular degeneration. *Nat. Genet.* 39, 1200–1201. doi:10.1038/ng2131
- Marmorstein, L. Y., Munier, F. L., Arsenijevic, Y., Schorderet, D. F., McLaughlin, P. J., Chung, D., et al. (2002). Aberrant accumulation of EFEMP1 underlies drusen formation in Malattia Leventinese and age-related macular degeneration. *Proc. Natl. Acad. Sci. U.S.A.* 99, 13067–13072. doi:10.1073/pnas.202491599
- Mehta, H., Tufail, A., Daien, V., Lee, A. Y., Nguyen, V., Ozturk, M., et al. (2018). Real-world outcomes in patients with neovascular age-related macular degeneration treated with intravitreal vascular endothelial growth factor inhibitors. *Prog. Retin. Eye Res.* 65, 127–146. doi:10.1016/j.preteyeres.2017.12.002
- Nandhu, M. S., Hu, B., Cole, S. E., Erdreich-Epstein, A., Rodriguez-Gil, D. J., and Viapiano, M. S. (2014). Novel paracrine modulation of notch-DLL4 signaling by fibulin-3 promotes angiogenesis in high-grade gliomas. *Canc. Res.* 74, 5435–5448. doi:10.1158/0008-5472.CAN-14-0685
- Newman, A. M., Gallo, N. B., Hancox, L. S., Miller, N. J., Radeke, C. M., Maloney, M. A., et al. (2012). Systems-level analysis of age-related macular degeneration reveals global biomarkers and phenotype-specific functional networks. *Genome Med.* 4, 16. doi:10.1186/gm315
- Rivera, A., Fisher, S. A., Fritsche, L. G., Keilhauer, C. N., Lichtner, P., Meitinger, T., et al. (2005). Hypothetical LOC387715 is a second major susceptibility gene for age-related macular degeneration, contributing independently of complement factor H to disease risk. *Hum. Mol. Genet.* 14, 3227–3236. doi:10.1093/hmg/ddi353
- Roybal, C. N., Marmorstein, L. Y., Vander Jagt, D. L., and Abcouwer, S. F. (2005). Aberrant accumulation of fibulin-3 in the endoplasmic reticulum leads to activation of the unfolded protein response and VEGF expression. *Invest. Ophthalmol. Vis. Sci.* 46, 3973–3979. doi:10.1167/iov.05-0070
- Sadr-Nabavi, A., Ramser, J., Volkmann, J., Naehrig, J., Wiesmann, F., Betz, B., et al. (2009). Decreased expression of angiogenesis antagonist EFEMP1 in sporadic breast cancer is caused by aberrant promoter methylation and points to an impact of EFEMP1 as molecular biomarker. *Int. J. Canc.* 124, 1727–1735. doi:10.1002/ijc.24108
- Schmidt-Erfurth, U., and Waldstein, S. M. (2016). A paradigm shift in imaging biomarkers in neovascular age-related macular degeneration. *Prog. Retin. Eye Res.* 50, 1–24. doi:10.1016/j.preteyeres.2015.07.007
- Seeliger, H., Camaj, P., Ischenko, I., Kleespies, A., De Toni, E. N., Thieme, S. E., et al. (2009). EFEMP1 Expression promotes *in vivo* tumor growth in human pancreatic adenocarcinoma. *Mol. Canc. Res.* 7, 189–198. doi:10.1158/1541-7786.MCR-08-0132
- Smith, W., Assink, J., Klein, R., Mitchell, P., Klaver, C. C., Klein, B. E., et al. (2001). Risk factors for age-related macular degeneration: pooled findings from three continents. *Ophthalmology*. 108, 697–704. doi:10.1016/s0161-6420(00)00580-7
- Sohn, E. H., Patel, P. J., MacLaren, R. E., Adatia, F. A., Pal, B., Webster, A. R., et al. (2011). Responsiveness of choroidal neovascular membranes in patients with R345W mutation in fibulin 3 (Doyle honeycomb retinal dystrophy) to anti-vascular endothelial growth factor therapy. *Arch. Ophthalmol.* 129, 1626–1628. doi:10.1001/archophthol.2011.338
- Song, E. L., Hou, Y. P., Yu, S. P., Chen, S. G., Huang, J. T., Luo, T., et al. (2011). EFEMP1 expression promotes angiogenesis and accelerates the growth of cervical cancer *in vivo*. *Gynecol. Oncol.* 121, 174–180. doi:10.1016/j.ygyno.2010.11.004
- Stanton, J. B., Marmorstein, A. D., Zhang, Y., and Marmorstein, L. Y. (2017). Deletion of Efemp1 is protective against the development of sub-RPE deposits in mouse eyes. *Invest. Ophthalmol. Vis. Sci.* 58, 1455–1461. doi:10.1167/iov.16-20955
- Stone, E. M., Lotery, A. J., Munier, F. L., Heon, E., Piguet, B., Guymer, R. H., et al. (1999). A single EFEMP1 mutation associated with both Malattia Leventinese and Doyle honeycomb retinal dystrophy. *Nat. Genet.* 22, 199–202. doi:10.1038/9722
- Wang, X., Sun, X., Qu, X., Li, C., Yang, P., Jia, J., et al. (2019). Overexpressed fibulin-3 contributes to the pathogenesis of psoriasis by promoting angiogenesis. *Clin. Exp. Dermatol.* 44, e64–e72. doi:10.1111/ced.13720
- Wong, W. L., Su, X., Li, X., Cheung, C. M., Klein, R., Cheng, C. Y., et al. (2014). Global prevalence of age-related macular degeneration and disease burden projection for 2020 and 2040: a systematic review and meta-analysis. *Lancet Glob. Health.* 2, e106–116. doi:10.1016/S2214-109X(13)70145-1
- Yang, Z., Camp, N. J., Sun, H., Tong, Z., Gibbs, D., Cameron, D. J., et al. (2006). A variant of the HTRA1 gene increases susceptibility to age-related macular degeneration. *Science*. 314, 992–993. doi:10.1126/science.1133811
- Zarepari, S., Reddick, A. C., Branham, K. E., Moore, K. B., Jessup, L., Thoms, S., et al. (2004). Association of apolipoprotein E alleles with susceptibility to age-related macular degeneration in a large cohort from a single center. *Invest. Ophthalmol. Vis. Sci.* 45, 1306–1310. doi:10.1167/iov.03-1253
- Zhang, Y., and Marmorstein, L. Y. (2010). Focus on molecules: fibulin-3 (EFEMP1). *Exp. Eye Res.* 90, 374–375. doi:10.1016/j.exer.2009.09.018

Conflict of Interest: The authors declare that the research was conducted in the absence of any commercial or financial relationships that could be construed as a potential conflict of interest.

Copyright © 2021 Cheng, Chen, Guo, Liu, Zhao, Lu, Yu and Xu. This is an open-access article distributed under the terms of the Creative Commons Attribution License (CC BY). The use, distribution or reproduction in other forums is permitted, provided the original author(s) and the copyright owner(s) are credited and that the original publication in this journal is cited, in accordance with accepted academic practice. No use, distribution or reproduction is permitted which does not comply with these terms.

Advantages of publishing in Frontiers



OPEN ACCESS

Articles are free to read
for greatest visibility
and readership



FAST PUBLICATION

Around 90 days
from submission
to decision



HIGH QUALITY PEER-REVIEW

Rigorous, collaborative,
and constructive
peer-review



TRANSPARENT PEER-REVIEW

Editors and reviewers
acknowledged by name
on published articles

Frontiers

Avenue du Tribunal-Fédéral 34
1005 Lausanne | Switzerland

Visit us: www.frontiersin.org

Contact us: frontiersin.org/about/contact



REPRODUCIBILITY OF RESEARCH

Support open data
and methods to enhance
research reproducibility



DIGITAL PUBLISHING

Articles designed
for optimal readership
across devices



FOLLOW US

@frontiersin



IMPACT METRICS

Advanced article metrics
track visibility across
digital media



EXTENSIVE PROMOTION

Marketing
and promotion
of impactful research



LOOP RESEARCH NETWORK

Our network
increases your
article's readership